Hot Topics in Thermal Analysis and Calorimetry 11

Jaroslav Šesták
Pavel Hubík
Jiří J. Mareš *Editors*

Thermal Physics and Thermal Analysis

From Macro to Micro, Highlighting Thermodynamics, Kinetics and Nanomaterials

Springer

Thermal Physics and Thermal Analysis

Hot Topics in Thermal Analysis and Calorimetry

Volume 11

Series editor

Judit Simon, Budapest, Hungary

More information about this series at http://www.springer.com/series/6056

Jaroslav Šesták · Pavel Hubík · Jiří J. Mareš
Editors

Thermal Physics and Thermal Analysis

From Macro to Micro, Highlighting Thermodynamics, Kinetics and Nanomaterials

Springer

Editors
Jaroslav Šesták
New Technologies Research Centre
(NTC-ZČU)
University of West Bohemia
Pilsen
Czech Republic

Pavel Hubík
Division of Solid-State Physics
Institute of Physics, Czech Academy
of Sciences
Prague
Czech Republic

Jiří J. Mareš
Division of Solid-State Physics
Institute of Physics, Czech Academy
of Sciences
Prague
Czech Republic

ISSN 1571-3105 ISSN 2542-4505 (electronic)
Hot Topics in Thermal Analysis and Calorimetry
ISBN 978-3-319-45897-7 ISBN 978-3-319-45899-1 (eBook)
DOI 10.1007/978-3-319-45899-1

Library of Congress Control Number: 2016963609

Printed on acid-free paper

This Springer imprint is published by Springer Nature
The registered company is Springer International Publishing AG
The registered company address is: Gewerbestrasse 11, 6330 Cham, Switzerland

Dedication and Acknowledgements

This book fulfillment was greatly supported by Dr. Pavel Holba (1940–2016), one of the most talented world thermodynamists, who unfortunately passed away during this volume completion, so that we are contented to dedicate this work to his memory.

The present book completion as well as the accomplishment of individual chapters was supported by Institutional Research Plan of Institute of Physics ASCR, v.v.i., while developed at its Join Research Laboratory with the New Technologies Centre of the University of West Bohemia in Pilsen. The financial assistance was provided by the CENTEM project (NTC, ZČU), reg. no. CZ.1.05/2.1.00/03.0088 that is co-funded from the ERDF as a part of the MEYS—Ministry of Education, Youth and Sports OP RDI Program and, in the follow-up sustainability stage supported through the CENTEM PLUS LO 1402.

The multi-institutional cooperation during the drafting of this book is greatly acknowledged, and the contributions by distinguished experts from an international array of world renowned scientists are recognized.

The present book is a stretchy continuation of the previous Volume 8 (*Glassy, Amorphous and Nano-Crystalline Materials: Thermal Physics, Analysis, Structure and Properties*—ISBN 9789048128815) and Volume 9 (*Thermal Analysis of Micro-, Nano-, and Non-Crystalline Materials: Transformation, Crystallization, Kinetics and Thermodynamics*—ISBN 9789048131495), complementing thus a coherent triptych with authoritative overview of cutting-edge themes of material science focused on solid-state chemistry, thermal physics, and analysis of various states of matter. It provides a new farsightedness of various concepts, often avant-garde and mostly not published yet.

Distinctive chapters featured in the book include, among others, calorimetry on timescales, glass transition phenomena, nonstoichiometry, kinetics of non-isothermal processes, kinetic phase diagrams, thermal inertia and temperature gradients, thermodynamics of nanomaterials, selforganization and econophysics, significance of temperature and entropy, hyperfree energy and Ehrenfest equations

of higher order, biomaterials and microtextiles, significance of scientific works, and infiniteness. Advanced undergraduates, postgraduates, researchers, and academicians working in the field of thermal analysis and calorimetry, thermophysical measurements, thermodynamics and material sciences will find this contributed volume invaluable.

This is the third volume of the triptych volumes on thermal behavior of materials; the previous two (volumes 8 and 9) received over twenty thousands of downloads guaranteeing their worldwide impact ranking them between the twenty best books by Springer.

Initial Volume 8 was appreciatively instigated by thermoanalytical legends as US Professors A. Angel and B. Wunderlich, Bulgarian I. Avramov, Brazilian E. Zanotto or Japanese H. Suga and further based on the Czech and Slovak studies not so well internationally known yet but influential, among others mentioning N. Koga, M. Liška, J. Málek or P. Šimon.

The editors are pleased to present this forward-thinking compendium to public judgment convinced that the innovative ideas will serve duly the coming generation of thermal scientists.

Foreword

The Eyewitness's Recollections on Thermal Analysis Maturity; the Half-Century Anniversary of Formation of the New Field, which is Now Due for Revision

The historic part of this preface is more than a recollection of the pertaining chronology. The present state of thermal analysis, as an inseparable part of thermal physics [1], is "resting on the shoulders" of its pioneers and their previous problems, controversies, and fallibilities. That gives us a relative perspective that our present achievements are neither absolute nor the last. A more detailed description than just a chronological enumeration of events was needed to link the previous ways of thinking with ours. This humbleness aside, we should be feeling lucky and happy that we are a part of this discipline, so uniquely diversified and bridging refined theory with technical applications, and the curious insight into materials with methodological inventiveness. The most exciting thermoanalytical discoveries, fundamental revisions of the theories, and enormous expansions of the research areas, are still ahead of us.

Thermal analysis is a research method which studies, in dynamic, time-related ways, the relationships between temperature and some selected properties. This method dates back well into the nineteenth century, and it was initially called thermography. The term "thermal analysis" (TA) was introduced at the turn of twentieth century by Tammann [2] who was recording cooling curves in phase-equilibrium studies of binary systems. He was followed by others [3], performing more exhaustive study of the effect of experimental variables on the shape of heating curves, as well as the influence of temperature gradients and heat fluxes taking place within both the furnace and the sample. The associated differential thermal analysis (DTA) was initially an empirical technique, and its early quantitative studies were semi-empirical and based on intuitive reasoning. Though some theoretical understanding was build [3], it was Berg, using the Newton's cooling law, who gave the initial theoretical bases for DTA [4], later improved within the renowned Russian thermoanalytical school [5]. DTA became gradually the center of attention [6], thermogravimetry being the second, thanks to its quantitative benefits.

Fig. 1 Those who instigated the underpinning new fields of thermal physics and its indispensable branch of thermal analysis: Strouhal Čeněk (Vincenc) (1858–1922, Bohemia [15]), Berg [4] (1896–1974, USSR), Mackenzie [9, 16] (1920–2000, Scotland), who also helped for the formation of ICTA (International Confederation of Thermal Analysis); William Wesley Wendlandt [11, 17] (1927–2000, USA, the architect of Thermochimica Acta [18]), Keattch and Dollimore [19] (1920–2000, UK–USA, the initiator of the sister organization ESTAC—European Symposium of thermal Analysis and Calorimetry) and Cornelius Bernard Murphy [20] (1918–1994, USA, the first elected ICTA President)

It is high time now to recognize heat as an "instrumental reagent." Vold [7] was the first to take account of sample's thermal inertia, an essential factor of kinetic evaluation. That improvement, however, was repudiated by Borchard and Daniels [8] and that had a deleterious effect [10] on the subsequent DTA kinetic studies, persisting even now. Those improvements [6–7] remained largely ignored in the ensuing key books [9–11] and in many related papers. Therefore, the progress in this area (equation manipulation, thermal effects) can be best seen in the sphere of kinetic papers. The six most important founders of thermal analysis are shown in Fig. 1. There are certainly other noteworthy "architects" who could not be listed here, but most of them have been mentioned elsewhere [12–14].

As the result of WW2, Europe was divided into the free West, and the East occupied by USSR, with a profoundly deep split between them—political, military, economic, and cultural. Information coming from the free world had a disruptive potential for the communist doctrine, so the East-European science became a victim of the all-encompassing censorship and restrictions. Because of that, the East-European science, including thermal analysis, was developing to a great extent independently from that in the West. For this reason, the history of thermal analysis in the second half of the twentieth century needs to be told in two parts: in the West, and in the East, separately.

The Western Course of Thermal Analysis Advancement, and Foundation of Thermochimica Acta

The development of the Western stream of thermal analysis matured at the first International Symposium on Thermal Analysis [12] which was held at the Northern Polytechnic in London (organized by B.R. Currel and D.A. Smith, April 1965), consisting of about 400 mostly international participants. The choice of the invited

lectures offered the first account of thermal analysts who founded the field's progress, such as B.R. Currell, D.A. Smith, R.C. Mackenzie, P.D. Garn, M. Harmelin, W.W. Wendlandt, J.P. Redfern, D. Dollimore, C.B. Murphy, H.G. McAdie, L.G. Berg, M.J. Frazer, W. Gerard, G. Lombardi, C.J. Keattch, and G. Berggren. The remarkable key lectures were read by P.D. Garn, G. Guiochon, and J.P Redfern, on kinetic studies, also by W.W. Wendlandt and M. Hermelin on the methods of thermoanalytical investigations. The organizers invited scientist from the informationally isolated countries of the Soviet Block, then represented by F. Paulik and J. Šesták giving the key lectures on the standardization of experimental condition and errors of kinetic data. This event was followed by the Aberdeen conference (September 1965) organized by J.P. Redfern and R.C. Mackenzie (Scotland), with the help of US C.B. Murphy, Czech R. Barta, Russian L.G. Berg, and Hungarian L. Erdey, with almost identical personal attendance.

During those conferences, culminating at the first ICTA conference in Worcester (USA 1968) [21], the Elsevier publishing house, advocated by Prof. W.W. Wendlandt (USA), realized the need to create an international journal covering thermal analysis. And so in early 1970s, the journal Thermochimica Acta (TCA) started the publishing

Fig. 2 Editorial Board meeting of Thermochimica Acta in Grado (6th ESTAC, September 1994). *Upper from left* T. Ozawa (Kyoto), J. Šesták (Prague), J. Hay (one time TCA Editor, Birmingham), W. Hemminger (one-time TCA Editor, Brunswick), E.L. Charsley (Leeds), J. Dunn (Pearth), part-hidden M. Richardson (Teddington), V.B. Lazarev (Moscow), part-hidden P.K. Gallagher (Columbus), J. Rouquerol (Marseilles). *Sitting from left*: L. Whiting, (one time TCA Editor, Midland), G. Arena (Catalania), G. DelaGatta (Torino), H. Suga (Osaka). In 1990s, several more renowned thermal analysts participated at the TCA EB such as J.R. Allan (Edinburgh, V. Balek (Řež), E.H.P. Cordfunke (Petten), G. D'Ascenzo (Rome), D. Dollimore (Toledo, USA), C.M. Earnest (Rome), W. Eysel (Aachen), J.H. Flynn (Washington), A.K. Galwey (Belfast), F. Grønvold (Oslo), J.-P.E. Grolier [Aubiere), L.D. Hansen (Provo), K. Heide (Jena), L.G. Hepler (Edmonton), R.-H. Hu (Beijing), R.B. Kemp (Aherystwyth), A. Kettrup (Paderborn), I. Lamprecht (Berlin), F. Paulik (Budapest), O.T. Sorensen (Roskilde), or S.St.J. Warne (Newcastle)

process, which continued for twenty-five years by its founder [18] and legendary editor Wesley W. Wendlandt (1920–1997), with the help of the group of already renowned scientists, making the first international TCA Editorial Board: B.R. Currell, T. Ozawa, L. Reich, J. Šesták, A.P. Gray, R.M. Izatt, G. Beech, M. Harmelin, H.G. McAdie, H.G. Wiedemann, E.M. Barrall, T.R. Ingraham, R.N. Rogers, J. Chiu, H. Dichtl, P.O. Lumme, R.C. Wilhoit, G. Pannetier, G.M. Lukaszewski, E. Sturm, G.A. Vaughan, with support of D.A. Smith, S. Seki, M.J. Frazer, C.J. Keattch, and/or G. Berggren (Fig. 2). The journal had its seat in Huston (Texas, USA) gradually joining the best established and recognized international periodicals. Only one of those authors of the earliest TCA board is remaining now as a yet active member.

TCA grew fast, and during the first ten years of its existence it increased the number of pages tenfold. The credit largely belongs to the editor [18], whose scientific reputation and guidance, as well as his own articles substantially contributed to the success. The TCA publications focused on the hot topics identified during the former conferences, especially those dealing with the theoretical basis of general thermoanalytical kinetics [22–26]. Unfortunately, less attention was paid to DTA theory [27] which later became more abundant [28, 29], but its treatment mostly overlooked the factor of sample's thermal inertia [7, 30] ignoring the first kinetic software which did address sample's heat inertia [33]—the readers were probably apprehensive to be overwhelmed by the complexity of the problem which would require a revision of the commonly practiced procedures. Five papers [22–26] from the first two years of TCA's existence are worth highlighting. They analyzed the consequences of the Garn's book [10], which provided the early core of non-isothermal kinetic studies. Those papers have received an abundant citation response, namely (Scopus) 29, 282, 70, 802, and 8, respectively. They altogether provided a starting point to the subsequent kinetic studies, resulting in books [31–33], the latest of which just preserved mathematical exploitation of kinetic equations, but paying not enough attention to other critical assessments [34–36]. The ICTAC's Kinetics Committee issued "Recommendations" [37], which received a high citation response ($\sim$800), but that may be seen rather relative since they advise how to precisely evaluate and correctly publish not fully truthful kinetic numbers [36]. Hundreds of valuable kinetic publications and some more recent TCA papers received equally high citation response such as [38] with 180 or [39] with 230 citations.

We should appreciate the pioneering role of TCA having published the first concise paper coining the term "heat inertia" and showing its effect on kinetics [30]. It is not a fault of the journal that paper [30] was overlooked and was not incorporated in further kinetic software. Moreover, the historical data clearly show the key influence of kinetic studies on the TCA publication scope [36, 37], recently touching advanced treatises providing detailed characterization of samples by averaging the temperature values at different locations within the sample [40], incorporation of a cooling constant [41], merging the impact of gradient [42] necessary to better direct future research of modern kinetics [33].

In 1969, Paul D. Garn, a pioneer of thermoanalytical kinetics (then of the Akron University, Ohio), founded the North American Thermal Analysis Society (NATAS), becoming its first president. Presently, NATAS is a large organization,

with many sections, and remaining very active for the last 47 years. It organizes conferences annually, publishing their proceedings as NATAS Notes. Information about NATAS, and links to the other national thermoanalytical organizations, can be found at [43]. Garn's scientific life was not happy. He disagreed with the mainstream of the thermoanalytical kinetics, criticized it relentlessly [34], and he was logically deconstructing its fundamental faults, so his arguments were systematically ignored. The other researchers were unwilling to revise their most basic assumptions and "start from scratch." Only now, long after his death, his line of thinking seems to be getting some traction.

Several Japanese researchers (Ihmory, Takagi, Honda) developed their original designs much earlier than the first European (Nernst, Škramovský, Guichard, Duval) and American (anonymous, later Cahn) thermobalance instruments became commercially available in 1950s [13, 14]. Those Japanese designs pioneered the technique in several ways: Saito's TG was top loading, Shibata and Fukushima used electromagnetic force. It was followed by other masterminds as Ozawa (non-isothermal kinetics) and Suga (calorimetry and non-crystallinity) which was detailed in our previous historical chapter [14].

The Eastern Stream of Thermoanalytical Progress and Foundation of Journal of Thermal Analysis

The other Eastern branch became active in the difficult times when persecution and discrimination of politically active scientist was common in those countries. The science in the so-called Eastern Block had to work in almost full isolation from the thermal analysis of the rest of the world. From late 1940s to late 1980s, most of the scientists in the Soviet Block were neither allowed to communicate with the West, nor permitted to travel there. The Western literature was only scarcely available; purchasing Western instrumentation was generally out of question. That resulted in a "schism," into the "Western" thermal analysis and "Eastern" one [12–14, 44]. Paradoxically, that isolation from the West created some benefits by forcing the Eastern thermal analysts to build their own instruments, e.g., the famous Hungarian Derivatograph (T+DTA+TG+DTG) [45], the only relatively easily available thermoanalytical instrument in Eastern Europe, or "Pyrometr Kurnakova" (DTA), thousands of which were manufactured in USSR, primarily for geological exploration.

The contributions to the thermoanalytical theory by scientists from USSR should not be overlooked [4, 5, 46] to mention just these of the hundreds who combined broad scientific background with practical attitude. The mainstream thermoanalytical theory could benefit from both, but their books and articles, published mostly in the Cyrllic font, remain almost completely unknown in the West.

Cut-off from the West by the communist "Iron Courtain," the East-European thermal analysts were actively working toward acquiring scientific, cultural, social and political information from the free world. Contacts with Western thermal analysts were performed by letters, joint publications, and participation in international meetings. The very difficult access to publish internationally dictated the need to find local forum for thermoanalytical publications. One of them turned out to be the Czechoslovak scientific journal "Silikáty" founded by R. Barta as early as 1956 and long edited by Šatava [47]. It became famous for promoting publications in the sphere of thermal analysis [44]. Since those papers, naturally for the circumstances, were published in the Czech language, they did not get the international attention they deserved. However, some of them did contribute to acquiring initial insight into the role of temperature gradients in kinetic evaluations [48].

Journal "Silikaty" originated from the first Czechoslovak (more or less first international) conference on thermal analysis, mostly dealing with DA. It was organized by R. Barta in Prague as early as 1955 (titled "Thermography Discussions") [47]. That was followed by a series of thermoanalytical conferences, such as the first Thermography Day (1958 in Bratislava) and the 2nd Conference on Thermography (1961 in Prague, already with an international participation including Dr. R.C. Mackenzie. The most important of those events was the first international thermoanalytical conference behind the iron curtain: the 4th ICTA in Budapest 1974, where the thermoanalytical West and the East had a chance to work together, underpinning the bases of various advanced methods (cf. Fig. 3.).

Worth noting are the Soviet conferences on thermal analysis [55] (formerly named "thermography") starting in Kazan 1953 and 1957, followed by the All-Union conferences in Riga 1962 and continued in Moscow 1969, etc. In early 1970s, other major TA conferences took place in Germany, Hungary, and Poland. In 1972, jointly with J.P. Redfern and G. Liptay, R.C. Mackenzie started publishing a periodical Thermal Analysis Abstracts (TAA), prepared by a team of reviewers covering the East- and West-European countries. After 20 years, that service was stopped in 1991 due to the proliferation of computers. Several books and articles [31, 32, 46, 51, 54–58] largely contributed to the growth of thermal analysis.

Despite severe political difficulties, Judit Simon and Eva Buzagh followed the example of the "Silikáty" and fashioned a team consisting of renowned L. Erdey, the F. and J. Paulik brothers, J.P. Redfern, R. Bárta, L.G. Berg, G. Lombardi, R.C. Mackenzie, C. Duval, P.D. Garn, S.K. Bhattacharyya, A.V. Nikolaev, C.B. Murphy, T. Sudo, D.J. Swaine, W.W. Wendlandt, J.F. Johanson, and consulting editors F. Szabadvary and G. Liptay (of this group, only three remain now), publishing thus the first thermoanalytical-focused journal, in a record-short time [59]. It helped to facilitate the communication between the East and West.

Kinetics became an important subject [60–63] of the two first JTA volumes, but again little attention was paid to DTA's theory [64]. Thermal inertia was practically absent in JTA, and only passingly mentioned elsewhere [48]. The early JTA issues contained articles on modern kinetics [65–68], including its critique [69, 70].

Fig. 3 Young scientists participating at 1974 ICTA in Budapest who represented a new groundswell for the rising field of thermal analysis; *from left* Jean Rouquerol (*1937) [49] France, Hemminger (*1937) [50], Germany, Schultze (*1937), [51] Germany, Jaroslav Šesták (*1938), [17, 52] Czechoslovakia, Simon (*1937) [53] and Ferenc Paulik (1922–2005), [45, 54] both from Hungary

The 1985 ICTA in Bratislava, cf. Fig. 4, became the topmost achievement of the Czech–Slovak thermal analysts, who bravely prepared and carried out an open international conference in then communistic Czechoslovakia; such initiatives were "strongly discouraged" by authorities. The geopolitical split of thermal analysis into "East" and "West" lasted forty years, the length of a typical active period in the life of a scientist. That schism ceased to exist in 1989, the Soviet Army withdrew from stationing in the Eastern Europe, so communism in Europe was allowed to collapse and most countries of these two "blocks" merged.

Fig. 4 Celebrating the 20th anniversary of ICTA foundation: The ICTA Council meeting in the castle Liblice (near Prague) taking place at the occasion of the 8th ICTA Conference in Bratislava 1985 (former Czechoslovakia). *From left* Giuseppe Della Gatta (Persuading additional term Calorimetry in ICTAC, Italy), Erwin Marti (Switzerland), Jaroslav Šesták (8 ICTA program chair, Czechia), *behind* Klaus Heide (Germany), Slade St.J. Warne (ICTA Vice-president, Australia), Hans-Joachim Seifert (ICTA President, Germany), Patric K. Gallagher (ICTA Past-president, USA), Joseph H. Flynn (USA), Tommy Wadsen (Sweden), John Crighton (England), John O. Hill (Australia), Paul D. Garn (USA), Vladislav V. Lazarev (Russia), Walter Eysel (Germany), Bordas S. Alsinas (Spain), Edward L. Charsley (England, former president), *behind* Shmuel Yariv (Izrael, secretary)

Fig. 5 Budapest, Hungary, March 2015. Honorary celebration and farewell to the long-running JTAC editor-in-chief, Professor Judit Simon. *From left* Petru Budrugeac (Romania), Peter Šimon (Slovakia), Alfred Kállay-Menyhárd (Deputy JTAC editor-in-chief since 2014), Judit Simon (Honorary JTAC Editor), György Liptay (Honorary consulting Editor), Jaroslav Šesták (Czechia), and Imre Miklós Szilágyi (JTAC co-editor since 2014)

As the field of thermal analysis broadened its scope, the journal changed its name to Journal of Thermal Analysis and Calorimetry (JTAC) with Judit Simon managing it as the editor-in-chief until, unbelievably, 2013, see Fig. 5, almost twenty years longer than the legendary TCA editor W.W. Wendlandt. Four international publishing companies (Heyden, Wiley, Kluver, and now Springer) and the Hungarian Academic Publisher have been engaged in printing the journal, and the original impact factor of 0.2 has grown to the present 2.2, reaching that of TCA. JTAC became also famous in presenting on its pages the proceedings of the most important conferences (ICTAC, ESTAC, and recent CEEC TA).

Thermal Analysis has Reached Adult Status; Time for Revisions

On wrapping up the history, it seems clear that the process of developing the theory of thermal analysis [3–11, 47–58] has not been completed yet, and it needs a revision and upgrading, which may not be welcomed by some orthodox users. For instance, the phenomenological theory of kinetics [8, 10, 17, 22–26, 31–39] demonstrates inclination to mathematical sophistication and disregard to physical meaning or usefulness. One such neglected aspects are the thermal inhomogeneities inside samples, unavoidable even in the smallest ones, since in thermal analysis temperature is constantly changing.

The logistic approach [66] provides an alternative insight into the reacting interfaces, based on the propagation of defects, which, interestingly, resembles

progression of infectious diseases. New strategies such as [66], and others [65, 68–70], are welcome, but we lack in more fundamental things, in first place we are in need of understanding the processes related to heat and temperature, taking place inside thermoanalytical samples [71–74]. The fact that transferring heat takes time has been known since Newton's cooling law [75] and from the fundamental Tian's calorimetric equation [76]. That knowledge has not been incorporated into thermoanalytical theoretical treatises as much as it deserves [30, 37, 78]. On top of that knowledge, experiments have shown that gradients of temperature [40, 72] and of gaseous decomposition products (if any) are inescapable even in submilligram samples [77], so ignoring them is not justifiable. Those gradients, interwoven with the thermal inertia, with the chemical equilibria, phase transitions and reaction fronts [10, 78], reflect the complex and dynamically changing situation inside thermoanalytical samples. Such difficulties are especially severe at the high cooling rates of novel chip microcalorimetry [79, 80], important in the new field of kinetic phase diagrams [81]. This vast range of problems has been glossed over by the thermoanalytical mainstream [33, 37, 50]. A new proposition for thermal analysis theory, addressing this complexity [30, 40, 71–74], as well as the new meaning of temperature while changing at ultrafast rates [80, 81], is expected to get underway.

In the area of theory, a two-pronged effort is needed: abandoning some unjustifiable practices and improving the legitimate ones. Of the unjustifiable practices, calculating activation energy [34–36, 69] and temperature [79] in situations where it is not sure whether such calculations are legitimate at all, should be stopped by researchers and rejected by reviewers and publishers. Calculating activation energy for transport-controlled processes (which we often do, while no undergraduate student of chemical engineering would) or reporting temperature values with several decimal places when the error margin may be one hundred degrees or more (in ultrarapid quenching) is a futile "academic" exercise. The common practice of adding qualifiers "formal," "apparent," or "of no real meaning" to activation energy is a lame excuse for using inadequate models. Thermal analysis can help some technical disciplines such as geopolymers [82], semiconductors [83, 84], biocompatible inorganic [85], and building materials and catalysts [86] in solving their problems, but trust will not be possible without proving the reliability of the results and the legitimacy of the underlying theories.

A broader definition of thermogravimetry extends beyond materials characterization and includes such uses as modeling of thermo-chemical fabrication of advanced materials or optimization of thermochemical processing of materials and parts. At present, most researchers who are trying to optimize processes such as CVD or steel carburization, either do not use weight recording at all, or merely apply it in the "before-and-after" mode. Catalysis offers a rich opportunity for insightful thermogravimetry [86]. Reactive analytical thermogravimetry, by imposing chemical reactions with gases onto the sample, determines the percentage of the components. However, this vast R&D potential requires expansion of capabilities of the instrumentation. There are two classes of TG users: one is those who want problem-free, quick results; the other class is those who want to use TG instruments for advanced research. The first group are satisfied by the present "push

button" design of TG's, and they do not mind that the instrument's software denies the user chances to review its algorithms—allegedly because of trade secrets. The elegant, compact styling hides the "guts" of the instrument and discourages the users from experimenting because they are afraid to damage that costly piece of equipment. The second class of users needs capabilities which are not offered now. It is highly desirable that TG instruments match the requirements of these two classes of users: one for routine analyses mostly required by industrial laboratories, and another that would be better suited for the scientific and industrial research. In addition to the present "push-button" class of TG instruments, manufacturers may consider adding an advanced, "transparent," and flexible class. On top of this, specialized versions of TG's could address several areas of specific applications; the desired features can be found in [86].

The present shape and structure of thermal analysis was neither obvious at its conception, nor are we sure that it is the best possible. We believe that progress means practice-verified improvements, which not just changes. Since what counts in science is "better" rather than "new," then returning to some older thermoanalytical concepts mentioned here, could result in additional progress.

Authors of this preface are happy to have been parts of thermal analysis for fifty years and contributing to it by their publications ranging from some old, groundwork articles [12, 13, 17, 30, 77, 86] of which the "SB equation" [25] became the best cited paper in thermoanalytical history, to the recent "hot topics" ones, related to heat inertia and thermal gradients [72–74], to reliability of experimentally observed temperature under its fast changes [80, 81], to equilibrium background conditions [78] and to the summarizing books and articles [10, 11, 17, 19, 33, 46, 49–52, 56–58].

Two books provide a broader view on thermal analysis: the underlying bibliographical book by Wunderlich [87] (1930–2012, citation response >17,000, H-index >70) thoroughly chronicles it, while Sestak's memoirs [88], present thermal analysis as an widespread themes connected to econophysics, environment, interdisciplinary science and even philosophy (see Fig. 6), showing also author´s accomplishment in art photography.

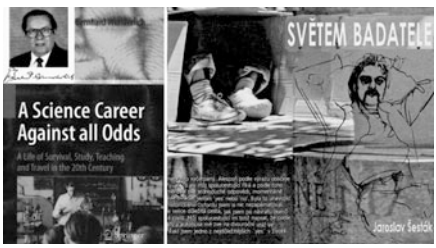

Fig. 6 Book covers of recent biographical publications related to thermal analysis

It is worth noting that the previous two books [89, 90] in this series "Hot topics of thermal analysis" [53] (Vols. 8 and 9) reached a high popularity; they were ranked by Springer among the 20 best downloaded and cited publications. We are convinced that this third continuation, Volume 11, will perform equally nicely.

Prague, Czech Republic/La Habra, USA
May 2016

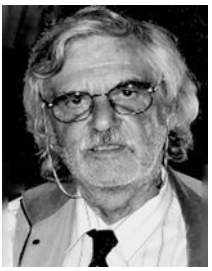

Prof. Ing. Jaroslav Šesták, D.Sc. Dr.h.c
(*1938, thermodynamics) Emeritus,
Westbohemian University in Pilsen
and New York University, branch in Prague

Ing. Věra Šestáková, MS (USA)
(*1945, crystal growth technologist),
Formerly with the Institute of Physics and then with the
Prague Municipal House (famous of Art Nouveau)

Dr. Jerry P. Czarnecki
(*1937, Chemist and Designer
of Thermogravimetric Systems),
Emeritus, Formerly with Cahn Instruments

References

[1] Tykodi RJ (1967) Thermodynamics of steady state. MacMillan, New York; and Kroemer H, Kittel C (1980) Thermal physics, 2nd edn. Freeman, New York; and Callen HB (1985) Thermodynamics and an introduction to thermostatistics, 2nd edn. Wiley, New York

[2] Tammann G (1897) Über die Grenzen des festen Zustandes. Wied Ann 16:280–299

[3] Burgess GK (1908) Methods of obtaining cooling curves. Bull. Bur Stand (S99) 5:199–225; and White WP (1909) Melting point determinations. Am J Sci. 28:453–473; and Sykes C (1935) Methods for investigating thermal changes occurring during transformations in solids. Proc R Soc A 148:422–446

[4] Berg GL Nikolaev AV, Ya RE (1944) Термография (Thermography). Izd. AN SSSR Moskva/Leningrad; and Berg LG (1952) Быстрый количественный фазовый анализ. (Rapid Quantitative Phase Analysis). Akad. Nauk, Moscow; and Berg LG (1961) Введение в термографию (Introduction to Thermography). Akad. Nauk, Moscow

[5] Popov MM (1954) Термометрия и калориметрия (Thermometry and calorimetry). Nauka, Moskva; and Piloyan FO (1964) Введение в термографию (Introduction to thermography). Nauka, Moskva

[6] Boersma SL (1955) Theory of DTA and new methods of measurement and interpretation. J Am Cer Soc 38:281–284; and Borchadt HJ (1956) Differential thermal analysis. J Chem Educ 33:103–109

[7] Vold MJ (1949) Differential thermal analysis (DTA). Anal Chem 21:683–688

[8] Borchard HJ, Daniels F (1957) The application of DTA to the study of reaction kinetics. J Am Chem Soc 79:41–46

[9] Mackenzie RC (1957) The differential thermal investigation of clays. Mineralogical Society, London; and Mackenzie RC (ed) (1966) Handbook of DTA. Chemical Publishing, New York

[10] Garn PD (1964) Thermoanalytical methods of investigation. Academic, New York

[11] Wendlandt WW (1964) Thermal methods of analysis. Wiley, New York

[12] Šesták J (2005) Some historical aspects of thermal analysis: origins of Termanal, CalCon and ICTA. In: Klein E, Smrčková E, Šimon P (eds) Thermal analysis. Proceedings of international conference on thermal analysis "Termanal". Publishing House of the Slovak Technical University, Bratislava, pp 3–11

[13] Šesták J, Hubík P, Mareš JJ (2011) Historical roots and development of thermal analysis and calorimetry. In: Šesták J, Mareš JJ, Hubík P (eds) Glassy, amorphous and nano-crystalline materials (Chapter 21). Hot topics of thermal analysis (published as Vol. 8 of the series) (edited by J. Simon). Springer, Berlin, pp 347-370.

[14] Šesták J, Mareš JJ (2007) From caloric to statmograph and polarography. J Thermal Anal Calor 88:763–771; and Šesták J, (2013) Thermal science and analysis: history, terminology, development and the role of personalities. J Thermal Anal Calor 113:1049–1054

[15] Strouhal Č (1908) Thermika (Thermics ≡ Thermal Physics), JČMF, Praha (in Czech)

[16] Mackenzie RC (ed) (1970) Differential thermal analysis, vol 2. Academic Press, London; 1972 vol. 2; and Mackenzie RC (1974) Highways and byways in thermal analysis. Analyst 99:900–912

[17] Šesták J, Šatava V, Wendlandt WW (1973) The study of heterogeneous processes by thermal analysis. Monograph as a special issue of Thermochimica Acta, vol 7. Elsevier, Amsterdam

[18] Wendlandt WW (1981) How thermochmica acta began: some reflections. Thermochim Acta 50:1–5

[19] Keattch J, Dollimore D (1975) Introduction to thermogravimetry. Heyden, London; and Brown ME, Dollimore D (eds) (1980) Reactions in the solid state. Elsevier, Amsterdam; and Dollimore D, Lerdkanchanaporn S (1998) Thermal analysis. Anal Chem 70:27–36

[20] Murphy CB (1958) Thermal analysis. Anal Chem 30:867–872 (published bi-annually until (1980) Anal Chem 52:106R–112R)

[21] Mackenzie RC (1984) History of thermal analysis. Monograph as a Special issue of Thermochimica Acta, vol 73. Elsevier, Amsterdam; and Mackenzie RC (1993) Origin and development of the international conference for thermal analysis (ICTA). J Therm Anal 40:5–28
[22] Vachuška J, Vobořil M (1971) Kinetic data computation from non-isothermal thermogravimetric curves of non-uniform heating rate. Thermochim Acta 2:379
[23] Šatava V (1971) Mechanism and kinetics from non-isothermal TG traces. Thermochim Acta 2:423
[24] Šesták J (1971) On the applicability of the p(x)-function to the determination of reaction kinetics under non-isothermal conditions. Thermochim Acta 3:150–154
[25] Šesták J, Berggren G, (1971) Study of the kinetics of the mechanism of solid-state reactions at increasing temperatures, Thermochim. Acta 3:1–12,
[26] Carroll B, Manche EP (1972) Kinetic analysis of chemical reactions for non-isothermal procedures 3:449–459
[27] Sturm E (1972) A systematic error and quantitative differential thermal analysis 4:461–470
[28] Lölich KR (1994) On the characteristics of the signal curves of heat flux calorimeters in studies of reaction kinetics: a contribution to desmearing techniques. Thermochim Acta 231:7–20
[29] Kempen ATW, Sommer F, Mittemeijer EJ (2002) Calibration and desmearing of DTA measurements signal upon heating and cooling. Thermochim Acta 383:21–30
[30] Holba P, Nevřiva M, Šesták J (1978) Analysis of DTA curve and related calculation of kinetic data using computer technique. Thermochim Acta 123:223–231
[31] Koch E (1977) Non-isothermal reaction kinetics. Academic Press, New York
[32] Segal E, Fatu D (1983) Introduction to nonisothermal kinetics. Editura Academie RSF, Bucharest (in Romanian)
[33] Vyazovkin S (2015) Isoconversional kinetics of thermally stimulated processes. Springer, Berlin/Heidelberg
[34] Garn PD (1961) Thermal analysis—a critique. Anal Chem 33:1247–1255; and Garn PD (1974) Non-isothermal kinetics. J Therm Anal 6:237–239; and Garn PD (1978) Kinetic parameters—a review. J Therm Anal 13:581–593; and Garn PD (2008) Kinetic investigations by techniques of thermal analysis. Critical Rev Anal Chem 3:65–111
[35] Galway AK (2004) Is the science of thermal analysis kinetics based on solid foundations? A literature appraisal. Thermochim Acta 413:139–183
[36] Šesták J (2015) The quandary aspects of non-isothermal kinetics beyond the ICTAC kinetic committee recommendations. Thermochim Acta 611:26–35
[37] Vyazovkin S, Burnham AK, Criado JN (2011) ICTAC kinetics committee recommendations for performing kinetic computations on thermal analysis data. Thermochim Acta 520:1–19; and Vyazovkin S, Chrissafis K, DiLorenzo ML, Koga N, Pijolat M, Roduit MB, Sbirrazzuoli N, Suñol JJ (2014) ICTAC kinetics committee recommendations for collecting experimental thermal analysis data for kinetic computations. Thermochim Acta 590:1–23
[38] Madhusudanan PM, Krishna K, Ninan KN (1986) New approximation for the p(x) function in the evaluation of non-isothermal kinetic data. Thermochim Acta 97:189
[39] Vyazovkin S, Wight CA (1999) Model-free and model-fitting approaches to kinetic analysis of isothermal and nonisothermal data. Thermochim Acta 341:53–68
[40] Lyon RE, Safronova N, Senese J, Stoliarov SI (2012) Thermokinetic model of sample response in nonisothermal analysis. Thermochim Acta 545:82–89
[41] Mouchina E, Kaisersberger E (2009) Temperature dependence of the time constants for deconvolution of heat flow curves. Thermochim Acta 492:101–109
[42] Sanchez-Rodrigues D, Eloussifi H, Farjas J, Roura P, Dammak M (2014) Thermal gradients in thermal analysis experiments: criterion to prevent inaccuracies when determining sample temperature and kinetic parameters. Thermochim Acta 589:37–46; and Farjas J, Roura P

(2014) Exact analytical solution for the Kissinger equation: determination of the peak temperature and general properties of thermally activated transformations. Thermochim Acta 508:51–58
[43] North American Thermal analysis Society. http://www.natasinfo.org/
[44] Holba P, Šesták J (2012) Czechoslovak footprints in the development of methods of thermometry, calorimetry and thermal analysis. Ceramics-Silikaty 56:159–167
[45] Paulik F, Paulik J (1981) Simultaneous thermoanalytical examination by means of derivatograph. Elsevier, Amsterdam
[46] Rozovskii AY (1974) Кинетика топо-химическихреакций (Kinetics of topo-chemical reactions). Khimija, Moscow; and Boldyrev VV (1958) Методы изучения кинетики термического разложения твердых веществ (Methods of studying of kinetics of thermal decomposition solids). Томск/Tomsk; and Logvinenko VA, Paulik F, Paulik J (1989) Квазиравновесная термогравиметрия всовременной неорганической химии (Quasi-quilibrium thermogravimetry in inorganic chemistry). Новосибирск, Наука
[47] Šatava V (1957) Documentation on the thermographic methods: a review. Silikáty (Prague) 1: 240 (in Czech)
[48] Proks I (1961) Influence of rate of temperature increase on the quantities important for the evaluation of DTA curves. Silikáty 5:114; and Šesták J (1963) Temperature effects influencing kinetic data accuracy obtained by thermographic measurements under constant heating. Silikáty 7:125 (both in Czech)
[49] Rouquerol J (1994) Characterization of porous solids, vol I. Elsevier, Amsterdam (1982) series of five books published till; and Sørensen OT, Rouquerol J (2003) Sample controlled thermal analysis. Kluwer, Dordrecht
[50] Hemminger W, Höhne GWH (1979) Grundlagen der Kalorimetrie. Verlag Chemie Weinheim; and Hemminger W, Höhne GWH (1984) Calorimetry: fundamentals and practice. Verlag Chemie, Weinheim
[51] Schultze D (1969) Differentialthermoanalyze. VEB, Berlin (Polish translation 'Różnicowa analiza termiczna'. PWN, Warsaw 1974)
[52] Šesták J (1984) Thermophysical properties of solids: theoretical thermal analysis. Elsevier, Amsterdam (Russian translation 'Těoretičeskij těrmičeskij analyz'. Mir, Moscow 1988)
[53] Simon J (ed) Hot topics of thermal analysis and calorimetry. Series of eleven consequent books by Springer (since 2001 when published Vol. 1: Brown ME, Introduction to Thermal Analysis: Techniques and Applications)
[54] Paulik F (1995) Special trends in thermal analysis. Wiley, Chichester
[55] Šesták J, Holba P, Gavrichev KS (1995) Reinstatement of thermal analysis tradition in Russia and related interactions. J Therm Anal Calorim 119(2015):779–784
[56] Heide K (1979) Dynamische thermische analysenmethoden. VEB, Leipzig; and Widemann G, Riesen R (1987) Thermal analysis: terms, methods, applications. Hüthig, Heidelberg; and Hemminger WF, Cammenga HK (1989) Methoden der Thermischen Analyse. Springer, Berlin; and Smykatz-Kloss W (1991) Thermal analysis in the geosciences. Springer, Berlin
[57] Swietosławski W (1933 & 1956) Microcalorimetrie. Mason, Paris; and Bretsznajder S (1971) Prediction of transport and other physical properties. Perganon, New York; and Zielenkiewicz W, Margas E (1990) Podstawy teoretyczne kalorymetrii dynamicznej (Theoretical fundamentals of dynamic calorimetry). Ossolineum, Wroclaw
[58] Proks I (1991) Evaluation of the knowledge of phase equilibria—Chapter 1. In: Chvoj Z, Šesták J, Tříska A (eds) Kinetic phase diagrams: nonequilibrium phase transitions. Elsevier, Amsterdam, pp 1–54; and Proks I (2012) The whole is simpler than its parts: chapters from the history of exact sciences. Veda-Academy, Bratislava (in Slovak)
[59] Šulcová P, Šesták J, Menyhárd A, Liptay G (2015) Some historical aspects of thermal analysis on the mid-European territory. J Therm Anal Calorim 120:239–254
[60] Zsakó J (1970) Kinetic analysis of thermogravimetric data—I. J Therm Anal 2:145–149 (later II and III)

[61] Ozawa T (1970) Kinetic analysis of derivative curves in thermal analysis. J Therm Anal 2:301–324
[62] Škvára F, Šatava V (1970) Kinetic data from DTA measurements. J Therm Anal 2:325–335
[63] Simon J, Debreczeny E (1971) 1/T—heating program in reaction kinetic studies. J Therm Anal 3:301–305
[64] Berg LG, Egunov VP (1969) Quantitative thermal analysis—I. J Therm Anal 1:5 (later II and III)
[65] Serra R, Nomen R, Sempere J (1998) Non-parametric kinetics: a new method for kinetic study. J Therm Anal Calorim 52:933
[66] Avramov I, Šesták J (2014) Generalized kinetics of overall phase transition explicit to crystallization. J Therm Anal Calorim 118:1715–1720
[67] Criado JM, Perez-Maqueda LA, Gotor FJ, Málek J, Koga N (2003) A unified theory for the kinetic analysis of solid state reactions under any thermal pathway. J Therm Anal Calorim 72:901–906
[68] Dubaj T, Cibulková Z, Šimon P (2015) An incremental isoconversional method for kinetic analysis based on the orthogonal distance regression. J Comput Chem 3:6392–6398
[69] Reading M, Dollimore D, Whitehead R (1991) The measurements of meaningful kinetic parameters for solid-state decompositions. J Therm Anal 37:2165–88; and Galwey AK (2006) What theoretical and/or chemical significance is to be attached to the magnitude of an activation energy determined for a solid-state decomposition by thermal analysis? J Therm Anal Calor 86:267–286
[70] Šimon P (2005) Single-step kinetics approximation employing non-Arrhenius temperature functions. J Therm Anal Calorim 79:703–708; and Šimon P (2007) The single-step approximation: attributes, strong and weak sides. J Therm Anal Calorim 88:709–715
[71] Gray AP (1968) Simple generalized theory for analysis of dynamic thermal measurements. In: Porter RS, Johnson JF (eds) Analytical calorimetry, vol 1, pp 209–18. Plenum Press, New York
[72] Holba P, Šesták J, Sedmidubský D (2013) Heat transfer and phase transition at DTA experiments—Chapter 5. In: Šesták J, Šimon P (eds) Thermal analysis of micro-, nano- and non-crystalline materials. Springer Berlin, pp 99–134
[73] Šesták J (2005) Thermometry and calorimetry—Chapter 12. In: Science of heat and thermophysical studies: a generalized approach to thermal analysis. Elsevier, Amsterdam, pp 344–376
[74] Šesták J, Holba P (2013) Heat inertia and temperature gradient in the treatment of DTA peaks: existing on every occasion of real measurements but until now omitted. J Therm Anal Calorim 113:1633–1643; and Holba P, Šesták J (2015) Heat inertia and its role in thermal analysis. J Therm Anal Calor 121:303–307
[75] Newton I (1701) Scale graduum Caloris. Calorum Descriptiones & Signa. Philosophical Trans 22:824–829
[76] Tian A (1933) Recherches sue la calorimétrie. Généralisation de la méthode de compensation électrique: microcalorimetrie. J de Chimie-Physiq 30:665–708
[77] Kemula W, Czarnecki J (1978) Kinetics of heterogeneous thermal decomposition with special reference to the complex Ni (NCS) 2 (gamma-picoline) 4. Pol J Chem 52:613
[78] Holba P, Šesták J (1972) Kinetics with regard to the equilibrium of processes studied by non-isothermal techniques. Zeit physik Chem N F 80:1–20; and Holba P (2015) Ehrenfest equations for calorimetry and dilatometry. J Therm Anal Calorim 120:175–181
[79] Adamovsky AS, Minakov AA, Schick C (2003) Scanning microcalorimetry at high cooling rate. Thermochim Acta 403:55–63; and Minakov AA, Schick C (2015) Dynamics of the temperature distribution in ultra-fast thin-film calorimeter sensors. Thermochim Acta 603:205–217
[80] Šesták J (2016) Measuring “hotness”; should the sensor’s readings for rapid temperature changes be named “tempericity”? J Therm Anal Calorim 125:991–999

[81] Šesták J (2015) Kinetic phase diagrams as a consequence of radical changing temperature or particle size. J Thermal Anal Calorim 120:129–137
[82] Davidovits J (1989) Geopolymers and geopolymeric materials. J Therm Anal 35:429–441; and Davidovits J (1991) Geopolymers: inorganic polymeric materials. J Therm Anal 37:1633–1656; and Šesták J, Foller B (2012) Some aspects of composite inorganic polysialates. J Therm Anal Calor 109:1–5
[83] Šestáková V, Štěpánek B, Šesták J (1993) Comparative analysis of single-crystal growth techniques. Inorg Mater 29:1210–1215; and Šestáková V, Štěpánek B, Šesták J (1996) Various methods for the growth of single crystals. J Cryst Growth 165:159–162; and Šestáková V, Štěpánek B, Šesták J (1996) Properties of doped GaSb single crystals grown by the Czochralski method. Cryst Res Technol 31:929–934
[84] Štěpánek B, Šestáková V, Šesták J (1995) Copper solubility and distribution in doped GaSb single crystals. J Therm Anal 43:389–397; and Šestáková V, Šesták J, Štěpánek B (1999) Doping limits and growth thermodynamics of GaSb crystals. J Therm Anal Calorim 56:749–754; and Šestáková V, Štěpánek B, Šesták J (2003) Thermal conditions of growth and the necking evolution of Si, GaSb and GaAs. J Therm Anal Calorim 72:165–172
[85] Koga N, Strnad J, Strnad Z, Šesták J (2003) Thermodynamics of non-bridging oxygen in silica bio-compatible glass-ceramics: mimetic material for the bone tissue substitution. J Therm Anal Calorim 71:927–937; and Strnad J, Strnad Z, Šesták J (2007) Physico-chemical properties and healing capacity of potentially bioactive titanium surface. J Therm Anal Calor 8:775; and Šesták J, Strnad Z, Strnad J, Holeček M, Koga N (2008) Biomedical thermodynamics and implantology aspects of biocompatible glass-ceramics and other inorganic materials. Adv Mater Res 39/40:329–333
[86] Czarnecki J, Koga N, Šestáková V, Šesták J (1992) Factors affecting the experimentally resolved TG curves. J Therm Anal 38:575; and Czarnecki J, Šesták J (2015) From recording balances to thermogravimetric instruments and back. J Therm Anal Calor J Therm Anal Calorim 120:157–166; and Czarnecki J (2015) Precision thermogravimetry. J Therm Anal Calorim 120:139–147
[87] Wunderlich B (2010) Science careers against all odds: a life of survival, study, teaching and travel in the 20th Century. Springer, Heidelberg; and Wunderlich B (1990) Thermal analysis academic. Boston, till (2005) Thermal analysis of polymeric materials. Springer, Heidelberg
[88] Šesták J (2014) Through the world of explorer: on the frontier of science and philosophy of Nature. OPS, Plzeň and second edition Plzeň 2015 ("Světem badatele"—in Czech. Available on the author's website www.fzu.cz/∼sestak together with other scientific books)
[89] Šesták J, Mareš JJ, Hubík P (eds) (2011) Glassy, amorphous and nano-crystalline materials: thermal physics, analysis, structure and properties, vol 8. Springer, Berlin/Heidelberg, ISBN 978-90-481-2881-5
[90] Šesták J, Šimon P (eds) (2013) Thermal analysis of micro-, nano- and non-crystalline materials: transformation, crystallization, kinetics and thermodynamics, vol 9. Springer, Berlin/Heidelberg, ISBN 978-90-481-3149-5

Contents

About the Editors

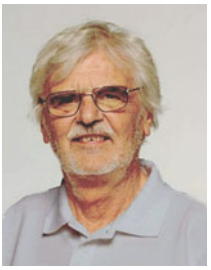

Jaroslav Šesták Emeritus Scientist of Academy of Sciences, Doctor Honoris Causa, Honorary Citizen of Prague 5, New Technologies, Research Centre of the Westbohemian Region, University of West Bohemia, Universitní 8, CZ-30114 Pilsen.

Pavel Hubík Principle Scientists, Executive of Quantum and Mesoscopic Thermodynamic Conferences, Division of Solid-State Physics, Institute of Physics, v.v.i., Academy of Sciences of the Czech Republic, Cukrovarnická 10, CZ-16200 Prague.

Jiří J. Mareš Deputy Director of the Institute of Physics, Honorary citizen of Prague 4, Division of Solid-State Physics, Institute of Physics, v.v.i., Academy of Sciences of the Czech Republic, Cukrovarnická 10, CZ-16200 Prague.

Chapter 1
Local Thermal Analysis by Structural Characterization (TASC)

Mike Reading, Sheng Qi and Muqdad Alhijjaj

Abstract Thermal analysis by structural characterization (TASC) is a new thermal technique that is based on image analysis combined with hot-stage microscopy (HSM, also called thermomicroscopy). The image analysis algorithm is sensitive to any change in structure as seen by digital optical microscopy. A key feature of the algorithm is that it accounts for any sample movement. Due to thermal expansion of the sample or the sample chamber, there is, at high magnification, usually some sample displacement and this needs to be removed, so the measurement is purely one of structural change. HSM has a variety of uses but struggles with opaque samples (such as filled samples) and cannot routinely detect glass transitions. TASC, when used with an imposed structure such as an indentation, can routinely measure glass transition temperatures because, when the sample softens, the indentation disappears. This is true even when analyzing opaque samples. TASC can also be used to measure melting temperatures, transitions in small (microgram) samples, dissolution behavior, and heterogeneity.

1.1 The Development of Methods for Local Thermal Analysis

The first approach to local thermal analysis (LTA) was proposed by Hammiche et al. [1]. It was based on a scanning thermal microscope (SThM) (a type of scanning probe microscope (SCM) [1]); in this technique, a thermal probe that is capable of measuring temperature and, in some cases, also capable of being heated,

M. Reading (✉)
Department of Chemical Sciences, University of Huddersfield,
Queensgate, Huddersfield NR4 7TJ, UK
e-mail: m.reading@hud.ac.uk; mike@mike-reading.com

S. Qi · M. Alhijjaj
School of Pharmacy, University of East Anglia,
Norwich, Norfolk NR4 7TJ, UK
e-mail: Sheng.Qi@uea.ac.uk

J. Šesták et al. (eds.), *Thermal Physics and Thermal Analysis*,
Hot Topics in Thermal Analysis and Calorimetry 11,
DOI 10.1007/978-3-319-45899-1_1

over the surface of a sample. In this way, a map of the surface topography is generated together with a simultaneous map of some aspect of the sample's thermal properties. There are two basic types of thermal probe; a thermocouple that measures local temperature and a resistance thermometer, such a platinum filament, that can measure temperature and, by Joule heating, increase the local temperature. It is the latter that is used for thermal analysis. The first local thermal analysis instrument used a probe, called a Wollaston wire probe, which had a tip made of platinum that could be heated to temperatures in excess of 500 °C. Local thermal analysis was achieved by placing the tip on a selected location and heating it so that its temperature was a linear function of time. If the material beneath the tip softened, the tip would indent into the surface and this was measured using the defection of a laser beam (a description of the details of how a SThM works can be found in [1]). The softening event would usually be a consequence of a glass transition or melting; thus, a local transition temperature was determined. This technique came to be called initially Micro-TA then, as spatial resolution improved, Nano-TA [2]. The Wollaston wire probe had a tip with a contact area of the order of square microns and this limited the lateral spatial resolution. This type of probe has now been superseded; in modern instruments, the thermal probe is a micromachined device with a tip with a radius of circa 10 nm. This enables a spatial resolution of, in favorable cases, 100 nm for LTA. The applications for this type of local thermal analysis capability are now legion [3, 4] and a number of instrument manufacturers offer this capability. However, this type of SThM-based approach has its limitations; scanning probe microscopes are expensive and not easy to use. They are typically limited to imaging a maximum area of 100 μ × 100 μ with a height limitation of 10 μ; while this type of microscopy has the advantage that it can achieve nanometer spatial resolution, this is not always what is needed. Sometimes the structure of interest has features that are of the order of 10 μ or larger. When this is the case, using a scanning probe microscope is time-consuming and perhaps not possible if the surface is too rough. There are also issues related to accuracy and precision. Localized heating necessarily creates very sharp temperature gradients around the point of contact. The character of these gradients is affected by the topography in the immediate vicinity of the tip; if it is at the bottom of a depression, then the quality of the thermal coupling between the tip and the sample is different from when the tip is at the apex of a "hill." This means that, on a rough surface, the scatter of results for a pure pharmaceutical compound is of the order of 10 °C or more [3], i.e., an order of magnitude worse than conventional thermal techniques. Furthermore, conventional temperature calibrants, such as indium, cannot be used because their high thermal conductivity gives rise to temperature gradients that they are so far removed from those experienced with organic samples that calibration curves obtained with these materials cannot be relied on when analyzing polymers, pharmaceuticals, etc. To overcome this difficulty, polymer calibrants are used and these are not primary standards.

A solution to the problems encountered by micro-/nano-TA has recently been proposed in the form of thermal analysis by structural characterization or TASC [5–7]. A simple example of this technique is that of analyzing a structure imposed

on the surface of an amorphous polymer. A typical experiment is as follows: a sample has a small indentation made in its surface using a dissection needle, it is placed in a hot-stage microscope and the indentation is brought into the field of view of a digital camera. The sample is heated and when its glass transition temperature is reached, it softens which leads to the disappearance of the indentation under the action surface tension. This is illustrated in Fig. 1.1.

The TASC value is calculated by subtracting a selected area within the first image from the corresponding areas in each subsequent image; thus, any change in appearance will result in a change in the TASC curve. The algorithm is able to compensate for any movement by the sample; this is essential because heating a sample under high magnification is almost certain to result in shifts in its position due to thermal expansion by the sample and the sample chamber. These are not of interest so eliminating them is a requirement for the analysis to work. Clearly, the absolute values of the TASC calculations are dependent on the size of the area that is chosen so TASC curves are normalized to the highest value. Details of the algorithm can be found in [6]. The areas of application can be categorized as follows:

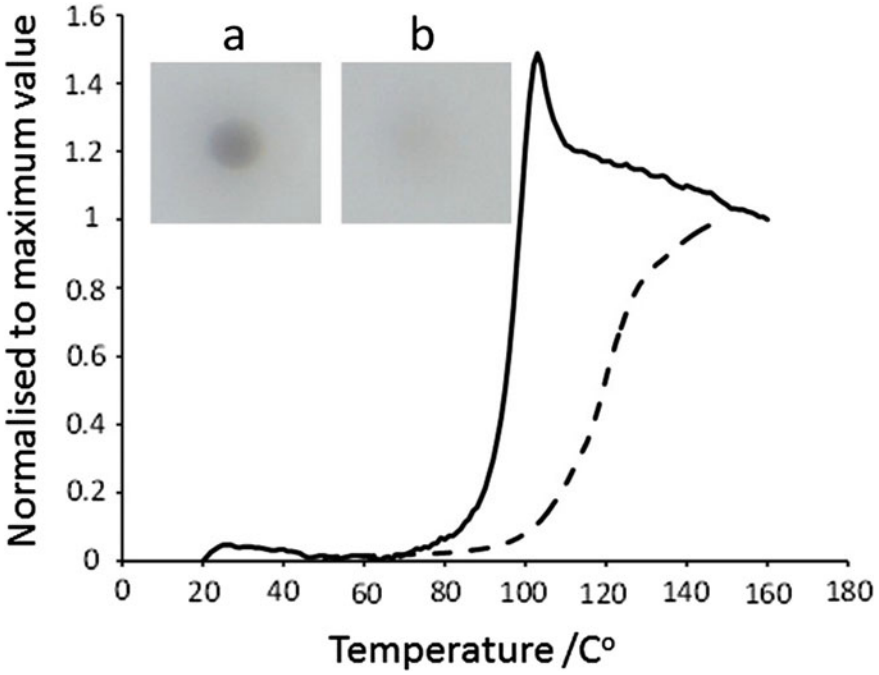

Fig. 1.1 An illustration of a TASC experiment with a DSC measurement for comparison. The image **a** size 1 mm × 1 mm is an indentation in a filled polystyrene sample prior to heating. Image **b** is the same area after heating to 160 °C. The *dashed line* is the TASC curve and the *solid line* is a DSC experiment for the same sample (normalized to final value)

- A general tool of measuring transition temperatures,
- Local thermal analysis including surface analysis,
- Measuring heterogeneity

These are considered below.

1.2 Measuring Transition Temperatures and Local Thermal Analysis

Figure 1.1 gives us an example on measuring a glass transition. Clearly, this is a localized measurement because it monitors the change in viscosity in the immediate vicinity of the indentation. How this can be exploited to measure differences in transition temperatures in different locations has been demonstrated [5]. Similarly, the melting temperatures of individual crystals can be determined. This is illustrated in Fig. 1.2.

Particles made of amorphous materials also change shape upon being heated above their glass transition. This type of experiment complements traditional thermal measurements. Analyzing a mixture of particles of the order of tens of microns using, for example, DSC can provide information on the constituents and their relative amounts. However, it is only by making measurements on individual components that it can be established whether these material are within each particle or each particle is a different material. The components might only be a few micrograms and could not, therefore, be analyzed by conventional means. TASC provides an easy and convenient means of analyzing a large number of such small samples in a single experiment.

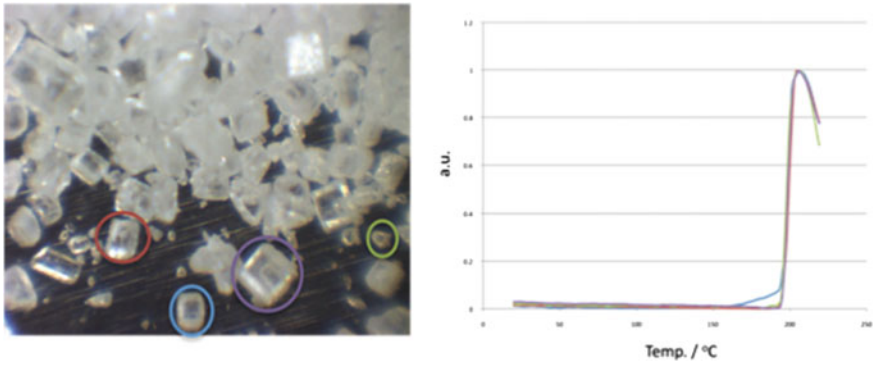

Fig. 1.2 Above *left* is a micrograph of sugar crystals; *right* are the TASC results for the crystals indicated by the *colored circles*. There is excellent agreement for the onset of the principle event. For the crystal highlighted by the *blue circle,* there is a suggestion of a preliminary process (further work would be needed to confirm this). This is illustrative of how TASC provides discrete information rather than the global data obtained by conventional methods

Another aspect of this type of localized measurement is that, in most cases, it is a form of surface analysis. Figure 1.3 is a measurement made on the surface of a foodstuff coated in carnauba wax.

It might be argued that this measurement could be made using thermomechanical analysis in penetration mode, but it would usually not be possible to be sure whether the transition arose from the surface or somewhere deeper.

For complex systems, TASC has demonstrated the ability to detect "hidden" transitions that are often difficult to measure by conventional thermal methods such as DSC. Two examples of such cases are detection of the dissolution of crystalline material into matrices upon heating and the development of metastable polymorphs with rapid kinetic transformation during the thermal ramp. Alhijjaj and coworkers reported the use of TASC to study a series of complex pharmaceutical formulations containing three semicrystalline excipients (poly(ethylene glycol), poly(ethylene oxide), and D-α-tocopheryl polyethylene glycol succinate) with low melting points (37–70 °C) and a model drug (felodipine) with a melting point of 145 °C [8]. These formulations were manufactured using hot melt extrusion methods, and the semicrystalline excipients were fully melted and recrystallized during preparation. The physical state of the drug in the formulations is highly dependent on the drug loading, and accurate identification of the physical state of both the drug and excipients is extremely important for predicting the stability of such products. However, the rapid thermal dissolution behavior of the crystalline drug that occurred during DSC heating, prevented the detection of drug melting as shown in Fig. 1.4a. In contrast for the formulations with high drug loading, TASC detected an additional transition (lower than the crystalline drug melting) to all melting transitions of the excipients in the formulations that was not detected by DSC (Fig. 1.4c). The confirmation of the presence of crystalline drug in these formulations by PXRD and ATR-FTIR indicated this additional transition detected by TASC is associated with onset of the thermal dissolution of crystalline drug into the molten excipients. The full recovery of the TASC signal at the end of the experiment (shown as a plateau at a normalized TASC value of 1) is a good indication of the completion of all thermal melting behavior (Fig. 1.4b). The samples containing crystallized drug did not reach a plateau. This is a result of the incomplete melting of the drug at the end temperature of the experiments. With increasing the end

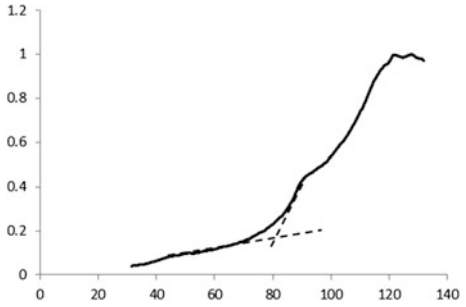

Fig. 1.3 This is an example of a TASC measurement on the surface of a piece of candy. The surface is coated in carnauba wax, and its melting temperature can be determined as being 80 °C

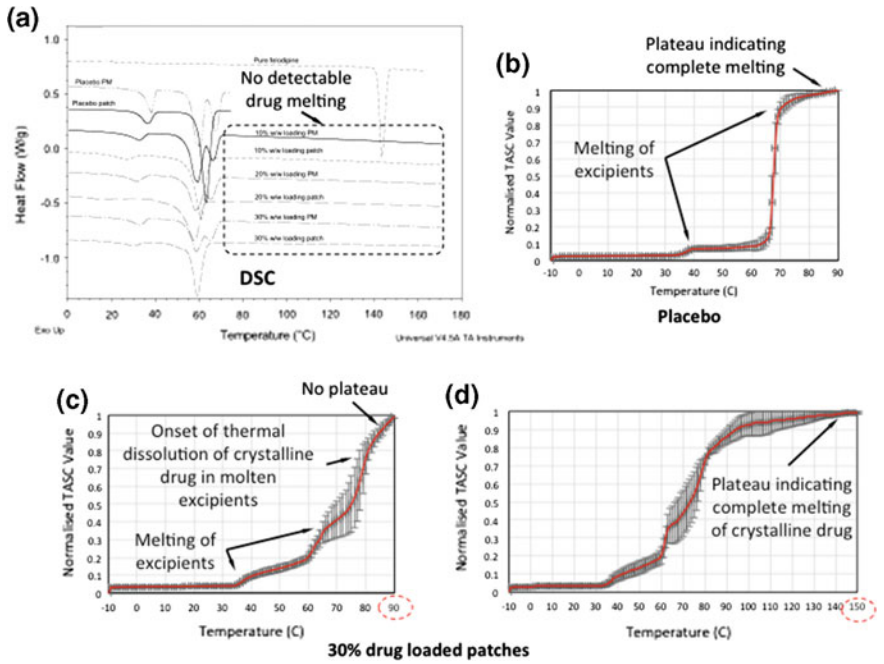

Fig. 1.4 An illustration of the detection of the thermal dissolution of crystalline drug (with melting point at 145 °C) in complex polymeric matrices by TASC **a** DSC results of the formulations show no indication of melting of the crystalline drug due to thermal dissolution; **b** TASC results of placebo formulations demonstrate the clear detection of thermal melting of excipients and a plateau region indicating the complete melting of all materials in the formulations; **c** TASC results of formulations containing crystalline drug show onset of thermal dissolution of the crystalline drug which is not detectable by DSC, but without the plateau due to the incomplete melting/thermal dissolution of the drug at 90 °C; **d** The clear detection of the plateau indicating the complete melting of drug at 150 °C which is above the melting point of the crystalline drug. (Reproduced from Ref. [7] with permission)

temperature of the TASC test above the melting of the pure crystalline drug, as shown in Fig. 1.4d, a clear plateau can be obtained implying the complete dissolution and melting of crystalline drug in the molten excipient matrices. This can be used as an evidence of the presence of crystalline drug in the original formulation which could not be detected by DSC.

Evidence of the high sensitivity of TASC for detecting metastable polymorphs has been demonstrated through investigating the behavior of melt-cooled PEG and PEO mixtures. In the literature, it is well documented that the stable polymorph of PEG and PEO mixed systems consists of extended polymer chains with the metastable form having folded chains [8]. Melt-cooling is one method that can induce the formation of the metastable form of PEG and PEO which can convert to stable form upon thermal treatment or aging [9]. When relatively low quantities of PEG and PEO are used in pharmaceutical formulations, it is often difficult to detect

the presence of the metastable form using conventional DSC (as shown in Fig. 1.5a). However, the presence of the metastable form may cause a long-term stability issue with the formulations. TASC was used to study melt-cooled formulations containing PEG and PEO (with less than 50% total weight of the formulations) [6, 7]. Highly reproducible double transitions were detected by TASC which is believed to be associated the presence of both folded and extended forms of PEG and PEO (Fig. 1.5d), whereas only a single transition was observed in DSC results of the same samples tested using the same heating rate. In the melt-cooled PEG and PEO mixture, the metastable form with a lower melting point would soften and melt prior to the recrystallization and melting of the stable form. The subtle heat capacity change of this process was not detected by standard DSC, but confirmed by MTDSC and VT-ATR-FTIR measurements on the same samples [6].

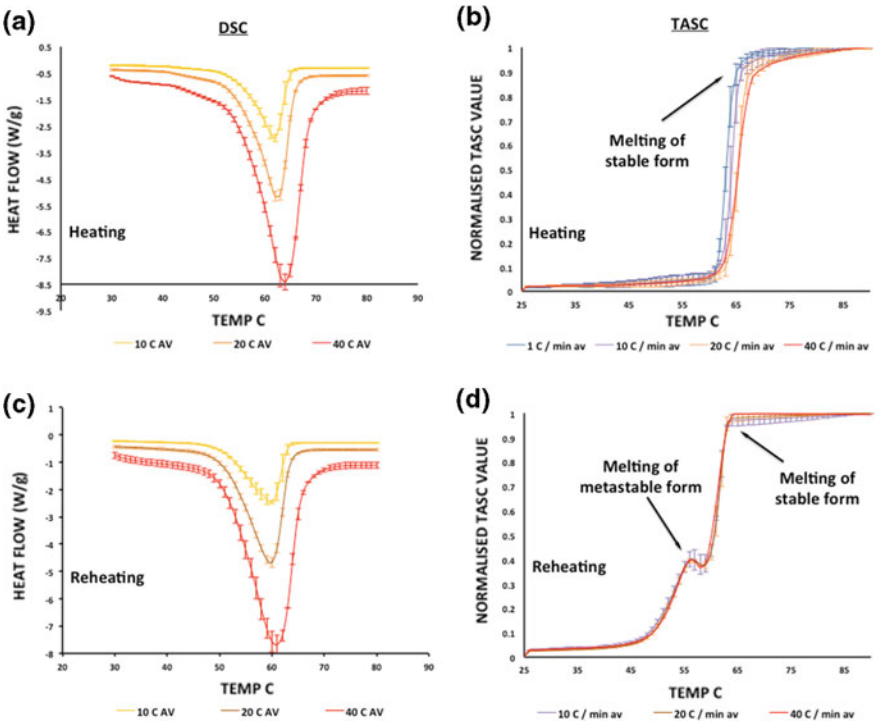

Fig. 1.5 An example of the detection of metastable forms by TASC which are not detectable by DSC: **a** and **c** DSC results with heating rate ranging from 10 to 40 °C/min of formulations containing PEG and PEO during first heating (**a**) and reheating (**c**) after cooling. Single melting transitions of the mixture of PEG and PEO is shown for both heating and reheating at all heating rates; **b** and **d** TASC results of the same samples show clear shoulder peaks associated with the melting of the metastable form of PEG and PEO during heating (**b**) and reheating (**d**) cycle. TASC results also show a lower heating rate effect on the resolution of the results than those obtained by DSC. (Reproduced from Ref. [6] with permission)

This sequence of thermal behavior has rather fast kinetics. As the working mechanism of TASC is based on imaging analysis, it can follow the consequences of changing structure on a micron length scale that conventional DSC cannot directly interrogate. The results also demonstrated another advantage of TASC in comparison with conventional DSC, which is a much lower heating rate effect on the sensitivity and resolution of the results. As shown in Fig. 1.5, heating rates of 10–40 °C/min show good similarity in the transition temperatures and the shape of the curves, whereas the change of heating rate from 10 to 40 °C/min changed the resolution of the DSC detected melting peak.

1.3 Measuring Heterogeneity

Heterogeneity of the distribution of ingredients is an undesirable feature in many consumer products. For pharmaceuticals, heterogeneity may be an indicator of poor product quality. If undetected, it can lead to serious issues such as product instability over its shelf life and dose inconsistency which can significantly reduce the therapeutic effectiveness of the treatment. As TASC is by nature an imaging-based technique, it has the flexibility of altering the size of the region of interest (ROI). Using this feature of TASC, one can judge the heterogeneity of a sample by the reproducibility of transitions detected by TASC for different ROI with a range of sizes. For a homogenous sample, highly reproducible TASC results should be expected regardless of the location and size of the ROI. However, inconsistent results would be expected in heterogeneous samples. This is because random selection of location and size of the ROI raises the chances of capturing more or less of the ingredient of interest within the ROI. This has been demonstrated with a set of pharmaceutical patches containing a range of drug concentrations [6, 7]. At low drug concentration, the drug was melted and homogenously distributed in the excipient polymers during the manufacturing process (which is hot melt extrusion and injection molding in this particular case). However, when the drug was too concentrated in the formulation, a population of crystalline drug was observed to be scattered in the formulation. These drug crystals were either undissolved/melted during manufacturing or generated through recrystallization following aging as a result of supersaturation of the drug in the matrices. It is shown in Fig. 1.6a, b that the reproducibility of the data (presented as error bars at each data point) collected by analyzing small ROIs (approximately between 2.5×10^{-3} and 10×10^{-3} mm^2) is lower than that obtained from larger ROIs (between 40×10^{-3} and 90×10^{-3} mm^2). This indicates that at the micron scale, the sample is highly heterogeneous. This is not detectable by DSC in which the samples were tested as a bulk material with localized information not being obtainable (Fig. 1.6c). TASC's unique capability of identifying the heterogeneity of the samples at the scale of interest has great potential in quality control of pharmaceutical products.

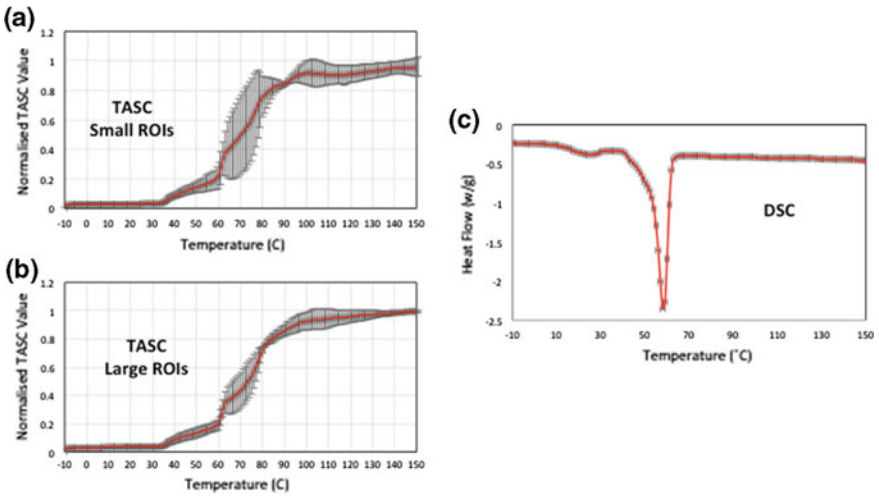

Fig. 1.6 An illustration of detection of heterogeneity in pharmaceutical formulations by altering the size of ROIs **a** TASC results of a set of ROIs on the formulations with small areas showing low reproducibility as suggested by the large error bars. This implies the heterogeneity of the sample at the scale of tested size of ROI; **b** TASC results of a set of ROIs on the same sample formulations as tested in (**a**) but with larger tested areas. The *error bars* for this set of ROIs are smaller than the ones in (**a**) indicating less heterogeneity when the sizes of the ROIs are increased; **c** DSC results of the same formulation show high reproducibility due to the nature of the DSC measurement relating to the bulk sample. (Reproduced from Ref. [7] with permission)

1.4 Conclusions

The ability to make localized thermal measurements has been available since the invention of micro (then nano)-thermal analysis. However, the high cost of atomic force microscopes and their limitations in terms of the range of length scales they can access has limited the use of spatially resolved thermal analysis. Working at the nanoscale remains the preserve of scanning probe microscopy for this type of study, but there many cases where microns to millimeters is the range of interest. When this is the case, TASC provides an alternative that is, in many ways, more powerful because a large amount of data can be easily and retrospectively obtained by analyzing the images provided by hot-stage microscopy. Local thermal analysis is made more accessible using this approach and localized measurements are often needed to correctly interpreting the data provided by more conventional means.

References

1. Price D, Reading M, Hammiche A, Pollock HM (2000) Micro-thermal analysis: scanning probe microscopy and localized thermal analysis. Int J Pharm 192(1):85–95

2. Harding L, King WP, Dai X, Reading M (2007) Nanoscale characterization and imaging of partially amorphous materials using local thermomechanical analysis and heated tip AFM. Pharm Res 24(11):2048–2054
3. Xuan D, Moffat JG, Wood J, Reading M (2011) Thermal scanning probe microscopy in the development of pharmaceuticals. Adv Drug Deliv Rev 64(5):449–460
4. Gorbunov V, Grandy D, Reading M, Tsukruk V (2008) Micro and nanoscale local thermal analysis. In: Thermal analysis of polymers, fundamentals and applications, pp 615–649. doi:10.1002/780423837.ch7
5. Reading M, Morton M, Antonijevic MD, Lacey AA (2014) New methods of thermal analysis and chemical mapping on a micro and nano scale by combining microscopy with image analysis. In: Mendez-Villas A (ed) Microscopy advances in scientific research and education, vol 2. Formatex Research Centre, pp 1083–1089
6. Alhijjaj M, Reading M, Belton P, Qi S (2015) Thermal analysis by structural characterization as a method for assessing heterogeneity in complex solid pharmaceutical dosage forms. Anal Chem 87:10848–10855
7. Alhijjaj M, Yassin S, Reading M, Zeitler JA, Belton P, Qi S (2016) Characterization of heterogeneity and spatial distribution of phases in complex solid dispersions by thermal analysis by structural characterization and X-ray micro computed tomography. Pharm Res 2016:1–19
8. Buckley CP, Kovacs AJ (1976) Melting behaviour of low molecular weight poly (ethylene-oxide) fractions. Colloid Polym Sci 254:695–715
9. Lloyd GR, Craig DQM, Smith A (1997) An investigation into the melting behavior of binary mixes and solid dispersions of paracetamol and PEG 4000. J Pharm Sci 86:991–996

Chapter 2
Sample Controlled Thermal Analysis (SCTA) as a Promising Tool for Kinetic Characterization of Solid-State Reaction and Controlled Material Synthesis

Jose M. Criado, Luis A. Pérez-Maqueda and Nobuyoshi Koga

Abstract The historical development of the thermal analysis methods that imply an intelligent control of the reaction temperature by the own sample (SCTA) is outlined. It has been shown that the precise control of the reaction rate involved in SCTA enables a control, either direct or indirect, of both the partial pressure of the gases generated/consumed by the reaction and the heat evolution/adsorption rate associated to the reaction. This control allows to minimize the influences of heat and mass transfer phenomena and to obtain real kinetic parameters of the forward reaction that occur under the conditions far from the equilibrium. Moreover, it is shown that the shape of α–T plots obtained under constant rate of transformation (CRTA) is strongly dependent on the kinetic model, while the α–T plots obtained using the conventional linear nonisothermal method represent a sigmoidal shape irrespective of the kinetic model. Thus, CRTA has a considerably higher resolution power for discriminating the kinetic model obeyed by the reaction. The applications of SCTA methods both for the kinetic analysis of solid-state reactions and for the synthesis of materials with controlled texture and/or structure have been reviewed. The chapter contains 202 references.

2.1 Introduction to Sample Controlled Thermal Analysis

Sophisticated controls of material synthesis processes are necessary for obtaining the functional materials with desired chemical and physical properties. Among others, thermal treatments involving calcination and annealing processes are of

J.M. Criado (✉) · L.A. Pérez-Maqueda
Instituto de Ciencias de Materiales de Sevilla, Centro Mixto Universidad de Sevilla—C.S.I.C, c/Américo Vespucio 49, 41092 Seville, Spain
e-mail: jmcriado@icmse.csic.es

N. Koga
Chemistry Laboratory, Department of Science Education, Graduate School of Education, Hiroshima University, Higashi-Hiroshima 739-8524, Japan

J. Šesták et al. (eds.), *Thermal Physics and Thermal Analysis*,
Hot Topics in Thermal Analysis and Calorimetry 11,
DOI 10.1007/978-3-319-45899-1_2

paramount importance in the synthesis of materials. For developing well-controlled synthesis procedure of the advanced materials via the thermal treatments of precursor materials, the chemical and physical processes that occur in the solid state should be characterized in details. Thermal analysis methods such as thermogravimetry (TG), differential thermal analysis (DTA), differential scanning calorimetry (DSC), and evolved gas analysis (EGA) are extensively used in material characterization including the kinetic analysis of solid-state reactions. In general, all thermal treatments are performed under isothermal or linearly increasing temperature (linear nonisothermal) conditions. Another alternative to perform thermal treatments can be designed by controlling the rate of thermally induced transformation according to predetermined rules, resulting in a smart temperature control where the transformation kinetics of the reaction governs the temperature profile during the course of the process. This technique with the inverse concept of thermal analysis is generally named Sample Controlled Thermal Analysis (SCTA). This alternative approach is realized by monitoring the rate of thermally induced variation of a physical property of the sample that is proportional to the reaction rate. By using a feedback control system, the regulation of variation rate of such property according to predetermined rules determines the temperature profile during the reaction. We will refer along this chapter to one of the SCTA methods, that is, the most generally used technique to control the temperature in such a way that the reaction rate is maintained constant all over the process. The SCTA technique is known as Constant Rate Thermal Analysis (CRTA).

Probably, the first CRTA instrument was that proposed by Smith in 1940s [1]. This method referred to as "Smith Thermal Analysis" [2] used a differential thermocouple to establish a constant temperature difference between sample and furnace wall and is continuously employed even in a modernized form to study alloys systems [3]. The sensitivity of this method has been dramatically improved by Charsley et al. [2], by applying the advantages of CRTA to DSC, named "Sample Controlled Differential Scanning Calorimetry (SCDSC)" [2]. However, the great boost of SCTA methods was driven in the 1960s and 1970s because of the works of two groups, one in France and the other in Hungary. In France, Rouquerol developed that called "Constant Rate Thermal Analysis (CRTA)" [4–6]. This method uses the partial pressure of the evolved gases for monitoring the transformation rate and as feedback signal for controlling sample temperature. Conversely, the Paulik brothers, in Hungary, used the derivative TG (DTG) signal for the same purpose and used the term "quasi-isothermal" for describing the working conditions of their device [7–9]. Different devices for maintaining the reaction rate to be constant during the course of the process have been described in literatures [10–13]. Since then, other approaches have been proposed in literatures, it is worth citing that of Sørensen, called "Stepwise Isothermal Analysis" [14]. In this method, the sample temperature is increased at a constant heating rate until the reaction rate reaches a pre-set limit, then the temperature remains constant until the reaction rate reaches a lower pre-set limit, when the heating is reassumed. Parkes et al. [15] proposed another approach, in which the sample temperature is maintained at a constant, while the partial pressure of the reactive gas is adjusted so as to keep the

reaction rate to be constant. Other authors have proposed a new form where the reaction rate is steadily accelerated, providing better resolution for kinetic analysis [16, 17]. Recently, most of commercially available thermal analysis devices are equipped with the SCTA methodologies in their most modern instruments, while proposing new modified approaches such as high-resolution thermal analysis (High-Res™) introduced by TA Instruments® [18] or Max-Res™ included in the software of Mettler®.

The developments of SCTA techniques are expected to expand the application of the quantitative analysis for the changes in the physico-chemical properties of materials during thermally induced transformation process to the complex process by realizing the higher experimental resolution for deconvoluting partially overlapping multistep reaction. An illustrative example is the application of SCTA to the compositional analysis of multicomponent polymeric materials. Figure 2.1 compares the mass-change curves recorded in flowing N_2 under the conventional linear heating condition at a heating rate β of 1 K min^{-1} and under CRTA control at a C (= dα/dt) of 3.0 × 10^{-3} min^{-1} for PVC blended with a plasticizer, DINCH (1, 2cyclohexane dicarboxylic acid, diisononyl ester) [19]. The temperature profile of CRTA apparently indicates well separated two-step mass-change process composed of the evaporation of the plasticizer and the thermal degradation of the polymer, while the two-step process cannot be distinguished in the conventional TG. Thus, SCTA can be used to determining the percentage of plasticizers contained in blended polymers, as well as chromatographic techniques [20, 21].

SCTA is also promising for solving long-discussed methodological problems inherent in the kinetic analysis of solid-state reaction using thermal analysis and for precisely controlling the morphology and structure of solid products in the material synthesis via the thermal treatment of solid precursors. In this chapter, the merits of SCTA for applying to the kinetic analysis of solid-state reactions and to the morphological and structural controls of solid products during the solid-state reactions are described as exemplified by some practical examples.

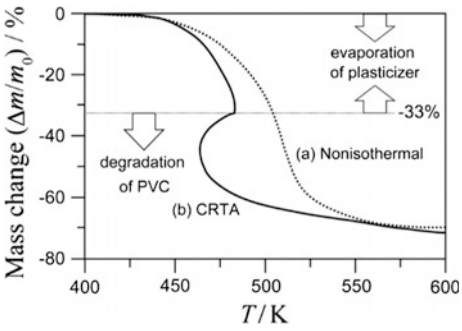

Fig. 2.1 Comparison of mass-change traces of a blended PVC–DINCH recorded in flowing N_2: **a** under linear heating condition at β of 1 K min^{-1} and **b** under constant transformation rate condition at C (= dα/dt) of 3.0 × 10^{-3} min^{-1} [19, 22]

2.2 Advantages of SCTA for Recording Kinetic Rate Data

The kinetic analysis of the solid-state reactions is a scientific methodology constructed with different components involving the measurement of kinetic rate data, kinetic theory, and kinetic calculation [23]. As the measurement technique, various thermal analysis methods have widely been used for tracking of the reaction processes of solid-state reactions. The simplified kinetic equation with the assumption of the single step reaction regulated by a specific rate-limiting step is used in many kinetic studies [24, 25].

$$\frac{\mathrm{d}\alpha}{\mathrm{d}t} = A \exp\left(-\frac{E_\mathrm{a}}{RT}\right) f(\alpha) \tag{2.1}$$

where α is the reacted fraction at time t; E_a is the apparent activation energy; A is the pre-exponential factor of Arrhenius; T is the absolute temperature; and $f(\alpha)$ is a function depending on the physico-geometrical mechanism of the reaction [26]. Many different calculation methods have been proposed for determining the kinetic parameters, i.e. E_a, A, $f(\alpha)$, and kinetic exponents in $f(\alpha)$, by applying Eq. (2.1) to the analysis of experimentally resolved thermoanalytical curves [27, 28]. The experimentally determined kinetic parameters are used for discussing the kinetic characteristics of the reaction, for evaluating possible change in the kinetics depending on reaction conditions, and for comparing the kinetic characteristics among a series of samples and reactions. In this scheme, any drawbacks in each methodological component possibly affect the physical significance of the apparent kinetic parameters. Therefore, further developments of each methodological component are necessary for promoting the methodology to be more powerful tool for researches in modern material sciences [23, 25]. At the same time, each methodological component should compensate the drawbacks in the others for establishing the logically coordinated methodology for kinetic analysis that is fully supported by chemistry and physics.

The measurement of kinetic rate data is essential for the reliable kinetic analysis. The precise measurements realized using modern thermoanalytical instruments do not necessarily provide the reliable kinetic rate data. This relates to the other methodological components, that is, the kinetic theory illustrated by the fundamental kinetic equation and the kinetic calculation method employed for the data analysis. In the fundamental kinetic equation Eq. (2.1), the reaction rate is expressed only as the functions of T and α, and no other factors that affect the reaction rate is assumed. This simplified assumption is rarely realized in the actual solid-state reactions, because of the heat evolution/absorption and generation/consumption of gases during the reaction. The apparent reaction rate is more or less influenced by the self-generated reaction conditions and those changes during the reaction, which is not considered in the fundamental kinetic equation. Therefore, careful considerations of the sample and measurement conditions are

requested for minimizing the influences of mass and heat transfer phenomena on the apparent reaction rate behaviour [29]. SCTA have important advantages for tracking of the kinetic rate data of solid-state reactions with regard to the conventional linear nonisothermal and even isothermal methods. The precise control of the reaction rate involved in SCTA enables a control, either direct or indirect, of both the partial pressure of the gases generated/consumed by the reaction and the associated heat evolution/adsorption rate during the course. This control allows to minimize the influences of heat and mass transfer phenomena and to obtain real kinetic parameters of the forward reaction that occur under the conditions far from the equilibrium.

Figure 2.2 compares the TG–DTG curves for the thermal decomposition of $NaHCO_3$ under isothermal, linear nonisothermal, and CRTA conditions [30] drawn as a function of time, which is in accordance with that illustrated conceptually by Reading [31, 32] and clearly describes the differences of the experimentally resolved thermoanalytical data as a source of kinetic rate data in view of the control of self-generated reaction conditions during the reaction. The shape of the DTG curves is directly correlated to the variations in the rates of gaseous evolution and heat exchange during the reaction. It is thus apparent that the variations in the rates of gaseous evolution and heat exchange are the most significant for the thermoanalytical data recorded under linear nonisothermal conditions, although the magnitudes change depending on the applied measurement conditions involving sample mass, heating rate, flow rate of inert gas, and so on. The variations are largely

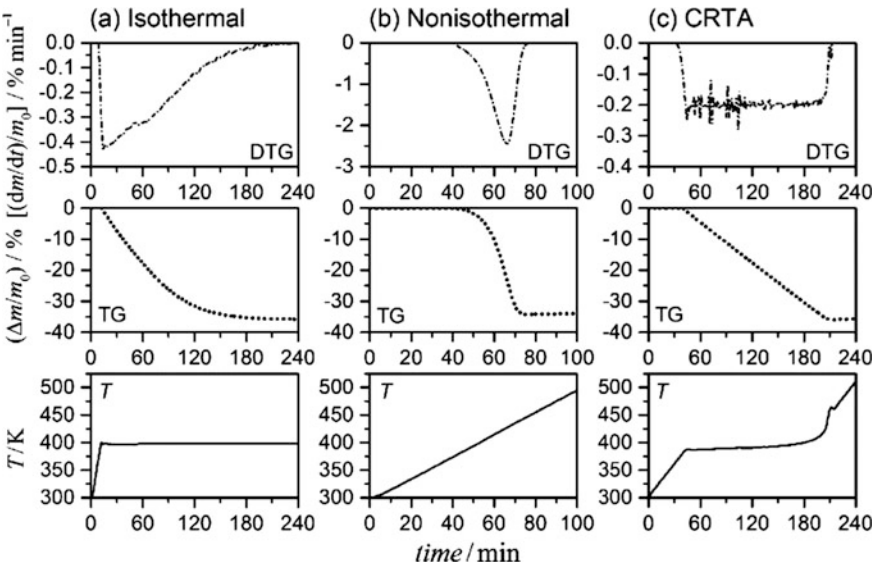

Fig. 2.2 TG–DTG curves for the thermal decomposition of $NaHCO_3$ (100–170 mesh, sample mass m_0 = 5.0 mg, in flowing N_2 (80 cm^3 min^{-1})) recorded under **a** isothermal (T = 398 K), **b** linear nonisothermal (β = 2 K min^{-1}), and **c** CRTA (C = 10.0 μg min^{-1}) conditions [30]

diminished in the isothermal measurements, but still cannot be ignored. If the variation rate of a physical property for a single step reaction, mass-change rate in the example of Fig. 2.2, was controlled to be constant as in CRTA, no variations of the rates of gaseous evolution and heat exchange are practically found. The differences among the thermoanalytical data recorded under different temperature control modes produce different self-generated reaction conditions during the reaction and possibly cause the different influences of the mass and heat transfer phenomena on the apparent kinetic behaviour. Even under such different reaction conditions produced by the reaction, all of the kinetic rate data recorded under different temperature control modes are equally useful for the kinetic analysis based on Eq. (2.1), if the reaction rate of a single step reaction was not sensitive to the variations in the partial pressure of the evolved gas, and the appropriate measurement conditions were selected for realizing negligible temperature gradient within the sample. The establishment of the ideal situation is confirmed by examining the isoconversional relationship (Eq. 2.2) among the data points at a fixed α extracted from a series of kinetic rate data recorded under different temperature control modes and the constancy of the evaluated E_a values at different α during the course of reaction, because Eq. (2.1) is applicable to all of the kinetic rate data under different temperature controlled modes [33, 34].

$$\ln\left(\frac{d\alpha}{dt}\right)_{\alpha} = \ln[Af(\alpha)] - \frac{E_a}{RT_{\alpha}} \tag{2.2}$$

Such ideal kinetic behaviour in view of simplicity of the kinetic analysis is actually observed in the practical reactions as is illustrated in Fig. 2.3 for the kinetic analysis of the thermal decompositions of $NaHCO_3$ [30], $In(OH)_3$ [35], and $Na_2CO_3 \cdot (3/2)H_2O_2$ [36]. In these examples, the isoconversional plot of $\ln(d\alpha/dt)$ versus T^{-1}, known as the Friedman plot [37], for the data points at the fixed α are appreciably linear and the E_a values are practically constant in a wide range of α. In the isoconversional kinetic relationship, the data points obtained from the measurements using CRTA take over the lower reaction rate and temperature part in the kinetic relationship. In general, the lower the reaction rate is the higher the chance to diminish the gradients of temperature and partial pressure of evolved gas in the sample matrix. Therefore, the data points of CRTA can be used as the reference for examining the applicability of the thermoanalytical data recorded using the conventional isothermal and linear nonisothermal methods and appropriate range of the temperature program parameters, T and β.

The advantage of CRTA in terms of maintaining constant the partial pressure of product gas and the reaction rate at a possibly small constant value is of paramount importance in the case of the kinetic analysis of reversible reactions in the thermal decomposition of solids; A(s) $\rightleftarrows$ B(s) + C(g). In such a case, the reaction rate should be expressed by considering the partial pressure, P, of the gaseous product and the equilibrium pressure, P_{eq}, of the reaction [24, 38]:

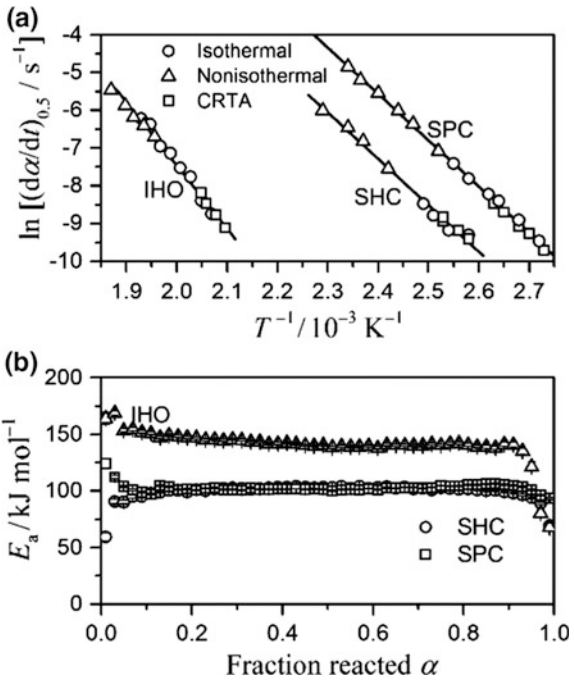

Fig. 2.3 Isoconversional kinetic analyses for the thermal decompositions of $NaHCO_3$ (SHC) [30], $in(OH)_3$ (IHO) [35], and $Na_2CO_3 \cdot (3/2) H_2O_2$ (SPC) [36]: **a** Friedman plots at $\alpha = 0.5$ and **b** E_a values at different α

$$\frac{d\alpha}{dt} = A \exp\left(-\frac{E_a}{RT}\right) f(\alpha) \left(1 - \frac{P}{P_{eq}}\right) \text{ with } P_{eq} = \exp\left(\frac{\Delta_r S}{R}\right) \exp\left(-\frac{\Delta_r H}{RT}\right) \quad (2.3)$$

where $\Delta_r S$ and $\Delta_r H$ are the entropy and the enthalpy of the reaction, respectively. It is clear from Eq. (2.3) that the term $(1 - P/P_{eq})$ should be maintained close to unity in order to obtain reliable kinetic parameters for the forward reaction represented by Eq. (2.1). If the value of P were strictly controlled or precisely measured through the overall reaction, it would be possible to carry out a meaningful kinetic analysis using Eq. (2.3), for which SCTA is a proper method. On the other hand, the isothermal and linear nonisothermal temperature control methods (Fig. 2.2) would lead to significant changes in the reaction rate and in the partial pressure of the product gas, which generally cannot be controlled and could modify the shape of the thermoanalytical curves leading to a meaningless interpretation of the reaction mechanism. Owing to the good control of both the atmosphere surrounding the sample and the real temperature of the sample bed exerted by SCTA methods, the E_a values determined for either reversible [39–52] or irreversible [53] thermal decompositions of solids were sometimes independent of the starting sample mass m_0 in a wider range, while a similar behaviour was not observed when the measurements under linear nonisothermal conditions were concerned. For example, Criado et al. [39] reported that the E_a value for the thermal decomposition of $CaCO_3$; $CaCO_3 \rightleftarrows CaO + CO_2$, as determined under a high dynamic vacuum

using SCTA experiments, was independent of m_0 in the investigated range, i.e. from 0.5 to 50 mg. However, the E_a value determined from conventional linear heating TG curves under high vacuum is strongly depending on the experimental conditions. For obtaining the relevant E_a value with reference to that determined using SCTA, the measurement conditions using m_0 less than 2 mg and β lower than 1 K min^{-1} were necessary in the linear nonisothermal measurement. These results are consistent with those reported later by Reading et al. [42] for the same reaction. Koga and Criado [51] investigated more critically the range of m_0 where the influence of the mass transfer phenomena is practically negligible during CRTA measurements for the thermal decomposition of $CaCO_3$ under high vacuum, in which a series of CRTA curves under high vacuum was recorded by controlling the evolution rate of CO_2 to be a fixed constant value and by changing m_0. As shown in Fig. 2.4, the effect of the mass transfer phenomena on the apparent kinetic behaviour appears to be practically negligible in a smaller m_0 range ($m_0 < 10$ mg), where the isoconversional relationship was actually established. This ideal situation was suddenly broken due to the influence of the mass transfer phenomena when m_0 was attained a certain value, although the critical m_0 value is the empirical value that varies with the size of sample pan, sampling conditions, and controlled vacuum.

In the case of the thermal decomposition of $CdCO_3$ and $PbCO_3$, it was further difficult to obtain E_a values independent of m_0 and β from conventional linear nonisothermal measurements, while the E_a values obtained from SCTA were practically constant in a wide range of m_0 [41]. The similar conclusion was derived by Ortega et al. [44, 49] through the kinetic study of the thermal decomposition of dolomite. From those results, SCTA can be recognized as one of the most reliable approaches for obtaining meaningful kinetic parameters for the thermal decomposition of solids. The influence of the partial pressure of the product gas around the sample on the kinetic results analyzed by several authors [46, 55, 56] indicated that, in the case of reversible reaction, a poor control of the pressure would lead to

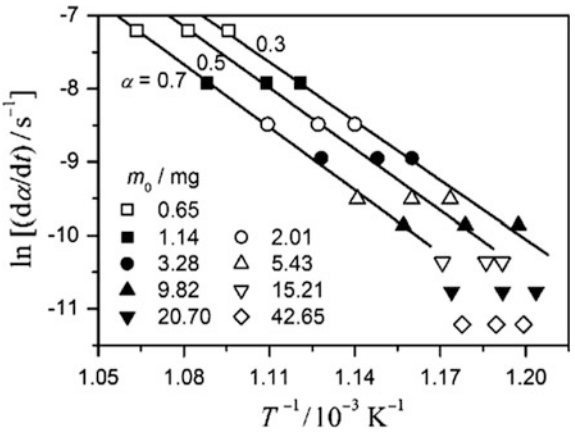

Fig. 2.4 Friedman plots at different α for the thermal decomposition of $CaCO_3$ under high vacuum (5.0×10^{-3} Pa) examined for a series of CRTA curves recorded by controlling the transformation rate to be a fixed constant value and by changing m_0 [51, 54]. (Reproduced from [54] with permission)

artificially high E_a values as is expected from Fig. 2.4, although reliable kinetic parameters of the forward reaction could be obtained by introducing an accommodation function for the partial pressure of product gas [56] in the general kinetic equation as in Eq. (2.3), if the partial pressure of the product gas around the sample is known or measured.

Rouquerol et al. [57, 58] proved that even a relatively small change of the partial pressure of the product gas in the high vacuum range could influence on the reaction mechanism of the thermal dehydration of inorganic hydrates. This behaviour would explain that the E_a values obtained from SCTA methods are independent of m_0 in an appreciably wide range, while the kinetic parameters obtained from conventional linear nonisothermal method very often depend on m_0 and β. This is because all the kinetic analyses of reversible reactions referred in the previous paragraph had been carried out using experimental SCTA data recorded under vacuum and at a low constant partial pressure of the product gas during the course of reaction. The ideal reaction conditions were realized by employing instruments based on the method originally developed by Rouquerol [4–6], where the sample temperature was regulated so as to control the residual pressure to be a low constant value. As the results, the influence of the mass transfer phenomena on the experimentally resolved thermoanalytical curve is minimized and the accommodation function for the partial pressure of the product gas in Eq. (2.3), $(1 - P/P_{eq})$, can be treated approximately as unity or a constant. It has been shown by Criado et al. [39] that it is difficult to maintain the partial pressure of CO_2 during the thermal decomposition of $CaCO_3$ to be a constant in the conventional linear nonisothermal measurement, even if a dynamic starting vacuum of 2.6×10^{-4} Pa was applied using a high pumping rate vacuum system. For example, when the TG curve for the thermal decomposition of $CaCO_3$ with m_0 of 21 mg was measured at a β of 10 K min^{-1} in the dynamic vacuum system, the partial pressure of CO_2 increased up to approximately 10^{-1} Pa. To keep the starting pressure of 2.6×10^{-4} Pa during the thermal decomposition, m_0 and β should be decreased to 1 mg and 0.5 K min^{-1}, respectively. However, mass-loss curves at a constant pressure as low as 5×10^{-4} Pa during entire course of the thermal decomposition were recorded, under SCTA conditions, irrespective of m_0. Furthermore, the thermal decomposition of $BaCO_3$ was studied using SCTA under constant residual partial pressures of CO_2 lower than 10^{-5} Pa by using a high vacuum system equipped with a mass spectrometer attached to a thermobalance [59]. In this case, the partial pressure of CO_2 evolved by the reaction was directly monitored during the entire experiment by means of the mass spectrometer, and even partial pressures lower than the total limit vacuum of the system are used for the feedback control of the sample temperature. Using this procedure, the thermal decompositions of very stable compounds with low equilibrium pressures could be studied in conditions far from equilibrium. Further complex cases can be found for the thermal decomposition of solids that evolves more than one gas and each evolved gas influences differently on the apparent kinetic behaviour. Koga et al. [13, 54, 60–63] approached to the complex kinetic behaviour observed for the thermal decompositions of $NaHCO_3$, $Cu_2CO_3(OH)_2$ (synthetic malachite), and $Zn_5(CO_3)_2(OH)_6$ (synthetic hydrozincite),

using an instrument of constant rate EGA (CREGA) coupled with TG, in which the concentrations of CO_2 and H_2O in the inlet gas to TG were systematically varied and the changes in CO_2 and H_2O concentrations in the outlet gas from TG were controlled to be constant values using CRTA technique. Through examining the thermal decomposition processes that simultaneously evolve CO_2 and H_2O under systematically varied conditions of applied and controlled concentrations of CO_2 and H_2O, it was revealed for the thermal decompositions that CO_2 indicates normal effect on the apparent kinetic behaviour in view of chemical equilibrium, while H_2O exhibits the inverse effect.

The possible thermal gradient within the sample matrix induced by self-cooling or self-heating by the enthalpy of the reaction and the influences of heat transfer phenomena on the experimentally resolved shape of thermoanalytical curves can also be diminished by the application of SCTA. This advantage is used for studying significant exothermic reactions that lead ignition of the sample under conventional thermal analysis method. In SCTA, the self-heating effect by the exothermic reaction can be regulated by controlling the transformation rate during the entire course of the reaction; therefore, preventing thermal runaway and ignition as was demonstrated by Charsley et al. [2] in the study of metal–oxidant pyrotechnics. Paulik [64] has reviewed the successful applications of SCTA for the study of exothermic reactions.

Despite of the problems concerning mass and heat transfer phenomena, application of periodical rate jump during the CRTA measurement proposed by Rouquerol [65–67] can be used for determining reliable E_a value even using a larger m_0. The CRTA jump method imposes periodical jumps between two pre-set reaction rates, C_1 and C_2, and records the accompanied change in the sample temperature from T_1 to T_2. Because the transformation rate is originally controlled at a low constant rate in CRTA, the fraction reacted at times just before and after the rate jump can be approximated to a constant value. Then, using the two data sets of controlled rate and temperature, (C_1, T_1) and (C_2, T_2), the E_a value can be calculated in an isoconversional scheme.

$$E_a = \frac{RT_1T_2}{T_2 - T_1} \ln \frac{C_2}{C_1} \tag{2.4}$$

As in the Friedman plot based on Eq. (2.2), the kinetic model function is cancelled between the two states. It was reported in many kinetic studies of the thermal decomposition of solids, the E_a values at different rate jump points are practically constant and reasonable in comparison with other data sources [44, 68], indicating the practical usability to determine the E_a value from a single CRTA rate jump measurement.

The above review results support our primary statement concerning the advantage of SCTA and allow us to conclude that SCTA methods are a more reliable approach than conventional linear nonisothermal methods in order to obtain reliable E_a values for the thermal decomposition of solids.

2.3 Merits of Kinetic Calculation Using CRTA Curves

The resolution power of SCTA for discriminating among the reaction kinetic models of solid-state reactions listed in Ref. [24] is somewhat more favourable than that of isothermal methods and considerably higher than that of conventional linear nonisothermal methods. This analysis will be mainly based on CRTA that has been the most extensively and systematically studied among different SCTA methods in literatures, as shown in previous reviews on the topic [31, 32, 69]. The characteristic of CRTA is especially important when a single thermoanalytical curve is subjected to the kinetic analysis. However, various kinetic calculation methods using a single thermoanalytical curve recorded under linearly increasing temperature have been proposed and widely used because of less laborious procedure. However, the single run methods have an apparent drawback of mutually correlated apparent variations of calculated kinetic parameters involving E_a, A, and $f(\alpha)$ [70]. This problem is clearly illustrated by curve fittings of a single α–T plot under linear nonisothermal condition using different kinetic models as shown in Fig. 2.5 [71, 72]. By assuming F1, A2, and A3 models, the uniform α–T plot can be reproduced within an error lower than 10^{-5}%, where different sets of Arrhenius parameters, E_a and A, are estimated for the respective $f(\alpha)$ assumed. Therefore, the mutual correlation of the calculated kinetic parameters leads the distortion of the calculated E_a and A values due to the wrong choice of $f(\alpha)$ and a superficial linear correlation between E_a and ln A values calculated by assuming different kinetic model functions [70, 73–77]. The distortion of the Arrhenius parameters by the wrong choice of the kinetic model function can be explained as a simple mathematical relationship using an approximation of exponential temperature integral under linearly increasing temperature condition [78, 79].

$$\frac{E_{\mathrm{dis}}}{E_a} = \frac{f(\alpha_p)F'(\alpha_p)}{F(\alpha_p)f'(\alpha_p)} \text{ with } f'(\alpha) = \frac{\mathrm{d}f(\alpha)}{\mathrm{d}\alpha} \text{ and } F'(\alpha) = \frac{\mathrm{d}F(\alpha)}{\mathrm{d}\alpha} \tag{2.5}$$

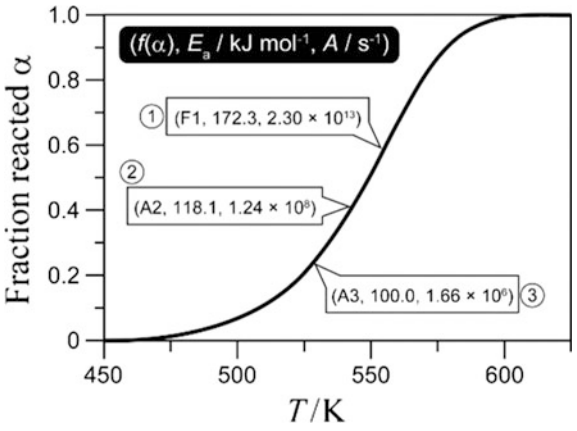

Fig. 2.5 A single TG curve at β of 1 K min^{-1} drawn by assuming three different kinetic models with different Arrhenius parameters ($f(\alpha)$, E_a/kJ mol^{-1}, A/s^{-1}) = (F1, 172.3, 2.30 × 10^{13}), (A2, 118.1, 1.24 × 10^{8}), and (A3, 100.0, 1.66 × 10^{6}) [71, 72, 84]

$$\ln\left(\frac{A_{\mathrm{dis}}}{A}\right) = \frac{E_{\mathrm{a}}}{RT_{\mathrm{p}}}\left[\frac{f(\alpha_{\mathrm{p}})F'(\alpha_{\mathrm{p}}) - F(\alpha_{\mathrm{p}})f'(\alpha_{\mathrm{p}})}{F(\alpha_{\mathrm{p}})f'(\alpha_{\mathrm{p}})}\right] + \ln\frac{f(\alpha_{\mathrm{p}})}{F(\alpha_{\mathrm{p}})} \tag{2.6}$$

where E_{dis} and A_{dis} are the distorted Arrhenius parameters caused by the use of wrong kinetic model function $F(\alpha)$. The subscript p denotes the values at the peak top of the transformation rate under linearly increasing temperature condition. To avoid this problem, it is generally recommended to use a two-step kinetic calculation procedure using a series of thermoanalytical data recorded under different measurement conditions, which is composed of the determination of E_{a} value as the first step using the isoconversional method and subsequent determination of A and $f(\alpha)$ using the master plot method [28, 34, 80–82]. The single step kinetic calculation based on Eq. (2.1) using multiple thermoanalytical data proposed by Pérez-Maqueda et al. [83] as the combined kinetic analysis method is also useful to avoid the problem. In connection with this problem, the higher power of CRTA for discriminating the kinetic model function provides the possible opportunity of the determination or estimation of the kinetic model function in the first step using a single CRTA curve.

Because in CRTA, the transformation rate is kept constant at a programmed value C, Eq. (2.1) can be rewritten in the following form

$$C = A\exp\left(-\frac{E_{\mathrm{a}}}{RT}\right)f(\alpha) \tag{2.7}$$

In the scheme of constant transformation rate, the shape of CRTA curves characterized by T–α plots (inverse to α–T plots of linear nonisothermal measurements because of inverse measurement logics) are strongly depending on the typical kinetic model functions for the solid-state reactions [71, 85], while the α–T plots obtained using the conventional linear nonisothermal method at a β represent a sigmoidal shape irrespective of the kinetic model. Thus, it is quite impossible to discern the reaction mechanism from the shape analysis of a single TG curve recorded under linear nonisothermal condition [86–93]. The shape analysis of T–α plots of CRTA curves with respect to different $f(\alpha)$ would be very illustrative for demonstrating the power of CRTA for discriminating the most appropriate $f(\alpha)$ from a single experimental curve. Figure 2.6 compares the shapes of T–α plots of CRTA curves drawn by assuming different $f(\alpha)$ functions [54, 72, 94]. It is clearly seen that the T–α plots for the phase boundary controlled models (Rn) are concave with regards to α axis, while those of diffusion controlled models (Dn) present an inflection point. From the difference in the shape of T–α plots, the reactions that obey to Rn and Dn models are distinguishable. However, this observation is applicable to the reaction of the uniformly sized reactant particles, because the shape of CRTA curves for the reaction of interface shrinkage type including Rn and Dn changes depending on the degree of distribution in the particle size [95, 96].

The T–α plots for the Avrami–Erofeev (Am) equation that describes a nucleation-growth model show a minimum temperature midway through the

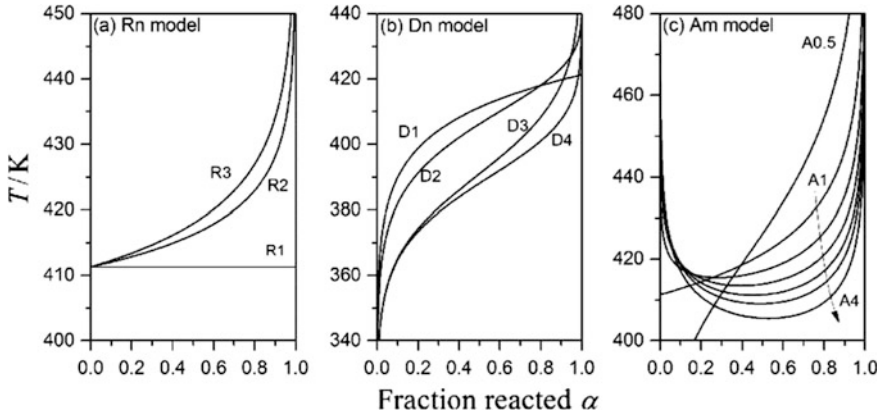

Fig. 2.6 T–α profiles of CRTA curves corresponding to different kinetic models simulated assuming E_a = 100 kJ mol^{-1}, A = 5.0 × 10^8 s^{-1}, and C (= dα/dt) = 1.0 × 10^{-4} s^{-1} [54, 72, 94]. (Reproduced from [54] with permission)

reaction when $m > 1$. By this characteristic of the shape of CRTA curve, the reaction of Am models can be distinguished from Rn and Dn models. The α value at the minimum temperature (α_m) has the specific values for respective Am equations with different kinetic exponents (α_m = 0.393; 0.486; and 0.528 for the models A2, A3 and A4, respectively) [71]. The α_m values calculated for CRTA curves for Am model are perfectly in agreement with the calculated α value at the maximum transformation rate under isothermal conditions [38, 97]. The relationship between the rate behaviour under isothermal condition and the T–α profile of CRTA for Am models was clearly described by Tiernan et al. [98]. The initial temperature decreasing part in the T–α profile of CRTA would correspond to the acceleratory period under isothermal condition, where the total area of the reaction interface increases by the nucleation and growth of the nuclei. In CRTA, the acceleration would be offset by a diminution of the temperature in order to maintain the transformation rate constant. The later rising temperature stage of CRTA would correspond to the decay period under isothermal condition, where the reaction rate decelerated by the overlapping of the growing nuclei. The deceleration must be compensated by increasing the temperature in CRTA. The specific value of α_m for each Am model can be used for discriminating the most appropriate kinetic exponent among different Am models. A similar T–α profile with the minimum temperature midway through the reaction would be observed for the reaction that indicates a sigmoidal mass-change trace under isothermal condition. The typical examples are the consecutive surface reaction and subsequent shrinkage of the reaction interface towards the centre of the reacting particle as have been formalized under isothermal condition by Mampel [99], autocatalytic reaction formalized by Prout and Tompkins [100, 101], and random scission mechanism of the thermally induced polymer degradation [102, 103]. For effectively using the model discrimination power of CRTA, different master plot methods applicable to shape analysis of CRTA curves have been proposed as reviewed previously [72].

Many practical examples substantiate the higher model discrimination power of CRTA. For example, the thermal decomposition of anhydrous nickel nitrate obeys Am model with $m = 2$ under isothermal conditions [104]. As shown in Fig. 2.7a, the T–α profile of CRTA for the reaction apparently indicates the minimum temperature midway through the reaction at $\alpha_m = 0.38$ [71], which closely corresponds to the specific α_m value for A2 model ($\alpha_m = 0.393$). The T–α profiles of CRTA that are characteristic for Am models have been very often reported in literature for different reactions [57, 58, 62, 64, 105–113], which involves the thermal dehydration of uranyl nitrate trihydrate reported by Bordère et al. [58] as shown in Fig. 2.7b.

Barnes et al. reported an example that effectively utilized the deconvolution power of partially overlapping reaction processes and the discrimination power of kinetic models of SCTA for the thermally induced successive reduction of V_2O_5 to V_2O_3 in hydrogen atmosphere [106, 114]. The reaction steps involved cannot be separated in the conventional linear nonisothermal measurement, while possible three reaction steps, $V_2O_5 \rightarrow V_4O_9 \rightarrow VO_2 \rightarrow V_2O_3$, are expected from the overall α–T profile of CRTA as shown in Fig. 2.8. At the same time, Am models are estimated for the respective reaction steps, because the α–T profiles of all the

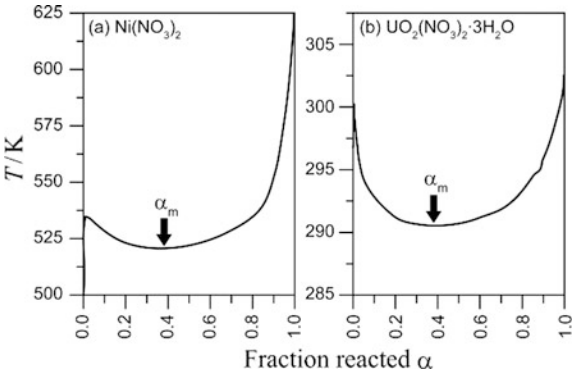

Fig. 2.7 T–α profiles of CRTA for **a** the thermal decomposition of anhydrous nickel nitrate under vacuum at $C\,(= d\alpha/dt) = 4.17 \times 10^{-5}\ s^{-1}$ [71] and **b** thermal dehydration of uranyl nitrate trihydrate under vacuum at $C\,(= d\alpha/dt) = 2.77 \times 10^{-6}\ s^{-1}$ [58]

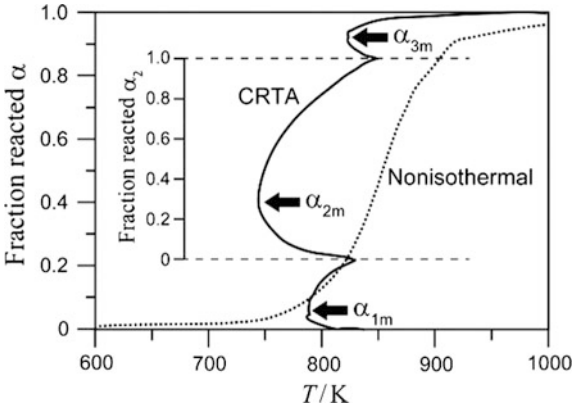

Fig. 2.8 α–T profiles of thermally induced hydrogen reduction of V_2O_5 under linear nonisothermal condition at $\beta = 1\ K\ min^{-1}$ and under CRTA condition at $C\,(= d\alpha/dt) = 1.8 \times 10^{-5}\ s^{-1}$ [106, 114]

reaction steps indicate the characteristic shape for Am model with the minimum temperature midway through the reaction. Tierman et al. [98] have reported the similar effective use of CRTA in their comparative study for the thermal reduction of different iron oxides involving hematite and magnetite. The thermal reduction of hematite to metal iron under conventional conditions are recorded as two overlapping processes, while in CRTA, the two reaction steps are observed separately as a complete conversion to magnetite before the reduction of magnetite to iron takes place. It was also revealed that the reductions of hematite to magnetite and of magnetite to metal iron follow an Rn model and an Am model, respectively. Similarly, the thermal reductions of NiO and CuO have also been studied using CRTA by the same authors, concluding that the shape of the curves is characteristic of an Am model [98, 115].

In some kinetic studies of the thermal decomposition of inorganic solids reported recently, the characteristic T–α profile in CRTA curves with the minimum temperature midway through the reaction were interpreted in relation to physico-geometrical reaction mechanisms other than Am models. For the thermal decomposition of $FeC_2O_4{\cdot}2H_2O$ [116], the T–α profile of CRTA was explained by the consecutive process of surface reaction regulated by the first order law (F1) and subsequent phase boundary reaction with two dimensional shrinkage of the reaction interface (R2), which is expressed by a kinetic equation of Mampel type under isothermal conditions.

(a) $t \leq 1/k_{\mathrm{PBR}}$

$$\frac{\mathrm{d}\alpha}{\mathrm{d}t} = -2k_{\mathrm{PBR}}\left[\left(1+\frac{k_{\mathrm{PBR}}}{k_{\mathrm{SR}}}\right)\exp(-k_{\mathrm{SR}}t) + k_{\mathrm{PBR}}t - \left(1+\frac{k_{\mathrm{PBR}}}{k_{\mathrm{SR}}}\right)\right] \tag{2.8}$$

(b) $t \geq 1/k_{\mathrm{PBR}}$

$$\frac{\mathrm{d}\alpha}{\mathrm{d}t} = -2k_{\mathrm{PBR}}\exp(-k_{\mathrm{SR}}t)\left[1+\frac{k_{\mathrm{PBR}}}{k_{\mathrm{SR}}} - \frac{k_{\mathrm{PBR}}}{k_{\mathrm{SR}}}\exp\left(\frac{k_{\mathrm{SR}}}{k_{\mathrm{PBR}}}\right)\right] \tag{2.9}$$

where k_{SR} and k_{PBR} are the rate constants for the surface and phase boundary reactions, respectively. Differently, the similar T–α profile of CRTA observed for the thermal decomposition of $Na_2CO_3{\cdot}(3/2)H_2O_2$ was interpreted by a physico-geometrical model that assumes the acceleration of linear advancement rate of reaction interface in the scheme of contracting geometry [36]. This type of reaction also indicates a sigmoidal shape of the integral kinetic curve (α–t) under isothermal conditions and expressed by the kinetic model function originally proposed by Galwey and Hood [117].

$$f(\alpha) = 2n(1-\alpha)^{1-1/n}\left[1-(1-\alpha)^{1/n}\right]^{1/2} \tag{2.10}$$

where n is the dimension of interface shrinkage. Many other examples of the successful use of SCTA and CRTA for the study of kinetics and mechanisms of solid-state reaction can be found in literatures [10, 13, 22, 50, 61, 63, 118–144], which involve the kinetic studies of solid–gas reactions in the framework of the CO_2 capture from the atmosphere [136, 137].

SCTA methods have also been applied to the thermal degradation of polymers [84, 103, 145–154]. The T–α profile of CRTA for the typical reaction mechanism of polymer degradation known as the random scission mechanism is similar to those of Am models [103, 149]. The reaction mechanism of the thermal degradation of polybutylene (PBT) has been characterized as a random scission of the polymer chains using CRTA [146]. Another example of the polymer degradation studied using CRTA is for polyvinyl chloride (PVC). In many previous studies that used the conventional thermal analysis [155–160], F1 model has been selected as the most appropriate kinetic model for the dehydrochlorination reaction. However, the α–T profile of CRTA does not fit to F1 model as shown in Fig. 2.9 [11, 146] and clearly indicate the two-step feature of the process, which cannot be deconvoluted in the conventional linear nonisothermal method. The α–T profile of CRTA for the first reaction step is characterized by the appearance of the minimum temperature midway through the reaction. Therefore, the reaction mechanism of the first reaction step of the thermal dehydrochlorination of PVC can be interpreted either by an Am model [11, 146] or a random scission model [150].

The potential of CRTA for the kinetic model discrimination would be approved by the above review. Once the appropriate kinetic model function was selected from a single CRTA curve through the shape analysis of T–α profile of CRTA and using available master plot methods, the Arrhenius parameters can separately be determined based on Eq. (2.1) from the same CRTA curve [85, 161]. In addition, the reliability of the calculated Arrhenius parameters can be confirmed by the comparison with the E_a value determined using the rate jump CRTA method [65–67]. Therefore, two CRTA measurements, one is the ordinal and the other is the rate jump measurements, are the minimum requirement for the kinetic analysis. Of

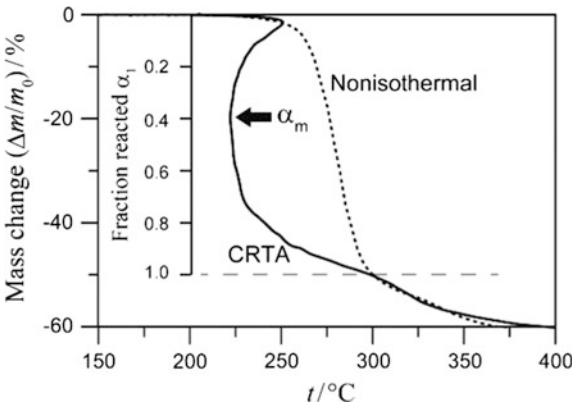

Fig. 2.9 Comparison of mass-change traces for the thermal dehydrochlorination of PVC recorded under linear nonisothermal condition at $\beta = 2$ K min^{-1} and CRTA condition at C (= dα/dt) = 5 × 10^{-4} s^{-1} [11, 84, 146]

course, a systematic kinetic approach with the measurements of a series of CRTA curves under different measurement conditions of m_0 or C are preferable. Using the series of CRTA curves, the recommended two-step kinetic analysis, determination of E_a by the isoconversional method and the subsequent analysis of the experimental master plot for determining $f(\alpha)$ and A, can be performed using the universally applicable procedures of kinetic calculation [28, 34, 80–82].

2.4 Application of SCTA to Material Synthesis

2.4.1 Controls of Porosity and Specific Surface Area

The potential of SCTA to control the self-generated reaction conditions in a sophisticated manner can be applied to the synthetic reactions of materials. The application of SCTA to material synthesis was first attempted by Rouquerol et al. [162, 163] for the thermal decomposition of $Al(OH)_3$ (gibbsite) crystals to form Al_2O_3, where the influence of partial pressure of the self-generated water vapour on the variation of specific area of reacting sample was examined using CRTA under vacuum. The thermal decomposition process was controlled at a constant decomposition rate C (= $d\alpha/dt$) of 5.5×10^{-4} min^{-1} under different residual pressures of water vapour within the range from 5.3 to 667 Pa. As shown in Fig. 2.10a, the variation of specific surface area of the reacting sample largely depends on the residual pressure of water vapour, where the initial increase in the specific surface area dramatically increases with increasing the residual pressure. The maximum value of the specific surface area attained during the thermal decomposition varied from 40 m^2 g^{-1} at 5.3 Pa up to 450 m^2 g^{-1} at 667 Pa. On further heating, the specific surface area turns to decrease at the temperature in the range of 250–300 °C irrespective of the residual pressure. The diminution of the specific surface also depends on the residual pressure, indicating the higher the residual pressure is the lower the decrease degree. As the results, the final product of Al_2O_3 with the larger specific surface area was obtained when the sample was decomposed at a constant reaction rate under higher residual pressure of water vapour. The phenomena were lately reconfirmed by Stacey [164, 165] and Barnes and Parkes [166] for the thermal decompositions of $Al(OH)_3$ (gibbsite) and AlO(OH) (boehmite) and explained with experimental evidence of the formations of slit-shaped micropores, mesopores, and macropores and the variations of those contributions to the specific surface area depending on the residual pressure of water vapour during the course of reaction. With decreasing the residual pressure, the specific surface area attributed to the microporosity increases accompanied with a decrease in the width of the slit pores, while the specific surface area attributed to mesoporosity and macroporosity decreases. The significant low specific surface area when the thermal decomposition was subjected under lower residual pressure was interpreted by the formation of slit pores with narrow width that cannot be accessed by nitrogen during the measurement of specific surface area using the Brunauer–Emmett–Teller

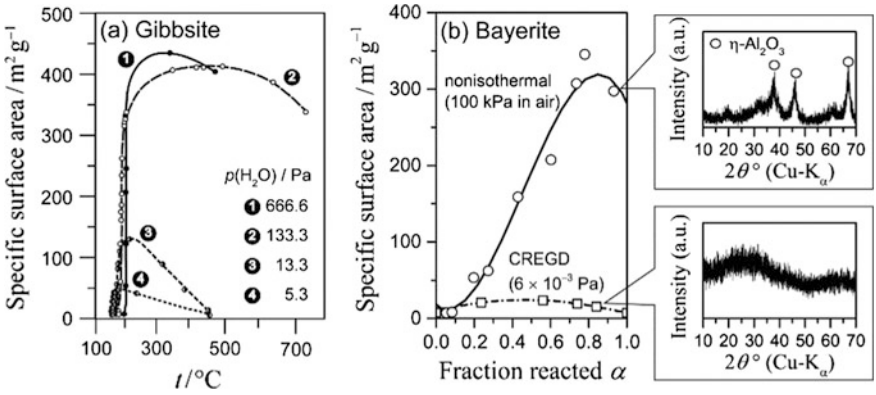

Fig. 2.10 Variation of the specific surface area during the thermal decompositions of $A1(OH)_3$: **a** gibbsite (grain size 1 μm) at a constant reaction rate C (= dα/dt) of 5.5×10^{-4} min^{-1} under different water vapour pressures [162] and **b** bayerite (m_0 = 300 mg) under linear heating condition at β = 2 K min^{-1} in air and under CRTA at a controlled water vapour pressure of 6.0×10^{-3} Pa (C = 18.4 μg min^{-1}), together with the powder XRD patterns of the product solids [138, 167]

(BET) method. The decrease in the specific surface area on further heating the sample at a temperature higher than 300 °C has been explained by the effective annealing temperature for the microporosity being lower than that of mesopores and macropores. A comparison of the changes in the specific surface area during the thermal decomposition of synthetic bayerite ($Al(OH)_3$) under linear heating condition in air (100 kPa) and under CRTA condition of controlled residual pressure at 6.0×10^{-3} Pa also indicated the lower maximum specific surface area under the CRTA condition in reduced pressure (Fig. 2.10b), where the maximum specific surface area of each process was approximately 350 m^2 g^{-1} at α = 0.9 and 25 m^2 g^{-1} at α = 0.4 under the linear heating condition and the CRTA condition, respectively [138, 167]. η-Al_2O_3 was obtained as the decomposition product under the linear heating condition, while the product was amorphous to XRD under the CRTA condition.

Possible control of porosity of reacting sample during the thermal decomposition of solids under vacuum was also demonstrated by controlling the decomposition rate and residual pressure of water vapour for the thermal decomposition of α-FeO(OH) (goethite to form α-Fe_2O_3 (hematite) [168, 169], in which an independent control of both constant reaction rate and constant residual pressure of water vapour was applied using SCTA. By the SCTA control under vacuum, the porosity of the hematite product can be controlled by the formations of two different types of pore structures as shown in Fig. 2.11. Those are the isolated round pores formed at higher residual pressures (Fig. 2.11a) and slit pore channels oriented along the c-lattice axis (the long axis of the particle) formed at very low water vapour pressures (Fig. 2.11b). The specific surface area of the produced hematite was significantly increased with decreasing the controlled residual pressure of water vapour during

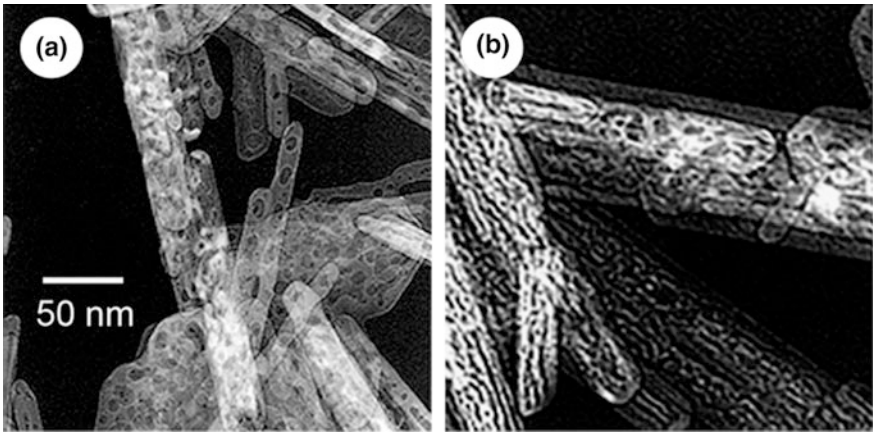

Fig. 2.11 TEM micrographs of the hematite products obtained by the thermal decomposition of goethite under CRTA conditions: **a** $P = 1.1$ kPa and $C = 7.6 \times 10^{-4}$ min^{-1} and **b** $P = 7.3 \times 10^{-3}$ Pa and $C = 3.3 \times 10^{-3}$ min^{-1} [168, 169]

the thermal decomposition of goethite [168, 169]. A similar behaviour was also found for the thermal decomposition of γ-FeOOH (lepidocrocite) to form γ-Fe_2O_3 (maghemite) when both the rate and the water vapour pressure were controlled during the thermal decomposition using CRTA [170]. However, the trend of the residual pressure-specific surface area relationship observed for the thermal decomposition of goethite and lepidocrocite is apparently opposite to those described above for the thermal decompositions of gibbsite, bayerite, and hematite, although the respective hydroxides and oxyhydroxides have the similar crystal structures. It is noteworthy to point out that the microporosity increases in both isostructural oxyhydroxides by decreasing the water partial pressure during the dehydroxylation reaction, but the size of the slit-shaped microporous generated from iron oxyhydroxides are larger than those generated from aluminium oxyhydroxides; therefore, they are accessible to the nitrogen adsorption. This behaviour would explain that the BET surface of iron oxides obtained from the dehydration of oxyhydroxides increases by increasing the microporosity, contrarily what occurs in the case of the alumina obtained from aluminium oxyhydroxide. The size of the structural microporous generated during the dehydroxylation of these compounds perhaps would be controlled by the cation size in such a way that the lower is the cation radius the lower is the size of the microporous.

The potential of SCTA for controlling the porosity and specific surface area of the oxides produced by the thermal decomposition of precursor compounds under controlled vacuum and reaction rate can be applicable to the syntheses of adsorbents and catalysts as have been reported in many works [113, 124, 171–177]. Those works have previously been reviewed by Llewellyn et al. [178], Fesenko et al. [114], and Pérez-Maqueda et al. [179].

2.4.2 Controls of Particle Morphology, Size, and Phase Composition

The SCTA control of both the residual pressure under dynamic vacuum and the reaction rate has also been applied to the synthesis of barium titanate ($BaTiO_3$) from the thermal decomposition of its oxalate and citrate precursors [180–183] and it was reported the successful controls of particle morphology, particle size, and phase composition of $BaTiO_3$ polymorphs. The crystal size and the stabilization of the cubic phase with regards to the tetragonal phase of $BaTiO_3$ were controlled by changing the controlled residual pressure to different constant values in the range from 10^{-2} Pa to 10 kPa, in which the crystal size of $BaTiO_3$ was decreased and the cubic phase was stabilized by decreasing the constant residual pressure. Figure 2.12 shows the electron microscopic views of the citrate precursor (Fig. 2.12a) and $BaTiO_3$ products (Fig. 2.12b–d). Round powder particles of $BaTiO_3$ were obtained by the conventional isothermal annealing treatment (Fig. 2.12b). Under some selected conditions of constant residual pressure and reaction rate using CRTA method, $BaTiO_3$ fibres constituted by welded nanocrystals (Fig. 2.12c, d) were obtained through the thermal decomposition of acicular shaped particles of barium titanyl citrate [184].

A successful control of the phase composition and the crystal and particle sizes has also been reported for the synthesis of Si_3N_4 through the carbothermal nitridization of silica using SCTA by controlling both the reaction rate and the partial pressure of CO generated by the carbothermal reduction of silica [185–187]. Figure 2.13 compares the SEM images of two Si_3N_4 products obtained through the carbothermal reduction of silica in flowing a mixed N_2–H_2 gas (95% N_2) and by controlling the reaction rate to be constant at C (= $d\alpha/dt$) of 1.1×10^{-3} min^{-1} under different controlled partial pressures of CO generated by the carbothermal reduction of silica, which was subsequently annealed isothermally at 1450 °C for 5 h in flowing the mixed gas [187]. The Si_3N_4 produced by the thermal decomposition at the lowest constant residual concentration of CO is constituted by a mixture of β-Si_3N_4 ribbons and small hexagonal crystallites of α-Si_3N_4 (Fig. 2.13a), while that obtained at the higher residual CO concentration is constituted by hexagonal crystallites of pure α-Si_3N_4 with homogeneous size (Fig. 2.13b). The application of SCTA to the synthesis of other ceramic materials has also been reported [188–193].

2.4.3 Controls of Debinding and Curing Processes

Multilayer capacitors (MLCs) or in general multilayer actuators (MLAs) constituted by layers of ferroelectric ceramics separated by electrode metal layers are manufactured by stacking the different layers by a tape casting technology, generally using an organic binder, followed by debinding and sintering processes by co-firing

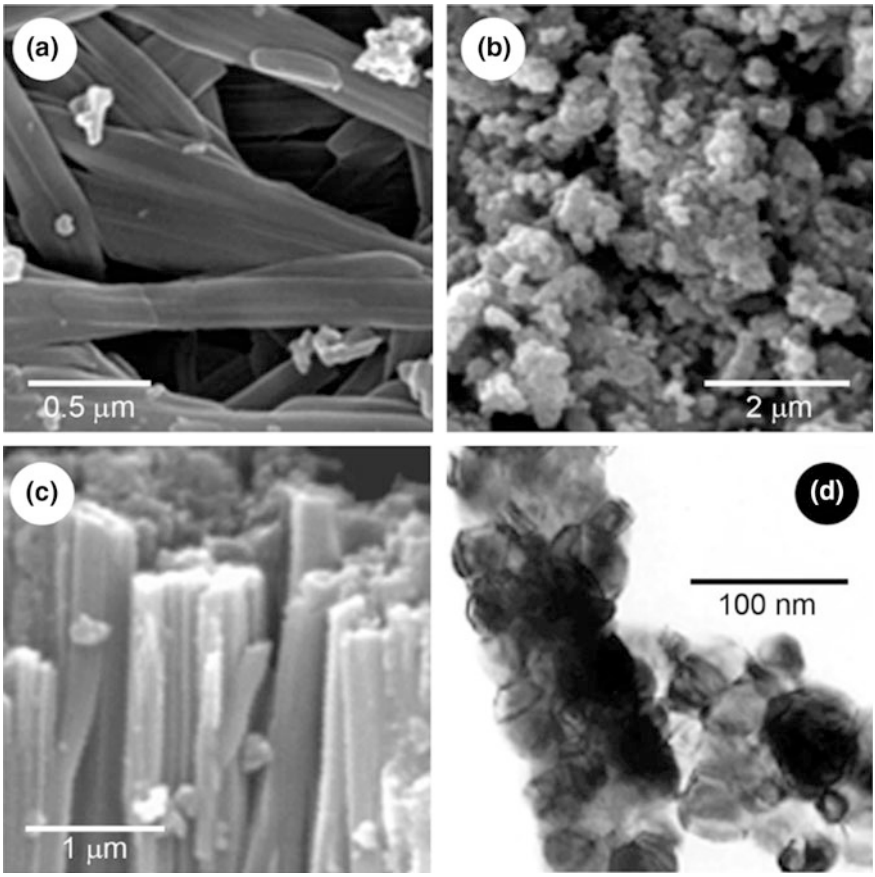

Fig. 2.12 Electron microscopic views of the citrate precursor and its thermal decomposition product, $BaTiO_3$: **a** barium titanyl citrate (SEM); **b** $BaTiO_3$ obtained by isothermal annealing at 700 °C for 5 h (SEM). **c** $BaTiO_3$ obtained by the thermal treatment under CRTA conditions ($P = 1.3 \times 10^{-3}$ Pa) and subsequent isothermal annealing at 700 °C for 5 h (SEM) **d** as in (**c**) (TEM) [184]

treatment. The possible crack formation during the co-firing treatment is the main problem in the manufacturing of these devices. Therefore, the debinding process is a rather cumbersome process that very often takes several weeks [194]. The control of debinding rate at a low constant rate using SCTA is one of the possible solutions for avoiding the crack formation as demonstrated by Speyer et al. [194, 195]. Figure 2.14 illustrates the optical microscopic views of the polished surfaces of MLAs obtained by debinding at different controlled rates. It is clearly shown that the delaminating damage is dramatically reduced by decreasing the debinding rate.

The SCTA technique has also been applied to the thermal curing of concretes [196]. During the curing process, crystallization of xonotlite and other hydrates can be hindered by the control of the thermal dehydration rate at a low constant rate and

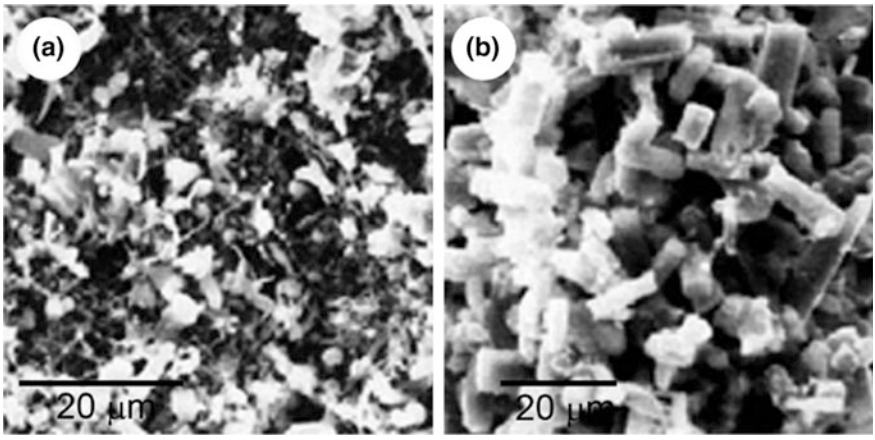

Fig. 2.13 SEM images of Si_3N_4 obtained from carbothermal reduction of silica at the constant reaction rate C (= dα/dt) of 1.1×10^{-3} min^{-1} under different constant concentration of CO: **a** 20 Pa and **b** 1 kPa [187]

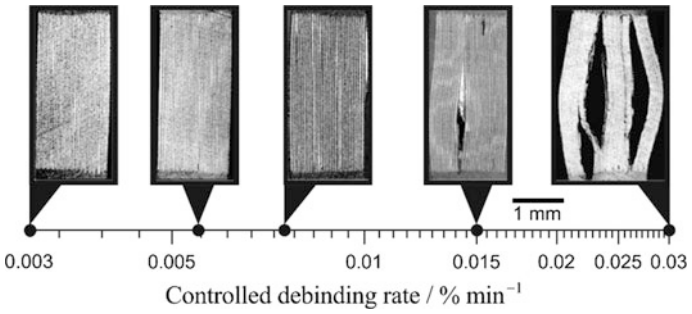

Fig. 2.14 Optical microscopic views of the polished surfaces of MLAs obtained under different controlled debinding rates [195]

maintain the partial pressure of water vapour in the close vicinity of the samples at a lower value. SCTA techniques were also useful for controlling the interfibre porosity and for eliminating the structural microporosity of sepiolites [197] and for synthesising oxide systems with tailored specific surface [198–200]. A study of the thermal dehydration of the hydrated rare earth polyphosphates using SCTA for obtaining the anhydrous salts, which is of great interest as catalysts and luminescent materials, has been reported in literature [201, 202]. A novel $Ce(PO_3)_3$ phase with a crystal structure, different from those of the other lanthanide polyphosphates, has been obtained by controlling the thermal dehydration at a constant reaction rate so as to maintain the partial pressure of self-generated water vapour to be a constant value of 5 kPa [201].

2.5 Conclusions

In addition to the higher resolution power for the thermally induced multistep processes, SCTA techniques represent higher potentials for applying to the kinetic analysis of the solid-state reactions and polymer degradations and for controlling the synthetic and manufacturing processes of materials and devices. The special performance of SCTA to control the reaction rate at a small constant value and the partial pressure of the evolved gas at a low constant value offers the measurements of the kinetic rate data for the reaction under the controlled reaction conditions involving the conditions self-generated by the reaction itself. In modern SCTA instruments, the reaction rate is controlled precisely even for the process with a small total change of the measured physical properties, for example several hundred μg in TG. The SCTA measurement using a small amount sample provides ideal kinetic rate data, in which the gradients in temperature and partial pressure within the sample matrix are largely diminished in comparison with conventional isothermal and linear nonisothermal measurements. When applying the data to kinetic calculation, the T–α profile of CRTA are characteristic for the respective kinetic models; therefore, the appropriate kinetic model function can easily be estimated using available master plot methods. This is the significant merit to avoid possible distortions of the calculated Arrhenius parameters by the wrong choice of the kinetic model function. In applying SCTA for material synthesis processes, both the reaction rate and the partial pressure of gases can be controlled to be different constant values in wide ranges by changing the applied reaction atmosphere, pumping rate to vacuum, sample mass, controlled transformation rate, and so on. The performance of SCTA can be used for obtaining the solid products with the desired chemical and physical properties in the more sophisticated manner in comparison with the empirical annealing treatments. The advantages of SCTA have been evidenced by the previous works reviewed in this chapter, and the techniques can further contribute to the promising advancement of modern material sciences.

References

1. Smith CS (1940) A simple method of thermal analysis permitting quantitative measurements of specific and latent heats. Trans AIME 137:236–245
2. Charsley EL, Laye PG, Parkes GMB, Rooney JJ (2010) Development and applications of a sample controlled DSC system. J Therm Anal Calorim 105(2):699–703
3. Saccone A, Macciò D, Robinson JAJ, Hayes FH, Ferro R (2001) Smith thermal analysis of selected Pr–Mg alloys. J Alloys Compd 317–318:497–502
4. Rouquerol J (1970) L'analyse thermique a vitesse de decomposition constante. J Therm Anal 2(2):123–140
5. Rouquerol J (1997) Controlled rate evolved gas analysis: 35 years of rewarding services. Thermochim Acta 300(1–2):247–253
6. Rouquerol J (1964) Methode d'analyse thermique sous faible pression et a vitesse de decomposition constante. Bull Soc Chim Fr:31–32

7. Paulik J, Paulik F (1971) "Quasi-isothermal" thermogravimetry. Anal Chim Acta 56(2):328–331
8. Paulik F, Paulik J (1986) Thermoanalytical examination under quasi-isothermal—quasi-isobaric conditions. Thermochim Acta 100(1):23–59
9. Paulik F (1999) Thermal analysis under quasi-isothermal–quasi-isobaric conditions. Thermochim Acta 340–341:105–116
10. Barnes PA, Parkes GMB, Charsley EL (1994) High-performance evolved gas analysis system for catalyst characterization. Anal Chem 66(14):2226–2231
11. Diánez MJ, Pérez-Maqueda LA, Criado JM (2004) Direct use of the mass output of a thermobalance for controlling the reaction rate of solid-state reactions. Rev Sci Instrum 75 (8):2620–2624
12. Criado JM, Pérez-Maqueda LA, Diánez MJ, Sánchez-Jiménez PE (2007) Development of a universal constant rate thermal analysis system for being used with any thermoanalytical instrument. J Therm Anal Calorim 87(1):297–300
13. Koga N, Yamada S (2005) Influences of product gases on the kinetics of thermal decomposition of synthetic malachite evaluated by controlled rate evolved gas analysis coupled with thermogravimetry. Int J Chem Kinet 37(6):346–3549
14. Sørensen OT (1981) Quasi-isothermal methods in thermal analysis. Thermochim Acta 50(1–3):163–175
15. Parkes GMB, Barnes PA, Charsley EL (1998) Gas concentration programming—a new approach to sample controlled thermal analysis. Thermochim Acta 320(1–2):297–301
16. Ortega A, Pérez-Maqueda LA, Criado JM (1994) Simultaneous determination of the activation energy and the reaction kinetic model from the analysis of a single curve obtained by a novel method. J Therm Anal 42(2–3):551–557
17. Ortega A, Pérez-Maqueda LA, Criado JM (1994) Shape analysis of the α–T curves obtained by CRTA with constant acceleration of the transformation. Thermochim Acta 239:171–180
18. Gill PS, Sauerbrunn SR, Crowe BS (1992) High resolution thermogravimetry. J Therm Anal 38(3):255–266
19. Sánchez-Jiménez PE, Pérez-Maqueda LA, Crespo-Amoros JE, Lopez J, Perejon A, Criado JM (2010) Quantitative characterization of multicomponent polymers by sample-controlled thermal analysis. Anal Chem 82(21):8875–8880
20. Wang FC-Y (2000) Polymer additive analysis by pyrolysis–gas chromatography. J Chromatogr A 891(2):325–336
21. Peris-Vicente J, Baumer U, Stege H, Lutzenberger K, Gimeno Adelantado JV (2009) Characterization of commercial synthetic resins by pyrolysis-gas chromatography/mass spectrometry: application to modern art and conservation. Anal Chem 81(8):3180–3187
22. Pérez-Maqueda LA, Criado JM, Sánchez-Jiménez PE, Perejón A (2013) Kinetic studies in solid state reactions by sample-controlled methods and advanced analysis procedures. J Therm Anal Calorim 113(3):1447–1453
23. Koga N (2015) Kinetic characterization of the inorganic solid-state reactions using thermal analysis. Netsu Sokutei 42(1):2–9
24. Koga N, Šesták J, Simon P (2013) Some fundamental and historical aspects of phenomenological kinetics in the solid state studied by thermal analysis. In: Šesták J, Simon P (eds) Thermal analysis of micro, nano- and non-crystalline materials. Springer, Berlin, pp 1–28
25. Koga N (2013) Ozawa's kinetic method for analyzing thermoanalytical curves. J Therm Anal Calorim 113(3):1527–1541
26. Koga N, Tanaka H (2002) A physico-geometric approach to the kinetics of solid-state reactions as exemplified by the thermal dehydration and decomposition of inorganic solids. Thermochim Acta 388(1–2):41–61
27. Khawam A, Flanagan DR (2006) Basics and applications of solid-state kinetics: a pharmaceutical perspective. J Pharm Sci 95(3):472–498

28. Vyazovkin S, Burnham AK, Criado JM, Pérez-Maqueda LA, Popescu C, Sbirrazzuoli N (2011) ICTAC Kinetics Committee recommendations for performing kinetic computations on thermal analysis data. Thermochim Acta 520(1–2):1–19
29. Vyazovkin S, Chrissafis K, Di Lorenzo ML, Koga N, Pijolat M, Roduit B, Sbirrazzuoli N, Suñol JJ (2014) ICTAC kinetics committee recommendations for collecting experimental thermal analysis data for kinetic computations. Thermochim Acta 590:1–23
30. Koga N, Maruta S, Kimura T, Yamada S (2011) Phenomenological kinetics of the thermal decomposition of sodium hydrogencarbonate. J Phys Chem A 115(50):14417–14429
31. Reading M (1992) Controlled rate thermal analysis and beyond. In: Charsley EL, Warrington SB (eds) Thermal analysis-techniques and applications. Royal Society of Chemistry, Cambridge, pp 126–155
32. Reading M (1998) Controlled rate thermal analysis and related techniques. In: Brown ME (ed) Handbook of thermal analysis and calorimetry, vol 1. Elsevier, Amsterdam, pp 423–443
33. Ozawa T (1986) Applicability of Friedman plot. J Therm Anal 31:547–551
34. Koga N (1995) Kinetic analysis of thermoanalytical data by extrapolating to infinite temperature. Thermochim Acta 258:145–159
35. Koga N, Kimizu T (2008) Thermal decomposition of indium(III) hydroxide prepared by the microwave-assisted hydrothermal method. J Am Ceram Soc 91(12):4052–4058
36. Wada T, Koga N (2013) Kinetics and mechanism of the thermal decomposition of sodium percarbonate: role of the surface product layer. J Phys Chem A 117(9):1880–1889
37. Friedman HL (1964) Kinetics of thermal degradation of cha-forming plastics from thermogravimetry. Application to a phenolic plastic. J Polym Sci C 6:183–195
38. Garner WE (1955) Chemistry of the solid state. Butterworths, London
39. Criado JM, Rouquerol F, Rouquerol J (1980) Thermal decomposition reactions in solids—comparison of the constant decomposition rate thermal analysis with the conventional TG method. Thermochim Acta 38(1):109–115
40. Criado JM (1980) Study of the thermal decomposition of double strontium and barium carbonates using a new technique: constant rate thermal analysis (CRTA). Mater Sci Monogr 6:1096–2001
41. Criado JM (1982) Determination of the mechanism of thermal decomposition of $MnCO_3$, $CdCO_3$, and $PbCO_3$ by using the TG and the cyclic and constant decomposition rate of thermal analysis. In: Miller B (ed) Thermal analysis, The 7th international conference on thermal analysis, 1982. Wiley, pp 99–105
42. Reading M, Dollimore D, Rouquerol J, Rouquerol F (1984) The measurement of meaningful activation energies. J Therm Anal 29(4):775–785
43. Criado JM, Ortega A, Rouquerol J, Rouquerol F (1987) A new method of thermal analysis: thermal analysis under controlled rate. II Kinetic analysis. Bol Soc Esp Cerám 25:3–11
44. Ortega A, Akhouayri S, Rouquerol F, Rouquerol J (1990) On the suitability of controlled transformation rate thermal analysis (CRTA) for kinetic studies. Thermochim Acta 163:25–32
45. Criado JM, Dianez MJ, Macias M, Paradas MC (1990) Crystalline structure and thermal stability of double strontium and barium carbonates. Thermochim Acta 171:229–238
46. Reading M, Dollimore D, Whitehead R (1991) The measurement of meaningful kinetic parameters for solid state decomposition reactions. J Therm Anal 37(9):2165–2188
47. Criado JM, Ortega A (1991) Kinetic study of thermal decomposition of dolomite by controlled transformation rate thermal analysis (CRTA) and TG. J Therm Anal 37(10):2369–2375
48. Málek J, Šesták J, Rouquerol F, Rouquerol J, Criado JM, Ortega A (1992) Possibilities of two non-isothermal procedures (temperature- or rate-controlled) for kinetical studies. J Therm Anal 38(1–2):71–87
49. Ortega A, Akhouayri S, Rouquerol F, Rouquerol J (1994) On the suitability of controlled transformation rate thermal analysis (CRTA) for kinetic studies. Part 3. Discrimination of the reaction mechanism of dolomite thermolysis. Thermochim Acta 247(2):321–327

50. Laureiro Y, Jerez A, Rouquérol F, Rouquérol J (1996) Dehydration kinetics of Wyoming montmorillonite studied by controlled transformation rate thermal analysis. Thermochim Acta 278:165–173
51. Koga N, Criado JM (1998) The influence of mass transfer phenomena on the kinetic analysis for the thermal decomposition of calcium carbonate by constant rate thermal analysis (CRTA) under vacuum. Int J Chem Kinet 30(10):737–744
52. Hatakeyama T, Zhenhai L (1998) Handbook of thermal analysis. Wiley, Chichester
53. Finaru A, Salageanu I, Segal E (2000) Non-isothermal kinetic study of the heterogeneous thermal decomposition of a Mannich compound. J Therm Anal Calorim 61(1):239–242
54. Koga N, Criado JM, Tanaka H (2000) Kinetic analysis of inorganic solid-state reactions by controlled rate thermal analysis. Netsu Sokutei 27(3):128–140
55. Criado JM, Ortega A, Rouquerol J, Rouquerol F (1994) Influence of pressure on the shape of TG and controlled transformation rate thermal analysis (CRTA) traces. Thermochim Acta 240:247–256
56. Criado J, González M, Málek J, Ortega A (1995) The effect of the CO_2 pressure on the thermal decomposition kinetics of calcium carbonate. Thermochim Acta 254:121–127
57. Rouquerol F, Laureiro Y, Rouquerol J (1993) Influence of water vapour pressure on the thermal dehydration of lithium sulphate monohydrate. Solid State Ionics 63–65:363–366
58. Bordère S, Rouquérol F, Llewellyn PL, Rouquérol J (1996) Unexpected effect of pressure on the dehydration kinetics of uranyl nitrate trihydrate: an example of a Smith-Topley effect. Thermochim Acta 282–283:1–11
59. Pérez-Maqueda LA, Criado JM, Gotor FJ (2002) Controlled rate thermal analysis commanded by mass spectrometry for studying the kinetics of thermal decomposition of very stable solids. Int J Chem Kinet 34(3):184–192
60. Koga N, Criado JM, Tanaka H (1999) Apparent kinetic behavior of the thermal decomposition of synthetic malachite. Thermochim Acta 340–341:387–394
61. Yamada S, Koga N (2005) Kinetics of the thermal decomposition of sodium hydrogen carbonate evaluated by controlled rate evolved gas analysis coupled with thermogravimetry. Thermochim Acta 431(1–2):38–43
62. Koga N, Criado JM, Tanaka H (2000) Kinetic analysis of the thermal decomposition of synthetic malachite by CRTA. J Therm Anal Calorim 60(3):943–954
63. Yamada S, Tsukumo E, Koga N (2009) Influences of evolved gases on the thermal decomposition of zinc carbonate hydroxide evaluated by controlled rate evolved gas analysis coupled with TG. J Therm Anal Calorim 95(2):489–493
64. Paulik F (1995) Special trends in thermal analysis. Wiley, Chichester
65. Rouquerol J (1985) Recent developments in the calorimetric and thermoanalytical approaches to problems related to fossil-fuels (genesis, extraction and use). Pure Appl Chem 57(1):69–77
66. Rouquerol F, Rouquerol J (1971) Activation energy of a thermolysis: conditions for significant measurements under very low pressure. In: Wiedemann HG (ed) Thermal analysis, Proceedings of the 3rd international conference on thermal analysis, Davos, 1971. Birkhauser Verlag, pp 373–377
67. Rouquerol F, Regnier S, Rouquerol J (1975) Activation energy of the dehydration of a silica gel between 200 and 1000 °C. In: Buzas I (ed) Thermal analysis, Proceedings of the 4th international conference on thermal analysis, Budapest, 1975, vol 1. Akademiai Kiadó and Heyden & Sons, pp 313–318
68. Reading M (1988) The kinetics of heterogeneous solid state decomposition reactions. Thermochim Acta 135:37–57
69. Sørensen OT, Rouquerol J (2003) Sample controlled thermal analysis: origin, goals, multiple forms, applications and future. Kluwer, Dordrecht
70. Koga N (1994) A review of the mutual dependence of Arrhenius parameters evaluated by the thermoanalytical study of solid-state reactions: the kinetic compensation effect. Thermochim Acta 244(1):1–20

71. Criado JM, Ortega A, Gotor FJ (1990) Correlation between the shape of controlled-rate thermal analysis curves and the kinetics of solid-state reactions. Thermochim Acta 157:171–179
72. Criado JM, Pérez-Maqueda LA (2003) SCTA and kinetics. In: Sørensen OT, Rouquerol J (eds) Sample controlled thermal analysis: origin, goals, multiple forms, applications and future. Kluwer, Dordrecht, pp 62–101
73. Criado JM, Gonzalez M (1981) The method of calculation of kinetic parameters as a possible cause of apparent compensation effects. Thermochim Acta 46(2):201–207
74. Tanaka H, Koga N (1988) Kinetic compensation effect between the isothermal and non-isothermal decomposition of solids. J Therm Anal 34(3):685–691
75. Koga N, Tanaka H (1991) A kinetic compensation effect established for the thermal-decomposition of a solid. J Therm Anal 37(2):347–363
76. Koga N, Šesták J (1991) Kinetic compensation effect as a mathematical consequence of the exponential rate-constant. Thermochim Acta 182(2):201–208
77. Koga N, Šesták J (1991) Further aspects of the kinetic compensation effect. J Therm Anal 37 (5):1103–1108
78. Koga N, Šesták J, Málek J (1991) Distortion of the Arrhenius parameters by the inappropriate kinetic-model function. Thermochim Acta 188(2):333–336
79. Málek J, Criado JM (1992) Empirical kinetic models in thermal analysis. Thermochim Acta 203:25–30
80. Málek J (1992) The kinetic analysis of non-isothermal data. Thermochim Acta 200:257–269
81. Gotor FJ, Criado JM, Málek J, Koga N (2000) Kinetic analysis of solid-state reactions: the universality of master plots for analyzing isothermal and nonisothermal experiments. J Phys Chem A 104(46):10777–10782
82. Criado JM, Pérez-Maqueda LA, Gotor FJ, Malek J, Koga N (2003) A unified theory for the kinetic analysis of solid state reactions under any thermal pathway. J Therm Anal Calorim 72 (3):901–906
83. Pérez-Maqueda LA, Criado JM, Sánchez-Jiménez PE (2006) Combined kinetic analysis of solid-state reactions: a powerful tool for the simultaneous determination of kinetic parameters and the kinetic model without previous assumptions on the reaction mechanism. J Phys Chem A 110(45):12456–12462
84. Pérez-Maqueda LA, Criado JM, Sánchez-Jiménez PE, Diánez MJ (2015) Applications of sample-controlled thermal analysis (SCTA) to kinetic analysis and synthesis of materials. J Therm Anal Calorim 120(1):45–51
85. Criado JM (1979) On the kinetic analysis of thermoanalytical diagrams obtained with the "quasi-isothermal" heating technique. Thermochim Acta 28(2):307–312
86. Criado JM, Morales J (1976) Defects of thermogravimetric analysis for discerning between first order reactions and those taking place through the Avrami-Erofeev's mechanism. Thermochim Acta 16:382–387
87. Criado JM, Morales J (1980) On the evaluation of kinetic parameters from thermogravimetric curves. Thermochim Acta 41(1):125–127
88. Criado JM, Dollimore D, Heal GR (1982) A critical study of the suitability of the Freeman and Carroll method for the kinetic analysis of reactions of thermal decomposition of solids. Thermochim Acta 54(1–2):159–165
89. Flynn JH (1988) Thermal analysis kinetics—problems, pitfalls and how to deal with them. J Therm Anal 34(1):367–381
90. Agrawal RK (1988) Analysis of irreversible complex chemical reactions and some observations on their overall activation energy. Thermochim Acta 128:185–208
91. Vyazovkin S, Wight CA (1998) Isothermal and non-isothermal kinetics of thermally stimulated reactions of solids. Int Rev Phys Chem 17(3):407–433
92. Vyazovkin SV, Lesnikovich AI (1989) On the methods of solving the inverse problem of solid-phase reaction kinetics. J Therm Anal 35(7):2169–2188
93. Brown ME, Maciejewski M, Vyazovkin S, Nomen R, Sempere J, Burnham A, Opfermann J, Strey R, Anderson HL, Kemmler A, Keuleers R, Janssens J, Desseyn HO, Li C-R, Tang TB,

Roduit B, Malek J, Mitsuhashi T (2000) Computational aspects of kinetic analysis. Thermochim Acta 355(1–2):125–143
94. Pérez-Maqueda LA, Ortega A, Criado JM (1996) The use of master plots for discriminating the kinetic model of solid state reactions from a single constant-rate thermal analysis (CRTA) experiment. Thermochim Acta 277:165–173
95. Koga N, Criado JM (1997) Influence of the particle size distribution on the CRTA curves for the solid-state reactions of interface shrinkage. J Therm Anal 49(3):1477–1484
96. Koga N, Criado JM (1998) Kinetic analyses of solid-state reactions with a particle-size distribution. J Am Ceram Soc 81(11):2901–2909
97. Criado JM (1981) On the determination of the activation energy of solid-state reactions from the maximum reaction rate of isothermal runs. J Therm Anal 21(1):155–157
98. Tiernan MJ, Barnes PA, Parkes GMB (2001) Reduction of iron oxide catalysts: the investigation of kinetic parameters using rate perturbation and linear heating thermoanalytical techniques. J Phys Chem B 105(1):220–228
99. Mampel KL (1940) Time conversion formulas for heterogeneous reactions at the phase boundaries of solid bodies I: the development of the mathematical method and the derivation of area conversion formulas. Z Phys Chem A 187:43–57
100. Prout EG, Tompkins FC (1944) The thermal decomposition of potassium permanganate. Trans Faraday Soc 40:488–497
101. Prout EG, Tompkins FC (1946) The thermal decomposition of silver permanganate. Trans Faraday Soc 42(6–7):468–472
102. Simha R, Wall LA (1952) Kinetics of chain depolymerization. J Phys Chem 56(6):707–715
103. Sánchez-Jiménez PE, Pérez-Maqueda LA, Perejón A, Criado JM (2010) A new model for the kinetic analysis of thermal degradation of polymers driven by random scission. Polym Degrad Stab 95(5):733–739
104. Criado JM, Ortega A, Real C (1987) Mecahnism of the thermal decomposition of anhydrous nickel nitrate. React Solids 4:93–103
105. Paulik J, Paulik F (1981) Simultaneous thermoanalytical examinations by means of derivatograph. Wilson-Wilson's Comprehensive Analytical Chemistry, vol XII. Elsevier, Amsterdam
106. Barnes PA, Parkes GMB, Brown DR, Charsley EL (1995) Applications of new high resolution evolved-gas analysis systems for the characterisation of catalysts using rate-controlled thermal analysis. Thermochim Acta 269–270:665–676
107. Gomez F, Vast P, Llewellyn P, Rouquerol F (1997) Dehydroxylation mechanisms of polyphosphate glasses in relation to temperature and pressure. J Non-Cryst Solids 222:415–421
108. Gomez F, Vast P, Llewellyn P, Rouquerol F (1997) Characterization of polyphosphate glasses preparation using CRTA. J Therm Anal 49(3):1171–1178
109. Badens E, Llewellyn P, Fulconis JM, Jourdan C, Veesler S, Boistelle R, Rouquerol F (1998) Study of gypsum dehydration by controlled transformation rate thermal analysis (CRTA). J Solid State Chem 139(1):37–44
110. Gomez F, Vast P, Baebieux F, Llewellyn P, Rouquerol F (1998) Controlled transformation rate thermal analysis: an inverse method allowing the characterisation of the thermal behaviour of polyphosphate glasses. High Temp.-High Pressures 30(5):575–580
111. Fulconis JM, Morato F, Rouquerol F, Fourcade R, Feugier A, Rouquerol J (1999) CRTA study of the reduction of UO_2F_2 into UO_2 by dry H_2. J Therm Anal Calorim 56(3):1443–1446
112. Ichihara S, Endo A, Arii T (2000) Analysis of thermal decomposition behaviors with consecutive reactions by TG. Thermochim Acta 360(2):179–188
113. Fesenko EA, Barnes PA, Parkes GMB, Dawson EA, Tiernan MJ (2002) Catalyst characterisation and preparation using sample controlled thermal techniques—high resolution studies and the determination of the energetics of surface and bulk processes. Top Catal 19(3/4):283–301

114. Fesenko EA, Barnes PA, Parkes GMB (2003) SCTA and catalysis. In: Sørensen OT, Rouquerol J (eds) Sample controlled thermal analysis: origin, goals, multiple forms, applications and future. Kluwer, Dordrecht, pp 174–225
115. Tiernan MJ, Barnes PA, Parkes GMB (1999) New approach to the investigation of mechanisms and apparent activation energies for the reduction of metal oxides using constant reaction rate temperature-programmed reduction. J Phys Chem B 103(2):338–345
116. Ogasawara H, Koga N (2014) Kinetic modeling for thermal dehydration of ferrous oxalate dihydrate polymorphs: a combined model for induction period-surface reaction-phase boundary reaction. J Phys Chem A 118(13):2401–2412
117. Galwey AK, Hood WJ (1979) Thermal decomposition of sodium carbonate perhydrate in the solid state. J Phys Chem 83(14):1810–1815
118. Koga N, Criado JM, Tanaka H (2002) A kinetic aspect of the thermal dehydration of dilithium tetraborate trihydrate. J Therm Anal Calorim 67(1):153–161
119. Criado JM (1980) Determination of the mechanism of thermal decomposition reactions of solids by using the cyclic and constant decomposition rate thermal analysis method. In: Wiedemann HG (ed) Thermal analysis, Proceedings of the 6th international conference on thermal analysis, Bayruth, 1980. Brikhauser Verlag, Basel, pp 145–148
120. Dion P, Alcover JF, Bergaya F, Ortega A, Llewellyn PL, Rouquerol F (1998) Kinetic study by controlled-transformation rate thermal analysis of the dehydroxylation of kaolinite. Clay Miner 33(2):269–276
121. Tiernan MJ, Barnes PA, Parkes GMB (1999) Use of solid insertion probe mass spectrometry and constant rate thermal analysis in the study of materials: determination of apparent activation energies and mechanisms of solid-state decomposition reactions. J Phys Chem B 103(33):6944–6949
122. Parkes GM, Barnes PA, Charsley EL (1999) New concepts in sample controlled thermal analysis: resolution in the time and temperature domains. Anal Chem 71(13):2482–2487
123. Barnes PA, Tiernan MJ, Parkes GMB (1999) Sample controlled thermal analysis: temperature programmed reduction of bulk and supported copper oxide. J Therm Anal Calorim 56(2):733–737
124. Fesenko EA, Barnes PA, Parkes GMB, Brown DR, Naderi M (2001) A new approach to the study of the reactivity of solid-acid catalysts: the application of constant rate thermal analysis to the desorption and surface reaction of isopropylamine from NaY and HY Zeolites. J Phys Chem B 105(26):6178–6185
125. Tiernan MJ, Fesenko EA, Barnes PA, Parkes GMB, Ronane M (2001) The application of CRTA and linear heating thermoanalytical techniques to the study of supported cobalt oxide methane combustion catalysts. Thermochim Acta 379(1–2):163–175
126. Arii T, Fujii N (1997) Controlled-rate thermal analysis kinetic study in thermal dehydration of calcium sulfate dihydrate. J Anal Appl Pyrol 39(2):129–143
127. Cai XE, Shen H, Zhang CH, Wang YX, Kong Z (2000) Application of constant reaction rate TG to the determination of kinetic parameters by Hi-Res TG. J Therm Anal Calorim 60 (2):623–628
128. Ortega A (1997) CRTA or TG? Thermochim Acta 298(1–2):205–214
129. Rouquerol J (1989) Controlled transformation rate thermal analysis: the hidden face of thermal analysis. Thermochim Acta 144(2):209–224
130. Ortega A, Akhouayri S, Rouquerol F, Rouquerol J (1994) On the suitability of controlled transformation rate thermal analysis (CRTA) for kinetic studies. Part 2. Comparison with conventional TG for the thermolysis of dolomite with different particle sizes. Thermochim Acta 235(2):197–204
131. Reading M, Dollimore D (1994) The application of constant rate thermal analysis to the study of the thermal decomposition of copper hydroxy carbonate. Thermochim Acta 240:117–127
132. Criado JM, Pérez-Maqueda LA (2005) Sample controlled thermal analysis and kinetics. J Therm Anal Calorim 80(1):27–33

133. Nahdi K, Rouquerol F, Trabelsi Ayadi M (2009) $Mg(OH)_2$ dehydroxylation: a kinetic study by controlled rate thermal analysis (CRTA). Solid State Sci 11(5):1028–1034
134. Gotor FJ, Macias M, Ortega A, Criado JM (2000) Comparative study of the kinetics of the thermal decomposition of synthetic and natural siderite samples. Phys Chem Miner 27 (7):495–503
135. Sánchez-Jiménez PE, Criado JM, Pérez-Maqueda LA (2008) Kissinger kinetic analysis of data obtained under different heating schedules. J Therm Anal Calorim 94(2):427–432
136. Valverde JM, Sánchez-Jiménez PE, Perejon A, Pérez-Maqueda LA (2013) Constant rate thermal analysis for enhancing the long-term CO_2 capture of CaO at Ca-looping conditions. Appl Energy 108:108–120
137. Valverde JM, Sánchez-Jiménez PE, Perejon A, Pérez-Maqueda LA (2013) Role of looping-calcination conditions on self-reactivation of thermally pretreated CO_2 sorbents based on CaO. Energy Fuels 27(6):3373–3384
138. Koga N (2005) A comparative study of the effects of decomposition rate control and mechanical grinding on the thermal decomposition of aluminum hydroxide. J Therm Anal Calorim 81(3):595–601
139. Kimura T, Koga N (2011) Thermal dehydration of monohydrocalcite: overall kinetics and physico-geometrical mechanisms. J Phys Chem A 115(38):10491–10501
140. Koga N, Suzuki Y, Tatsuoka T (2012) Thermal dehydration of magnesium acetate tetrahydrate: formation and in situ crystallization of anhydrous glass. J Phys Chem B 116 (49):14477–14486
141. Koga N, Yamada S, Kimura T (2013) Thermal decomposition of silver carbonate: phenomenology and physicogeometrical kinetics. J Phys Chem C 117(1):326–336
142. Kitabayashi S, Koga N (2014) Physico-geometrical mechanism and overall kinetics of thermally induced oxidative decomposition of Tin(II) oxalate in air: formation process of microstructural Tin(IV) Oxide. J Phys Chem C 118(31):17847–17861
143. Wada T, Nakano M, Koga N (2015) Multistep kinetic behavior of the thermal decomposition of granular sodium percarbonate: hindrance effect of the outer surface layer. J Phys Chem A 119(38):9749–9760
144. Stacey MH, Shanon MD (1985) The decomposition of Cu-Zn hydroxi-carbonate solid solutions. Mater Sci Monogr 28:713–718
145. Sánchez-Jiménez PE, Pérez-Maqueda LA, Perejón A, Pascual-Cosp J, Benítez-Guerrero M, Criado JM (2011) An improved model for the kinetic description of the thermal degradation of cellulose. Cellulose 18(6):1487–1498
146. Sánchez-Jiménez PE, Pérez-Maqueda LA, Perejón A, Criado JM (2009) Combined kinetic analysis of thermal degradation of polymeric materials under any thermal pathway. Polym Degrad Stab 94(11):2079–2085
147. Sánchez-Jiménez PE, Pérez-Maqueda LA, Perejón A, Criado JM (2011) Constant rate thermal analysis for thermal stability studies of polymers. Polym Degrad Stab 96(5):974–981
148. Sánchez-Jiménez PE, Perejón A, Criado JM, Diánez MJ, Pérez-Maqueda LA (2010) Kinetic model for thermal dehydrochlorination of poly(vinyl chloride). Polymer 51(17):3998–4007
149. Sánchez-Jiménez PE, Pérez-Maqueda LA, Perejón A, Criado JM (2010) Generalized kinetic master plots for the thermal degradation of polymers following a random scission mechanism. J Phys Chem A 114(30):7868–7876
150. Arii T, Ichihara S, Nakagawa H, Fujii N (1998) A kinetic study of the thermal decomposition of polyesters by controlled-rate thermogravimetry. Thermochim Acta 319 (1–2):139–149
151. Sánchez-Jiménez PE, Pérez-Maqueda LA, Perejón A, Criado JM (2013) Generalized master plots as a straightforward approach for determining the kinetic model: the case of cellulose pyrolysis. Thermochim Acta 552:54–59
152. Sánchez-Jiménez PE, Pérez-Maqueda LA, Perejón A, Criado JM (2012) Nanoclay nucleation effect in the thermal stabilization of a polymer nanocomposite: a kinetic mechanism change. J Phys Chem C 116(21):11797–11807

153. Perejón A, Sánchez-Jiménez PE, Gil-González E, Pérez-Maqueda LA, Criado JM (2013) Pyrolysis kinetics of ethylene–propylene (EPM) and ethylene–propylene–diene (EPDM). Polym Degrad Stab 98(9):1571–1577
154. Sánchez-Jiménez PE, Pérez-Maqueda LA, Perejón A, Criado JM (2013) Limitations of model-fitting methods for kinetic analysis: Polystyrene thermal degradation. Resour Conserv Recycl 74:75–81
155. Miranda R, Yang J, Roy C, Vasile C (1999) Vacuum pyrolysis of PVC I. Kinetic study. Polym Degrad Stab 64(1):127–144
156. Miranda R, Yang J, Roy C, Vasile C (2001) Vacuum pyrolysis of commingled plastics containing PVC I. Kinetic study. Polym Degrad Stab 72(3):469–491
157. Kim S (2001) Pyrolysis kinetics of waste PVC pipe. Waste Manag 21(7):609–616
158. Jiménez A, Berenguer V, López J, Sánchez A (1993) Thermal degradation study of poly (vinyl chloride): kinetic analysis of thermogravimetric data. J Appl Polym Sci 50(9):1565–1573
159. Wu C-H, Chang C-Y, Hor J-L, Shih S-M, Chen L-W, Chang F-W (1994) Two-stage pyrolysis model of PVC. Can J Chem Eng 72(4):644–650
160. Slapak MJP, van Kasteren JMN, Drinkenburg AAH (2000) Determination of the pyrolytic degradation kinetics of virgin-PVC and PVC-waste by analytical and computational methods. Comput Theor Polym Sci 10(6):481–489
161. Rouquerol J (1973) Critical examination of several problems typically found in the kinetic study of thermal decomposition under vacuum. J Therm Anal 5(2–3):203–216
162. Rouquerol J, Ganteaume M (1977) Thermolysis under vacuum: essential influence of the residual pressure on thermoanalytical curves and the reaction products. J Therm Anal 11 (2):201–210
163. Rouquerol J, Rouquerol F, Ganteaume M (1975) Thermal decomposition of gibbsite under low pressures I. Formation of the boehmitic phase. J Catal 36(1):99–110
164. Stacey MH (1985) Applications of thermal methods in catalysis. Anal Proc 22(8):242–243
165. Stacey MH (1987) Kinetics of decomposition of gibbsite and boehmite and the characterization of the porous products. Langmuir 3(5):681–686
166. Barnes PA, Parkes GMB (1995) A new approach to catalyst preparation using rate controlled temperature programme techniques. Stud Surf Sci Catal 91:859–868
167. Koga N, Yamada S (2004) Controlled rate thermal decomposition of synthetic bayerite under vacuum. Solid State Ionics 172(1–4):253–256
168. Pérez-Maqueda LA, Criado JM, Real C, Subrt J, Bohacek J (1999) The use of constant rate thermal analysis (CRTA) for controlling the texture of hematite obtained from the thermal decomposition of goethite. J Mater Chem 9(8):1839–1845
169. Pérez-Maqueda LA, Criado JM, Subrt J, Real C (1999) Synthesis of acicular hematite catalysts with tailored porosity. Catal Lett 60(3):151–156
170. Chopra GS, Real C, Alcalá MD, Pérez-Maqueda LA, Subrt J, Criado JM (1999) Factors influencing the texture and stability of maghemite obtained from the thermal decomposition of lepidocrocite. Chem Mater 11(4):1128–1137
171. Salles F, Douillard JM, Denoyel R, Bildstein O, Jullien M, Beurroies I, Van Damme H (2009) Hydration sequence of swelling clays: evolutions of specific surface area and hydration energy. J Colloid Interface Sci 333(2):510–522
172. Belgacem K, Llewellyn P, Nahdi K, Trabelsi-Ayadi M (2008) Thermal behaviour study of the talc. Optoelectron Adv Mat 2(6):332–336
173. Rockmann R, Kalies G (2007) Characterization and adsorptive application of ordered mesoporous silicas. Appl Surf Sci 253(13):5666–5670
174. Llewellyn P, Rouquerol J (2003) SCTA and adsorbents. J Therm Anal Calorim 72(3):1099–1101
175. Sicard L, Llewellyn PL, Patarin J, Kolenda F (2001) Investigation of the mechanism of the surfactant removal from a mesoporous alumina prepared in the presence of sodium dodecylsulfate. Microporous Mesoporous Mater 44–45:195–201

176. Dufau N, Luciani L, Rouquerol F, Llewellyn P (2001) Use of sample controlled thermal analysis to liberate the micropores of aluminophosphate $AlPO_4$ II: evidence of template evaporation. J Mater Chem 11(4):1300–1304
177. Chevrot V, Llewellyn PL, Rouquerol F, Godlewski J, Rouquerol J (2000) Low temperature constant rate thermodesorption as a tool to characterise porous solids. Thermochim Acta 360 (1):77–83
178. Llewellyn P, Rouquerol F, Rouquerol J (2003) SCTA and Adsorbents. In: Sørensen OT, Rouquerol J (eds) Sample controlled thermal analysis: origin, goals, multiple forms, applications and future. Kluwer, Dordrecht, pp 135–173
179. Pérez-Maqueda LA, Sánchez-Jiménez PE, Criado JM (2007) Sample controlled temperature (SCT): a new method for the synthesis and characterization of catalysts. Curr Top Catal 6:1–17
180. Criado JM, Gotor FJ, Real C, Jimenez F, Ramos S, Delcerro J (1991) Application of the constant rate thermal-analysis technique to the microstructure control of $BaTiO_3$ yielded from coprecipitated oxalate. Ferroelectrics 115(1–3):43–48
181. Criado JM, Dianez MJ, Gotor F, Real C, Mundi M, Ramos S, Delcerro J (1992) Correlation between synthesis conditions, coherently diffracting domain size and cubic phase stabilization in barium-titanate. Ferroelectrics Lett 14(3–4):79–84
182. Gotor FJ, Real C, Dianez MJ, Criado JM (1996) Relationships between the texture and structure of $BaTiO_3$ and its tetragonal → cubic transition enthalpy. J Solid State Chem 123 (2):301–305
183. Gotor FJ, Pérez-Maqueda LA, Criado JM (2003) Synthesis of $BaTiO_3$ by applying the sample controlled reaction temperature (SCRT) method to the thermal decomposition of barium titanyl oxalate. J Eur Ceram Soc 23(3):505–513
184. Pérez-Maqueda LA, Diánez MJ, Gotor FJ, Sayagués MJ, Real C, Criado JM (2003) Synthesis of needle-like $BaTiO_3$ particles from the thermal decomposition of a citrate precursor under sample controlled reaction temperature conditions. J Mater Chem 13 (9):2234–2241
185. Alcalá MD, Real C, Criado JM (1992) Application of constant rate thermal analysis (CRTA) to the synthesis of silicon nitride by carbothermal reduction of silica. J Therm Anal 38 (3):313–319
186. Alcalá MD, Criado JM, Real C (2002) Preparation of Si_3N_4 from carbothermal reduction of SiO employing the CRTA method. Mater Sci Forum 383:25–30
187. Alcalá MD, Criado JM, Real C (2002) Sample controlled reaction temperature (SCRT): controlling the phase composition of silicon nitride obtained by carbothermal reduction. Adv Eng Mater 4(7):478–482
188. Real C, Alcalá MD, Criado JM (1997) Synthesis of silicon carbide whiskers from carbothermal reduction of silica gel by means of the constant rate thermal analysis (CRTA) method. Solid State Ionics 95(1–2):29–32
189. Ortega A, Roldan MA, Real C (2006) Carbothermal synthesis of vanadium nitride: kinetics and mechanism. Int J Chem Kinet 38(6):369–375
190. Ortega A, Roldan MA, Real C (2005) Carbothermal synthesis of titanium nitride (TiN): kinetics and mechanism. Int J Chem Kinet 37(9):566–571
191. Real C, Alcalá MD, Criado JM (2004) Synthesis of silicon nitride from carbothermal reduction of rice husks by the constant rate thermal analysis (CRTA) method. J Am Ceram Soc 87(1):75–78
192. Alcalá MD, Criado JM, Real C (2001) Influence of the experimental conditions and the grinding of the starting materials on the structure of silicon nitride synthesised by carbothermal reduction. Solid State Ionics 141–142:657–661
193. Schaf O, Weibel A, Llewellyn PL, Knauth P, Kaabbuathong N, Vona MLD, Licoccia S, Traversa E (2004) Preparation and electrical properties of dense ceramics with NASICON composition sintered at reduced temperatures. J Electroceram 13(1–3):817–823
194. Dwivedi A, Speyer RF (1994) Rate-controlled organic burnout of multilayer green ceramics. Thermochim Acta 247(2):431–438

195. Nishimoto MY, Speyer RF, Hackenberger WS (2001) Thermal processing of multilayer PLZT actuators. J Mater Sci 36(9):2271–2276
196. Feylessoufi A, Crespin M, Dion P, Bergaya F, Van Damme H, Richard P (1997) Controlled rate thermal treatment of reactive powder concretes. Adv Cem Based Mater 6(1):21–27
197. Grillet Y, Cases JM, Francois M, Rouquerol J, Poirier JE (1988) Modification of the porous structure and surface area of sepiolite under vacuum thermal treatment. Clays Clay Miner 36 (3):233–242
198. Bordère S, Floreancing A, Rouquerol F, Rouquerol J (1993) Obtaining a divided uranium oxide from the thermolysis of $UO_2(NO_3)_2{\cdot}6H_2O$: outstanding role of the residual pressure. Solid State Ionics 63–65:229–235
199. Llewellyn PL, Chevrot V, Ragai J, Cerclier O, Estienne J, Rouquerol F (1997) Preparation of reactive nickel oxide by the controlled thermolysis of hexahydrated nickel nitrate. Solid State Ionics 101:1293–1298
200. Arii T, Taguchi T, Kishi A, Ogawa M, Sawada Y (2002) Thermal decomposition of cerium (III) acetate studied with sample-controlled thermogravimetric–mass spectrometry (SCTG—MS). J Eur Ceram Soc 22(13):2283–2289
201. Nahdi K, Férid M, Ayadi MT (2009) Thermal dehydration of $CeP_3O_9{\cdot}3H_2O$ by controlled rate thermal analysis. J Therm Anal Calorim 96(2):455–461
202. Chehimi-Moumen F, Llewellyn P, Rouquerol F, Vacquier G, Hassen-Chehimi DB, Ferid M, Trabelsi-Ayadi M (2005) Constant transformation rate thermal analysis of $HGdP_2O_7{\cdot}3H_2O$. J Therm Anal Calorim 82(3):783–789

Chapter 3
What Is the Physical and Operational Meaning of Temperature and Its Self-Measurability During Unsteady Thermal Processes Within Thermodynamic Concepts?

Miroslav Holeček, Jiří J. Mareš, Jaroslav Šesták and Pavel Hubík

Abstract Historical maturity of terms temperatura and thermoscope is sketched. Problem of temperature definition and observation (measurement) is studied in detail. Temperature is a typical averaged quantity clear-cut under equilibrium only. A self-measurability condition is implied, and some consequences are outlined. Physical and operational meaning of temperature and its self-measurability during unsteady thermal processes is analysed. Particular case of thermal analysis often idealized under constant temperature changes is thermodynamically examined. For extreme temperature changes as that during quenching, a novel term "tempericity" is proposed. Branched view to the spheres of alternative thermodynamics is shown locating thermal analysis as thermotics and quenching as thermokinetics. Non-equilibrium thermodynamics under a non-constant rate of temperature changes is analysed. Practical aspects of non-equilibrium temperatures due to heat inertia and thermal gradients are specified including cases of modulated experiments. Textbook thermodynamic description under the perceptible impact of second temperature derivatives becomes ambiguous and associated tabular values are unclear. Thermotics, thermokinetics, and the validity of the first and second thermodynamic laws are discussed bringing another dimension of the thermodynamic legacy. The concept of equivalence of work and heat is questioned. The chapter contains 126 references.

M. Holeček · J. Šesták (✉)
New Technologies Research Centre (NTC-ZČU), University of West Bohemia, Universitní 8, 30114 Pilsen, Czech Republic
e-mail: sestak@fzu.cz

M. Holeček
e-mail: holecek@ntc.zcu.cz

J.J. Mareš · P. Hubík
Division of Solid-State Physics, Institute of Physics, Czech Academy of Sciences, Prague, Czech Republic
e-mail: hubik@fzu.cz

J. Šesták et al. (eds.), *Thermal Physics and Thermal Analysis*,
Hot Topics in Thermal Analysis and Calorimetry 11,
DOI 10.1007/978-3-319-45899-1_3

3.1 Historical Introduction

In modern physics, temperature usually pretends to be a well-defined concept, intelligible for all and if not so, at least for experts. For instance, even such a critic and sceptic were par excellence as C. Truesdell, founder of rational thermodynamics, explains this term by writing [1] that *"The body is at each time assigned a real number called temperature. This number is a measure of how hot the body is*"—a definition which is not too far from a plain tautology. On the other hand, more sophisticated definitions of temperature, based on statistical physics [2] or an axiomatic approach to phenomenology [3], are rather difficult to understand and relevant to non-trivial experimental situations (involving, e.g., quantum interference).

Modern thermal physics [4, 5] started to develop in the seventeenth century with the invention of the thermometer enabling quantitative studies of thermal phenomena to be made. This statement should not, however, be interpreted as that there was no scientific theory dealing with heat effects before this date. Equally wrong is the widely spread opinion that after the thermometer became a popular instrument, the then scholars had a clear idea of what temperature is and, by making experiments with thermometers, were aware of what they were actually doing.

It may be quite surprising that a very essential part of ancient natural philosophy consisted just of what we now call thermal physics and that the theories and hypotheses worked out by these philosophers were more than one and a half centuries after the invention of thermometer still active. How was it possible to build up the predicative theory of thermal phenomena ignoring such a quantity as temperature? To give an answer to this question, it is worth saying a few words about these peculiar theories.

The most representative theory of this type, formulated by Aristotle in the fourth century B.C., is based on the well-known doctrine of four Elements. According to this theory, all objects in the nature are created of four Elements called Water, Earth, Fire and Air, by means of the action of four Qualities, namely Coldness, Dryness, Hotness and Humidity. Everybody thus consists of passive Matter and active Form, the Matter being a proper mixture of the Elements and the Form a mixture of the said Qualities (presently used in the derived term "*in-form-ation*"). Every Element has a tendency towards its natural place in the surrounding world and permanently possesses two Qualities, one of which is active (coldness, hotness) and the other passive (dryness, humidity) and the one of which is dominant (primary Quality) and the other submissive (secondary Quality). It was believed that formal manipulation with graphical symbols could be helpful for the solution of particular problems (touching to the modern theory of graphs). The hypothetical structure of matter, based on such a scheme, brings about an important consequence—the potential and/or intrinsic "thermal" property of all existing substances. Thus, e.g., alcohol, gunpowder and pepper are intrinsically hot substances, active with respect to other bodies, while opium and snow are examples of intrinsically cold materials. Moreover, the antagonistic nature (so-called *contraria*) of different Elements and Qualities ensures eternal

changes and movements of all things in the universe, in close analogy with well-known effects due to the combination such as love-hate in human society. These changes are, however, not completely free, but are submitted to the remarkable principle of *antiperistasis* controlling the relationship between two active Qualities (coldness and hotness). The principle can be verbalized in the following way: the properties of everything which are bound up with coldness/hotness tend to increase where the body is surrounded by a hot/cold environment. This principle is akin to the more modern Le Chatelier–Braun principle which provides, in many cases, correct qualitative predictions concerning the direction of thermal processes. A typical example consistent with the principle of *antiperistasis* originates from Oenopides of Chios (fifth century B.C.), i.e.: "Water in a deep well shows in winter the smallest degree of coldness, while in very hot days it is extraordinarily cold". Interestingly, this statement keeps actually valid and is not only a consequence of our subjective feelings, but has been confirmed by hydrological studies. There are numerous successful applications of the principle of *antiperistasis*, but there are also cases where it completely failed. For example, the dissolution of black gunpowder containing saltpetre led, contrary to expectation, not to the warming up but to cooling. Such exceptions were either neglected or used for discussion of other weak points of the doctrine. The most important problem, crucial for the theory, was the so-called problem of *primum frigidum*. While there was no doubt in which Element the hotness dwells (of course in fire), the primary seat of the coldness remained uncertain. This made the conclusions of the theory not to be very plausible. The problem of *primum frigidum* was never solved and disappeared only with the whole theory.

3.2 Temperatura and Thermoscope

In spite of the fact, as we have seen that the concept of temperature was superfluous for the general description of natural processes within the framework of Aristotle's theory, the term *temperatura* was frequently used by ancient physicians well before Avicenna (eleventh century A.D.). Such a temperatura was in a close connection with the individual temperament (later used in the concept of econophysics) and was given by a certain mixture of four Qualities which was necessary to maintain the Form of the tissues of the human body in a proper healthy state—*homeostasis*. But, in fact, these ancient physicians did not know how to determine this evidently crucial parameter. Probably, the first attempt to define the state of the human body by objective physical measurements came from a group of Italian scientists at the beginning of the seventeenth century. For example, Sanctorius (Santorio) studied experimentally the forces exerted by muscles, the content of various fluids in the body and the frequency of pulses using a *pulsologium*—an apparatus devised by Galileo. He tried, also, to measure an immediate characteristic of temperament, i.e. temperature, by means of a modified version of a very old device called a *thermoscope*, which had already been described by Philon of Byzantine (third century

B.C.) and Heron of Alexandria (first century A.D.). The thermoscope enabled Sanctorius to judge the degree of the patient's temperature and then to choose the proper medical treatment. This conversion of a curious toy into a measuring device and the intentional application of the data obtained for some purpose have all the features of an effective discovery. However, during the second half of the seventeenth century, there were in use an advanced form of thermometers for medical and meteorological purposes, namely those constructed by Guericke and by the members of *Accademia del Cimento* in Florence who also invented the closed fluid-type thermometer. Besides research reports, a box with original instruments was discovered in the last century by Antinori. The following peripatetic (i.e. Aristotelian) explanation of a thermometer function was put forward. Coldness in the external air activates the hotness inside the bulb which then escapes most likely into the solid wall of the bulb. This process changes the ratio between the Qualities of the enclosed air, in other words its Form. The depleted Form of the air has obviously a smaller volume, and the resulting empty space has to be immediately filled by water due to the *horror vacui*—nature's abhorrence of a vacuum.

There is a long story [1–18] describing the connotation development of thermoscope and thermoscopic states, adjusting fixed temperature points and bringing into play the important Mach's postulates [19] saying that fixed points can be ordered, to every fixed point can be ever found a fixed point which is lower/higher and the interlaying fixed point can be ever constructed in terms of mathematical set theory [20]. These free Mach's postulates were put into a more condensed form by Mareš [17, 18] declaring that the set of fixed points is an infinite countable ordered dense set having no first and no last point. Thus, the hotness series and empirical temperature scales were defined [17–22]; later on, Kelvin's scale was established by applying Carnot's principle and Kelvin's proposition [23, 24] or by using the ideal gas scale. The whole story was discussed in our previous papers [9–18], including a special Chap. 20 of our previous book—Volume 8 [17].

3.3 Temperature Definition

A thermodynamic temperature was probably firstly defined by Maxwell [25] in the second half of nineteen century by the words: "The temperature of a body is its thermal state considered with reference to its power of communicating heat to other bodies that body which gives out heat is said to have a higher temperature than that which receives heat from it". Further, a thermal equilibrium was defined as "If when bodies are placed in thermal communication neither of them loses heat or gains heat, two bodies are said to have equal temperatures or the same temperature. The two bodies are then said to be in thermal equilibrium". This definition became, often unwritten, part of early thermodynamics [26–30]. The geometrical flavour of which can be noticed with the formulation of the zeroth law of thermodynamics defines temperature without addressing thermal equilibrium. That is, "if bodies b_1, b_2 and b_3 are in equilibrium states it signifies that if b_1 is in thermal equilibrium with b_2, and b_2 with b_3, then b_3 is in equilibrium with b_1". This law strongly resembles the first

axiom of Euclidean geometry (≈300 B.C.) that is "things equal to the same thing are equal to one another". This historical, so-called Carathéodory's scheme [3, 31–33] of the classical thermodynamics representation for closed systems postulates the concept of an "equilibrium state" following Gibbs (legendary Gibbs spoke routinely of a "thermodynamic state") though neither explicitly using the phrase "thermodynamic equilibrium", nor explicitly postulating the existence of a "temperature" which would require a certain definition [28, 29, 34]. Therefore, if three or more systems are in thermal contact with each other and all are in a mutual equilibrium, then any two taken separately are in equilibrium with one another. Consequently, if one of the three systems could be an instrument calibrated to measure the temperature, i.e. a thermometer [22, 35, 36] which is placed in thermal contact with a measured system reaching the required thermal equilibrium, we then possess a quantitative thermometric measure of the temperature of the system in the succession of being its physical property/quantity. This clearly shows that if they are not in a static (collective) equilibrium, then the thermometer produces incorrect reading. In other words, thermometer is only measuring its own temperature-like state, being hardly of a scientific interest. This is a clear indictment of the nowadays popular temperature scanning used in rapid-quenching methods [37, 38].

The measuring of temperature is thus an operation that is very deeply related to the temperature equalling called equilibration [26–29]. When putting a thermometer into a medium, the temperature of an active part of the thermometer (e.g. a vessel with a liquid whose current volume is calibrated in the temperature degrees) usually has a different temperature than that of the surrounding medium. We must wait for a moment till the active part of the thermometer reaches the temperature of the medium. Then, the figures read at the thermometer may be identified with the temperature of the medium. This is a very familiar experience well known to everybody (remember measuring the body temperature via a classical medical thermometer).

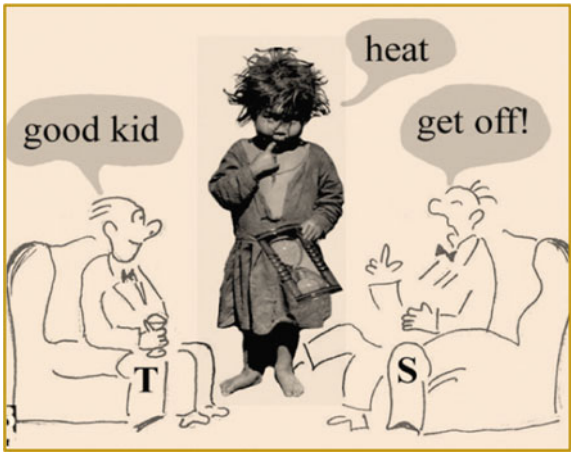

Many "definitions" of temperature are "hand-waving" but plainly hollow; examples are "temperature is well acknowledged from the basic courses of physics" [4, 19, 21, 26–29] or even "temperature is known intuitively". A shockingly frank definition says: "Temperature is the digital numeral, read on the temperature-sensor's display". The progress in the sensitivity of temperature sensors (from materials volume expansion (glass-mercury) to single thermocouples, thermopiles, printed circuits, to the latest integrated chips) is tremendous. However, this progress in sensitivity (even down to several decimal digits) by no means has been matched by improvements in accuracy. Actually, that gap is widening, due to the unresolved problems of the heat transfer during measuring temperature. This is an area awaiting a serious research.

Even when analysing simple cases, we reveal several problematic points of the temperature measurement [18, 19, 22, 26, 30]. First, the active part of the thermometer should be small in comparison with the measured (part of) system. Namely, if it were not so the original temperature of the thermometer, itself could influence significantly the measured value. Second, the slower the equilibration of the thermometer with its surrounding, the more problematic may be the figures given by the thermometer if the temperature of the measured medium is varying. Namely, then there is no time enough for equilibrating, and the reading given by thermometer may not express the medium temperature correctly.

The both problems seem to have the solution consisting in the assumption that the active part of the thermometer is negligibly small. Nevertheless, such an assumption cannot be generally used since the active part of the thermometer should have an unambiguously "definable" temperature, which is a macroscopic concept. In other words, it cannot be arbitrarily small. It reveals another problem, namely, if the temperature of the thermometer is ever defined. If the active part of thermometer is not in equilibrium, what is then the meaning of the "thermometer's temperature"? In fact, the temperature as a quantity measured by a (macroscopic) thermometer is some way an "averaged" concept.

If we accept that the thermometer can be hardly a point-like structure, we should take much care of the problem of measuring the temperature in speedy thermal processes. This question plays an essential role, for instance, in the thermal analysis [39] where the relation of structural or other material changes and the precise value of a current temperature of the sample is very important. The crucial problem in situations when the measured thermal field is rapidly changing is the fact that we cannot simply identify a taken reading of the thermometer with the temperature of a piece of the medium at the same moment. To determine a time delay may be an important task for practice (e.g. when evaluating rapid measurements in thermal analysis).

The calculation exploited further on reveals a more general viewpoint. Namely, when noticing that any small part of the medium may be understood as some (natural) thermometer, we discover the concept of self-measurability. The fact that the temperature field may become a measure of itself is deeply related to the process of equilibration during the heat transfer. The condition of self-measurability thus may be used as a constitutive law that can be much more general than the Fourier

law. The general questions concerning self-measurability [40] are under investigation. As a non-trivial example, we outline the problem of very rapid thermal processes when the Fourier law cannot be applied.

3.4 Temperature as an "Averaged" Concept

The fact that the thermometer is not a point-like structure has an important consequence, namely that the temperature is generally an *averaged quantity*. The averaging need not mean only a step from microscopic description to macroscopic one—e.g. by using the procedures of statistical physics—but also various operations at the macroscopic level. For example, the measuring of temperature is more or less an averaging procedure (at macroscopic or middle so-called mesoscopic scale). As a simple example, let us imagine a familiar thermometer: a vessel with mercury is emerged in a liquid and we measure the change of the volume of the mercury so that the pressure in the vessel may be supposed to be constant. The scale is calibrated in "degrees of temperature" by using some formulas of equilibrium thermodynamics relating the density of mercury, ρ, with its temperature under a given pressure, $T = f_V(\rho)$, $(p = \text{const})$. There are various thermal processes in liquid (e.g. the temperature of the air varies from place to place during a day), and no perfect thermodynamic equilibrium can be assumed within a finite (confined) region at a moment.

The thermometer's vessel is a small (but a finite) part of the system, and thus, the temperature within it cannot be supposed to be constant. Nevertheless, we can measure the volume of the mercury regardless if it is or is not in thermal equilibrium. Let $\theta(x)$ be the temperature field within the thermometer's vessel. It corresponds with the local density $\rho(x) = f_V^{-1}(\theta(x))$. The measured temperature is thus an averaged value

$$T = f_V\left(V^{-1}\int \rho \mathrm{d}V\right) = f_V\left(V^{-1}\int f_V^{-1}(\theta(x))\mathrm{d}V\right). \tag{3.1}$$

Let us notice that the assumption of a local temperature field $\theta(x)$ plays no meaning in the measured procedure—we measure the averaged density regardless if it is related to a temperature field. In the other words, the first part of formula (3.1) defines an averaged quantity which is identified with the temperature.

Another example is more theoretical than of a practical use. In any non-equilibrium situation in a rigid heat conductor, we can assign the temperature to any (finite) part of the medium at any time t by the following procedure: let us isolate this part adiabatically from its surrounding at the time t and wait till the region gets into equilibrium. Its temperature, $T = f_E(E/V)$, where E is internal energy of the region, then defines the temperature at t (i.e. in past). Because the internal energy of the region cannot change during the adiabatic isolation, this temperature is in fact identified by the formula

$$T(t) = f_E\left(V^{-1}\int u(x,t)\mathrm{d}V\right) \tag{3.2}$$

where $u(x,t)$ is the field of the volume density of internal energy. The both examples lead to the same averaging formula, namely

$$T = f\left(V^{-1}\int \phi(x,t)\mathrm{d}V\right). \tag{3.3}$$

There are also definitions of temperature by a measuring procedure defined not over a spatial region but over a surface. For example, we assign the temperature to a region in thermal non-equilibrium as follows: we put the region at time t in the full contact (along the whole boundary) with an equilibrium bath, whereas the temperature of the bath is chosen in a such way that the current (total) heat flux between the bath and the region is zero at this moment. Then, the temperature of the heat bath is assigned to the region at t and is called the contact temperature [41, 42]. Assuming that the thermal interaction is local, the contact temperature depends on an average of a quantity (or quantities) on the surface of the region.

3.5 The Self-Measurability

Let us imagine a thermometer with a spherical active part. This part is finite and has the radius, l, and the volume V_l. We assume that the thermal field $T(x',t)$ continuously goes through the medium as well as the active part of the thermometer. The reading given by the thermometer, T^{th}, is an average of this field over the active part. Being motivated by the formula (3.3), we define simply the temperature measured by the thermometer whose centre is at the point x,

$$T^{\mathrm{th}} \equiv \langle T\rangle_l(x,t) = V_l^{-1}\int_{B_l(x)} T(x',t)\mathrm{d}V, \tag{3.4}$$

where $B_l(x)$ is a ball with the centre x and the radius l.

When assuming the continuity of the thermal field on the border of the active part [43, 44], we may identify the temperature of the medium around the thermometer, T^{surr}, with the other averaged quantity, namely

$$T^{\mathrm{surr}} \equiv \langle T\rangle_l^b(x,t) = S_l^{-1}\int_{\partial B_l(x)} T(x',t)\mathrm{d}S, \tag{3.5}$$

where $\partial B_l(x)$ is the boundary of the ball $B_l(x)$ with the surface S_l.

Now, we use the Taylor expansion in spatial coordinates of the averaged quantities $\langle T\rangle_l^b$ and $\langle T\rangle_l$ and get the important formula,

$$\langle T\rangle_l^b(x,t) - \langle T\rangle_l(x,t) = l^2 N^{-1}(N+2)^{-1}\Delta T(x,t) + o\left(l^4\right), \tag{3.6}$$

where N is the spatial dimension of the studied system, usually $N = 3$.

Let us assume that the temperature field in the active part of the thermometer obeys the heat equation, $\frac{\partial T}{\partial t} = \kappa\nabla^2 T$. Since $\langle T\rangle_l = T + o(l^2)$, we can use the heat conduction equation on the right-hand side of (3.6) and identify $\frac{\partial T}{\partial t}$ with $\frac{\partial\langle T\rangle_l}{\partial t}$. As a result, we get

$$\langle T\rangle_l^b(x,t) = \langle T\rangle_l(x, t+\delta t(l)) + o\left(l^4\right), \tag{3.7}$$

where

$$\delta t(l) \sim \kappa^{-1} N^{-1}(N+2)^{-1} l^2. \tag{3.8}$$

The formula (3.7) has a clear meaning: the measured datum, T^{th}, corresponds with the (averaged) temperature of the medium, T^{surr}, with the time delay $\delta t(l)$.

As expected, this delay tends rapidly to zero when $l \to 0$. That means that the datum of the thermometer with a small active part gives a good approximation of the current temperature of the surrounding medium. Nevertheless, this conclusion is valid only if the assumption of the validity of the Fourier law may be used. That it cannot be the general case is simply seen from the condition (3.8). Namely, it implies that a typical velocity of this equilibrating,

$$v_{\text{eq}} \approx \frac{l}{\delta t(l)}, \tag{3.9}$$

tends to infinity when $l \to 0$ since $\delta t(l) \sim l^2$. It would correspond to the fact that heat propagates at infinite speed.

It implies that the diffusion equilibrating of temperatures is a useful approximation that cannot be, however, strictly valid. This problem is well known for many years. More than fifty years ago, Cattaneo [45] proposed a correction of the Fourier law, $q + \tau\frac{\partial q}{\partial \mathrm{t}} = -\lambda\nabla T$, leading to the hyperbolic heat conduction equation,

$$\frac{\partial T}{\partial t} + \tau\frac{\partial^2 T}{\partial t^2} = \kappa\Delta T. \tag{3.10}$$

The Eq. (3.7) may be written simply in the form

$$T^{\mathrm{th}}(t+\delta t) = T^{\mathrm{surr}}(t). \tag{3.11}$$

It says that the temperature given by thermometer at any time moment t is a correct temperature of the surrounding medium at a slightly delayed time $t - \delta t$. In other words, the equilibration may be understood as a certain "*transfer*" of information about the temperature of the medium into the thermometer. It takes a time δt that depends on the characteristic dimension l and possibly on other parameters of the active part of thermometer. Notice that the presence of a real thermometer (or its active part being in contact with the medium) plays no role. In other words, we may do the derivation for an arbitrarily small spherical piece of the medium.

The thermal equilibration within the medium thus provides some self-measurability [40, 43] of the field T: small pieces of media keep at any time moment t information about the averaged value of the field T in their nearest surroundings at a previous moment $t - \delta t$. The equilibration thus guarantees that pieces of media work as measuring device giving continuously delayed information about their surroundings.

The problem is, however, that the Fourier law may not be valid in special situations or for special materials. In gases, for instance, the molecules at places with higher temperature carry higher kinetic energy and thus the random molecular movement gives, at average, a net flux of energy (the heat flux) opposite to the temperature gradient as predicted by the Fourier law. This flux, however, is lagged by a time τ of the order of magnitude of the mean free flight that corrects the Fourier law as $q(t+\tau) \approx -\lambda \nabla T(t)$. If the time τ plays a role in our experimental set-up, this lag cannot be neglected and we get different kind of equilibration described by the Cattaneo law [45]. Similar lagging arguments may be used in solids (see, e.g., a comprehensive review in Ref. [46]). A special situation occurs in metals when the electron gas is immediately heated up while the metal lattice remains cold. A highly non-equilibrium state thus arises and the process of equilibration includes also a complicated thermal interaction between the electron and phonon gas [47, 48]. This equilibration cannot be described by the simple Fourier law, too.

The self-measurability condition is, however, much more general than the Fourier law of equilibration and can be used in the above-mentioned situations [43]. Independently of which constitutive law governs the heat conduction, there are always situations at which the self-measurability condition has to be identified at certain times and points. At standard diffusion processes, this condition is fulfilled at all situations, but the class of processes having this property is much broader. For example, if the sign of the averaged temperature gradient over the ball surface, $\int n \nabla T \, \mathrm{d}S$, implies the opposite sign of the current heat flux from the ball, the self-measurability condition becomes valid at all situations [40]. A very important situation when the self-measurability condition has a non-trivial meaning is as follows. After a sudden heat impact of a piece of metal by a short-pulse laser, the electron gas is immediately heated up while the metal lattice remains cold. A highly non-equilibrium state [49] thus arises, and the process of relaxation—the

equilibration between the electron and phonon gas—gets going [47]. Using the self-measurability condition, we get a hold of the hyperbolic heat conduction law [43, 48, 50] which falls beyond the scope of this chapter.

3.6 Particularity of Thermal Analysis

Let us recall that temperature is established as an *intensive quantity*, $\Im \equiv T$, and heat is characterized as the *extensive quantity,* $X \equiv \varsigma$, quantified as caloric, ς, casing thus a couple of *conjugate variables* when obeying dimensional equation of the form: [Energy] = [T] × [ς]. This approach was well described in our previous papers [23, 24] on alternative thermodynamics. Similarly, the 1848 Kelvin's proposition [51] is somehow innovative towards the definition of temperature scale, and it is independent on the type of thermometer and the thermometric substance. Kelvin proposes to treat Carnot's theorem as a fundamental postulate pointing out that the purpose of a Carnot's function is to modify the difference of temperature measured in a particular empirical temperature scale in such a way that it could serve as a exact proportionality factor between the work, ΔL, and heat, ς (in textbook thermodynamics normalized to an integration competent fraction, Q/T, called *entropy*, S [23, 24, 51–53]). As this factor, ΔL, according to Carnot's postulate, has to be the same for all substances, Kelvin suggested defining a universal (in his terminology "absolute") temperature scale just by prescribing a proper analytical form of Carnot's function.

Furthermore, the heat exchange rate is a primary attribute [53] determining the basic conditions of all thermoanalytical measurements [54–56]. As such, when defining our extended thermodynamic system, the principal quantities (temperature T or others like pressure P) must be also expressed as functions of time if needed, i.e. $T = \boldsymbol{T}(t)$, $P = \boldsymbol{P}(t)$ or generally any intensive parameter $\Im \equiv \Im(t)$. Therefore, in the so-called *dynamic thermal analysis* [54, 57], a description of the sample's environment, to be adequate, requires inclusion of not only the values of T or P and other $\Im$, but also of their time derivative, namely that of temperature T' (= dT/dt = *constant* β). Please note that the apostrophe ($'$) signifies time derivatives, and the bold italic letters ($\Im, \boldsymbol{T}, \boldsymbol{P}$) represent functions. Let us assume that under standard (even if idealized) thermoanalytical conditions of constant heating/cooling rates, $T' = \beta$, the generalized thermodynamic function Φ [54] (alike the standard Gibbs energy, G, but extended) of a given thermal state is specified by the set of intensive parameters T, P and $\Im$. For thermal analysis, in the first approximation, satisfactorily defined Φ reads as $\Phi = \boldsymbol{f}(T, T', P, \Im)$. Worth of attention is the fact that function significance of this constitutive thermodynamic potential Φ is not distorted by including the first temperature derivative, T'. So it keeps its legitimacy [54, 56] as

$$\Phi = f(T, P, \Im) \equiv f(T, T', P, \Im). \tag{3.12}$$

However, it is invalid for any further inclusion of higher derivatives of T'' such as $f(T, T', T'', P, \Im)$ [40, 41]. This process is certainly applicable for any other derivatives of intensives P, $\Im$, etc. It follows that for whichever experimental inconstancy where anticipated β become $\neq \mathrm{d}T/\mathrm{d}t$, the state function, Φ, *must* encompass the second derivative of temperature, T'', i.e. $f(T, T', T'', P, \Im)$. This, however, does not allow the customary amalgamation of established thermodynamic laws and their conventional mathematical processing. Moreover, in such a case, the meaning of temperature (as well as of its derivatives T', T'') may become inexact and thus questionable when taking into account the above definition of temperature. Similarly, the thermodynamic data obtained under extreme condition (like rapid temperature changes during quenching), such as C_p or ΔH, may not possess traditionally designed figures and thus should be presented under special connotation. However, this fact stays often unnoticed in most practical cases of extreme thermoanalytical experiments. Even the steady temperature reading of heating furnace/thermostat is used, time and again, as the actual temperature of the heated sample instead of the true temperature measured, e.g., on the sample surface.

It is worth declaring the yet unfamiliar term "thermokinetics" [10, 57] (derived from Greek word κινηση = motion, movement) which shares out states neither in equilibrium nor under steady states. For such off-equilibrium states, the temperature field $T(\boldsymbol{x})$ in the sample (local interior temperatures) changes with time [58]. All such states existing during heating or cooling are unsteady variable states so that usual thermoanalytical experiments are based on unsteady states and, as a consequence, on measuring the non-equilibrium temperatures [42, 49, 59–61]. Using heat transfer equations, we are able to estimate the temperature field (radial profile) for the applied linear heating rate (i.e. $\beta = \mathrm{d}T/\mathrm{d}t$) in a thermally inert (without transitions or reactions initiated mere by the change of temperature) sample [56, 59] as "a stabilized temperature profile" (dependence of temperature on coordinates)—e.g. for the coordinate r (= radial distance from the rotation axis in a cylindrical sample with infinite height) as

$$T(r,t) = T(t_0) + \beta\left[(t - t_0) - \left(R^2 - r^2\right)/4a\right] \tag{3.13}$$

assuming $T(R, t) = T(t_0) + \beta\,(t - t_0)$, where R is the external radius of cylinder, T_0 is the initial temperature at time t_0, and $a = \lambda/(\rho C)$ is the thermal diffusivity, respectively. The instantaneous average (weighted) temperature $T_\mathrm{ave}\,(t)$ through all volume of the sample is then given as [57]

$$T_\mathrm{ave} = T(R,t) - \beta R^2/8a \tag{3.14}$$

We are able to indicate only temperature on and near to the sample surface $T_{sS} = T(R, t)$, and it follows that the difference between the surface and the average temperature is proportional to the product of heating rate and sample radius, βR^2.

3.7 Introducing a Novel Term "Tempericity" for Extreme Temperature Changes and Tykodi's Classification of Thermal Science

During the intact course of special techniques applying rapid thermal changes during, e.g., quenching [37, 38], the above premises (i.e. $\Phi = f(T, T', P, \Im)$, when T' is constant) are evidently violated since a significant amount of heat is flowing between the bodies under study. It is raising the question where is the reliability limit of such a separated but also built-in measurement of heat and temperature under a process of their mutually linked rapid alteration. In a way, we can perceive a certain similarity to the Heisenberg quantum limit (which precludes simultaneous determination of a fast-moving particle's velocity and position) so that a simultaneous measurement of both heat and temperature may be unfeasible when conducting measurements under an extremely rapidly changing temperature [62]. For the cases that measured temperatures are changing extremely rapidly, a formulation of new terminology may be necessary [59], namely when inaugurating an *operational quantity* (the sensor's thermoscopic reading) instead the traditional *physical quantity*. Such a new operational term for extraordinarily off-equilibrium temperature can still be based on the Latin root "temper" producing term "tempericity" [56, 59]. Many new terms sounded strange initially, when they were proposed. However, looking at Table 3.1, tempericity does not seem to be an odd term.

It is worth attention that tempericity brings a narrowed relevance than the temperature, being just applicable under extraordinarily extreme conditions (e.g. quenching). Another nickname *tolerance* (introduced in a generalized connotation of temperature as a mean property) is complying with the increase of forbearance along with the parallel increase of temperature. Tolerance becomes relevant to the degree of disorder in the hierarchical, democratic and anarchical states of tolerance towards chaos. Tolerance has found application in modelling societal life within new field of the so-called thermodynamic economy (≈econophysics) [63, 64], which again goes beyond the scope of this chapter and is detailed in Chap. 23.

In respect of such special treatments, we should recall somehow forgotten and unfamiliar proposition of *thermotics* (resembling the traditional terminology as "mathematics" [10, 57, 65]) residing behind the science of heat and based also on the Greek origin, apparently used as early as in 1837 [65]. American physical chemist R. Tykodi (1925–2015) made an attempt to recharge the term thermotics in 1960s [66–68] as a term which could be put in a wider usage becoming on a par with the 1946 term idiom for "energetics". The latter term was provided by the Danish physical chemist J. N. Brønsted (1879–1947) [67] and closely connected

Table 3.1 Branched view to the spheres of alternative thermodynamics

Thermometry, calorimetry	Steady transport processes	Thermal analysis	Processes involving rapid changes
Sadi Carnot Clapeyron	Fourier, Fick, Ohm	Golding, Tykodi, Brønsted	Schick's "chip" fast-scanning calorimetry
Carnot line (dissipationless work)	Fourier line (workless dissipation)	Tykodi line (adjoining near-equilibrium thermodynamics)	Rapid temperature changes (off-equilibrium)
Clausius (classically based on thermodynamic laws)	Stokes and Kelvin particularities	Brønsted and Tykodi particularities	Newton cooling law (non-steady gradients, thermal inertia)
Thermostatics Gibbs—phase equilibrium	*Thermodynamics* Clausius-Duhem inequality of irreversible reprocesses	*Thermotics* generalized reprocesses irreversibility	*Thermokinetics* instable states, unsteadiness (unsolved yet)
T = constant with ideally zero changes $\mathrm{d}T/\mathrm{d}t = 0$	$\mathrm{d}T/\mathrm{d}t$ = constant $\cong \beta$, $\mathrm{d}T^2/\mathrm{d}t^2 = 0$	β ideally constant but often $\mathrm{d}T/\mathrm{d}t$ varying, at least $\mathrm{d}T^2/\mathrm{d}t^2 \Rightarrow 0$	$\mathrm{d}T/\mathrm{d}t$ arbitrary $\neq \beta$ *but equal to* $(\lambda/C)\nabla T \Rightarrow (\lambda/C)\nabla^2 T$ $\mathrm{d}T^2/\mathrm{d}t^2 > 0$
Temperature	Temperature	Up till now yet temperature	Novel tempericity
Calorimetry, elderly DTA theory (by Boersma, Borchadt, Vold, Berg, Soule)	Onsager relations	DTA theory involving gradients and thermal inertia (Gray, Holba)	Updated theories Sertorio, Jou, etc. (yet waiting development)

with the connotation of temperature. In this view, the "thermotics" has managed to survive as a thermal science comprised of three sub-branches [10, 57]: *thermostatics* (pertaining to the ordinary classical equilibrium aspects of temperature), while exploited *thermodynamics* (relevant to those aspects for which time variation is important) and finally *thermostaedics* (concerning the aspects that become temporally steady). The latter is another somehow forgotten sphere suitable to envelop the growing field of thermal analysis [5, 10–12, 57, 69]. Regretfully, thermal analysis [6, 7, 55], with its challenges of coupling temperature and heat flow under non-equilibrium conditions [53, 58], was never appropriately situated within the fields of the traditional thermodynamics [21, 25–30], and its proper position can be figured out in Table 3.1.

3.8 Thermodynamics Under a Non-constant rate of Temperature Changes: Methods of Observing Sample Quenching

Let us analyse more special cases of rapid temperature processing [37, 38, 62] which became now a popular method of the so-called ultrafast isothermal calorimetry using thin-film sensors [62]. Although the kinetic phase diagrams [5, 70–72] are configured as a stabilized consequence of previous quick temperature changes (≈quenching [56, 71]), we are anyhow focusing our attention on the resultant low-temperature measurement of the constrained high temperature (i.e. staying at periphery states excluding process of quenching). Even if declaring the experimental details of quenching process we do not include them in the entire description of our thermal scrutiny by any detailing the route of temperature changes—it is just a manner of experiential preparation. The analyses of individually elaborated states are consequently done by standard (so-called low-temperature) thermoanalytical methods where thermodynamic principles are yet "preserved" [55, 56, 70–72]. Certainly, it includes the expected problems induced by temperature transfer [43], thermal inertia [73, 74] and formation of temperature gradients [42, 72, 75], which was already noticed in the past paper by Smyth [75] and approved in detail in our book chapter [74] in the previous Volume 9.

Experimentalists are often proud of their ability of measuring temperature under extremely quick changes [62, 76–78]. Some thermoanalytical papers provide the measuring precision with many decimal places, but the accuracy is commonly of a lesser concern. It applies to special methods, too, even if weighted up. In other words, the temperature values that we produce and observe in rapidly changing processes are precisely repeatable, alas, far from the real values; moreover, we do not know how far. We need to have full knowledge of the structure of the transport processes [53, 79] including temperature measurements in such extreme conditions and being aware of the specificity of novel chip measurements [80]. Some of the needed improvements are elementary, e.g. measuring true sample temperature instead that of the simplified outer heat zone of the furnace, working out the mean sample temperature instead its surface's value [74, 81, 82], etc; that, however, falls beyond the subject of this paper. Of special interest are those phenomena which are especially active during the transient temperature changes. At first, we need to analyse the fluxes needed for such an irreversible off-equilibrium processes [58, 79, 83–90].

The relationships in these fluxes resemble those well known in areas other than thermal research detailed in our previously published chapter [79], i.e.

- the basic Newton laws display motional (x) momentum p related to the product of mass, m, velocity, $v = \mathrm{d}x/\mathrm{d}t$, and force, F, further linked to acceleration $a = \mathrm{d}^2x/\mathrm{d}t^2$,
- the essential law of heat transfer $q = \lambda\ \nabla T$ (Fourier [83, 84]),
- the parallel laws of diffusion $J = D\ \nabla c$ (Fick [85]), and
- of the analogous electric flow $I = r\ \nabla u$ (Ohm [86]).

The symbol ∇ is used for gradients of temperature ∇T, electrical potential ∇u and concentration ∇c together with the thermal conductivity λ, diffusion D and electrical resistivity r. These can be easily found in the literature [53, 79, 84] as well as in the well-known Onsager reciprocal relations for the area of irreversible processes [58, 88–90] steady processes.

In spite of practically identical forms [79] of these fundamental relationships providing a class of linear phenomenological transport equations [79, 83–89], there remain large differences in their physical content; such a large diversity in the nature of the processes described by the same mathematical form should serve as a serious warning before making superficial analogies, or before rushing to conclusions about a process mechanism. Impact of transport constitutive relations to the generalized carrying behaviour is detailed in our book chapter [79], in limit being affected by quantum features of diffusion [81].

It is worth of a remark that the most difficult part of establishing Fourier's and other similar fundamental relationships was not finding their mathematical form (which appears to be rather simple [79]) but finding the definitions and the physical interpretation of the quantities involved, or even the proof of their very existence [79]. In a way, they resemble the above-mentioned Newton law of momentum of movement [73, 74, 91] $p = mv$ and can be applied to explain the thermal inertia, too, where the mass m is replaced by the material heat capacity C_p and the velocity by heat rate $(\mathrm{d}\Delta T/\mathrm{d}t)$ [55, 57, 91]. However, the obvious resulting impact of omnipresent thermal inertia is so far neglected in thermoanalytical experiments and literature [92, 93] with the exception of [39, 94–96].

The empirically determined prefactor in Fourier equation is repeatedly dissected into the product of quantities having more straightforward or already known physical interpretations. For example, the thermal conductivity is usually written in the form $\lambda = a/(C_\mathrm{p}\rho_\mathrm{m})$, where a means the thermal diffusivity introduced by Kelvin as an analogue of diffusion constant, C_p specific heat capacity at constant pressure and ρ_m the density of the material. In such a way, it is commonly applied in thermal analysis for describing the condition of ideal cooling [72], where we assume infinitely high coefficient of heat transfer. Thus, the cooling rate β becomes dependent on the sample thickness d as $\beta \sim 1/d^2$, while for the Newtonian cooling mode, which is controlled by the phase boundary, β correlates with $1/d$ only. In practice, we may adopt the power relation $\beta = 1/d^n$ (where $1 \leq n \leq 2$ is an experimental constant). For illustration, we may present the example of cooling, which is close to ideal, with the proportionality coefficient, $\Lambda = 10^4$ (J m^{-2} K^{-1} s^{-1}), frequently displayed for several real materials. We can guess the limiting lowest cooling rates of 10^2, 10^6 and 10^9 (K/s) for the critical sample thicknesses d of the respective 10, 5.10^{-2} and 10^{-3} (mm). The latter value of thickness is very small, scarcely attainable even by intensive laser glazing [97], which works with very thin layers and assures intimate contact of the in situ melt sticking on the surface of the solid support. In fact, it is imagined by the surface-printed microchips used in sophisticated calorimetry [77, 78, 80, 81].

In that novel method of high cooling rate, thin-film-chip nanocalorimetry [77] makes available the direct analysis of the quenching process exhibiting the rates of the observed temperature changes of the order of 10^4 K/s which is possible. The design of a thin-film microchip cell opened extensive capabilities in reading normally hidden aspects of ultrafast processes. Such a measuring cell consists of a thin-film heater deposited on a silicon nitride membrane. The heater simultaneously serves as a resistive thermometer [62, 80]. The samples are considered necessary to be premelted and thus thinly spread on the microchip surface which is used for detecting temperature. Thus, the heat capacity of ultrathin films is negligible, and even when impaired by, e.g., the added polymer crystals, as well as by any nanoparticles and nanostructures, it is small enough to enable investigation at ultrafast heating rates, up to the astonishing 10^5 K/s.

Near-adiabatic conditions were achieved when the cell was additionally placed in vacuum. Historically, in the pioneering days, sensors were self-constructed, but at present, a number of commercially available microchip modules [80] can be widely utilized as sensors for such an updated thin-film nanocalorimetry. Consensually, the measurements at controlled heating and cooling rates at around 10^4 K/s were performed and published while studying processes of recrystallization [98].

A question arises about such extraordinary fast temperature changes whether the detected values keep the meaning of a *true sample temperature* and how to calibrate temperature under such extreme changes, since the danger of deep undercooling [71] and disturbing metastability occurrence was noticed as early as in early 1970s [99]. Despite the apparent successfulness of these special microchip techniques providing a new insight into material behaviour (otherwise unattainable), we must query the reliability of figures provided by such temperature sensors. They reflect the temperature to a *limited degree,* while displayed sensor's numbers are identified with the meaning of temperature by the labourer only. For that reason, we proposed to call such sensors reading as *tempericity* [57, 59] and declared that "temperature called" data obtained at the astonishing rates of million Kelvin's per second [38] may be rightfully questioned [56–59, 70, 82].

3.9 Practical Aspects of Off-equilibrium Temperatures Due to Heat Inertia and Thermal Gradients

Immediate and local values of thermodynamic variables under off equilibrium are a long lasting enquiry [41, 42, 58, 60, 61]. A frequent displaying non-equilibrium temperature [41, 42] is due to time delay, i.e. hindered temperature adaption of any coupled object under study to the imposed temperature of environment. In the framework of conventional thermal research, this phenomenon, often known as *heat inertia* effect, has an analogous impact as mechanical inertia having sample mass replaced by its thermal capacity and acceleration by factually acting the

second derivative of temperature (first of temperature difference ΔT) [91]. Its impact is usually ignored at the processing of outputs of thermoanalytical experiment despite its legitimacy well known since the Newton cooling law [95, 100, 101]. In the other words, it is a delay of the sample (and/or reference) temperature with respect to a temperature demanded by the externally applied heating programme. At DTA (as well as spontaneous heat flux DSC), the simplest refinement means [73] making use of the adequate equation including often absent term $\mathrm{d}\Delta T/\mathrm{d}t$, i.e. for DTA:

$$\Delta T = R_{\mathrm{eff}}(-C_s \mathrm{d}\Delta T/\mathrm{d}t - \Delta H \mathrm{d}\alpha/\mathrm{d}t) \Rightarrow \mathrm{d}\alpha/\mathrm{d}t \neq -\Delta T/A_{\mathrm{DTA}} \tag{3.15}$$

where ΔT ($= T_s - T_r$) is the difference between sample and reference temperatures, $\mathrm{d}\Delta T/\mathrm{d}t$ is the time derivative of this difference, R_{eff} (T) is the effective thermal resistance of heat flux, C_s is the heat capacity of sample, ΔH is integral change of enthalpy (corresponding to the process occurring inside the sample), α is the degree of the conversion of this process, $\mathrm{d}\alpha/\mathrm{d}t$ is then the rate of the process, and $A_{\mathrm{DTA}} = \int \Delta T \, \mathrm{d}t \equiv R_{\mathrm{eff}} \Delta H$ is the area of DTA peak (in Ks units). It worth attention that for a spontaneous heat flux DSC the following relations take place: $J_q = -C_s \, \mathrm{d}J_q/\mathrm{d}t - \Delta H \, \mathrm{d}\alpha/\mathrm{d}t \Rightarrow \mathrm{d}\alpha/\mathrm{d}t \neq -J_q/A_{\mathrm{DSC}}$, where ΔT is transformed (calibrated) into heat flux J_q (in W) between the sample and reference. So that $\mathrm{d}J_q/\mathrm{d}t$ is then the time derivative of this heat flux using R_{eff} (T) which is determined by the calibration at several temperatures, and $A_{\mathrm{DSC}} = \int J_q \, \mathrm{d}t \equiv \Delta H$ is the area of DSC peak (in W). During any process inside the sample, the temperature of the sample T_s is not equilibrium temperature as it differs from that linearly increasing or decreasing reference T_r (or other temperature T_{env} representing thermal state of the sample surroundings (e.g. T_{block} at DSC) as a consequence of self-cooling or self-heating due to the running process inside the sample.

The corrections included in Eq. (3.10) are not quite sufficient because also in the case of no self-heating or self-cooling (at $\alpha = 0$), the temperature in sample centre T_c is other than the temperature on sample surface T_{sS} as it is shown in [74]. This is a reason why at compensation DSC (Perkin-Elmer) method, the displayed temperature of sample is neither fully representing the temperature of sample although no correction on thermal inertia is necessary and the condition $\Delta T = 0$ (or $J_q = 0$) is guaranteed by compensating device. Generally, the temperature of sample surface does not represent the temperature of sample when temperature field inside sample is not uniform. It occurs due to self-cooling or self-heating but also due to nonzero heating or cooling rate. Besides at thermogravimetry, where thermometric (thermal) contact with the sample is usually far from being perfect, we do not know the true temperature and the form of TG curve can be, moreover, determined by the rate of heat transfer between the surroundings and the sample as it was well noted by Gray [102].

Best example of a non-trivial choice of what is a true sample temperature is illustrated in Fig. 3.1, where various representations of the workable temperature scanning are revealed including the impact of inertial term. First, let us account on the customary experimental set-up of so far standard reading of the difference

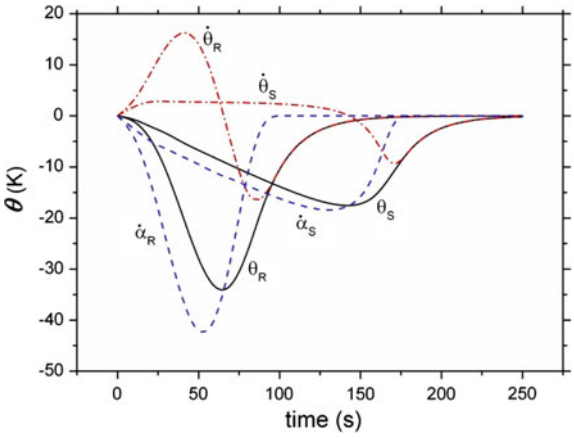

Fig. 3.1 Illustrative model outline of two possible temperature depictions adjusted during DTA measurements. The curve labeled with symbol θ_R is a standard DTA record providing heat inertia background $\dot{\theta}_R(\equiv \theta'_R)$ and consequential reaction rate $\dot{\alpha}_R$ while the curves with subscript S are based on the innovative approach where the temperature difference is related to the sample factual temperature alone and has evidently flatter course

between temperatures of the sample surface S and that of reference R, i.e. $T_S - T_R = \Delta T \Rightarrow \theta_R$. It is worth reminding that T_R is regularly identified with the heating programme, i.e. the temperature of furnace surface. This standard reading output can be corrected on the heat inertia θ'_R and transformed to the reaction rate, α'_R. However, this ordinary procedure does not truly account on the factual sample temperature which (in the first approximation) is just T_S (not assuming gradients yet), but not that imposed by external heating T_R. Therefore, another more truthful reading ought to be related to the factual difference θ_S between the sample surface temperature T_S and the averaged temperature of the sample T_{ave} which is related to the truthful sample temperature itself. Such a true but yet unusual approach understandably changes the standard reading θ_R providing a "deformed" but true θ_S distorting the previous reaction picture and providing the dissimilar rate values, α'_S. Certainly, this new portrait is leaving an unanswered question what kind of data we have ever kept measuring and publishing. It follows that any consequent calculation of specific kinetic data (typically activation energy values) with several decimal places is inconsequential as such an ordinary reporting temperature measure θ_R involves the error margin reaching perhaps several degrees or more (not talking about ultrarapid quenching). The common practice of adding qualifiers "formal", "apparent" or "of no real meaning" to published data is an irrelevant excuse for using inadequate practice of temperature observation.

It touches the quandary of ever involved temperature gradients in the studied solid samples which is known for long as early exposed by Smyth [75]. His particular 1951 model was analysed in more detail in our previous chapter [74] the computer calculation of which provided almost identical temperature profile for given instant, as documented in Fig. 3.2. Moreover, the chapter [74] deals

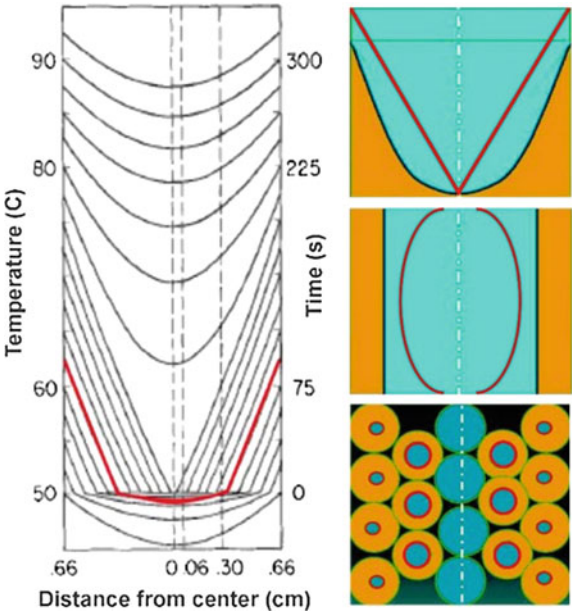

Fig. 3.2 *Left* is the Smyth's 1951 sketch of gradients added by our own calculation of one line (*thick red*). *Right* is a schematic pattern of some abridged cases of temperature gradients possibly participating in a solid-state transformation (shown within simple spherical images where *light blue* areas are reacted and *orange* areas are initial non-reacted material)

systematically with particular cases of modelling of temperature gradients so that it is not necessary to reiterate. Worth noting are three individually treated models depicted on the right-hand side of Fig. 3.2, drawing attention to its practical operate under a strict and/or a continual separation of temperature allocations. It was emphasized that the mean effect of temperature gradient and its variability inside the sample (the term proportional to the rate $\mathrm{d}\theta_{\mathrm{Smean}}/\mathrm{dt}$ of the difference θ_{Smean} between the outwardly measured temperature of sample holder T_{R} and the temperature T_{ave} which is averaged over its whole volume [74]) is practicable and capable for the introduction to both the private and commercial practice of instrumentally available software.

The gradient affairs are important in practical evaluation while forming a specific part of kinetically aimed analysis. The thermokinetic model by Lyon at all [81] describes the effect of thermal diffusion, internal energy generation and chemical kinetics on the sample response in differential, non-isothermal analysis. The distorted reaction rate results from internal energy generation and thermal diffusion and is interpreted as kinetic effects. In terms of the maximum reaction rate, the thermokinetic model provides a simple analytic relationship between the sample mass and heating rate, while the measurement error for chemically reacting solids in non-isothermal analyses has been found consistent with numerical calculations.

Farjas and Roura [82, 103] shown that in non-isothermal kinetic studies during the processes taking place at the same temperature range, the separation between peaks obtained at different heating rates increases steadily when the activation energy diminishes. They have also shown that in non-isothermal analysis, the different heating rates should be equidistant in a logarithm scale. In addition, the

temperature range analysed by non-isothermal measurements is relatively narrow, typically few hundreds of Kelvin while the heating rate is varied over three decades. Papers [103, 104] criticized the widely cited treaty on kinetic evaluation by Kissinger [105], which is also the subject of a parallel Chap. 10 of this volume.

Regarding the manifestation of temperature gradients in case of the fast scanning calorimeter (FSC), Svoboda [106] has shown that even for the micrometre-sized samples, significant temperature gradients can be established either within the sample or on the borderline between the sample and the calorimeter chip. This is especially true for the samples with poor thermal contact such as micrograins or flocks (in contrast to premelted thin films directly attached to the chip, representing an ideal thermal contact), where in addition to the always present air gaps, certain liquids are often used to supposedly enhance the thermal contact. The major distortion of the FSC structural relaxation signal obtained for amorphous Se [106] was explained in terms of the temperature gradients occurring within the hemispherical sample. The FSC signal was deconvoluted by using the theoretically modelled a–Se relaxation curve (with the parameters obtained from conventional DSC) as a deconvolution function. The weighing coefficient distribution obtained from the deconvolution was found to agree well with the heat propagation profile derived for the following simplified assumptions: linear temperature gradient, roughly similar heat conduction and radiation and negligible self-cooling effect. In this regard, the diffusion-less structural relaxation phenomena appear to be suitable for identifying and quantifying the thermal gradients under extreme conditions.

Another unreciprocated dilemma is the true temperature during the so-called modulated temperature measurements where temperature stepwise changes are imposed underlining the otherwise constant heating. Practically, the standard

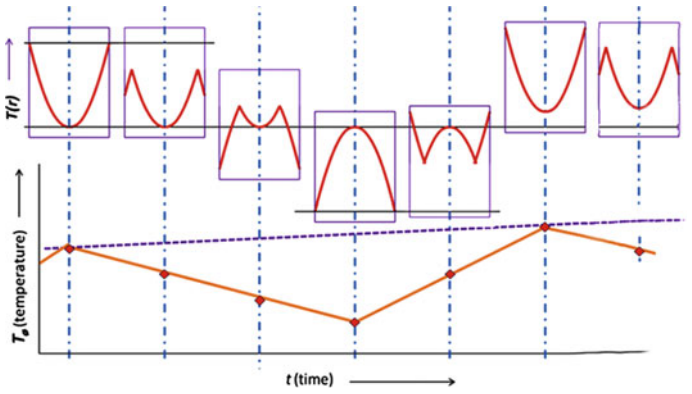

Fig. 3.3 Bottom are shown standard records of steady increasing temperature (*blue dashed*) and imposed recurring temperature changes (one period—*thick orange*), while above is revealed the true variance of temperatures inside the sample bulk (*red*)

heating is modified by externally applied variation on steady temperature profile adjusting its immediate profile to become often sinusoidal and/or stepwise deviations. However, the factual temperature profile [74] in the sample was calculated for a model sample showing its minute changes and true inner temperature profile switching up and down inside a real body. Despite this reflection, the widely popular methods involving modulations are providing valuable results. The true temperature outline relevant to the modulated temperature measurement is worth of a further reflection, see Fig. 3.3, in order to approve its validity.

A special attention needs the process of calibration applied to DTA peak profiles using externally launched heat pulses, inserted either by Joule resistivity heat inside the sample bulk [107–110] or by externally applied flashed laser pulses [110–113]. The analysis of which has been widely examined [95, 112] is becoming a standard equipment for the determination of solid-state thermal properties. It was graphically shown in our previous papers [91, 114] and specifically in the parallel Chap. 15 of this volume. In particular, the as-measured DTA feedback on the externally applied heat pulse was corrected by the instrumental software of our providence [108] and that by the company Netzsch [111] yielding a rectified peak comparable with the input shape when using the corrections inserted by differential method [107–110] and matching integral method [110–113]. It returns us to the beginning of this paragraph showing the inevitability of such corrections yet not familiar in the thermoanalytical practice [73, 114].

3.10 Thermotics and Thermokinetics

The measurement of temperature is not so trivial procedure as it may be seen from everyday accustomed thermoanalytical practice. Such measured values depend on the fact that ever-existing thermal field has a permanent tendency to disappear (equilibrate). In normal everyday situations, the process of temperature equilibration (such as the interaction of active part of the thermometer with its surrounding) is often faster than a typical duration of the change of thermal field—nevertheless, we have to *wait* for it. Moreover, a small error connected with an imperfect equilibrating is negligible. However, the situation becomes different when the precise value of the temperature has to be identified at a given moment of progressing time and temperature which is a typical situation in thermal analysis, better saying thermotics. Besides, a sample of material may be both macroscopic cells or miniature chips. The inside temperature field is in both cases in various degree inconstant, inside the sample as well as across its contacts with holder. It is very important but difficult to correlate chemical, structural or phase changes at any small part of the sample with relevant precise temperature. That is why the

procedure of the temperature measurement should be studied in more detail [74, 78, 82, 91] and not assumed customarily trivial.

The same appraisal uncertainty applies for the validity conditions of textbook thermodynamics when taking care about inherent non-equilibrium, i.e. equality of a thermodynamic function $f(T, P, ...)$ and its yet justifiable thermotic extension $f(T, T', P, P', ...)$ where the first derivatives T', P', etc., have got to be constant (e.g. $T'' = 0$). For small deviations ($T'' \to 0$), the standard formulae of thermodynamics are yet effective and productive for applications. For higher changes (e.g. $\left| T'' \right| > 0$), the standard thermodynamic description becomes indefinite and mathematically ambiguous [1, 41, 42, 48, 58, 60, 61]. Accordingly, the standard thermodynamic values (ΔH, C_p, λ, …) lose their classical meaning (e.g. tabulated data) which may turn out to become a subject of improper interpretation.

Heat transfer under extreme rates as well as for ultrathin and nanoscale media (e.g. nanocellular foams) may even drastically increase as a result of nanodimensionality where radius and volume cannot be fully functional as independent thermodynamic variables to characterize the nanosystem behaviour becoming dependent on another (independent) variables (pressure, temperature, composition, surface tension) [115]. Furthermore, ballistic and scattering effects, phonon tunnelling, Brownian action, etc. [48, 50], may turn out to be effectual which, however, falls beyond the scope of this chapter. Temperature alterations due to nanoscale thermodynamics are a subject of Chaps. 5 and 18 in this volume.

Anyhow, we should stay conscious that data displayed on thermometer under conditions of constant (non-isothermal) heating and/or cooling are not fully standard (i.e. equilibrium), but temperatures ensue correspondence to the zeroth law of thermodynamics. However, it is not the outermost case of temperatures observed under every occasion when the second derivatives T'' become influential and thus difficult to be interpreted as temperature. In such case of distinctive measurements under extreme temperature irregularities, the innovatively proposed term "tempericity" may sound strange initially but does not seem to be an odd term at all when regarding historical development of terms and also looking at Table 3.1 [57].

Moreover, the routinely observed temperature of a studied solid sample T_S is not equal to the programmed (ideally simplified) temperature T_R adjusted by heating regime since the sample shows some positional and internal characteristics and thermal inertia due to its heat capacity. Furthermore, its temperature is influenced by self-cooling and/or self-heating due to the process running inside the sample. Therefore, a classical DTA set-up is producing certain idealization even though it well characterizes the sample thermal changes. For integral analysis (calorimetry), it emerges satisfactorily due to the mere account on the starting end stages. However, for kinetic interpretation of true transformation, such an idealized choice of temperature location may bring a confusing impact (cf. Fig. 3.1) and we should cope with the special discipline thermokinetics [10, 57].

Factually, standard information on the temperature of solid sample, T_s, at a given time t does not represent its instantaneous and intimate thermal state (i.e. rational thermoscopic state) nor its average (weighted) temperature, T_{ave}. Often, it is merely temperature detected on the spot/range of sample surface. True thermal state of the solid sample can be represented by momentary temperature field inside [74, 81], which can be expressed for a given point with coordinate r (e.g. radial distance from vertical rotation axis) of infinite cylindrical sample, simply as $T_{(r)}$. Such a temperature field depends on size/dimensions of sample and on heating/cooling mode and becomes mutually connected with the space distribution of transition degree $\alpha_{(r)}$.

Perceptively, true knowledge of the thermal state of solid sample would be necessary for the construction of new generation of kinetic models (which we may call thermokinetic models, see Table 3.1) expressing local kinetic equations in a specified form

$$\mathrm{d}\alpha_{(r)}/\mathrm{d}t = F(\alpha_{(r)}, T_{(r)}). \tag{3.16}$$

The modified Fourier law [83, 84] (still assuming a simplified form of infinite cylinder [74]) should be applied for the relation between the local transition rate $\mathrm{d}\alpha_{(r)}/\mathrm{d}t$, local degree of transition $\alpha_{(r)}$ and local temperature $T_{(r)}$ (where λ_s, C_s and ΔH are, respectively, standard sample heat conductivity, sample heat capacity and integral enthalpy of transition. Then, [57]

$$(\mathrm{d}\alpha_{(r)}/\mathrm{d}t) = \left\{\left[\mathrm{d}^2T_{(r)}/\mathrm{d}r^2(1+1/r)\right](\lambda_s/C_s) - \mathrm{d}T_{(r)}/\mathrm{d}t\right\}/(\Delta H/C_s), \tag{3.17}$$

The actual form may become appropriate when fittingly applied for any position of r. However, such an innovative approach to non-isothermal kinetics would require not only a newly inspired researcher philosophy but also a novel experimental techniques allowing verification of such spatial kinetic models. This proposition returns factually to the early call for an alternative kinetic route as to provide, instead of single values of activation energy, its spatially distributed sequence [114].

3.11 Discussion of the Legacy of Thermodynamics

The determination of temperature penetrated even to other domains of thermal physics and particularly astrophysics [116]. As we shown earlier [16, 116], the most of the arguments placed in favour of opposite formulae existing in the theory of relativistic transformation of temperature had paradoxically the common starting point, the postulating of the covariance of the first and the second law of thermodynamics under the Lorentz transformations. This assumption was made without

giving plausible theoretical reasons and without any experimental verification. However, as we are convinced, just this unjustified extrapolation of laws of classical thermodynamics, together with spectacularly contradicting consequences, has revealed their weakness and principal inconsistency. In this context, one must revise the concept of heat and especially the first law of thermodynamics which is probably the most harmful statement in thermal physics [117]. Of course, it is generally believed and many mainstream authors claim that the first law of thermodynamics is nothing but the formulation of the general principle of conservation of energy and thermal phenomena including the principle which can only hardly be contested. However, just opposite is true. The first law is in fact fully dependent on validity of Joule–Mayer's postulate of equivalence of heat and work, which is in fact nothing but quite an arbitrary statement about the nature of heat [23]. In order to support such a not very usual view, let us make a short digression to the early history of Joule–Mayer's "principle" of equivalence.

The principle of equivalence of work and heat (PE) is usually proclaimed to be an experimental fact, being, nevertheless, quite an arbitrary postulate without any experimental support. We are aware that such a statement is in total contradiction with practically all modern college texts on thermodynamics, where the PE is considered to be one of the "greatest achievements of experimental science" [118]. The inspection of Joule's paper [119], where the PE is reputedly proved by experiment, shows, however, that the work is fully devoted to another subject, viz. to the determination of "mechanical equivalent of heat" (J) by various experimental methods. The merit of the work is thus quite different from that usually reported; Joule first assumed that the heat unit calorie is a unit of work (energy) and then determined the conversion factor J ($J = 4.2$ J/cal) between calorie and mechanical units. Indeed, the PE was originally the main conclusion of the paper, but under the influence of Faraday, who was the referee of this paper [120], it was omitted. Faraday, recognizing the circular reasoning, rated PE as a "strange conclusion" which was "deduced most illogically" from the experiments and rejected the paper in this form. Nevertheless, the amended paper finally appeared (without PE!) in Phil. Trans., and due to the good deal of experimental work involved, it became very famous. Following the publication of this paper, J. P. Joule was elected to fellowship in the Royal Society, and his reputation as a scientist was firmly established.

Later, probably on the basis of private communications, the PE treated as an experimental fact was pushed through by authorities in dynamical theory of heat (Kelvin and Clausius). In order to complete the picture, it should be stressed here that the determination of mechanical equivalent of heat is not firmly connected with PE. For example, a similar figure for this factor ($J \sim 4.2$ (J/cal)) was much earlier obtained by Carnot [121] using considerations fully belonging to the caloric theory of heat which is absolutely incompatible with PE. Also, all the later experiments devoted to the more precise determination of J, which followed the line of

published Joule's paper, are thus, on the same grounds, also irrelevant for the proof of PE. Mayer's speculation leading to the formulation of PE is even more untenable [122]. It is fully based on a logically doubtful "philosophical principle" (used already by Descartes for the scientific proof of God's existence) *causa aequat effectum*, which means that if the cause c has the effect e, then $c = e$. Accordingly, interpreting the last "equation" verbatim, cause and effect are inevitably the same entities having the same physical nature, dimension and magnitude. Taking then into account the qualitative observation that, in some cases, the motion disappears giving rises to heat and vice versa, Mayer inferred that motion and heat are physically identical. (It is astonishing to recognize such a dangerous type of deduction just by Mayer who was physician!) The very fact that the existence of a certain experimentally measurable coefficient called "mechanical equivalent of heat" does not imply the validity of Joule–Mayer's postulate may be clearly illustrated by means of the "prethermodynamics" operational definition of heat unit which is due to Fourier [83]. Accordingly, "Different quantities of heat are measured by determining how many times they contain a fixed quantity which is taken as the unit. Suppose a mass of ice having as a definite weight (a kilogramme) to be at temperature 0°, and to be converted into water at the same temperature 0° by the addition of certain quantity of heat: the quantity of heat thus added is taken as the unit of measure. Hence the quantity of heat expressed by a number C contains C times the quantity required to melt a kilogramme of ice at the temperature zero into a mass of water at the same zero temperature". From this quotation, it is evident that Fourier in his definition, playing a role of a standard in Carnot's times, does not need to distinguish the actual physical dimension of heat, measured simply in kilograms of melted ice. Indeed, as the latent heat of fusion of ice in contemporary energy units is $\sim 3.34 \times 10^5$ J/kg, we can compute, according to Fourier's prescription above, different "units of heat" which may thus have either a dimension of energy (1 unit = 3.34×10^5 J) or of entropy (1 unit = 1.22×10^3 J/K = 1.22×10^3 Ct). Summarizing, it can be claimed that there is no experimental proof of the PE at all.

The idea that measurement of heat is a matter of our decision was about one hundred years later, in pregnant way, formulated also by Lunn [123] who discussed especially the mathematical aspects of the problem. Therefore, as we believe, from this exposition, it might be obvious that the experimental determination of a conversion factor between arbitrary chosen units of heat cannot be interpreted as an experimental proof of the "true" dimension of the heat or even of its physical nature.

Another serious conceptual problem invoked by PE is that in contrast to all other kinds of energy, the Joule–Mayer's heat is not fully convertible to another form of energy. This anomaly, which is in fact the very subject of the second law of thermodynamics, leads already E. Mach to the suspicion that the heat is not a form

of energy at all [124]. Moreover, the statement proclaimed in many modern textbooks of thermodynamics (see, e.g., [125, 126]) that the only attribute distinguishing the heat from other forms of energy is its movement (heat is defined as "the energy in transit") is also somewhat questionable. There are, namely, many cases where the energy moves obviously without having attributes of heat; transfer of energy through driving shaft from engine to car wheels may serve as a good example.

3.12 Conclusion

In this contribution, we tried to show that the concept of temperature which plays a decisive role in the fields of thermal physics, thermodynamics and thermal analysis is often underestimated. We hope that above paragraphs shed some light on the various aspects of temperature, especially its standing within wide-ranging concepts of thermodynamics and helped transfigure the widespread opinion that the measured temperature is something trivial. Despite the prevailing confidence in the classical roots of thermodynamics, we must not be afraid of dialogue, even though it can bring unusual changes.

Acknowledgements The work was developed at the Join Research Laboratory of the Institute of Physics CAS, v.v.i., and the New Technologies Centre (NTC) of the University of West Bohemia in Pilsen and supported by the CENTEM project, reg. no. CZ.1.05/2.1.00/03.0088 that is cofunded from the ERDF as a part of the MEYS—Ministry of Education, Youth and Sports OP RDI Program, and, in the follow-up sustainability stage, supported through the CENTEM PLUS LO 1402.

References

1. Truesdell C (1969) Rational thermodynamics. McGraw-Hill, New York, p 6
2. Tolman RC (1938) The principles of statistical mechanics. Oxford University Press, London, pp 93 and 655; and Terletskii YP (1966) Statistical physics, Izd. Vysshaya Shkola, Moscow, p 47 (in Russian); and Kittel C, Kroemer H (1980) Thermal physics, 2nd edn. Freeman Company, pp 391–397
3. Carathéodory C (1909) Untersuchungen über die Grundlagen der Thermodynamik. Math Ann 67:355
4. Müller I (2007) A history of thermodynamics. Springer, Berlin
5. Proks I (1991) Evaluation of the knowledge of phase equilibrium. In: Chvoj Z, Šesták J, Tříska A (eds) Kinetic phase diagrams: nonequilibrium phase transitions. Elsevier, Amsterdam, pp 1–49
6. Šesták J, Mackenzie RC (2001) The heat/fire concept and its journey from prehistoric time into the third millennium. J Therm Anal Calorim 64:129–147
7. Barnett MK (1956) The development of thermometry and the temperature concept. Osiris 12:269–341
8. Cardillo P (2002) A history of thermochemistry through the tribulations of its development. J Therm Anal Calorim 72:7
9. Šesták J, Mareš JJ (2007) From caloric to stathmograph and polarography. J Therm Anal Calorim 88:763
10. Šesták J (2013) Thermal science and analysis: terms connotation, history, development, and the role of personalities. J Therm Anal Calorim 113:1049–1054
11. Šesták J (2011) Some historical features focused back to the process of European education revealing some important scientists, roots of thermal analysis and the origin of glass research. In: Šesták J, Holeček M, Málek J (eds) Thermodynamic, structural and behavioural aspects of materials accentuating noncrystalline states. ZČU-OPS, Pilsen, pp 30–58
12. Šesták J, Hubík P, Mareš JJ (2011) Historical roots and development of thermal analysis and calorimetry. In: Šesták J, Mareš JJ, Hubík P (eds) Glassy, amorphous and nano-crystalline materials. Springer, London, pp 347–370
13. Mackenzie R, Proks I (1985) Comenius and Black as progenitors of thermal analysis. Thermochim Acta 92:3–12
14. Proks I (2012) The whole is simpler than its parts: chapters from the history of exact sciences. Veda-Slovak Academy of Sciences, Bratislava (book in Slovak)
15. Mareš JJ (2000) On the development of temperature concept. J Thermal Anal Calor 60:1081
16. Mareš JJ (2011) Phenomenological meaning of temperature. In: J. Šesták, Holeček M, Málek J (eds) Thermodynamic, structural and behavioural aspects of materials accentuating noncrystalline states ZČU-OPS, Pilsen, pp 60–78. ISBN 978-80-87269-20-6
17. Mareš JJ (2011) Hotness manifold, phenomenological temperature and other related concepts of thermal physics. In: Šesták J, Mareš JJ, Hubík P (eds) Glassy, amorphous and nano-crystalline materials. London, Springer, pp 327–345
18. Mareš JJ (2015) Do we know what temperature is? J Thermal Anal Calorim 120:223–230
19. Mach E (1896) Die Prinzipien der Wärmelehre. Verlag von J.A. Barth, Leipzig
20. Huntington EV (1917) The continuum and other types of serial order. Harvard University Press, New York
21. Epstein PS (1954) Textbook of thermodynamics. Wiley, New York
22. Boyer CB (1942) Early principles in the calibration of thermometers. Am J Phys 10:176–180
23. Mareš JJ, Hubík P, Šesták J, Špička V, Krištofik J, Stávek J (2008) Phenomenological approach to the caloric theory of heat. Thermochim Acta 474:16–24
24. Šesták J, Mareš JJ, Hubík P, Proks I (2009) Contribution by Lazare and Sadi Carnot to the caloric theory of heat and its inspirative role in alternative thermodynamics. J Thermal Anal Calor 97:679–683

25. Maxwell JC (1871) Theory of heat. Longmans Green, London
26. Van der Waals J, Kohnstamm P (1927) Lehrbuch der Thermostatik. Verlag von J.A. Barth, Leipzig
27. Landsberg PT (1956) Foundations of thermodynamics. Rev Mod Phys 28:363–392
28. Callen HB (1960) Thermodynamics: an introduction to thermostatics. Wiley, New York
29. Tribus M (1961) Thermostatics and thermodynamics: an introduction to energy, information and states of matter. Nostrand, New York
30. McGee TD (1988) Principles and methods of temperature measurement. Wiley, New York
31. Sears FW (1963) A simplification of Carathéodory's treatment of thermodynamics. Am J Phys 31:747–752
32. Turner LA (1963) Temperature and Carathéodory's treatment of thermodynamics. J Chem Phys 38:1163–1167
33. Pogliani L, Berberan-Santos MN (2000) Carathéodory and the axiomatic thermodynamics. J Mathemat Chem 28:1–3
34. Gibbs JW (1902) Elementary principles in statistical mechanics. Yale University Press, New Haven
35. Quinn STJ (1983) Temperature. Academic Press, London. ISBN 0-12-569680-9
36. Temperature definition: https://en.wikipedia.org/wiki/Thermodynamic_temperature
37. Efremov MY, Olson EA, Zhang M, Schiettekatte F, Zhang Z, Allen LH (2004) Ultrasensitive, fast, thin-film differential scanning calorimeter. Rev Sci Instrum 75:179–191; and Zhuravlev E, Schick C (2010) Fast scanning power compensated differential scanning nano-calorimeter: the device. Thermochim Acta 505:14–21
38. Adamovsky AS, Minakov AA, Schick C (2003) Scanning microcalorimetry at high cooling rate. Thermochim Acta 403:55–63; and Minakov AA, Schick C (2007) Ultrafast thermal processing and nanocalorimetry at heating and cooling rates up to 1 MK/s. Rev Sci Instr 78:073902(10)
39. Šesták J (2005) Science of heat and thermophysical studies: a generalized approaches to thermal analysis. Elsevier, Amsterdam, pp 379–401
40. Holeček M (2009) Diffusion and the self-measurability. Appl Comput Mech 3:51–62
41. Muschik W (1977) Empirical foundation and axiomatic treatment of non-equilibrium temperature. Arch Rat Mech Anal 66:379–401
42. Casas-Vazquez J, Jou D (2003) Temperature in non-equilibrium states: a review of open problems and current proposals. Rep Prog Phys 66:1937–2013
43. Holeček M (2015) Self-measurability in rapid thermal processes. J Thermal Anal Calor 120:217–221
44. Voldřich J (2002) Averaging over N-dimensional balls and Cauchy problem for equations of mathematical physics. J Math Anal Appl 272:582
45. Cattaneo C (1958) Sur une forme de l'équation de la chaleur éliminant le paradoxe d'une propagation instantanée. C R Hebd Seances Acad Sci 247:431–433
46. Joseph DD, Preziosi L (1989) Heat waves. Rev Mod Phys 61:41
47. Tzou DY (1996) Macro- to microscale heat transfer. Taylor & Francis, Washington
48. Volz S (ed) (2007) Microscale and nanoscale heat transfer. Springer, Heidelberg
49. Vilar JMG, Rubí JM (2001) Thermodynamics "beyond" local equilibrium. Proc Natl Acad Sci USA 98:11081–11084
50. Holeček M (1992) Heat conduction equations as the continuum limits of the scale dependent hydrodynamics theory. Phys A 183:236–246
51. Thomson W (Lord Kelvin of Largs) (1848) On the absolute thermometric scale founded on Carnot's theory of the motive power of heat. Phil Mag 33:313
52. Callendar HL (1911) The caloric theory of heat and Carnot's principle. Proc Phys Soc London 23:153
53. Zemansky MV (1968) Heat and thermodynamics. McGraw-Hill, Kogakusha, Tokyo
54. Šesták J (1979) Thermodynamic basis for the theoretical description and correct interpretation of thermoanalytical experiments. Thermochim Acta 28:197–227

55. Šesták J (1984) Thermophysical properties of solids: theoretical thermal analysis. Elsevier, Amsterdam. ISBN 0 444 99653. Czech original by Academia, Praha 1982 and Russian translation by Mir, Moscow 1988
56. Šesták J (2015) Kinetic phase diagrams as a consequence of sudden changing temperature or particle size. J Thermal Anal Calor 120:129–137
57. Holba P (2016) Šesták's proposal of term "tempericity" for non-equilibrium temperature and modified Tykodi's thermal science classification with regards to methods of thermal analysis. J Therm Anal Calorim. doi:10.1007/s10973-016-5659-4; and (2017) Temperature dependence of activation energy of endothermic processes and related imperfections of non-isothermal kinetic evaluations. J Therm Anal Calorim doi: 10.1007/s10973-017-6088-8
58. Lebon G, Jou D, Casas-Vásquez J (2008) Understanding non-equilibrium thermodynamics. Springer, Berlin
59. Šesták J (2016) Measuring "hotness", should the sensor's readings for rapid temperature changes be named "tempericity"? J Therm Anal Calorim 125:991–999
60. Sertorio L (1991) Thermodynamics of complex systems. World Scientific, Singapore
61. Jou D, Casas-Vazquez J, Lebon G (1993) Extended irreversible thermodynamics. Springer, Berlin
62. Adamovsky SA, Schick C (2004) Ultra-fast isothermal calorimetry using thin film sensors. Thermochim Acta 415:1–7; and Minakov AA, Adamovsky SA, Schick C (2005) Non-adiabatic thin-film-chip nanocalorimetry. Thermochim Acta 432:177–185
63. Šesták J (2004) Thermodynamics and society—laws versus feelings. Chapter 18 in his book "Heat, Thermal Analysis and Society". Nucleus, Hradec Kralove. ISBN 8-86225-54-2, pp 298–302
64. Šesták J (2005) Thermodynamics, econophysics and societal behavior. Chapter 8 in his book "Science of heat and thermophysical studies: a generalized approach to thermal analysis". Elsevier, Amsterdam. ISBN 444 51954 8, pp 230–246
65. Golding B (1839) Two chapters on thermotics, in book "Elements of natural philosophy: the study of the physical sciences". John Churchill, London
66. Tykodi RJ (1967) Thermodynamics of steady state. MacMillan, New York
67. Brønsted J (1955) Principles and problems in energetics. Interscience, New York
68. Tykodi RJ (1968) Correspondence: thermodynamics—thermotics as the name of the game. Ind Eng Chem 60:22
69. Parker PM (ed) (2012) Thermal analysis: Webster's timeline history, 1909–2007. Icon Group International
70. Šesták J, Chvoj Z (1987) Thermodynamics of kinetic phase diagrams. J Thermal Anal 32:325–333
71. Chvoj Z, Šesták J, Tříska A (eds) (1991) Kinetic phase diagrams: non-equilibrium phase transitions. Elsevier, Amsterdam. ISBN 0-444-88513-7
72. Šesták J, Queiroz CA, Mareš JJ, Holeček M (2011) Some aspects of quenching, vitrification, amorphization, disordering and the extent of nano-crystallinity. In: Šesták J, Mareš JJ, Hubík P (eds) Chapter 4 in Glassy, amorphous and nano-crystalline materials. Springer, Berlin, Heidelberg, pp 59–76
73. Šesták J, Holba P (2013) Heat inertia and temperature gradient in the treatment of DTA peaks: existing on every occasion of real measurements but until now omitted. J Thermal Anal Calorim 113:1633–1643
74. Holba P, Šesták J, Sedmidubský D (2013) Heat transfer and phase transition at DTA experiments. In: Šesták J, Šimon P (eds) Chapter 5 inThermal analysis of micro-, nano- and non-crystalline materials. Springer, Berlin, pp 99–134
75. Smyth HT (1951) Temperature distribution during mineral inversion and its significance in DTA. J Amer Cer Soc 34:221–224
76. Kornilov VV, Makarov BI (1963) Measurement of rapidly changing temperatures of conducting solid bodies by means of thermocouples. Measur Tech 6:849–851
77. Minakov AA, van Herwaarden AW, Wien W, Wurm A, Schick C (2007) Advanced nonadiabatic ultrafast nanocalorimetry and superheating phenomenon in linear polymers.

Thermochim Acta 461:96–106; and Salinga M, Carria E, Kaldenbach A, Bornhöfft M, Benke J, Mayer J, Wuttig M (2013) Measurement of crystal growth velocity in a melt-quenched phase-change material. Nat Comm 4:2371
78. Minakov A, Morikawa J, Hashimoto T, Huth H, Schick C (2006) Temperature distribution in a thin-film chip utilized for advanced nanocalorimetry. Meas Sci Technol 17:199–207; and Minakov AA, Schick C (2015) Dynamics of the temperature distribution in ultra-fast thin-film calorimeter sensors. Thermochim Acta 603:205–217; and Minakov AA, Schick C (2015) Dynamics of the temperature distribution in ultra-fast thin-film calorimeter sensors. Thermochim Acta 603:205–217
79. Mareš JJ, Šesták J, Hubík P (2011) Transport constitutive relations, quantum diffusion and periodic reactions. In: Šesták J, Mareš JJ, Hubík P (eds) Chapter 14 in: Glassy, amorphous and nano-crystalline materials Springer, Berlin, pp 227–244
80. Lerchner JA, Wolf G, Wolf J (1999) Recent developments in integrated circuit calorimetry J Therm Anal Calorim 57:241; and Merzlyakov M (2003) Integrated circuit thermopile as a new type of temperature modulated calorimeter. Thermochim Acta 403:65
81. Lyon RE, Safronova N, Senese J, Stoliarov SI (2012) Thermokinetic model of sample centred response in non-isothermal analysis. Thermochim Acta 545:82–89
82. Sánchez-Rodríguez D, Eloussifi H, Farjas J, Roura P, Dammak M (2014) Thermal gradients in thermal analysis experiments: criterions to prevent inaccuracies when determining sample temperature and kinetic parameters. ThermochimActa 589:37–46
83. Fourier JBJ (1822) Théorie analytique de la chaleur. Paris (English transl.: The Analytical Theory of Heat). Dover Publications, Mineola, New York 2003
84. Fuchs HU (2010) The dynamics of heat. Springer, New York
85. Fick AE (1855) Über diffusion. Ann Phys Chem von Poggendorff 94:59
86. Ohm GS (1827) Die galvanische Kette, mathematisch bearbeitet. J. G. F. Kniestdt for T. H. Riemann, Berlin
87. Kirchhoff G (1849) Über eine Ableitung der Ohm'schen Gesetze, welche sich an die Theorie der Elektrostatik anschliest. Ann Phys 154:506–513
88. Onsager L (1931) Reciprocal relations in irreversible processes I and II. Phys Rev 37:405–426; Phys Rev 38:2265–2279
89. Miller DG (1960) Thermodynamics of irreversible processes: experimental verification of the Onsager reciprocal relations. Chem Rev 60:15–37
90. Stöckel H (1983) Linear and nonlinear generalizations of Onsager's reciprocity relations treatment of an example of chemical reaction kinetics. Fortsch Physik—Progr Phys 31:165–184
91. Holba P, Šesták J (2015) Heat inertia and its role in thermal analysis. J Thermal Anal Calor 121:303–307
92. Schultze D (1969) Differential thermo analyse. VEB Deutscher Verlag, Berlin; and Polish translation (1974) Różnicowa analiza termiczna. PWN, Warsaw
93. Hemminger W, Höhne GWH (1979) Grundlagen der Kalorimetrie. Verlag Chemie, Weinheim; and (1984) Calorimetry: fundamentals and practice. Verlag Chemie, Weinheim
94. Chen R, Kirsh Y (1981) Analysis of thermally stimulated processes. Pergamon Press, Oxford, pp 109–110
95. Šesták J (2005) Science of heat and thermophysical studies: a generalized approach to thermal analysis. Elsevier, Amsterdam
96. Boerio-Goates J, Callen JE (1992) Differential thermal methods. In: Rossiter BW, Beatzold RC (eds) Chapter 8 in Determination of thermodynamic properties. Wiley, New York, pp 621–718
97. Kittl JA, Reitano R, Aziz MJ, Brunco DP, Thompson MO (1993) Time-resolved temperature measurements during rapid solidification of Si–As alloys induced by pulsed-laser melting. J Appl Phys 73:3725–3733
98. Zhuravlev E, Schmelzer JWP, Wunderlich B, Schick C (2011) Kinetics of nucleation and crystallization in poly(3-caprolactone). Polymer 52:1983–1997

99. Flynn JH (1970) An analytical evaluation of DSC observing metastability. In: Menis O (ed) Status of thermal analysis. Special NBS publication no. 338, p 119
100. Newton I (originally anonymously) (1701) Scale graduum caloris. Calorum descriptiones & signa. Philos Trans 22:824–29
101. Grigull U (1984) Newton's temperature scale and the law of cooling. Wärme Stoffübertragung 18:195–199
102. Gray AP (1968) Simple generalized theory for analysis of dynamic thermal measurements. In: Porter RS, Johnson JF (eds) Compendium: analytical calorimetry, vol. 1. Plenum Press, New York, pp 209–213
103. Farjas J, Roura P (2014) Exact analytical solution for the Kissinger equation: determination of the peak temperature and general properties of thermally activated transformations. Thermochim Acta 508:51–5894
104. Holba P, Šesták J (2014) Imperfections of Kissinger evaluation method and crystallization kinetics. Glass Phys Chem 40:486–49
105. Kissinger HE (1957) Reaction kinetics in differential thermal analysis. Anal Chem 29:1702–1706
106. Svoboda R (2015) Glass transition kinetics measured by fast scanning calorimetry: effect of thermal gradients. J Therm Anal Calorim 122:985–995
107. Svoboda H, Šesták J (1974) A new approach to DTA calibration by predetermined amount of Joule heat via rectangular pulses. In: Buzas I (ed) Thermal analysis, proceedings of the 4th ICTA, Akademia Kiado, Budapest, pp 726–731
108. Holba P, Nevřiva M, Šesták J (1978) Analysis of DTA curve and related calculation of kinetic data using computer technique. Thermochim Acta 23:223–231
109. Kirchner R, Seidel K, Wolf G (1998) Electrical calibration and testing of calorimeters with simulated, time-variable reaction power. Thermochim Acta 310:19–24
110. Barale S, Vincent L, Sauder G, Sbirrazzuoli N (2015) Deconvolution of calorimeter response from electrical signals for extracting kinetic data. Thermochim Acta 615:30–37
111. Mouchina E, Kaisersberger E (2009) Temperature dependence of the time constants for deconvolution of heat flow curves. Thermochim Acta 492:101–109
112. Kubičár Ľ (1990) Pulse method of measuring basic thermophysical parameters. Elsevier, Amsterdam
113. Blumm J, Opfermann J (2002) Improvement of the mathematical modeling of flash measurements. High Temp—High Pres 34:515
114. Šesták J, Holba P (2017) Quo Vadis of nonisothermal kinetics (in the course of preparation); and (2016) Piloyan method to determine the activation energy from DTA is defective in addition to other methods which do not take into account the thermal inertia. J Anal Bioanal Tech 7:331 (open access doi:10.4172/2155-9872.1000331)
115. Cantwell PR, Tang M, Dillon SJ, Luo J, Rohrer GS, Harmer MP (2014) Grain boundary complexions (overview No. 152). Acta Mater 62:1–48; and Kaptay G (2016) Modeling equilibrium grain boundary segregation, grain boundary energy and grain boundary segregation transition by the extended Butler equation. J Mater Sci 51:1738–1755
116. Mareš JJ, Hubík P, Šesták J, Špička V, Krištofik J, Stávek J (2010) Relativistic transformation of temperature and Mosengeil-Ott's antinomy. Physica E 42:484–487
117. Job G, Lankau T (2003) How harmful is the first law? Ann Acad NY Sci 988:171–181
118. Shamos MH (1953) Great experiments in physics. Dover Publications Inc, New York
119. Joule JP (1850) On the mechanical equivalent of heat. Phil Trans Roy Soc London 140:61–82
120. Smith CW (1976) Faraday as referee of Joule's royal society paper "On the mechanical equivalent of heat". Isis 67:444–449
121. Carnot S (1824) Réflexions sur la puissance motrice du feu et sur les machines propres à développer cette puissance. Bachelier, Paris; Germ. Transl. (1909) Ostwald's Klassiker 37. Engelmann, Leipzig
122. Mayer JR (1842) Bemerkungen über die Kräfte der unbelebten Natur. Ann Chem Pharm 42:233–240; Reprint and English translation (1929) Isis 13:18–44

123. Lunn AC (1919) The measurement of heat and the scope of Carnot's principle. Phys Rev 14:1–19
124. Mach E (1923) Populär-Wissenschaftliche Vorlesungen. Verlag J.A. Barth, Leipzig
125. Blundell SJ, Blundell KM (2006) Concepts in thermal physics. Oxford University Press, New York
126. Wang L-S (2017) The function of heat: thermodynamics as a predicative entropic theory of heat. Springer, Book in the course of preparation; and (2017) The second law: from Carnot to Thomson-Clausius, to the theory of exergy, and to the entropy-growth potential principle. Entropy 57:2–19; doi: 10.3390/e19020057

Chapter 4
What Is Entropy—A Generalized Outlook and Application to Living Systems

F. Maršík, P. Novotný and M. Tomáš

Abstract Thermodynamics of open systems offers a new concept for description of real material objects including the living systems. The second law of thermodynamics can be interpreted as an evolution law of all material systems, which are in interaction with surroundings. The most important quantity is entropy, which is defined by balance of entropy. The production of entropy gives information about the processes in the systems. The convexity of entropy informs about the stability of the system states. Under the appropriate outer conditions, the fluctuations can force the systems to instability. Consequence is the creation or decay of new dissipative structures. When the new dissipative structure appears, the system is going out of the thermodynamic equilibrium to the new stable state. However, if the dissipative structure disappears, the systems will tend to the thermodynamic equilibrium. From the biological point of view, the thermodynamic equilibrium equals to death.

4.1 Introduction

Thermodynamics deals with states of systems and processes running inside and around systems. There are two kinds of the processes: reversible processes and irreversible processes, respectively. Study of these processes leads to the conclusion that every effect has its cause. This simple conclusion defines causality [1]. Let us suppose that all of the processes run according to the causality, so that the effects can be predicted. Problem of determinism related to this assumption defines an

F. Maršík (✉) · P. Novotný · M. Tomáš
New Technologies—Research Centre, University of West Bohemia,
Univerzitni 8, 306 14 Pilsen, Czech Republic
e-mail: marsik@it.cas.cz

P. Novotný
e-mail: novotnyp@ntc.zcu.cz

M. Tomáš
e-mail: mtomas@ntc.zcu.cz

J. Šesták et al. (eds.), *Thermal Physics and Thermal Analysis*,
Hot Topics in Thermal Analysis and Calorimetry 11,
DOI 10.1007/978-3-319-45899-1_4

accuracy of the effect prediction. Supposing further that the same conclusion, i.e., the prediction that has to be reached independently on position of an observer, exists. This assumption is called an objectivity [1, 2].

The balance laws, i.e., balance of mass, balance of energy, and balance of force, describe all of these properties of a system evolution and prediction. However, balance law formulations do not provide sufficient information on all of utilized variables. As an example can be mentioned the heat flux and diffusion flux, the chemical reaction rate, the dependency of the pressure on density and of the stress tensor on a strain tensor, respectively. These relations are known as the constitutive relations or the state equations, which define properties of the (material) systems. Knowledge of these constitutive relations is crucial to determine the prediction of the system evolution. Formulation and deep analysis of these constitutive relations are subjects of thermodynamics [3–6].

Thermodynamics results from the general outcomes of energy and matter transformation, so that it can be considered as a dialectics of matter and field. Thermodynamics deals with real objects, i.e., *thermodynamic systems*, consisted of many interacting parts, i.e., thermodynamic subsystems such as atoms, molecules, and even cells, genes, etc. [7]. The elementary thermodynamic subsystem used in the continuum mechanics is a material point, e.g., solid bodies, fluids, biological system, or its parts and/or ecological system (see, e.g., [6, 8]). The interaction is understood as effects between bodies in the nature, such as energy transformation, momentum changes, and matter exchange. The elementary terms used in thermodynamics are temperature, energy, entropy, and work [9]. These terms are used to derive the fundamental thermodynamic laws, which are depicted as follows [9]:

- *The zeroth law of thermodynamics*: the concept of temperature,
- *The first law of thermodynamics*: the conservation of the total energy,
- *The second law of thermodynamics*: production of entropy is always positive, and
- *The third law of thermodynamics*: the unattainability of the zero temperature.

Temperature has two interpretations. The first interpretation is well-known phenomenological one, i.e., data of the calibrated thermometer. The second one is the interpretation on subsystems level, i.e., molecules and atoms. On the subsystems level, temperature is a measure of energy mean value that is interchanged by subsystems [10]. Benefits of this interpretation are obvious in description of biological and ecological systems, where changed energy has different forms (form of energy can be literary money). Microscopic interpretation of entropy is a measure of an accidental nature during system evolution. Usual interpretation is connected with losses during transformations of different forms of energy. Furthermore, stability of systems evolution can be interpreted by entropy, concretely by the second differential of entropy. The second differential of entropy is interpreted as mean value of fluctuations of variables (temperature, density, concentration, etc.) around mean (equilibrium or reference) values [4]. Thus, the second differential of entropy is crucial for the description of stability of state and processes in more general sense, where process is represented by a time sequence of states.

The second law of thermodynamics is usually interpreted by two independent statements [10–12]:

(i) *Time irreversibility of processes*: A system non-interacting with surroundings is unable itself to reach an original state.
(ii) *The most probability of state*: A system occupies the most probable state with respect to the specific conditions.

The variable of entropy, S [J K^{-1}], is not explicitly mentioned in these statements. In general, entropy is defined as a macroscopic variable characterizing properties of the matter and describing a measure of randomness in the system evolution. Furthermore, it is possible to implicitly describe all of the real systems in terms of entropy. Moreover, entropy is usable to characterize even the non-material systems out of the field of thermodynamics.

Sir A.S. Eddington pronounced very interesting view on entropy that sounds [13]: "I cannot read any significance into a physical world when it is held before me upside down. For that reason I am interested in entropy not only because it shorten calculations which can be made by other methods, but because it determines an orientation which cannot be found by other methods."

Historical concept and interpretation of entropy are summarized in Table 4.1, where author's name with the symbol * stands for the Nobel Laureate in chemistry.

Table 4.1 Historical concept and interpretation of entropy

Name (year)	Interpretation
R. Clausius (1865)	Phenomenological approach: $\mathrm{d}S \geq \text{đ}Q / \mathrm{d}T$, đ$Q$ is the heat added to the system [14]
J.W. Gibbs* (1884)	Probabilistic approach: $S = k \ln \Gamma$, the system is in the most probable state defined by Γ, and k is the Boltzmann constant [15]
L. Boltzmann (1886)	Microscopic approach: $S = -k \int f \ln \mathrm{d}\lvert\mathbf{v}\rvert, f(\lvert\mathbf{v}\rvert)$ is the distribution function of molecular velocity $\mathbf{v}$ [16]
A. Einstein (1910)	Maximum entropy condition $\mathrm{d}^2 S < 0$; entropy of the system decreases due to fluctuations near the equilibrium state [17]
L. Onsager* (1933)	The entropy production $P(S) = \sum_i J_i X_i > 0$ is always positive; the thermodynamic fluxes $J_i = \sum_j L_{ij} X_j$ depend on the thermodynamic forces, where X_i, L_{ij} is reciprocal relation [18, 19]
E. Schrödinger (1945)	There is a negative entropy flux $-\bar{J}(S) = P(S) > 0$ that keeps the biological system in the thermodynamic non-equilibrium [20]
I. Prigogine* (1947)	Formulation of the minimal production of entropy $\mathrm{d}P(S)/\mathrm{d}t \geq 0$ (valid for systems in the dynamical equilibrium) [4]
M. Eigen* (1957)	According to the principle of the minimal production of entropy, i.e., $\min P(S)$, a competition of complex molecules during the recycling process leads to the finite number of amino acids [21, 22]
I. Prigogine* (1977)	The open system is in the stable dynamical equilibrium with the maximal thermodynamic efficiency [12]

The (Clausius) definition of entropy is in more detail discussed in the following sections

4.2 Entropy

4.2.1 *Balance of Entropy—System Entropy Near an Equilibrium State*

Stability of states and dissipative processes in a system are closely related to the existence of that system and to time irreversibility of the system evolution. Number of the non-dissipative system states is constant with time evolution, so that the time evolution of the system is reversible. On the contrary, the number of the real system states decreases with time evolution. Moreover, instabilities can occur in the time evolution for the real nonlinear systems [4, 23]. A decrease of the system states number does not allow determination of a system initiate state, which is the consequence of the time irreversibility of the system evolution (see, e.g., [5]). A macroscopic state of a system in thermodynamic equilibrium corresponds to the maximum number of microscopic states without any mutual correlations. This statement is not valid for the system in thermodynamic non-equilibrium, in which non-equilibrium is maintained due to the interaction with surroundings. The non-equilibrium is exhibited by the decrease of the number of microscopic states due to mutual correlations [12].

These mentioned assumptions are quantified via following variables—total entropy of the system S, entropy flux into the system $\overline{J}(S)$, and production of entropy inside the system $P(S)$. Changes of the system are characterized by the time change (derivative) of entropy $\dot{S}$, which is a consequence of an interaction of the system with surroundings by the entropy flux $\overline{J}(S)$ and internal processes in the system generating the entropy production $P(S)$. A specific expression of these variables is obtained by the balance laws depending on the system structure, i.e., balance of mass, balance of momentum, and balance of angular momentum.

An elementary evolution law can be written in terms of balance of entropy

$$\dot{S} - \overline{J}(S) = P(S) \geq 0, \tag{4.1}$$

where the non-dissipative processes obey a condition $P(S) = 0$, and the dissipative processes obey a condition $P(S) > 0$. The system of a volume V bounded by a surface A is described as follows

$$S = \int_V \rho s \mathrm{d}v, \quad \overline{J}(S) = -\int_A \mathbf{j}_{\mathrm{eq}}(S)\mathrm{d}\mathbf{a}, \quad P(S) = \int_V \sigma(S)\mathrm{d}v, \tag{4.2}$$

where the variables are specific entropy s [J kg^{-1} K^{-1}], density ρ [kg m^{-3}], density of entropy flux $j_{\mathrm{eq}}(S)$ [J m^{-2} K^{-1}], and density of entropy production $\sigma(S)$ [J m^{-3} K^{-1}], respectively. The entropy production depends on the balance laws, i.e., balance of mass, balance of momentum, balance of angular momentum, balance of mechanical energy, balance of internal energy, and balance/definition of entropy.

Table 4.2 Thermodynamic fluxes and forces for Gibbs definition of entropy (4.20) in local equilibrium states

Thermodynamic flux J_i	Thermodynamic force X_i
Heat conduction $\mathbf{j}_q$	$\nabla 1/T$
Thermodiffusion $\mathbf{j}_{D\alpha} h_\alpha$	$\nabla 1/T$
Diffusion $\mathbf{j}_{D\alpha}$	$\nabla \mu_\alpha/T$
Electric flux $\mathbf{j}_{e,\alpha}$	$\mathbf{F}_\alpha/T = -[(z_\alpha F)/(M_\alpha T)]\nabla\phi$
Viscoplastic processes	
(i) for solids $\mathbf{t}_{\text{dis}}(T, \mathbf{d}, \dot{\mathbf{t}}_{\text{dis}})$	$\mathbf{d}/T$
(ii) for fluids p_{dis}	$(\nabla \cdot \mathbf{v})/T$
(iii) viscosity $\mathbf{t}_{\text{dis}} - \sum_\alpha \rho_\alpha \mathbf{v}_{D\alpha} \otimes \mathbf{v}_{D\alpha}$	$\overset{(0)}{\mathbf{d}} \Big/ T$
Swelling $\mathbf{v}_{D\alpha}$	$\mathbf{t}_{\text{dis}\,\alpha} \cdot \nabla(1/T)$
Capillary flux $\mathbf{j}_{Dc}$	$\mathbf{\Gamma}_c/T = (1/T)\nabla(\sigma \cdot a)$
Chemical reactions and phase transitions $\dot{\xi}_\rho$	A_ρ/T

The Gibbs definition of entropy (4.20) is frequently used, and then, the entropy production is expressed as

$$P(S) = \int_V \sigma(S)\mathrm{d}v, \quad \text{for} \quad \sigma = \sum_i J_i X_i, \tag{4.3}$$

where the thermodynamic forces X_i and the thermodynamic fluxes J_i are summarized in Table 4.2 and in [3, 5, 23, 24].

But according to the Boltzmann relation, measure of the state probability is entropy of the system, where the states with higher entropy are the more probable states (see (4.7)). All real systems are in the state with maximum entropy, and hence, in the most probable state, see the statement (ii) of the second law of thermodynamics.

4.2.2 *Relations Between Fluctuations and Change of Entropy*

Time evolution of the thermodynamic system can be characterized among others by a stability condition, e.g., by Lyapunov function [4, 12]. It is impossible to theoretically derive an exact form of this function from mutual atomic and molecular interactions. This function can be estimated from macroscopic point of view. The form of the demanded Lyapunov function has to be connected to the probability of changes of the macroscopic state. Moreover, this function has to change sign in the points of instabilities with respect to fluctuations of the macroscopic variables.

A starting point is a relation for probability of fluctuation near an equilibrium state of the system. It is usually assumed that the relation for the probability of fluctuation (4.7) is valid even far from the state of local equilibrium, so that supposal of the equilibrium state of the system is not necessary.

The probability of fluctuation of a macroscopic variable is related to the total change of the system entropy caused by the fluctuation ΔS and is expressed by the Einstein relation [10]

$$\mathrm{Pr} \approx \exp \frac{\Delta S}{k}. \tag{4.4}$$

The Einstein relation is derived by the following assumptions. There is number of all microscopic system realizations in the equilibrium state Γ_{eq}, and the system maximum entropy is described as

$$S_{\mathrm{eq}} = k \ln \Gamma_{\mathrm{eq}}. \tag{4.5}$$

The number of the microscopic system realizations Γ_{noneq} decreases out of the equilibrium state, and the system entropy drops to the value S. The system can leave the equilibrium state spontaneously by internal processes, e.g., thermal motion of molecules, as a result of chemical reactions. So that, analogically to (4.5), it is possible to write

$$S = k \ln \Gamma_{\mathrm{noneq}}. \tag{4.6}$$

Probability of fluctuation of the macroscopic state is defined as a ratio

$$\mathrm{Pr} = \frac{\Gamma_{\mathrm{noneq}}}{\Gamma_{\mathrm{eq}}}$$

and usage of (4.5) and (4.6) allows to write following expression

$$\mathrm{Pr} = \exp \frac{S - S_{\mathrm{eq}}}{k} = \exp \frac{\Delta S}{k}, \quad S - S_{\mathrm{eq}} = \mathrm{d}S_{\mathrm{eq}} + \frac{1}{2}\mathrm{d}^2 S_{\mathrm{eq}} + \cdots, \tag{4.7}$$

where $\Delta S < 0$ is the total change of entropy caused by a fluctuation. Entropy reaches the local maximum in the equilibrium state, hence $\mathbf{d}S_{\mathrm{eq}} = 0$ and $(1/2)\mathrm{d}^2 S_{\mathrm{eq}} < 0$.

Relation (4.4) is useful mainly for the systems in the local thermodynamic equilibrium. Moreover, entropy has a physical meaning even in the local non-equilibrium states that is connected to the stability of the system state. Timescale of the fluctuations rising spontaneously inside the system is much lower than timescale of changes generated by boundary conditions. It is pragmatic to suppose that condition $(1/2)\mathrm{d}^2 S_{\mathrm{eq}} < 0$ involves an influence of the correlations between the fluctuations. The correlations are excluded in the case of the equilibrium states, which is valid even for the local equilibrium states in atomic and

molecular level. On the other hand, these correlations are crucial for the real systems and play key role in instabilities of the system states and the processes. All of above-mentioned assumptions are very useful to determine ΔS in (4.4) even for the open systems.

4.2.3 Thermodynamic Definition of Entropy

Entropy is defined implicitly by the Clausius inequality

$$\oint \frac{\text{đ}Q}{T} = \int_{t_1}^{t_2} \frac{\dot{Q}}{T}\,\mathrm{d}t \le 0\,. \tag{4.8}$$

This inequality means, that for each cycling process taking place in the system of a volume V, in which it is possible to measure temperature T, remains an amount of heat, which is necessary to remove from the system ($-\text{đ}Q > 0$ is added heat). The cyclic process consists of an irreversible part (real part) and a reversible part (equilibrium part) (see Fig. 4.1)

$$\oint \frac{\text{đ}Q}{T} = \underbrace{\int_1^2 \frac{\text{đ}Q}{T}}_{\text{ir} \Leftrightarrow \text{đ}Q = 0} + \underbrace{\int_2^1 \frac{\text{đ}Q}{T}}_{\text{eq} \Leftrightarrow T\mathrm{d}S_{eq} = \text{đ}Q} = S(1) - S(2) \le 0 \text{ or } S(2) \ge S(1)\,. \tag{4.9}$$

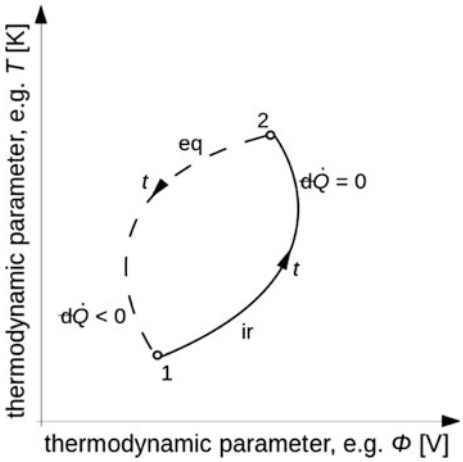

Fig. 4.1 Entropy is defined by the reversible part of a process "eq". On the contrary, entropy increases even without any interactions with surroundings in the irreversible part of a process "ir", e.g., without exchange of heat, mass, energy, and momentum. Moreover, a closed cycle requires removing of an amount of heat from the cycle

Entropy $\mathrm{d}S_{\mathrm{eq}}$ is defined for the reversible processes by exchange of heat $\mathrm{d}\!\!\!^{-}Q$. There is no dependency on a way between the states "1" and "2" in case of reversible processes (see Fig. 4.1). Independency of a way between states complies a function, whose differential is the total differential. Hence, entropy $\mathrm{d}S_{\mathrm{eq}}$ must be the total differential of independent variables [25], e.g., internal energy U and volume V. The system state with the equilibrium entropy S_{eq} is just a hypothetical state. Generally, all of the real systems are in the non-equilibrium state with entropy S.

Entropy and the total entropy flux close to the equilibrium state can be expanded into the Taylor series

$$S = S_{\mathrm{eq}} + (\delta S)_{\mathrm{eq}} + \frac{1}{2}\left(\delta^2 S\right)_{\mathrm{eq}} + \cdots, \tag{4.10}$$

$$\overline{J}(S) = \mathrm{J}\left(S_{\mathrm{eq}}\right) + \underbrace{\delta\overline{J}\left(S_{\mathrm{eq}}\right) + \delta^2\overline{J}(S)_{\mathrm{eq}} + \cdots}_{\overline{J}\left(S_{\mathrm{eq}}\right)}. \tag{4.11}$$

Here, δ means a differential representing even a small (negligible) fluctuation. The total entropy flux is split in two parts—the flux $\mathrm{J}\left(S_{\mathrm{eq}}\right)$ maintaining the equilibrium state and the flux $\overline{J}\left(S_{\mathrm{eq}}\right)$ forcing the system out of the equilibrium state. Relation (4.10) is rewritten in terms of time derivatives to employ the balance equations of entropy for open systems (4.1)

$$\dot{S} = \dot{S}_{\mathrm{eq}} + \dot{\overline{\delta S_{\mathrm{eq}}}} + \frac{1}{2}\dot{\overline{\delta^2 S_{\mathrm{eq}}}} + \cdots \tag{4.12}$$

and with respect to Eq. (4.11), the balance of entropy changes to following expression

$$\underbrace{\dot{S}_{\mathrm{eq}} + \mathrm{J}\left(S_{\mathrm{eq}}\right)}_{=0\,\text{equilibrium state}} = \underbrace{-\dot{\overline{\delta S_{\mathrm{eq}}}} - \frac{1}{2}\dot{\overline{\delta^2 S_{\mathrm{eq}}}} + \bar{J}\left(S_{\mathrm{eq}}\right) + P(S)}_{\to 0\,\text{non-equilibrium state}}. \tag{4.13}$$

The equilibrium state and the equilibrium entropy S_{eq} define the left side of this expression, whereas the entropy change of the non-equilibrium state and stability of the equilibrium state describe the right side of this expression. The reference state in the equilibrium state is defined by condition

$$\dot{S}_{\mathrm{eq}} = \mathrm{J}\left(S_{\mathrm{eq}}\right). \tag{4.14}$$

Stability of the reference state is ensured by

$$\frac{1}{2}\dot{\overline{\delta^2 S_{\mathrm{eq}}}} = P(S) + \bar{J}\left(S_{\mathrm{eq}}\right) - \dot{\overline{\delta S_{\mathrm{eq}}}} \geq 0. \tag{4.15}$$

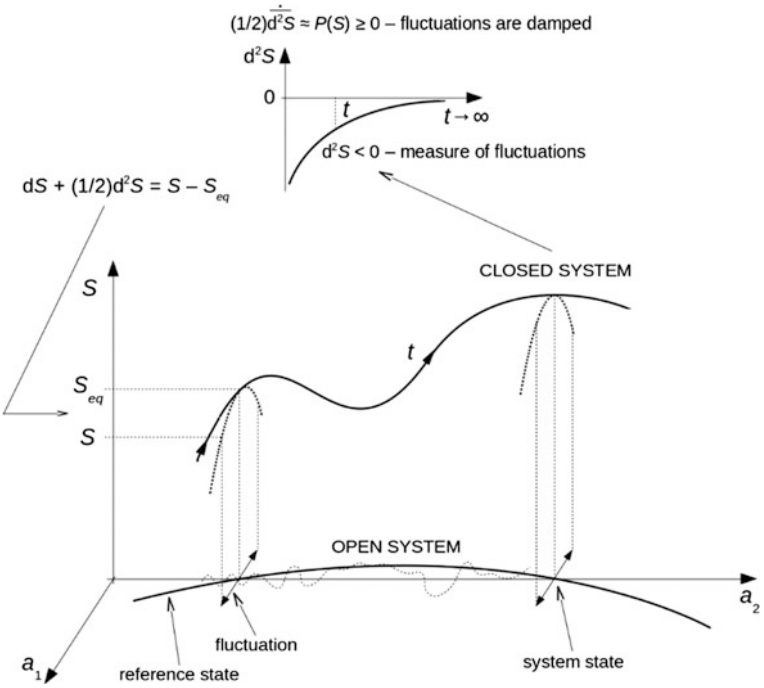

Fig. 4.2 The entropy defines a convex surface over all of the processes. The system state (entropy S) is, in general, given by coordinates a_1 and a_2. A stability of the states ensures the entropy production $P(S) > 0$

Thermodynamic justification of condition (4.15) follows from the stability condition of fluctuations (4.7) (see Fig. 4.2). Time change of the equilibrium state is slow; however, time change of the fluctuations in atomic and molecular level is fast ($\dot{S}_{\mathrm{eq}} \ll \overline{\dot{\delta S}_{\mathrm{eq}}}$). If the fluctuation is neglected, i.e., $(1/2)\,\overline{\dot{\delta S}_{\mathrm{eq}}} = 0$, condition (4.15) will be a relation for the balance of entropy in the non-equilibrium state (4.1), where $\overline{\dot{\delta S}_{\mathrm{eq}}} = \dot{S}$ is used.

Despite these facts, the general form of the balance of entropy (4.1) can be rewritten as

$$\frac{\mathrm{d}S}{\mathrm{d}t} = \frac{\mathrm{d}}{\mathrm{d}t}S_{\mathrm{eq}} + \frac{\mathrm{d}}{\mathrm{d}t}\delta S_{\mathrm{eq}} + \frac{1}{2}\frac{\mathrm{d}}{\mathrm{d}t}\delta^2 S_{\mathrm{eq}} = \mathrm{J}\left(S_{\mathrm{eq}}\right) + \bar{J}(S) + P(S) \tag{4.16}$$

and is used to define the equilibrium entropy (4.18), i.e., entropy of the equilibrium states. The balance of entropy (4.16) is then changed into

$$\frac{\mathrm{d}S}{\mathrm{d}t} = \frac{\mathrm{d}}{\mathrm{d}t}\delta S_{\mathrm{eq}} = \bar{J}(S) + P(S) \quad \text{for} \quad \frac{1}{2}\frac{\mathrm{d}}{\mathrm{d}t}\delta^2 S_{\mathrm{eq}} \to 0, \tag{4.17}$$

which gives the usual form (4.1).

The equilibrium entropy (4.14) defines only the equilibrium state of the system, so

$$\frac{\mathrm{d}}{\mathrm{d}t}S_{eq} = \mathrm{J}\left(S_{eq}\right) = \int_A \mathbf{j}_{eq}\left(S\right)\mathrm{d}\mathbf{a} = \frac{1}{T}\frac{\mathrm{d}\!\!\!^{-}Q}{\mathrm{d}t} \text{ assuming } P\left(S_{eq}\right) = \int_V \sigma\left(S\right)\mathrm{d}v = 0\,, \tag{4.18}$$

where $\dot{Q} = \mathrm{d}\!\!\!^{-}Q/\mathrm{d}t$ represents heat added into the system during the equilibrium processes. Moreover, the equilibrium processes and the equilibrium state are not real and serve just as a reference frame that describes the real systems. Furthermore, time is a parameter of change in the equilibrium processes, which symbolizes that each change has to run in a time. Equation (4.18) is the Clausius definition of entropy $\mathrm{d}S_{eq} = \mathrm{d}\!\!\!^{-}Q/T$ (see (4.9)) and is usually written in the Gibbs form [3, 15, 25]

$$\mathrm{d}S_{\mathrm{eq}}(U,V) = \frac{\mathrm{d}U}{T} + \frac{p}{T}\mathrm{d}V - \sum_{\alpha}\frac{\mu_\alpha}{T}\mathrm{d}N_\alpha \quad \text{with} \quad P\left(S_{\mathrm{eq}}\right) = 0 \tag{4.19}$$

for the total equilibrium system with a volume V and similarly

$$\mathrm{d}s(u,\rho) = \frac{\mathrm{d}u}{T} + \frac{p}{T}\mathrm{d}\left(\frac{1}{\rho}\right) - \sum_{\alpha}\frac{\mu_\alpha}{T}\mathrm{d}w_\alpha \quad \text{with} \quad P(S) \geq 0 \tag{4.20}$$

for the local equilibrium system—a material point (usually referred to unit of mass). Here, N_α [mol] is the total number of moles in a volume V, μ_α [J mol^{-1}] is the chemical potential, and w_α [–] is the mass fraction. Correlations inside the material point are also neglected in these cases. The nonzero production of entropy (4.3) is caused by non-equilibrium between the material points.

In case of mixtures, all of extensive variables depend on mass fraction

$$w_\alpha = \frac{\rho_\alpha}{\rho}, \quad \text{for} \quad \rho_\alpha = M_\alpha c_\alpha, \quad \rho = \sum_{\alpha}\rho_\alpha, \tag{4.21}$$

where ρ_α [kg m^{-3}] is the density, c_α [mol m^{-3}] is the molar concentration, and M_α [kg mol^{-1}] is the molar mass of a chemical component α. Energy of mutual interactions (energetic bonds) of the subsystems (atoms, molecules, etc.) is described by the chemical potential. The chemical potential is denoted by μ_α [J mol^{-1}] in a global approach and by $\mu_\alpha \to \mu_\alpha/M_\alpha$ [J kg^{-1}] in a local equilibrium approach

$$\mu_\alpha = u_\alpha - \left(\frac{\mathbf{t}_{\mathrm{el}}}{\rho}\right) : (\rho v_\alpha \mathbf{e}) - Ts_\alpha = \bar{\mu}_\alpha(T, \mathbf{t}_{\mathrm{el}}) + RT \ln w_\alpha \text{ for solids,} \tag{4.22}$$

$$\mu_\alpha = u_\alpha + pv_\alpha - Ts_\alpha = \bar{\mu}_\alpha(T, p) + RT \ln w_\alpha \text{ for ideal fluids,} \tag{4.23}$$

where $\bar{\mu}_\alpha(T, \mathbf{t}_{\mathrm{el}})$ and $\bar{\mu}_\alpha(T, p)$ are the chemical potential at given standard state, i.e., at elastic stress (Cauchy stress tensor) $\mathbf{t}_{\mathrm{el}}$, at pressure p, and at temperature T. Hereby, defined variables are used to express thermodynamic fluxes and forces as shown in Table 4.2.

Definition of entropy (4.19) in the following form

$$T\mathrm{d}S_{eq}\left(U, V\right) = \cancel{\mathrm{d}Q} = \mathrm{d}U + \mathrm{d}W = \mathrm{d}U + p\mathrm{d}V - \sum_\alpha \mu_\alpha \mathrm{d}N_\alpha \tag{4.24}$$

is the equivalent form of the law of conservation of energy for the total system. Heat converted into mechanical energy is represented by $\mathrm{d}W$. Moreover, $\mathrm{d}W$ includes also the chemical energy or electrical energy, respectively, which flows out of the system. Analogically, expression (4.20) is the balance of energy for the material point.

These definitions of entropy are alternatives of the first law of thermodynamics. However, evolution of the material points (systems) is described by the second law of thermodynamics as shown in the statements (i) and (ii).

4.3 Stability

4.3.1 Stability of the Equilibrium System

Definitions of entropy (4.19) and (4.20) are valid for the equilibrium or the local equilibrium states. Non-equilibrium states are described by fluctuations of entropy δS_{eq} (see the Eq. (4.15)). Time change of the global entropy (4.1) may be by the definition of the equilibrium state (4.18) modified into suitable form for description of the non-equilibrium systems

$$\dot{S} = \frac{\mathrm{d}}{\mathrm{d}t}\delta S_{\mathrm{eq}} = \bar{J}\left(S_{\mathrm{eq}}\right) + \int_V \sigma(S)\mathrm{d}v \quad \text{for} \quad -\frac{1}{2}\frac{\mathrm{d}}{\mathrm{d}t}\delta^2 S_{\mathrm{eq}} \to 0. \tag{4.25}$$

An interpretation of the entropy flux and entropy production differs from an interpretation used in expression (4.1). Here, $\bar{J}\left(S_{\mathrm{eq}}\right)$ characterizes the entropy flux through a surface A in case of system that deviates out of the equilibrium state. It is represented by the conductive heat flux and the mass diffusion flux, e.g., exchange of reactants and products that are necessary for chemical reactions. This entropy flux is given from boundary conditions relating the specific system (energetic

devices, chemical reactor, etc.). The total entropy production $P(S) > 0$ is generated by the transfer of energy and transfer of mass and is not connected to equilibrium transformation of non-heat forms of energy, e.g., chemical energy to electrical energy, chemical energy to mechanical energy, and potential energy to kinetic energy (assuming no friction) [3, 5].

Non-equilibrium processes taking place in the system are included in $\sigma(S) > 0$ that denotes the density of entropy production due to the non-equilibrium processes. The entropy production in case of the local thermodynamic equilibrium (4.20) is caused by non-equilibrium between the material points and is equal to $P(S) > 0$. The entropy production ensures stability of the system state, so that the system in the dynamical equilibrium, i.e., $\bar{J}(S) = 0$, complies $(1/2)(\mathrm{d}/\mathrm{d}t)\delta^2 S_{\mathrm{eq}} \approx P(S) > 0$ (see Fig. 4.2). It is difficult to determine a form of the entropy production for more complicated systems with many mutual interacting processes, e.g., unknown degradation processes and metastable states of chemical reactions and phase transitions. Existence of these processes is included in the term $(\mathrm{d}/\mathrm{d}t)\delta^2 S_{\mathrm{eq}}$ that is related to fluctuations around the equilibrium entropy S_{eq}. Therefore, this term may be interpreted as an additional entropy production. This additional entropy production characterizes dissipative (relaxation) processes that are not included in the thermodynamic fluxes and the thermodynamic forces (Table 4.2) and that do not affect explicitly the entropy flux on system boundaries. Furthermore, the additional entropy production may include even non-specified interactions of the subsystems. Explicit form of the density of entropy production and the density of entropy flux depends on the balance laws of all relevant variables (see, e.g., [3, 4]). These above-mentioned statements are an alternative formulation of Braun–Le Châtelier principle that sounds [3, 4, 26]: "If a chemical system (in general thermodynamic system; *note added by authors*) in equilibrium is subjected to a perturbation (stress), the equilibrium will be shifted (a reaction will occur) such as to partially undo this perturbation (oppose the stress)."

The real entropy flux is always caused by gradients of the relevant variables, e.g., temperature, pressure, and concentration, and usually has the form [3, 4]

$$\bar{J}\left(S_{\mathrm{eq}}\right) = -\int_A \left[\frac{\mathbf{j}_q}{T} - \sum_{\alpha=1}^{r}\left(\frac{\rho_\alpha \mu_\alpha \mathbf{v}_{D\alpha}}{T}\right)\right]\mathrm{d}\mathbf{a}. \tag{4.26}$$

Assuming the steady state of the system, i.e., $\dot{S} = \overline{\dot{\delta S}}_{\mathrm{eq}} = 0$, it can be due to the balance of entropy (4.25) and the stability condition (4.15),which is written as

$$\frac{1}{2}\frac{\mathrm{d}}{\mathrm{d}t}\left(\delta^2 S\right)_{\mathrm{eq}} = \int_V \sigma(S)\mathrm{d}v + \bar{J}\left(S_{\mathrm{eq}}\right) \geq 0. \tag{4.27}$$

This expression means that a dissipation is given by the entropy production and by the outward entropy flux. The outward entropy flux can eliminate this dissipation

insofar as the system becomes unstable, which implies that entropy is not further a local convex function (see Fig. 4.2).

From this point of view, the Clausius definition of entropy can be interpreted as a condition of the local extreme of entropy. The stability condition (4.15) for the isolated systems $\bar{J}(S_{\mathrm{eq}}) = 0$ can be understood as a condition of fluctuations damping (see Fig. 4.2)

$$\frac{1}{2}\frac{\mathrm{d}}{\mathrm{d}t}\left(\delta^2 S\right)_{\mathrm{eq}} = \int_V \sigma(S)\mathrm{d}v = P(S) \geq 0. \tag{4.28}$$

Gibbs derivation of the thermodynamic stability conditions is based on a time integration of condition (4.28) (see [10]). So that, the following relation can be obtained

$$\frac{1}{2}\frac{\mathrm{d}}{\mathrm{d}t}\left(\delta^2 S\right)_{\mathrm{eq}} = \int_{t_{\mathrm{eq}}}^{t_{\mathrm{eq}}+\Delta t} P(S)\mathrm{d}t = \Delta_{\mathrm{ir}} S \geq 0, \tag{4.29}$$

from which results a deviation from the equilibrium state (a fluctuation) is not able to satisfy inequality (4.29), because entropy maximum satisfies the equilibrium state. The fluctuation in the equilibrium state decreases entropy of the system, and therefore, the reverse inequality is valid (see Fig. 4.3). This reverse inequality (4.30) is called the general stability condition of the equilibrium state [4]

$$\frac{1}{2}\frac{\mathrm{d}}{\mathrm{d}t}\left(\delta^2 S\right)_{\mathrm{eq}} = \Delta_{\mathrm{ir}} S \geq 0. \tag{4.30}$$

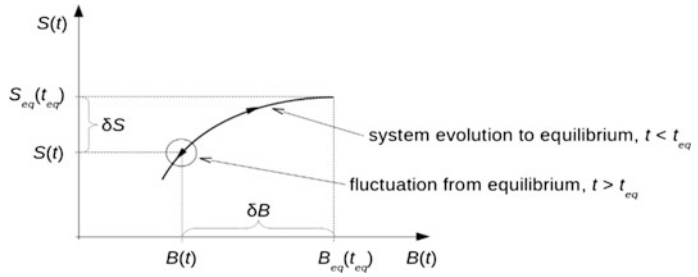

Fig. 4.3 Scheme of stability of the equilibrium state. $B = (U, V\ldots)$ is macroscopic state of the system; ΔB and ΔS are fluctuations of the state and entropy, respectively; and t_{eq} is a time, in which the system reached the equilibrium

It is possible to write $\Delta_{ir}S \doteq P(S)\Delta t \leq 0$ for small Δt, and moreover, the production of entropy $P(S) > 0$ leads to $\Delta t < 0$. Hence, the system returns by the fluctuations from the equilibrium state to the past.

Assuming dissipative processes in the system, i.e., $\mathrm{d}S = \left(\mathrm{d}_{eq}S + \mathrm{d}_{ir}S\right)$ and $\mathrm{d}_{ir}S = \mathrm{d}S - \mathrm{d}Q/T \geq 0$—classical formulation of the second law of thermodynamics, and using the first law of thermodynamics in the form $\mathrm{d}Q = \mathrm{d}U + p\mathrm{d}V$ the following relation, is derived

$$T\mathrm{d}_{ir}S = T\mathrm{d}S - \mathrm{d}U - p\mathrm{d}V > 0. \tag{4.31}$$

For the system approaching the equilibrium, in Fig. 4.3, inequality (4.31) is valid and for the system in equilibrium is $\mathrm{d}_{ir}S = 0$. Fluctuations from the equilibrium state in the isolated system are not able to satisfy inequality (4.31) because in the equilibrium state, entropy has its maximum. So that, if the fluctuations do not obey condition (4.31), the fluctuations will have to comply $T\mathrm{d}_{ir}S < 0$. This condition can be written as

$$\delta U + p\delta V - T\delta S > 0. \tag{4.32}$$

Condition (4.32) represents the Gibbs–Duhem stability condition of the equilibrium state.

The second law of thermodynamics in terms of the Clausius definition of entropy (4.28), the definition of the equilibrium state (4.18), and the general stability condition (4.30) is schematically shown in Fig. 4.3. It presents that the condition for maximum of a function in B_{eq} is relation (4.30) and that entropy of the system is decreased by the fluctuation δB.

Here, presented assumptions of thermodynamics avoid one elementary property of subsystem fluctuations, namely correlations between fluctuations. All of macroscopic variables are in the fact mean values of many mutual interactions of individual subsystems (collisions, action of forces, etc.), so that the correlations between individual actions were neglected. Despite this, the correlations between actions are crucial for the systems on the stability limits (boundary). As an example serves a bubble in water at room temperature cropping up spontaneously, however immediately dissolves. However, a bubble close to the boiling point, or in case of the superheated water, expands and leads water (the system) to phase transition (instability). A question still remains. What will be properties of the system in unstable region, where constitutive relations are not valid? The subsystems (atoms, molecules, species, etc.) in the unstable region remain the same, but the relations between the subsystems changed.

4.3.2 Thermodynamic Stability Condition for Non-living Open System

Generally, probability distribution of the fluctuations of variable b_i near the equilibrium state $b_{i\,\mathrm{eq}}$ (4.6) can be written as

$$\Pr \approx \exp\left[-\frac{\left(b_i - b_{i\,\mathrm{eq}}\right)^2}{2\beta_i}\right] \approx \exp\left(\frac{\mathrm{d}^2 s}{2R}\right), \tag{4.33}$$

where R [J kg^{-1}K^{-1}] is the gas constant. This expression represents normal (Gaussian) distribution, so that the mean quadratic deviation of the variable $\overline{\left(b_i - b_{i\,\mathrm{eq}}\right)^2} = \beta_i$.

Condition (4.30) can be rewritten in both cases: in the global (integral) variables (4.19) and in the local equilibrium state (4.20). In case of the local equilibrium state, the second differential of entropy has form [4, 10]

$$\delta^2 s = \delta\frac{1}{T}\delta u + \delta\left(\frac{p}{T}\right)\delta\left(\frac{1}{\rho}\right) - \sum_{\alpha=1}^{r}\delta\left(\frac{\mu_\alpha}{T}\right)\delta w_\alpha, \tag{4.34}$$

which can be for $v = 1/\rho$ modified to quadratic form that is used to describe stability of the real systems

$$\delta^2 s = -\frac{1}{T}\left[\frac{c_v}{T}(\delta T)^2 + \frac{\rho}{\chi}(\delta v_{w\alpha})^2 + \sum_{\alpha=1}^{r}\left(\frac{\partial \mu_\alpha}{\partial w_{\alpha'}}\right)_{T,p,w\alpha}\delta w_\alpha, \delta w_{\alpha'}\right] < 0. \tag{4.35}$$

Here, c_v is the specific heat at constant volume, and $\delta v_{w\alpha}$ is the differential of specific volume at constant chemical composition, which is given as

$$\delta v_{w\alpha} = \left(\frac{\partial v}{\partial T}\right)_{p,w\alpha}\delta T + \left(\frac{\partial v}{\partial p}\right)_{T,w\alpha}\delta p, \quad \chi = -\rho\left(\frac{\partial 1/\rho}{\partial p}\right)_T = \frac{1}{\rho}\left(\frac{\partial \rho}{\partial p}\right)_T = \frac{1}{\rho c_T^2} > 0, \tag{4.36}$$

where χ is isothermal compressibility factor, and c_T is isothermal speed of sound. Assuming (4.33), mean values of the fluctuations of temperature, density, and concentration can be found. The local equilibrium system (material point in continuum mechanics) is stable, if

$$\overline{(\delta T)^2} = \frac{RT^2}{c_v}, \quad c_v > 0, \tag{4.37}$$

$$\overline{(\delta v_{w\alpha})^2} = \frac{RT}{\rho^2 c_T^2}, \quad c_T^2 > 0, \tag{4.38}$$

$$\sum_{\alpha,\alpha'}^{r}\left(\frac{\partial\mu_\alpha}{\partial w_\alpha}\right)_{T,p,w\alpha'}\delta w_\alpha\delta w_{\alpha'}>0\,,$$
$$\overline{(\delta w_\alpha)^2}=RT\left(\frac{\partial\mu_\alpha}{\partial w_\alpha}\right)^{-1}_{T,p}=RT\left(\frac{\partial w_\alpha}{\partial\mu_\alpha}\right)_{T,p}=w_\alpha>0. \tag{4.39}$$

Thermodynamic stability conditions are usable to determine properties of the material systems. Thus, these inequalities characterize thermal stability condition (4.37), mechanical stability condition (4.38), and diffusion stability condition (4.39), which is the consequence of (4.23) and represents a preliminary outcome that concentration fluctuation equals to concentration. Moreover, these inequalities provide relations between properties of the real systems and the stability condition (4.30). Inequality (4.37) leads to the conditions for specific heats that is valid for gases, i.e., $c_v>0$, $c_p>0$, and furthermore to the important relation $c_p=c_v+\left(9T\alpha_T^2\right)/(\rho\chi)$, where $3\alpha_T=\rho(\partial v/\partial T)_p$ is the volumetric thermal expansion coefficient.

Condition (4.38) transformed to relation for isothermal speed of sound, i.e., $c_T^2=(\partial p/\partial\rho)_T$, is crucial for instabilities study. An instability can occur in case, when the change of pressure with respect to density at constant temperature is negative; in this case the fluctuations of density increase. As an example can serve, a phase transition in fluids (evaporation, explosion of liquid oversaturated by gas, condensation) or solid materials failures (cracks initiation and propagation).

Mixture stability condition (4.39) has a special relevance. It can be related to the either different chemical compounds (atoms and molecules are distinguishable) or chemical compounds of the same kind (particles, atoms, and molecules in the same energetic state are indistinguishable). Number of particles N_k in the energetic state U_k with degeneration G_k may be determined by the statement (ii) of the second law of thermodynamics [10]

$$N_k=\frac{G_k}{\exp\left(\frac{U_k-\mu}{kT}\right)\pm1}\qquad -\text{ for bosons},\quad +\text{ for fermions}. \tag{4.40}$$

This relation for particle energy is higher than energy of chemical bonds, i.e., $U_k\gg\mu$, transformed to

$$N_k=G_k\exp\left(\frac{\mu-U_k}{kT}\right)\text{ Boltzmann distribution}. \tag{4.41}$$

Relation (4.39) serves to determine the mean value of fluctuations replacing the concentration by number of particles. The definition of entropy (4.19), or analogically (4.20), for the system with constant volume can be used for the derivation of the stability condition (4.39) in the form

$$\overline{(\Delta N_k)^2} = \overline{\left(N_k - N_{k,\mathrm{eq}}\right)^2} = \overline{N^2} - N_{k,\mathrm{eq}}^2 = kT\left(\frac{\partial N_k}{\partial \mu}\right)_T > 0. \tag{4.42}$$

This condition is useful for description of mixtures including mutual interactions and phase transitions. It also provides the following interpretations

$$\left(\frac{\partial N_k}{\partial \mu}\right)_T = \frac{\overline{(\Delta N_k)^2}}{kT} = N_k\left(1 \mp \frac{N_k}{G_k}\right) \quad + \text{ for bosons, } - \text{ for fermions,}$$
$$= N_k \text{ Boltzmann distribution.} \tag{4.43}$$

This expression for bosons was derived by A. Einstein and was used for the determination of photon fluctuations radiated by the black body, which was described by the Planck's radiation law [17].

4.3.3 Thermodynamic Stability Condition for Living Open System

Living biological systems are in the dynamical equilibrium, so that $\dot{S} = 0$. The system is maintained in the stationary non-equilibrium state by the nonzero negative entropy flux, see the balance of entropy (4.1) and [12, 20]

$$-\bar{J}(S) = P(S) > 0 \quad \text{inequality is ensured by interactions with surroundings.} \tag{4.44}$$

In general, this system is the material system and is described by the first law of thermodynamics and by the balance laws. The stability of living systems is often considered as an immunity (disease resistance, resistance against changes of a system, etc.).

The state in the dynamical equilibrium is denoted by subscript "0" and symbolizes a reference state. Its stability with respect to the fluctuations in time $t = t_0$ is characterized by the constant entropy $\dot{S}\big|_0 = 0$, i.e., $S(t_0) = S_0 = \text{const}$. Value of the constant entropy is determined from (4.1) as

$$-\bar{J}(S_0) = P(S_0) \geq 0. \tag{4.45}$$

Entropy is constant despite the system interacts with surroundings, so that the system is non-conservative $\bar{J}(S) \neq 0$. Necessary condition for stable equilibrium is an elimination of the fluctuation by dissipative processes inside the system (see Fig. 4.3). This fluctuation can be either spontaneous or generated from outside, which can the entropy of the system only decrease due to local maximum value of the total entropy. But dissipative processes increase entropy back to the value S_0.

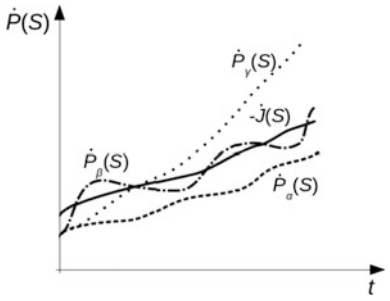

Fig. 4.4 Scheme of evolution of the open systems with respect to interactions with surroundings. $\dot{P}_\alpha$ is the stable evolution; $\dot{P}_\beta$ is the dynamical evolution; and $\dot{P}_\gamma$ is unstable evolution

Entropy can be expanded into the series in time, and then, its value in time close to t_0 is given as

$$S(t) - S_0 = \dot{S}_0(t - t_0) + \ddot{S}_0 \frac{(t - t_0)^2}{2} + \cdots = \ddot{S}_0 \frac{(t - t_0)^2}{2} + \cdots < 0. \tag{4.46}$$

The stability condition is a sign of the second time derivative of entropy, i.e., $\ddot{S}_0 < 0$, which is analogical to condition (4.15). The stability condition of open systems is then formulated as a combination of relation (4.27) and the balance of the total entropy (4.1), which is as follows

$$\begin{aligned} \ddot{S}_0 = \dot{\overline{J}}(S_0) + \dot{P}(S_0) < 0 \quad & \text{for stable evolution,} \\ > 0 \quad & \text{for unstable evolution .} \end{aligned} \tag{4.47}$$

The system state with maximal entropy, i.e., $S_0 = S_{\max}$, is defined by the sign "<". Assuming (4.47), a satisfactory stability condition of that state is

$$-\dot{\overline{J}}(S_0) > \dot{P}(S_0). \tag{4.48}$$

Thus, the open system will be stable, if the time change of the negative entropy flux is greater than the time change of the entropy production. The entropy flux is usually defined by (4.26), which consists of the heat flux and the diffusive fluxes of chemical compounds (it is useful food for biological system).

According to the condition of stable evolution (4.48), the evolution of the open system can be split as follows (see Fig. 4.4).

α The permanent sustainable evolution is ensured by condition $-\dot{\overline{J}(S)} > \dot{\overline{P(S)}}$, so that increase of the entropy production is always lower than increase of interaction of the system with surroundings. Interaction with surroundings (added food and products formation) is represented by the negative entropy flux;

β The dynamical evolution is characterized by alternation of stable and unstable periods (periodic occurrence of crisis); and

γ The unstable evolution leads to destruction of the system, which is characterized by permanent increase of entropy that is not compensated by the negative entropy flux. Assuming the balance of entropy (4.48), this statement can be formulated as

$$0 < \left(\overline{\dot{J}(S)} + \overline{\dot{P}(S)} \right) \mathrm{d}t = \frac{\mathrm{d}\dot{S}}{\mathrm{d}t} \mathrm{d}t, \quad \Rightarrow \mathrm{d}\dot{S} > 0, \quad \Rightarrow \int_{t_0}^{t} \mathrm{d}\dot{S} = \dot{S}(t) - \dot{S}(t_0) > 0. \tag{4.49}$$

The total entropy of the system increases with respect to time, and the system approaches the thermodynamic equilibrium state. From the biological point of view, the thermodynamic equilibrium state is identical to death.

4.3.4 Application of Thermodynamic Stability Condition for Living Open System

An effort to survive and exist is the basic instinct of all living systems. Consequence of this effort is then competition for space and resources. Rivalry on the level of ecological and social systems is an example of results of this competition. Thus, knowledge of suitable processes of energy and matter transformation respecting surroundings and inner structure can be an advantage in the evolution. Modern evolution biology shows that driving force of evolution is intraspecific competition on level of species, but also on level of smaller units, e.g., genes, bacteria, and viruses [7]. This competition results from a general principle, e.g., minimum of the Gibbs free enthalpy (for chemical reactions), the total enthalpy (for thermomechanical systems), and even the entropy production together with the stability for particular conditions (in general, for open systems).

The Sun is the primary source of energy for the Earth. Energy received by the Earth is $\bar{J}(E_S) = 3.5 \times 10^{24}$ J year^{-1}. Energy obtained by Earth cooling represents only 0.0027% of the received energy. Moreover, due to green cover (vegetation), energy of 5.5×10^{21} J year^{-1} is needed to form a new biomass, which is just 0.16% of the received energy [8]. The Earth is in the long-term dynamical equilibrium (4.45). Thus, the same amount of heat is radiated back to the universe. and the balance of entropy (4.1) is

$$\begin{aligned} \bar{J}(S_E) &= \frac{4}{3} \bar{J}(E_S) \left(\frac{1}{T_S} - \frac{1}{T_E} \right) = \frac{4}{3} \times 3.5 \times 10^{24} \left(\frac{1}{5770} - \frac{1}{288} \right) \\ &= -P(S_E) = -1.54 \times 10^{22} \text{ J K}^{-1} \text{ year}^{-1} < 0. \end{aligned} \tag{4.50}$$

Temperature of the Sun is T_S = 5770 K, which corresponds to wavelength of green light (≈550 nm), and an effective temperature of the Earth is $T_{E,\text{eff}}$ = 252 K. For the balance of energy, a mean temperature T_E = 288 K respecting the greenhouse effect is more crucial. Relative absorbency of the Earth atmosphere is very low close to this temperature, which corresponds to wavelengths ≈700 nm and ≈8–9 μm. This assures an energetic balance of the Earth. Increase of CO_2, NO_2, H_2O, and other so-called greenhouse gas concentration would affect the energetic balance of the Earth that would result in the increase of temperature of the Earth.

Flux of energy $5.5 \cdot 10^{21}$ J year^{-1} used to form the new biomass is consumed by photosynthesis from 99%

$$n\text{CO}_2 + 2n\text{H}_2\text{O} + mhv \rightarrow (\text{CH}_2\text{O})n + n\text{O}_2 + n\text{H}_2\text{O}. \tag{4.51}$$

CO_2 fixation needs the Gibbs free energy ΔG = 450 kJ mol^{-1} and 8 − 12 photons in range of wavelengths 400–700 nm with energy in range 300–170 kJ mol^{-1} [27]. The total enthalpy needed for the release of one molecule of oxygen is ΔH = 1360–8400 kJ mol^{-1}. In case of n = 1, the product of photosynthesis is CH_2O (formaldehyde). Higher carbohydrates can be produced by higher energy, e.g., for glucose $C_6H_{12}O_6$ are parameters n = 6 and m = 6 (8 − 12). Maximal efficiency of photosynthesis is $\eta_{ps} = \Delta G/\Delta H = 450/1360 = 0.33$. But it is necessary to note that photosynthesis runs on wavelengths 400–700 nm, whereon it is radiated only 45% of the total solar energy.

Vegetation covers just smaller part of the Earth, so that only 0.16% of coming energetic flux $\bar{J}(E_S)$ reaches green cover, which is able to form the new biomass. Assuming that 60% of energy used by photosynthesis is immediately consumed for respiration, there is only 40% of energy for forming of the new biomass (the net annual production of biosphere, NPB). Thus, the energetic flux $\bar{J}(\text{NPB}) = 0.0016 \times 0.4 \times 3.5 \times 10^{24} = 2.2 \times 10^{21}$ J year^{-1} is consumed to form the new biomass. This flux represents an energetic base for all of living being on the Earth [8]. Technical civilization generates energy of 5.7×10^{20} J year^{-1} (data for 2013), from which just 15% is generated by renewable sources and rest of energy is produced by fossil fuels [28]. So, human civilization is able to produce energy, which is equal to 40% of the energetic flux $\bar{J}(\text{NPB})$ provided by the Sun in the long term. It seems that this additional energetic flux can influence even biosphere. Homo sapiens is part of biosphere with estimated energetic consumption of 4×10^9 J year^{-1}, so that for population of six billions, humans consumption is equal to 2.4×10^{19} J year^{-1} [8]. At present time, human civilization consumes approximately 1.1% of the total energetic flux needed to form biosphere, which was utilized by all of living being on the Earth in the past. Here, presented values of the energetic fluxes can serve for the determination of the next evolution on the Earth.

4.3.4.1 Energetic Limitations of Population Growth

An important consequence of the non-equilibrium thermodynamics is the law of mass action, which follows from the production of entropy $\dot{\varsigma}_\rho A_\rho \geq 0$ of chemical reactions (see Table 4.2 and [3, 4]). This law is usable for description of dynamics of population biology, e.g., cells and species. Moreover, this law can be even used to study dynamics of ecological systems.

Simply, description of population growth can be written as an analogy to autocatalysis in chemistry in the following form

$$\mathrm{EI} + \mathrm{X} \underset{k_{-1}}{\overset{k_{+1}}{\rightleftarrows}} 2\mathrm{X} + \mathrm{E'I} - \bar{J}(\mathrm{X}), \tag{4.52}$$

where EI is the surrounding interaction of individual X before reproduction and E′I is the surrounding interaction of individual X after reproduction. Rate of reproduction characterizes rate constant k_{+1}, and rate of cessation characterizes rate constant k_{-1}. This model is correct for species that are reproduced by proliferation, e.g., cells. Note that the cessation means the cessation of all vital phenomena without capability of resuscitation, either in animals or in plants.

It is assumed for species with sex reproduction that individual X is represented by pair male and female. So that population growth can be described as

$$\mathrm{EI} + \mathrm{X} \underset{k_{-1}}{\overset{k_{+1}}{\rightleftarrows}} g\mathrm{X} + \mathrm{E'I} - \bar{J}(\mathrm{X}), \tag{4.53}$$

where parameter g complies condition $g \geq 3, 4, \ldots$ and depends on number of descendants. Number g has not to be integer because not every descendant is able to reproduce again. Leaving of descendants from place of origin is characterized by flux $\bar{J}(\mathrm{X})$. According to the law of mass action, time change of the number of individuals is given as

$$\begin{aligned} \frac{\mathrm{d}N}{\mathrm{d}t} &= k_{+1} N\, N_{\mathrm{EI}} - k_{-1} N^2\, N_{\mathrm{E'I}} - \bar{J}(\mathrm{X}) \quad \text{or} \\ \frac{\mathrm{d}N}{\mathrm{d}t} &= k_{+1} N\, N_{\mathrm{EI}} - k_{-1} N^g\, N_{\mathrm{E'I}} - \bar{J}(\mathrm{X}). \end{aligned} \tag{4.54}$$

Here, N is the number of individuals, N_{EI} is consumption of energy and matter before reproduction, and $N_{\mathrm{E'I}}$ is the production of energy and matter after reproduction. The thermodynamic equilibrium of chemical reaction, which is valid even for dynamical equilibrium, is characterized by an equilibrium constant K_{X}. This constant is connected with enthalpy of the reaction ΔH_{X} and with the change of entropy ΔS_{X}

$$K_{\mathrm{X}} = \frac{k_{+1}}{k_{-1}} = \exp\left(\frac{-\Delta G_{\mathrm{X}}}{RT}\right) = \exp\left(\frac{\Delta S}{R} - \frac{\Delta H_{\mathrm{X}}}{RT}\right). \tag{4.55}$$

Change of the Gibbs free enthalpy ΔG_{X} represents the limit of the growth of every species, see further. Assume that leaving of individuals is proportional to their quantity (concentration in given place), i.e., $\bar{J}(\mathrm{X}) = N/R_{\mathrm{X}}$, where R_{X} is resistance of surroundings. Stationary state of the system is then expressed as

$$N_0 = K_{\mathrm{X}} \frac{N_{\mathrm{EI}}}{N_{\mathrm{E'I}}} - \frac{K_{\mathrm{X}}}{k_{+1} N_{\mathrm{E'I}} R_{\mathrm{X}}}, \quad \text{or} \quad N_0^{g-1} = K_{\mathrm{X}} \frac{N_{\mathrm{EI}}}{N_{\mathrm{E'I}}} - \frac{K_{\mathrm{X}}}{k_{+1} N_{\mathrm{E'I}} R_{\mathrm{X}}}. \tag{4.56}$$

A population curve can be obtained by the integration of Eq. (4.54) using initial condition $N(t = 0) = N_1$

$$N(t) = \frac{N_0}{1 + \left(\frac{N_0}{N_1} - 1\right) \exp(-at)} \quad \text{for} \quad a = k_{+1} N_{\mathrm{EI}} - \frac{1}{R_{\mathrm{X}}}. \tag{4.57}$$

Crucial parameters of the population curve are the rate of reproduction characterized by $k_{+1} N_{\mathrm{EI}}$ [s^{-1}], and a stationary value N_0, which due to the equilibrium constant K_{X}, Eq. (4.55), relates to energy (in general to sources) that is necessary for reproduction. In ecology, the variable N_0 is called carrying capacity and describes number of individuals, which are sustained by surroundings [29]. Then, the first expression form Eq. (4.54) is formulated as

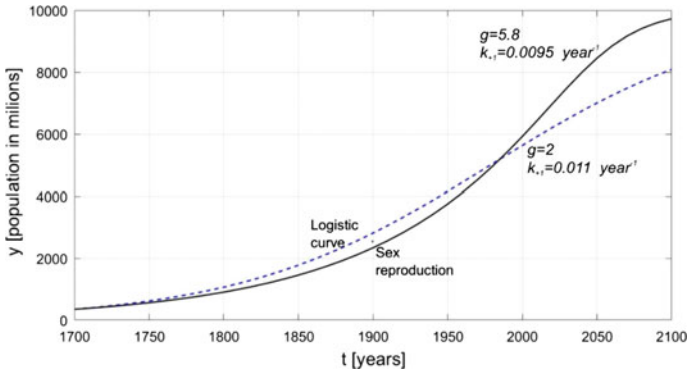

Fig. 4.5 Two population models applied to evolution of the Earth. Supposed stationary state is 10 billions. Sex reproduction curve is fitted to data from world population prospects [29]

$$\begin{aligned}\frac{\mathrm{d}N}{\mathrm{d}t} &= k_{+1}N_{\mathrm{EI}}N\left(1-\frac{N}{N_0}\right),\\ \frac{\mathrm{d}N}{\mathrm{d}t} &= k_{+1}N_{\mathrm{EI}}N\left(1-\frac{N^{g-1}}{N_0^{g-1}}\right) \quad \text{with no migration } \bar{J}(\mathrm{X})=0.\end{aligned} \tag{4.58}$$

Stationary state of reproduction by proliferation is the same as stationary state of sex reproduction for $g = 2$, where two pairs rise from pair male to female. Stationary state (4.56) is reached faster in case of $g > 2$ (see comparison of both of the models for case of human population in Fig. 4.5).

Assume a fluctuation of the stationary state N_0 in the form of $\delta N(t) = \delta N_0 \exp(\omega t)$. Then, actual state value is $N(t) = N_0 + \delta N(t)$, which is put into Eq. (4.54). Using the definition of the stationary state (4.56) and the condition of zero migration, i.e., $\bar{J}(\mathrm{X}) = 0$, the following expression for ω (ω_P for logistic curve and ω_S for sex reproduction curve) is obtained

$$\begin{aligned}\omega_P &= k_{+1}N_{\mathrm{EI}}\left(1-\frac{2N_0N_{\mathrm{E'I}}}{K_{\mathrm{X}}N_{\mathrm{EI}}}\right) = -k_{+1}N_{\mathrm{EI}},\\ \omega_S &= k_{+1}N_{\mathrm{EI}}\left(1-\frac{gN_0^{g-1}N_{\mathrm{E'I}}}{K_{\mathrm{X}}N_{\mathrm{EI}}}\right) = -(g-1)k_{+1}N_{\mathrm{EI}}.\end{aligned} \tag{4.59}$$

It is obvious that the stationary state is stable for negative ω, because of deviation decrease. Variable $-\omega$ represents population rate, and sex reproduction is always higher.

In case of the interaction of individual with surrounding is the same before reproduction and after reproduction, i.e., $N_{\mathrm{EI}} = N_{\mathrm{E'I}}$, crucial influence has the Gibbs free enthalpy (4.56) bounded to proliferation of one cell or one pair for sex reproduction. In the stationary state (in dynamical equilibrium for $\omega = 0$) are these two types of reproduction comparable to consumption estimation of the Gibbs free enthalpy. Due to the condition of the stationary state (4.56), the following expression is valid

$$\ln N_{0p} = -\frac{\Delta G_{\mathrm{X}p}}{RT}, \quad \text{or} \quad (g-1)\ln N_{0s} = -\frac{\Delta G_{\mathrm{X}s}}{RT}, \tag{4.60}$$

where ΔG_{Xp} is the Gibbs free enthalpy of proliferation, and ΔG_{Xs} is the Gibbs free enthalpy of sex reproduction. For two systems with the same number of individuals, i.e., $N_{0\mathrm{p}} = N_{0\mathrm{s}}$, the following condition is derived

$$(g-1)\Delta G_{\mathrm{X}p} = \Delta G_{\mathrm{X}s}. \tag{4.61}$$

Relations (4.60) can be used for the estimation of the Gibbs free enthalpy to reach the stationary state. Assume simple population model for proliferation, which is identical with population model for sex reproduction in case of $g = 2$. An estimation is determined for human population that has $N_0 = 7.6 \times 10^9$ individuals and rate of growth (reproduction) $k_{+1}N_{\mathrm{EI}} = 0.011\ \mathrm{year}^{-1}$ in 2014. Assume, moreover, that N_0 is the stationary state (according to [29], the stationary state is supposed to be $N_0 = 10 \times 10^9$ in 2080) then

$$\ln N_{0p} = \ln 7.6 \times 10^9 = 22.8 = -\frac{\Delta G_{\mathrm{X}p}}{RT}, \quad \text{so that } \frac{\Delta G_{\mathrm{X}s}}{RT} < 0. \tag{4.62}$$

Thus, reproduction process is spontaneous process with increase of entropy $T\Delta S_{\mathrm{Xp}} = \Delta H_{\mathrm{Xp}} - \Delta G_{\mathrm{Xp}} > 0$, $\Delta H_{\mathrm{Xp}} > 0$, which is compensated by negative entropy flux from the Sun, as given in Eq. (4.50). Actual values of ΔG_{Xp} and ΔG_{Xs} for specific population have to be determined experimentally. As a good way, how can be determined experimental value of probability of mean quadratic deviation of entropy, follows from the relation (4.33). From value of d^2S, a parameter R, i.e., "a gas constant," can be estimated, which is well defined on atom and molecular level. Unfortunately, this value is for specific ecological system still unknown.

From thermodynamic point of view, sex reproduction is more advantageous for $g > 4$ (more than 2 descendants). Because ΔG_{Xp} and ΔG_{Xs} are negative (processes are spontaneous), it is written as

$$\Delta G_{\mathrm{Xp}} > \Delta G_{\mathrm{Xs}} \quad \text{or} \quad -\Delta G_{\mathrm{Xp}} < -\Delta G_{\mathrm{Xs}} \quad \text{for } g > 4. \tag{4.63}$$

Thus, the same number of descendants produced by sex reproduction is reached by the lower Gibbs free enthalpy, and it is probably the reason why sex reproduction is evolutionarily advantageous (compared with cell division).

4.3.4.2 Dynamics of Ecological System with Migration

Influence of reproduction and migration dynamics is evident on example of two competitive ecological systems (in general two autocatalytic reactions) of type predator (X_3) and prey (X_2). Kinetics of that system can have the form as follows

$$\begin{aligned} &\mathrm{EI} + \mathrm{X}_2 \underset{k_{-1}}{\overset{k_{+1}}{\rightleftarrows}} g_1\mathrm{X}_2 - \bar{J}(\mathrm{X}_2) && (\rho = 1),\\ &\mathrm{X}_2 + \mathrm{X}_3 \underset{k_{-2}}{\overset{k_{+2}}{\rightleftarrows}} g_2\mathrm{X}_3 - \bar{J}(\mathrm{X}_3) && (\rho = 2),\\ &\mathrm{X}_3 \underset{k_{-3}}{\overset{k_{+3}}{\rightleftarrows}} \mathrm{E'I} && (\rho = 3). \end{aligned} \tag{4.64}$$

EI and E′I represent interaction with surrounding before and after reaction. It is a classical Lotka–Volterra model that is a base of other ecological models [8, 12].

$\bar{J}(\mathrm{X}_2), \bar{J}(\mathrm{X}_3) > 0$ show leaving of individuals out of place (migration). The first two reactions model reproduction, and the third reaction models cessation of predator. These reactions describe very simplified food chain. Reaction rates are expressed by the law of mass action

$$\begin{aligned} \dot{\varsigma}_1 &= k_{+1} N_{\mathrm{EI}} N_2 - k_{-1} N_2^{g1}, \\ \dot{\varsigma}_2 &= k_{+2} N_2 N_3 - k_{-2} N_3^{g2}, \\ \dot{\varsigma}_3 &= k_{+3} N_3 - k_{-3} N_{\mathrm{E'I}}. \end{aligned} \tag{4.65}$$

Assuming rates of reversed reactions equal to zero (it is just reproduction), the rate of the origin of individuals is

$$\begin{aligned} \frac{\partial N_2}{\mathrm{d}t} &= \dot{\varsigma}_1 - \dot{\varsigma}_2 - \bar{J}(\mathrm{X}_2) = k_{+1} N_{\mathrm{EI}} N_2 - k_{+2} N_2 N_3 - \bar{J}(\mathrm{X}_2), \\ \frac{\partial N_3}{\mathrm{d}t} &= \dot{\varsigma}_2 - \dot{\varsigma}_3 - \bar{J}(\mathrm{X}_3) = k_{+2} N_2 N_3 - k_{+3} N_3 - \bar{J}(\mathrm{X}_3). \end{aligned} \tag{4.66}$$

Due to the neglect of reversed reactions, the parameters of rate of reproduction g_1 and g_2 do not affect the final number of N_2 (prey) and N_3 (predator) individuals. Crucial influence has migration. Migration is described in the cylindrical coordinates by diffusive flux, that represents leaving of individuals as a consequence of their infestation in a place, r is the distance from a center

$$\bar{J}(\mathrm{X}_2) = -\frac{D_2}{r}\frac{\partial}{\partial r}\left(\frac{r\partial N_2}{\partial r}\right), \quad \bar{J}(\mathrm{X}_3) = -\frac{D_3}{r}\frac{\partial}{\partial r}\left(\frac{r\partial N_3}{\partial r}\right). \tag{4.67}$$

Stationary values N_{20} and N_{30} are obtained from the following expressions

$$\begin{aligned} 0 &= k_{+1} N_{\mathrm{EI}} N_{20} - k_{+2} N_{20} N_{30} + \frac{D_2}{r}\frac{\partial}{\partial r}\left(\frac{r\partial N_{20}}{\partial r}\right), \\ 0 &= k_{+2} N_{20} N_{30} - k_{+3} N_{30} + \frac{D_3}{r}\frac{\partial}{\partial r}\left(\frac{r\partial N_{30}}{\partial r}\right). \end{aligned} \tag{4.68}$$

Solution of these equations is the Bessel functions of the first kind, which describe changing and decreasing concentration $N_{20}(r)$ and $N_{30}(r)$ from a center (epicenter). Further, presented solution represents simplified case, which is given by the sum of Eq. (4.68)

$$k_{+1} N_{\mathrm{EI}} N_{20} - k_{+3} N_{30} + \frac{1}{r}\frac{\partial}{\partial r}\left(\frac{r\partial(D_2 N_{20} + D_3 N_{30})}{\partial r}\right) = 0. \tag{4.69}$$

This expression is now split into two parts. The first part describes reproduction and competition, when the second part describes migration

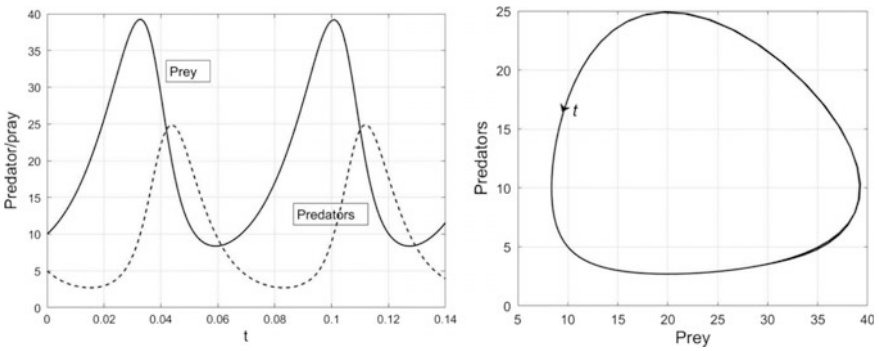

Fig. 4.6 Dynamics of ecological model predators (N_{30})–prey (N_{20}), for stationary values $N_{30} = 10$, $N_{20} = 20$, with rate constant $k_{+1}N_{EI} = 70$, $k_{+2} = 7$ and time period $\tau = 0.064$. Thermodynamically correct evolution is in the *direction of arrow* because just evolution in this direction produces positive entropy

$$k_{+1}N_{EI}N_{20} - k_{+3}N_{30} = 0, \quad \frac{1}{r}\frac{\partial}{\partial r}\left(\frac{r\partial(D_2N_{20} + D_3N_{30})}{\partial r}\right) = 0. \tag{4.70}$$

Solutions of Eq. (4.70) are

$$N_{20} = \frac{k_{+3}N_{30}}{k_{+1}N_{EI}} \quad \text{or} \quad N_{20} = \frac{k_{+3}}{k_{+2}}, \quad N_{30} = \frac{k_{+1}N_{EI}}{k_{+2}}, \tag{4.71}$$

$$D_2N_{20} + D_3N_{30} = P = \text{const.}\left[(\text{number of Prays and Predators})\text{s}^{-1}\right]$$
$$\text{for } N_{20}\left[(\text{number of Prays})\text{m}^{-2}\right] \quad \text{and} \quad N_{30}\left[(\text{number of Predators})\text{m}^{-2}\right], \tag{4.72}$$

where the migration part is equal to zero, i.e., migration fluxes are compensated $\bar{J}(X_2) = -\bar{J}(X_3)$, and moreover, singular solution with term ln r is omitted. Relations (4.71) are stationary solutions of Eq. (4.68) with compensated migration, and relations (4.72) represent local distribution of prey and predators. Variable P expresses dynamics of change of species number and moreover is constant in space and time. Specific calculations are given by rate constant (4.59) of reactions (4.68) and by values of migration (diffusive) coefficients D_2 and D_3 [m^2 s^{-1}]. An example of dynamical behavior of two competitive population with compensated migration, see Fig. 4.6, is described by Eq. (4.68), which for the stationary state (4.71) have the form

$$\begin{aligned} \frac{dN_2}{dt} &= k_{+1}N_{EI}N_2\left(1 - \frac{N_3}{N_{30}}\right), \\ \frac{dN_3}{dt} &= k_{+2}N_3(N_2 - N_0). \end{aligned} \tag{4.73}$$

Stability of Ecological System with Migration

Stability of system can be studied by the fluctuation dynamics of stationary state (4.68) in the form of traveling wave in direction r from center

$$\begin{aligned} N_2(r,t) &= N_{20}(r) + \delta N_2(r,t), \quad \delta N_2(r,t) = \delta \bar{N}_2 \exp(\omega t - ikr), \\ N_3(r,t) &= N_{30}(r) + \delta N_3(r,t), \quad \delta N_3(r,t) = \delta \bar{N}_3 \exp(\omega t - ikr), \quad \omega = \omega_r + i\omega_{im}. \end{aligned} \tag{4.74}$$

The equation describing fluctuation is given by Eq. (4.74) with Eq. (4.68) and using stationary solution (4.68). Then, the fluctuation is described by following expression

$$\begin{pmatrix} -\omega + k_{+2}\Delta N_{30} - D_2(k^2 + ik/r) & -k_{+2}N_{20} \\ k_{+2}N_{30} & -\omega + k_{+2}\Delta N_{20} - D_3(k^2 + ik/r) \end{pmatrix} \begin{pmatrix} \delta N_2 \\ \delta N_3 \end{pmatrix} = \begin{pmatrix} 0 \\ 0 \end{pmatrix}. \tag{4.75}$$

Deviations from the stationary solution with compensated migration (or with no migration), Eq. (4.71), are denoted by

$$\Delta N_{20} = N_{20} - \frac{k_{+3}}{k_{+2}}, \quad \Delta N_{30} = \frac{k_{+1}}{k_{+2}} N_{\mathrm{EI}} - N_{30}. \tag{4.76}$$

Existence condition of nonzero fluctuations is zero determinant of Eq. (4.75). The simplified stationary case, Eqs. (4.71) and (4.72), is given by $\Delta N_{20} = \Delta N_{30} = 0$. The specific stationary state (4.71) is maintained by permanent leaving of prey $D_2 = D > 0$ and by permanent arrival of predators $D_3 = -D_2 < 0$. Using these assumptions in the migration terms (4.69) and then by putting the matrix into Eq. (4.75) and by splitting the final expression into the real and imaginary parts, the relation of the frequency of traveling wave is obtained

$$\begin{aligned} &\omega_r^2 - \omega_{im}^2 - D^2\left(k^4 - \frac{k^2}{r^2}\right) + k_{+2}^2 N_{20} N_{30} = 0, \\ &\omega_r = \frac{D^2 k^3}{\omega_{im} r}. \end{aligned} \tag{4.77}$$

In the case of no migration (for $D = 0$), Eq. (4.73), the frequency of fluctuation of number individuals $\omega_{im0} = \sqrt{k_{+1}k_{+3}N_{\mathrm{EI}}}$ depends on the conditions of surroundings and rate constants of prey reproduction and decay rate of predators (see Fig. 4.6).

The next simple solution is obtained for the case of long distance from origin, i.e., for $r \to \infty$

$$\omega_{im} = \frac{2\pi}{\tau} = \pm\sqrt{k_{+1}k_{+3}N_{\mathrm{EI}} - D^2k^4}. \tag{4.78}$$

Thus, the migration decreases the frequency of dynamical state of system. Due to the migration, this dynamical state can change to the stationary state when time period is high enough, i.e., $\tau \to \infty$. In this case, it is possible to determine a distance, where this change of states occurs. So that, the traveling wave stops and its wavelength λ is

$$\lambda = 2\pi\sqrt{\frac{D}{\omega_{im0}}} = 2\pi\sqrt{\frac{D}{\sqrt{k_{+1}k_{+3}N_{\mathrm{EI}}}}}. \tag{4.79}$$

Number of prey decreases significantly at this distance. Moreover, the relation (4.79) is usable for the determination of parameters of the studied ecological model.

4.3.4.3 Basal Metabolism of Human Body

The dynamical state, Eq. (4.45), for biological system, e.g., human body, can be in its simplest terms, which is written as

$$-\bar{J}(S_0) = -\int_A \frac{-\mathbf{j}_q}{T}\,\mathrm{d}\mathbf{a} - \int_A \sum_{\alpha=1}^{r}\left(\frac{\rho_\alpha\mu_\alpha\mathbf{v}_{D\alpha}}{T}\right)\mathrm{d}\mathbf{a} = \frac{\dot{\overline{\Delta Q}}}{T_{\mathrm{surroundings}}} + \frac{\dot{\overline{\Delta G}}}{T_{\mathrm{body}}} = P(S) > 0. \tag{4.80}$$

Note that, for integration is used an outer normal of the system (body) surface, is used, i.e., $\dot{\overline{\Delta Q}} > 0$ for heat added through the system surface (it was added more heat than removed heat) and $\dot{\overline{\Delta G}} > 0$ for consumed Gibbs enthalpy by the system.

Chemical reactions during digestion have to be spontaneous, so the Gibbs enthalpy has to be negative. In other words, the food has to be digestible. For human organism, the purest energy is glucose added by infusion. Molar mass of glucose $C_6H_{12}O_6$ is 180 g mol^{-1}. The Gibbs enthalpy of glucose is -2880 kJ mol^{-1} for aerobic metabolism. Furthermore, the Gibbs enthalpy of products of complex reaction cycle leaving an organism is -1740 kJ mol^{-1}. There are chemical reactions in human organisms, which are not spontaneous, i.e., $\Delta G > 0$. These non-spontaneous chemical reactions, satisfying mainly sustainability of the ions non-equilibrium on cell membranes and for proteins production, are supported by ATP (adenosine triphosphate). Human organisms produce for these reactions 38 mol of ATP from the Gibbs enthalpy $\Delta G = 1140$ kJ mol^{-1}.

Glucose consumption of organism that does not do work ($p\mathrm{d}V = 0$), e.g., on intensive care unit, is according to the balance of energy (4.24) assuming an isothermal system ($\mathrm{d}U = 0$), sketched in (4.81). So that, the heat power (approximately 75 W) determines amount of consumed glucose

$$\begin{aligned} &\dot{\overline{\Delta Q}}(-75\ \mathrm{W}) = -\dot{\overline{\Delta G}} \\ &\left(\text{up to 4 mg s}^{-1}\text{ of glucose}\right) \rightarrow \text{basal metabolism 6347 kJ day}^{-1}. \end{aligned} \tag{4.81}$$

Value of basal metabolism 6347 kJ day^{-1} is used as an assumed limit value. This problem is depicted in more details in [30].

The entropy production of a human being in basal metabolism state at ambient temperature 18 °C is given from the stability condition of the dynamical equilibrium (4.80) assuming the balance of energy in form (4.81)

$$\begin{aligned} P(S) &\approx -\frac{\dot{\overline{\Delta Q}}}{273+18} - \frac{\dot{\overline{\Delta Q}}}{273+37} = -(-75)\left(\frac{1}{273+18} + \frac{1}{273+37}\right) \\ &= 0.5\ \mathrm{W\ K^{-1}} > 0. \end{aligned} \tag{4.82}$$

This minimal entropy production needs to be maintained for keeping the thermodynamic non-equilibrium (figuratively "preservation of life") and depends strongly on the temperature of surroundings. In relation (4.82), the heat $\dot{\overline{\Delta Q}}$ has to be lower than zero, which corresponds to removed heat. But condition (4.82) would fail in case of the insufficient removed heat, as shown in (4.80), where absolute value of the term $\dot{\overline{\Delta G}}$ decreases faster than heat that is removed. The balance of energy (4.81) is still valid, but due to finite relaxing time, entropy increases irreversibly.

References

1. Truesdell C (1984) Rational thermodynamics. Springer, New York
2. Eringen AC (1975) Continuum physics, Vol. II: continuum mechanics of single-substance bodies. Academic Press, New York
3. de Groot SR, Mazur P (1962) Non-equilibrium thermodynamics. North-Holland, Amsterdam
4. Glansdorff P, Prigogine I (1971) Thermodynamic theory of structure, stability and fluctuations. Wiley-Interscience, New York
5. Jou D, Casas-Vázquez J, Lebon G (2010) Extended irreversible thermodynamics, 4th edn. Springer, Berlin
6. Woods LC (1975) The thermodynamics of fluid systems. Bristol, Oxford
7. Dawkins R (2006) The selfish gene, 3rd edn. Oxford, Oxford
8. Jorgensen SE, Svirezhev YM (2004) Towards a thermodynamic theory for ecological systems. Elsevier Ltd., Amsterdam
9. Atkins P (2010) The laws of thermodynamics: a very short introduction. Oxford, New York
10. Landau LD, Lifshitz EM (1980) Statistical physics. Pergamon Press, Oxford
11. Callen HB (1985) Thermodynamics and an introduction to thermostatistics. Wiley, Singapore

12. Prigogine I (1980) From being to becoming. W. H. Freeman and Company, San Francisco
13. Eddington AS (1929) The nature of the physical world. The Maxmillan Company, New York
14. Clausius R (1854) Über eine veränderte Form des zweiten Hauptsatzes der mechanischen Wärmetheorie. Annalen der Physik und Chemie 93(12):481–506
15. Gibbs JW (1884) On the fundamental formula of statistical mechanics, with applications to astronomy and thermodynamics. In: Proceedings of the American Association for the Advancement of Science, vol 33, pp 57–58. Reproduced in The Scientific Papers of J. Willard Gibbs, Vol II, pp 16 (1906)
16. Boltzmann L (1974) Theoretical physics and philosophical problem (trans: Brush SG). Reidel, Boston (Original work published 1886)
17. Einstein A (1909) Zum gegenwärtigen Stand des Strahlungsproblems. Physikalische Zeitschrift 10:185–193
18. Onsager L (1931) Reciprocal relations in irreversible processes I. Phys Rev 37:405–426
19. Onsager L (1931) Reciprocal relations in irreversible processes II. Phys Rev 38:2265–2279
20. Schrödinger E (1967) What is life. Cambridge Press, Cambridge
21. Eigen M (1971) Selforganization of matter and the evolution of biological macromolecules. Naturwissenschaften 58:465–523
22. Voet D, Voet JG (1995) Biochemistry, 2nd edn. Wiley, New York
23. Kjelstrup S, Bedeaux D (2008) Non-equilibrium thermodynamics of heterogeneous systems. World Scientific Publishing, Singapore
24. Pavelka M, Maršík F, Klika V (2014) Consistent theory of mixtures on different levels of description. Int J Eng Sci 78:192–217
25. Atkins P, de Paula J (2006) Physical chemistry, 8th edn. Oxford University Press, Oxford
26. De Heer J (1957) The principle of Le Châtelier and Braun. J Chem Educ 34(8):375–380
27. Kazuhisa M (1997) Renewable biological systems for alternative sustainable energy production [online]. Food and Agriculture Organization of the United Nations (seen 14 Jan 2016). Available at: http://www.fao.org/docrep/w7241e/w7241e06.htm
28. Key World Energy Statistics (2015) [online] The International Energy Agency (seen 18 Jan 18 2016). Available at: http://www.iea.org/publications/freepublications/publication/KeyWorld_Statistics_2015.pdf
29. World population prospects (2016) [online] United Nations, Department of Economic and Social Affairs, Population Division (seen 20 Jan 2016). Available at: http://esa.un.org/unpd/wpp/
30. Henry CJK (2005) Basal metabolic rate studies in humans: measurement and development of new equations. Public Health Nutrition 8(7A):1133–1152

Chapter 5
Kinetic Phase Diagrams as an Enforced Consequence of Rapid Changing Temperature or Diminishing Particle Size: Thermodynamic Fundamentals and Limits

Jaroslav Šesták

Abstract The innovative sphere of kinetic phase diagrams as a special domain of routine thermodynamic determined diagrams is re-evaluated while accentuating its specificity and practical impact when studying system under rapid changes of temperature (e.g., cooling). Requirement for a certain driving force in order to accomplish transformations is explored. It involves merger of heating–cooling as a nonequilibrium thermodynamic state of a certain sample 'autonomy.' The meaning of temperature is discussed when measured during inconstant thermal experiments. Thermodynamic legitimacy when assuming the effect of programmed temperature changes at the constant heating rate is examined and approved. Query about the implication of the term 'temperature' under rapid quenching results in a proposal of new tem 'tempericity.' Size as another degree of thermodynamic freedom is observed and investigated for the issue of nanomaterials providing the apparent analogy between the temperature-dependent kinetic phase diagrams and those obtained for diminishing particle size. Specific behavior of nanocomposites is explored regarding the particle curvature, temperatures of transformation, dissolution or phase separation, etc. Extension of kinetic phase diagram to the nanostate determinability, involving thermodynamics expanded by 'one dimension' as a result of severely contracted particle surface, is dealt with. The chapter contains 92 references.

5.1 Introducing Equilibrium and Off-Equilibrium Thermodynamics

In view of a nonstationary character of near-equilibrium conditions of thermal analysis, we have to discriminate three gradual stages of our thermodynamic description related to the intensive, $\Im$ [1], and extensive, X, parameters. This case is

J. Šesták (✉)
New Technologies Research Centre (NTC-ZČU), University of West Bohemia,
Universitní 8, 30114 Pilsen, Czech Republic
e-mail: sestak@fzu.cz

J. Šesták et al. (eds.), *Thermal Physics and Thermal Analysis*,
Hot Topics in Thermal Analysis and Calorimetry 11,
DOI 10.1007/978-3-319-45899-1_5

predominantly associated with temperature, T, and its linearly programmed changes, $\beta = \mathrm{d}T/\mathrm{d}t$ [1]:

(Classical) equilibrium	Near-equilibrium	Off-equilibrium
$\Im, (\mathrm{d}\Im \to 0)$	$\Im, (\Delta\Im, \mathrm{d}\Im/\mathrm{d}t = \text{const})$	$\Im, (\mathrm{d}\Im/\mathrm{d}t, \mathrm{d}^2\Im/\mathrm{d}t^2 \neq \text{const})$
$T, (\mathrm{d}T \to 0)$	$T, (\Delta T, \mathrm{d}T/\mathrm{d}t = \beta)$	$T, (\mathrm{d}T/\mathrm{d}t, \mathrm{d}^2T/\mathrm{d}t^2 \neq \text{const})$

Any closed system under investigation is defined and described by the energy-conserving approach to equilibrium, which in its limit subsists factually a state of 'thermal death.' The counterpart in thermoanalytical dynamics brings the reality of external fields which give and take away energy to the system without being modified. Still further, we can consider thermodynamics of an open system with two thermal baths providing the possibility of thermal cycles. We may go on assuming several baths getting closer and closer to the description of a real multiplicity situation in nature through the so-called irreversible thermodynamics [2] which, however, is not easy for everyday application.

Therefore, in classical thermodynamics (understood in the yet substandard notation of 'thermostatics' [3]), we generally accept for processes the nonequality in terms of entropy $\mathrm{d}S \geq \mathrm{d}Q/T$ accompanied by a statement to the effect that although $\mathrm{d}S$ is a total differential, being completely determined by the states of system, the counterparty heat $\mathrm{d}Q$ is not implicating that heat is not a true energy which is incongruity of thermodynamic laws [4] (see Chap. 3). This has its very important consequence that in an isolated system, $\mathrm{d}Q = 0$, entropy has to increase; however, processes move toward equilibrium and the equilibrium state corresponds to maximum entropy. In actual nonequilibrium thermodynamics, the local entropy follows the formalism of extended thermodynamics where gradients are included and small corrections to the local entropy appear due to flows, making $\mathrm{d}S/\mathrm{d}t \geq \mathrm{d}Q/\mathrm{d}t(1/T)$. In continuous systems, the local increase in entropy can be then defined using the local production of entropy density, $\sigma(r, t)$. For the total entropy change, $\mathrm{d}S$, consisting of internal changes and contributions due to interaction with the surroundings (source, *i*), we can define the local production of entropy as $\sigma(r, t) \equiv \mathrm{d_i}S/\mathrm{d}t \geq 0$. Irreversible processes [2] obey the Prigogine evolution theorem on the minimum of the entropy production and hence $S = S^{\mathrm{dis}} + \sum^{\mathrm{source}}$, where $\sum^{\mathrm{source}} > 0$.

We can produce disequilibrium operating from the outside at the expense of some external work, $\Delta W^{\mathrm{ext}} > 0$ (using the classical Gibbs terminology and function, Φ), and once the system is taken away from its equilibrium, we can consider ΔW^{ext} as $\Delta \Phi^{\mathrm{max}}$, now understood as the maximum obtainable work. We can relate the ratio of ΔW^{ext} to $\Delta \sum^{\mathrm{source}}$ as the inequality greater than zero. For $\Delta W^{\mathrm{ext}} \to 0$, we can assume the ratio limit to catch the equality $\Delta \sum^{\mathrm{source}} / \Delta W^{\mathrm{ext}} = 1/\mathrm{T} (= \partial S/\partial U$, where U is the standard internal energy). It is important saying that the arrow of thermodynamics goes in the direction of the increased entropy (or dissipated energy) that was embedded in the disequilibrium situation. This is

another representation of the second law of thermodynamics leading us in a natural way to think in terms of disequilibrium potency. If there is no disequilibrium, we must spend energy to generate it granting to bring alive the needed driving force. Nevertheless, if disequilibrium is already given, we may think of extracting energy from it. As a result, the ratio $\Delta\sum^{\text{source}}/\Delta W^{\text{ext}}$ can be understood in terms of heat flow in view of the efficiency of Carnot's ideal conversion $\eta = 1-T_2/T_1$ to become $\Delta\sum^{\text{flow}}/\Delta W^{\text{ideal}} = 1/T_2$. An advanced equation for the efficiency η of a semi-ideal heat engine operating at maximum power under irreversible heat transfer becomes, however, $\eta = 1-\sqrt{T_2}/\sqrt{T_1}$ [4, 5]. It comes up with a new content: Before we talked of energy that was dissipated, we have to point out the energy, which is actually extracted. Thermodynamics is thus a strange science because it teaches us simultaneously: *how both the Nature and our active artifact system behave*.

5.2 Thermodynamic Legitimacy When Assuming the Effect of Programmed Temperature Changes at the Constant Heating Rate

Let us first talk about the standard procedures applied to thermoanalytical experiments under the orthodox constant heating, β. A primitive self-assurance of the reliability of these traditional thermoanalytical examinations can be based on the quotation of heat exchange $Q'(=\mathrm{d}Q/\mathrm{d}t)$ between the sample and its surroundings. It is thus customized as a fundamental feature, specifying experimental conditions of all thermal measurements [1–4]. As such, it must be reflected by the fundamental quantities when defining our extended system; i.e., the principal quantities (temperature, T or pressure P) must be also expressed as functions of time, i.e., $T = T(t), P = P(t)$ or generally any intensive $\Im = \Im(t)$. Therefore, a sufficient description of the sample environment in the so-called *dynamic thermal analysis* requires specification, not only the traditional values of T or P (and other $\Im$) but needing also the particular inclusion of the time derivative of temperature, $T'(=\mathrm{d}T/\mathrm{d}t = \beta)$, respecting thus the kind of dynamic environment. Please note that the apostrophe $'$ signifies derivatives and the bold italic letters $(\Im, T, P)$ functions.

Hence, the state of material can be characterized in terms of material (*constitutional*) functions [1, 3] of the following type $= V(T, T', P), S = S(T, T', P)$, or generally, $\Phi = \phi(T, T', P)$. Let us write the basic energy equation in forms of fluxes, i.e., $U' = Q'-PV'$ or as a general inequality relation, $0 \geq U' + TS'-PV'$, where primes again represent the time derivatives. Substituting the generalized thermodynamic potential, Φ, the above inequality, eventually complemented with another pair of $(\boldsymbol{\mathcal{J}} \leftrightarrow X')$, is changed to $0 \geq \Phi' + ST'-VP')$. Now, we can substitute the partial derivatives from material relations into the inequality of the state function, $\phi(T, T', P)$, or $0 \geq [\partial\phi/\partial T + S]T'[\partial\phi/\partial P-V]P' + [\partial\phi/\partial T']T''$.

According to the permissibility rule, the above relation must hold for *any* allowed process and for all values T and P (and further $\Im$), as well as for their

derivatives, which can thus be chosen arbitrarily and independently. For $T = 0$ and $P = 0$, it is reduced to its last term, i.e., $0 \geq [\partial\phi/\partial T]T$, which can be solved for all T only if $[\partial\phi/\partial T] = 0$. Consequently, the constitutive *state function* $\phi(T, T', P)$ *cannot depend on temperature derivatives* T' and its form reduces to the simple initial $\phi(T, P)$ known from textbook thermodynamics. The term *temperature remains here fully justified*. In the same way, we can eliminate the second P and any other term $\Im$ by accounting the pairs $T-P$ or generally $T-\Im$. It, however, does not apply to the inclusion of the second derivative $T'' = \mathrm{d}^2T/\mathrm{d}t^2$ (i.e., inconstant $T' = \mathrm{d}T/\mathrm{d}t \neq \beta$) and the new-fangled state function $\phi(T, T', T'', P)$ which does not allow the application of standard thermodynamic relations, and thus, the entire term of temperature may request a revision.

However, the analysis of the entropy term of the first expression is more difficult [1–3] because it can be split into two parts, i.e., equilibrium-related entropy, $S_{\mathrm{eq}} = \mathbf{S}(T, T' = 0, P)$, and the complementary term, $S_i = S-S_{\mathrm{eq}}$, or $0 \geq [\partial\phi/\partial T + S_{\mathrm{eq}}]T' + [S-S_{\mathrm{eq}}]T'$. For the fixed values of T and P, it takes the form of an analytical relationship, $0 \geq aT' + b(T')T'$, involving variable T', with $b(T')$ approaching zero, if $T' \to 0$. Such an inequality can be satisfied for arbitrary T only if $a = 0$ and if $b(T')T' \geq 0$, i.e., if $\partial\phi/\partial T = S_{\mathrm{eq}}$ and $[S-S_{\mathrm{eq}}]T' \leq 0$. The resultant relation represents the *dissipation inequality*—providing the *term* $S = \boldsymbol{S}(T, T', P)$ is negligible or, at least, sufficiently small. This is a reasonable portrayal of a *quasistatic process* for which the standard relationships of classical (equilibrium) thermodynamics are valid to an agreeable degree [2]. In conclusion, we can emphasis that we do not need to make any special notional adjustments for thermoanalytical experiments carried out under $\beta =$ constant. However, this presumption (of $\beta =$ constant) *is not perpetually legitimate* because of the real experimental arrangement and involved heat obstruction, e.g., sample gradients and inertia, and difference between temperatures of the sample acceptor and the furnace source, and the steady change of later is often misused as the sample true temperature for kinetic calculation [1, 3].

5.3 Requirement for a Certain Driving Force in Order to Accomplish Transformations

Any system to carry on a transformation needs to include a certain driving force [3–8] which in the focus of solid-state transformations is usually located from an overheating or undercooling, $\pm\Delta T$, embedded between the equilibrium temperature, T_o and that of an immediate state, T. This is well exampled for crystallization of melts graphically portrayed in Fig. 5.1.

The widespread representation of such a thermodynamic process needs incorporating time, t, often represented by the form of so-called ***T-T-T*** diagrams (transformation–temperature–time) [8–10]. However, for continual temperature

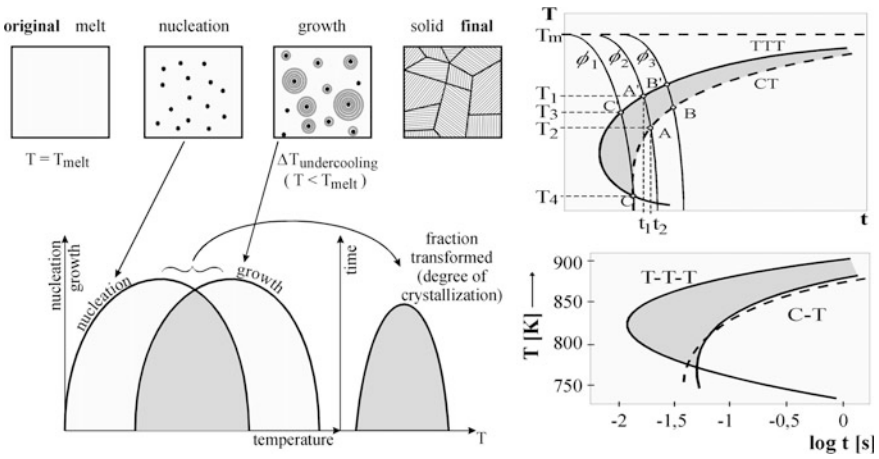

Fig. 5.1 (*left*) inclusive diagram of the mutually overlapping patterns of nucleation and growth showing that if nucleation curve goes first before the growth curve (*bottom left*), the overall crystallization process (*bottom right*) is straightforward (*upper*) toward the formation of solid crystalline product upon cooling. However, if their sequence is opposite (growth curve preceding nucleation), the crystallization becomes difficult because the early process of growth is hindered by lack of nuclei so that such a case requests seeding to trigger growth, which appeals for greater undercooling. The cooperative position of the curves, and the degree of their mutual overlapping, then determines the feasibility of overall processing, e.g., the ease of crystallization and/or opposite process of vitrification, for in the latter, the nucleation curve should be delayed behind the growth curve as much as possible. Entire dependence of ΔG for the new phase formation on the nucleus radius, r, under temperature, T, by way of the increasing undercooling, $\Delta T(=T - T_{\mathrm{eg}})$, provides certain the critical values. That is, the threshold size necessary to uphold the nuclei to exist (*circles*) decreases (*dashed line*) as the change $\Delta G^{1\to 2}$ is generally proportional to the ratio $\Delta T/T_{\mathrm{eq}}$. Assuming $T_{\mathrm{eq}} \cong T_{\mathrm{melt}}$ and introducing reduced values $T_r = T/T_{\mathrm{melt}}$ and $\Delta T_r = (T - T_{\mathrm{melt}})/T_{melt}$, the common approximate solutions can be developed convenient for practical application

Model	ΔH	ΔS	ΔG	Surface energy, γ	Critical ΔG_{crit}
Constant	ΔH_r	$\Delta H_r/T_r$	$\Delta H_r/\Delta T_r$	ΔH_r	$\Delta H_r/(\Delta T_r)^2$
Linear	$\Delta H_r T_r$	$\Delta H_r\, T_r/T_r$	$\Delta H_r/\Delta T_r\, T_r$	$\Delta H_r\, T_r$	$\Delta H_r\, T_r/(\Delta T_r)^2$ or $\Delta H_r/(\Delta T_r\, T_r)^2$

Right scheme of the construction of the nonisothermal C-T curves (*upper*) from the known shape of the isothermal T-T-T diagram in the coordinates of temperature (*vertical*) and logarithm of time (*horizontal*). Shade areas put on view the difference between both treatments. Below there are shown two real cases, C-T curves calculated by the approximate method of *Grange* and *Kiefer* [10] (*dashed line*) and by the direct method suggested by *MacFarlane* [9] (*solid lane*). The curves are drawn in the comparison with their associated, classical T-T-T curves derived for the following sample alloys of $Pd_{82}Si_{18}$ using the data for its critical cooling rate, $\phi_{\mathrm{crit}} = 2 \times 10^7$[K/s], and right $-Au_{72}Ge_{14}Si_9$ with $\phi_{\mathrm{crit}} = 7 \times 10^3$[K/s] [8]

changes, it is transformed to ***C-T*** diagrams (cooling–temperature), see the right part of Fig. 5.1. It was found that the characteristic ratio of temperature of the curve nose (T_{nose}) to its value of melting T_m falls in the range from 0.74 to 0.82 with the value 0.77 being most typical. Illustrative cases of a detailed analysis applied to experimentally well-known system anticipating incorporation of various approximations and material characteristics are available in Refs. [7, 8]. The methods evaluating solidification behavior from cooling curve were practically treated as an assortment of methods [7–9] such as computer-aided cooling curve thermal analysis (CA-CCA) [11, 12], thus becoming an important topic endeavor.

5.4 Innovative Sphere of 'Kinetic Phase Diagrams' When Incorporating Radical Temperature Changes

A quarter century ago, we coined a new field called *kinetic phase diagrams* [7, 8, 14–18] as a continuation of the previous attempts [7–9] to describe phase relations of systems studied irregularly under extreme changes of the externally imposed experimental conditions. It has become an extension of the standard theory of phase equilibria [6, 7] applied to phase boundaries giving confidence to the development of experimental methods used for such 'nonstandard' investigations [8, 15]. It gave the impetus to the extensive physical–chemical program aimed at the compilation, tabulation, and interpretation of phase diagrams of substances in practically all the fields of natural science and technology [19– 27].

The theoretical foundation of thermodynamic analysis of the metastable equilibria occurring due to martensitic transformation was laid in late thirties of the twentieth century when transformation of austenite to martensite was calculated for the given content of carbon (to include strain energy of the crystal network rearrangement, interfacial energy, undercooling, as well as under the use of activities instead concentration). It changed the classical view to a 'true equilibrium' approach by admitting that the shape of experimentally determined phase diagrams can be affected by the 'degree of equilibration' altered during the experiment itself. The best example is the history of $SiO_2-Al_2O_3$ phase diagram which was continuously studied two hundred years. The interpretation of its high alumina regions varied from experiment to experiment according to the duration of the system annealing (from hours to weeks and even years) and was indicated to exhibit both the incongruent and the congruent melting points. This experiment can be generalized that the resulting data can be prejudiced by the experimentalists' view on what is appropriate experimental arrangement and adequate processing of the system resonance in order to attain equilibration in the reasonable time. In fact, a really true equilibrium is ideally achievable only during almost limitless 'geological-like' processes. Actually available rates of experimental measurements

fall, however, within the boundary area of the so-called thermodynamically imposed (somehow intense) conditions. The introduction of real conditions to the existing thermodynamic description must refer, to the state of local equilibrium, whether the rates of changes of state (macroscopic variables) are comparable with the rates of elementary (molecular) processes, which determine the state of the system at the microscopic level. It is often related to the ratio of $\Delta T/\Delta t \ll \langle T\rangle/\tau_T$ and/or $\Delta T/\Delta x \ll \langle T\rangle/\lambda$ where ΔT is the variation of temperature at macroscopic level during the time interval, Δt (or over the distance, Δx), and τ_T is the matching period of the elementary thermal motion of molecules or their mean free path, λ, at the given average temperature $\langle T\rangle$.

It was perceived granted that any new phase can be formed only under certain *nonequilibrium* conditions of a definite driving force, $\Delta\mu > 0$, aware that *at the equilibrium, no new phase can ever originate*. The conditions of particular points at which the phase transformation takes place are further determined by the transport of energy (heat) and mass (diffusion). Thus, we must study both the temperature and concentration changes (and distribution) in the system under a real investigation and their time adjustments in connection with the initial state, experimental impact, and boundary conditions (interfaces). So there arises a question how to correctly interpret the experimentally determined phase diagrams which do not fully comply with equilibrium conditions, the divergence being dependent on the experimental routine when approximating to the factually applied and thermodynamically mandatory conditions. It would require deeper knowledge of *metastable and unstable phase equilibria*, which would also promote the application of the thermodynamics of irreversible processes in new branches of science and technology and may bring about the discoveries of new phases and of the yet unknown (often longed-for) properties.

Hence, it follows that the existing phase diagrams can generally fall into three groups regarding their practical validity and applicability. There can be located those having the relevance in order of the following:

1. *Scientific age*, suitable for the tabulation of equilibrium data, adjusted with respect to the achieving as equilibrated state as experimentally realizable. It is often assumed that the equilibrium be arrived from both sides of equilibration, e.g., upon heating and cooling, too.
2. *Livelihood*, good enough for everyday use of a scientific generation in the sequence of years and wholly functional to prepare materials durable long enough to be defined as *stable* and measurable under experimentally accessible conditions.
3. *Given instant* relevant for a given experimental purpose, respecting particularity of a given arrangement and often freeze-in functionality (*kinetic phase diagrams)* to get the ready-to-use material of unusual properties to last for a certain limited period. It becomes a subject to the method of experimental observations (see. 2).

5.5 Intensive Cooling as a Nonequilibrium Thermodynamic Status of a Certain Sample 'Autonomy'

Current metallurgy bears the long-known consequences of certain nonequilibrium effects arising during equilibrium solidification, i.e., phenomena recognized as *metastable phase formation* and specific *coring* and *surroundings* (see Fig. 5.2). They indubitably occur in the vicinity of all characteristic (e.g., invariant) points [7, 8, 13–20] of phase diagrams. In the case of coring, the melt under solidification does not include sufficient time to follow equilibration process along the balanced curve of solidus, which is caused by insufficient mass transport toward the phase interface. The precipitated grains, whose centers are closer to the equilibrium composition than their core layers grown later, are the typical result. In the second case of surroundings, the originally precipitated phase starts to react with the remaining melt on reaching the peritectic temperature developing a new peritectic phase. It requires the atoms of one component to diffuse out from the melt to reach the phase interface. The thicker the layer to cross, the slower the diffusion proceeds, particularly if the atoms of the second component must diffuse in the opposite direction through the solid layers to counterpart the reaction. This, evidently, must imply certain nonequilibrium conditions even if assumed under the equilibrium solidification and the consequent modification of the notion: phase 'equilibrium' composition, which is gradually becoming irregular (often layered [28–32]), regularly affected by the diffusion-driven self-organization [28]. Supplementary elimination of such nonequilibrium concentration gradients is usually accomplished by subsequent thermal treatment to allow equilibrating rearrangement. Similar phenomena are regularly accoutered when single crystals are grown from foreign melts, their concentration gradients being dependent on the concentration changes

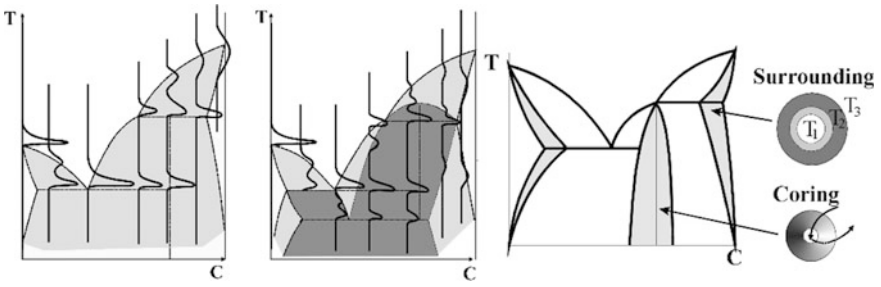

Fig. 5.2 *Left* Hypothetical α ↔ β binary eutectic–peritectic phase diagram showing critical points and phase separation lines (*thick solid*). Light shadow reveals equilibrium areas, while dark shadow areas are affected by metastability which, e.g., affects the experimentally observed DTA peak thermal responses. Prolonged *thin lines* with *arrows* reveal possible tendency of a metastability contour extension. *Right* The shadow areas are depicting equilibrating processes of due to mass transfer resulting in consequential grains layering in the vicinity of hyperperitectic (*above*) and peritectic (*below*) sites

in the matrix melt. These gradients are again a subject of secondary removal often by specific thermal treatment or by melt agitation.

On the other hand, practical aspects of mastering successfully the technology of rapid cooling are long known in material science (instigated in metallurgy and tailored for glassy metals). It deals with the so-called *rapid solidification* (or simply the process of *quenching*) where the meaning 'rapid' can be taken to imply a short-time interval between initiation and completion of solidification and high velocity of propagation of the advancing solidification front [14, 20, 28, 29]. It occurs either directly as a result of coupling between external heat extraction and the transport of latent and specific heat required to propagate the solidification front, or indirectly during the recalescence that follows nucleation of solidification at large undercooling.

For a system that cannot follow the experimentally enforced (usually rapid) temperature changes, the boundary lines shift almost freely along both the concentration and the temperature axes. Thereby, the regions of unstable phases are formed to be described in terms of the *kinetics of the physical–chemical processes* (especially fluxes of mass and heat). Such a truly kinetic phase diagram is fully dependent upon the experimental conditions applied (cooling rate, sample geometry, external fields, measuring conditions) and can portray materials, which state become fixed at room temperature by suitable *freeze-in* techniques [14, 15, 30]. It is best treated exactly in the case of a near-stationary process conditioned by, e.g., *Fokker–Planck* equation, *Monte-Carlo* method, or other stochastic process theory [14, 15] requiring higher state of mathematics such as the linear kinetic segregation model by comparing its predictions with the results of *Monte-Carlo* simulations for both a well-mixing systems and a phase separating structure [14, 15, 31, 32].

It is complicated by the introduction of local cooling rates and degrees of undercooling in bulk and at interfaces, and a mathematical solution requires very complicated joint solution of the equations for heat and mass transfer under given boundary conditions as well as that for the internal kinetics associated with phase transition on the solidification front [6, 20]. Evaluation yields interesting dependences between the undercooling, concentration, linear growth rate, and cooling rate, as simply demonstrated in Table 5.1 adding together with the effect of particle size discussed in the following paragraph.

A global view to the gradual development of a nonequilibrium phase diagram is illustrated in Fig. 5.3, exhibiting thus the consequence of intensified experimental processing, i.e., the gradual impact of more extreme temperature conduct. For lower cooling rates, it results in the slight refocus of phase boundary only, i.e., the implementation of curves extension (dotted extrapolation) called *metastability* which are yet thermodynamically 'loyal' regions. Faster cooling, however, forces the system to enter true 'kinetic status,' controlled by the rates of transport processes so that whole boundary setup (thick lines, new shadowed areas) are shifted away from the originally equilibrium pattern (thin lines). Finally, at the extreme temperature changes, the entire state becomes relocated to a highly nonequilibrium

Table 5.1 Some qualitative dependence of the solidification/melting parameters on the extreme external and internal alterations (assuming three orders changes)

Resulting change ⇒	T_f	ΔT	$C_{\text{liq}}\Delta \sim C_{liq} - C_{\text{solid}}$	G	Growth rate
Inserted increase ⇓ Internally adjusted diffusion transport					
$D \sim 10^{-6} \rightarrow 10^{-3}\text{m}^2/$	Decrease	Increase	Increase	Decrease	Increase
Externally applied cooling rate					
$\Phi \sim 10^3 \rightarrow 10^6\text{K/s}$	Increase	Increase	Increase	Decrease	Increase
Internally adjusted size of particles					
$r \sim 10^5 \rightarrow 10^2\text{nm}$	Decrease	Increase	Increase	Decrease	Increase

where $T_f, \Delta T, C_{\text{liq}}$, $\Delta \sim C_{\text{liq}} - C_{\text{solid}}$ and growth rate G are, respectively, the temperature on the solidification front, $T_f - T_{\text{eq}} = \Delta T$ temperature undercooling, attuned concentration of the liquid phase, resulting concentration difference in the solidification front, and the growth rate of solid-phase formation. Changed parameters are diffusion coefficient, D, cooling rate, Φ, and particle size, r

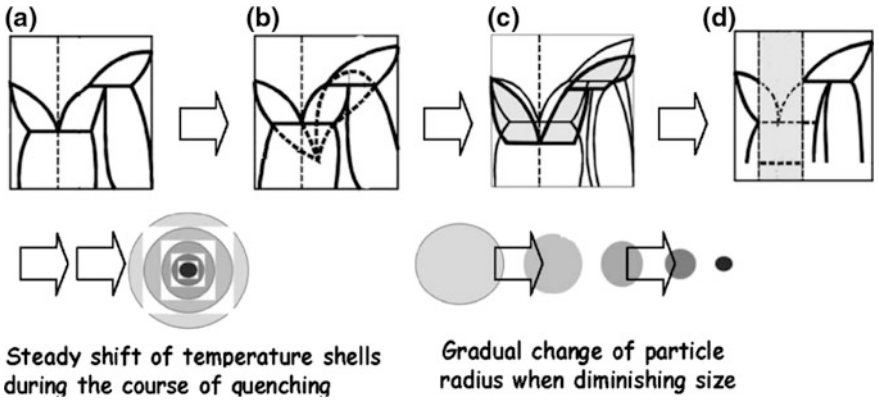

Fig. 5.3 The portrayal of state sequences (axis: temperature ↑ vs. concentration→) is illustrated along the increasing cooling impact from (**a**) to (**d**) likely affecting the particle core by stepwise de-enveloping (*below left*) which is compared with a mechanical process of gradual reduction of grain size (similarly diminishing the interface, *below right*). *Shaded areas* on *left* display the shifted nonequilibrium areas in limit, resulting in disordered (*glassy*) state, which in diminishing nanoparticles yields a similar crystal-order-less state, and it is clear that the consideration based on a single particle approach is simplified and inaccessible in practice of compact samples composed of assembled particles. The heat transfer is thus carried out through the sample bulk hitting progressively individual particles

condition, where the material structure cannot match the transport processes, which is a kind of forceful immobilization, i.e., establishment of a frozen-in state of glassiness or amorphousness, where the actual phase boundary is missing (or being featureless, shaded). Such a region is factually characterized by nonequilibrium

parameter called *glass transformation* [30, 33], cf. horizontal broken line in (d) of Fig. 5.3.

A portrayal of above pattern can be imaged in the form of concentric spheres (particles) in which heat is gradually withdrawn from the interior putting consequently a collectively temperature-gradient shell-like structure which is reminding the shrinking core model. It may evoke the mechanical procedure when a particle sphere is gradually reduced reminiscent to the progression of top-down nanoparticles formation discussed in the foregoing paragraph.

5.6 Query About the Implication of the Term 'Temperature' During Rapid Quenching—What About 'Tempericity' as an Alternative?

For experimental evidence, we can compare various cooling rates approximately anticipated for quenching of the melt of silicates down from the temperature of about 1200 °C. The maximum cooling rate subsists in the neighborhood of 104–5 K/s applying either the melt pressing between two moving metallic surfaces that form a ribbon with the thickness of about 0.2 mm or the melt disintegration to drops of about 0.5 mm in diameter and their centrifugation and splashing against metallic walls. Generally, drawing a fiber into liquid bath (with a diameter less than 0.5 mm) decreases the cooling rate by more than one order of magnitude and would become similar to the helium fast-flow cooling of thin layers or wires. When dropping droplets of melt ($\sim$3 mm in diameter) into suitable heat absorbing medias (oil), a cooling rate is experienced to about 102–3 K/s. The increasing quenching rate can cause the diminishing grain size, increase chemical inhomogeneities and origin supersaturation making easier the formation of disordered (glassy, amorphous) states. Chemically, it is usually achievable in the systems exhibiting as many components as possible situated in the vicinity of deep eutectics [29, 30].

An empirical relation in the form of a power law often holds for the dependence of the distance, d, of dendrites on the local solidification time, τ, or on the average cooling rate, ϕ, i.e., $d = a\,\phi^{-n} = a_0\tau^n$, where a, $a_{o,}$ and the exponent n are the characteristic constants. The local conditions of solidification to form constraint glasses upon the melt vitrification give up its specific heat, whereas coupled crystallization is accompanied by additional release of the heat of crystallization. The glass-forming ability is related to the ratio of $T_g/T_m = T_{\mathrm{gr}}$, the so-called reduced lass temperature, where T_g and T_m are the temperatures of glass transformation and melting, respectively [33]. The higher the value of T_{gr}, the lower the required critical cooling rate. Moreover, the cooling rate, ϕ, is essentially predisposed by the heat transfer coefficient, Λ, and the thickness of cooled sample, d, and relatively less by its entire temperature, and the estimated gradient is then matching $\sim \phi d/\Lambda$. At the condition of ideal cooling, where we assume infinitely high coefficient of heat transfer, the cooling rate ϕ is proportional to $1/d^2$, while for the

Newtonian cooling mode, which is controlled by the phase boundary, ϕ correlates with $1/d$ only. In practice, we may adopt the power relation $\phi = 1/d^n$ (where $1 \leq n \leq 2$ is an experimental constant). For illustration, we may present the example of cooling, which is close to ideal, with the proportionality coefficient, $\Lambda = 10^{-4}\,\mathrm{Jm^{-2}\,K^{-1}\,s^{-1}}$, frequently displayed for several real materials. We can guess the limiting (minimum) cooling rates of 10^2, 10^6, and 10^9 K/s for the critical sample thicknesses of respective 10, 5×10^{-2}, and 10^{-3} mm [30]. The latter value of thickness is very small, hardly attainable even by intensive laser glazing, which works with very thin layers and assures intimate contact of the in situ melt with the surface of solid support. It, however, lies within the possible rates assumed for vapor/gas deposition onto the solid surface, i.e., within about $\approx 10^9$ K/s. In the novel method of high cooling rate chip microcalorimetry [35, 36], the rate of the observed temperature changes reaches the order of 10^4 K/s for samples premelted and thinned on the microchip surface.

During all extraordinary fast temperature changes, there, however, arise a question whether the detected values sustain the meaning of a real sample temperature [31, 34–37] and how to ever calibrate temperature under such extreme changes when the danger of deep undercooling and disturbing metastability occurrence was noticed as early as in the turn of seventies [38]. Despite the successfulness of a special microchip technique particularly developed to study system behavior when undergoing rapid quenching [35, 36], we must question the reliability of figures provided by a *T*-measuring sensors which always display some numbers making thus possible to monitor processing temperature at as speedy cooling rates as 10^6 K/s [31, 34, 39].

It is well known that the temperature as a physical quantity is a numerical measure of hot and cold (hotness manifold), the measurement of which is realized by the way of instrumental detection [33]. Temperature and its measurement must stay in accordance with the thermodynamic law, declaring that measured physical systems are in thermal equilibrium and assuring that no heat flows between bodies involved in the measurement when they are connected by a path well permeable to heat [4, 40, 41]. During quenching, this premise is evidently violated as a significant amount of heat is flowing between the considered bodies arising the question where is the capability limit of such a separated measurement of heat and temperature under a cooperative process of their linked rapid changes. There may be present a similar threshold known as a *Heisenberg quantum limit* preventing a detached detection of a particle motion from its position. Similarly, there can exist limit for a parallel measurement of heat and temperature when taking place very far from required thermal equilibrium [34].

In such a case of experimentally not a well-'defined' temperature, cf Fig. 5.4 when being detected under crucially extreme heat conditions, one may instigate a novel terminology instituting an *operational quantity* instead the traditionally mandatory *physical quantity*. For popular scanning microcalorimetry at ultra-high cooling rate, we may coin a new term for the operational characterization of distinguishing temperatures derived on basis of 'melting-melt,' such as *melticity* even

if it would sound strange. Similarly, we can proceed originating a new term for operational temperature by using basis of 'temper' for coining a new term: *tempericity* [31, 34]. However, this falls beyond the scope of this chapter sounding moreover as desired music of future.

5.7 Size as Another Degree of Thermodynamic Freedom for the Issue of Nanomaterials

Novel-*nanostructured materials* and their description encompass a rich history beginning with a colloidal solution—heterogeneous mixtures in which the particle size of the substance is intermediate between a true solution and a suspension, i.e., between 1 and 1000 nm. Some properties of nanoparticles were investigated using the term microclusters (which term was used for the first time in 1661 by English chemist R. Boyle associated with Alchemist process of multiplied splitting up by division) and further including structural code or even inorganic gene [42]. It became close to the topic of chemistry beyond the molecule [43] and specially associated with a behavior in terms of superatoms exhibiting the quantum properties of nanoclusters (i.e., quantum nature of nanostates [44, 45]). Nanoparticles can be defined as aggregates of $<10^4$ atoms linking with a notion of the so-called Planck's mass which amounts to about $2{,}17 \times 10^{-5}$ g, both thus specifying the boundary of interfering quantum world [28, 44, 45].

Nanoworld thermodynamic groundwork [45–56] unfolds from a single-phase division, i.e., splitting up into two (α and β) separated phased by introducing new interfaces, eventually accompanied by elastic deformation (strain) and predominantly the curvature requesting the higher pressure on the concave side with respect to the surrounding, p, i.e., $p_\alpha > p_\beta = p$ (Young–Laplace effect) [56–58]. It follows that any *nanosystem possesses an extra degree of freedom*, which is the *size*, the study of which equilibrium requires a revision of traditional thermodynamics when transferring from macro- to nanoworld [37, 42–48]. Everything factually originates from the *Kelvin* 1805 historical relation, $\ln p/p_\infty = 2V\gamma/(RTr)$, and the related *Thomson* (1888) equation for temperatures, $T/T_\infty = 2V\gamma/(\Delta Hr)$, where $V, \gamma, \Delta H$, and r are the volume, surface tension, enthalpy change, and radius, respectively (sometimes called Gibbs–Thomson equation [57–59]).

In the other words, it means that if we want to create any equilibrium modification for a variation of curvature [60–70] upon the change of external conditions (T, p), we have to change either pressure (from $p_{\beta\infty}$ to $p_{\beta r}$ under constant T_∞) or temperature (from T_∞ to T_r under constant p_∞).

Certainly, there exists further particularizing models such as *liquid skin melting* (LSM), assuming that melting starts on the particle surface creating thus a thing surface layer of the thickness δ (adjustable parameter) so that $T/T_\infty = 1-(2V\gamma/(\Delta H(r-\delta))$. Eventually, it may include further shape dependability by $T/T_\infty = 1-(A/V\Delta H)(\gamma_{\mathrm{sol}} - \gamma_{\mathrm{liq}})$ for the difference in surface tension

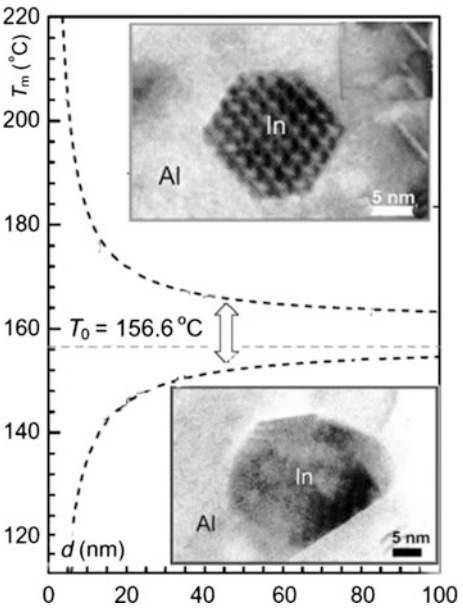

Fig. 5.4 *Upper plot* showing opposite temperature behavior when particle obtained by extreme melt fast quenching is firmly built-in the matrices having little volume flexibility and, bottom, loosely integrated particle produced by intensive ball milling having thus more space within the matrices, thus exhibiting classically assumed decrease in melting temperature upon the particle diameter (*d*). Evidently, there is a difference in the interface characteristics, not yet well understood, yielding an open space for further theory. Compiled and adapted on basis of data in Refs. [70, 71]

where for a sphere the ration of area versus volume, *A/V*, equals *3/r*. As a consequence, the crystallization temperature can be found dependent on both the particle diameter [63–69] and the experimentally implemented cooling rate [35, 72]. The first reveals an approach to a limiting value, while the second case discloses a sudden threshold of quenching where any crystallization becomes imperceptible. Another impact relates to the particle volume contraction, ΔV, due to the internal overpressure which may even result to the as-triggered internal phase transition. There, however, remains yet unsolved specifics of melting due to yet indefinite characteristic of the interface, such as coherent (with a small elastic deformation due to the small differences in atomic arrangements) and incoherent links (with a large elastic deformation due to the significant differences in atomic arrangements). Nanoworld brings new phenomena [53–69] linked to thermodynamics dependent on the shrinking particle size [46, 47].

As a curiosity, we can notice an experimentally observed variance on the temperature dependence of melting for nanoparticles of indium in the matrix of alumina prepared through different techniques (see above Fig. 5.4, [70, 71]). Furthermore, it is necessary to consider a supplementary effect of the particle versus matrix interface and consequent increase in inner pressure. In polymeric nanocomposites (wherein nanoobjects are nanofibers [61]), it forms a continuously surrounded rigid solid often under a various degree of core–shell structure. The core is often covered with a thin surface layer of an alternative material (chemically ached, oxidized, ion exchanged). Nevertheless, seldom happen that the inorganic filaments would show evidence of a lower melting temperature than the polymeric matrices, but it reveals the worth of interfaces' character on the interfaces contact strength.

Another worthy factor is the interior nanoparticles admixing where the routine *Ostwald-Freundlich* equation applies for dissolution of solid particles (of radius r) in liquids in contrast to bulk (∞) using molar ratios (x) in the form $\ln(x_r^m/x_\infty^m) = 1 - (2\gamma V)/(RT\,r)$. Another important upshot of nanodimensionality is the internal phase separation which in the particles can yield different appearance as shown for two limiting cases shown in Fig. 5.5 (left—core–shell and right—Janus models). It may undergo variety of configurations [53, 54] dependent on the surface tension and other internal dispositions typical for nanoworld. The Gibbs energy of mixing often comes to play because it becomes dependent on the particle interior dependent on the particle size and the atomic distribution varying from the simple flat surface due to the impact of curvature yielding surface interface segregation, cf. Fig. 5.5.

As a result, the phase diagrams of nanoparticles can exhibit various shapes providing similar characteristic images as that previously shown on temperature-affected kinetic phase diagrams [15]. Change in Gibbs energy of mixing due to the decreasing particle size will affect the degree of nonideality (boundary silhouette, cf. Fig. 5.6, upper) [72–77]. Irregular configuration becomes true when assuming internal metastable admixtures, while the factual kinetic diagrams with shifted boundaries become a result from contracting interfaces and expanded curvatures. The extremity state where the rapidly quenched systems looses it arrangement becoming noncrystalline (amorphous-like) is comparable with similar nanoworld manners where due to contraction particle size, the curved interface forces the lost of interior crystal ordering [46–48].

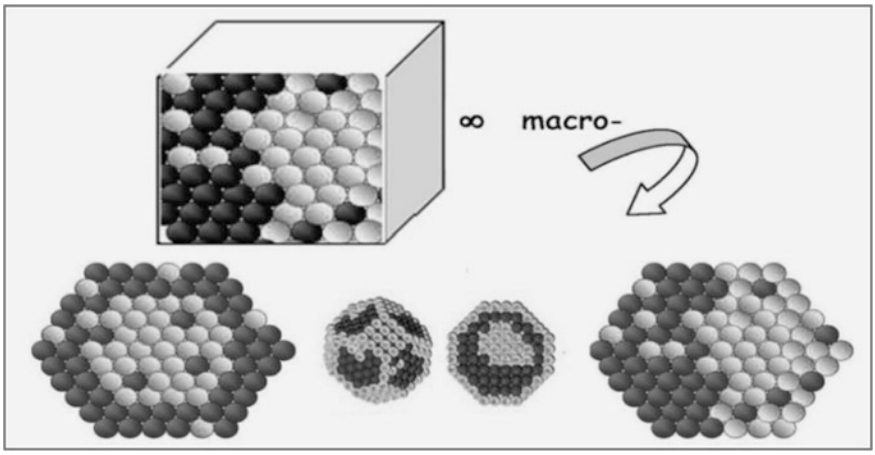

Fig. 5.5 Illustrative figure shoving the way of phase separation: going top-down from macrosystem to the sphere of nanoworld

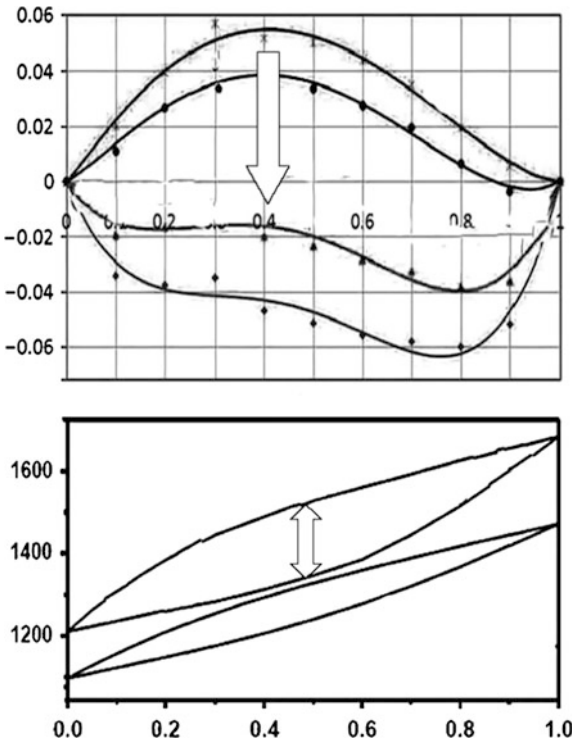

Fig. 5.6 *Upper* a model alloy ($\sim$Ag $\leftrightarrow$ Cu) showing decrement of mixing enthalpy for decreasing quantity of constituent atoms; *upper curves* with $\Delta H_{\text{mix}} > 0$ are valid for more than 2000 atoms in a clusters, while *below curves* with $\Delta H_{\text{mix}} > 0$ are relevant to those having clustered atoms below 600, moreover exhibiting a curved trend to indicating miscibility. In order to calculate the total energy of pure elements and the composition of the solution under standard conditions ($\sim T$), a classical molecular dynamics was employed and the size (number of atoms) of nanoparticles was taken into account by using a special correction factor [40–43]. It was designed according to the mixing Gibbs energy of a solid solution (modeled by Ag–Cu on the particle composition adjusted by different number of atoms [62–66]) and modified by rule for mixing and excess energy reliance while introducing relevant parameters on dimensions. For the case of a regular solution, the model by Jiang et al. [65] was considered. *Bottom* a model alloy phase diagram ($\sim$Ge $\leftrightarrow$ Si) assessed for both a macrosystem (bulk) and for a microsystem assembled by nanoparticles of diameter $\sim$10 nm [65–68]). Consequences of a yet further reduction in particle size subsists in almost merging both liquids and solids lines each other while reaching in limit a nonstructured cluster. Compiled and adapted on basis of data in Refs. [62–69]

5.8 Further Expansion of Kinetic Phase Diagram and Nanostate Determinability

It is a matter of curiosity that the phase description in the nanoworld of particles shows signs of similar characteristics as cooling-dependent kinetic phase diagram when assuming contracting interface impacts [31]. It seems that the experimentally

affected situation of rapid change in the temperature resembles similar layer-like outcome of the diminishing radius of particles assembling the sample under study. Returning to Fig. 5.3, we would like to accentuate again that the change in ideality in (a) can be achieved by shrinking the particle size, metastability in (b) results in the particle inner admixture, while the kinetically reallocated portrayal in (d) takes shape by the increased pressure effect of enveloping surfaces and its enlarged curvature. The end figure (d) is obtained in the limiting smallness when the particle interiors lose their crystallographic orderliness alike its counterparting glassiness.

Both forms of above-discussed phase diagrams need a special care when investigated by means of thermal analysis [78–84] particularly careful when applying DTA [85, 86] due to its overlooked effect of heat inertia [87]. Some assistance for a better understanding can be found in analyzing the processes by means of a thermodynamic background [88, 89]. A needed continuation should better reveal the interconnection of nanomaterial characterization and quantum phenomena [41, 44–46, 66].

So far, standard theories on size-dependent phase equilibria are based mostly on the formalism introduced by Gibbs [6, 15, 52, 53]. However, the nanosystem radius/volume cannot be used as an independent thermodynamic variable to characterize the size of nanosystems, as it is dependent on another independent variables (pressure, temperature, composition). Instead, the system total number of atoms/stable molecules is used as a new independent thermodynamic parameter capable to characterize the deviation of thermodynamic behavior of nanosystems from that of macrosystems as in novel theories [90, 91]. The contradiction between the critical nucleus size (Gibbs) and the so-called equilibrium melting point of nanocrystals (Gibbs–Thomson) is resolved if the Gibbs equation is jointly applied to study both the nucleation and the equilibration of nanocrystals. Thus, the difference in the behavior of nanosystems compared to macrosystems is due to their high specific surface area (Gibbs) and not to the high interface curvature (Kelvin). The modified versions of the Kelvin and Gibbs–Thomson equations are introduced [90, 91], showing a surprising contradiction between the classical nucleation theory of Gibbs and the proposed equilibrium of Gibbs–Thomson equation. Fluctuation theories challenging temperature of critical clusters is worth mentioning [92].

Acknowledgements The present work was also supported by Institutional Research Plan of Institute of Physics ASCR, v.v.i., as developed at its Join Research Laboratory with the New Technologies Centre of the University of West Bohemia in Pilzen (the CENTEM project, reg. no. CZ.1.05/2.1.00/03.0088 that is cofunded from the ERDF as a part of the MEYS—Ministry of Education, Youth and Sports OP RDI Program and, in the follow-up sustainability stage supported through the CENTEM PLUS LO 1402). Deep thanks are due to long-lasting collaboration activity by J.J. Mareš, P. Hubík, Z. Kožíšek, Z. Chvoj (Institute of Physics), P. Holba^{+}, M. Holeček (West Bohemian University), J. Málek (University of Pardubice), N Koga (Hiroshima University in Japan), J. Leitner (University of Chemical Technology in Prague), and P. Šimon (President of the Slovak Chemical Society with Technical University in Bratislava).

References

1. Šesták J (1979) Thermodynamic basis for the theoretical description and correct interpretation of thermoanalytical experiments. Thermochim Acta 28:197
2. Jou D, Casas-Vázquez J, Lebon G (1993) Extended irreversible thermodynamics. Springer, Berlin
3. Šesták J (1984) Thermophysical properties of solids: their measurements and theoretical thermal analysis. Elsevier, Amsterdam; and (1987) Teoretičeskij termičeskij analysis. Mir, Moscow (in Russian)
4. Šesták J, Mareš JJ, Hubík P, Proks I (2009) Contribution by Lazare and Sadi Carnot to the caloric theory of heat and its inspirative role in thermodynamics. J Thermal Anal Calorim 97:679–683
5. Curzon FL, Ahlborn B (1975) Efficiency of a Carnot engine a maximum power output. Am J Phys 43:22–24
6. Glicksmann ME (2011) Principles of solidification. Springer, Berlin
7. Šesták J, Chvoj Z (1987) Thermodynamics of kinetic phase diagrams. J Thermal Anal 32:325–333
8. Chvoj Z, Kožíšek Z, Šesták J (1989) Non-equilibrium processes of melt solidification and metastable phases formation. Thermochim Acta 153 (Spec Issue)
9. MacFarlane DR (1982) Continuous cooling (CT) diagrams and critical cooling rates: a direct method of calculation using the concept of additivity. J Non-Cryst Sol 53:61
10. Grange K, Kiefer J (1941) The transformation of austenite by continuous cooling and its relation to transformation at constant temperature. Trans ASM 29:85
11. Farahany S, Ourdjini A, Idris MH, Shabestari SG (2013) Computer aided cooling curve thermal analysis of near eutectic Al–Si–Cu–Fe alloy. J Therm Anal Calorim 114:705–717
12. Saleh AM, Clemente RA (2004) A simple model for solidification of undercooled metallic samples. Jpn J Appl Phys 43:3624–3628
13. Xu JF, Liu F, Zhang D, Jian ZY (2015) An analytical model for solidification of undercooled metallic melts. J Therm Anal Calorim 119:273–280
14. Šesták J, Chvoj Z, Proks I, Bárta Č (1990) Thermodynamic applications concerning constrained (kinetic) states. Institute of Physics- internal report, available on websites: http://www.fzu.cz/~sestak/yyx/KineticPhaseFullTx.pdf
15. Chvoj Z, Šesták J, Tříska A (eds) (1991) Kinetic phase diagrams: non-equilibrium phase transitions. Elsevier, Amsterdam
16. Chvoj Z, Šesták J, Fendrych F (1995) Nonequilibrium (kinetic) phase diagrams in the $PbCl_2$-AgCl eutectic system. J Therm Anal 43:439–448
17. Stefanescu DM, Upadhya G, Bandyopadhyay D (1990) Heat transfer solidification kinetics: modeling of solidification of castings. Metall Trans 21A:997–1005
18. Šesták J, Chvoj Z (2003) Irreversible thermodynamics and kinetic thermal state dynamics in view of generalized solid-state reactions. Thermochim Acta 388:427–439
19. Lipton J, Glicksman ME, Kurz W (1984) Dendritic growth into undercooled alloy melts. Mater Sci Eng 65:57–63
20. Elliot RS (1989) Eutectic solidification processing: crystalline and glassy alloys. Butterworth, London
21. Saunders N, Miodownik AP (1998) CALPHAD (Calculation of phase diagrams): a comprehensive guide. Elsevier, Amsterdam
22. Zhao J-C (2007) Methods for phase diagram determination. Elsevier, Amsterdam
23. Hillert M (2007) Phase equilibria, phase diagrams and phase transformations. Cambridge University Press, Cambridge
24. Šesták J (2000) Art and horizon of nonequilibrated states by quenching and the methods of formation. Glass Sci Tech 70C:153–161; and (2000) Miracle of reinforced states of matter Glasses: ancient and innovative materials for the third millennium. J Thermal Anal Calorim 61:305–323

25. Šesták J (1988) Thermophysical properties of solids: theoretical thermal analysis. Elsevier, Amsterdam (1984 and Russian translation: Mir, Moscow)
26. Rossiter BW, Beatzold RC (eds) (1992) Determination of thermodynamic properties. Wiley, New York
27. Herlach DM (1994) Non-equilibrium solidification of undercooled metallic melts. Mater Sci Eng R 12:177–272
28. Stávek J, Šesták J (2002) The application of the principle of least action to some self-organized chemical reactions. Thermochim Acta 388:441–450
29. Šesták J, Barta Č (2001) Invited plenary lecture: thermophysical research under microgravity: kinetic phase diagrams determination inspace lab. In: CD Proceedings of the 3rd IPMM (Inteligent Processing and Manufacturing of Materials, J. Meech. edt), Vancouver, Canada
30. Šesták J, Queiroz CA, Mareš JJ (2013) Some aspects of quenching, vitrification, amorphization, disordering and the extent of nano-crystallinity, Chapter 4 in the book "Glassy, Amorphous and Nano-crystalline Materials" (J. Šesták, J. Mareš, P. Hubík, editors). pp 59–76,. Springer, Berlin, ISBN 978-90-481-2881-5
31. Šesták J (2015) Kinetic phase diagrams as a consequence of radical changing temperature or particle size. J Thermal Anal Calor 120:129–137
32. Los JH, Van den Heuvel M, van Enckevort WJP, Vlieg E, Oonk HAJ, Matovic M, van Miltenburg JC (2006) Models for the determination of kinetic phase diagrams and kinetic phase separation domains. Calphad 30:216–224
33. Šesták J, Kozmidis-PetrovicA, Živković Ž. (2011) Crystallization kinetics accountability and the correspondingly developed glass-forming criteria. J Min Metall Sect B-Metall 47B:229–239; and Kozmidis-Petrovic A, Šesták J. (2012) Forty years of the Hruby' glass-forming coefficient via DTA when comparing other criteria in relation to the glass stability and vitrification ability. J Thermal Anal Calor 110:997–1004
34. Šesták J (2016) Measuring "hotness": should the sensor's readings for rapid temperature changes be named "tempericity"?. J Thermal Anal Calorim 125:991–999
35. Adamovsky AS, Minakov AA, Schick C (2003) Scanning microcalorimetry at high cooling rate. Thermochim Acta 403:55–63
36. Minakov A, Morikawa J, Hashimoto T, Huth H, Schick C (2006) Temperature distribution in a thin-film chip utilized for advanced nanocalorimetry. Meas Sci Technol 17:199–207
37. Šesták J (2010) Invited plenary lecture: Macro-, meso-, micro- and nano-world: significance of temperature and allied thermal physics. In: Joint Middle European GEFTA Symposium (Modeling and experiments for solving calorimetry and kinetics)) Dresden, (Abstracts pp 15–16)
38. Flynn JH (1970) An analytical evaluation of DSC. In: Menis O (ed) Status of thermal analysis. Special NBS Publication No. 338, p 119
39. Adamovsky S, Schick C (2004) Ultra-fast isothermal calorimetry using thin film sensors Thermochim Acta. 415:1–7
40. Mareš JJ, Hubík P, Šesták J, Špička V, Krištofik J, Stávek J (2008) A Phenomenological approach to the caloric theory of heat: an alternative thermodynamics. Thermochim Acta 474:16–24
41. Mareš JJ, Šesták J, Hubík P (2013) Transport constitutive relations, quantum diffusion and periodic reactions. In: Šesták J, Mareš J, Hubík P (eds) Glassy, amorphous and nano-crystalline materials: thermal physics, analysis, structure and properties. Springer, Berlin, pp. 227–245. ISBN 978-90-481-2881-5
42. Andeson S (1983) On the description of complex inorganic crystal structures. Angewandte Chem 22:69–81
43. Lehn JM (1995) Supramolecular chemistry: concepts and perspectives, Weiheim CWCH
44. Naivz O, Arndt M, Zeilinger A (2003) Quantum interference experiments with large molecules. Amer J Phys 7:319–325
45. Mareš JJ, Šesták J (2005) An attempt at quantum thermal physics. J Thermal Anal Calor 82:681–686

46. Šesták J, Mareš JJ (2014) Invited plenary lecture: composite materials and nanostructured systems thermodynamics. In: ICCE-22 international conference on composite nano-engineering). Saint J, Malta; and Šesták J (2015) at 20 RCCT (international conferewnce on chemical thermodynamics) Nizhni Novgord (Russia)
47. Šesták J (2014) Invited award lecture: peculiarities of nano-structured systems: thermodynamic (top-down) and quantum (bottom-up) issues. In: At the 40th anniversary GEFTA conference (Thermal analysis in industry and research), Berlin
48. Wautelet M, Shyrinian AS (2009) Thermodynamics: nano vs. macro. Pure Appl Chem 81:1921–1930
49. Schevchenko VYA (2011) Search in chemistry, biology and physics of the nanostate. Lema, St.Petersburg (Rusia)
50. Hill TL (2002) Thermodynamics of small systems. Courier Dover Publications
51. Jiang Q, Wen Z (2011) Thermodynamics of materials. In: Thermodynamics of interfaces., Springer, Berlin, p 207
52. Fiala J, Kraus I (2009) Povrchy a rozhraní (Surfaces and interfaces). ČVUT, Praha (in Czech)
53. Leitner J (2004) Nanothermodynamics: http://ltp.epfl.ch/files/content/sites/ltp/files/shared/Teaching/Master/04-AdvancedNanomaterials/lectures/Thermodynamic.pdf
54. Leitner J. (2011) http://www.vscht.cz/ipl/nanomaterialy/uvod.htm Structure of nanometarials (Struktura nanomateriálů), Textbook by the Prague Institute of Chemical Technology (in Czech)
55. Leitner J, Kamrádek M (2003) Termodynamický popis nanosytémů (Thermodynamic description of nanosystem) Chem. Listy 107:606–613 (in Czech)
56. Bustamante C, Liphardt J, Ritort F (2005) The nonequilibrium thermodynamics of small systems. Phys Today 58:43–48
57. Thomas Y (1805) An essay on the cohesion of fluids. Philos Trans R Soc Lond 95:65
58. Laplace PS (1805) Traité de Mécanique Céleste, vol 4. Courcier, Supplément au dixième livre du Traité de Mécanique Céleste, Paris, France, pp 1–79
59. Thomson JJ (1888) Applications of dynamics to physics and chemistry. Macmillan and Co., London
60. McDonald JE (1953) Homogeneous nucleation of supercooled water drops. J Meteorology 10:416–433
61. Křemenáková D, Mishra R, Militký J, Mareš JJ, Šesták J (eds) (2013) Selected properties of functional materials. OSP, Liberec-Plzeň. ISBN 978-80-87269-28-2
62. Bhushan B, Luo D, Schricker SR, Sigmund W, Zauscher S (eds) (2014) Handbook of nanomaterials properties. Springer, Berlin. ISBN 978-3-642-31107-9
63. Leitner J (2011) Teplota tání nanočástic (Melting temperatures of nanoparticles) Chem. Listy 105:174–185 (in Czech)
64. Roduner E, Cronin L (2006) Nanoscopic materials: size-dependent phenomena. RSC-Publications, Cambridge
65. Jiang Q, Yang CC (2008) Size effect on the phase stability of nanostructures. Curr. Nanosc. 4:179–200
66. Guisbiers G (2010) Size-dependent materials properties toward a universal equation. Nanoscale Res Lett 5:1132–1136
67. Wautelet M, Duvivier D (2007) The characteristic dimensions of the nanoworld. Er J Phys. 28:953–959
68. Babuk VA, Zelikov AD, Salimullin RM (2013) Nanothermodynamics as a tool to describe small objects of nature. Zhurnal Tekhnicheskoi Fiziki, 2013; 83, 1–7, transl. Tech Phys 58:151–157
69. Barnard AS, Zapol P (2004) A model for the phase stability of arbitrary nanoparticles as a function of size and shape. J. Chem Phys 121:4276–4283
70. Sheng HW, Xu J, Yu LG, Sun KX, Hu ZQ, Lu K (1996) Melting process of nanometer-sized in particles embedde in an Al matrix synthesized by ball milling. J Mater Res 11:2841–2851
71. Sheng HW, Ren G, Peng LM, Hu ZQ, Lu K (1997) Epitaxial dependence of the melting behavior of In nanoparticles embedded in an Al matrices. J Mater Res 12:119–123

72. Schick C (2014) Invited award lecture: calorimetry on scales from microseconds to days. In: At the 40th anniversary GEFTA conference (Thermal analysis in industry and research) Berlin
73. Xiao S, Hu W, Luo W, Wu Y, Li X, Deng H (2006) Size effect on alloying ability and phase stability of immiscible bimetallic nanoparticles. Eur Phys J B 54:479–484
74. Ouyang Q, Tan X, Wang CX, Yang GW (2006) Solid solubility limit in alloying nanoparticles. Nanotechnology 17:4257–4262
75. Martinez JMM, La Hoz De, Callejas Tovar R, Balbuena PB (2009) Size effect on the stability of Cu–Ag nanoalloys. Mol Simul 35:785–794
76. Qi WH, Huang BY, Wang MP (2009) Size and shape-dependent formation enthalpy of binary alloy nanoparticles. Phys B 404:1761–1765
77. Zhao M, Jiang Q (2010) Size effect on thermal properties in low-dimensional materials. Key Eng Mater 444:189–217
78. Romero M, Kováčová M, Rincón JMa.(2008) Effect of particle size on kinetics crystallization of an iron-rich glass. J Mater Sci 43:4135–4142
79. Höhne GWH (2003) Calorimetry on small systems a thermodynamic contribution. Thermochim Acta 403:25–36
80. Staszczuk P (2005) World of nanostructures nanotechnology, surface properties of chosen nanomaterials. J Thermal Anal Calor 79:545–554
81. Wunderlich B (2007) Calorimetry of nanophases of macromolecules. Int J Thermophys 28:958–967
82. Garden JL, Guillou H, Lopeandia AF, Richard J, Heron JS, Souche GM, Ong FR, Vianay B, Bourgeois O (2009) Thermodynamics of small systems by nanocalorimetry: From physical to biological nano-objects. Thermochim Acta 492:16–28
83. Perepezko JH, Glendenning TW, Wang J-Q (2015) Nanocalorimnetry measurements ofmetastable states. Thermochim Acta 603:24–28
84. Leitner J (2010) Využití kalorimetrie při studiu nanočástic (Use of calorimetry for studying nanoparticles) KS2011_Leitner.ppt http://old.vscht.cz/ipl/nanomaterialy/uvod.htm
85. Šesták J, Holba P (2013) Heat inertia and temperature gradient in the treatment of DTA peaks: existing on every occasion of real measurements but until now omitted. J Thermal Anal Calorim 113:1633–1643
86. Holba P, Šesták J (2014) Imperfections of Kissinger evaluation method and crystallization kinetics. Glass Physics and Chemistry. 40: 486–495. ISSN 1087–6596. doi:10.1134/S1087659614050058) and on Russian: Fizika I Khimiya Stekla, 2014; 40:645–657; and Šesták J, Holba P, Živkovič Ž, (2014) Doubts on Kissinger's method of kinetic evaluation based on several conceptual models showing the difference between the maximum of reaction rate and the extreme of a DTA. J Min Metall Sect B-Metall 50:77–81. doi:10.2298/JMMB130902006S
87. Holba P, Šesták J (2015) Heat inertia and its role in thermal analysis. J Thermal Anal Calor 121:303–307
88. Holba P (2013) Equilibrium background of processes initiated by heating and Ehrenfest's classification of phase transitions. In: Šesták J, Šimon P, (ed) Thermal analysis of micro, nano- and non-crystalline materials. Springer, Berlin, pp 29–52. ISBN 978-90-481-3149-5); and (2015) Ehrenfest equations for calorimetry and dilatometry. J Thermal Anal Calorim 120:175–181
89. Holba P, Šesták J (1972) Kinetics with regard to the equilibrium of processes studied by non-isothermal techniques. Zeit physik Chem N.F 80:1–20
90. Cantwell PR, Tang M, Dillon SJ, Luo J, Rohrer GS, Harmer MP (2014) Grain boundary complexions (overview No. 152). Acta Mater 62:1–48; and Kang YB (2015) Relationship between surface tension and Gibbs energy, and application of constrained Gibbs energy minimization. Calphad 50:23–31
91. Kaptay G (2008) A unified model for the cohesive enthalpy, critical temperature, surface tension and volume thermal expansion coefficient of liquid metals of bcc, fcc and hcp crystals. Mater Sci Eng A 495:19–26 and 501:255 as well as (2011) The extension of the phase rule to

nanosystems and on the quaternary point in one-component nano-phase diagrams. J Nanosci Nanotechnol 12:1–9; and (2016) Modeling equilibrium grain boundary segregation, grain boundary energy and grain boundary segregation transitive by the extended Butler equation. J Mater Sci 51:1738–175

92. Boltachev GS, Schmelzer WPJ (2010) On the definition of temperature and its fluctuations in small systems. J Chem Phys 133:134509; and Schmelzer WPJ, Boltachev GS, Abyzov AS (2013) Temperature of critical clusters in nucleation theory: generalized Gibbs' approach. J Chem Phys 139:034702. doi:10.1063/1.4813238

Chapter 6
Self-organized Periodic Processes: From Macro-layers to Micro-world of Diffusion and Down to the Quantum Aspects of Light

Jaroslav Šesták, Pavel Hubík, Jiří J. Mareš and Jiří Stávek

Abstract Self-similarity and the orderly crystal (often dendritic) growth are an important parts of nature as well as the source of solid-state thermal chemistry under nonequilibrium (undercooling) conditions providing theoretical roots of chemical swinging clock. Such oscillation processes known in chemistry and biology apply for systems far from equilibrium involving special cases of oscillations extending from the self-organized periodic chemical reactions (such as Liesegang's or Belousov–Zhabotinsky's reactions) to ordered solid-state processes, from liquids to atmosphere, from macro to micro, indispensable in biology. The chapter deals with a remarkable problem of thermal physics, unresolved for more than 70 years, concerning class of diffusion-controlled periodic chemical reactions, where macroscopically observed diffusion action attains, with appreciable accuracy, the value of Planck's quantum. Because the classical and quantum diffusions are processes, which are indistinguishable in the configuration space, a quantum criterion in terms of diffusion constants is valid. This criterion enables one to find out conditions under which the quantum behaviour of self-organized periodic reactions can be observed. Examples are shown for the subcritical and critical oscillatory regimes; a special kind of self-organized Liesegang's rings—annual growth rings of a trunk of larch tree is discussed. The text even involves a thinkable hypothesis of the light self-organization based on the previously analysed principle on least time

J. Šesták (✉)
New Technologies Research Centre (NTC-ZČU),
University of West Bohemia, Universitní 8, 30114 Pilsen, Czech Republic
e-mail: sestak@fzu.cz

P. Hubík · J.J. Mareš
Division of Solid-State Physics, Institute of Physics, Czech Academy of Sciences,
Prague, Czech Republic
e-mail: hubik@fzu.cz

J. Stávek
Laboratory of Diffusion Processes, Bazovského 1228, Prague 16300, Czech Republic
e-mail: stavek.jiri@seznam.cz

J. Šesták et al. (eds.), *Thermal Physics and Thermal Analysis*,
Hot Topics in Thermal Analysis and Calorimetry 11,
DOI 10.1007/978-3-319-45899-1_6

(Fermat) and of the least action (Maupertuis). It was already noticed by Galileo who opened this problem aware that the cycloid curve yields the quickest descent leading to the so-called brachistochrone. The chapter contains 130 references.

6.1 Introduction

Generally, the process of coordination arising out of the local interactions between smaller component parts of an initially disordered larger system is identified as *self-organization*. Such a principle is called "*order from noise"* as first formulated by the cyberneticist Heinz von Foerster in 1960 [1]. He noted that self-organization is facilitated by random perturbations (i.e. noise) that allow the system exploration throughout a variety of states in its state-space. This increases the chance of internal organization during the system influx into a set of certain (e.g. numerical) denominations towards which a system tends to evolve (called *attractor*). It is often triggered by random fluctuations that are amplified by positive feedback, which would then allow entering the attractor stipulation itself.

A similar principle was formulated by the thermodynamists *Ilya Prigogine* and named "*order out of chaos"* [2]. Consequently, Georgi and Georgiev [3] utilized the stationary principle of *least action* within the concept of physics defining inner organization of a complex system as the state of the constraints determining the total action of the individual elements in such a system. There simultaneously emerges an elementary constant which value can be identified as the *Planck quantum of action*. The mechanism of such a mode of self-organization sustains the interaction between the elements and constrains leading to the minimization of constraints [2]. This is consistent with the *Gauss*' *principle of least constraint* [4] saying that more elements minimize the constraints faster which is another aspect of the mechanism in the course of quantity accumulation. As a result, the paths of the elements are straightened, which is also consistent with the *Hertz's principle of least curvature* [5] recently applied elsewhere [6].

In the 1940s, the forward-looking concept of self-organization was innovatory discussed by the cyberneticist Ashby [7]. In 1992, it was followed by above mentioned Förster [1] within his ides of cybernetics of second order as well as by Heylighen [8]. During the 1990s, the idea was picked up by physicists and chemists while studying phase transitions and other phenomena of spontaneous ordering of molecules and particles [9–12]. These include Ilya Prigogine [2, 13] who received a Nobel Prize for his investigation of self-organization of dissipative structures and Haken [14] who dubbed his approach as *synergetics.* In the 1980s, this tradition was cross-fertilized with the emerging mathematics of nonlinear dynamics and theory of chaos [2, 12, 13], producing such an investigation of complex systems that comes up quantitative, mathematical and predictable by physicists. However, the same period saw the appearance of a parallel approach, research into so-called *complex adaptive systems* [10] taking its inspiration more from biology and the social sciences than from physics and chemistry, thus helping to create another new

disciplines of *artificial life* and *social simulation*, which falls beyond the scope of this chapter.

In the down-to-earth sphere of experimental chemistry, the naturally synchronized oscillating processes are among the most fascinating reactions [15, 16]. In one type of reaction, a mixture of chemicals goes through a sequence of colour changes, and this sequence repeats periodically; in another, the mixture periodically emits a burst of gas foaming up or even affects the stoichiometry of solid-state reactions. To many laypersons, these self-oscillating reactions are engaging examples of chemical magic; to others, having already some acquaintance with chemistry, these reactions still being the mystery and a challenge. Under a given set of conditions, experience tells us that chemical reactions go in only one direction rarely finding a chemical reaction that appears to reverse itself, much less to do so repeatedly. When we do encounter such a reaction, we may be inclined to draw an analogy to a simple physical oscillator such as a pendulum. A pendulum oscillates from side to another side through its equilibrium position, and these oscillations can be attributed to the inter-conversion between the potential and kinetic energy of the pendulum. Analogously to this physical process, the chemical oscillator may seems to swing through its equilibrium composition; but it contradicts to the second law of thermodynamics which asserts that, once a chemical system reaches equilibrium, it cannot deviate from that condition spontaneously. Therefore, oscillations in chemical reactions cannot be like the oscillations of a pendulum because chemical reactions cannot simply oscillate throughout the equilibrium condition. More links can be found between the oscillation processes and self-similar branching of dendrite arms resulting from unstable temperature and concentration gradients [17].

6.2 Self-Similarity and the Orderly Dendritic Growth

Rates of general processes are coupled with flows initiating growths, which associate off-equilibria subordinated with supersaturations, ΔC and undercoolings, ΔT. They are closely related by the functions whose forms depend upon the processes controlling transformation (atomic arrangement, heat and electrical conduction or mass and viscous flow) [17–20]. In each case, the growth rate increases with increasing degree of out-of-equilibrium and inherent perturbations on the reaction interface. The driving force for such an accelerated growth can be usually expressed by the negative value of the first derivative of the Gibbs energy change, ΔG, with respect to the reaction remoteness (from equilibrium), labelled as the distance, $\boldsymbol{r}$. For small undercooling, we can still adopt the concept of constancy of the first derivatives, so that $\mathrm{d}\Delta G$ equals to the product of the entropy change, ΔS, and the temperature gradient, ΔT, which is the difference between the thermodynamic temperature gradient (associated with transformation) and the heat-imposed gradient at the reaction interface as a consequence of external and internal heat fluxes. Because ΔS is often negative, a positive driving force will exist to allow perturbations to grow, only if ΔT is positive [20]. At the critical wavelength linked to

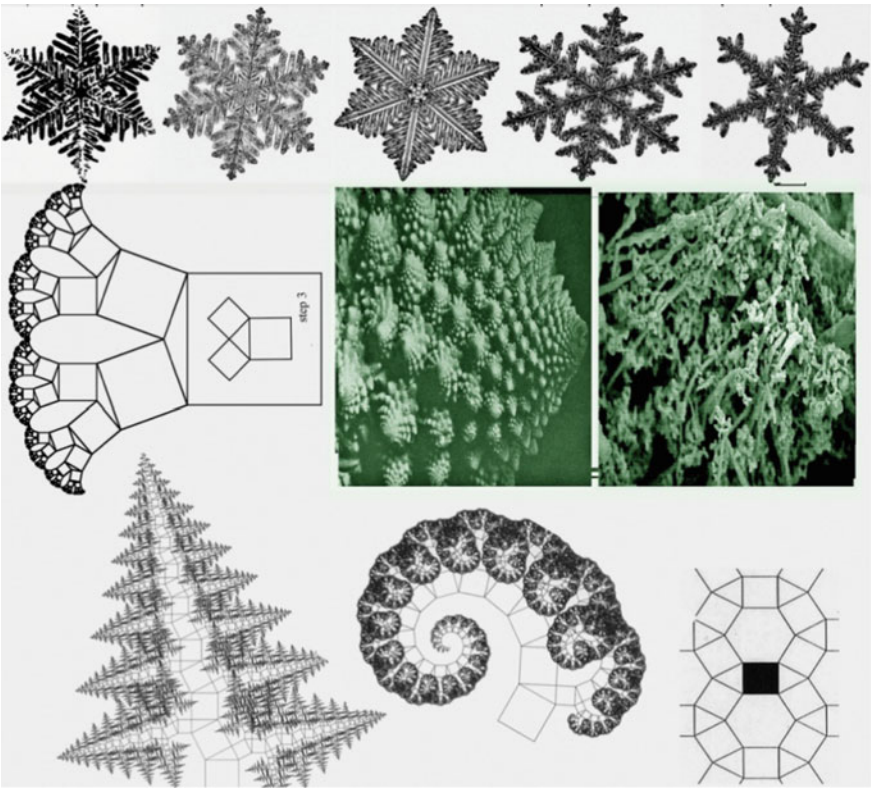

Fig. 6.1 *Upperline* growth of a snow crystal under near-constant weather conditions is primarily dependent on temperature, pressure, and vapour density and their interaction with environment. Growth [21] is based on a strong convexifying force up to micrometer size and three physically reasonable mechanisms: diffusion of water molecules off the crystal, exchange between attached and unattached molecules at the boundary and heat evolved interplay. Throughout dendritic crystallization, the lower vapour density first leads to lower frequency of side branches, then to sandwich instabilities and relatively thick plates. The melting rate regulates the ability of attached molecules at the boundary to detach. Other sketches and photos are described in the text

minimum undercooling at the solidification front depending on the surface tension thus lamellar eutectic oscillatory instability arises, leading to the formation of secondary arms called *dendrites* [17–20]. Illustrative view on self-similarity on the subject of such structures on gradual span ranking is best imagined by the sequential duplication of certain geometrical motives; see Fig. 6.1, simulating thus various natural objects.

Regimes displaying spatial or temporal order, we call *dissipative structures* [18], often associated with the formation of a dendrite which begins with the recurrent breakdown of an unstable planar solid/liquid interface. Perturbations are amplified

until a marked difference in growth of the tips and depressions occurs. The temperature gradient must be deformed in the liquid as the tip increases, therefore, more heat will flow into the tip and less will flow out of it. Moreover, the equilibrium temperature at the interface, determined mainly by intermediate composition C, is changed as a consequence of the local interface curvature. Because the tip can also reject the solute in lateral direction, it will tend to grow more rapidly than a depression which tends to accumulate the excess solute rejected by the tips. Therefore, the form of the perturbation is no longer (initially) oscillatory but adopts the form of cells which are ellipsoid-like crystals growing anti-parallel to the net flux direction. If the growth conditions continue close to the limit of constitutional undercooling of the corresponding planar interface, tree-like formation occurs and the cells rapidly change to dendrites, which then exhibit secondary arms and crystallographic governing growth directions [17–20]. This pseudo-thermodynamic approach gives the same result as that deduced from the concept of zone constitutional undercooling. Its analysis, important for the manufacturing of advanced materials (such as fine-metals, nano-composed assets, formation of quantum dots and composite whiskers and growth of oriented biological structures) falls, however, beyond the scope of this chapter. Self-similarity is caused by periodic processes but the true sphere of the formation of oscillating reactions is, however, due to another nonequilibrium factors as will be shown later.

Self-similarity (and/or self-affinity) is exhibited, in various scales, by all natural plants (broccoli is a right example) and by crystals. It can be simulated upon a geometrical construction by repeating and duplicating patterns of various bifurcation processes known in vegetation, tree growth, etc. The typical feature of this growth is the so-called *allometric* scaling, the logarithms of the inverse compass setting (precision) as linearly dependent on logarithm of the length (e.g. measuring the circumference of leafs, live organs or more traditional length of the coast). The popular construction of Pythagorean tree starts by simple children-like drawing of a square with an attached right-angled triangle. Then two squares are attached along the free sides of triangle followed by repeating attachment of squares and triangles, see Fig. 6.1, middle line, inset of the left sketch. It certainly can be modified in various ways; the triangles need not be right-angled providing another degree of freedom. After as many as 50 iterations, the results cannot look more different: when the applied angle is greater than 90° (see middle line, the large sketch on left), we can envisage the structures like broccoli in comparison with a natural broccoli; cf. the middle line of Fig. 6.1, left photo; while right is electrodeposited metallic tantalum. Bottom left is a fern or even a pine tree. In other cases, it can remind us of a spiralling leaf or decorated coiled shell (Fig. 6.1, bottom middle), worth noting that the size of triangles in the bottom are the same in both exampled portrayals.

6.3 Chemical Swinging Clock and the Emergence of Planck Constant

In certain solute concentrations range (often from $\sim 10^{20}$ to $\sim 10^{23}$ ions per dm^{-3}), the nonlinear coupling between chemical reaction and ionic diffusion leads under some circumstances to the appearance of succession of chemical waves. When a Russian scientist B.P. Belousov discovered in the year 1952 such an unpredictably spontaneous product of self-organization in the form of sequence changes of colour in some chemically reacting system; it took him several years to convince scientific officials to believe it. He was able to publish his finding in an obscure nonreviewed journal [22]. Belousov's research was followed and enhanced by Zhabotinsky [22] and Tyson [23]. They discovered mostly inorganic reactions, which surprisingly deny the traditional view on chemical kinetics (characterized by the natural tendency to reach by the shortest way the state of equilibrium). They were interpreted even as a precursor of life processes [24–26] (cf. Bautrieb due to the Lebenskraft [25]).

A well-defined periodic precipitation patterns were traditionally obtained by chemists a long time ago. In early nineteenth century, Fechner published [27] a report on the regular swinging in a chemical system, describing an electrochemical cell that produced an oscillating current. Later in nineteenth century, Ord [28] prepared 1D precipitation patterns and Pringsheim [29] introduced the concept of osmotic pressure to this field late in eighties. Famous is Liesegang [30] who prepared various 2D patterns (often called Liesegang rings) and Leduc [31] who developed the concept of osmotic pressure waves. There are many other researchers who contributed significantly better awareness of this subject. Creative incentive appeared already in middle of nineteenth century when Runge [32] shown substances interactions associated with various self-grown pictures; while in the 1930s, Nikiforov [33] proposed to characterize the spatial and temporal development of chemical waves by the *Principle of the least action*. It was expressed in 1744 by Maupertuis [34]: "*when some change takes place in nature*, *the quantity of action necessary for the change is the smallest possible*. *The quantity of action is the product obtained by multiplying the mass of the bodies by their velocity and the distance travelled*", factually extending the earlier Fermat's similarly attuned *principle of least time* [35–39].

Several research groups followed this approach and evaluated the quantities of action during the Liesegang rings formation [40–47]. They found that during the evolution of successive waves, the product of instantaneous propagation speed u and the wavelength λ converges to a constant value. It was found that this value depends on the type and the concentration of the used polymer. When trying to describe diffusing front of the process, a crucial role of a characteristic particle mass m was established. The product of the characteristic mass m, propagation speed u and the wavelength, λ, was termed as the *diffusion action* [37–39, 46, 47].

More than one hundred different combinations of cations and anions were utilized for the Liesegang rings formation from liquid phase, and the calculated values

of their diffusion action, $u\lambda m$, were in the order $\sim 10^{-34}$ Js. Küster [40] and Schaafs [44] analyzed periodic structures in various biological materials by means of the principle of least action and approved a very surprising coincidence with the quantum of the least action [37–39], too. Recently, Stávek et al. [46] evaluated the diffusion action during the diffusion of 1D Belousov–Zhabotinsky waves and found the value of diffusion action of these chemical waves self-organized to fall close to the Planck constant.

Several physicists [48–51] contributed to this topic and several decades of long experimental and theoretical research can be condensed into the following equation [37–39, 46–53]:

$$(K\kappa)m\,\lambda\,u = h \tag{6.1}$$

where K is the diffusivity factor, κ is the tortuosity factor, m is the particle mass, λ is the wavelength, u is the propagation speed and h is a characteristic constant of the diffusion action lying close to the value of Planck constant. The parameter K (diffusivity factor) describes the geometrical arrangement of the experiment. For one-dimensional space (thin glass tubes) $K = 1$, for two dimensional space (thin layer in a Petri dish) $K = 2$, in case of the three-dimensional experiment the value K depends on the space angle available for the diffusion of Brownian particles from their source. If the whole space is available for the propagation of the chemical waves, then $K = 4\pi$. Many studies of the dispersion relations were performed in gels, membranes, resin beads, glasses in order to prevent hydrodynamic disturbances from the reacting media. These media help to localize the propagating bands; on the other hand, they modify the diffusion path of ions. The diffusion field in these restricted environments changes upon the tortuosity factor κ, characterizing thus the diffusivity in permeable (porous) media.

There is no consensus concerning relation (6.1) in scientific community at all [37–40, 44, 46, 47]. It was found by various scholars to be either accidental without any deeper physical meaning (pointing to the experimental difficulties in the estimation of mass of diffusing units) or enigmatic, with something very important on behind. Such diversity in opinions is partially due to the traditional, rather subjective discrimination between *macroscopic* and *microscopic* phenomena. The quantities u and λ on the left-hand side of Eq. (6.1) stay explicitly in contrast to m which is essentially macroscopic; they are accessible to the observation by unaided eye, while the Planck quantum of action h, on the right-hand side of Eq. (6.1) is regarded to be characteristic of tiny quantum processes on an atomic scale. There are several attempts for its explanation, cf. Fig. 6.2.

For example, there is a very straightforward interpretation of relation (6.1) using a concept of the de Broglie wave known from elementary quantum mechanics [49–51] as a wave controlling the probability amplitude of a particle. Accordingly, we have reputedly to do with the de Broglie probability pilot wave of an abstract particle [49] of mass equal to the mass m of the end-product molecule moving with the speed of diffusion$\approx u$. It is further assumed ad hoc that the wavelength h/mu of this de Broglie-like wave [49] coincides with some integer multiple of the period of

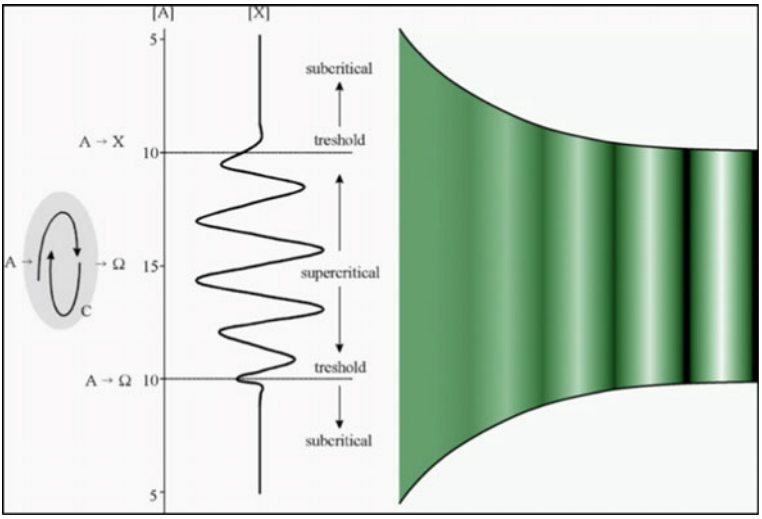

Fig. 6.2 A schematic diagram showing the subcritical and critical oscillatory regimes

precipitation, what is just that meets the want. Such a simplistic exploitation of quantum ideas and quite formal approach to the problem, tolerable in pioneering works, together with the obscure concepts involved is, as we believe, the very reason which has led to the scepticism aimed against the quantum theoretical interpretation of Eq. (6.1) and for years effectively damped the activities in this interesting field.

6.4 Diffusion Action of Brownian Particles

Curiosity of self-organization attracted deserved attention in a wider analysis of time-symmetry breaking associated with the emergence of time-periodic solutions known as limit cycles whose period and amplitude are stable and independent of the initial conditions. The importance of self-organization was approved, as they can constitute models of rhythmic phenomena observed in nature, such as chemical clocks in more important biological or other evolution processes [54–57]. It became a model focus in generalized theory of chaos expressing its minute ordering [58–60]. Curiously even the attempt to imagine a self-organizing ether (primeval matter) became also source of a related reaction-diffusion model of space-time creation [50] based on 1887 *Cu-t'ung* subatomic wave theory. He proposed the subnuclear wave theory of ether based on *Konfuciou's* idea of transmutation-bipolar ether of mutually transmuting states of "*Jin"* and "*Jang"*.

Let us turn our attention to the stable waves observed in this so-called yet-classical Belousov–Zhabotinsky [15, 22, 23] reactions resulting from the

possibility of cascade splitting (called *bifurcation* [17]) which opens the way to gradual increase in complexity by a mechanism of successive transitions, leading either to the loss of stability of a primary branch and the subsequent evolution to a secondary solution displaying asymmetry in space and/or in time. It is worth mentioning that such transitions are sometimes accompanied by some remarkable trends, e.g. certain classes of reaction-diffusion systems under zero-flux boundary conditions may exhibit no net entropy production change when the system switches from the thermodynamic branch to a dissipative structure [37]. On the other hand, there is a systematic decrease in entropy in the vicinity of bifurcation points known in the associated fields, e.g. chaos [13, 17, 57–59, 61] or even traditional field of predicting weather.

A lot of research was given to the detailed observation of properties of these chemical waves, and a great number of theories were proposed in order to characterize the behaviour of these structures. There can be applied a very useful criterion enabling one to decide whether a particular physical problem belongs to the domain of classical and/or quantum physics [62–73]. Making use of *A.J.W. Sommerfeld's* criterion [50, 51, 64, 68], we can assume that in every case where the quantity of type of action is relevant to a given physical problem occurring comparable with the Planck's quantum of action ($\sim h$), the problem can be solved consistently only within the frame of the quantum theory. There, however, is no further requirement put on the absolute scale of the system; it can be either of microscopic or macroscopic origin.

Assuming that the decisive process controlling the periodic precipitation or oscillating reactions is the diffusion of reactants (i.e. we consider the so-called Nernst–Brunner limit of chemical kinetics [51]); we need for the construction of the corresponding "relevant quantity of type action" the definition of something like the instant *speed of diffusion*. If we, for the sake of simplicity, confine ourselves only to one dimension, the diffusion can be described by the following differential equation (traditional Fick's law) $\partial n/\partial t = D\,(\partial^2 n/\partial x^2)$ leading to the relation for the position of extreme concentration $x^2 = 2Dt$ which in time derivative is $x\ u = D$, where $u = (\partial x/\partial t)$ has physical meaning of the instant speed of transfer of concentration maximum. It is quite reasonable just to call u the "instant speed of diffusion" [64–67].

These results can be identified as counterpart to random walk of a single Brownian particle (≈molecule) [68–73]. The only differences are that here is x no more the position of the concentration maximum but the mean square root $\sqrt{\langle x^2\rangle}$ of the position of a particular Brownian particle at time t and u has a meaning of its mean square root of stochastic speed $\sqrt{\langle U^2\rangle}$. For these quantities, the validity of the relation $\sqrt{\langle x^2\rangle}\,\sqrt{\langle U^2\rangle} \geq D$ can be easily proved [51]. The diffusion constants D must naturally be identical for the microscopic as well as for the macroscopic cases and simultaneously the relations $u = \sqrt{\langle U^2\rangle}$ and $x = \sqrt{\langle x^2\rangle}$ must be valid. We can thus conclude that a typical "average" Brownian particle [51, 70–72] follows the position of the concentration maximum or in other words that the most significant packet of diffusing molecules consists of average Brownian particles. Therefore, if the microscopic movement of a Brownian particle of mass m would be

controlled by a purely quantum process, where the diffusion constant in three dimensions should have Fürth's limiting value [69] of $D = D_Q = h/4\pi m$ which can formally attain the same form as empirical Eq. (6.1), i.e. $4\pi m\, ux = h$ provided that the experimentally observed quantities u and λ are identified with $u = \sqrt{\langle U^2 \rangle}$ (speed of diffusion) and $x = \sqrt{\langle x^2 \rangle}$ (distance spanned by diffusion), respectively.

It seems thus plausible that to prove the quantum nature of Eq. (6.1), it is sufficient to make clear conditions under which the numerical value of diffusion constant D attains Fürth's value D_Q [51]. The key is provided by the close analogy between the diffusion equation and Schrödinger equation proposed by Fürth [69]. Accordingly, these equations may be mapped one onto another by substituting for diffusion coefficient the value

$$iD_Q = ih/4\pi m \tag{6.2}$$

and/or identifying tentatively the universal noise source behind the assumed stochastic process with electromagnetic zero-point fluctuations of vacuum [63].

The fact that the Brownian and quantum diffusions are impossible to differentiate by intermittent examinations performed in configuration space which is just the equivalent of experimental techniques by means of which the periodic chemical reactions are investigated. It justifies the direct comparison of empirical diffusion coefficients with the Fürth's value $D_Q = h/4\pi m$. Assuming, namely, that the noise sources behind classical and quantum stochastic behaviour are independent, the resulting diffusion has to be given by a superposition of quantum and classical stochastic diffusions which are described by coefficients D_Q and D_S, respectively. Obviously, the diffusion coefficient attains its maximal value (theoretically $D \rightarrow \infty$) just if the ambient puts no constrains on the free movement of a particle, and consequently this quantity is formally analogous to working example of electric conductance [64]. Two simultaneous diffusion processes with coefficients D_S and D_Q are thus represented by a diffusion coefficient D corresponding to D_S and D_Q connected in series, i.e.:

$$D = D_S D_Q/(D_S + D_Q) \tag{6.3}$$

Then, it is easy to show by comparison with empirical data that there are numerous cases where $D \approx D_Q$ (e.g. H^+, Na^+, Ca^{2+} and Ag^+ ions in aqueous solutions at room temperature). Moreover, in accordance with formula (6.3), the accessibility of Fürth's limit may be formally expressed as follows [51]: $D_S > D_Q$. The very physical meaning of this condition is to provide a quantitative estimate for the partial decoupling of particle from the sources of classical noise, which is sufficient for reaching a quantum diffusion regime $D_S = kT/6\pi\eta R > h/4\pi m$ in a real system.

Although somewhat formal, the application of correspondence principle in terms of diffusion constant provides the superposition of quantum and classical diffusion again. While D_S is meaningful only to the mean-free path δ of the molecule

$$Mv_F\delta \leq h/2\pi, \tag{6.4}$$

if the mean-free path exceeds the de Broglie wavelength [49], the process is exclusively controlled by quantum effects only.

Very small Brownian particles (without observable persistency in motion) in medium of small viscosity, η, gives very high D_S, in other words they decouple from the stochastic environment and their quantum-like behaviour starts to be apparently observable. Rough estimate is valid for the quantum performance

$$D_S = kT/6\pi\eta R > h/4\pi m \tag{6.5}$$

Evaluation for ball-like molecules of effective radius R within aqueous solutions at room temperature (T = 300 K) and viscosity $\eta \approx 10^{-3}$ kg m^{-1} s^{-1}provides estimate of quantum behaviour for $7.0 \times 10^{-12} \geq R/m$. Supposing $m = 1.67 \times 10^{-27}$ kg multiplied by molecular weight of a given molecule we arrive to the same ion candidates of Na^+, Ca^{2+} and Ag^+ as above. Making an estimate for diffusion constant of H^+ ions (protons) which are the most active and mobile particles in aqueous solutions and applying Eq. (6.5) for an effective proton radius in water ($\approx 10^{-11}$ m) and for η ($\approx 10^{-3}$ kg m^{-1} s^{-1}), we obtain for the room temperature estimate of diffusion constant $D_S \approx 2.2 \times 10^{-8}$ m^2s^{-1} which is within an error comparable with the numerical value of quantum diffusion constant for protons with $m = 1.67 \times 10^{-27}$ kg providing $D_Q \approx 3.1 \times 10^{-8}$ m^2s^{-1}. It indicates that diffusion of protons needs to be treated by more extended, fully quantum approach.

Based on the classical Einstein–von Smoluchowski description of diffusion as a particular case of the Brownian motion and on the fact that the Brownian and quantum movements are indistinguishable by intermitted measurements in configuration space, we have shown [51–53] that a certain class of self-organized periodic reactions characterized by the empirical dispersion relation (6.1) are to be very likely controlled by the Fürth's quantum diffusion of reactants.

To conclude this section and to further illustrate a validity of Eq. (6.1), let us consider a nice example of growth with an evident oscillatory character [53], a saw off slab from an old tree (cut down in Šesták's owned forest), see Fig. 6.3. It is clear that we have to do with a special kind of Liesegang's reaction with a cylindrical symmetry for which the following variation of the Eq. (6.1) is expected

$$2m\lambda^2/\tau = h \tag{6.6}$$

where m is the molecular weight of precipitating cellulose, λ the distance between the neighbouring annual rings, τ the growth period and $h = 6.63 \times 10^{-34}$ Js is the Planck universal constant. Then, taking into account that the glucose-based polymer cellulose having empirical formula ($C_6H_{10}O_5$) N is known to create, in wood, the chains of average polymerization degree $N \approx 400$, its molecular weight may be determined immediately as $m \approx 400 \times 162 \times 1.67 \times 10^{-27} = 1.08 \times 10^{-22}$ kg.

Fig. 6.3 Cross-section of a trunk of larch tree showing annual growth rings, reputedly showing a special kind of self-organized Liesegang's rings [53]

Admitting further for the distance between annual rings a value $\lambda = 5 \times 10^{-3}$ m and for the duration of the season an estimate $\tau = 8 \times 10^{6}$ s, we obtain an incredibly exact figure for the Planck constant, namely $h = 6.7 \times 10^{-34}$ Js.

6.5 Oscillation Processes in Chemistry and Biology: Systems Far from Equilibrium

We should also focus our attention to a specific case often encountered when an experimentalist faces chaotic trends in his resulting data while studying chemical reactions in an apparently closed system. Such results are frequently refused by reasoning that the experiment was not satisfactorily completed due to ill-defined reaction conditions, unknown disturbing effects from surroundings, etc. This attitude has habitual basis in traditional view common in classical thermodynamics that the associated dissipation of energy should be steadily decelerated to reach its minimum (often close to zero) at a certain stable state (adjacent to equilibrium). In many cases, however, the reaction is initiated to start far away from its equilibrium or external contributions are effectual (in a partly open system), or reaction intermediates play a role of doorway agents (i.e. feedback catalysis). In such a case, the seemingly chaotic (in fact oscillatory) behaviour is not an artefact but real scientific output worth of a more detailed inspection where the reaction mechanism should not only be understood in its traditional terms of time-continuous progress, but also as a reflection of reaction time-rejoinder which feedback character yields rather complex structure of self-organization. Statistics show that the stability of nonequilibrium steady state is reflected in the behaviour of the molecular/atomic fluctuations that became larger and larger as the steady state becomes more and more unstable, finally becoming cooperative on a long-range order. In many cases,

this effect is hidden by our insensitive way of observations. Particularly it becomes apparent for those reactions that we let start far from equilibrium; which first exhibit nonequilibrium phenomena but later they either decay (disappear) close to their steady state or are abruptly stopped (freeze-in) by quenching phenomena (often forming the reinforced amorphous state of noncrystallites).

The oscillatory *Belousov–Zhabotinsky* processes [15, 22, 23] were also successfully simulated by the use of computers, and the most famous is a simple scheme known as "*Brussellator*" which is a theoretical model for a type of autocatalytic reaction proposed by Ilya Prigogine [2, 13] and his collaborators at the Université Libre de Bruxelles. It describes autocatalysis of the following variety: A $\rightarrow$ X; 2X + Y $\rightarrow$ 3X and B + X $\rightarrow$ Z + D; X $\rightarrow$ E which, however, can be simplified in the following scheme shown in Table 6.1 (left) as the so-called cross-catalytic reactions. It is involving two reactants A and B and two products Z and P with the intermediates X and Y. The catalytic loop is caused by multiplication of the intermediates X, well illustrating the input effect of reactant concentration within the given reaction mechanism (at the threshold concentration of A the steady subcritical region changes from the sterile to the fertile course of action capable of oscillations in supercritical region, see Fig. 6.2). Although first assumed hypothetically, it enabled to visualize the autocatalytic nature of many processes and gave to them the necessary practical dimension when applied to various reality situations: This scheme is typical for many biological systems such as the glycolytic energetic cycles where the oscillatory energy intermediates are adenosine-tri-phosphate (ATP) and adenosine-di-phosphate (ADP). It is also likely to explain the functioning of periodic flashes of the biogenic (cold) light produced by some microorganisms where the animated transformation is fed by oxygen whose energy conversion to light exhibit high efficiency [75]. Also the chromophore-assisted light inactivation offers the only method capable of modulating specific protein activities in localized regions and at particular times [76].

Another theoretical model is labelled "*Oregonator*" which is a simple realistic model of the chemical dynamics of the oscillatory processes [79–81]. The so-called *Lotka–Volterra* equations are known as the predator–prey equations in the form of a pair of first-order, nonlinear, differential equations frequently used to describe the dynamics of biological systems in which two species interact, one as a predator and

Table 6.1 Schematic portrait of the simplest self-organized reactions

reactants$\rightarrow$ A products	dA$\rightarrow$ diffusion $\rightarrow$dA
$\downarrow\uparrow$	$\downarrow$react $\Downarrow\downarrow$react
reactants$\rightarrow$ B + X $\rightarrow$ Z + Y	dB $\rightarrow$ diffusion $\rightarrow$ dB
$\uparrow\downarrow$	$\Downarrow$
products $\leftarrow$ P $\leftarrow$ 3X $\Leftrightarrow$ 2X + Y	reaction on interface

the other as prey. One of the basic schemas is the diffusional model, see the Table 6.1 right, which provides all-purpose source for oscillations [62, 64, 74].

Picturesque world of assorted bayaderes endowed with various seashells and other organized structures provided by different living organisms such as butterflies or animal skin ornamentation (zebra) was elaborated by cyberneticist Turing [81], formulating the hypothesis that such decorative patterns are, in general, the result of diffusion based reactions presented in Table 6.1 right, which are mostly functional at the early stages of the cell growth.

It is clear that the basic phenomenon of life [77–81] is a self-replicating mutable macro-molecular system capable to interact [77–80] inside itself as well as with its surroundings (supply of energy). It involves autocatalysis that is a process in which the given compound serves as a catalyst of its own synthesis. Certain biopolymers exhibit such an inquisitive property that is basis for self-reproduction, i.e. the feature enabling agglomerates of molecules (possessing similar starting capability—concentration) to develop preferentially for those molecules that grow to be dominant (morphogenesis [81]). It means that particular linear sequences of nucleotides must code for nonrandom sequences of amino acids having autocatalytic properties furthering their replication to a preferential reproduction. Other coding, providing less effective proteins, would have replicated more slowly. By mutual cooperative actions of autocatalytic reactions a larger self-regulating systems can be created by gastrulating to show the cyclic reproduction under its fixed repeating time—an important attribute of life. Most important role is played by enzymes that are big proteins molecules acting as biological catalysts and accelerating chemical reactions without being consumed themselves. Their activity is specific for a certain set of chemical substrates and it is dependent on various boundary conditions (concentration, acidity-pH, temperature, etc.). Such a system is again evidently far from equilibrium and its fertile behaviour cannot be explained by the classically viewed off-equilibrium thermodynamics that is sufficient to describe the formation of stable static structures (as crystals). Unlike standard equilibrium states, such self-catalysed states, that are far away from equilibrium, can be unstable because a small perturbation may lead precipitously to new states rich in their variety, seen not only within the above mentioned biologic systems, bust also in less known, but less significant physical and chemical systems of inorganic world. It is worth mentioning that such dynamic (dissipative) structures are linked with all kinds of flows shifting from linear (laminar) to nonlinear (turbulent) regimes, as for example, in fluid hydrodynamics (boundary friction), oscillations in electric gas discharges or in electron flow (local overheating known as the Kohler effect in resistors or mobility versus velocity control in semiconductors).

In order to find a best example in biology, the Ranvier nodes [82] (also known as myelin sheath gaps) can be exploited using the distance of the gap periodicity in the insulating myelin sheaths of myelinated axons where the axonal membrane is exposed to the extracellular space. This self-organization facilitates nerve conduction in myelinated axons, which is referred to as saltatory conduction (from the

Latin *saltare*, to hop or leap) because of the manner in which the action potential comes out jumping from one node to the next along the length of the axon.

Beside the above discussion of quantum diffusion, further notes on relation between biology and quantum phenomena should be added. Quantum effects in biology do not seem bizarre at all. There is no additional strangeness, just quantum approach applied to minute biological processes from the bird navigation to photosynthesis. The actual questions of why we need quantum physics rather than classical physics can be explained exploring how a cell can maintain quantum coherence (i.e. preserve of a quantum state necessary for quantum effects) long enough to allow the process to complete when physics labs cannot maintain quantum coherence for nearly as long despite massive equipment. Such a minute events can have a profound influence on living beings which are vastly bigger despite a general expectation that something tinier than a hair on a dog's tail could not possibly wag the dog. The recent innovative books [83, 84] show what is speculative and what has been supported by research conducted in labs around the world supporting ample reasoning to believe that quantum physics plays an important function in biological processes.

Quantum world represented by the Planck constant enters in chemistry and biology also when information aspect of the processes is considered. It is convenient to convert information coded, as usual, in binary units Γ_2 (bits) into the information Γ_p expressed in physical units [52]. This relation obviously reads as follows:

$$\Gamma_p = (k \ln 2)\Gamma_2 \tag{6.7}$$

where k is Boltzmann's constant ($k = 1.38 \times 10^{-23}$ J K^{-1}). We assume now that there is no information "*an sich"* or in other words information needs in all cases a material carrier [52]. From the point of view of macroscopic thermal physics there is, however, a fundamental difference between, e.g. genetic information inscribed in the DNA and information provided by a gravestone inscribed with personal data. Whereas in the former case for coding of information structural units on molecular level are used, which should be described by microscopic many-body formalism, to the latter case rather a macroscopic description in terms of boundary–value problem is adequate. To distinguish without ambiguity between these two extreme cases we need, however, a criterion which, having a sign of universality, specifies what the "molecular level" is. As far as we know, a good candidate for such a criterion is modified Sommerfeld's condition [68] distinguishing between classical and quantum effects [51–55]. It reads as $\Omega = 2\pi\hbar = h$, where Ω is phase space occupied by a structural unit (*qubit*) where minimally 1 bit information is stored and h is the Planck universal constant again. Direct computation of the action Ω corresponding to one atom built in an ordinary crystal, liquid or gas confirms the validity of condition (7) in these cases. It proves the fact that every atom together with its nearest neighbourhood should be treated as a quantum structural unit responsible for information storage on a "molecular level". Generalizing this result, we can

conclude that the very nature of the entropy-like quantity, Carnot's caloric [85] is the destructed information originally coded in occupied quantum states of structural units of which the macroscopic system under investigation consists.

6.6 Special Cases of Oscillation Processes: From Solid-State to Atmosphere

Oscillatory pattern can be found on various microscopic and mesoscopic cases of gemstones, shell ripening up to the macroscopic scale of geological sediment layers (see Fig. 6.4), and there arise a question why this separation is regular and what is its cause. Normally, we are looking for a reaction mechanism in the view of the processes sequences and its space distribution.

In some cases, the authors use for the description of autocatalytic reactions overall phenomenological models and fractal geometry [17, 86, 87]. However, inorganic solid-state reactions are not often assumed to proceed via branching [88] or oscillations. In order to show a kind of self-organization in solid phase, let us assume a simple synthesis of cement as an illustration of ideal and real reactions, supposed to follow processes taking place during cement formation [89]. There are two starting solid reactants A (CaO) and B (SiO_2) undergoing synthesis according the scheme below (left) to yield the final product AB ($CaSiO_3$) either directly or via transient products A_2B ($CaSi_2O_4$) and A_3B ($CaSi_3O_5$). The formation of these intermediate products depends, beside the standard thermodynamic and kinetic factors, on the local concentrations. If A is equally distributed and so covered by the corresponding amount of B, the production of AB follows standard kinetic portrayal (arrows in Fig. 6.5). For a real mixture, however, the component A may not be statistically distributed everywhere so that the places rich in A may affect the reaction mechanism preferring the formation of A_2B (or even A_3B) the later decomposition of which is due to delayed reacting with deficient B that is becoming responsible for the time prolongation of reaction completion. If the component A

Fig. 6.4 Self-organization in various scales from silica colloids in opals, to agates, from calcite in shells to geological layers (not in scale)

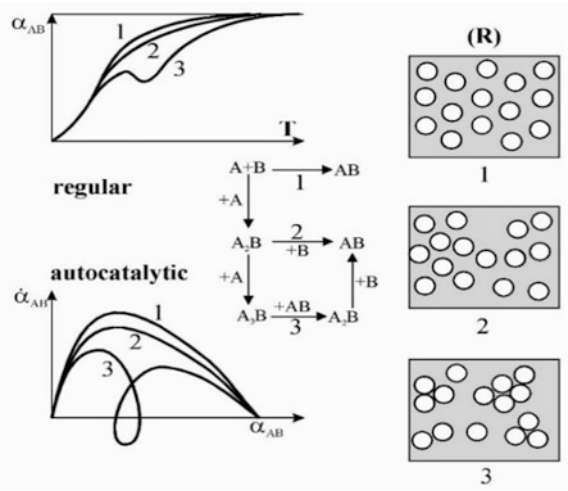

Fig. 6.5 Portrayal of ideal and actual courses of a potential solid-state reaction where two reactants, A and B, undergo synthesis to the product, AB, via transient products, A_2B and A_3B (*rights*). *Left*: the characteristic plots of reaction progress. The creation of the intermediates depends, besides the standard thermodynamic and kinetic factors, on the local concentration (particle closeness) dependent to the degree of segregation. If the agglomeration is effective, the synthesis becomes helpful to produce intermediates, self-organizes, and the entire course of reaction becomes self-catalysed, possibly exhibiting oscillatory character

tends to agglomerate the condition of synthesis of intermediates become more favourable taking thus the role of rate controlling process, and the entire course of reaction can consequently exhibit oscillation regime due to the temporary consumption of the final product AB. If intermediates act as the process catalyst, the oscillation course can even show a regular nature which localized micro-character is, however, difficult to be detected by direct macro-observations and can be assumed upon secondary characteristics of final morphology only. Introduction of diffusion is an important factor that may affect many of interface reaction (below scheme on right) to become oscillatory [88–91].

The entire course of reaction can consequently exhibit an oscillation regime due to the temporary consumption of the final product AB, which is limited to small neighbouring areas. If the intermediates act as the process catalyst, the oscillation course is pronounced showing a more regular nature. Their localized fluctuation micro-character is, however, difficult to be detected by direct physical macro-observations and can be only believed upon secondary characteristics read-out from the resulting structure (final morphology).

Similarly, some glasses may exhibit a crystallization pendulum [92]: after proceeding very fast in certain direction(s), the growth often stops due to the changes in concentration and converts into dissolution while in the other direction(s), where the growth rate was initially lower, it never becomes negative even if it decelerates

effectively. Hence, a competition between several simultaneous processes takes often place, typical for such a nonequilibrium system and leading to curious morphology (plate or needle-shaped crystals [92, 93]. Another working example is well known, resistor carrying large electrical current exhibiting negative differential resistance, i.e. currents that even decrease with increasing voltage supporting oscillations, rather than steady currents [39]. Instabilities also occur in thin wafers of certain semiconductors (GaAs, InP). If the electrical potential across the semiconductor exceeds a critical value the steady current that is stable at lower potentials, abruptly gives way to periodical changes in the current, often called Gunn oscillations [39, 94, 95]. There are other cases worth mentioning reaching the sphere of solid-state reactions [95–99].

Directional solidification of the $PbCl_2$-AgCl eutectic [39, 100] provides swinging lamellar structure separated regularly at almost equal severance which can be compared with dynamic structures caused by Bernoulli instabilities well known in hydrodynamics [39, 101]. Atmosphere is another source of oscillatory effects when billow clouds are created from instability associated with air flows having marked vertical shear and weak thermal stratification. The common name for these fluctuations is Kelvin–Helmholtz instability often visualized as a row of horizontal eddies aligned within this layer of vertical shear.

The Kelvin–Helmholtz instability results from a turbulence of two air layers lying close to each other, which move with different speed and/or direction. According to Bernoulli's principle, the pressure inside an air layer with the higher wind velocity is smaller than in the environment. Consequently, there is a force, which pulls the barrier shape (wave comb or hill summit) in the direction of the faster air flow [101]. Such an external perturbation may provide an oscillation of the vortex sheet where the pressure in concavities is higher than that in convexities. The amplitude of the oscillation grows up and the upper part of the sheet is carried by upper fluid instead the lower part of the sheet is carried by lower fluid. So a tautening of the front occurs, and there is a phenomenon of rolling up of the interface with a direction corresponding to the vorticity direction of the mixing layer. It is worth mentioning that such dynamic (dissipative) structures are linked with all kinds of flows shifting from linear (laminar) to nonlinear (turbulent) regimes; besides fluid hydrodynamics (boundary friction), they are oscillations in electric gas discharges or in electron flow (local overheating known as the Kohler effect in resistors or mobility versus velocity control efficient from semiconductors to traffic mentioned above [6, 94, 101–103]) (Fig. 6.6).

This approach may even touches spheres of thermal analysis [39]. Often experimental trouble was a noisy heat flow signal obtained by flow differential scanning calorimetry that appeared random but dependent on the sample mass (internal heat production) and seemingly too low in frequency to be of electric in origin. For a high-resolution temperature derivative, there was found a straightforward match to the "noise" in the heat flow signal. Instead standard way of eliminating such a kind of "fluctuations" by more appropriate tuning of instrument,

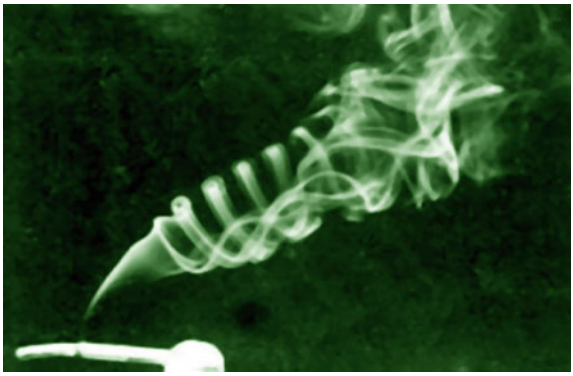

Fig. 6.6 Humorous picture of self-organized perturbation of cigarette smoke oscillations showing general impact of Bernoulli–Kelvin–Helmholtz instabilities proficient on any scale

the advanced but also more logical approach was to deliberately incorporate such fluctuations in a controlled and regular way to entire experimentation, i.e. the temperature oscillation were imposed on the heating curve and the response was evaluated through a deconvolution. Thus, received cyclic reaction could be treated in a manner known before and applied for the method of DMA.

6.7 Thinkable Hypothesis of the Light Self-Organization

When talking on the subject of light let us first mention the Michelson and Morley's article in the American Journal of Science which has been by some means portrayed as a most famous failed experiment in history instead providing insight into the properties of the aether. It compared the speed of light in perpendicular directions, in an attempt to detect the relative motion of matter through the stationary luminiferous aether. Although the small velocity was measured, it was considered far too small to be used as evidence of a speed relative to the aether, and it was understood to be within the range of an experimental error that would allow the speed to actually be zero [104, 105].

Now, we should first return to the previously noted *Fermat Principle* on least time, t [36–39] preceding the *Maupertuis Principle* of the least action [34]. It was already noticed by Galileo (1564–1642) who opened this problem by using formula $t = d/\sqrt{d_v} \times \sqrt{(2/g)}$ where d is direct distance, d_v is vertical distance and g is gravitational acceleration (9.8 ms^{-2}) aware that the cycloid curve yields the quickest descent. Historically this archetype problem introducing the calculus of variations is called "brachistochrone" (from Ancient Greek βράχιστοςχρόνος—*brakhistoskhrónos*), meaning shortest time which is consistent with the Fermat's principle. It interprets the actual path of a beam of light between two points taken by the one which is traversed in the least time. In 1697, *Johann Bernoulli* (1667–1748) already used this principle to derive the brachistochrone curve [106–110] by

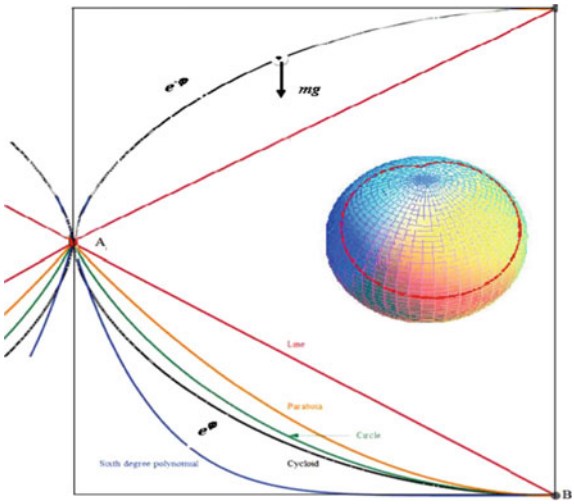

Fig. 6.7 Characteristic descending curves of a point mass free fall under the action of gravity (mg). Clearly, the *straight line* between the start A and the end B, the *violet line*, is the shortest distance, but it does not lead to the quickest descent. Below (*orange*) is parabola, below (*green*) is circle, yet below (*black*) is cycloid which has the fastest descent. At the bottom (*blue*) is a six order polynomial. Insert shows the characteristic (*red*) for the shortest time of travel along the brachistochrone on the Earth's surface. Any solution is, therefore, a compromise between travelling further and travelling faster due to gravitational acceleration so that as helping the expression for the time of travel along the brachistochrone between two points on Earth's surface [126, 127]

considering the trajectory of a beam of light in a medium where the speed of light increases following a constant vertical acceleration of gravity g. Supposing that a particle of mass m moves along some curve under the influence of gravity imagining that the mass point is like a bead that moves along a rigid wire without friction (Fig. 6.7).

The question is: What is the shape of the assumed wire for which the time to get from the start a to the end b is minimized? Whittaker [111] promoted the source of non-Euclidean geometry (e.g. Veričák's theory [112]) capable to show how to express relativity formulas using hyperbolic function in 3D space namely employing the Bolyai–Lobachevski geometry of hyperbolic function for rapidity, i.e. the inverse tangent in the form [112–114]

$$\varphi = \tan \mathrm{h}^{-1}(v/c), \tag{6.8}$$

giving way to the access of general formulas [109]

$$\mathrm{e}^{\varphi} = \sqrt{\{(1+v/c)/(1-v/c)\}} \text{ and } \mathrm{e}^{-\varphi} = \sqrt{\{(1-v/c)/(1+v/c)\}}, \tag{6.9}$$

Table 6.2 Three tuning mechanisms in the Doppler–Voigt–Einstein (DVE) self-organization [109, 116, 117]

Tuning of the light speed constancy, c
$c_{1,\ \mathrm{rel1}} == \lambda_1 f_1 == \sim \lambda_2 f_2 == c_{2,\ \mathrm{rel2}}$
Tuning of the Maupertuis equation $h == m\lambda\ c$
$h/c_{1,\ \mathrm{rel1}} == \lambda_1 m_1 == \sim \lambda_2 m_2 == h/c_{2,\ \mathrm{rel2}}$
Tuning of the energy equation $h\ f = mc^2$
$h/c^2_{1,\mathrm{rel1}} == m_1/f_1 == \sim m_2/f_2 == h/c^2_{2,\mathrm{rel2}}$

where φ is the rapidity, v is the velocity and c is the limiting speed of light following the Latin word "celerites" meaning "swiftness".

For the interpretation of the observed photon properties, the old concepts physics [109, 111, 115] is employed where the photon with mass m (Lavoisierian caloric mass m concept where $v_2/v_1 = m_1/m_2$ *and* $c_2/c_1 = m_1/m_2$) self-organizes its surroundings with the wavelength λ (Aristotelian space time t concept where $v_2/v_1 = t_2/t_1$ and $c_2/c_1 = \lambda_2/\lambda_1$) and the frequency f (Galilean time distance d concept where $v_2/v_1 = d_2/d_1$ *and* $c_2/c_1 = f_1/f_2$) assuming validity of $c_2/c_1 = (1 + v/c)/(1 - v/c)$. The so-called *Doppler–Voigt–Einstein* self-organization [109, 116, 117] transmits information about the relative velocity of the source and the observer. The photon as particle m moves simultaneously with its self-organized surroundings with wavelength λ and frequency f, and observable events are summarized in the Table 6.2.

In the redshifted DVE self-organization, one should observe the diffusion of caloric mass from the photon mass to the surface of the moving object. In the blueshifted DVE self-organization, one should observe the diffusion of the caloric mass from the moving object to the photon mass (the radiation of the moving particle). The total energy of a moving particle which is the total sum of energies of the redshifted and blueshifted self-organizations gives the identical result as it was found by Einstein [118–120]. Presumably, his enthusiasm would have been even greater had he known that the same curve describes radial gravitational freefall versus proper time in general relativity. Entanglement plays a fundamental role in the brachistochrone evolution of composite quantum probability density. Brownian motion under brachistochrone-type of metrics [121], quantum adiabatic brachistochrone [109, 122, 123] as well as the situation of dry ($\sim$Coulomb) and viscous friction with the coefficient that arbitrarily depends on speed [124–127] and other solutions [128–130]. The subject discussed in this last section is still under the progress; the study shown here is more or less a curiosity that probably would not be publishable elsewhere but is worth of attention.

Acknowledgements The results were developed and the book realized thanks to the resources made available by the financial support of the CENTEM project, reg. no. CZ.1.05/2.1.00/03.0088, jointly funded by the ERDF (within the OP RDI program of the Czech Ministry of Education, Youth and Sports).

References

1. von Foerster H (1960) On self-organizing systems and their environments. In: Yovits MC, Cameron S (eds), Self-organizing systems, Pergamon Press, London, pp 31–50; and (1992) Cybernetics. In: Skapiro SC (ed) The encyclopedia of artificial intelligence, 2nd edn, Wiley, New York, pp 309–312
2. Nicolis G, Prigogine I (1977) Self-organization in nonequilibrium systems: from dissipative structures to order through fluctuations. Wiley, New York
3. Georgiev GY, Georgiev IY (2002) The least action and the metric of an organized system. Open Syst Inform Dynam 9:371–380
4. Gauss CF (1829) Über ein neues allgemeines Grundgesetz der Mechanik. Crelle's J 4:232
5. Hertz H (1896) Principles of mechanics miscellaneous papers III. Macmillan, New York
6. De Sapio V, Khatib O, Delp S (2008) Least action principles and their application to constrained and task-level problems in biomechanics. Multibody Syst Dyn 19:303–322
7. Ashby WR (1947) Principles of the self-organizing dynamic system. J General Psych 37:125–128
8. Heylighen F (1990) Classical and non-classical representations in physics. Cyber Syst 21:423–444; and Heylighen F, Joslyn C (2001) Cybernetics and second order cybernetics. Encyclop Phys Sci Technol 4:155–1701
9. Heylighen F, Dewaele JM (1996) Complexity and self-organization. Cambridge Dictionary of Philosophy, 784–785
10. Kauffman SA (1993). The origins of order. Oxford University Press; and (2005) At home in the universe: the search for laws of self-organization and complexity. Viking, London
11. Bar-Yam Y (1997) Dynamics of complex systems: studies in nonlinearity. Westview Press
12. Waldrop MM (1992) Complexity: the emerging science at the edge of order and chaos. Viking, London
13. Prigogine I, Stengers I (1984) Order out of chaos. Bantam Books, New York
14. Haken H (2000) Information and self-organization: a macroscopic approach to complex systems. Springer, New York
15. Tyson J (1976) The Belousov-Zhabotinsky reactions. Springer, Heidelberg
16. Tockstein A, Treindl L (1986) Chemické oscilace (Chemical oscillations). Academia, Praha, (in Czech); and Gray P, Scot S (1990) Chemical oscillations and instabilities. Oxford Press
17. Šesták J (2004) Power laws, fractals and deterministic chaos: or how nature is smart. Chapter 13 in his book 'Heat, thermal analysis and society' Nucleus, Hradec Králové, pp 219–235
18. Glicksmann ME (2011) Principles of solidification. Springer, Berlin/Heidelberg
19. Chvoj Z, Kožíšek Z, Šesták J (1989) Non-equilibrium processes of melt solidification and metastable phase formation. Monograph as a special issue of Thermochim Acta, vol 153, Elsevier, Amsterdam
20. Glicksman ME, (1976) Curvature, composition and supercooling kinetics at dendrite growth. Metall Trans A A7:1747 and (1984) Mater Sci Eng 65:45–57
21. Gravner J (2009) Modeling snow crystal growth: a three-dimensional mesoscopic approach. Phys Rev 79:011601
22. Belousov BP, (1959) Collection of Short Papers on Radiation Medicine. Medical Publications, Moscow, pp 145–9; and (1985) In: Field RJ, Burger M (eds) Oscillations and travelling waves in chemical systems, Wiley, New York, pp 605–13
23. Zaikin AN, Zhabotinsky AM (1970) Concentration wave propagation in two-dimensional liquid-phase self-oscillating system. Nature 225:535
24. Winfree AT (1980) The geometry of biological time. Springer, New York; and (1987) The timing of biological clocks. Freeman, San Francisco
25. Runge FF, Liesegang RE, Belousov BP, Zhabotinsky AM (1987) In: Kuhnert L, Niedersen U (eds) Selbsorganisation chemischer Strukturen. Ostwald's Klassiker, Verlag H. Deutsch, Frankfurt am Main

26. Camazine D, Sneyd TB (2003) Self-organization in biological systems. Princeton University Press
27. Fechner GT (1831) Maassbestimmungen über die galvanische Kette. Leipzig, F.A, Brockhaus
28. Ord WM (1879) On the influence of colloids upon crystalline form and cohesion. E. Stanford, London
29. Pringsheim N (1895) Über chemische Niederschläge in Gallerte. Z Phys Chem 17:473
30. Liesegang RE (1896) Ueber einige Eigenschaften von Gallerten. Naturwiss. Wochenschrift 11 353; and Michaleff P, Nikiforoff VK, Schemjakin FM (1934) Uber eine neue Gesetzmässigkeit für periodische Rektionen in Gelen. Kolloid-Z. 66:197–200
31. Leduc S (1912) Das Leben in seinem physikalisch-chemischen Zusammenhang. L. Hofstetter Verlag, Halle
32. Runge FF (1855) Der Bildungstrieb der Stoffe: veranschaulicht in selbständig gewachsenen Bildern. Selbstverlag, Oranienburg, p 32
33. Nikiforov VK (1931) lectures at the Mendeleev chemical congress. Moscow
34. Maupertuis PLM (1768) Oevres de Maupertuis. Alyon: Paris, vol IV, p 36
35. Fermat P (1662) Synthesis ad reflexiones—a latter to de la Chambre in Oeuveres de P. Fermat, Tom 1, Paris 1891, p 173
36. Priogine I, Nicoli G, Baylogantz A (1972) Über chemische Niederschläge in Gallerte. Physics Today 25
37. Stávek J, Šípek M, Šesták J (2002) Application of the principle of least action to some self-organized chemical reactions. Thermochim Acta 388:440
38. Stávek J, Šípek M, Šesták J (2002) On the mechanism and mutual linking of some self-organized chemical reactions. Proc/Acta Western Bohemian University Pilsen 3:1
39. Šesták J (2004) The principle of lest action and self-organization of chemical reactions. Chapter 15 in his book 'Heat, thermal analysis and society' Nucleus, Hradec Králové, pp 260–273
40. Küster E (1931) Űber Zonenbildung in kolloiden Medien. Jena
41. Mikhalev P, Nikiforov VK, Schemyakin FM (1934) Űber eine neue Gesetzmässigkeit für periodische Reaktionen in Gelen. Kolloid Z 66:197
42. Christiansen JA, Wulf I (1934) Untersuchungen űber das Liesegang-Phänomen. Z Phys Chem B 26:187
43. C Raman V, Ramaiah KS (1939) Studies on Liesegang rings, Proc Acad Sci India 9A:455–478
44. Schaafs W (1952) Untersuchungen an Liesegangschen Ringen. Kolloid Z. 128:92
45. Joos G, Enderlein HD, Schädlich H (1959) Zur Kenntnis der rhythmischen Fällungen Liesegang-Ringe. Z Phys Chem (Frankfurt) 19:397
46. Stávek J, Šípek M (1995) Interpretation of periodic precipitation pattern formation by the concept of quantum mechanics. Cryst Res, Tech 30
47. Stávek J (2003) Diffusion action of chemical waves. Apeiron 10:183–193
48. Lafever R (1968) Dissipative structures in chemical systems. J Chem Phys 49:4977
49. de Broglie L (1926) Ondes et mouvements. Gauthier-Villars et Cie, Paris, p 1
50. LaViolette PA (1994) Subquantum kinetics. Staslane, New York
51. Mareš JJ, Stávek J, Šesták J (2004) Quantum aspects of self-organized periodic chemical reaction. J Chem Phys 121:1499
52. Mareš JJ, Šesták J (2000) An attempt at quantum thermal physics. J Thermal Anal Calor 80:681
53. Mareš JJ, Šesták J Stávek J, Ševčíková H, Hubík P (2005) Do periodic chemical reactions reveal Fürth's quantum diffusion limit? Physica E 29:145
54. Marek M, Ševčíková H (1988) From chemical to biological organization. Springer, Berlin
55. Stávek J, Mareš JJ, Šesták J (2000) Life cycles of Belousov-Zhabotinsky waves in closed systems. Proc/Acta Western Bohemian Uni Pilsen 1:1
56. Deneubourg C, Sneyd F, Bonabeau T (2003) Self-organization in biological systems. Princeton University Press
57. Ebeling W, Feistel R (2011) Physics of self-organization and evolution. Wiley, Weinheim

58. Epstein IR, Pojman JA (1998) An introduction to nonlinear chemical dynamics: oscillations, waves, patterns, and chaos. Oxford University Press, USA, p 3
59. Glendinning P (1994) Stability, instability, and chaos. Cambridge Press, New York
60. Field RJ, Schneider FW (1989) Oscillating chemical reactions and non-linear dynamics. J Chem Educ 66:195
61. Gulick L (1992) Encounters with chaos. McGraw-Hill, New York
62. Leblond J-M L, Balibar F (1990) Quantics-rudiments of quantum physics. North-Holland, Amsterdam
63. de la Peña L, Cetto AM (1996) The quantum dice—an introduction to stochastic electrodynamics. Academic, Dordrecht
64. Mareš JJ, Šesták J, Hubík P (2013) Transport constitutive relations, quantum diffusion and periodic reactions. Chapter 14 in book In: J. Šesták, J. Mareš, P. Hubík (eds) Glassy, amorphous and nano-crystalline materials: thermal physics, analysis, structure and properties. pp 227–245. Springer, Berlin (ISBN 978-90-481-2881-5)
65. Stávek J, Šípek M, Šesták J (2001) Diffusion action of waves occurring in the Zhabotinsky-Belousov kind of chemical reactions. Proc/Acta Western Bohemian Uni Pilsen 2:1
66. Kalva Z, Šesták J, Mareš JJ, Stávek J (2009) Transdisciplinarity of diffusion including aspects of quasiparticles, quantum diffusion and self-organized transport, chapter 20 in the book. In: Šesták J, Holeček M, Málek J (eds) Some thermodynamic, structural and behavior aspects of materials accentuating non-crystalline states, OPS-ZČU Plzen, pp 128–151 (ISBN 978-80-87269-20-6)
67. Kalva Z, Šesták J (2004) Transdiciplinary aspects of diffusion and magnetocaloric effect. J Thermal Anal Calor 76:1
68. Sommerfeld AJW (1929) Wave-mechanics: supplementary volume to atomic structure and spectral lines (trans: Henry L. Brose), Dutton
69. Fűrth R (1933) Űbereinige Beziehungenzwischen klassischer Statistik und Quantummechanik. Z Physik 81:143
70. Einstein A (1956) Investigations on the theory of the Brownian movement. In: Fürth R (ed), Dover Publications, New York
71. Smoluchowski MV (1916) DreiVorträgeüber Diffusion, BrownischeMolekularbewegung und Koagulation von Kolloidteilchen. Physik Zeitschr 17:557
72. Chung KL, Zhao Z (1995) From Brownian motion to Schrödinger´s equation. Springer Verlag, Berlin
73. Łuczka J, Rudnick R, Hanggi P (2005) The diffusion in the quantum Smoluchowski equation. Phys A 351:60–68
74. Field RJ, Noyes RM (1974) Oscillations in chemical systems. IV. Limit cycle behavior in a model of a real chemical reaction. J Chem Phys 60:1877–1884
75. Rebane KK (1992) Possibility of self-organization in photosynthetic light harvesting antennae. J Phys Chem 96:9583–9585
76. Surrey T, Elowitz MB, Wolf PE (1998) Chromophore-assisted light on activation and self-organization of microtubules and motors. Proc National Acad Sci USA 95:4293–4298
77. Lotka AJ (1910) Contribution to the Theory of Periodic Reaction. J Phys Chem 14:271–274
78. Chance B, Chost AK, Pye EK, Hess B (1973) Biological and biochemical oscillations. Academic, New York
79. Feltz B, Crommelinck M, Goujon P (eds) (2006) Self-organization and emergence in life sciences. Springer, Heidelberg
80. Lehn J-M (2002) Toward self-organization and complex matter. Science 295:2400–2403
81. Turing AM (1952) The chemical basis of morphogenesis. Phil Trans R Soc Lond B 237: 37–72
82. Ranvier L (1871) Contribution á l'histologie et á la physiologie des nerfs périphériques. C R Acad Sci 73:1168–1171

83. McFadden J, Al-Khalili J (2014) Life on the edge: the coming of age of quantum biology: a readable intro to the relation between quantum physics and biological processes. Dreamscape Media
84. Silverman A (2015) The vital question: energy evolution and the origins of complex life. Dreamscape Media
85. Šesták J, Mareš JJ, Hubík P, Proks I (2009) Contribution by both the Lazare and Sadi Carnots to the caloric theory of heat: its inspirative role in thermodynamics. J Thermal Anal Calor 97:679–683
86. Feng De-Jun, Lau Ka-Sing (2014) Geometry and analysis of fractals. Springer, Berlin/Heidelberg
87. Ozao R, Ochiai M (1993) Fractal nature and thermal analysis of powders. J Thermal Anal 40:1331
88. Galwey AK, Brown ME (1999) Thermal decomposition of ionic solids. Elsevier, Amsterdam; and Brown ME, Dollimore D, Galwey AK (1980) Reactions in the solid state. Elsevier, Amsterdam
89. Jesenák V (1985) Philosophy of the mechanism of diffusion controlled processes; Thermochim. Acta 92:39; and (1985) Thermal effects of oscillating solid-state reactions; Thermochim. Acta 95: 91
90. Logvinkov SM, Semchenko GD, Kobyzeva DA. (1998) On the self-mechanism of reversible chemical solid-phase reactions in the $MgO–Al_2O_3–SiO_2$ system, Russ. Ogneup. Tekh. Keram 8: 29–34; and (1999) Conjugated processes in the $MgO–Al_2O_3–SiO_2$ system and the oscillatory, autocatalized evolution of phase composition, Russ. Ogneup. Tekh. Keram, 9: 6–13
91. Osmialowski B, Kolehmainen E, Dobosz R, Rissanen K (2010) Self-organization of 2-Acylaminopyridines in the solid state and in solution. J Phys Chem A 114:10421–10426
92. Avramov I, Hoche T, Russel C (1999) Is there a crystallization pendulum? J Chem Phys 110:8676
93. Stávek J, Ulrich J (1994) Interpretation of crystal growth and dissolution by the reaction fractal dimensions. Cryst Res Technol 29:763–785; and Chubynsky MV, Thorpe MF (2001) Self-organization and rigidity in network glasses. Curr Opin Solid State Mater Sci 5: 525–532
94. Usychenko VG (2006) Electron self-organization in electronic devices in the light of principles of mechanics and thermodynamics. Russ. Zhurnal Tekhnicheskoĭ Fiziki, 76: 17–25; translated in Theoret. Mat Phys 51:409–417
95. Sze SM (1969) Physics of Semiconductor Devises. Wiley, London; and Teichert C (2002) Self-organization of nanostructures in semiconductor heteroepitaxy: a review. Phys Rep 365: 335
96. Janek J (2000) Oscillatory kinetics at solid/solid phase boundaries in ionic crystals. Solid State Ionics 131:129–142
97. Liu Ruey-Tarng, Liaw Sy-Sang, Maini PK (2007) Oscillatory Turing patterns in a simple reaction-diffusion systems. J Korean Phys Soc 50:234–238
98. Ren Jie, Zhang Xiaoyan, Jinzhang Gao, Yang Wu (2013) The application of oscillating chemical reactions to analytical determinations. Cent Eur J Chem 11:1023–1031
99. Betzler SB, Wisnet A, Breitbach B, Mitterbauer C, Weickert J, Schmidt-Mende L, Scheu C (2014) Template-free synthesis of novel, highly-ordered 3D hierarchical $Nb_3O_7(OH)$ superstructures with semiconductive and photoactive properties. J Mater Chem A 2:12005
100. Šesták J, Barta Č (2001) Invited plenary lecture: thermophysical research under microgravity: kinetic phase diagrams determination inspace lab. CD—Proceedings of the 3rd IPMM (Intell Process Manu Mater J Mech), Vancouver, Canada
101. Brandt L, Loiseau J-Ch (2015) General introduction to hydrodynamic instabilities. KTH Mechanics; and Curry JA, Webster PJ (1999) Thermodynamics of atmosphere. Academic, New York
102. Epstein IR, Showalter K (1996) Nonlinear chemical dynamics: oscillations and chaos. J Phys Chem 100:13132–13147

103. Orosz G, Wilson RE, Krauskopf B (2004) Global bifurcation investigation of an optimal velocity traffic model with driver reaction time. Phys Rev E 70:026207
104. Michelson AA, Morley EW (1886) Influence of motion of the medium on the velocity of light. Am J Sci 31: 377–386; and (1887) On the relative motion of the earth and the luminiferous aether. Am J Sci 34: 333–345
105. Caghill RT, Kitto K (2003) Michelson-Morley experiment revised and the cosmic background radiation preferred frame 10:104–117
106. Bernoulli J (1696) The brachistochrone problem for the shrewdest mathematicians. Acta Eruditorum
107. Erlichson H (1999) Johann Bernoulli's brachistochrone solution using Fermat's principle of least time. Eur J Phys 20:299–304
108. Haws L, Kiser T (1995) Exploring the brachistochrone problem. Amer Math Monthly 102:328–336
109. Stávek J (2014) On the brachistochrone problem in the Michelson-Morley experiment, Apeiron, unpublished as yet
110. Gjurchinovsi A (2004) Einstein´s mirror and Fermat´s principle of least time. J Phys 72:1325–1327
111. Whittaker RT (1910) History of theories of Aether and electricity. Lobngman, Dublin
112. Veričák V (1910) Anwendung der Lobatschewki Geometrie in der Relativitätstheorie. Phys Zeit 11:93–96
113. Barett JF (2010) The hyperbolic theory of special relativity. https://arxiv.org/ftp/arxiv/papers/1102/1102.0462.pdf
114. de Saxce G, Vallee C (2016) Galilean mechanics and thermodynamics of continua. Wiley-ISTE, London
115. Feynman R (2010) Feynman Lectures vol III. http://www.feynmanlectures.caltech.edu/III_toc.html; and (1985) QED—the strange theory of light and matter. Princeton University Press, Princeton
116. Stávek J (2006) Evaluation of self-organized photon waves. Apeiron 13:102–117; and (2010) Doppler-Voigt-Einstein self-organization–the mechanism for information transfer. Apeiron 17:214–222
117. Stávek J (2004) Diffusion of individual Brownian particles through Young´s double-slits. Apeiron 11:752–186; and (2005) Possible solar microwave background radiation. Galilean Electrodyn.16:31–38; and (2007) On the photon information constant. Apeiron, unpublished as yet
118. Einstein A (1905) Zur Elektrodynamikbewegter Körper. Ann der Physik 322:891–921
119. Sommerfeld A (1909) On the composition of velocities in the theory of relativity. Verh der DPG 21:577–582
120. Rybczyk JA (2008) Alternative versions of the relativistic acceleration composition formula, http://www.mrelativity.net/
121. Aryal PR (2014) A Study of the behavior of Brownian motion under brachistochrone-type metrics. New Mexico State University, Las Cruces
122. Rezakhani AT, Kuo W-J, Hamma A, Lidar D.A, Zanardi P (2009) Quantum adiabatic brachistochrone. Phys Rev Lett 103: 080502
123. Mareš JJ, Hubík P, Šesták J, Špička V, Krištofik J, Stávek J (2008) Phenomenological approach to the caloric theory of heat. Thermochim Acta 474:16–24
124. Ashby N, Brittin WE, Love WF, Wyss W (1975) Brachistochrone with coulomb friction. Am J Physics 43(10):902
125. Golubev YuF (2012) Brachistochrone with dry and arbitrary viscous friction. J. Comput Syst Sci Int 51:22–37
126. Benson DC (1969) An elementary solution of the brachistochrone problem. Am Mathem Monthly 76:889–890
127. Jeremić S, Šalinić A, Obradović Z, Mitrović Z (2011) On the brachistochrone of a variable mass particle in general force fields. Mathemat Comput Model 54:2900–2912

128. Manor G, Rimon E (2014) The speed graph method: time optimal navigation among obstacles subject to safe braking constraint. IEEE Int Conf Robot Automat 1155–1160
129. Perlick V (1991) The brachistochrone problem in a stationary space-time. J Math Phys 32:3148
130. Maleki M, Hadi-Vencheh A (2010) Combination of non-classical pseudospectral and direct methods for the solution of brachistochrone problem. Inter J Mathem Comp 87:1847–1856

Chapter 7
Clapeyron and Ehrenfest Equations and Hyper-free Energy for Partly Open Systems

Pavel Holba and David Sedmidubský

Abstract Following the approach applied by Clapeyron to describe sharp phase transitions in *P-T* diagrams of unary systems as well as that used by Ehrenfest for so-called second-order phase transitions, we derived a set of analogous equations for partly open binary and higher-order systems. These systems share one or more components with the surroundings (reservoir), and thus, their content in the system is given by their chemical potentials (activities, a_f) in the reservoir. Hence, in addition to *P-T* diagrams, the phase relations can be represented in T–a_f, P–a_f, and a_f–a_g phase diagrams and three additional Clapeyronian equations describe the corresponding borderlines delimiting the different phase fields. Moreover, it is shown that Ehrenfest equations cannot be applied for λ-transitions; however, their applicability is demonstrated for so-called partial phase transitions such as liquidus curves in closed binary systems. For partly open systems, 28 new Ehrenfestian equations are derived for partial phase transitions which involve, apart from the changes of heat capacity, thermal expansion and compressibility appearing in the original three Ehrenfest equations, the changes of newly defined quantities such as thermal, pressure, proper, and mutual plutabilities. The Clapeyronian and Ehrenfestian equations derived in this chapter can be useful for equilibrium studies and construction of thermodynamic models of non-stoichiometric phases as well as for the construction of simple phase diagrams reflecting the equilibrium phase relations under a given controlled atmosphere.

Pavel Holba—Deceased

P. Holba
New Technologies—Research Centre, University of West Bohemia,
Univerzitní 8, 30114 Pilsen, Prague, Czech Republic
e-mail: holbap@gmail.cz

D. Sedmidubský (✉)
Department of Inorganic Chemistry, University of Chemistry and Technology Prague,
Technická 5, 166 28 Pilsen-Prague, Czech Republic
e-mail: sedmidub@vscht.cz

J. Šesták et al. (eds.), *Thermal Physics and Thermal Analysis*,
Hot Topics in Thermal Analysis and Calorimetry 11,
DOI 10.1007/978-3-319-45899-1_7

7.1 Clapeyron Equation in Closed Systems

In 1888, Lehmann [1] suggested to distinguish between *enantiotropic* transitions (essentially reversible) and *monotropic* (irreversible) transitions. In unary systems, any phase transitions accompanied by a *complete* change of state of aggregation (melting/solidification, boiling/condensation, sublimation/deposition) as well as the vast majority of solid–solid transitions (e.g., transition of α—quartz to β—quartz) are enantiotropic processes, at which a substance in thermodynamically stable state transfers *fully* into another thermodynamically stable state at equilibrium transition temperature when heated as a closed system under isothermal isobaric conditions. By contrast, a transition is referred to as monotropic when a substance in a thermodynamically unstable (metastable) state reaching a certain temperature becomes able to overcome an energetic barrier hindering the path to thermodynamic stable state. The transition of aragonite to calcite can be given as an example of a monotropic process.

The *general Clapeyron equation* valid for *enantiotropic phase transitions* in unary system can be derived from Gibbs free energy change $\Delta_{st}G$ accompanying the *sharp transition* (alternatively denoted as *step transition*, index st). The name "sharp transition" has been coined by Hillert [2]. At sharp transition temperature $T_{st,}$ the initial phase φ is *fully* transformed into the final phase ψ and the Gibbs free energy integral change of the system remains zero

$$\Delta_{st}G(T_{st}) = G_m^{\psi}(T_{st}) - G_m^{\varphi}(T_{st}) = \Delta_{st}H - T_{st}\Delta_{st}S = \Delta_{st}U + P\Delta_{st}V - T_{st}\Delta_{st}S = 0 \tag{7.1}$$

Here, $\Delta_{st}H = H_m^{\psi}(T_{st}) - H_m^{\psi}(T_{st})$ and similarly $\Delta_{st}S, \Delta_{st}U$ and $\Delta_{st}V$ are, respectively, the integral changes of molar enthalpy, entropy, internal energy, and volume accompanying the sharp transition.

The triple product rule (valid for partial differentiation [3]) can be used to determine the change of transition temperature due to a small change of hydrostatic pressure:

$$\frac{dT_{st}}{dP_{st}} = -\frac{(\partial\Delta_{st}G/\partial P)_T}{(\partial\Delta_{st}G/\partial T)_P} = \frac{\Delta_{st}V}{\Delta_{st}S} = \frac{T_{st}\Delta_{st}V}{\Delta_{st}H} \tag{7.2}$$

A predecessor of Clapeyron equation was an equation derived by Clapeyron [4] in 1834 and popularized by Clausius [5] in 1850 and thus referred to as *Clausius–Clapeyron equation,* which is expressed by Eq. (7.3)

$$\frac{dT_{st}}{dP_{st}} = \frac{RT_{st}^2}{P_{st}\Delta_{st}H} \tag{7.3}$$

It is valid for transitions from a condensed into gaseous (vapor) phase where $\Delta_{st}V$ is substituted by the volume of gaseous phase $\Delta_{st}V \approx V_G$ (applying equation

of state for ideal gas $V_m^G(T_t) = RT_{st}/P_{st}$ and neglecting the volume of initial condensed phase).

The Clapeyron equation (7.2) (labeled here also as C1) can be also applied for some invariant transformations in binary and multicomponent systems when one or more original phases are completely transformed into one or more quite different phases as in the case of eutectic melting ($\varphi_1 + \varphi_2 \rightarrow L$) or monotectic melting ($\varphi \rightarrow L_1 + L_2$) as well as for eutectoid ($\varphi_1 + \varphi_2 \rightarrow \psi$) or monotectoid ($\varphi \rightarrow \psi_1 + \psi_2$) transitions where the composition of a binary system A − B is determined by molar fractions referred to the whole (total) system $X_T \equiv X_B^T$, and the composition of original phases at eutectic and eutectoid transition satisfies the balance equations $X_L = X_{\varphi_1} + \xi_{\varphi_2}(X_{\varphi_2} - X_{\varphi_1})$ and $X_\psi = X_{\varphi_1} + \xi_{\varphi_2}(X_{\varphi_2} - X_{\varphi_1})$, respectively, where the phase fraction ξ_{φ_2} is determined as $\xi_{\varphi_2} = (X_L - X_{\varphi_1})/(X_{\varphi_2} - X_{\varphi_1})$ and $\xi_{\varphi_2} = (X_\psi - X_{\varphi_1})/(X_{\varphi_2} - X_{\varphi_1})$.

The classification of transitions into the *first-order* (denoted as *sharp transitions* in this chapter) and *second-order transition* categories was first introduced by Ehrenfest [6] in 1933 in response to the report by Keesom et al. [7] who observed an unusual phase transition (*lambda transition*) in liquid helium. Based on the Clapeyron equation, Ehrenfest started to derive relations describing this new type of phase transitions observed by Keesom, for which the values ΔV and ΔH are equal to zero so that the right-hand side of Eq. (7.2) is represented by so-called *indefinite form* (zero divided by zero).

7.2 Ehrenfest Equations in Closed Systems

To calculate the limiting value of indefinite form, Ehrenfest used the l'Hopital rule [8]: "If the fraction of two functions $F(x, y)/G(x, y)$ is an indefinite form then its limit is determined as a fraction of their partial differentiations $(\partial F(x, y)/\partial x)_y/(\partial G(x, y)/\partial x)_y$ and/or $(\partial F(x, y)/\partial y)_x/(\partial G(x, y)/\partial y)_x$."

$$\lim_{F,G\rightarrow 0} \frac{F(x,y)}{G(x,y)} = \frac{(\partial F(x,y)/\partial x)_y}{(\partial G(x,y)/\partial x)_y} = \frac{(\partial F(x,y)/\partial y)_x}{(\partial G(x,y)/\partial y)_x} \tag{7.4}$$

Thus, the following three Ehrenfest equations can be derived from Clapeyron equation C1 (Eq. 7.2) for the second-order transitions within the original Ehrenfest scheme (denoted only by a subscript *t*):

(a) the first one by differentiation of numerator as well as of denominator in Eq. (7.2) with respect to temperature T (denoted as {EC1:T})

$$\frac{dT_t}{dP_t} = \lim_{\Delta_t V, \Delta_t H \rightarrow 0} \frac{\Delta_t V T_t}{\partial \Delta_t H} = T_t \frac{(\Delta_t V/\partial T)_P}{(\Delta_t H/\partial T)_P} = \frac{V_m T_t \Delta_t \alpha}{\Delta_t C_p} \tag{7.5}$$

where $\Delta_t\alpha = (\partial\Delta_t V/\partial T)_P/V_m$ means the isobaric thermal expansion change, and $\Delta_t C_p = T_t(\partial\Delta_t S/\partial T)_P$ means the molar isobaric heat capacity integral change,

(b) the second one by differentiation of numerator and denominator in Eq. (7.2) with respect to pressure P (denoted also as {EC1:P})

$$\frac{dT_t}{dP_t} = \lim_{\Delta_t V, \Delta_t S \to 0} \frac{\Delta_t V}{\Delta_t S} = \frac{(\Delta_t V/\partial P)_T}{(\partial\Delta_t S/\partial P)_T} = \frac{\Delta_t\beta}{\Delta_t\alpha} \tag{7.6}$$

where $\Delta_t\beta = -(\partial\Delta_t V/\partial P)_T/V_m$ stands for the integral change of isothermal compressibility, and Maxwell's relation [9] was used

$$-\left(\frac{\partial\Delta_t S}{\partial P}\right)_T = \left(\frac{\partial^2\Delta_t G}{\partial T\partial P}\right) = \left(\frac{\partial^2\Delta_t G}{\partial P\partial T}\right) = \left(\frac{\partial\Delta_t V}{\partial T}\right)_P = V_m\Delta_t\alpha \tag{7.7}$$

(c) the third one obtained by comparison between (7.5) and (7.6) (denoted as EC1: T–P)

$$\frac{V_m T_t \Delta_t\alpha}{\Delta_t C_p} = \frac{\Delta_t\beta}{\Delta_t\alpha} \rightarrow V_m T_t(\Delta_t\alpha)^2 = \Delta_t C_p \Delta_t\beta \tag{7.8}$$

As mentioned, the transitions with zero value of changes in the first-order derivatives of criterial function (e.g., Gibbs energy) were classified as the second-order transitions. This classification was immediately applied by Rutgers [10] to describe the transition between normal and superconducting state in metals.

In 1937, Landau suggested [11] the theory of phase transitions based on Taylor series of thermodynamic potential as a function of the order parameter. In 1944, Onsager [12] showed that his solution of Ising model for two-dimensional magnets did not observe the character expected for Ehrenfest second-order transitions.

The Ehrenfest classification became widely accepted after publishing of the classical book by A.B. Pippard in 1957 [13] where the existence of higher-order transitions has been also admitted. By contrast, the generalized thermodynamics established by Tisza [14] and Callen [15] found that from the thermodynamic point of view, only two types of transitions are possible—the first-order transition and the transition occurring when the system passes through its critical point, namely the critical phase transition.

In 1996, Matolcsi [16] wrote in his paper: "Second order phase transitions of Ehrenfest type are rarely observed in nature; on the contrary, λ-transitions which correspond to Tisza's classification, are common phenomena."

In summary, the attempts to experimentally verify the validity of Ehrenfest equations in unary systems were not successful; however, this validity was found in binary systems.

In fact, Ehrenfest equations could be applied to all transitions where the integral change of Gibbs free energy $\Delta G = G_{HT} - G_{LT}$ between the low-temperature state (index LT) and high-temperature state (index HT) is zero (much like for the sharp phase transition); however, also the integral change of thermodynamic quantities derived from Gibbs free energy as the first derivatives ($\Delta_t H = (\partial(\Delta_t G/T)/\partial(1/T))_P$, $\Delta_t U = (\partial(\Delta_t G/P)/\partial(1/P))_T$, $\Delta_t S = -(\partial\Delta_t G/\partial T)_P$, and $\Delta_t V = (\partial\Delta_t G/\partial T)_P$) is vanishing.

Hillert [2] in his excellent book distinguished between the sharp phase transition (with strictly defined equilibrium transition temperature T_t) and gradual phase transitions occurring in two-component (A–B) systems where a two-phase region arises due to different concentration dependences of G_m for phases φ and ψ (see Figs. 7.1 and 7.2). The compositions of coexisting phases [the original (φ) and the resulting (ψ)] are determined by common tangent rule (Fig. 7.1) in the temperature interval $T \in (T_{in}, T_{fin})$ (the initial temperature T_{in} and the final temperature T_{fin}) where T_{in}, X_T is the point on the borderline between one-phase region (φ) and two-phase region ($\varphi + \psi$), and T_{fin}, X_T is the point on the line separating two-phase region ($\varphi + \psi$) and one-phase region (ψ) (Fig. 7.2).

We can say that the gradual transition includes two *partial transitions* (the name *partial transition* has been coined in [17])—in its initial point at T_{in} (where the final phase (ψ) starts to precipitate and the amount of the original phase (φ) starts to decrease but remains nonzero) and the final point at T_{fin} (where the original phase φ disappears and the composition of high temperature phase (ψ) reaches X_T). During the gradual phase transition, the composition of phase φ changes gradually from $X_\varphi = X_T$ to $X_\varphi = X_\varphi^*$ and composition of phase φ is gradually changing from $X_\psi = X_\psi^*$ to $X_\psi = X_T$, and the phase fraction ξ_ψ of the two-phase state is changing according to lever rule as $\xi_\psi = (X_T - X_\varphi)/(X_\psi - X_\varphi)$.

Denoting the phase fraction of the precipitating phase ψ as ξ_ψ and the phase fraction of disappearing phase φ as $\xi_\varphi = 1 - \xi_\psi$, the **initial (low-temperature) partial phase transition point** (index *pt* from *partial transition*) can be viewed as a

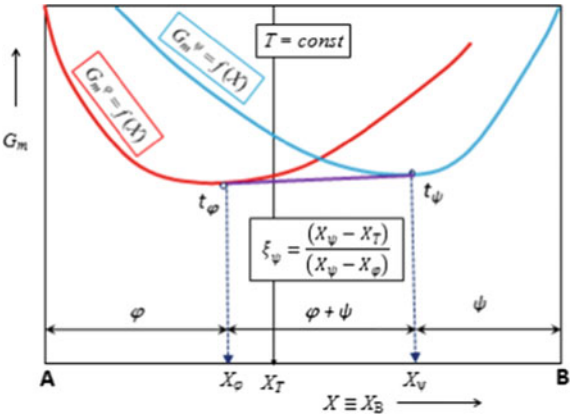

Fig. 7.1 The two-phase region (lentiform gap) in a binary system is formed by separation into two phases whose total Gibbs free energy reached the minimum value. The total composition X_T is distributed according to common tangent rule into two phases φ and ψ with compositions X_φ and X_ψ (corresponding to tangent points)

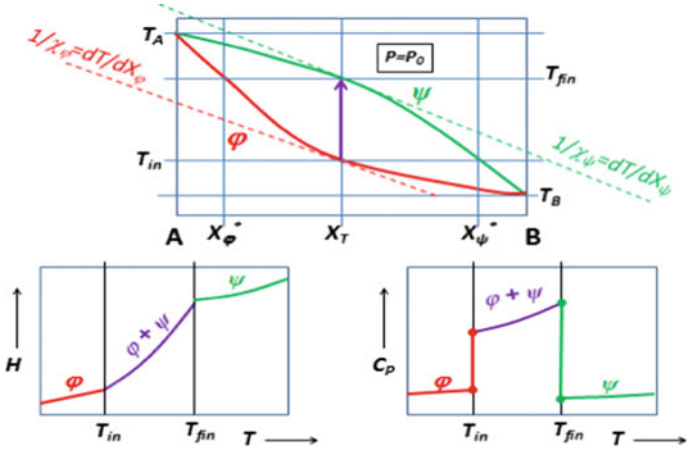

Fig. 7.2 Binary phase diagram with the lentiform two-phase field and the equilibrium background for enthalpy H and apparent heat capacity C_p at the gradual transition of sample with composition X_T

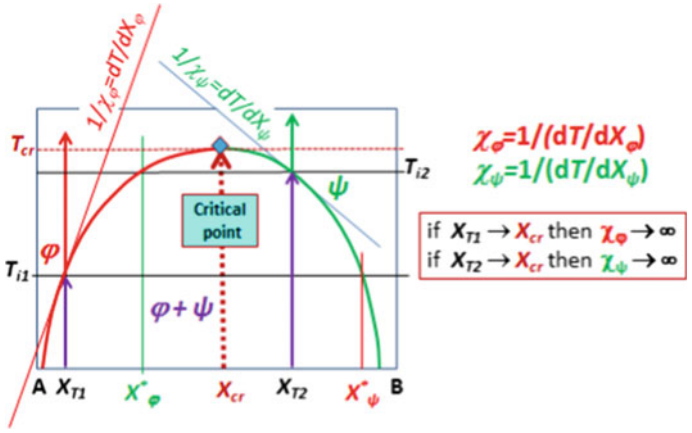

Fig. 7.3 Stand-alone final partial transition points occurring in the vicinity of critical consolution point on the boundary of bell-like miscibility gap in a binary $T - X$ diagram

point where temperature becomes T_{in}, phase fraction ξ_ψ becomes higher than zero, phase φ leaves its composition X_T, and the precipitating phase ψ adopts its neonatal composition X^*_ψ. The **final (high-temperature) partial phase transition point** is a point where temperature becomes T_{fin}, phase fraction ξ_ψ becomes unity, phase φ with its final composition X^*_φ disappears, and the ψ reaches the composition X_T.

Stand-alone final partial transition points occur in the vicinity of critical consolution point on the boundary of bell-like miscibility gap in a binary T-X diagram as shown in Fig. 7.3.

Regarding the use of Ehrenfest equations for the description of partial phase transition, it should be noted that the values of change in heat capacity $\Delta_{pt}C_p$, isobaric volume thermal expansion $\Delta_{pt}\alpha$, and isothermal volume compressibility $\Delta_{pt}\beta$ are different from those occurring in the indefinite expressions in fractions $\Delta_t\alpha/\Delta_t C_p$ (see Eq. 7.5) and $\Delta_t\alpha/\Delta_t\beta$ (see Eq. 7.6). Applications of Ehrenfest equations to partial phase transitions in closed binary systems have been shown in [17] including the expressions derived for $\Delta_{pt}C_p$, $\Delta_{pt}\alpha$, and $\Delta_{pt}\beta$ at the initial and final points. For instance, for a partial transition $\varphi(X_T) \rightarrow \varphi(X_T) + \psi(X_\psi^*)$ (the initial point), we end up with the relation [17]

$$\frac{dT_{pt}}{dP_{pt}} = \frac{V_\varphi T_{pt}\Delta_{pt}\alpha}{\Delta_{pt}C_p} = \frac{V_\psi\left(X_\psi^*\right) - V_\varphi(X_T)}{S_\psi\left(X_\psi^*\right) - S_\varphi(X_T)} \tag{7.9}$$

7.3 Hyper-free Energy in Partly Open Systems

Hyper-free energy Z has been first coined in and introduced in 1992 [18] for *partly open thermodynamic systems* sharing some components with their surroundings. This thermodynamic potential is defined as a Legendre transformation of Gibbs free energy G

$$Z = G - N_f\mu_f \tag{7.10}$$

where N_f is the molar content of free component f in the system and μ_f its chemical potential. Since the free component (index f) is supposed to be shared with the surrounding atmosphere serving as a reservoir, its chemical potential in the condensed system is equal to its chemical potential in the surroundings and is given as a sum of the standard chemical potential $\mu_f^\circ = G_f^\circ$ and the logarithmic term involving activity a_f

$$\mu_f = \mu_f^\circ + RT\ \ln\ a_f = G_f^\circ + RT\ \ln\ a_f \tag{7.11}$$

However, the idea to distinguish between mobile (free) components (shared with the surroundings) and inert (permanent, conservative) components belongs to geochemist Korzhinskiy [19] whose new thermodynamic potentials are used in physical geochemistry, but unfortunately not in the textbooks of chemical thermodynamics. In Fig. 7.4, the facsimile of two figures from Korzhinskiy's paper [19] presents, likely for the first time, a potential–potential diagram of quasiunary Fe–(O)–(S) system.

Generally, it is possible to construct hyper-free energies with any number of free components (up to $N - 1$, where N is the total number of components)

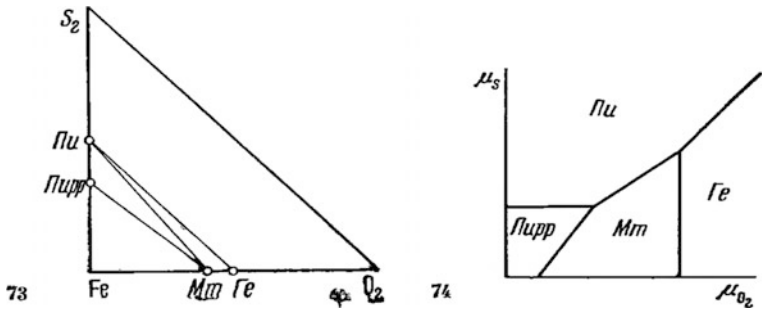

Fig. 7.4 Facsimile of Korzhinskiy's figures [19] published in 1957 with phase relations between *Пирр* Pyrrhotine, *Пи* Pyrite, *Mm* Magnetite, and *Ге* Hematite. *Left* Closed ternary system Fe–O_2–S_2. *Right* Quasiunary Fe–(O_2)–(S_2) system where an analogue of C5 (see Eq. 7.23), $d\mu_{S2}/d\mu_{O2} = \Delta Y_{O2}/\Delta Y_{S2}$, was applied

$$Z = G - \sum_i N_{fi}\left(\mu^{\circ}_{fi} + RT\ \ln\ a_{fi}\right) \tag{7.12}$$

and such potentials are useful for the description of nonstoichiometric phases behavior [20, 21].

For the thermodynamic analysis of partly open systems, it is appropriate to express the composition (e.g., composition of N components of which $N - 2$ are conservative components and two are free components—with the indices f and g) using *quasimolar fractions* Y_i which are derived from molar fraction X_i:

$$X_i = \frac{N_i}{\sum_{i=1}^{N} N_i}; \quad Y_i = \frac{N_i}{\sum_{i=1}^{N-2} N_i} = \frac{X_i}{1 - X_f - X_g}; \quad X_i = \frac{Y_i}{1 + Y_f + Y_g} \tag{7.13}$$

Similarly, it is convenient to use quasimolar quantities Q_q related to the amount of conservative components only (e.g., $C = N - 2$ conservative components) instead of molar quantities Q_m related to the amount of all components (e.g., N components = C conservative components + 2 free components)

$$Q_m = \frac{Q}{\sum_{i=1}^{N} N_i}; \quad Q_q = \frac{Q}{\sum_{i=1}^{N-2} N_i} = \frac{Q_m}{1 - X_f - X_g}; \quad Q_m = \frac{Q_q}{1 + Y_f + Y_g} \tag{7.14}$$

Hyper-free energy has been also used for the construction of crystallochemical models allowing to estimate the relations between the amount of crystal point effects and the equilibrium content of free component [22] and for the description of equilibrium behavior of nonstoichiometric phases [23, 24]. Moreover, this new thermodynamic potential gives us a possibility to derive new Clapeyronian and Ehrenfestian equations involving activities of free components.

7.4 Clapeyronian Equations for Partly Open Systems

The procedure applied to derive Clapeyron equation using Gibbs free energy G can be used to derive analogous Clapeyron-like (Clapeyronian) equations describing phase transitions in partly open systems in the space of adjustable intensive potential quantities (predictors)—T, p, a_f (the activity of free component a_f can be alternatively replaced by ln a_f, log a_f, or μ_f). As we are dealing with partly open systems, we have to employ hyper-free energy Z involving one (f) or more (f, g, …) free components. The change of hyper-free energy corresponding to a given phase transition, which can be considered as a decomposition (index d) due to an abrupt change of free component content, is defined as

$$\Delta_d Z_q(T_d) = Z_q^{\varphi}(T_d) - Z_q^{\varphi}(T_d) = \Delta U_q + P_d \Delta V_q - T_q \Delta S_q - \Delta Y_f (G_f^{\circ} + RT_d \ln a_f) = 0 \tag{7.15}$$

where ΔH_q, ΔS_q, ΔV_q, and ΔU_q are the integral changes expressed in terms of quasimolar quantities as defined in Eq. 7.14, ΔY_f is the change of free component content (expressed as quasimolar fraction, as defined in Eq. 7.13, and G_f° is the molar Gibbs free energy of the pure free component in its standard state

$$G_f^{\circ}(T) = H_f^{\circ}(T) - TS_f^{\circ}(T) = U_f^{\circ}(T) + PV_f^{\circ}(T) - T\,S_f^{\circ}(T). \tag{7.16}$$

Substituting (7.11) into (7.12) and introducing integral changes of extensive quantities on decomposition referred to nonvolatile (conservative) components of the system

$$\begin{aligned} \Delta_d H_q &= \Delta H_q - \Delta Y_f H_f^{\circ}; \quad \Delta_d S_q = \Delta S_q - \Delta Y_f S_f^{\circ}; \\ \Delta_d V_q &= \Delta V_q - \Delta Y_f V_f^{\circ}; \quad \Delta_d U_q = \Delta U_q - \Delta Y_f U_f^{\circ} \end{aligned} \tag{7.17}$$

we obtain

$$\begin{aligned} \Delta_d Z_q(T_d) &= Z_q^{\varphi}(T_d) - Z_q^{\varphi}(T_d) = \Delta_d H_q - T_d \Delta_d S_q - \Delta Y_f R T_d \ln a_f \\ &= \Delta_d U_q + P_d \Delta_d V_q - T_d \Delta_d S_q - \Delta Y_f R T_d \ln a_f = 0 \end{aligned} \tag{7.18}$$

A new Clapeyronian equation (denoted as C2) is obtained for constant pressure as

$$\left(\frac{\mathrm{d} \ln a_f}{\mathrm{d}(1/T_d)}\right)_P = -\frac{(\partial(\Delta_d Z_q/T)/\partial(1/T))_{a_f,P}}{(\partial(\Delta_d Z_q/T)/\partial \ln a_f)_{T,P}} = \frac{\Delta_d H_q}{R \Delta Y_f} \tag{7.19}$$

where the Gibbs–Helmholtz equation $\Delta H = d(\Delta G/T)/d(1/T)$ has been applied. The comparison between log a_f − $1/T$ plot for a partly open (quasiunary) system Fe–(O) and $T - X_f$ plot for the correspondingly closed binary system Fe–O is shown in Fig. 7.5.

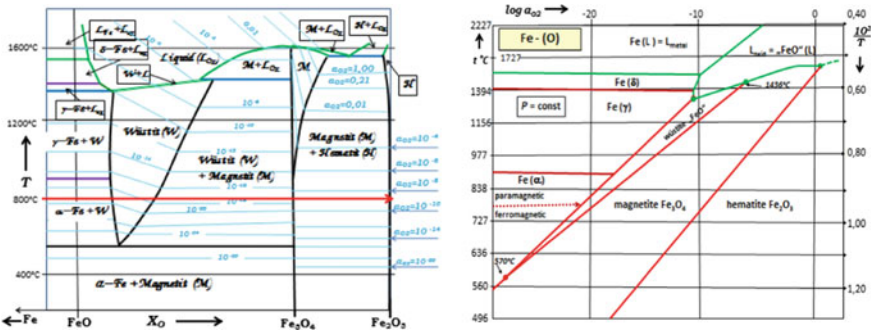

Fig. 7.5 *Left* Closed binary system Fe–O [25]; *Right* Quasiunary Fe–(O) system [26]

Another Clapeyronian equation (denoted as C3) can be derived for constant temperature

$$\left(\frac{\mathrm{d}\ln a_\mathrm{f}}{\mathrm{d}P_\mathrm{d}}\right)_\mathrm{T} = -\frac{(\partial\Delta_\mathrm{d}Z_\mathrm{q}/\partial P)_{\mathrm{T},a_\mathrm{f}}}{(\partial\Delta_\mathrm{d}Z_\mathrm{q}/\partial\ln a_\mathrm{f})_{\mathrm{T,P}}} = \frac{\Delta_\mathrm{d}V_\mathrm{q}}{\mathrm{R}T_\mathrm{d}\Delta Y_\mathrm{f}} \tag{7.20}$$

and the next one (denoted as C4) is derived for constant activity of free component a_f as

$$\left(\frac{\mathrm{d}T_\mathrm{d}}{\mathrm{d}P_\mathrm{d}}\right)_{a_\mathrm{f}} = -\frac{(\partial\Delta_\mathrm{d}Z_\mathrm{q}/\partial P)_{\mathrm{T},a_\mathrm{f}}}{(\partial\Delta_\mathrm{d}Z_\mathrm{q}/\partial T)_{\mathrm{P},a_\mathrm{f}}} = \frac{\Delta_\mathrm{d}V_\mathrm{q}T_\mathrm{d}}{\Delta_\mathrm{d}H_\mathrm{q}} \tag{7.21}$$

These three new Clapeyronian equations correlate the mutual variations (derivatives) between pairs of three intensive potential quantities (T, P, a_f) with the changes of several relative (quasimolar) quantities $\Delta_\mathrm{d}H_\mathrm{q}$, ΔY_f, and $\Delta_\mathrm{d}V_\mathrm{q}$. It means that from one Clapeyronian equation, we should be able to derive six Ehrenfestian equations (3 differentiations with respect to T, P, and a_f plus 3 comparisons between T–P, T–a_f, and P–a_f).

The last Clapeyronian equation (denoted as C5) is derived from hyper-free energy Z constructed for two different free components f and g:

$$\begin{aligned}\Delta_\mathrm{d}Z_\mathrm{q}(T_\mathrm{d}) &= Z_\mathrm{q}^{\psi}(T_\mathrm{d}) - Z_\mathrm{q}^{\varphi}(T_\mathrm{d}) = \Delta_\mathrm{d}H_\mathrm{q} - T_\mathrm{d}\Delta_\mathrm{d}S_\mathrm{q} - \Delta Y_\mathrm{f}\mathrm{R}T_\mathrm{d}\ \ln a_\mathrm{f} - \Delta Y_\mathrm{g}\mathrm{R}T_\mathrm{d}\ \ln a_\mathrm{g} \\ &= \Delta_\mathrm{d}U_\mathrm{q} + P_\mathrm{d}\Delta_\mathrm{d}V_\mathrm{q} - T_\mathrm{d}\Delta_\mathrm{d}S_\mathrm{q} - \Delta Y_\mathrm{f}\mathrm{R}T_\mathrm{d}\ \ln a_\mathrm{f} - \Delta Y_\mathrm{g}\mathrm{R}T_\mathrm{d}\ \ln a_\mathrm{g} = 0\end{aligned} \tag{7.22}$$

where $\Delta_\mathrm{d}H_\mathrm{q}$, $\Delta_\mathrm{d}S_\mathrm{q}$, $\Delta_\mathrm{d}V_\mathrm{q}$, and $\Delta_\mathrm{d}U_\mathrm{q}$ have the same meaning as defined in Eq. 7.17, but the original quantities are reduced with respect to two different free components.

Applying the differentiation with respect to logarithms of both activities for a constant temperature and pressure, we end up with the familiar form used for the construction of Kellogg potential phase diagrams [27] published in (1960)

$$\left(\frac{\mathrm{d}\ln a_\mathrm{f}}{\mathrm{d}\ln a_\mathrm{g}}\right)_{\mathrm{P,T}} = -\frac{(\partial(\Delta Z/T)/\partial\ \ln a_\mathrm{g})_{\mathrm{P,T,a_f}}}{(\partial(\Delta Z/T)/\partial\ \ln a_\mathrm{f})_{\mathrm{P,T,a_g}}} = -\frac{\Delta Y_\mathrm{g}}{\Delta Y_\mathrm{f}} \tag{7.23}$$

In this case, the hyper-free function Z includes four potential quantities (T, P, a_f, a_g) so that we can derive ten Ehrenfestian equations (4 differentiations with respect to T, P, $a_\mathrm{f,}$ and a_g plus 6 comparisons T–P, T–a_f, T–a_g, P–a_f, P–a_g, and a_f–a_g). A list of all derived Clapeyronian and Ehrenfestian equations including their symbols and the corresponding equation numbers is given in Table 7.1.

Table 7.1 List of 5 Clapeyron equation (CE) and 31 Ehrenfest equation (EE) symbols and numbers

System	CE		EE (a)		EE (b)	
	Symbol	Eq.	Symbol	Eq.	Symbol	Eq.
Closed unary system A	C1	(7.2)				
Closed binary system A-B			EC1:T	(7.5)	EC1:T–P	(7.8)
			EC1:P	(7.6)		
Quasiunary system A-(F)	C2	(7.19)				
Quasibinary system A-B-(F), P = const.			EC2:T	(7.28)	EC2:T–P	(7.32)
			EC2:P	(7.29)	EC2:T–a_f	(7.33)
			EC2:a_f	(7.30)	EC2:P–a_f	(7.34)
Quasiunary system A-(F)	C3	(7.20)				
Quasibinary system A-B-(F), T = const.			EC3:T	(7.35)	EC3:T-P	(7.39)
			EC3:P	(7.36)	EC3:T-a_f	(7.40)
			EC3:a_f	(7.37)	EC3:P-a_f	(7.41)
Quasiunary system A-(F)	C4	(7.21)				
Quasibinary system A-B-(F), a_F = const.			EC4:T	(7.42)	EC4:T-P	(7.45)
			EC4:P	(7.43)	EC4:T-a_f	(7.46)
			EC4:a_f	(7.44)	EC4:P-a_g	(7.47)
Quasiunary system A-(F)-(G)	C5	(7.23)				
Quasibinary system A-B-(F)-(G), T, P = const.			EC5:T	(7.48)	EC5:T-P	(7.52)
			EC5:P	(7.49)	EC5:T-a_f	(7.53)
			EC5:a_f	(7.50)	EC5:T-a_g	(7.54)
			EC5:a_g	(7.51)	EC5:P-a_f	(7.55)
					EC5:P-a_g	(7.56)
					EC5:a_f-a_g	(7.57)

(a) derived from CE using the predictors T, P, $a_\mathrm{f,}$ and a_g and (b) by comparison of the derived EE: (T–P), (T–a_f), (T–a_g), (P–a_f), (P–a_g), and (a_f–a_g)

7.5 Ehrenfestian Equations for Partly Open Systems

In order to derive the Ehrenfestian equations for partly open systems, it is useful to define the specific quantities representing the variation of free component composition with respect to predictors T, P, and a_f (a_g):

proper plutability (πλούτος = rich):

$$\kappa_{ff} = (\partial Y_f/\partial \ln a_f)_{T,P} \tag{7.24}$$

thermal plutability[1]:

$$\kappa_{fT} = (\partial Y_f/\partial T)_{P,a_f} \tag{7.25}$$

pressure plutability[2]:

$$\kappa_{fP} = (\partial Y_f/\partial P)_{T,a_f} \tag{7.26}$$

mutual plutability:

$$\kappa_{fg} = \left(\partial Y_f/\partial \ln a_g\right)_{T,P,a_f} \tag{7.27}$$

Since the variation of Y_f is a continuous but not a smooth function of predictors on the borderline delimiting a partial transition, ΔY_f is equal to zero at the transition point (we use index t instead of d); however, the plutabilities are discontinuous step functions with $\Delta\kappa_{fi} \neq 0$ at the transition.

From the Clapeyronian equation C2 (Eq. 7.19), we obtain the first Ehrenfestian equation (denoted as {EC2:T}) by differentiation at constant pressure with respect to temperature

$$\left(\frac{\mathrm{d}\ln a_f}{\mathrm{d}(1/T_t)}\right)_P = \lim_{\Delta_t H_q, \Delta Y_f \to 0} \frac{1}{R}\frac{\Delta_t H_q}{\Delta Y_f} = \frac{1}{R}\frac{\partial \Delta_t H_q/\partial T}{\partial \Delta Y_f/\partial T} = \frac{\Delta_t C_p}{R\Delta_t \kappa_{fT}} \tag{7.28}$$

The second Ehrenfestian equation (denoted as EC2:P) derived from C2 is obtained by the differentiation with respect to pressure

$$\begin{aligned}\left(\frac{\mathrm{d}\ln a_f}{\mathrm{d}(1/T_t)}\right)_P &= \lim_{\Delta_t H_q, \Delta Y_f \to 0} \frac{1}{R}\frac{\Delta_t H_q}{\Delta Y_f} = \frac{1}{R}\frac{\partial \Delta_t H_q/\partial P}{\partial \Delta Y_f/\partial P} \\ &= \frac{T_t\left(\partial \Delta_t S_q/\partial P\right)}{R\Delta_t \kappa_{fP}} = -\frac{T_t\left(\partial \Delta_t V_q/\partial T\right)}{R\Delta_t \kappa_{fP}} = -\frac{T_t V_q \Delta_t \alpha}{R\Delta_t \kappa_{fP}}\end{aligned} \tag{7.29}$$

[1] In our previous works [20, 21], the term thermal phtochability $\kappa_{fT} = -(\partial Y_f/\partial T)_{P,af}$ was used.

[2] In our previous work [21], the term pressure phtochability $\kappa_{fP} = -(\partial Y_f/\partial P)_{T,af}$ was used.

where the relation $(\partial H/\partial P)_{\mathrm{T}} = T(\partial \mathrm{S}/\partial P)_{\mathrm{T}} + V$ and the Maxwell's relation $(\partial \mathrm{S}/\partial P)_{\mathrm{T}} = -(\partial \mathrm{V}/\partial T)_{\mathrm{P}}$ were applied. Note that the respective changes of heat capacity and thermal expansion coefficient, $\Delta_{\mathrm{t}}C_{\mathrm{p}}$ and $\Delta_{\mathrm{t}}\alpha$ (as well as $\Delta_{\mathrm{t}}\beta$ below), involve not only the difference in the corresponding quantities of condensed phases but also the changes associated with free component release or uptake. For instance, for the heat capacity change, we find $\Delta_{\mathrm{t}}C_{\mathrm{p}} = \Delta C_{\mathrm{pq}} - \Delta Y_{\mathrm{f}} C^{\circ}_{\mathrm{pf}} + \Delta_{\mathrm{d}}\kappa_{\mathrm{fT}} H^{\circ}_{f}$.

The third Ehrenfestian equation (denoted as EC2:a_{f}) derived from C2 is obtained by the differentiation with respect to logarithm of free component activity

$$\left(\frac{\mathrm{d}\ln a_{\mathrm{f}}}{\mathrm{d}(1/T_{\mathrm{t}})}\right)_{\mathrm{P}} = \lim_{\Delta_{\mathrm{t}}H_{\mathrm{q}},\Delta Y_{\mathrm{f}}\to 0}\frac{1}{\mathrm{R}}\frac{\Delta_{\mathrm{t}}H_{\mathrm{q}}}{\Delta Y_{\mathrm{f}}} = \frac{\partial \Delta_{\mathrm{t}}H_{\mathrm{q}}/\partial \ln a_{\mathrm{f}}}{\mathrm{R}(\partial \Delta Y_{\mathrm{f}}/\partial \ln a_{\mathrm{f}})} = \frac{T_{\mathrm{t}}^2 \Delta_{\mathrm{t}}\kappa_{\mathrm{fT}}}{\Delta_{\mathrm{t}}\kappa_{\mathrm{ff}}} \tag{7.30}$$

where the Clairaut theorem [28]

$$\frac{\partial \Delta_{\mathrm{t}}H_{\mathrm{q}}}{\partial \ln a_{\mathrm{f}}} = \left(\frac{\partial^2(\Delta_{\mathrm{t}}Z_{\mathrm{q}}/T)}{\partial(1/T)\partial \ln a_{\mathrm{f}}}\right) = \left(\frac{\partial^2(\Delta_{\mathrm{t}}Z_{\mathrm{q}}/T)}{\partial \ln a_{\mathrm{f}}\partial(1/T)}\right) = -\mathrm{R}\frac{\partial \Delta Y_{\mathrm{f}}}{\partial(1/T)} = \mathrm{R}T^2\Delta_{\mathrm{t}}\kappa_{\mathrm{fT}} \tag{7.31}$$

was used to obtain Eq. (7.30). Three additional Ehrenfestian equations derived from C2 follow from the comparison of those previously derived, as given in Eqs. (7.28)–(7.30). The first one (denoted as EC2:*T*–*P*) is obtained by comparing (7.28) and (7.29)

$$\frac{\Delta_{\mathrm{d}}C_{\mathrm{p}}}{\Delta_{\mathrm{d}}\kappa_{\mathrm{fT}}} = -\frac{T_{\mathrm{t}}V_{\mathrm{q}}\Delta_{\mathrm{d}}\alpha}{\Delta_{\mathrm{d}}\kappa_{\mathrm{fP}}}, \tag{7.32}$$

the second one (denoted as EC2:*T*–a_{f}) as comparison of (7.28) and (7.30)

$$\frac{\Delta_{\mathrm{t}}C_{\mathrm{p}}}{\mathrm{R}\Delta_{\mathrm{t}}\kappa_{\mathrm{fT}}} = \frac{T_{\mathrm{t}}^2\Delta_{\mathrm{t}}\kappa_{\mathrm{fT}}}{\Delta_{\mathrm{t}}\kappa_{\mathrm{ff}}} \to \frac{\Delta_{\mathrm{d}}C_{\mathrm{p}}}{\mathrm{R}} = \frac{(T_{\mathrm{t}}\Delta_{\mathrm{t}}\kappa_{\mathrm{fT}})^2}{\Delta_{\mathrm{t}}\kappa_{\mathrm{ff}}} \tag{7.33}$$

and the third one (denoted as EC2:*P*–a_{f}) as comparison of (7.29) and (7.30)

$$-\frac{V_{\mathrm{q}}\Delta_{\mathrm{t}}\alpha}{\mathrm{R}\Delta_{\mathrm{t}}\kappa_{\mathrm{fP}}} = \frac{T_{\mathrm{t}}\Delta_{\mathrm{t}}\kappa_{\mathrm{fT}}}{\Delta_{\mathrm{t}}\kappa_{\mathrm{ff}}} \tag{7.34}$$

Starting from C3, we then obtain the following Ehrenfestian equations denoted as EC3:*T*, EC3:*P*, and EC3:a_{f},

$$\left(\frac{\partial \ln a_{\mathrm{f}}}{\partial P_{\mathrm{t}}}\right)_{\mathrm{T}} = \lim_{\Delta_{\mathrm{t}}V_{\mathrm{q}},\Delta Y_{\mathrm{f}}\to 0}\frac{1}{\mathrm{R}}\frac{\Delta_{\mathrm{t}}V_{\mathrm{q}}}{\Delta Y_{\mathrm{f}}} = \frac{1}{\mathrm{R}}\frac{\partial \Delta_{\mathrm{t}}V_{\mathrm{q}}/\partial T}{\partial \Delta Y_{\mathrm{f}}/\partial T} = \frac{1}{\mathrm{R}}\frac{\Delta_{\mathrm{t}}\alpha V_{\mathrm{q}}}{\Delta_{\mathrm{t}}\kappa_{\mathrm{fT}}} \tag{7.35}$$

$$\left(\frac{\partial \ln a_\mathrm{f}}{\partial P_\mathrm{t}}\right)_\mathrm{T} = \lim_{\Delta_\mathrm{t}V_\mathrm{q},\Delta Y_\mathrm{f}\to 0} \frac{1}{\mathrm{R}}\frac{\Delta_\mathrm{t}V_\mathrm{q}}{\Delta Y_\mathrm{f}} = \frac{1}{\mathrm{R}}\frac{\partial \Delta_\mathrm{t}V_\mathrm{q}/\partial P}{\partial \Delta Y_\mathrm{f}/\partial P} = \frac{1}{\mathrm{R}}\frac{\Delta_\mathrm{t}\beta V_\mathrm{q}}{\Delta_\mathrm{t}\kappa_\mathrm{fP}} \tag{7.36}$$

$$\left(\frac{\partial \ln a_\mathrm{f}}{\partial P_\mathrm{t}}\right)_\mathrm{T} = \lim_{\Delta_\mathrm{t}V_\mathrm{q},\Delta Y_\mathrm{f}\to 0} \frac{1}{\mathrm{R}}\frac{\Delta_\mathrm{t}V_\mathrm{q}}{\Delta Y_\mathrm{f}} = \frac{1}{\mathrm{R}}\frac{\partial \Delta_\mathrm{t}V_\mathrm{q}/\partial \ln a_\mathrm{f}}{\partial \Delta Y_\mathrm{f}/\partial \ln a_\mathrm{f}} = -\frac{T_\mathrm{t}\Delta_\mathrm{t}\kappa_\mathrm{fP}}{\Delta_\mathrm{t}\kappa_\mathrm{ff}} \tag{7.37}$$

where the Clairaut theorem

$$\frac{\partial \Delta_\mathrm{t}V_\mathrm{q}}{\partial \ln a_\mathrm{f}} = \frac{\partial^2 \Delta_\mathrm{t}Z_\mathrm{q}}{\partial P \partial \ln a_\mathrm{f}} = \frac{\partial^2 \Delta_\mathrm{t}Z_\mathrm{q}}{\partial \ln a_\mathrm{f} \partial P} = -\mathrm{R}T\frac{\partial \Delta Y_\mathrm{f}}{\partial P} = -\mathrm{R}T\Delta_\mathrm{t}\kappa_\mathrm{fP} \tag{7.38}$$

was used to derive Eq. (7.37), and three additional equations, EC3:T–P, EC3:T–a_f, and EC3:P–a_f, are obtained from the comparison of the previous three Eqs. (7.35)–(7.37):

$$\frac{\Delta_\mathrm{t}\alpha}{\Delta_\mathrm{t}\kappa_\mathrm{fT}} = \frac{\Delta_\mathrm{t}\beta}{\Delta_\mathrm{t}\kappa_\mathrm{fP}} \tag{7.39}$$

$$\frac{\Delta_\mathrm{t}\alpha V_\mathrm{q}}{\mathrm{R}T_\mathrm{t}\Delta_\mathrm{t}\kappa_\mathrm{fT}} = -\frac{\Delta_\mathrm{t}\kappa_\mathrm{fP}}{\Delta_\mathrm{t}\kappa_\mathrm{ff}} \tag{7.40}$$

$$\frac{\Delta_\mathrm{t}\beta V_\mathrm{q}}{\mathrm{R}T_\mathrm{t}\Delta_\mathrm{t}\kappa_\mathrm{fP}} = -\frac{\Delta_\mathrm{t}\kappa_\mathrm{fP}}{\Delta_\mathrm{t}\kappa_\mathrm{ff}} \to \frac{\Delta_\mathrm{t}\beta V_q}{\mathrm{R}T_\mathrm{t}} = -\frac{\left(\Delta_\mathrm{t}\kappa_\mathrm{fP}\right)^2}{\Delta_\mathrm{t}\kappa_\mathrm{ff}} \tag{7.41}$$

Starting from C4, we then obtain the following Ehrenfestian equations denoted as EC4:T, EC4:P, and EC4:a_f

$$\left(\frac{\mathrm{d}T_\mathrm{t}}{\mathrm{d}P_\mathrm{t}}\right)_{a_\mathrm{f}} = \lim_{\Delta_\mathrm{t}V_\mathrm{q},\Delta_\mathrm{t}H_\mathrm{q}\to 0} \frac{T_\mathrm{t}\Delta_\mathrm{t}V_\mathrm{q}}{\Delta_\mathrm{t}H_\mathrm{q}} = T_\mathrm{t}\frac{\partial \Delta_\mathrm{t}V_\mathrm{q}/\partial T}{\partial \Delta_\mathrm{t}H_\mathrm{q}/\partial T} = \frac{\Delta_\mathrm{t}\alpha T_\mathrm{t}V_\mathrm{q}}{\Delta_\mathrm{t}C_\mathrm{p}} \tag{7.42}$$

$$\left(\frac{\mathrm{d}T_\mathrm{t}}{\mathrm{d}P_\mathrm{t}}\right)_{a_\mathrm{f}} = \lim_{\Delta_\mathrm{t}V_\mathrm{q},\Delta_\mathrm{t}H_\mathrm{q}\to 0} \frac{T_\mathrm{t}\Delta_\mathrm{t}V_\mathrm{q}}{\Delta_\mathrm{t}H_\mathrm{q}} = T_\mathrm{t}\frac{\partial \Delta_\mathrm{t}V_\mathrm{q}/\partial P}{\partial \Delta_\mathrm{t}H_\mathrm{q}/\partial P} = -\frac{\Delta_\mathrm{t}\beta T_\mathrm{t}V_\mathrm{q}}{T_\mathrm{t}\left(\partial \Delta_\mathrm{t}V_\mathrm{q}/\partial T\right)} = -\frac{\Delta_\mathrm{t}\beta}{\Delta_\mathrm{t}\alpha} \tag{7.43}$$

where the Maxwell relation $\left(\partial \Delta_\mathrm{t}S_\mathrm{q}/\partial P\right)_\mathrm{T} = -\left(\partial \Delta_\mathrm{t}V_\mathrm{q}/\partial T\right)_\mathrm{P}$ is used to derive Eq. (7.43).

$$\left(\frac{\mathrm{d}T_\mathrm{t}}{\mathrm{d}P_\mathrm{t}}\right)_{a_\mathrm{f}} = \lim_{\Delta_\mathrm{t}V_\mathrm{q},\Delta_\mathrm{t}H_\mathrm{q}\to 0} \frac{T_\mathrm{t}\Delta_\mathrm{t}V_\mathrm{q}}{\Delta_\mathrm{t}H_\mathrm{q}} = T_\mathrm{t}\frac{\partial \Delta_\mathrm{t}V_\mathrm{q}/\partial \ln a_\mathrm{f}}{\partial \Delta_\mathrm{t}H_\mathrm{q}/\partial \ln a_\mathrm{f}} = \frac{-\mathrm{R}T_\mathrm{t}\Delta_\mathrm{t}\kappa_\mathrm{fP}}{\mathrm{R}T_\mathrm{t}^2\Delta_\mathrm{t}\kappa_\mathrm{fT}} = -\frac{\Delta_\mathrm{t}\kappa_\mathrm{fP}}{T_\mathrm{t}\Delta\kappa_\mathrm{fT}} \tag{7.44}$$

where Clairaut theorem [28] was applied twice according to Eqs. (7.31) and (7.38). Comparing Eqs. (7.42)–(7.44), three additional equations denoted, respectively, EC4:T–P, EC4:T–a_{f}, and EC4:P–a_{f}, are obtained:

$$\frac{T_{\mathrm{t}}V_{\mathrm{q}}}{\Delta_{\mathrm{t}}C_{\mathrm{p}}} = -\frac{\Delta_{\mathrm{t}}\beta}{\Delta_{\mathrm{t}}\alpha^2} \tag{7.45}$$

$$\frac{\Delta_{\mathrm{t}}\alpha T_{\mathrm{t}}^2 V_{\mathrm{q}}}{\Delta_{\mathrm{t}}C_{\mathrm{p}}} = -\frac{\Delta_{\mathrm{t}}\kappa_{\mathrm{fP}}}{\Delta_{\mathrm{t}}\kappa_{\mathrm{fT}}} \tag{7.46}$$

$$\frac{\Delta_{\mathrm{t}}\beta}{\Delta_{\mathrm{t}}\alpha} = \frac{\Delta_{\mathrm{t}}\kappa_{\mathrm{fP}}}{T_{\mathrm{t}}\Delta_{\mathrm{t}}\kappa_{\mathrm{fT}}} \tag{7.47}$$

The last set of 10 Ehrenfestian equations denoted as EC5:T, EC5:P, EC5:a_{f}, EC5:a_{g}, EC5:T–P, EC5:T–a_{f}, EC5:T–a_{g}, EC5:P–a_{f}, EC5:P–a_{g}, and EC5:a_{f}–a_{g} is obtained by the differentiation of indefinite form resulting from C5:

$$\left(\frac{\mathrm{d}\ln a_{\mathrm{f}}}{\mathrm{d}\ln a_{\mathrm{g}}}\right)_{\mathrm{T,P}} = \lim_{\Delta Y_{\mathrm{f}},\Delta Y_{\mathrm{g}}\to 0} -\frac{\Delta Y_{\mathrm{g}}}{\Delta Y_{\mathrm{f}}} = -\frac{\partial \Delta Y_{\mathrm{g}}/\partial T}{\partial \Delta Y_{\mathrm{f}}/\partial T} = -\frac{\Delta_{\mathrm{t}}\kappa_{\mathrm{gT}}}{\Delta_{\mathrm{t}}\kappa_{\mathrm{fT}}} \tag{7.48}$$

$$\left(\frac{\mathrm{d}\ln a_{\mathrm{f}}}{\mathrm{d}\ln a_{\mathrm{g}}}\right)_{\mathrm{T,P}} = \lim_{\Delta Y_{\mathrm{f}},\Delta Y_{\mathrm{g}}\to 0} -\frac{\Delta Y_{\mathrm{g}}}{\Delta Y_{\mathrm{f}}} = -\frac{\partial \Delta Y_{\mathrm{g}}/\partial P}{\partial \Delta Y_{\mathrm{f}}/\partial P} = -\frac{\Delta_{\mathrm{t}}\kappa_{\mathrm{gP}}}{\Delta_{\mathrm{t}}\kappa_{\mathrm{fP}}} \tag{7.49}$$

$$\left(\frac{\mathrm{d}\ln a_{\mathrm{f}}}{\mathrm{d}\ln a_{\mathrm{g}}}\right)_{\mathrm{T,P}} = \lim_{\Delta Y_{\mathrm{f}},\Delta Y_{\mathrm{g}}\to 0} -\frac{\Delta Y_{\mathrm{g}}}{\Delta Y_{\mathrm{f}}} = -\frac{\partial \Delta Y_{\mathrm{g}}/\partial \ln a_{\mathrm{f}}}{\partial \Delta Y_{\mathrm{f}}/\partial \ln a_{\mathrm{f}}} = -\frac{\Delta_{\mathrm{t}}\kappa_{\mathrm{gf}}}{\Delta_{\mathrm{t}}\kappa_{\mathrm{ff}}} \tag{7.50}$$

$$\left(\frac{\mathrm{d}\ln a_{\mathrm{f}}}{\mathrm{d}\ln a_{\mathrm{g}}}\right)_{\mathrm{T,P}} = \lim_{\Delta Y_{\mathrm{f}},\Delta Y_{\mathrm{g}}\to 0} -\frac{\Delta Y_{\mathrm{g}}}{\Delta Y_{\mathrm{f}}} = -\frac{\partial \Delta Y_{\mathrm{g}}/\partial \ln a_{\mathrm{g}}}{\partial \Delta Y_{\mathrm{f}}/\partial \ln a_{\mathrm{g}}} = -\frac{\Delta_{\mathrm{t}}\kappa_{\mathrm{gg}}}{\Delta_{\mathrm{t}}\kappa_{\mathrm{fg}}} \tag{7.51}$$

$$\frac{\Delta_{\mathrm{t}}\kappa_{\mathrm{gT}}}{\Delta_{\mathrm{t}}\kappa_{\mathrm{fT}}} = \frac{\Delta_{\mathrm{t}}\kappa_{\mathrm{gP}}}{\Delta_{\mathrm{t}}\kappa_{\mathrm{fP}}} \tag{7.52}$$

$$\frac{\Delta_{\mathrm{t}}\kappa_{\mathrm{gT}}}{\Delta_{\mathrm{t}}\kappa_{\mathrm{fT}}} = -\frac{\Delta_{\mathrm{t}}\kappa_{\mathrm{gf}}}{\Delta_{\mathrm{t}}\kappa_{\mathrm{ff}}} \tag{7.53}$$

$$\frac{\Delta_{\mathrm{t}}\kappa_{\mathrm{gT}}}{\Delta_{\mathrm{t}}\kappa_{\mathrm{fT}}} = \frac{\Delta_{\mathrm{t}}\kappa_{\mathrm{gg}}}{\Delta_{\mathrm{t}}\kappa_{\mathrm{fg}}} \tag{7.54}$$

$$\frac{\Delta_{\mathrm{t}}\kappa_{\mathrm{gP}}}{\Delta_{\mathrm{t}}\kappa_{\mathrm{fP}}} = \frac{\Delta_{\mathrm{t}}\kappa_{\mathrm{gf}}}{\Delta_{\mathrm{t}}\kappa_{\mathrm{ff}}} \tag{7.55}$$

$$\frac{\Delta_{\mathrm{t}}\kappa_{\mathrm{gP}}}{\Delta_{\mathrm{t}}\kappa_{\mathrm{fP}}} = \frac{\Delta_{\mathrm{t}}\kappa_{\mathrm{gg}}}{\Delta_{\mathrm{t}}\kappa_{\mathrm{fg}}} \tag{7.56}$$

$$\frac{\Delta_t \kappa_{gf}}{\Delta_t \kappa_{ff}} = -\frac{\Delta_t \kappa_{gg}}{\Delta_t \kappa_{fg}} \tag{7.57}$$

The Clapeyronian and Ehrenfestian equations derived in this chapter can be useful for equilibrium studies and construction of thermodynamic models of non-stoichiometric phases as well as for the construction of simple phase diagrams reflecting the equilibrium phase relations under a given controlled atmosphere [29]. Several examples of their application for the description of phase transitions in partly open systems and the construction of the respective potential phase diagrams are given in the following chapter "Nonstoichiometric phases—composition, properties and phase transitions."

Acknowledgements P. Holba acknowledges the support of Ministry of Education of the Czech Republic in the framework of CENTEM PLUS project (LO1402) operated under the "National Sustainability Programme I."

References

1. Lehmann O (1988) Molekularphysik 2. Engelmann, Leipzig, pp 398–415
2. Hillert M (1998) Phase equilibria, phase diagrams and phase transformation. Their thermodynamic basis. Cambridge University Press, Cambridge
3. Elliott JR, Lira CT. (1999) Introductory Chemical Engineering Thermodynamics, 1st Ed., Prentice Hall PTR: 184
4. Clapeyron E (1834) Puissance motrice de la chaleur, Journal de l'École Royale Polytechnique 14(23):153–190
5. Clausius R (1850) Über die bewegende Kraft der Wärme und die Gesetze, welche sich daraus für die Wärmelehre selbst ableiten lassen. Pogg Ann (Annalen der Physik) 79(368–397):500–524
6. Ehrenfest P (1933) Phasenumwandlungen im üblichen und erweiterten Sinn, classifiziert nach dem entsprechenden Singularitäten des thermodynamischen Potentiales, Verhandlingen der Koninklijke Akademie van Wetenschappen Amsterdam 36: 153–157; Communications from the Physical Laboratory of the University of Leiden, Supplement No. 75b
7. Keesom WH, de Haas WJ (1932) Die Umwandlung flüssiges Helium I-Helium II unter Druck. Verhandlingen der Koninklijke Akademie van Wetenschappen Amsterdam 34:605; Communications from the Physical Laboratory of the University of Leiden, Communication No. 216b
8. de l'Hôpital G (1696) Analyse des infiniment petits pour l'intelligence des lignes Courbes, Paris
9. Maxwell JC (1871) Theory of heat. Longmans, Green&Co, London, pp 165–168
10. Rutgers AJ (1934) Note on supraconductivity I. Physica 2:1055–1058
11. Landau LD (1937) On the theory of phase transitions. Zh Eksp Teor Fiz 7:19–32
12. Onsager L (1944) Crystal statistics. I. A two-dimensional model with an order-disorder transition. Phys Rev 65:117–149
13. Pippard AB (1957) Elements of classical thermodynamics. Cambridge University Press, Cambridge
14. Tisza L (1951) On the general theory of phase transitions. In Smoluchowski R et al (eds) Phase transitions in solids (Symposium at Cornell University, August, 1948). Wiley, New York, pp 1–37
15. Callen HB (1960) Thermodynamics. Wiley, New York

16. Matolcsi T (1996) On the classification of phase transitions. Z Angew Math Phys 47:837–857
17. Holba P (2015) Ehrenfest equations for calorimetry and dilatometry. J Thermal Anal Cal 120 (1):175–181
18. Holba P (1992) Thermodynamics of partially open systems. Czech J Phys B 42:549–575
19. Korzhinskiy DS (1957) Fizikochimikheskie osnovy analiza paragenesisov mineralov; Izd. Akad. nauk SSSR, Moscow: 184. English translation: (1959) Physicochemical basis of the analysis of the paragenesis of minerals, Consultants Bureau, New York
20. Holba P, Sedmidubský D (2013) Heat capacity equations for nonstoichiometric solids. J Therm Anal Calorim 113:239–245
21. Sedmidubský D, Holba P (2015) Material properties of nonstoichiometric solids. J Therm Anal Calorim 1120:183–188
22. Holba P, Sedmidubský D (2013) Crystal defects and nonstoichiometry contributions to heat capacity of solids, Chapter 3 in book: Thermal analysis of micro- nano- and non-crystalline materials: transformation, crystallization, kinetics and thermodynamics, Ed. J. Šesták & P. Šimon, Springer, pp 53–74
23. Nevřiva M, Kraus H, Sedmidubský D (1996) Phase equilibria study in the partially open Cu-(O) and Me-Cu-(O) (Me = Sr, Bi, Ba) systems. Thermochim Acta 282:205–224
24. Sedmidubský D, Strejc A, Nevřiva M, Leitner J, Martin C (2003) Structural and phase relations in the Sr-Mn-O System. Solid State Phenom 90–91(2003):427–432
25. Darken LS, Gurry RW (1945) The system iron-oxygen. I. The wüstite field and related equilibria. J Am Chem Soc 67:1378–1412. Darken LS, Gurry RW (1946) The system iron-oxygen. II. Equilibrium and thermodynamics of liquid oxide and other phases. J Am Chem Soc 68:789–816
26. Tretyakov YuD (1967) Termodinamika ferritov (in Russian). Izd. Chimiya, Leningradsk. Otdel. Moscow 1967.] Tretyakov YuD (1974) Chimiya nestechiometricheskikh okislov (in Russian). Izd. Moscow Univ 1974
27. Kellogg HH, Basu SK (1960) Thermodynamic properties of the system lead-sulfur-oxygen to 1100°K. Trans Metall Soc AIME 218:70–81
28. Clairaut AC (1743) Théorie de la figure de la terre, tirée des principes de l'hydrostatique, 2nd edn. (1808), Courcier, Paris
29. Sedmidubský D, Šesták J (2017) On the history and recent applications of hyperfree energy describing thermodynamics of mobile components in partly open ceramic systems - in memory of D.S. Korzhinskiĭ and P. Holba, Ceramics-Silikáty, submitted

Chapter 8
Nonstoichiometric Phases—Composition, Properties and Phase Transitions

David Sedmidubský and Pavel Holba

Abstract Nonstoichiometric phases constitute a large family of technologically important materials. Among them, the inorganic materials whose variable stoichiometry of some components originates from their exchange with surrounding atmosphere represent particular thermodynamic systems referred to a partly open system. The phase equilibria in these systems including the homogeneous crystallochemical reactions of the involved crystal defects can be effectively treated using the thermodynamic potential called hyper-free energy derived from the Gibbs free energy by Legendre transformation with respect to the amounts of free components. In this chapter, we focus on general thermodynamic description of systems with variable content of components shared with a dynamical atmosphere, their essential material quantities being influenced by variable stoichiometry, conditions for homogeneous crystallochemical equilibria as well as for phase transitions. The influence of variable stoichiometry on material properties such as isobaric thermal expansion, isothermal compressibility and in particular heat capacity is analyzed and divided into two parts: the direct effect on conventional isoplethal quantities due to deviation from stoichiometry, and so-called saturation contributions determining the difference in material properties measured under isoplethal and isodynamical conditions (constant activities of free components). In the last part, the construction of phase diagrams of partly open systems is demonstrated on several examples of oxide systems, and the relevant phase transitions are classified and discussed.

Pavel Holba—Deceased

D. Sedmidubský (✉)
Department of Inorganic Chemistry, University of Chemistry and Technology Prague,
Technická 5, 166 28 Praha 6, Czech Republic
e-mail: sedmidub@vscht.cz

P. Holba
New Technologies—Research Centre, University of West Bohemia,
Univerzitní 8, 30114 Pilsen, Prague, Czech Republic
e-mail: holbap@gmail.cz

J. Šesták et al. (eds.), *Thermal Physics and Thermal Analysis*,
Hot Topics in Thermal Analysis and Calorimetry 11,
DOI 10.1007/978-3-319-45899-1_8

8.1 Introduction

The term "stoichiometry" was introduced into chemistry in 1792 by Benjamin Richter to point out an experimental finding that substances combine together in fixed weight ratios. Richter's results were then attached to German translation of Berthollet's treatise "*Recherches sur les lois de l'affinite*" (1801) and became (together with works by Proust) an impulse to formulate the law of definite proportions which provided an important support for Dalton's atomic hypothesis. Berthollet, however, did not accept the general validity of this law and contended that fixed ratios are rather an exception and generally the variable ratios between chemical elements in compounds should be expected.

After one century, the first nonstoichiometric compound—palladium hydride—was discovered in 1895 [1]; however, intermetallic phases were not considered as compounds at these times. The considerations on the relations between the terms phase, compound, and solution became a concern of Czech analyst in metallurgy Wald (1861–1930). His ideas (e.g., [2, 3]) inspired Kurnakov (1860–1941) (see also [4, 5]) to publish a paper [6] where he proposed to distinguish between the compounds respecting the definite proportions law as "daltonides" and the nonstoichiometric compounds as "berthollides" in honor of the scientist who called into question the general validity of definite proportions law more than one century before.

The phenomenon of nonstoichiometry became important for chemists in 1920s when Chaudron [7] discovered the formation of ferrous oxide from metallic iron and magnetite (Fe_3O_4) at temperatures higher than 570 °C and when its great deviation from stoichiometry was found (FeO_{1056}) without any possibility of reaching a homogeneous stoichiometric oxide FeO [8]. X-ray diffraction (discovered in 1912) then enabled to develop the concepts of structure of mixed crystals and in 1930 Wagner and Schottky [9] proposed a physical model, including the idea of crystal lattice point defects and their crystallochemical equilibria. This model formed a basis for "crystal defect chemistry" in 1950s which was a theoretical support for the development of the first semiconductors.

In 1940s, Darken and Gurry [10, 11] devoted a systematic attention to nonstoichiometry which resulted in their excellent study on equilibria in Fe–O system, including experimental methods (e.g., method of controlled atmosphere) for investigation of equilibria between condensed systems and their gaseous surroundings. Nonstoichiometry has been also reported for actinide oxides used in the first nuclear power plants, for magnetic ferrites, solid electrolytes, high T_C superconducting cuprates, metallic hydrides, etc.

Inorganic materials exhibiting various degrees of nonstoichiometry are currently being employed in a multitude of technical applications such as structural materials, refractories, energy conversion, functional parts in electronics and optoelectronics, protective coatings, heterogeneous catalysis, and many others [12–16]. In the vast majority of these applications, the material properties and phase stability play a crucial role by directly determining the primary functionality of a given material

and by limitations posed on the conditions under which it can be safely and effectively operated.

Material properties can be dramatically affected by the presence of defects and disorder, and in many instances a controlled introduction of defects is a key to tailoring the resulting material characteristics. Compared to other materials such as metals or polymers, a particular feature of many inorganic materials such as oxides, nitrides, hydrides, and others is the variable stoichiometry of some components originating from their exchange with surrounding atmosphere and imposing formation of two kinds of defects: the primary defects establishing the departure from stoichiometry (vacancies, interstitials), and compensating defects providing the charge balance (mixed valency, charge polarons). From the thermodynamic point of view, such systems are classified as partly open systems, since the content of shared components in the condensed system is not stable and can be in principle controlled by the state of surrounding atmosphere.

In this chapter, we intend to focus on fundamental thermodynamic properties of nonstoichiometric phases, addressing particularly the general thermodynamic description of systems with variable content of components shared with a dynamical atmosphere, essential material quantities being influenced by variable stoichiometry conditions for homogeneous crystallochemical equilibria as well as for phase transitions.

8.2 Composition of Nonstoichiometric Phases

Nonstoichiometric condensed phases consists of conservative (fixed) components, whose contents (amounts) are invariable with respect to the equilibrium with gaseous atmosphere and of free (volatile) components whose content depends on the composition of the controlled atmosphere and should correspond to an equilibrium with this atmosphere.

Let us consider a binary nonstoichiometric phase with a single conservative component (index *c*) and another free component (index *f*). It is favorable to express the composition of such phase using *quasimolar* (*molal*) *fraction* of free component Y_f derived from *molar fractions* X_c or *molar amounts* N_c and N_f by the relation:

$$Y_f = N_f/N_c = X_f/X_c = X_f/(1 - X_f). \tag{8.1}$$

Moreover, the *quasimolar fraction of free component* Y_f can be written in terms of nonstoichiometry quotients γ or Δ reflecting the deviation from stoichiometry for a nonstoichiometric phase given by the formula $A_mX_{n+\gamma}$ or $A_{m-\Delta}X_n$:

$$Y_f = (n+\gamma)/m = n/(m-\Delta) \tag{8.2}$$

where $\gamma = n\Delta/(m - \Delta)$ and $\Delta = m\gamma/(n + \gamma)$. It is favorable to transform all composition variants of a given phase into a reference formula $AX_{n/m+\delta}$, where $AX_{n/m}$

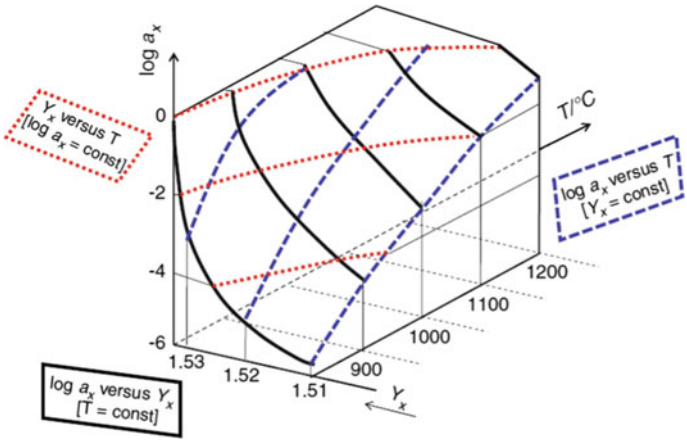

Fig. 8.1 Free component content $Y_f = (n + \gamma)/m$ as a function of free component activity a_f and temperature T within the homogeneity field of a nonstoichiometric phase $A_mX_{n+\gamma}$ (with free component X)

expresses the chemical formula of a strictly stoichiometric phase (so-called daltonian composition point), and $\delta = \gamma/m = Y_f - n/m = n\Delta/m/(m - \Delta)$ expresses a deviation from the strict stoichiometry.

The equilibrium content of free component Y_f in a condensed phase depends on temperature T, pressure P, and activity of free component a_f adjusted by the composition of controlled atmosphere $Y_f = f(T, P, a_f)$, eventually $Y_f = f(1/T, P, \log a_f)$ so that we can display equilibrium deviation from stoichiometry δ as a surface in the space with coordinates T, P, a_f or $1/T$, p, $\log a_f$. An isobaric section of such dependence (Y_f, T, $\log a_f$) is shown in Fig. 8.1.

The functional dependences for Y_f (and similarly for δ) can be defined as:

$$Y_f = f\left(T, P, \log a_f\right) \rightarrow \mathrm{d}Y_f = \left(\partial Y_f/\partial T\right)_{P,af}\,\mathrm{d}T + \left(\partial Y_f/\partial P\right)_{T,af}\,\mathrm{d}P + \left(\partial Y_f/\partial \log a_f\right)_{P,T}\,\mathrm{d}\log a_f \tag{8.3}$$

where the partial derivatives represent additional material properties of a nonstoichiometric phase referred to as

thermal plutability ($\pi\lambda o\acute{\upsilon}\tau o\varsigma$ = rich):

$$\kappa_{fT} = \left(\partial Y_f/\partial T\right)_{P,af} \tag{8.4}$$

pressure plutability:

$$\kappa_{fP} = \left(\partial Y_f/\partial P\right)_{T,af} \tag{8.5}$$

proper plutability:

$$\kappa_{ff} = (\partial Y_f / \partial \log a_f)_{P,T} \tag{8.6}$$

In the case of ternary or other multicomponent phases with more conservative and free components, the invariant composition (independent on the reached equilibrium with gaseous phase) is always given by *quasimolar fractions* of conservative components Y_{ci} so that the substance with chemical formula $A_aB_bC_cF_fG_g$ where A, B, and C are the conservative and F, G the free components should be expressed as $A_{1-Yb-Yc}B_{Yb}C_{Yc}F_{Yf}G_{Yg}$, where quasimolar fractions Y_i are derived from the molar fractions X_I using

$$\begin{aligned} Y_b &= X_B/(X_A + X_B + X_C) = X_B/(1 - X_F - X_G); \\ Y_c &= X_C/(X_A + X_B + X_C) = X_B/(1 - X_F - X_G) \end{aligned} \tag{8.7}$$

$$\begin{aligned} Y_f &= X_F/(X_A + X_B + X_C) = X_F/(1 - X_F - X_G); \\ Y_g &= X_G/(X_A + X_B + X_C) = X_G/(1 - X_F - X_G) \end{aligned} \tag{8.8}$$

From a thermodynamic viewpoint, a system sharing one or several components with its surroundings cannot be classified as a closed system but as a partly open system.

8.3 Equilibrium Crystallochemical Composition

For a given set of adjustable quantities (predictors), T, P, Y_c, and a_f, the equilibrium quasimolar fraction Y_f or the deviation from stoichiometry δ can be found by minimizing the free energy of the nonstoichiometric phase with respect to Y_f or δ. For partly open systems with free component activities a_f acting as predictors, it is expedient to use a thermodynamic potential Z denoted as *hyper-free energy* [17] and derived from the Gibbs free energy G by Legendre transformation with respect to free component content n_f.

$$Z = G - n_f \frac{\mathrm{d}G}{\mathrm{d}n_f} = G - n_f \mu_f = n_f \left(\mu_f^\circ + RT \ln a_f \right) \tag{8.9}$$

where $\mu_f^\circ = G_f^\circ$ is the standard Gibbs energy of free component in gaseous state. The activity a_f can be optionally replaced by relative partial pressures p_f in case of ideal gas behavior.

As mentioned, the variable stoichiometry of free components is related to primary and compensating crystal defects representing crystallochemical species. Based on the knowledge of crystal structure including occupancies of different crystallographic sites

by atoms with specific valencies, a thermodynamic crystallochemical model of a given phase can be constructed. The Gibbs energy in Eq. (8.9) can be expressed as a sum

$$G = \sum_j n_j \mu_j = -\sum_j n_j \left(\mu_j^\circ + RT \ln a_j \right) \tag{8.10}$$

over all species j with chemical potentials μ_j, standard potentials μ_j°, referring to a complete occupation of a given sublattice by j, and activities a_j that can be substituted by site occupancies u_j in case of ideal behavior or by $u_j \gamma_j$ (γ_j standing for activity coefficient). Applying balances of mass (chemical elements), charge, and crystallographic sites, the mole amounts of the individual species can be expressed in terms of equilibrium conversion degrees λ_r of R independent crystallochemical reactions and integer coefficients v_j°, v_{jr} and v_{jf} resulting from balance equations:

$$n_j = v_j^\circ + \sum_r^R v_{jr} \lambda_r + v_{jf} \delta \tag{8.11}$$

where the last term represents the particular reaction associated with the deviation from stoichiometry δ. Substituting Eq. (8.11) into (8.10) and minimizing the Gibbs energy with respect to λ_r yields R equations in a form of mass action law for the homogeneous equilibria with the corresponding equilibrium constants K_r and standard Gibbs energy changes ΔG_r°:

$$\left(\frac{\partial G}{\partial \lambda_r} \right)_{\delta, \lambda_s} = \sum_j v_{jr} \mu_j^\circ + RT \sum_j v_{jr} \ln a_j \equiv \Delta G_r^\circ + RT \ln K_r = 0 \tag{8.12}$$

Similarly, minimizing the hyper-free energy (Eq. 8.9) with respect to nonstoichiometry coefficient δ, we derive the last equilibrium condition describing the equilibrium with the surrounding atmosphere:

$$\left(\frac{\partial Z}{\partial \delta} \right) = \Delta G_{If}^\circ + RT \ln K_f + \sum_r \kappa_{r\delta} \left(\Delta G_r^\circ + RT \ln K_r \right) = 0 \tag{8.13}$$

where ΔG_{If}° and K_f are, respectively, the standard Gibbs energy change and equilibrium constant for a selected (dominating) free component incorporation reaction (involving G_f° and a_f), and $\kappa_{r\delta} = (\partial \lambda_r / \partial \delta)$ are so-called interconnectivity coefficients relating the intrinsic defect contents with the overall free component nonstoichiometry. Solving Eqs. (8.12) and (8.13) simultaneously for a given T and a_f, we obtain the equilibrium value δ_{eq} as well as the distribution of the individual crystallochemical species (intrinsic defects).

Let us show the oxygen-deficient perovskite $SrMnO_{3-\delta}$ as an example [18]. The structure is depicted in Fig. 8.2, including the unit cell which involves 5 formula units as well as the oxygen sites where the vacancies are predominantly formed.

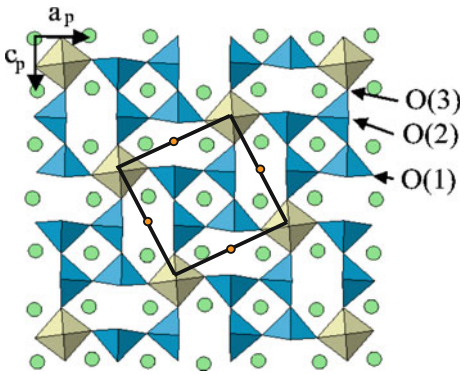

Fig. 8.2 Structure of the oxygen-deficient perovskite $SrMnO_{3-\delta}$. *Orange circles*—sites of predominant vacancy formation (q)

This would correspond to a point defect model $[Sr_5]\ [Mn^{4+}_{5-4q}]\ [O_{13}]\ [O_{2-2q}(Va\ Mn^{3+}_2)_{2q}]$ in which each oxygen vacancy is bound to two compensating Mn^{3+} ions. Such model would allow for a maximum oxygen nonstoichiometry $\delta = 0.4$; however, the real oxygen deficit was found even higher. A more general model describing this situation corresponds to a formula $[Sr_5]\ [Mn^{4+}_{5-4q}]\ [O_{12}]\ [O_{2-2q}(Va\ Mn^{3+}_2)_{2q}]\ [O_{1-r}(Va\ Mn^{3+}_2)_r]$ with two different vacancy sites (the other one at the vertices of complete octahedra). The respective vacancy concentration fractions q and r are related to the overall nonstoichiometry by mass balance equation, $\delta = (2q + r)/5$. The remaining two equations are derived by minimizing Z with respect to δ and r yielding two homogeneous equilibrium conditions:

$$\begin{aligned}\left(\frac{\partial Z}{\partial r}\right) &= \Delta\mu^{\circ}_{rq} + RT\ \ln\frac{r(2-5\delta+r)}{(1-r)(5\delta-r)} = 0\\ \left(\frac{\partial Z}{\partial \delta}\right) &= \Delta\mu^{\circ}_{q} - \frac{1}{2}G^{\circ}_{Of} + T\ \ln\frac{(2-5\delta+r)}{(5\delta-r)p^{\frac{1}{2}}_{O2}} = 0\end{aligned} \tag{8.14}$$

where the first one (equivalent to Eq. (8.12)) corresponds to vacancy–oxygen exchange reaction between the two sites ($\Delta\mu^{\circ}_{rq}$ = 59 kJ mol^{-1} is the difference in oxygen chemical potentials), while the second one (equivalent to Eq. (8.13)) represents the equilibrium for oxygen incorporation reaction into the first oxygen site $2Mn^{3+}\ \ Va + 0.5O_2(g) \rightarrow 2Mn^{4+} + O^{2-}$ with $\Delta\mu^{\circ}_{q} = -97.2 + 0.0643T$ kJ mol^{-1}. Both parameters, $\Delta\mu^{\circ}_{rq}$ and $\Delta\mu^{\circ}_{q}$, were optimized in order to reproduce the structure refinement from neutron diffraction data.

Fig. 8.3 shows the calculated distribution of vacancies r and q on two oxygen sublattices and the variation in macroscopic oxygen nonstoichiometry parameter δ with temperature and partial pressure of oxygen in the surrounding atmosphere. Note that the population of vacancies on the second, energetically less favorable sublattice, increases with rising temperature while at lower temperatures $q \approx \delta$ and $r \approx 0$ up to $\delta = 0.4$.

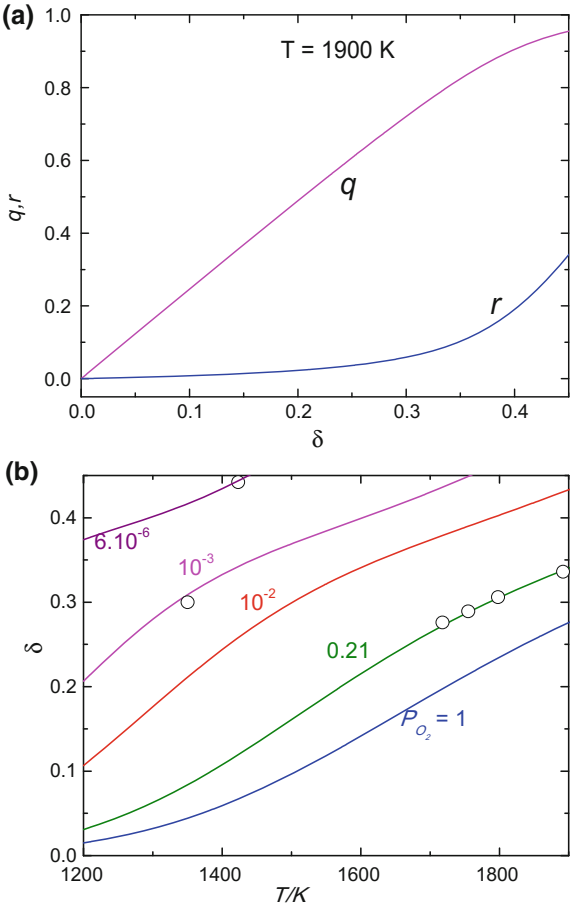

Fig. 8.3 Oxygen-deficient perovskite $SrMnO_{3-\delta}$: **a** distribution of oxygen vacancies as a function of overall nonstoichiometry δ for T = 1900 K and **b** oxygen deficiency δ as a function of temperature and oxygen partial pressure in the surrounding atmosphere. *Circles* represent the experimental points

8.4 Material Properties

From the thermodynamic point of view, the fundamental material properties are intensive thermodynamic parameters, which are specific for a given material and are related to a second-order differential of a Gibbs free energy. For a single component system, the essential thermodynamic properties are isobaric heat capacity C_p, coefficient of thermal expansion α, and isothermal compressibility β defined, respectively, as

$$C_p = \left(\frac{\partial H}{\partial T}\right)_P = T\left(\frac{\partial S}{\partial T}\right)_P = -T\left(\frac{\partial^2 G}{\partial T^2}\right)_P \tag{8.15}$$

$$\alpha = \frac{1}{V}\left(\frac{\partial V}{\partial T}\right)_P = \frac{1}{V}\left(\frac{\partial^2 G}{\partial P \partial T}\right) \tag{8.16}$$

$$\beta = -\frac{1}{V}\left(\frac{\partial V}{\partial P}\right)_T = -\frac{1}{V}\left(\frac{\partial^2 G}{\partial P^2}\right)_T \tag{8.17}$$

where of the isobaric heat capacity C_p is related to isochoric heat capacity C_V (usually described within harmonic crystal approximation) by an additive term $\Delta_{dil}C$, involving both the thermal expansion and the isothermal compressibility.

$$C_p = C_V + \Delta_{dil}C = C_V + \frac{V\alpha^2}{\beta}T \tag{8.18}$$

All these properties are defined for materials with a fixed composition (isoplethal conditions of a closed system) invariant of the state of surrounding atmosphere. However, it has been shown recently [19, 20] that heat capacity, thermal expansion, and compressibility can be also redefined for isodynamical conditions (conditions of partly open systems). In case of nonstoichiometric phases, it was pointed out [20, 21] that the heat capacity $C_{p,af}$ measured at constant pressure and isodynamical conditions (under controlled atmosphere with a fixed activity of free component, a_f) differs from that defined for standard isoplethal conditions, $C_{p,Yf}$ by an additive term $\Delta_{sat}C_p$ denoted as saturation contribution

$$\Delta_{sat}C_p = C_{p,a_f} - C_{p,Y_f} = \overline{H}_f \kappa_{fT} = \left(H_f^0 + \Delta\overline{H}_f\right)\kappa_{fT} \tag{8.19}$$

where $\overline{H}_f$ is the partial molar enthalpy of free component. The relative partial molar enthalpy $\Delta\overline{H}_f$ referred to the standard state of gaseous-free component that can be derived from a crystallochemical thermodynamic model calculating the equilibrium of crystallochemical species in the crystal lattice of a nonstoichiometric phase [21]. $\Delta\overline{H}_f$ can vary substantially upon changing the mechanism of free component incorporation within a given crystallochemical model; however, it can be assessed experimentally by taking use of its relation to thermal and proper plutability

$$\Delta\overline{H}_f = -RT^2\left(\partial \ln a_f/\partial T\right)_{P,Y_f} = (\ln 10)RT^2\left(\kappa_{fT}/\kappa_{ff}\right) \tag{8.20}$$

To calculate the value of isoplethal heat capacity C_p corresponding to nonstoichiometry Y_f from a value valid for another nonstoichiometry Y_f° (the difference being expressed as $\delta \equiv Y_f - Y_f^\circ$), the correction called *deviation contribution* has to be applied.

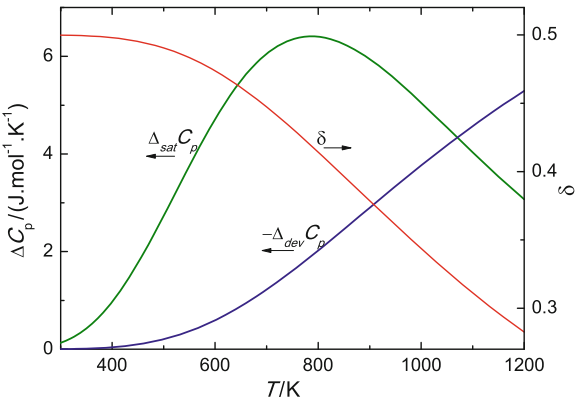

Fig. 8.4 $Bi_2Sr_2CoO_{6+\delta}$: oxygen nonstoichiometry δ measured by TGA in air atmosphere, saturation contribution $\Delta_{sat}C_p$ to isodynamical heat capacity and the difference in isoplethal heat capacity $\Delta_{dev}C_p = C_{p,\delta} - C_{p,\delta=0}$

$$\Delta_{dev}C_p = \delta C^0_{p,f} + \int_0^{\delta} \left(\partial \Delta \overline{H}_f(\delta, T)/\partial T\right)_P \mathrm{d}\delta \tag{8.21}$$

To demonstrate the effect of variable oxygen stoichiometry on heat capacity measured at isodynamical conditions, we refer to cobalt analogue of superconducting cuprate, $Bi_2Sr_2CoO_{6+\delta}$. As seen from Fig. 8.4, this phase exhibits an oxygen excess δ with respect to purely stoichiometric form, $Bi_2Sr_2CoO_6$, ranging from 0 to 0.5 [22]. Assuming a simple crystallochemical model with a single partly occupied oxygen site per unit cell comprising two formula units and, as in the model of $SrMnO_{3-\delta}$ discussed above, the Co^{2+} ions bound to oxygen vacancies, we can use the resulting equilibrium condition

$$\Delta \overline{H}_O - T\Delta \overline{S}_O + RT \ln \frac{\delta}{(2-\delta)p_{O2}^{1/2}} = 0 \tag{8.22}$$

to evaluate the relative partial molar enthalpy $\Delta\overline{H}_O$ and entropy $\Delta\overline{S}_O$ by fitting the thermogravimetry $\delta(T)$ data and to calculate the saturation contribution $\Delta_{sat}C_p$ to isodynamical heat capacity as well as the correction term $\Delta_{dev}C_p$ for recalculation of isoplethal heat capacity from actual nonstoichiometry δ to stoichiometric end-members $Bi_2Sr_2CoO_6$ or $Bi_2Sr_2CoO_{6.5}$.

Similarly to heat capacity, the coefficients of thermal expansion α and compressibility β_T of a nonstoichiometric phase are affected by the content of volatile component [20]. In a controlled atmosphere with a given activity of shared component, the coefficient of thermal expansion differs from that obtained at constant composition, and the same applies to isothermal compressibility.

For the difference between isodynamical and isoplethal thermal expansions, we find, in analogy to Eq. (8.19),

$$\Delta_{sat}\alpha = \alpha_{a_f} - \alpha_{Y_f} = (1/V)\overline{V}_f\kappa_{fT} = (1/V)\left(V_f^0 + \Delta\overline{V}_f\right)\kappa_{fT} \tag{8.23}$$

where $\overline{V}_f$ is the partial molar volume of the volatile component f which can be expressed as a sum of the molar volume of pure component f (in its standard state) and the relative partial molar volume $\Delta\overline{V}_f$.

Likewise the difference between isodynamical and isoplethal compressibility reads:

$$\Delta_{sat}\beta = \beta_{a_f} - \beta_{Y_f} = -(1/V)\overline{V}_f\kappa_{fP} = -(1/V)\left(V_f^0 + \Delta\overline{V}_f\right)\kappa_{fP} \tag{8.24}$$

In analogy to $\Delta\overline{H}_f$, Eq. (8.20), the relative partial molar volume $\Delta\overline{V}_f$ is an experimentally accessible quantity as seen from its relation to pressure and proper plutability:

$$\Delta\overline{V}_f = RT\left(\partial \ln a_f/\partial P\right)_{T,Y_f} = -(\ln 10)\,RT\left(\kappa_{fP}/\kappa_{ff}\right) \tag{8.25}$$

Moreover, comparing (8.20) and (8.25), we find a relation between $\Delta\overline{H}_f$ and $\Delta\overline{V}_f$,

$$\left(\kappa_{fT}/\kappa_{fP}\right) = \left(\partial P/\partial T\right)_{a_f,Y_f} = -\left(\Delta\overline{H}_f/T\Delta\overline{V}_f\right) \tag{8.26}$$

which is analogous to Clapeyron equation, since it describes the slope of temperature versus pressure dependence which must be kept constant at a given activity a_f in order to maintain a given free component content Y_f in the condensed phase at constant value. Equation (8.25) can be also used to calculate the pressure plutability κ_{fP} (which might not be readily accessible from experiment) from the known values of thermal plutability and relative partial molar volume and enthalpy.

As in the case of deviation contribution to C_p, Eq. (8.21), the difference in thermal expansion coefficient α and isothermal compressibility β brought about by the difference $\delta = Y_f - Y_f^\circ$ can be, respectively, written as:

$$\Delta_{dev}\alpha = \delta\alpha_f^0 + (1/V)\int_0^\delta \left(\partial\Delta\overline{V}_f(\delta,T)/\partial T\right)_P \mathrm{d}\delta \tag{8.27}$$

$$\Delta_{dev}\beta = \delta\beta_f^0 + (1/V)\int_0^\delta \left(\partial\Delta\overline{V}_f(\delta,T)/\partial p\right)_T \mathrm{d}\delta \tag{8.28}$$

with $\alpha_f^0 = \left(\partial \ln V_f^0/\partial T\right)_P$ and $\beta_f^0 = -\left(\partial \ln V_f^0/\partial P\right)_T$ standing for the thermal expansion and compressibility of pure free component f in its standard state.

8.5 Phase Transitions

The phase relations in partly open systems can be conveniently visualized in basic representation involving the intensive quantities (T, P, μ_f, or a_f) as predictors, while the stoichiometry of conservative components is either uniquely given (single conservative component) or kept fixed. In the former case, the dimensionality D of the coexistence field of P phases in C component system is determined by Gibbs phase rule

$$D = C - P + 2 - I \tag{8.29}$$

where I means the number of fixed predictors, lowering the total dimension $C + 1$ of the phase diagram.

As seen from the example of Co–O system shown in Fig. 8.5, the T–log p_f phase diagram (Fig. 8.5a) of a binary system with one free and one stable component resembles the T–P diagrams of unary systems, including the occurrence of triple points and a critical point. The phase relations can be also visualized in T–X_O phase diagram; however, since the content of free component is not an adjustable quantity, the heating in dynamical atmosphere follows the isoactivity lines as shown in Fig. 8.2b with the abrupt changes of free component content on phase transitions. By contrast, the phase transitions in the basic representation correspond to lines constituting the boundaries between the respective phase fields. The boundary lines, $T = f(p_{O2})$, can be determined from the condition of equality of hyper-free energies at the point of phase transition, $\Delta Z = 0$. For nonstoichiometric phases, additional conditions for equilibrium content of free component δ_{eq} (Eq. (8.13)) have to be included into the set of equations to be solved. To extrapolate the boundary line from a single calculated point, the second Clapeyron equation (see the previous chapter, Eq. (8.19))

$$\left(\frac{\mathrm{d}\ \ln a_f}{\mathrm{d}(1/T)}\right)_P = \frac{\Delta_d H_q}{R\Delta Y_f} \tag{8.30}$$

can be conveniently used. For systems with two or more free components, the potential phase diagrams (activity versus activity or Kellogg diagrams) are useful for the graphical representation of phase equilibria at fixed temperature, pressure and content of conservative components. For their construction, the fifth Clapeyron equation (see the previous chapter, Eq. (7.23))

$$\left(\frac{\mathrm{d}\ \ln a_f}{\mathrm{d}\ \ln\ a_g}\right)_P = -\frac{\Delta Y_g}{\Delta Y_f} \tag{8.31}$$

can be applied. Fig. 8.6 shows the log p_{Hg}–log p_{O2} potential phase diagram involving the superconducting cuprate, $Hg_{0.9}Ba_2CuO_5$, that can be reproducibly synthesized only under a simultaneous control of p_{Hg} and p_{O2} [23].

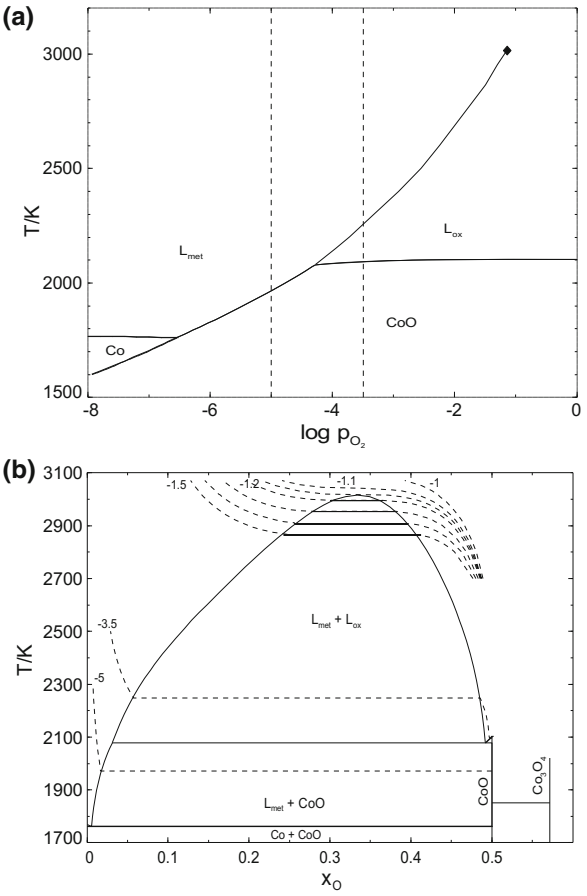

Fig. 8.5 **a** T versus log p_{O2} phase diagram of Co–O system with one stable (Co) and one shared (O) component and **b** the corresponding T versus X_O phase diagram with isoactivity lines (*dashed*)

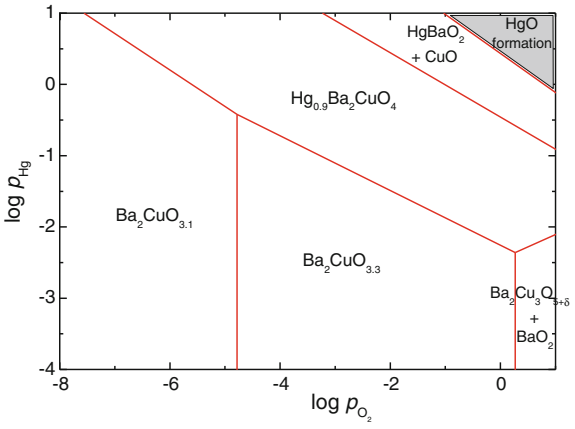

Fig. 8.6 Potential (Kellogg) phase diagram of Hg–Ba–Cu–O system for fixed ratio Ba: Cu = 2:1, T = 700 K

The crossover through a miscibility gap between the metal and oxide melt shown in Fig. 8.5b represents a particular case of phase transition. Since Eq. (8.13) has two solutions, their difference determines the amount of free component release or uptake at the transition point. As the isoactivity lines approach the critical point, this difference tends to zero and the whole process changes its character from sharp transition to a gradual variation in the essential quantities which can be regarded as a result of homogeneous equilibrium within a single phase. For log $p_{O2} = -1.15$, the isoactivity line passes through the critical point, the temperature dependences of oxygen content (Fig. 8.7a), and enthalpy becomes continuous and their temperature derivatives, κ_{fT} and C_p, diverge to infinity (Fig. 8.7b). If we have more than one stable component, their composition replaces the respective chemical potential in the set of predictors, and we need to use an extended representation for displaying the phase relations. For a system with S stable components, we need $R = S - 1$ such replacements. In such case, the corresponding phase field has the dimension:

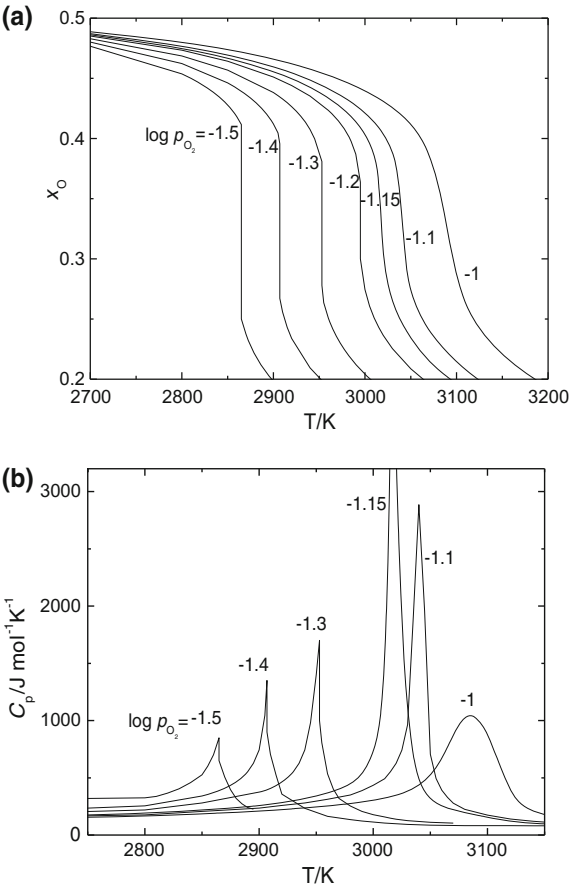

Fig. 8.7 **a** Variation in oxygen stoichiometry and **b** heat capacity of CoO_x melt

$$D = C - P + 2 - I + R$$
$$\text{and} \tag{8.32}$$
$$D = C + 1 - I$$

for $P > R$ and $P \leq R$, respectively.

Nevertheless, if we fix the composition of all stable components, then the phase relations can be still displayed in the T–log a_f–(log a_g) coordinate system, and the resulting phase diagrams retain the essential topological features of the T–log a_f diagrams of binary systems [24]. In fact the Kellogg diagram in Fig. 8.6 belongs to this category, since $R = 1$, but I is increased by one due to fixing the Ba:Cu ratio. As a consequence of Eq. (8.32), the two-dimensional phase fields are represented by a single-phase or two-phase assemblies. If all involved phases are stoichiometric with respect to stable components, the phase transitions are sharp and we can apply the same equilibrium conditions as in the previous case ($\Delta Z = 0$ and Eq. (8.13)).

By contrast, if there are some solution phases with respect to stable components in the system, then the phase field boundaries and the respective phase transitions are either sharp or gradual (the reader is referred to the classification given in the previous chapter). In the latter case, the amount of one phase gradually decreases when approaching the phase boundary and reaches zero at the borderline (partial transition). In the example of Ca–Co–O system [25] presented in Fig. 8.8a, it is the lower lying borderline between the solution phase $Ca_3Co_{3.9+x}O_{9.2}$ and the two-phase region of this phase and $Ca_3Co_2O_6$ whose content is vanishing when crossing the boundary. Let us note that the phase equilibria in such three-component system can be also represented in a quasibinary phase diagram as shown in Fig. 8.8b which exhibits exactly the same topological characteristics as conventional binary phase diagrams of closed systems. Also the equilibrium conditions that can be used for mapping the phase boundaries are quite analogous except for the Gibbs free energy being replaced by hyper-free energy. For instance, the composition of a solution phase Y_{sol} coexisting with a stoichiometric phase of composition Y_{st} can be found by minimizing the thermodynamic potential with respect to Y_{sol}, yielding well-known relation:

$$\frac{\mathrm{d}Z_{sol}}{\mathrm{d}Y_{sol}} = \frac{Z_{sol} - Z_{st}}{Y_{sol} - Y_{st}} \tag{8.33}$$

which is to be solved (combined with homogeneous equilibrium conditions) for a given T and a_f to find the unknown Y_{sol} in the quasibinary phase diagram T–Y_c (a_f = const.). To determine the transition point in the corresponding T–log a_f (Y_c = const.) phase diagram, we solve the same Eq. (8.33) for selected Y_c and a_f and unknown T. Since the variation in enthalpy and free component content is continuous but not a smooth function at the onset of gradual transition, Eq. (8.30) cannot be applied for the calculation of such borderline. However, the Ehrenfest equations:

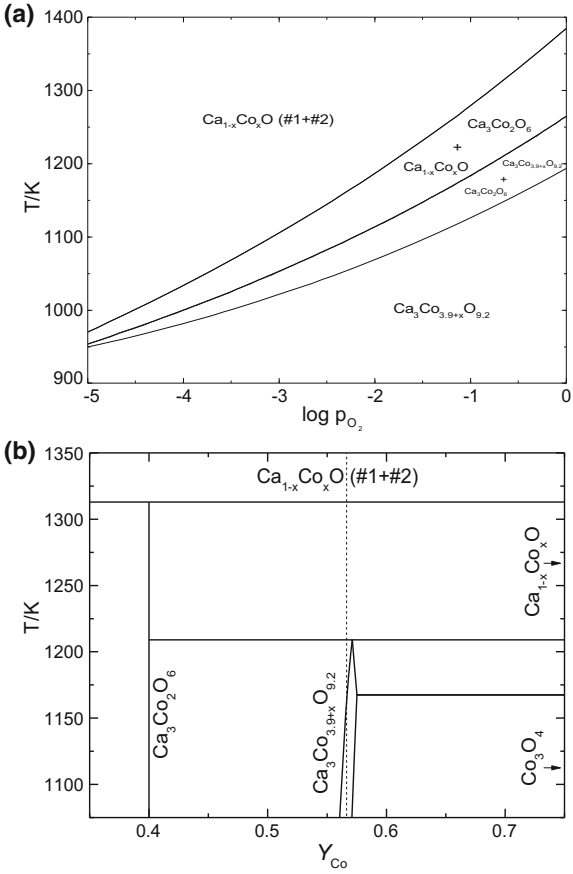

Fig. 8.8 **a** T versus log p_{O2} phase diagram of Ca–Co–O system for Ca:Co = 3:3.9 and **b** T versus Y_{Co} isoactivity section (p_{O2} = 0.21) of Ca–Co–O phase diagram (*dashed line* isoplethal section shown in (**a**))

$$\left(\frac{\mathrm{d}\ \ln a_f}{\mathrm{d}(1/T_t)}\right)_P = \frac{\Delta_t C_p}{R\Delta_t \kappa_{fT}} \quad \text{or} \quad \left(\frac{\mathrm{d}\ \ln a_f}{\mathrm{d}(1/T_t)}\right)_P = T_t^2 \frac{\Delta\kappa_{fT}}{\Delta\kappa_{ff}} \tag{8.34}$$

as derived in the previous chapter (Eqs. (7.28) and (7.30)) are suitable for this purpose.

The sharp transitions involving solution phases such as $Ca_3Co_{3.9+x}O_{9.2} \rightarrow Ca_3Co_2O_6 + Ca_{1-x}Co_xO$ and $Ca_3Co_2O_6 \rightarrow Ca_{1-x}Co_xO$ (#1 + #2) (miscibility gap for rock salt solid solution $Ca_{1-x}Co_xO$) are invariant toward Y_c, and the same approach can be thus applied to identify a given transition point on the isoplethal and isoactivity sections of the T–Y_c–a_f phase diagram. A simultaneous solution of two independent equations (e.g., Eq. (8.33) and $\Delta Z = 0$), alternatively combined with Eq. (8.13), is necessary in this case.

Acknowledgements P. Holba acknowledges the support of Ministry of Education of the Czech Republic in the framework of CENTEM PLUS project (LO1402) operated under the "National Sustainability Programme I."

References

1. Hoitsema C (1895) Palladium und Wasserstoff. Z Phys Chem 17:1–42
2. Wald F (1897) Elementare chemische Betrachtungen. Z Phys Chem 24:633–650
3. Wald F (1899) Was ist ein chemisches Individuum. Z Phys Chem 28:13–16
4. Holba P (2015) Termodynamický popis tepelných kapacit v nestechiometrických fázích (In Czech). Chemické Listy 109:113–116
5. Šesták J, Holba P, Gavrichev K (2014) Reinstatement of thermal analysis tradition in Russia and related East European interactions. J Therm Anal Cal 119:779–784
6. Kurnakov NS (1914) Compound and chemical individuum. Bull Acad Imp Sci de St Pétersbourhg 321–328
7. Chaudron G (1921) Reversible reactions of hydrogen and carbon monoxide on metallic oxides. Ann Chem 16:221–281
8. Schenck R, Dingmann T (1927) Gleichgewichtsuntersuchungen bei der Reduktions, Oxydations und Kohlungsvorgänge beim Eisen III. Z Anorg Chem 166:113–154
9. Schottky W, Wagner C (1930) Theorie der geordneten Mischphasen. Z Phys Chem (Leipzig) B 11:163–220
10. Darken LS, Gurry RW (1945) The system iron–oxygen. I. The Wüstite field and related equilibria. J Am Chem Soc 67:1398–1412
11. Darken LS, Gurry RW (1946) The system iron–oxygen. II. Equilibrium and thermodynamics of liquid oxide and other phases. J Am Chem Soc 68:798–816
12. Aricò AS, Bruce P, Scrosati B, Tarascon J-M, Van Schalkwijk W (2005) Nanostructured materials for advanced energy conversion and storage devices. Nat Mater 4:366–377
13. O'regan B, Grätze M (1991) A low-cost, high-efficiency solar cell based on dye-sensitized colloidal TiO_2 films. Nature 353:737–740
14. Ohta H, Hosono H (2004) Transparent oxide optoelectronics. Mater Today 7(6):42–51
15. Keller F, Hunter M, Robinson D (1953) Structural features of oxide coatings on aluminum. J Electrochem Soc 100:411–419
16. Weckhuysen BM, Keller DE (2003) Chemistry, spectroscopy and the role of supported vanadium oxides in heterogeneous catalysis. Catal Today 78:25–46
17. Holba P (1992) Thermodynamics of partially open systems. Czech J Phys B 42:549–575
18. Sedmidubský D, Strejc A, Nevřiva M, Leitner J, Martin C (2003) Structural and phase relations in the Sr–Mn–O system. Solid State Phenom 90–91:427–432
19. Holba P, Sedmidubský D (2013) Heat capacity equations for nonstoichiometric solids. J Therm Anal Calorim 113:239–245
20. Sedmidubský D, Holba P (2015) Material properties of nonstoichiometric solids. J Therm Anal Calorim 1120:183–188
21. Holba P, Sedmidubský D (2013) Crystal defects and nonstoichiometry contributions to heat capacity of solids, Chapter 3 in book: thermal analysis of micro- nano- and non-crystalline materials: transformation, crystallization, kinetics and thermodynamics. In: Šesták J, Šimon P (eds) Springer, pp 53–74
22. Jankovský O, Sedmidubský D, Sofer Z, Rubešová K, Růžička K, Svoboda P (2014) Oxygen non-stoichiometry and thermodynamic properties of $Bi_2Sr_2CoO_{6+\delta}$ ceramics. J Eur Ceram Soc 34:1219–1225
23. Sedmidubský D, Leitner J, Knížek K, Strejc A, Veverka M (2000) Phase equilibria in Hg–Ba–Cu–O systém. Phys C 329:191–197

24. Voňka P, Leitner J, Sedmidubský D (2008) Topology of potential phase diagrams of partially open condensed systems. Collect Czech Chem Commun 73(3):372–387
25. Sedmidubský D, Jakeš V, Jankovský O, Leitner J, Sofer Z, Hejtmánek J (2012) Phase equilibria in Ca–Co–O system. J Sol St Chem 194:199–205

Chapter 9
How Do Crystals Nucleate and Grow: Ostwald's Rule of Stages and Beyond

Jürn W.P. Schmelzer and Alexander S. Abyzov

Abstract W. Ostwald predicted with the "rule of stages" formulated by him that phase formation processes in complex condensed matter systems may proceed step by step via different evolution paths involving a discrete series of metastable states, which can be formed in a macroscopic form at the given thermodynamic conditions, until finally, the most stable phase will be reached. Advancing this idea, it was shown in recent years by us that in condensation and boiling, as well as in segregation and crystallization processes in multi-component liquid and solid solutions, critical clusters may be formed and evolve via a continuous sequence of states with properties which may differ from the properties of any of the macroscopic phases present in the respective phase diagram. The kinetics of nucleation proceeds hereby via a scenario similar to spinodal decomposition, i.e., via a continuous amplification of density and/or composition differences accompanied eventually by sequential discrete changes of the structure of the system. The basic ideas and results of this theoretical approach developed by us are described in the present chapter. Recently published experimental results on crystal nucleation are discussed in detail giving additional confirmation of these conclusions. As a second man topic devoted also to the theoretical description of crystal nucleation, the relevance of the concepts of fragility of the liquid for the understanding of crystal nucleation and growth in glass-forming liquids is explored. Finally, a number of directions of research are discussed which may lead to new insights into the complex phenomena of crystal formation and growth processes.

J.W.P. Schmelzer (✉)
Institute of Physics, University of Rostock, 18051 Rostock, Germany
e-mail: juern-w.schmelzer@uni-rostock.de

A.S. Abyzov
National Scientific Centre, Kharkov Institute of Physics and Technology,
61108 Kharkov, Ukraine

J. Šesták et al. (eds.), *Thermal Physics and Thermal Analysis*,
Hot Topics in Thermal Analysis and Calorimetry 11,
DOI 10.1007/978-3-319-45899-1_9

9.1 Introduction

The properties of materials are significantly affected by the volume fraction, shape, size distribution, orientation, and degree of dispersion of the different phases formed during their fabrication. Crystallization is particularly important in glass technology, where, in addition to the aforementioned features, the rates of crystal nucleation and growth of the glass-forming melts determine whether a given liquid can be vitrified or is likely to crystallize on the cooling path to a glass. By this reason, a detailed knowledge of the laws governing crystal nucleation and growth is of basic relevance.

The theoretical interpretation of crystal nucleation and growth experiments is performed till now in most cases based on the classical thermodynamic theory of heterogeneous systems as developed by Gibbs [1] in the period 1875–78. In the subsequent decades, van der Waals advanced an alternative continuum's approach to the description of heterogeneous systems. In discussing his results, in 1893/94, van der Waals [2, 3] described his work and stated that in its main consequences, his theory is equivalent to Gibbs' approach, however, much wider applicable. In particular, he noted: "*Schon von Gibbs ist eine thermodynamische Theorie der Kapillarität aufgestellt worden. Ein grosser Teil seiner Abhandlung*" *On the equilibrium of heterogeneous substances "ist der Kapillarität gewidmet … In einer Fußnote … bemerkt Gibbs, dass man die Erscheinungen in ganz anderer Weise würde behandeln können. Wirklich haben Umstände … mich dazu geführt, die Theorie der Kapillarität in ganz anderer Weise in Angriff zu nehmen … Dazu kommt noch, dass die Gibbssche Theorie die kapillaren Erscheinungen als von der Voraussetzung der Diskontinuität bedingt betrachtet … Im Gegensatz dazu ist die Methode, welche ich in den folgenden Seiten zu entwickeln wünsche, nur dann anwendbar, falls eine kontinuierliche Dichteänderung angenommen wird*", or, in the English translation, "*A thermodynamic theory of capillarity has already been developed by Gibbs. His paper 'On the equilibrium of heterogeneous substances', is in the main devoted to these phenomena … According to Gibbs' theory, capillarity phenomena are present only if there is a discontinuity between the portions of fluid that are face-to-face … In contrast, the method that I propose to develop … is not a satisfactory treatment unless the density of the body varies continuously at and near its transition layer. It will not be without interest to show that the two apparently contradictory hypotheses lead to values of the same order of magnitude for the capillary tension and energy.*"

In this statement, van der Waals emphasizes as an advantage of his treatment that it is more accurate as compared to Gibbs' approach since it refers more appropriately to the real situation. Similar statements can be found also in the modern literature supposing that Gibbs' theory is not correct since it does not account, as a rule, for the continuous change of density and/or composition in the transient interfacial layer between both considered phases. However, such statement is not correct. Gibbs was, of course, fully aware of the real situation. But he describes heterogeneous systems in terms of a model system consisting of two homogeneous

phases divided by a mathematical surface of zero thickness. All thermodynamic parameters are considered as the sum of the contributions of the two homogeneous phases and appropriate correction terms assigned to the mathematical interface. This approach allows one to employ the well-established laws of thermodynamics for homogeneous equilibrium systems. The main problem is then to compute appropriately the correction terms. So, Gibbs' approach is fundamentally correct, and the only problem remains is to account correctly for the above-mentioned corrections due to the existence of the interface. Provided Gibbs would have really assumed that systems consist of two homogeneous phases, there would not be need to introduce the correction terms, in particular, for the number of particles of the different components. In order to compute mentioned correction terms, Gibbs introduced a fundamental equation for the superficial quantities interconnecting the mentioned superficial thermodynamic parameters. In his approach, Gibbs restricted his considerations to systems in thermodynamic equilibrium. We have developed a different more general approach as compared to the classical Gibbs' method as described in more detail in the chapter allowing one to remove several severe limitations of the classical Gibbs' approach in application to the description of the kinetics of phase formation.

Despite his critical remarks concerning Gibbs' classical theory, van der Waals mentioned that in their consequences—describing the properties of planar interfaces—his and Gibbs' methods lead to similar results. However, as can be shown, in application to nucleation and growth of small clusters, Gibbs' and van der Waals' methods lead to highly different consequences [4, 5]. These differences can be removed as shown by us by generalizing Gibbs' classical method. This generalization accounts also for the need to have a tool to describe clusters which are not in equilibrium with the ambient phase. Such thermodynamic treatment is however essential in order to describe the growth and decay of the clusters. In addition, it is also a prerequisite to appropriately determine the properties of the critical clusters, i.e., of the cluster being in unstable equilibrium with the ambient phase and determining the nucleation rate. The description of the basic ideas of the generalized Gibbs' approach as it is denoted by us and an illustration of its power in application to recent experimental investigations of crystal formation is the first aim of the present chapter.

The second part of the chapter is devoted to another aspect of the theoretical description of crystallization connected with the interplay of glass transition and crystallization-growth processes. It is devoted to the concept of fragility and its relevance to the understanding of crystallization. Based on a detailed analysis of crystallization processes in glass-forming melts, it is demonstrated that classical fragility in the form as introduced by Angell can be relevant for the understanding of the crystallization behavior only if several severe conditions are fulfilled that are rarely met. However, as shown as well, introducing an appropriate modification of the classical definition, fragility becomes one of the main factors determining the temperatures and magnitudes of the maxima of nucleation, growth, and overall crystallization rates. In addition, an analysis is performed specifying the conditions at which classical fragility can be considered as a measure of deviations of the

viscosity from an Arrhenius type of temperature dependence. Finally, a number of directions of research are discussed which may lead to new insights into the well-established but anyway intensively developing field of experimental and theoretical research devoted to crystal formation and growth processes.

9.2 Ostwald's Rule of Stages and Its Generalization

In Ref. [6], the results of sophisticated experiments on the crystallization behavior of metal phosphates are presented. In this transformation, an amorphous material transforms into a stable crystalline phase via a sequence of intermediate crystalline phases. The authors assert—supported by [7]—that these experimental results directly prove the validity of Ostwald's rule of stages formulated by W. Ostwald in the form [8] "*in the course of transformation of an unstable* (*or meta-stable*) *state into a stable one the system does not go directly to the most stable conformation* (*corresponding to the modification with the lowest free energy*) *but prefers to reach intermediate stages* (*corresponding to other possible meta-stable modifications*) *having the closest free energy difference to the initial state.*" In the discussion in [7], it is also noted that a number of problems remain open as follows: (i) Is such type of behavior always to be expected in crystallization in complex systems? (ii) Can there be given a sound theoretical basis for such general principle as Ostwald's rule of stages? (iii) Is a similar behavior also observed for phase formation from the melt? A variety of other questions can be added. A very important additional one is—to our opinion—the following problem.

The classical theory of nucleation and growth assumes—in agreement with the theory of heterogeneous systems developed by Gibbs [1]—that the bulk properties of the critical clusters, the embryos of the newly evolving phases (see Fig. 9.1a), coincide widely with the properties of the respective macroscopic phases. In such a description, clusters of the new phase form and grow by changing its size with nearly size-independent bulk and surface properties. This classical model of phase formation is illustrated in Fig. 9.1a. However, in particular, since the work of Hillert [9], and then Cahn and Hilliard [10] on phase separation processes in solid solutions, employing the same density functional approach as developed earlier by van der Waals [2, 3], it is well-established that the properties of the critical clusters deviate, and as a rule considerably, from the properties of the respective macroscopic phases. So, the question arises why the existence of different metastable or stable macroscopic phases can affect nucleation at all once anyway the properties of the critical clusters differ from the properties of the respective macroscopic phases?

This and a variety of related problems could be resolved generalizing the classical Gibbs' method of description of heterogeneous systems [4, 5]. In this generalization, the classical method of description as developed by Gibbs is basically retained, but it is extended (first new element in the generalization) to clusters being not in equilibrium with the ambient phase (Gibbs restricted his analysis—as evident already from the title of his publications—to "equilibrium of heterogeneous

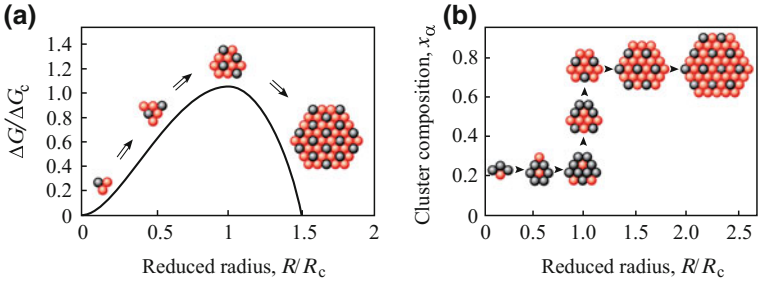

Fig. 9.1 Comparison of the classical model of phase separation in multi-component solutions illustrated in (**a**) with the scenario as developed based on the generalized Gibbs' approach (**b**). According to the classical picture (**a**), clusters evolve by changing its size, R (it is assumed here that the clusters are of spherical shape with a radius, R), retaining nearly the same density, composition, and structure. The critical cluster (specified by the subscript c) corresponds to the maximum of the Gibbs' free energy, ΔG. Clusters with sizes $R > R_c$ are capable to a further deterministic growth representing in this way "embryos" of the newly evolving phase, cluster with a size $R < R_c$ decay. According to the generalized Gibbs' approach (**b**), crystals are formed via amplification of composition differences to the ambient phase supplemented by discrete changes in the structure. Here, the thermodynamic potential barrier in nucleation is overcome mainly via changes of the state of the precursors of the new phase at nearly constant size

substances", exclusively; cf. also [11, 12]). Hereby, it is taken into account (second new element in the generalization) that the specific interfacial energy of the clusters of the new phase has to depend, in general, on the properties of both the clusters and the ambient phase. Based on this more general thermodynamic approach, in the next step, the properties of critical clusters are determined. As it turns out, the respective predictions differ from the predictions of the classical Gibbs' approach, and they are in agreement with the predictions of density functional computations [13].

This method of determination of critical cluster properties was based originally on a postulate we denoted as "***generalized Ostwald's rule of stages***." It reads in the formulation given by us in [4]: "*In phase transformation processes, the structure and properties of the critical nucleus may differ qualitatively from the properties of the evolving macroscopic phases. Those classes of critical clusters determine the process of the transformation, which correspond to a minimum of the work of critical cluster formation* (*as compared with all other possible alternative structures and compositions, which may be formed at the given thermodynamic constraints*)." Some similarity in this approach with the classical explanation of Ostwald's rule of stages in its original form as given by Stranski and Totomanov [14] is evident. However, our approach is more general not restricting the selection rule for the properties of the critical clusters to different stable or metastable phases which can be formed in a macroscopic form at the given thermodynamic constraints but allowing for the occurrence of a much wider spectrum of possible states not realized for macroscopic samples.

As we became aware about a decade after the publication of Ref. [4], similar ideas have been expressed already in 1951 by Scheil [15] and Hobstetter [16] in application to nucleation-growth processes in metal physics, where this approach is denoted as Scheil–Hobstetter model [17]. As it turned out, this suggestion was fully correct. Indeed, Scheil started his paper of 1950 with the observation of Gerlach [18] that in segregation of nickel–gold particles from a solid solution, as a rule, particles are formed which do not have the equilibrium composition. He cited also the observation of Masing [19] in his book on metal physics that such effect—the difference between the composition of the clusters and the composition of the macroscopic phases—is not an exception but the rule in metal physics. Employing, similar to our analysis in Ref. [4], Becker's equation [20] for the description of the interfacial energy in dependence on composition, he came to the conclusion again in full agreement with our approach that the critical cluster composition is, in general, different from the equilibrium composition of macroscopic samples and determined by the condition of the minimum of the work of critical cluster formation; i.e., he had really expressed the same idea as advanced by us 50 years later not being aware then of this earlier work. However, Scheil presumably did not recognize that this approach is in deep conflict to Gibbs' classical theory which leads—if correctly employed—to different results. Consequently, in the analysis of Scheil, the question remains unanswered: How one can employ on one side Gibbs' theory but replace one of its inherent consequences by a different assumption contradicting the conclusions of Gibbs' classical approach? The solution to these problems has been given by us by developing the generalization of Gibbs' approach mentioned above.

By the way, as mentioned by Scheil as well, Becker, developing and employing the relation for the description of the surface tension in dependence on composition, employed in the analysis Gibbs' classical theory; i.e., he identified the composition of the newly evolving critical clusters with the composition of the newly forming macroscopic phase. In addition, Scheil supposed that eventually, the state of the critical cluster may refer to some metastable phase which under certain conditions may be formed macroscopically remaining in this way to some extent at the level of the classical Ostwald's rule of stages (but leaving open also the possibility that such metastable states may not exist). According to our treatment formulated in the generalized Ostwald's rule of stages, the composition of the critical clusters is from the very beginning supposed to refer to transient states (composition, density, structure etc.) having, as the rule, no macroscopic analog.

In contrast to the classical Gibbs' approach, the generalized Gibbs' theory allows one to describe also phase formation processes in solutions proceeding from unstable initial states [21], and the results are in agreement with the predictions of the Cahn–Hilliard theory and more advanced density functional computations. In addition, a variety of experimental data on crystal nucleation of glass-forming melts could be explained straightforwardly, which cannot be interpreted in classical terms. An overview on these results is given in [22, 23], and some others are described below.

In addition to the understanding of crystal nucleation, the process of formation of critical clusters, the generalized Gibbs' approach allows one to determine the most probable whole path of evolution of the clusters in size-composition space [23, 24]. For segregation processes in solutions, we come to the conclusion that the evolution to the new phase does not proceed via the classical picture, illustrated in Fig. 9.1a, but in a way as shown in Fig. 9.1b. In a certain region of the ambient solution with spatial dimensions of the critical cluster size, an amplification of cluster composition is observed. Only after this process is completed, the further evolution is governed by the classical picture, again, i.e., by a change in size with nearly constant bulk parameters of the clusters. So, according to the generalized Gibbs' approach nucleation-growth processes in solutions and similar systems proceed via a scenario to some extent typical for processes known as spinodal decomposition.

A direct experimental verification of the predictions of the generalized Gibbs' approach as illustrated in Fig. 9.1b is shown in Fig. 9.2 [25, 26]. It was intentionally designed and performed as a test of these predictions. On this figure, the results of ASAXS investigations of the primary crystallization of Ni(P) particles in a hypoeutectic Ni-P amorphous alloy are shown. It is evident that—in agreement with the predictions of the generalized Gibbs' approach—the crystals change their composition continuously at nearly constant sizes of the crystals. Only after this process is completed, classical growth processes (change in size with nearly constant composition) start to dominate the growth behavior. So, the evolution to the new phase proceeds here via a continuous sequence of states not realized for macroscopic samples at the given thermodynamic constraints.

Having now a close look at the data given in Ref. [6] on the crystallization behavior of metal phosphates it becomes evident that as the initial step of the transformation, the first phase crystallizes from the amorphous phase. As we can see from Fig. 9.1 in Ref. [6], a cluster consolidation process takes place (which is related to the disappearance of lattice defects—stacking faults). It is followed by a successive change of the crystallographic structure of the cluster (Fig. 9.2 in [6]). Note that all these transformations occur without significant changes in the cluster size; that is, cluster evolution mainly proceeds via changing its structure. Only after the formation of the stable olivine crystallographic structure is completed, clusters

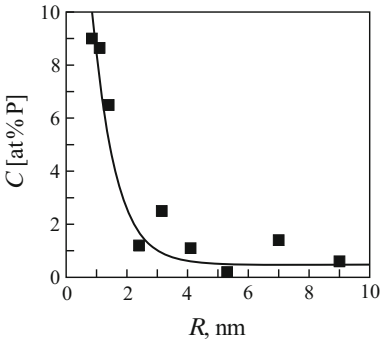

Fig. 9.2 Size dependence of the cluster composition (C is here the content of phosphorus) for the case of primary crystallization of Ni (P) particles in a hypoeutectic Ni-P amorphous alloy as obtained via small-angle scattering of polarized neutrons (for the details see [25, 26], where the data are taken from)

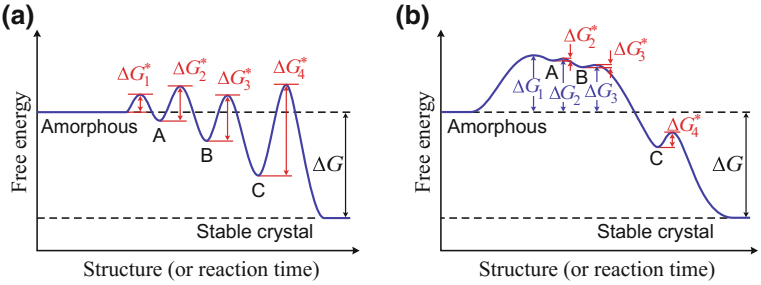

Fig. 9.3 Schematic diagram showing the free energy change during the crystallization process as discussed in [6]: (**a**) scenario as proposed in Ref. [6] (see Fig. 6 in [6]) and (**b**) scenario derived via the generalized Gibbs approach

begin to grow in size, again. Obviously, this sequence fits much better the scenario given in Fig. 9.1b here and then, a sequence of processes evolving via the classical picture is shown in Fig. 9.1a preferred by the authors of Ref. [6].

In more detail, a schematic diagram showing the most probable free energy change during this crystallization process is shown in Fig. 9.3b of the present contribution (Fig. 6 from [6] has been reproduced in Fig. 9.3a for comparison giving the interpretation of the authors of Ref. [6]). Here, ΔG_i are the free energy barrier values for the intermediate crystalline phases referred to the amorphous state level, ΔG_i^* are the activation barriers for the formation of the next in the sequence crystalline phase (for the first phase, $\Delta G_1 = \Delta G_1^*$). We see that this scenario (Fig. 9.3b) is very different from the scenario as proposed in [6] (see Fig. 9.3a): instead of the inequalities $\Delta G_1^* < \Delta G_2^* < \Delta G_3^* < \Delta G_4^*$, the inequalities $\Delta G_1^* > 0, \Delta G_{2,3}^* \approx 0, \Delta G_4^* < \Delta G_2^*$ hold. Ostwald's rule of stages in its classical form can be employed for the interpretation only for the transition $3 \rightarrow 4$ in the third series of experiments in [6], but for the transitions amorphous state $\rightarrow 1 \rightarrow 2 \rightarrow 3$ (and for the whole cycle in the second series of experiments reported in [6]), the generalized Gibbs' approach gives a more adequate interpretation: Near to the critical size, the cluster structure (corresponding to composition as the appropriate parameter for phase formation in a solution) is changing without significant changes in the cluster size, and only after the formation of the structure, which corresponds to the bulk phase, the cluster begins to grow in size. The difference to segregation processes in solutions is here merely that the intensive state parameter (composition) describing the state of a solution and the developing from it clusters is changing continuously. For crystallization, such parameter variations are supplemented by changes in the type of the crystal structure of the newly evolving phase, which can vary only in discrete steps. In general, both changes in crystal structure and composition will govern the behavior as realized in the example of primary crystallization of Ni(P) particles shown here in Fig. 9.2, and the spectrum of states the system may evolve through is much wider as suggested by the classical formulation of Ostwald's rule of stages. A more detailed overview on the basic ideas

of the generalized Gibbs' approach to crystal nucleation and growth processes and its application to different phase formation processes can be found in Refs. [27–30].

The topics discussed up to now refer to thermodynamic aspects of nucleation-growth processes. Here, we would like to analyze also another topic—connected with kinetic parameters determining crystal nucleation and growth—which is of major current interest in the analysis of crystal nucleation and growth processes, the possible correlation between crystallization intensity and fragility index.

9.3 Crystal Nucleation and Growth, and Fragility

The concept of fragility index introduced by Angell (cf. [31, 32]) and related questions (cf. [33–42]) have been widely discussed in the literature with controversial conclusions concerning the ability of the classically defined fragility index to describe appropriately the crystallization tendency of glass-forming melts. By this reason, a critical analysis of this problem is of basic scientific interest and has been performed in [40–42]. Here, we give first a brief review of the basic ideas and results in order to further advance some of the considerations outlined in these papers.

The fragility index $m = m\left(T_g\right)$ was originally defined by Angell as follows:

$$m = \frac{d \log \eta}{d\left(\frac{T_g}{T}\right)}. \tag{9.1}$$

Hereby, m has to be identified with the value of the derivative taken at the temperature, T, equal to the glass transition temperature T_g. Moreover, as will be discussed in detail below, implicitly, it is supposed that T_g has to be defined in a particular way corresponding to Tammann's definition of the glass transition temperature [43].

The viscosity η can be generally expressed as

$$\eta = \eta_0 \exp\left(\frac{E_\eta}{k_B T}\right). \tag{9.2}$$

Here, $E_\eta = E_\eta(T)$ is the activation energy for the viscous flow depending in general on T, the temperature, k_B the Boltzmann constant, and η_0 a kinetic pre-factor only weakly dependent on temperature as compared to the exponential term in Eq. (9.2). From the conventional definition of fragility, we obtain then

$$m = (\log \mathrm{e})\left(\frac{E_\eta^{(eff)}\left(T_g\right)}{k_B T_g}\right). \tag{9.3}$$

The effective activation energy for viscosity, $E_\eta^{(eff)}(T)$, is hereby defined as

$$E_\eta^{(eff)}(T) = E_\eta(T) - T\frac{dE_\eta(T)}{dT}. \tag{9.4}$$

For the specification of the classical fragility index, it has to be computed at $T = T_g$.

The possible correlations of fragility and crystallization behavior are intensively discussed in the literature (cf., e.g., [33–35]). On the other hand, it is well known that, in general, diffusion is the main kinetic factor affecting both crystal nucleation and growth described by a diffusion coefficient, which can be generally expressed similar to Eq. (9.2) as

$$D = D_0 \exp\left(-\frac{E_D(T)}{k_B T}\right). \tag{9.5}$$

So, the first principal limitation in the applicability of fragility concepts in the traditional form is that it is not the activation energy for viscosity but the activation energy for diffusion, $E_D(T)$, which primarily determines crystal nucleation and growth. By this reason, it is the activation energy for diffusion and not the effective activation energy for viscosity which should determine the crystallization behavior. Only in cases when the Stokes–Einstein–Eyring (SEE) equation (allowing one to replace the diffusion coefficient D by the inverse of the Newtonian viscosity) holds, the diffusion coefficient can be replaced by viscosity. In such cases, viscosity can be considered as the main kinetic factor affecting both crystal nucleation and growth. Usually, such replacement is possible above a certain decoupling temperature, T_d, located frequently in the range $T \geq T_d \cong 1.15 - 1.25T_g$ (where T_g is determined by typical experimental methods in conventional laboratory time and size scales). But even in such cases, it is not the *effective activation energy* for viscosity but the *activation energy* which seems to be basically relevant for the description of both nucleation and diffusion. From such considerations, it becomes highly questionable whether fragility can be of relevance at all, even more, taking into account that its value is supposed to be taken at T_g.

However, as shown in Refs. [40–42], the location and magnitude of the maxima of the rates of nucleation, growth, and overall crystallization are determined in addition to the thermodynamic factors not only by the activation energy but also by the effective activation energy of diffusion and, in the range of temperatures where the SEE relation holds, also of viscosity (in this range, the activation energies for diffusion and viscosity coincide). So, for these maxima fragility concepts really enter the description but in order to arrive at correct correlations, fragility has to be defined in a new way. This new definition of the fragility index as proposed in Ref. [41] based on the results of the analysis performed in Ref. [40] is characterized by three new elements as compared to the classical definition as given by Eq. (9.1): (i) We define the fragility index for both diffusion coefficient and viscosity to include all possible cases. (ii) We take as a measure of temperature not the ratio

T_g/T but T_m/T, i.e., replace T_g by the thermodynamically well-defined melting or liquidus temperature, T_m. (iii) We do not connect the fragility with its value at glass transition but compute it for the specific temperatures of maximum rates of nucleation, growth, and overall crystallization in dependence on the particular process analyzed. Following such considerations, the modified diffusion fragility index was defined as [41]

$$m_D^{(m.d.)}(T) = -\frac{d\log D}{d\left(\frac{T_m}{T}\right)} = \frac{E_D^{(eff)}(T)}{k_B T_m} \tag{9.6}$$

and the modified viscosity fragility as

$$m_\eta^{(m.d.)}(T) = \frac{d\log \eta}{d\left(\frac{T_m}{T}\right)} = \frac{E_\eta^{(eff)}(T)}{k_B T_m}. \tag{9.7}$$

It is shown in [41] that the modified diffusion fragility is one of the main factors determining magnitude and location of the maxima of nucleation, growth, and overall crystallization rates. In cases that the SEE equation holds, the modified diffusion fragility can be replaced by the modified viscosity fragility. Even in latter case, the modified viscosity fragility computed at the temperatures referring to the maxima of the respective different processes will be quite different from the classical fragility computed at $T = T_g$. Consequently, as a rule, classical fragility will be of very minor relevance to the crystal nucleation and growth.

9.4 Fragility Index and Deviations from Arrhenius-Type Temperature Dependence of Viscosity

Long ago, Tammann [44] stated that "*the higher the melt viscosity at the melting temperature, the lower its crystallizability*" (cf. also Fig. 9.5a in [34] which provides additional support to Tammann's suggestion). However, as we have demonstrated here, crystallizability is affected not only by the activation energy at the melting temperature but also by the rate of change of the activation energy with temperature. By this reason, one could expect possibly some qualitative correlation of classical fragility and nucleation-growth behavior if the classical fragility index would appropriately describe changes in activation energy of diffusion and viscosity in the case that the SEE relation holds. In this connection, we consider it of interest to examine in more detail whether this is the case or not, i.e., whether classical fragility is really a measure of deviations from Arrhenius-type temperature dependence of the viscosity.

Indeed, frequently, one comes across statements such as "*the fragility of a supercooled liquid quantifies the extent to which the viscosity of the liquid has an Arrhenius temperature dependence*" ([44], cf., e.g., also [40, 45]). This statement is

true but only under certain conditions specified below. First of all, the classical fragility index refers to one particular temperature, the glass transition temperature. Consequently, it can be correlated with the activation energy and its temperature derivatives, i.e., with deviations from Arrhenius-type behavior, strictly speaking, only at $T = T_g$. Second, the fragility index in Angell's definition is proportional to the effective activation energy for viscosity (cf. Equations (9.1)–(9.4)) taken both at $T = T_g$. Consequently, it depends on the sum of the activation energy, $E_\eta(T_g)$, and an additional term, $-T\frac{dE_\eta(T_g)}{dT}$. This second term, which is proportional to the temperature derivative of the activation energy, is the primary measure of deviations of the temperature dependence of the viscosity from Arrhenius-type behavior. Consequently, the fragility in Angell's definition can be a measure of deviations from Arrhenius-type behavior only if the first term, the activation energy at T_g, has widely the same value for all glass-forming systems. If this condition is not fulfilled, then classical fragility is, in general, not a measure of mentioned deviations of the viscosity from Arrhenius-type behavior.

As will be shown below, the second criterion is fulfilled exclusively for a very special specification of the glass transition temperature. Consequently, fragility is, in general, not a measure of the deviations of the viscosity from Arrhenius-type behavior: (i) It refers to one particular temperature, the glass transition temperature, T_g; (ii) it holds only if a very specific definition of the glass transition temperature is employed.

The above-cited statement concerning the correlation of fragility and deviations from Arrhenius-type behavior appears at a first glance to be plausible by examining the so-called Angell plot (cf. Fig. 9.4) giving the dependence of the Newtonian viscosity, η, on the ratio T_g/T. It is assumed, however, in these plots, that for all systems and cooling and heating conditions, T_g refers to the same value of viscosity, $\eta = 10^{12}$ Pa s. Only at such assumption, all viscosity curves coincide at T_g. Consequently, this representation utilizes implicitly the definition of the glass transition temperature proposed by Tammann [30, 43] (identifying the glass transition temperature with values of the viscosity of the order of $\eta\left(T_g^{(12)}\right) = 10^{12}$ Pa s). In this case, $\eta\left(T_g\right)$ and, consequently, $E_\eta\left(T_g\right)$, in Eq. (9.2), have nearly the same values for all glasses. In such situations (but only for them), the differences in the fragility index defined in the classical way are then really caused by the derivatives of the activation energy with respect to temperature at T_g.

In general, however, T_g can be realized for different cooling rates at very different values of the viscosity [30, 45, 46] and, consequently, at different values of the activation energy of viscous flow. In these more general situations, the statement mentioned above concerning the existence of a direct correlation between classical fragility m at T_g and deviation from Arrhenius behavior ceases to be true. The classical fragility index m, when calculated at a viscosity $\eta\left(T_g^{(12)}\right) = 10^{12}$ Pa s, can be correlated with departures from an Arrhenius behavior but, at mentioned more general conditions, $T_g^{(12)}$ does not correspond to the glass transition temperature.

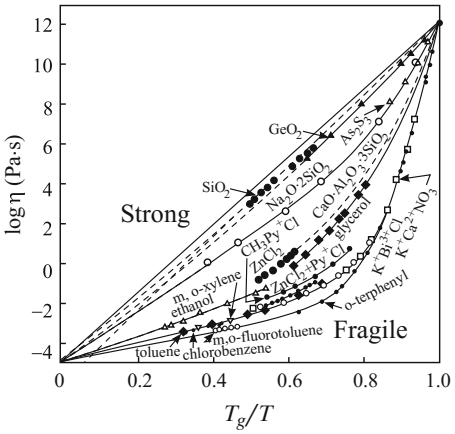

Fig. 9.4 Viscosity of several glass-forming melts in coordinates, $\log \eta$ versus T_g/T. Note the "strong"-type rheological behavior of SiO_2 and GeO_2. The "fragile"-type change of the viscosity is characterized by temperature-dependent activation energies of viscous flow, $E_\eta(T)$. Note as well that in drawing these curves, it is assumed that the glass transition takes place for all systems at the same value of viscosity following the definition of the glass transition temperature as suggested long ago by Tammann [43]. Conclusions drawn from this figure hold consequently only for the case that this additional assumption is fulfilled

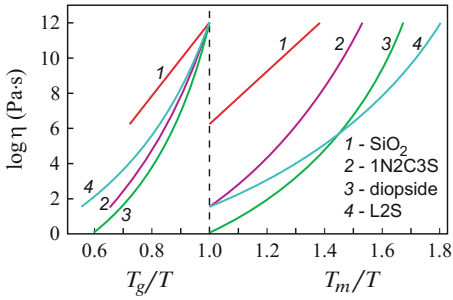

Fig. 9.5 Dependence of viscosity on the ratios T_g/T and T_m/T for four glass-forming melts. The latter dependencies, $\eta = \eta(T_m/T)$, of the equilibrium viscosity on T_m/T hold independently on any particular specification of the glass transition temperature, T_g

For illustration, in Fig. 9.5, the dependence of viscosity with respect to both reduced temperatures, T_g/T and T_m/T, is shown. Reduced coordinates T_g/T have been employed earlier already by Oldekop [36], Laughlin and Uhlmann [37]. Laughlin and Uhlmann presented viscosity data for different systems as functions of both these reduced variables. These authors classified the presentation of viscosity in terms of T_m/T as a "*superior normalization*" of viscosity data but went over then to T_m/T considering it as "*difficult to rationalize* a priori *the dependence of liquid on characteristics other than those of the liquid phase alone.*" For the analysis of nucleation and growth processes, it is shown here, however, that the description of the temperature dependence of diffusion and viscosity in terms of T_m/T is preferable.

9.5 Summary of Results and Discussion

In the present chapter, a critical overview on some of the basic assumptions of the classical theory of crystal nucleation and growth is given. It is shown how the classical theory can be generalized in order to overcome contradictions between theoretical predictions and experimental data. The generalizations discussed here refer in the first part of our analysis to the method of determination of the work of formation of clusters of sub-, super-, and critical sizes being essential ingredients of the theoretical description of nucleation-growth phenomena. In particular, generalizing the classical Gibbs' theory of heterogeneous systems to thermodynamic non-equilibrium states, it is shown that the properties of the clusters change significantly in dependence on their sizes. In particular, it is shown that the properties of the critical clusters deviate, as a rule, from the properties of the newly evolving macroscopic phases. As a result, it turns out that the classical nucleation theory assuming validity of the capillarity approximation overestimates the work of critical cluster formation and underestimates the value of the steady-state nucleation rate [5]. As an additional consequence, it follows that the temperature of the critical clusters may differ from the temperature of the ambient phase where the phase formation proceeds [46, 47]. In addition, it allows one to describe in a new way heterogeneous nucleation accounting for changes of the wetting angle in dependence on the bulk state parameters of the critical clusters [48]. As demonstrated here as well by analyzing several new experimental results, the application of the generalized Gibbs' approach to the phase formation allows one in addition a new interpretation of a variety of phenomena in crystallization processes of glass-forming melts, which could not be given a satisfactory explanation in terms of the classical theory so far, retaining on the other side the advantages of the classical approach.

It is shown further, in the present chapter, why fragility concepts—defined in a new way—may be of relevance to the understanding of crystal nucleation and growth processes. This correlation is due to the fact that the location and the magnitude of the maximum rates of nucleation, growth, and overall crystallization are determined by the expressions where the effective activation energy computed at the respective maximum temperatures is one of the main factors determining these maxima. The classical definition of fragility can, as shown, be of relevance only if a set of conditions is fulfilled which are however rarely met. Classical fragility is shown, in addition, to be not a parameter describing properties of the glass-forming liquids at glass transition. It can be a measure of deviations of the temperature dependence of viscosity from an Arrhenius law only if for all considered systems the glass transition proceeds at the same value of viscosity, restricting its applicability in latter respect to cases when Tammann's classical definition of the glass transition temperature is appropriate. Taking into account the dependence of the glass transition temperature on cooling and heating rates [30, 45, 49], the glass transition will not proceed as a rule at temperatures corresponding to Tammann's definition. Consequently, the fragility computed at a viscosity $\eta\left(T_g^{(12)}\right) = 10^{12}\,\mathrm{Pa\,s}$ can be

correlated with departures from an Arrhenius behavior but, at mentioned more general conditions, $\boldsymbol{T}_{\boldsymbol{g}}^{(12)}$ does not correspond to the glass transition temperature.

There exist some further problems the solution of which is expected to shed some new light on crystal nucleation and growth processes as follows (cf. also [50]): (i) description of the driving force of critical cluster formation accounting for the deviations of the bulk (structure, composition, density) and surface properties of critical nuclei; (ii) determination of the kinetics of change of the bulk and surface properties of sub- and supercritical crystals in their evolution to the critical size, respectively, to the macroscopic phase; (iii) description of the temperature dependence of the crystal nucleus–liquid interfacial energy and the degree of validity of the Stefan–Skapski–Turnbull equation; (iv) applicability of the Stokes–Einstein–Eyring relation in calculating the effective diffusion coefficients that control the crystal nucleation and growth; (v) account of the effect of decoupling on characteristic size parameters entering classical nucleation theory; (vi) a clear understanding of the causes of the breakdown of the SEE equation reported to occur for the crystal growth somewhat above T_g; (vii) a deeper understanding of the relationship, if any, between the molecular structure of glass-forming melts and the nucleation and growth mechanisms [51]; (viii) the relation between the sizes of supercritical nuclei vis-à-vis the sizes of co-operatively rearranging regions (CRRs) of the configurational entropy theory and of the domains of heterogeneous dynamics (DHD) envisaged in the structure of viscous liquids [52]; (ix) development of sufficiently accurate analytical expressions for the description of crystallization at cooling and heating. Consequently, not only with respect to the analysis of the properties of glasses and the glass transition [53] but also with respect to crystallization, "*the melody still lingers on*"!

References

1. Gibbs JW (1928) On the equilibrium of heterogeneous substances, Trans. Connecticut Academy of Sciences 3, 108, 343 (1875–79); The collected works, vol 1, Thermodynamics. Longmans, New York—London—Toronto
2. van der Waals JD (1894) Verhandel. Konink. Akad. Weten. Amsterdam (sect. 1), 1, 56 (1893); Z Phys Chemie 13:657
3. Rowlinson JS (1979) Translation of J. D. van der Waals' The thermodynamic theory of capillarity under the hypothesis of a continuous variation of density. J Stat Phys 20:197
4. Schmelzer JWP, Gutzow IS, Schmelzer J Jr (2000) J Chem Phys 112:3820
5. Schmelzer JWP, Boltachev GSh, Baidakov VG (2006) J Chem Phys 114:194502
6. Chung S-Y, Kim Y-M, Kim J-G, Kim Y-J (2009) Nat Phys 5:68
7. Billinge SJL (2009) Nat Phys 5:13
8. Ostwald W (1897) Z Phys Chemie 22:289
9. Hillert M (1956) A theory of nucleation of solid metallic solutions. Sc.D. Thesis, Massachusetts Institute of Technology
10. Cahn JW, Hilliard JE (1959) J Chem Phys 28, 258 (1958); 31:688
11. Nishioka K, Kusaka I (1992) J Chem Phys 96:5370
12. Debenedetti PG, Reiss H (1998) J Chem Phys 108:5498

13. Baidakov VG, Boltachev GSh, Schmelzer JWP (2000) J Colloid Interface Sci 231:312
14. Stranski IN, Totomanov D (1933) Z Phys Chemie A 163:399
15. Scheil E (1952) Z Metallkunde 43:40
16. Hobstetter JN (1949) Trans. American Inst Min (Metall) Eng 180:121
17. Burke J (1965) The kinetics of phase transformations in metals. Pergamon Press, New York
18. Gerlach W (1949) Z Metallkunde 40:281
19. Masing G (1950) Lehrbuch der Allgemeinen Metallkunde. Springer, Berlin
20. Becker R (1938) Ann Phys 32:128
21. Abyzov AS, Schmelzer JWP (2007) J Chem Phys 127:114504
22. Fokin VM, Zanotto ED, Yuritsyn NS, Schmelzer JWP (2006) J Non-Cryst Solids 352:2681
23. Schmelzer JWP, Gokhman AR, Fokin VM (2004) J Colloid Interface Sci 272:109
24. Schmelzer JWP, Abyzov AS, Möller J (2004) Chem Phys 121:6900
25. Tatchev D, Hoell A, Kranold R, Armyanov S (2005) Phys B 369:8
26. Tatchev D, Goerigk G, Valova E, Dille J, Kranold R, Armyanov S, Delplancke J-L (2005) J Appl Crystallogr 38:787
27. Schmelzer JWP, Abyzov AS (2007) J Eng Thermophys 16:119
28. Schmelzer JWP (2009) Generalized Gibbs thermodynamics and nucleation-growth phenomena. In: Rzoska S, Drozd-Rzoska A, Mazur V (eds) Proceedings of the NATO advanced research workshop "metastable systems under pressure", Odessa, Ukraine, 4–8 Oct 2008. Springer, pp 389–402
29. Schmelzer JWP, Fokin VM, Abyzov AS, Zanotto ED, Gutzow IS (2010) Int J Appl Glass Sci 1:16
30. Gutzow IS, Schmelzer JWP (2013) The vitreous state: thermodynamics, structure, rheology, and crystallization, 1st edn. Springer, Berlin-Heidelberg, 1995; Second enlarged edition. Springer, Heidelberg
31. Angell CA (1995) Science 267:1924
32. Martinez L-M, Angell CA (2001) Nature 410:663
33. Gallo LSA, Mosca TM, Teider BH, Polyakova IG, Rodrigues ACM, Zanotto ED, Fokin VM (2014) J Non-Cryst Solids 408:102
34. Orava J, Greer AL (2014) J Chem Phys 140:214504
35. Wilde G (2014) Early stages of crystal formation in glass-forming metallic alloys. In: Schmelzer JWP (ed) Glass: selected properties and crystallization. de Gruyter, Berlin, pp 95–136
36. Oldekop W (1957) Glastechnische Berichte 30:8
37. Laughlin WT, Uhlmann DR (1972) J Phys Chem 76:2317
38. Nemilov SV (1995) Thermodynamic and kinetic aspects of the vitreous state. CRC Press, Boca Raton
39. Ediger MD, Harrowell P, Yu L (2008) J Chem Phys 128:034709
40. Schmelzer JWP, Abyzov AS, Fokin VM, Schick C, Zanotto ED (2015) J Non-Crystalline Solids 429:24
41. Schmelzer JWP, Abyzov AS, Fokin VM, Schick C, Zanotto ED (2015) J Non-Crystalline Solids 428:68
42. Schmelzer JWP, Abyzov AS, Fokin VM, Schick C, Zanotto ED (2015) J Non-Crystalline Solids 429:45
43. Tammann G (1933) Der Glaszustand. Leopold Voss Verlag, Leipzig
44. Tammann G (1904) Z Elektrochemie 10:532
45. Schmelzer JWP, Gutzow IS (2011) Glasses and the glass transition. Wiley-VCH, Berlin-Weinheim
46. Boltachev GSh, Schmelzer JWP (2010) J Chem Phys 133:134509
47. Schmelzer JWP, Boltachev GSh, Abyzov AS (2013) J Chem Phys 139:034702
48. Abyzov AS, Schmelzer JWP (2014) J Chem Phys 138, 164504 (2013); 140:244706
49. Schmelzer JWP (2012) J Chem Phys 136:074512
50. Zanotto ED, Schmelzer JWP, Fokin VM, Nucleation, growth, and crystallization in inorganic glasses, submitted to publication

51. Wright AC (2013) Int J Appl Glass Sci 5:31
52. Johari GP, Schmelzer JWP (2014) Crystal nucleation and growth in glass-forming systems: some new results and open problems. In: Schmelzer JWP (ed) Glass: selected properties and crystallization. de Gruyter, Berlin, pp 531–590
53. Cooper AR (1982) J Non-Cryst Solids 49:1

Chapter 10
Imperfections of Kissinger Evaluation Method and the Explanation of Crystallization Kinetics of Glasses and Melts

Jaroslav Šesták and Pavel Holba

Abstract The famous Kissinger's kinetic evaluation method (see Anal. Chem. 1957) is examined with respect to both the relation between the DTA signal $\theta(t)$ and the reaction rate $r(t) \equiv \mathrm{d}\alpha/\mathrm{d}t$, the requirements on reaction mechanism model $f(\alpha)$, and the relation of starting kinetic equation to the equilibrium behavior of sample under study. Distorting effect of heat inertia and difference between the temperature T_p of extreme DTA deviation and the temperature T_m at which the reaction rate is maximal are revealed. DTA equation of Borchard and Daniels is criticized regarding the neglection of heat inertia correction. The kinetic equations respecting the influence of equilibrium temperature T_{eq}, especially fusion/melting temperature T_f, are tested as bases for a modified Kissinger-like evaluation of kinetics. Crystallization kinetics on melt solidification is examined under integration of undercooling and needed Gibbs approximations are explored. This chapter provides a new insight into the routine practice of nonisothermal kinetics showing forward-looking outlook and encompasses hundreds of references.

10.1 Introduction

The method of kinetic parameter evaluation based on the treatment of experimental curves obtained by differential thermal analysis (DTA) [1–4] was published by Kissinger in 1957 [5] ($\sim$8000 citations). The method has been habitually used up to the present

Pavel Holba—Deceased

J. Šesták (✉) · P. Holba
New Technologies Research Centre (NTC-ZČU),
University of West Bohemia, Universitní 8, 30114 Pilsen, Czech Republic
e-mail: sestak@fzu.cz

J. Šesták
Division of Solid-State Physics, Institute of Physics, v.v.i. Czech Academy of Sciences,
Cukrovarnická Str.10, 16200, Prague, Czech Republic

J. Šesták et al. (eds.), *Thermal Physics and Thermal Analysis*,
Hot Topics in Thermal Analysis and Calorimetry 11,
DOI 10.1007/978-3-319-45899-1_10

times and became a base for the standardization method by ASTM [1] for testing of explosives. The method was applied not only to DTA/DSC studies but also to other thermoanalytical (primarily thermogravimetric) measurements. The original Kissinger paper [5] was esteemed in [3]; no one, however, paid more detailed attention to its inertia instigated heat transfer. It received numerous modifications and upgrading [1–25] as well as countless citation responses [26]. If the label "Kissinger" is searched to be a part for the relevant papers either Journal of Thermal Analysis or Thermochimica Acta, it provides almost one thousand rejoinders. The so-called Kissinger equation has become widely and routinely applicable [1–25], providing easy attainable values of activation energies even though these values may not be correct anybody, however, bother about.

In spite of this long-standing popularity in community of thermoanalysts [1–25], the method [5] comprises some overlooked but substantial imperfections consisting generally in two points. At first, it is the fact that the relation between the measured DTA temperature deviation ΔT (or θ in Kissinger's original article [5]) and the reaction rate $\boldsymbol{r} = \mathrm{d}\alpha/\mathrm{d}t$ (where α is the extent of reaction or degree of conversion and t is time on which the method is established) does not respect the distorting influence of heat inertia [27–29] even if it was noticed almost ten years in advance [30] of [5]. The second point is connected with the use of kinetic equation $\boldsymbol{r} = F(T, \alpha) = k(T)\, f(\alpha)$ as the starting point of the method. The mentioned kinetic equation assumes the function $F(T, \alpha)$ which is expressing the reaction rate is as a product of two mutually independent functions: temperature dependent $k(T)$ and $f(\alpha)$ dependent on the extent of reaction (modeling the reaction mechanism) which cannot be true as both variables are permanently and reciprocally affected [4, 31]. Moreover, the temperature-dependent function is customarily expressed by the Arrhenius equation $k(T) = Z.\exp(-E/RT)$ where E is activation energy, R is universal gaseous constant, and Z is frequency factor. Both the above-mentioned assumptions—the separability of $F(\alpha, T)$ [4, 31] as well as a mutual dependency of variables E ⇔ Z in Arrhenius equation [32–34]—have been questioned for long [31]. One of the practical imperfections of the kinetic usage of Kissinger equation is, however, the fact, that the equation does not respect the changes of stable equilibrium state of sample when temperature is changing [35, 36]. Due to this fact, the processes taking place at the vicinity of equilibrium transition temperature cannot be evaluated regularly by Kissinger method [36–41], which is also the subject of further analysis.

The purpose of this chapter is to determine and explain the effect of heat inertia [27–30] on the applicability of Kissinger method to DTA/DSC measurements and to recognize ways to relate kinetic equation to stable equilibria of sample—to the so-called equilibrium background [35, 36] of the process under kinetic study.

10.2 Reminding the Method Proposed by Kissinger

As early as in 1955 while studying kinetics of thermal decomposition of clays Murray and White [4, 6] introduced the second derivative of a standard rate equation [42–46]

$$\boldsymbol{r}(T,\alpha) = \mathrm{d}\alpha/\mathrm{d}t = F(T,\alpha) = k(T)f(\alpha) = A\exp(-B/T)\mathrm{f}(\alpha) \tag{10.1}$$

in a widespread form [3, 4, 32]:

$$\mathrm{d}(\mathrm{d}\alpha/\mathrm{d}t)/\mathrm{d}t \equiv \mathrm{d}\alpha^2/\mathrm{d}t^2 = \mathrm{d}\alpha/\mathrm{d}t[B/T^2\mathrm{d}T/\mathrm{d}t + \mathrm{d}f(\alpha)/\mathrm{d}\alpha A\exp(-B/T)] \tag{10.2}$$

where r, α, t, T, E, A, and B (=E/R) are the standard abbreviations of reaction rate, degree of conversion, time, temperature, activation energy, pre-exponential factor, and a B-constant comprising the ratio of activation energy, E, and universal gas constant, R, *respectively*.

The second derivative [42–46] $\mathrm{d}\alpha^2/\mathrm{d}t^2$ should be equal to zero at the moment of maximum reaction rate ($\mathrm{d}\alpha_m/\mathrm{d}t$) occurring at the temperature, T_m. Under conditions of a constant heating rate, $\beta = \mathrm{d}T/\mathrm{d}t$, the Eq. (10.2) can be rewritten as follows:

$$(\mathrm{d}\alpha/\mathrm{d}t)[B\beta/T_m^2 + \mathrm{d}f(\alpha_m)/\mathrm{d}\alpha A\exp(-B/T_m)] = 0 \tag{10.3}$$

where $\mathrm{d}f(\alpha_m)/\mathrm{d}\alpha$ is always negative if, e.g., $f(\alpha) = (1 - \alpha)^n$. Because the term ($\mathrm{d}\alpha/\mathrm{d}t$) is never zero, the condition of maximum is always fulfilled if the expression in square brackets is equal to zero

$$[B\beta/T_m^2 + \mathrm{d}f(\alpha_m)/\mathrm{d}\alpha A\exp(-B/T_m)] = 0 \tag{10.4}$$

The final form of which equals to a well-known equation

$$\beta/T_m^2 = -\mathrm{d}f(\alpha_m)/\mathrm{d}\alpha(A/B)\exp(-B/T_m) \tag{10.5}$$

and its logarithmic form encompasses the famous *Kissinger equation* [6]

$$\ln(\beta/T_m^2) = -B/T_m + \mathrm{const} \tag{10.6}$$

where const = ln [$-\mathrm{d}f(\alpha_m)/\mathrm{d}\alpha$ (A/B)] and [$-\mathrm{d}f(\alpha_m)/\mathrm{d}\alpha > 0$].

Equations (10.5) and (10.6) have undergone various mathematical modifications and applicability upgrading [1–25] in order to improve data fitting of individual experimental measurements while endorsing reliability of evaluated activation energies [47–49]. It is worth mentioning that the Kissinger method [5] received according to the databases WOS as many as about 5000 citation responses [26]. The most widespread variant of the method by Augis and Bennet [8] from 1978 became one of the best time-honored papers of the Journal of Thermal Analysis with about 500 citations [26]. There have been published numerous papers employing this method for experimental data evaluation, thus producing plentiful numerical values of so far published activation energies—mostly as a major subject of publications. However, only few papers analyzed the true meaning of evaluated data, such as activation energies [46–49] with almost no deeper examination of mathematical and physical background of this approach under specific conditions of nonisothermal study. In this respect, it is worth noting that the ongoing recommendations of the

ICTAC Kinetic Committee have been somehow contra-productive while declaring unchanged guidance literally, suggesting how to precisely evaluate and correctly publish [50] fictitious kinetic data [46].

It was shown that the Kissinger equation formally holds for any kinetic model [14] based on Eq. (10.1), which can be mathematically adjusted [4, 7, 14, 18, 20–25, 43–45] and which is generally symbolized by the function $f(\alpha)$. However, despite the apparent linearity of the Kissinger plots, we should stay aware that the sensitivity of the required linear plot is severely reduced by the use of logarithmic scale, and thus, the data may not be fully representative for the fortitude of a reaction profile. The original derivation [2–5] is based on a simplest model of reaction order, n, i.e., $f(\alpha) = (1 - \alpha)^n$. The evaluation, however, cannot fully discriminate the category of any model in question while the model itself affects the values of activation energies insignificantly. Moreover, the evaluation is strictly dependent on the progressive shifts of rate maxima (T_m) along with the increasing heating rate (habitually provided by *JMAYK* [42–46, 51–54] or *SB crystallization models* [54–56]).

For some special cases of the cold crystallization of nanostructured glasses [45, 57, 58] or near-equilibrium processes of solidification [35–40], Kissinger method resides inappropriate. It is particularly worth mentioning for the case of "finemet" category of metallic glasses with a very fine nanocrystalline structure [45], the crystallization of which follows the *Atkins NNG model* [57, 58] of so-called normal crystal growth, see Fig. 10.1. There is not gradual shift of the peak apex making furthermore difficulty to adjust appropriate values of associated glass-forming

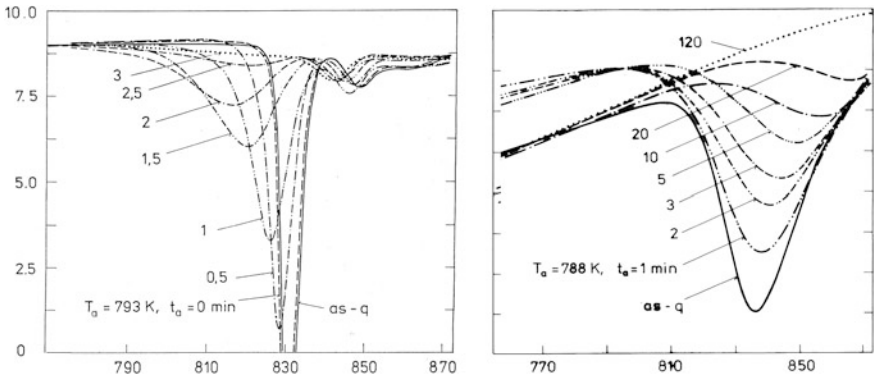

Fig. 10.1 Not all crystallization processes reveal the shift of DTA peak apex upon change of heating. *Left*, the quenched alloy composed of conventional stoichiometry $Fe_{75}Si_{15}B_{10}$ and annealed at temperature 793 K while right is the quenched alternative fine metal of almost comparable composition $Fe_{74}Cu_1Nb_3Si_{13}B_9$ which, however, does not reveal peak shifting. The figure shows DSC traces (first run) for the crystallization of glassy ribbons freeze-in by the method of rapidly rotating drum and DTA samples have in weight of about 15 mg, composed of 10–20-μm-thick and 10-mm-wide ribbons cut in several pieces and pressed in a Pt cell, heating 40 K/min under nitrogen inert atmosphere under the progressively increased annealing time t_o [36]. Courtesy of *Emilie Illeková*, Bratislava, Slovakia

coefficients [41, 43, 45, 59, 60]. The subject of a mathematical incorporation of various reaction models became a popular theme of the various modifications of Kissinger equation [1–25]; we, however, are not intending to appraise them, thus abandoning any deeper examination of existing literature.

10.3 Choice of Reaction Mechanism, Isothermal and Nonisothermal Degree of Conversion, and the Impact of Equilibrium Background

Degree of conversion, α, can be experimentally measured by a range of thermoanalytical measurements, an important point of which is a true definition of the system under investigation when also accounting on its equilibrium background [36, 37, 61–68] which is often disregarded [46]. For example, Svoboda and Málek [2, 64] shown that the values of (apparent) activation energies, E, determined for the process of glass transformation by means of the Kissinger method, occured in a disagreement with the original values used for simulation, even if the activation energies corresponded to the perceptible linear dependences. It was caused by the impact of thermal history of glassy samples and their evidently constrained nonequilibrium states [45, 60]. Orava and Greer [67] pointed out that the changing rate of nucleation may result in curved Kissinger plot. Therefore, the cases of crystallization, either "cold" on reheating or "true" on the melt solidification, will be dealt out in more details in the following paragraph 6.

The disturbing effect when studying the alternative processes during melting and/or solidification in multi-phase diagrams is seldom anticipated [35–38]. The variability of the degree of conversion was introduced by Holba and Šesták [35, 36] because in such cases it is expedient to introduce a novel so-called *nonisothermal degree of conversion*, λ, in the form [31, 35, 36]

$$\lambda = \alpha\, \lambda_{eq}(T), \tag{10.7}$$

where α represents the classical "isothermal" degree, while $\lambda_{eq}(T)$ stands for the equilibrium degree of conversion for a given temperature T (the so-called the *equilibrium background* [35, 36]). It signifies that the momentary degree is pushed toward the end of the process by thermodynamic equilibration, only. The correlated nonisothermal rate of overall reaction progress, $\mathrm{d}\lambda/\mathrm{d}t$, is then given as a two-part sum often called Holba–Sestak equation [37]:

$$\mathrm{d}\lambda/\mathrm{d}t = \alpha(\mathrm{d}\lambda_{eq}/\mathrm{d}t) + \lambda_{eq}(\mathrm{d}\alpha/\mathrm{d}t), \tag{10.8}$$

Which transformed in the logarithmic form reads

$$\mathrm{d}\ \ln \lambda/\mathrm{d}t = (\mathrm{d}\ \ln \lambda_{eq}/\mathrm{d}t) + (\mathrm{d}\ \ln \alpha/\mathrm{d}t). \tag{10.9}$$

Upon substituting $\mathrm{d}\ \ln\ \lambda_{eq}/\mathrm{d}t = \beta.\ \mathrm{d}\ \ln\ \lambda_{eq}/\mathrm{d}T$ (where $\beta = \mathrm{d}T/\mathrm{d}t$), we obtain the expression for the maximum of nonisothermal rate ($\mathrm{d}\lambda/\mathrm{d}t = \max$) [25]

$$\mathrm{d}^2\lambda/\mathrm{d}t^2 = (\mathrm{d}\lambda/\mathrm{d}t).[\beta(\mathrm{d}\ \ln \lambda_{eq}/\mathrm{d}T) + (\mathrm{d}\ \ln \alpha/\mathrm{d}t)] + \lambda.(\mathrm{d}^2 \ln \alpha/\mathrm{d}t^2) = 0. \tag{10.10}$$

The term λ_{eq} can be derived on the basis of an experimentally measured extensive property Z (e.g., enthalpy) [4, 35, 36], the observation of which starts from the initial value, Z_0, gradually attaining its maximum value, Z_∞, at the end of the process. For an isothermal course, the degree accomplishes its intermediate value $Z_{eq}(T)$ corresponding to the equilibrium at the given operation temperature, T. Therefore, we can write

$$\lambda_{\mathrm{eq}}(\mathrm{T}) = \big(\mathrm{Z_{eq}}(\mathrm{T}) - \mathrm{Z_o}\big)/(\mathrm{Z_\infty} - \mathrm{Z_o}). \tag{10.11}$$

The further analysis aiming such adaptation of the extended Kissinger-like plot requires the analysis of supplementary λ-complications, the detailed solution of which falls, however, beyond the framework of this contribution.

10.4 The Apex of Maximum Temperature Deviation at a DTA Peak Is not the Point of Its Maximum Reaction Rate

Original 1957 Kissinger derivation starts from the temperature distribution in the differential thermal analysis specimen holders obeying the general heat flow equation (see Eq. {1} in the original Kissinger's paper [5])

$$\partial \mathrm{T}/\partial \mathrm{t} - (\mathrm{k}/\rho\mathrm{c})\nabla^2\mathrm{T} = (1/\rho\mathrm{c})(\mathrm{dq}/\mathrm{dt}), \tag{10.12}$$

where $(\mathrm{d}q/\mathrm{d}t)$ is the rate of *heat generation* (in W) due to a chemical reaction, k is thermal conductivity (in Wm/K), ρ is density (kg/m^3), and c is specific heat capacity (J/K/kg). Kissinger assumed such conditions wherein the temperature of the outside of the holder rises at a linear rate, β (expressed by φ in Kissinger paper [5]), the solution of which is expressing the temperature at the centers of the reference T_r and of the sample T_s in the form (see Eqs. {3} and {4} in the original [5])

$$T_r = T_0 + \varphi t - (\rho c/k)(\varphi\, a^2/4);\ T_s = T_0 + \varphi t - f(\mathrm{d}q/\mathrm{d}t) \tag{10.13}$$

a is a diameter of cylindrical reference holder and $f\,(\mathrm{d}q/\mathrm{d}t)$ is a function of the reaction rate (including also any secondary effects of the reaction).

The disparity temperature, θ, is the difference in temperature of the centers of the two samples. According to Kissinger [5], this difference, $\theta = T_s - T_r$, is then given by

$$\theta = T_s - T_r = f(\mathrm{d}q/\mathrm{d}t)_{\mathbf{sample}} - (\rho c/k)(\varphi a^2/4)_{\mathbf{reference}} \tag{10.14}$$

and after the differentiation with respect to time (see his Eq. {6} in [5]) it reads

$$\mathrm{d}\theta/\mathrm{d}t = \mathrm{f}'(\mathrm{dq}/\mathrm{dt})\left(\mathrm{d}^2\mathrm{q}/\mathrm{dt}^2\right). \tag{10.15}$$

It follows that apostrophe (′) means derivative, i.e., $f' = \mathrm{d}f/\mathrm{d}t$ so that $\mathrm{d}\theta/\mathrm{d}t = (\mathrm{d}f/\mathrm{d}t)\ (\mathrm{d}q/\mathrm{d}t)\ (\mathrm{d}^2q/\mathrm{d}t^2)$.

Equation (10.15) (and Eq. {6} in Ref. [5]) states that the peak differential deflection occurs when the reaction rate is a maximum.

This approach, however, evidently ignored the effect of a true heat transfer, which is responsible for the DTA peak mounting [27–29], and which extreme point —*apex,* is the maximum deviation θ_p at temperature T_p, perceptibly influenced by the sample *heat inertia* [29]. According to the equation originally derived by *Vold* almost ten years earlier (see her Eq. {5} in [30]) than that by Kissinger [5], we can ensue the Vold equation [30] as

$$-\mathrm{d}\theta/\mathrm{dt} = -(\mathrm{K}/\mathrm{C_s})\theta + (1 - \mathrm{C_r}/\mathrm{C_s})\beta + (\mathrm{dq}/\mathrm{dt})/\mathrm{C_s} + \Delta\mathrm{K(T)}/\mathrm{C_s}. \tag{10.16}$$

The symbol K is the instrumental constant (in W/K), Cs are heat capacities of the sample (s) and reference (r), and $\Delta K(T)$ reflects the difference between heat transfer conditions between the sample and the reference, so that after differentiation of Eq. (10.16) with respect to time and the rearrangement we reach

$$\mathrm{d}\theta/\mathrm{dt} - (\mathrm{Cs}/\mathrm{K})\mathrm{d}^2\theta/\mathrm{dt}^2 = \left(\mathrm{d}^2\mathrm{q}/\mathrm{dt}^2\right)/\mathrm{K}, \tag{10.17}$$

which is in contrary to the Kissinger's final Eq. {6} in [5] (see the above Eq. (10.15)) where the term with $\mathrm{d}^2\theta/\mathrm{d}t^2$ is missing.

Substituting

$$(\mathrm{d}q/\mathrm{d}t) = -H(\mathrm{d}\alpha/\mathrm{d}t) \tag{10.18}$$

where H is the reaction enthalpy change ($H < 0$ at exothermic process when heat is generated inside the sample) and neglecting the second and the fourth right-side terms ($C_r \approx C_s$ and $\Delta K \approx 0$) we rearrange Eq. (10.16) into the form

$$-(\mathrm{d}\theta/\mathrm{dt}) = -(\mathrm{K}/\mathrm{C_s})\theta - (\mathrm{H}/\mathrm{C_s})(\mathrm{d}\alpha/\mathrm{dt}) \tag{10.19}$$

It follows from Eq. (10.19) that at maximum deviation of temperature difference $|\theta_p|$ = max at the temperature of apex T_p we have $\mathrm{d}\theta_p/\mathrm{d}t = 0$, so that

$$\left(\mathrm{d}\alpha_p/\mathrm{d}t\right) = -(K/H)\theta_p \tag{10.20}$$

Upon rearranging Eq. (10.19), we generally have

$$(\mathrm{d}\alpha/\mathrm{d}t) = (C_s/H)(\mathrm{d}\theta/\mathrm{d}t) - (K/H)\theta \tag{10.21}$$

and after its differentiation we find

$$\left(\mathrm{d}^2\alpha/\mathrm{d}t^2\right) = (C_s/H)(\mathrm{d}^2\theta/\mathrm{d}t^2) - (K/H)(\mathrm{d}\theta/\mathrm{d}t) \tag{10.22}$$

or

$$(C_s/H)(\mathrm{d}^2\theta/\mathrm{d}t^2) = (K/H)(\mathrm{d}\theta/\mathrm{d}t) + \left(\mathrm{d}^2\alpha/\mathrm{d}t^2\right) \tag{10.23}$$

The condition of a maximum reaction rate ($\mathrm{d}\alpha_m/\mathrm{d}t$ = max) at temperature T_m, for the temperature difference $\mathrm{d}\theta_m$ and extent of reaction α_m from Eq. (10.22) is found

$$\left(\mathrm{d}^2\alpha_m/\mathrm{d}t^2\right) = (C_s/H)(\mathrm{d}^2\theta_m/\mathrm{d}t^2) - (K/H)(\mathrm{d}\theta_m/\mathrm{d}t) - = 0 \tag{10.24}$$

so that

$$(C_s/H)(\mathrm{d}^2\theta_m/\mathrm{d}t^2) = (K/H)(\mathrm{d}\theta_m/\mathrm{d}t) \tag{10.25}$$

If the temperature of the peak apex T_p and the temperature of maximum reaction rate T_m would occur identical ($T_p = T_m = T_{mp}$, $\theta_p = \theta_m = \theta_{mp}$, $\alpha_p = \alpha_m = \alpha_{mp}$), then we can write the Eq. (10.24) in the form

$$(C_s/H)(\mathrm{d}^2\theta_{mp}/\mathrm{d}t^2) = (K/H)(\mathrm{d}\theta_{mp}/\mathrm{d}t) + \left(\mathrm{d}^2\alpha_{mp}/\mathrm{d}t^2\right) \tag{10.26}$$

However, for the case ($\mathrm{d}\theta_{mp}/\mathrm{d}t$) = ($\mathrm{d}\theta_p/\mathrm{d}t$) = 0 and (at the same time ($\mathrm{d}^2\alpha_{mp}/\mathrm{d}t^2$) = ($\mathrm{d}^2\alpha_m/\mathrm{d}t^2$) = 0) we find that ($\mathrm{d}^2\theta_{mp}/\mathrm{d}t^2$) should be zero. It follows from Fig. 10.2 that ($\mathrm{d}^2\theta/\mathrm{d}t^2$) cannot reach zero value in a surrounding of the apex point of peak (T_p, θ_p, α_p) because for the point with maximum value of temperature difference θ_p the value of ($\mathrm{d}^2\theta_p/\mathrm{d}t^2$) can be never zero

$$(\mathrm{d}^2\theta_p/\mathrm{d}t^2) \neq 0 \rightarrow T_p \neq T_m, \quad \theta_p \neq \theta_m, \alpha_p \neq \alpha_m \tag{10.27}$$

Despite a long-lasting history of kinetic evaluation, it is clear that such an important part of DTA peak analysis [4, 27, 28] has been overlooked at everyday applications. It is possibly caused by the apparent methods simplicity, which provoke easy publishable values of activation energies. It is surprising that anyone who implicated various alternatives of the Kissinger method [7–24] did not come across any reasons for its disapproval due to the heat inertia effect.

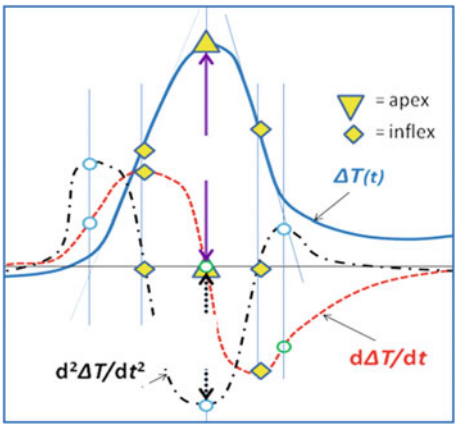

Fig. 10.2 Illustrative scheme of a DTA curve ($\Delta T \equiv \theta$) and its first ($d\Delta T/dt \equiv d\theta/dt$) and the second ($d^2\Delta T/dt^2 \equiv d^2\theta/dt^2$) derivatives as function of time t during a thought endothermic process at heating

10.5 DTA Equation of Borchard and Daniels and the Heat Inertia Correction

Inquisitively even well-written books on DTA [69–73] did not persuaded this quandary of heat inertia design [27, 28] into a more widely accepted understanding because the influence of heat inertia on the whole peak area is realistically negligible so that it possesses practically no impact on the enthalpy measurements. This negligibility is due to the fact that the contribution of heat inertia at the onset stage of DTA peak is nearly compensated by the reversed contribution at the attenuation (rundown) stage of the peak. The effect of thermal inertia is actually represented by *s-shaped* curve [27, 28] and its addition to original DTA does not change the value of peak area but its profile. Moreover, for the determination of various thermal criteria (such a glass-forming coefficients) this inertia term comprises negligible effect [59, 60]. In many theoretical treaties, the second derivative $d^2\Delta T/dt^2$ was identified [72, 74, 75] but not auxiliary contemplated until the detailed scrutiny in books [4, 76, 77].

Factually the above-mentioned inertia term was in 1957 incorporated on the study by Borchard and Daniels [78] (≈900 WOS citations [26]) who employed DTA to the kinetic study of homogeneous reactions in well-stirred liquid samples. They starts with the balance equation (see their Eq. {3} in Ref [78])

$$dH = C_S\, d\theta + K.\theta\, dt \tag{10.28}$$

where $dH = -H\, d\alpha$, and θ, C_s, K have the same meaning as in Eqs. (10.14–10.27), although Borchard and Daniels used ΔT instead of θ and C_p instead of C_s. The correction with respect to heat inertia was included (cf. their Eq. {13} in [78]), thus expressing the rate constant k of a homogeneous reaction as

$$k = (C_s(\mathrm{d}\theta/\mathrm{d}t) + K\theta)/(K(A - a) - C_s\theta) \tag{10.29}$$

(A is total area of peak and a is a part of this area for time interval $t - t_0$), and this correction is included in other consequent equations (from {12} to {15} in Ref. [78]). However, the heat inertia term was then neglected (referring the original equations {17}, {19}, {21}, and {22} see Ref. [78]) upon the authors' argumentation [78]: "… the quantities (C_s dθ/dt) and $C_s\,\theta$ are usually an order of magnitude smaller than the quantities to which they are added and subtracted…" (as translated into the symbols used in this paper). The results [78] showed, however, that the term: "C_s dθ/dt varies from 0.634 … to −2.70" while the term $K\,\theta$ "varies from 4.67 to 13.1 going through a maximum of 28.1." For that reason, the above negligence seems to be rather incorrect because the heat inertia term has a significant influence (being asymmetrical on the level approaching the curve inflection points—differing at least 10% from the original signal). The resulting shape of kinetic curve and the derived kinetic parameters are thus extremely sensitive to this heat inertia consequence.

Blumberg [79] (≈50 WOS citations [26]) applied DTA to the kinetic study of heterogeneous reaction of silica with HF in a linearly heated bath. He used also a theoretical background with a thermal inertia term as it follows (e.g., from his Eq. {8} in Ref. [79]). Nevertheless, at the same time Kissinger [3, 5] proposed a kinetic evaluation particularly based on the shift of the DTA peak apexes along with increased heating rates, thus omitting the above-mentioned studies. Ten years later, it was criticized, but the characteristic temperatures were directly substituted by the reaction rates derived from the slope of mounting part of a DTA peak by Piloyan [80, 81] (≈400 WOS citations [26]), however, missing the heat inertia term again.

The detailed evaluation waited until the late 1970s in the comprehensive studies by Holba et al. [82–86]), thus piloting the true (full-size) DTA equation (after translation into symbols of the present paper) in the form:

$$\theta = [\Delta K(T_W - T_r) - (C_s - C_r)\beta - C_s(\mathrm{d}\theta/\mathrm{d}t) - H.\mathrm{d}\alpha/\mathrm{d}t]/K \tag{10.30}$$

where θ = difference between temperature of proper sample (T_s) and that of reference sample (T_s); T_W = temperature of furnace wall; ΔK = difference between coefficients of heat transfer between the furnace and sample holder (K_s) and between the furnace and reference holder (K_r); $\beta = \mathrm{d}T_r/\mathrm{d}t$ = externally applied linear heating rate); K = (in J/K s) the so-called apparatus constant of a given DTA instrument (depending on temperature T_r and heating rate β); H = integral enthalpy change due to transition/reaction inside sample and α = extent of transition (conversion). The recalculation of experimental DTA curve according to Eq. (10.25) gives an illustrative peak *rectification* (which is graphically shown in Fig. 10.3, thus illustrating the shift of the top of DTA peak).

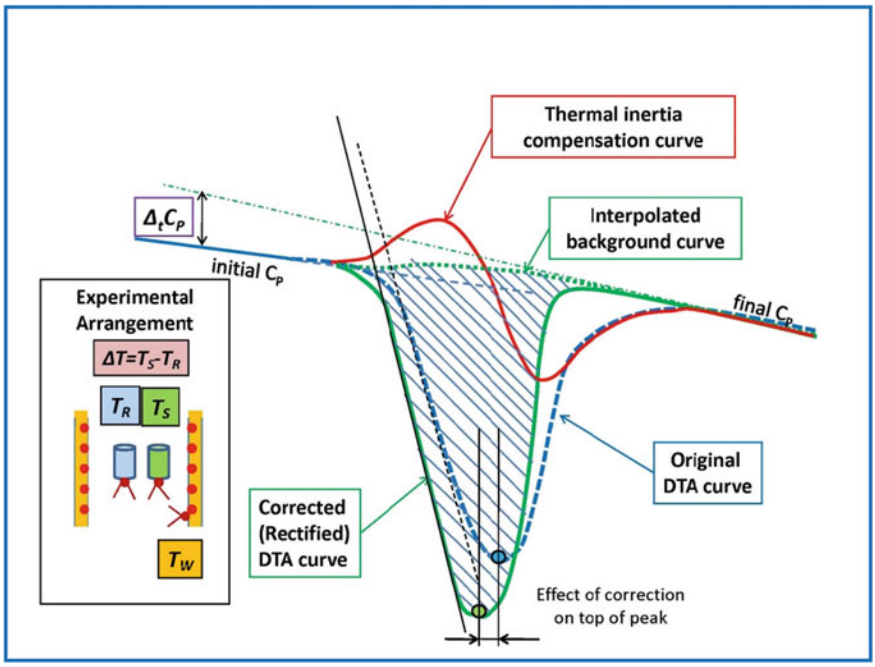

Fig. 10.3 Graphical representation of individual contributions composing a DTA peak assuming the standard DTA setup with samples (T_S and T_R) heat from the outside (T_W), left insertion, cf Eq 10.30. Then, the *misfit* between T_m and broadly implemented value of the DTA apex, T_p is explicitly shown. It could be deduced that difference between temperatures T_p and T_m increases with a sharpness (higher curvature) of the peak apex

As an example of the adjusted obtaining the activation energy for phase transition of $BaCO_3$ (at 810 °C), the experimental DTA records were exploited upon using two relations for the transformation of DTA curve into transition rate values [82, 83]: (a) the equation without any heat inertia correction: $\mathrm{d}\alpha/\mathrm{d}t = (K/H)\theta$ (b) and the same including the simple heat inertia correction: $\alpha/\mathrm{d}t = -(K/H)\theta + (K/C_s)\mathrm{d}\theta/\mathrm{d}t$.

Using some assumptions on transition mechanisms, the ensuing values of activation energy were obtained diverged, namely 87 kcal/mol and 38 kcal/mole for the uncorrected and the corrected cases, respectively.

Even though the authoritative software proposal appeared in a respected journal of Thermochimica Acta long ago [85], the perceptible effect of thermal inertia has not been accredited until today with few exceptions [76, 77] not mentioning the detailed description in the recent books by Šesták [4, 42, 60, 87].

10.6 Kinetic Equations when Involving Equilibrium Temperature (e.g., Melting Temperature)

A number of recent executions of the Kissinger equation have been concerned with a nonisothermal crystallization of melts upon cooling, while temperature is decreasing with time the negative values of β are subsequent. This fact means mathematically that in Eq. (10.4) we have at

$$\left[B\beta/T_m^2 + (\mathrm{d}f(\alpha_m)/\mathrm{d}\alpha)A\exp(-B/T_m)\right] = 0$$

mutually negative terms. However, $[(\mathrm{d}f(\alpha_m)/\mathrm{d}\alpha$ is negative only if $f(\alpha) = (1 - \alpha)^n$ and $B\beta/T_m^2$ are negative and if $B = E/R$ is positive (note that β is negative at cooling which should give jointly the zero value). The simplest way to avoid this problem is to use (by incorrect way, of course) the absolute value of heating rate $|\beta|$ instead of β in Eq. (10.4). This case was numerically analyzed by Vyazovkin [88] showing that such simulated data provided mistaken and almost absurd results which in a way was a contra-productive consent.

The correct way how to avoid the mentioned nonsense result of Eq. (10.4) is to start from kinetic equation dissimilar of Eq. (10.1) and employing kinetic equation which would respect the relation of reaction rate to the corresponding equilibrium state. For a more rigorous derivation, we have to employ a modified rate equation where the simple form of Eq. (10.1) is supplemented by additional factor of a thermodynamic driving force mounting along with the melt undercooling, δT [4, 25, 35, 60, 89, 90], as happen below equilibrium fusion (melting) temperature, T_f, due to the process of nucleation. In such a case, we substitute temperature-dependent Arrhenius $k(T) = A.\exp(-B/T)$ by a factor $k_{cr}(T, \delta T)$ which depends not only on temperature T but also on the difference between this temperature T and the temperature of equilibrium melting (fusion) T_f through quantity of undercooling $\delta T = (T_f - T)$ as proposed by Suňol et al. [89] in the form

$$k_{cr}(T, \delta T) = A\exp\{-B_{cr}/(T\delta T^2)\} \tag{10.31}$$

where $B_{cr} = \sigma^3/\Delta S_f^2$ (σ is surface energy between crystal nucleus and liquid melt, ΔS_f is entropy of fusion). The starting kinetic equation has the following form

$$r(T, \alpha) = \mathrm{d}\alpha/\mathrm{d}t = k(T)f(\alpha) = A\exp\left(-B_{cr}/(T\delta T^2)\right)\mathrm{f}(\alpha) \tag{10.32}$$

The differentiation of k_{cr} with respect to T gives

$$\mathrm{d}k_{cr}/\mathrm{dT} = -B_{cr}(2T - \delta T)/(T^2\delta T^3)A\exp(-B_{cr}/(T\delta T^2)) \tag{10.33}$$

$$\mathrm{d}k_{cr}/\mathrm{dT} = -B_{cr}\left(3T - T_f\right)/\left(T^2(T_f - T)^3\right)A\exp\left(-B_{cr}/\left(T(T_f - T)^2\right)\right)$$

and instead of Eq. (10.2), we have

$$\begin{aligned} \mathrm{d}(\mathrm{d}\alpha/\mathrm{d}t)/\mathrm{d}t = \mathrm{d}\alpha/\mathrm{d}t[-B_{cr}(2T-\delta T)/(T^2\delta T^3)\mathrm{d}T/\mathrm{d}t \\ + \mathrm{d}f(\alpha)/\mathrm{d}\alpha A\exp(-B_{cr}/(T\delta T^2))] \end{aligned} \tag{10.34}$$

and Eq. (10.4) should be substituted by

$$\left[-B_{cr}\beta/\left(3T_m - T_f\right)/\left(T_m^2(T_f - T_m)^3\right) + \mathrm{d}f(\alpha_m)/\mathrm{d}\alpha A\exp\left(-B_{cr}/\left(T_m(T_f - T_m)^2\right)\right)\right] = 0 \tag{10.35}$$

where the first term is positive at cooling (i.e., at negative heating). The value of B_{cr} could be then evaluated using logarithmic form (compare Eq. (10.6))

$$\ln\left[-\beta/\left(3T_m - T_f\right)/\left(T_m^2\left(T_f - T_m\right)^3\right)\right] = -B_{cr}/\left(T_m\left(T_f - T_m\right)^2\right) + \text{const} \tag{10.36}$$

where const = ln $[-\mathrm{d}f(\alpha_m)/\mathrm{d}\alpha\ (A/B_{cr})]$ and $[-\mathrm{d}f(\alpha_m)/\mathrm{d}\alpha > 0]$.

The imperfection of the Eq. (10.31) is a conflict with a general requirement of dimensionless argument in exponential function when dimension of B_{cr} is J K^2 (dimension of entropy of melting ΔS_f is J K^{-1} m^{-3}) and then the dimension of the complete argument is J K^{-1}.

There is a range of various thermodynamic models involving extent of undercooling (see Appendix 1); the most common is another equilibrium-dependent kinetic model proposed by Turnbull [90] for the nucleation rate $I = (k_I/\eta)\exp[-B_n/(T_r\ \delta T_r^2)$ where $T_r = T/T_f$ is reduced temperature and $\delta T_r = 1 - T_r$ is reduced undercooling.

A more general way for introducing an influence of equilibrium state to reaction rate is multiplying the original kinetic Eq. (10.1) by a driving force $D(T, T_{eq})$

$$\boldsymbol{r}(\alpha, T, T_{eq}) = \mathrm{d}\alpha/\mathrm{d}t = k(T)f(\alpha)D\left(T, T_{eq}\right) = A\exp(-B/T)f(\alpha)D\left(T, T_{eq}\right) \tag{10.37}$$

The driving force should be chosen as a dimensionless difference between logarithm of activity of the initial state of sample ln a_0 and logarithm ln a_f of final activity (activity of a state of sample which is reached by a process under study)

$$D\left(T, T_{eq}\right) = \ln a_0 - \ln a_f = -\ln\left(a_f/a_0\right) = -\left(G_f - G_0\right)/RT = -\Delta G(T)/RT \tag{10.38}$$

Quantity ΔG can be expressed through enthalpy change ΔH and entropy change ΔS, $\Delta G(T) = \Delta H - T\Delta S$, and for *enantiotropic* processes [36], the equilibrium temperature T_{eq} exists at which $\Delta G(T_{eq}) = \Delta H - T_{eq}\Delta S$, and if temperature

dependences of ΔH and ΔS are neglected, then $\Delta G(T) = \Delta H(1 - T/T_{eq}) = \Delta H (T_{eq} - T)/T_{eq} = \Delta H \cdot \Delta T/T_{eq}$ so that

$$D\left(T, T_{eq}\right) = -DH\left(T_{eq} - T\right)/\left(RTT_{eq}\right) = (DH/RT_{eq})\left(T - T_{eq}\right)/T \tag{10.39}$$

Substituting Eq. (10.39) and using Arrhenius equation for $k(T)$, the Eq. (10.37) arrives at the form

$$\mathrm{d}\alpha/\mathrm{d}t = f(\alpha)A\exp(-B/T) \cdot (DH/RT_{eq})\left(T - T_{eq}\right)/T \tag{10.40}$$

Defining new constant $L = A\Delta H/RT\Delta H_{eq}$ which is positive for endothermic process ($\Delta H > 0$) and negative for exothermic process (< 0) and using $B = E/R$, the Eq. (10.40) is transposed into

$$\mathrm{d}\alpha/\mathrm{d}t = f(\alpha)L\exp(-E/RT) \cdot \left(T - T_{eq}\right)/T \tag{10.41}$$

For isothermal reaction rate and assuming $f(\alpha) = (1 - \alpha)$, we then have the simplest kinetic model which is exploitable as the continuous model of enantiotropic phase transition, see Ref. [41]

$$\mathrm{d}\alpha/\mathrm{d}t = k_T(1 - \alpha)\left(T - T_{eq}\right) \tag{10.42}$$

Differentiating Eq. (10.41) with respect to time and after rearrangement by using $\mathrm{d}T/\mathrm{d}t = \beta$, we obtain

$$\begin{aligned}\mathrm{d}^2\alpha/\mathrm{d}t^2 = (\mathrm{d}\alpha/\mathrm{d}t)[(\mathrm{d}f(\alpha)/\mathrm{d}\alpha)L\exp(-E/RT) \cdot \left(T - T_{eq}\right)/T + E\beta/RT^2 \\ + \beta\left(T_{eq}/T\right)/\left(T - T_{eq}\right)]\end{aligned} \tag{10.43}$$

For the point (α_m, T_m) of maximum reaction rate ($\mathrm{d}^2\alpha/\mathrm{d}t^2 = 0$), we find

$$\begin{aligned}0 = (\mathrm{d}f(\alpha_m)/\mathrm{d}\alpha)L\exp(-E/RT_m)\left(T_m - T_{eq}\right)/T_m \\ + E\beta/RT_m^2 + \beta\left(T_{eq}/T_m\right)/\left(T_m - T_{eq}\right)]\end{aligned} \tag{10.44}$$

which after multiplying by $(T_m/L)/(T_m - T_{eq})$ gives

$$-(\mathrm{d}f(\alpha_m)/\mathrm{d}\alpha)\exp(-E/RT_m) = \left(\beta/\left(T_m - T_{eq}\right)\right)(1/L)(E/RT_m + T_{eq}/\left(T_m - T_{eq}\right)) \tag{10.45}$$

By substitution $\beta = |\beta|\ \mathrm{sgn}(\beta)$ and upon using logarithm of Eq. (10.45), we obtain

$$-E/RT_m = \ln(|\beta|) - \ln\left[\left(T_m - T_{eq}\right)L\right] + \ln\left[\mathrm{sgn}(\beta)\left(E/RT_m + T_{eq}/\left(T_m - T_{eq}\right)\right)\right] - \ln[-(\mathrm{d}f(\alpha_m)/\mathrm{d}\alpha)] \tag{10.46}$$

The above argument $(T_m - T_{eq})L$ is positive if $[(L > 0 \wedge T_m > T_{eq})$ or $(L < 0 \wedge T_{eq} > T_m)]$ at endothermic process $(L > 0)$ and the maximum reaction rate is observed at a temperature higher than T_{eq} but at exothermic process $(L < 0)$, the maximum reaction rate is displayed at $T_m < T_{eq}$.

Differentiating Eq. (10.46) with respect to $(1/T_m)$, the following equation is found:

$$-E/R = \mathrm{d}\,\ln|\beta|/\mathrm{d}(1/T_m) + LT_m^2/\left(T_m - T_{eq}\right) + C \tag{10.47}$$

where $C = \mathrm{sgn}(\beta)[-E/R - T_{eq}T_m^2/(T_m - T_{eq})^2)]/[E/RT_m + T_{eq}/(T_m - T_{eq})]$ if $(\mathrm{d}f(\alpha_m)/\mathrm{d}\alpha)$ is assumed to be independent on T_m.

10.7 Conclusions

Reviewing problems at applications of Kissinger methods, we can come to the following closing stages:

There is a problem that the relation between TA signal and reaction rate is not as simple as it is assumed by the expedient procedure of Kissinger.

Application of Kissinger method on DSC curves measured by compensation DSC method (Perkin–Elmer) is, however, correct since such DSC signal is not distorted by heat inertia.

Application of Kissinger method on DTA curves uncorrected with respect to heat inertia is erroneous. The same is valid for curves obtained by heat flux DSC (i.e., calibrated DTA).

Application of Kissinger method on DTA as well as heat flux DSC curves is accepted when the as-cast curves are additionally corrected with respect to the heat inertia effect [27–29] or by impact of time lag [22, 91].

In some apparatus setups, the resulting DTA signal subsists an inbuilt experimental (software) adjustment already involving the heat inertia but correlated to the measure of time lag [22, 29, 91].

Application of Kissinger method on reaction rates obtained from TG curves (through differentiation with respect to time—DTG curve) is also capable of above fine-tuned rectification. Kinetic evaluations should conquer optimal experimental procedures [92], see Appendix 2.

There is a problem that Kissinger method based on standard kinetic Eq. (10.1) needs special requirements on the reaction mechanism model exploited for f(α). Equation (10.4) shows that Kissinger method based on Eq. (10.1) can be applied only if the derivative $\mathrm{d}f(\alpha)/\mathrm{d}\alpha$ and heating rate $\beta = \mathrm{d}T/\mathrm{d}t$ have different signs. For

processes studied at heating ($\beta > 0$), the value of $df(\alpha)/d\alpha$ has to be negative, and for processes taking place at cooling (such as crystallization of melt), the value of $df(\alpha)/d\alpha$ has to be positive. For any other cases, the condition of maximum reaction rate of Eq. (10.4) cannot be fulfilled.

For modifying standard kinetic equation in order to respect impact of equilibrium temperature (e.g., melting temperature, T_f), no simple relation has been obtained for condition of maximum reaction rate.

Generally, it seems that the Kissinger method is suitable for study of samples in thermodynamically metastable state (e.g., explosives and some glasses) where the exothermic process (reaction) is initiated by heating. Studies of sample which starting state is thermodynamically stable and becomes unstable after reaching the equilibrium temperature are not suitable for application of Kissinger method although the processes taking place at heating seem to give reasonable results. This impression is due to the fact that the higher equilibrium temperature is in standard kinetic model (cf Eq. 10.1) reflected in a higher value of activation energy because the standard model is not respecting equilibrium. If the Kissinger method is based on the standard kinetic model, then its application on processes taking place at cooling is impossible (because Eq. 10.4 cannot be fulfilled).

In general, it appears that description of the kinetics of the processes in solid state based on the standard kinetic Eq. (10.1), i.e., $\boldsymbol{r}(\alpha, T) = f(\alpha)\, k(T)$, is insufficient not only because of failure regarding its equilibrium background but predominantly because these processes, whether releasing or consuming heat, cause a nonuniform temperature field with steep thermal gradients. If the speed of the process depends on temperature, then it ought to depend on the whole set of local temperatures, too, and not on the single temperature measured on the sample holder, only.

For the better knowledge of the thermal state of solid sample, we should observe the necessity to introduce a novel generation of kinetic models (called as *thermokinetic models* [93]) expressing local kinetic equations in a form:

$$\mathbf{r}(\mathrm{T},\alpha) = \mathrm{F}(\mathrm{T},\alpha) = \mathrm{k}(\mathrm{T})\mathrm{f}(\alpha) \neq \mathrm{r}\{\alpha(\mathrm{r}),\mathrm{T}(\mathrm{r})\} \Rightarrow \mathrm{d}\alpha(\mathrm{r})/\mathrm{dt} = \Upsilon\{\alpha(\mathrm{r}),\mathrm{T}(\mathrm{r})\} \tag{10.48}$$

where the modified second Fourier law (for sample in the form of an infinite cylinder, r) along with the relation between the local transition rate $d\alpha(r)/dt$, localized degree of transition $\alpha(r)$, and resident spot-immediate temperature $T(r)$.

Acknowledgements The present work was developed at the Join Research Laboratory of the Institute of Physics CAS and the New Technologies Centre of the University of West Bohemia in Pilsen (the CENTEM project, reg. no. CZ.1.05/2.1.00/03.0088 that is co-funded from the ERDF as a part of the MEYS—Ministry of Education, Youth and Sports OP RDI Program and, in the follow-up sustainability stage supported through the CENTEM PLUS LO 1402). The abandoned support by the Grant Agency of ČR for the projected grant 'Thermal inertia and its significance for the analysis of DTA measurements' (No 17-21840S-2016) is worth mentioning as an example of fatal misunderstanding of current needs of thermal science. Deep thanks are due to long-lasting collaboration activity by J.J. Mareš, P. Hubík (Institute of Physics), J. Málek (University of Pardubice), N. Koga (Hiroshima University in Japan) and P. Šimon (The President of the Slovak Chemical Society, with Technical University in Bratislava).

Appendix 1: Gibbs Energy Approximations

For theoretical study on nucleation and crystal growth during solidification, the difference in Gibbs free energy between liquid and solid is usually expressed by various authors as ΔG, thus emerging in several theoretical formulations in phase transfer phenomena [4, 60, 94–96]. By definition, ΔG, is given by $\Delta G = \Delta H - T\Delta S$ which can be expanded using the popularly known expressions for ΔG and ΔS as

$$\Delta G = \Delta H_m \frac{\Delta T}{T_m} - \int_T^{T_m} \Delta C_p dT + T \int_T^{T_m} \Delta C_p \frac{dT}{T}$$

leading to $\Delta G = \Delta H\ \Delta T/T_{eq} + \Delta Cp\ (\Delta T)^2/2T\ (1 - \Delta T/6T)$.

While the enthalpy of melting, ΔH_m, is readily available for most materials, the difference in solid–liquid specific heats, ΔCp, is not, because its experimental measurements is difficult due to the liquid metastability. Hence, having ΔCp neglected and after approximating a meaningful value of ΔG, it gives simple $\Delta S_m\ \Delta T$ which is the most convenient and widely used expressions attributed to Turnbull [90] and valid over small undercooling (conventional solidification processes like casting). The value of ΔG is therefore overestimated which was approved by Thompson and Spaepen [97] for a linear ΔCp approximation yielding after simplification the more workable $\Delta G = \Delta S_m\ T\ \ln\ (T_m/T)$ which after expanding the logarithmic term can be extended to feasible $\Delta G = \Delta S_m\ \Delta T\ (2T/(T_m + T)$.

More recent attempts involve expansions involving higher powers of undercooling and incorporating theoretical quantities like *Kauzmann* temperature [60]. A noteworthy example and one that is applied in this work is a simple looking expression obtained by Lad et al. [98] upon using the series expansion, $\ln\left(1 - \frac{\Delta T}{T_m}\right) = \frac{\Delta T}{T_m} - \frac{\Delta T^2}{2T_m^2} + \frac{\Delta T^3}{3T_m^3} \ldots$ as to obtain a parabolic approximation for ΔG, leading to [98]

$$\Delta G = \Delta S_m \Delta T \left(1 - \frac{\Delta T}{2T_m}\right) \tag{10.49}$$

In the classical study by Hoffmann [60, 99], the constant ΔC_p was also assumed arriving at a simple approximation $\Delta G = \Delta H\ \Delta T/T_{eq}\ (T/T_{eq})$ while Dubay and Ramanchadro [100] proposed another specification as $\Delta G = \Delta H\ \Delta T/T_{eq}\ (2T)/(T_{eq} + T)$. By incorporating the third-order term in the TS-approximation, Ji and Pan [101] obtained more recently a new relation

$$\Delta G = 2\Delta S_m \Delta T \left(\frac{T}{T_m + T} - \frac{\Delta T^2 T_m}{3(T_m + T)^3}\right) \tag{10.50}$$

Pillai and Málek [96] used the arithmetic averaging to obtain an innovative approximation as

$$\Delta G = \Delta S_m \Delta T \left(\frac{T}{T_m + T} + \frac{T}{2T_m} \right) \tag{10.51}$$

In conclusion, it follows that for small undercoolings, the simplest form of the Turnbull [90] (see Paragraph 4) or Hoffmann [99] approximations can be readily used [60, 96]. However, when the liquid is deeply undercooled the other approximations should be preferred in conjunction with testing [60, 96]. In extreme when the liquid is undercooled down to the glass transition temperature (or even lower), the simple utilization of Turnbull becomes incorrect, thus recommending the arithmetic mean values such as Eq. (10.51).

Appendix 2: Experimental

Numerical evaluation and analysis of transformation kinetics is just an end consequence of specific experimental study often related to the so-called macro-system, i.e., giving way to analysis of bulk samples of certain property and treated under ordinary heat conditions often provided by commercial instruments. ICTAC Kinetic committee [50] presented a manual for kinetic analysis staying, however, on the surface of the problem citing. "The temperature used in the kinetic analysis must be that of the sample. Thermal analysis instruments control precisely the so-called reference temperature (T), whereas that of sample can deviates from it due to the limited thermal conductivity of the sample or due to the thermal effect of the process that may lead to self-heating/cooling." There is no comment that such a T-deviation is a factual instrumental response which is exploited for kinetic data determination [27, 28] under appeal of proper analyzing alongside with the impact of heat inertia [29]. Further "Typical approaches to diminishing the deviation of the sample temperature from the reference temperature are decreasing the sample mass as well as the heating rate" brining no clarification on the sample factual temperature due to both the gradients and the grain size structure. Neglecting the customary quandary towards the sample makeup (sample holder, mutual thermal contacts, in-weight, averaging, powdering, etc.) most important is the upcoming prospect of thermal analysis going down to the nano-dimensions and, in limit, to quantum world [102–105]. The experimentation may extend to the novel features touching the significance of temperature [93] during the ultrafast T-changes (see Chap. 3). Accordingly, we would need to recognized specialized fields of heat micro-transfer [104] exhibiting unusual assets still regarding validity of constitutive equations [105] but paying attention to the novel techniques based on highly sensitive thin microchips enabling rapid scanning microcalorimetry [67, 106, 107]. Particularity of the emerging area of nanomaterials can be studied by alteration calorimetry [108–112] forcing us to learn about its specificity (see Chap. 18)

providing extra dimension in thermodynamic description [113, 114]. The overall examination was the subject of our invited lectures [115, 116]. Moreover, it brought some unexpected consequences of non-constancy of certain thermodynamic values when severally diminishing particle curvature [117, 118]. It is just a short inventory of material basis wherein the kinetic analysis is employed and which should be kept in the researchers' attention in order to carry on a respectable kinetic study [46].

References

1. Standard Test Method for Arrhenius Kinetic Constants for Thermally Unstable Materials by DSC using Kissinger method (2001) ASTM International, 100 Barr Harbor Drive, PO Box C700, West Conshohocken, PA 19428-2959, United States
2. Svoboda R, Málek J (2014) Is the original Kissinger equation obsolete today? J Therm Anal Calorim 115:1961–1967; and Šesták J (2014) Is the original Kissinger equation obsolete today—not obsolete the entire non-isothermal kinetics? J Therm Anal Calorim 117:1173–1177
3. Blaine RL, Kissinger HE (2012) Homer Kissinger and the Kissinger equation. Thermochim Acta 540:1–6; and Kissinger HE (1956) Variation of peak temperature with heating rate in DTA. J Res Natl Bur Stand 57(4):217–221
4. Šesták J (1984) Thermophysical properties of solids: theoretical thermal analysis. Amsterdam: Elsevier and Russian translation: 'Těoretičeskij těrmičeskij analyz' Moscow: Mir 1988
5. Kissinger HE (1957) Reaction kinetics in differential thermal analysis. Anal Chem 29:1702–1706
6. Murray P, White J (1955) Kinetics of the thermal decomposition of clay; Part 4: Interpretation of DTA to thermal analysis of clays. Trans Brit Ceram Soc 54:204–237
7. Matusita K, Sakka S (1978) Kinetic study of crystallization by DTA: criterion and application of Kissinger plot. J Non-Cryst Sol 39:741–746; and (1979) Kinetic study of crystallization of glass by differential thermal analysis: criterion on application of Kissinger plot. Phys Chem Glasses 20:81–84
8. Augis JA, Bennet JE (1978) Calculation of Avrami parameters for heterogeneous solid-state reactions using a modification of Kissinger method. J Thermal Anal 13:283–292
9. Balarin M (1979) Is Kissinger's rule true? Thermochim Acta 33:341–343
10. Boswell PG (1980) On the calculation of activation energies using a modified Kissinger method. J Thermal Anal 18:353–358; and Elder JP (1985) The general applicability of the Kissinger equation in thermal analysis J Thermal Anal 30:657–669
11. Chen X, Gao D, Dollimore D (1993) A generalized form of the Kissinger equation. Thermochim Acta 215:109–117
12. Taylor SM, Fryer PJ (1992) Numerical study of the use of the Kissinger analysis of DSC thermograms to obtain reaction kinetic parameters. Thermochim Acta 209:111–125
13. Shishkin YuL (1985) Reaction kinetics calculated by the single-point method: a synthesis of DTA theory by Kissinger. J Thermal Anal 30:557–577
14. Llópiz J, Romero MM, Jerez A, Laureiro Y (1995) Generalization of the Kissinger equation for several kinetic models. Thermochim Acta 256:205–211
15. Sánchez-Jiménez PE, Criado JM, Pérez-Maqueda LA (2008) Kissinger kinetic analysis of data obtained under different heating schedule. J Thermal Anal Calor 94:427–432
16. Budrugeac P, Segal E (2007) Applicability of the Kissinger equation in thermal analysis. J Therm Anal Calor 88:703–707

17. Starink MJ (2007) Activation energy determination for linear heating experiments: deviations due to neglecting the low temperature end of the temperature integral. J Mater Sci 42:483; and Starink MJ (2004) Analysis of aluminium based alloys by calorimetry: quantitative analysis of reactions and reaction kinetics: a review. Int Mater Rev 49:191
18. Criado JM, Ortega A (1988) Nonisothermal transformation kinetics in relation to Kissinger method. J Non-Cryst Sol 87:302–311; and Koga N, Criado JM (1999) Application of the Kissinger method to solid-state reactions with a particle size distribution. J Min Metal 35:171–185
19. Budrugeac P (2007) The Kissinger law and the IKP method for evaluating the non-isothermal kinetic parameters. J Therm Anal Calor 89:111
20. Liu F, Liu XN, Wang Q (2009) Examination of Kissinger's equation for solid-state transformation. J Alloys Com 473:152–156; and Yi C, Yanchun L, Yunlong H (2010) Supplement on applicability of the Kissinger equation in thermal Analysis. J Therm Anal Calorim 102:605–608
21. Roura P, Farjas J (2009) Analytical solution for the Kissinger equation. J Mater Res 24:3095; and Farjas J, Butchosa N, Roura P (2010) A simple kinetic method for the determination of the reaction model from non-isothermal experiments. J Thermal Anal Calorim 102:615–625
22. Farjas J, Roura P (2014) Exact analytical solution for the Kissinger equation: determination of the peak temperature and general properties of thermally activated transformations. Thermochim Acta 508:51–58
23. Peng C, Chen ZH, Zhao XY, Zhang AL, Zhang KL, Chen D (2014) Crystallization kinetics of $Zr_{60}Cu_{25}Fe_5Al_{10}$ bulk metallic glass. J Non-Cryst Sol 405:7–11
24. Huang C, Mei X, Cheng Y, Li Y, Zhu X (2014) A model-free method for evaluating theoretical error of Kissinger equation. J Therm Anal Calorim 116:1153–1157; and (2010) Supplement on applicability of the Kissinger equation in thermal analysis. J Therm Anal Calorim 102: 605–608
25. Holba P, Šesták J (2014) Imperfections of Kissinger evaluation method and crystallization kinetics. Glass Phys Chem 40:486–549
26. Šesták J (2012) Citation records and some forgotten anniversaries in thermal analysis. J Thermal Anal Calor 109:1–5
27. Holba P., Šesták J, Sedmidubský D (2013) Heat transfer and phase transition at DTA experiments. In: Šesták J, Šimon P (eds) Thermal analysis of Micro-, nano- and non-crystalline materials. Springer, Berlin, pp 99–134 (Chapter 5) (ISBN 978-90-481-3149-5)
28. Šesták J, Holba P (2013) Heat inertia and temperature gradient in the treatment of DTA peaks existing on every occasion of real measurements but until now omitted. J Therm. Anal Calorim 113:1633–1643
29. Holba P, Šesták J (2015) Heat inertia and its role in thermal analysis. J Thermal Anal Calor 121:303–307
30. Vold MJ (1949) Differential thermal analysis. Anal Chem 21:683–688
31. Šesták J (2012) Rationale and fallacy of thermoanalytical kinetic patterns: how we model subject matter. J Thermal Anal Calor 110:5–16
32. Zsako J (1996) Compensation effect in heterogeneous non-isothermal kinetics. J Therm Anal 47:1679–1690
33. Koga N, Šesták J (1991) Kinetic compensation effect as a mathematical consequence of the exponential rate constant. Thermochim Acta 182:201–208
34. Galwey AK, Mortimer M (2006) Compensation effects and compensation defects in kinetic and mechanistic interpretations of heterogeneous chemical reactions. Int J Chem Kinet 38:464–473
35. Holba P, Šesták J (1972) Kinetics with regard to the equilibrium of processes studied by non-isothermal techniques. Zeit physik Chem NF 80:1–20
36. Holba P (2013) Equilibrium background of processes initiated by heating and the Ehrenfest classification of phase transitions. In: Šesták J, Šimon P (eds) Thermal analysis of micro-,

nano- and non-crystalline materials. Springer, Berlin, pp 29–52 (Chapter 2) (ISBN 978-90-481-3149-5)
37. Mianowski A (2009) Consequences of Holba-Šesták equation reflecting processes equilibria. J Thermal Anal Calorim 96:507–513
38. Mianowski A (2003) The Kissinger law and isokinetic effect: most common solution and thermokinetic equation. J Thermal Anal Calorim 74:953–973; and (2004) The Kissinger law and isokinetic effect: experimental analysis. J Thermal Anal Calor 75:355–373
39. Agresti F (2013) Extended Kissinger equation for near-equilibrium solid-gas heterogeneous transformations. Thermochim Acta 566:214–217
40. Baumann W, Leineweber A, Mittermeijer EJ (2010) Failure of Kissinger (-like) method for the determinative of activation energies of phase transitions. J Mater Sci 45:6075–6082
41. Yao Z, Qiao JC, Zhang C, Yao Y (2015) Non-isothermal crystallization transformation kinetics analysis and isothermal crystallization kinetics in super-cooled liquid region of bulk metallic glasses. J Non-Cryst Sol 415. Doi:10.1016/j.jnoncrysol.2015.02.017; and Gong P, Zhao S, Wang X, Yao K (2015) Non-isothermal crystallization kinetics and glass-forming ability of $Ti_{41}Zr_{25}Be_{28}Fe_6$ bulk metallic glass investigated by differential scanning calorimetry. Appl Phys A 120. Doi:10.1007/s00339-015-9182-4
42. Šesták J (2005) Nonisothermal kinetics by thermal analysis. Chapter 11 in his book: science of heat and thermophysical studies: a generalized approach to thermal analysis. Elsevier, Amsterdam, pp 318–343 (ISBN 0-444-51954-8)
43. Šesták J, Kozmidis-Petrović A, Živković Ž (2011) Crystallization kinetics accountability and the correspondingly developed glass-forming criteria. J Min Metall Sect B-Metall 47:229–239
44. Koga N, Šesták J, Šimon P (2013) Some fundamental and historical aspects of phenomenological kinetics in solid-state studied by thermal analysis. In: Šesták J, Šimon P (eds) Thermal analysis of micro-, nano- and non-crystalline materials. Springer, Berlin, pp. 1–45 (Chapter 1) (ISBN 978-90-481-3149-5)
45. Illeková E, Šesták J (2013) Crystallization of metallic micro-, nano- and non-crystalline glasses. In: Šesták J, Šimon P (eds) Thermal analysis of Micro-, nano- and non-crystalline materials. Springer, Berlin, pp 257–290 (Chapter 13) (ISBN 978-90-481-3149-5)
46. Šesták J (2015) The quandary aspects of non-isothermal kinetics beyond the ICTAC kinetic committee recommendations. Thermochim Acta 611:26–35
47. Illeková E (1984) On the various activation energies at crystallization of amorphous metallic materials. J Non-Cryst Sol 68:153–216
48. Galwey AK (2003) What it meant by the term 'variable activation energy' when applied in the kinetic analysis of solid state decompositions? Thermochim Acta 397:49–268
49. Galwey AK (2006) What theoretical and/or chemical significance is to be attached to the magnitude of an activation energy determined for a solid-state decomposition? J Therm Anal Calor 86:267–286
50. Vyazovkin S, Burnham AK, Criado JN, Perez-Maqueda LA, Popescu C, Sbirrazzuoli N (2011) ICTAC Kinetics Committee recommendations for performing kinetic computations on thermal analysis data. Thermochim Acta 520:1–19
51. Málek J, Criado JM (1992) Empirical kinetic models in thermal analysis. Thermochim Acta 203:25–30
52. Málek J (1995) The applicability of Johnson-Mehl-Avrami (JMAYK) model in the thermal analysis of crystallization kinetics of glasses. Thermochim Acta 267:61–73
53. Mamleev V, Bourbigot S, LeBras M, Duquesne S, Šesták J (2000) Modeling of nonisothermal kinetic mechanism in thermogravimetry. Phys Chem Chem Phys 2:4708–4716
54. Avramov I, Šesták J (2014) Generalized kinetics of overall phase transition explicit to crystallization. J Therm Anal Calorim 118:1715–1720
55. Šimon P (2011) Forty years of Šesták-Berggren equation. Thermochim Acta 520:156–157
56. Šesták J (2015) The Šesták-Berggren equation: now questioned by formerly celebrated—what is right? J Therm Anal Calorim. Doi:10.1007/s10973-015-4998-x; and Militký J,

Šesták J (2016) On the eliminating attempts toward Sestak-Berggren equation. J Therm Anal Calorim. Doi:10.1007/s10973-016-5848-1
57. Atkinson HV (1988) Theories of normal grain growth in pure single phase systems. Acta Metall 36:469–491
58. Illeková E (2001) Finemet-type nano-crystallization kinetics. Thermochim Acta 387:47–56
59. Kozmidis-Petrovic AF, Šesták J (2013) Forty years of Turnbul reduced glass transition temperature and Hrubý glass-forming coefficient and their current perception ib glass characterization. In: Šesták J, Šimon P (eds) Thermal analysis of micro-, nano- and non-crystalline materials. Springer, Berlin, pp 75–98 (Chapter 4) (ISBN 978-90-481-3149-5)
60. Šesták J (1991) Phenomenology of glass crystallization. In: Chvoj Z, Šesták J, Tříska A (eds) Kinetic phase diagrams: nonequilibrium phase transitions. Elsevier, Amsterdam, pp 169–176 (Chapter 6) (ISBN 0-444-88513-7)
61. Ruitenberg FG (2003) Applied Kissinger analysis to the glass transition peak in amorphous metals. Thermochim Acta 404:2007–2011
62. Soliman AA (2007) Derivation of the Kissinger equation for nonisothermal glass transition peaks. J Thermal Anal Calorim 89:389–392
63. Mehta M, Kumar A, Pratap A (2007) Applicability of Kissinger relation in the determination of activation energies of glass transition processes. J Optoelect Adv Mater 7:1473–1478; and (2012) Kinetics of crystallization of $Zr_{52}Cu_{18}Ni_{14}Al_{10}Ti_6$ metallic glass. J Therm Anal Calor 17:159–165; and (2012) Study of kinetics of glass transition of metallic glasses. J Therm Anal Calor 110:567–571
64. Svoboda R, Čičmanec P, Málek J (2013) Kissinger equation versus glass transition phenomenology. J Therm Anal Cal 114:285–293
65. Zhang Z, Chen J, Liu H (2014) Applicability of Kissinger model in nonisothermal glass crystallization using a computer simulation method. J Therm Anal Calorim 117:783–787; and Gong P, Zhao S, Ding H, Yao K, Wang X (2015) Nonisothermal crystallization kinetics, fragility and thermodynamics of $Ti2_0Zr_{20}Cu_{20}Ni_{20}Be_{20}$ high entropy bulk metallic glass. J Mater Res 30:2772–2782; and Zhu M, Li J, Yao L (2013) Non-isothermal crystallization kinetics and fragility of $(Cu_{46}Zr_{47}Al_7)_{97}Ti_3$ bulk metallic glass investigated by differential scanning calorimetry. Thermochim Acta 565:132–136
66. Holba P, Šesták J (2014) Imperfections of Kissinger evaluation method and its impact on crystallization kinetics. Russian Fizika i Khimiya Stekla 40:645–657
67. Orava J, Greer AL (2015) Kissinger method applied to the crystallization of glass-forming liquids: regimes revealed by ultra-fast-heating calorimetry. Thermochim Acta 603:63–68
68. Zhao B, Li L, Lu F, Zhai Q, Yang B, Schick C, Gao Y (2015) Phase transitions and nucleation mechanisms in metals studied by nanocalorimetry: a review. Thermochim Acta 603:2–23
69. Schultze D (1969) Differentialthermoanalyze. VEB, Berlin
70. Smykats-Kloss W (1974) Differential thermal analysis. Springer, Berlin
71. Pope MI, Judd MD (1977) Differential thermal analysis. Heyden, London
72. Höhne GWH, Hemminger W, Flammersheim HJ (2010) Differential scanning calorimetry. Springer, Dortrecht
73. Egunov VP (1996) Введение в термический анализ (Introduction to thermal analysis) Samara
74. Wendlandt WW (1964) Thermal methods of analysis. Wiley, New York
75. Šesták J, Šatava V, Wendlandt WW (1973) The study of heterogeneous processes by thermal analysis, monography as a special issue of Thermochimica Acta, vol 7. Elsevier, Amsterdam
76. Chen R, Kirsh Y (1981) Analysis of thermally stimulated processes. Pergamon Press, Oxford, pp 109–110
77. Boerio-Goates J, Callen JE (1992) Differential thermal methods. In: Rossiter BW, Beatzold RC (eds) Determination of thermodynamic properties. Wiley, New York, pp 621–718 (Chapter 8)

78. Borchadt HJ. (1956) Differential thermal analysis. J Chem Educ 33:03–109; and Borchard HJ, Daniels F (1957) The application of DTA to the study of reaction kinetics. J Amer Chem Soc 79:41–46
79. Blumberg AA (1959) DTA and heterogeneous kinetics: the reactions of vitreous silica with HF. J Phys Chem 63:1129
80. Piloyan GO (1964) Введение в теорию термического анализа (Introduction in theory of thermal analysis), Izd. Nauka, Moskva
81. Piloyan GO, Ryabchikov IO, Novikova SO (1966) Determination of activation energies of chemical reactions by DTA. Nature 3067:1229
82. Holba P, Nevřiva M, Šesták J (1974) Utilization of DTA for the determination of heats of the transformation of solid-solutions Mn_3O_4-Mn_2CrO_4. Izv. AN SSSR, Neorg. Materialy 10:2007–2008 (in Russian)
83. Šesták J, Holba P, Bárta R (1976) Teorie a praxe termoanalytických metod založených na indikaci změn tepelného obsahu (Theory a practice of thermoanalytical methods based on indication of heat content changes) Silikáty 20:83–95
84. Šesták J, Holba P, Lombardi G (1977) Quantitative evaluation of thermal effects: theory and practice. Anal Chim 67:73–87
85. Holba P, Nevřiva M, Šesták J (1978) Analysis of DTA curve and related calculation of kinetic data using computer technique. Thermochim Acta 23:223–231
86. Holba P (1987) Processing of thermoanalytical curves and exact use of thermal analysis Thermochimica Acta 110:81–85; and Šesták J (1979) Thermodynamic basis for the theoretical description and correct interpretation of thermoanalytical experiments. Thermochim Acta 28:197–227
87. Šesták J (2005) Thermometry and calorimetry. Chapter 12 in his book: science of heat and thermophysical studies: a generalized approach to thermal analysis. Elsevier, Amsterdam, pp 344–375 (ISBN 0-444-51954-8)
88. Vyazovkin S (2002) Is the Kissinger equation applicable to the processes that occur on cooling? Macromol Rapid Commun 23:771–775
89. Sunol JJ, Berlanga R, Clavaguera-Mora MT, Clavaguera N (2002) Modeling crystallization processes and transformation diagrams. Acta Mater 50:4783–4790A
90. Turnbull D (1969) Under what conditions can a glass be formed? Contemp Phys 10:473–488; and (1950) Kinetics of heterogeneous nucleation. J Chem Phys 18:198–203
91. Mouchina E, Kaisersberger E (2009) Temperature dependence of the time constants for deconvolution of DSC heat flow curves. Thermochim Acta 492:101–109
92. Šesták J (2015) Kinetic phase diagrams as a consequence of radical changing temperature or particle size. J Thermal Anal Calor 120:129–137
93. Šesták J (2016) Measuring "hotness": should the sensor's readings for rapid temperature changes be named "tempericity"? J Thermal Anal Calorim 125:991–999; and Holba P (2016) Šesták's proposal of term "tempericity" for non-equilibrium temperature and modified Tykodi's thermal science classification with regards to methods of thermal analysis. J Thermal Anal Calor. Doi:10.1007/s10973-016-5659-4
94. Vehkamäki H (2006) Classical nucleation theory in multicomponent systems. Springer, Berlin/Heidelberg
95. Glicksmann ME (2011) Principles of solidification. Springer, Berlin/Heidelberg
96. Pillai SKS, Málek J (2014) On approximating of thermodynamic driving force in deeply undercooled melts. Sci Papers University Pardubice, Series A20:263–272
97. Thompson C, Spaepen F (1979) On the approximation of the free energy change on crystallization. Acta Metall 27:1855
98. Lad K, Raval K, Pratap A (2004) Estimation of Gibbs free energy difference in bulk metallic glass forming alloys. J Non Cryst Solids 335:259
99. Hoffman JD (1958) Thermodynamic driving force in nucleation and growth processes. J Chem Phys 29:1192
100. Dubey SK, Ramachandrarao P (1984) On the free energy change accompanying crystallization of undercooled melts. Acta Metal 32:91

101. Ji X, Pan Y (2007) Gibbs free energy difference in metallic glass forming liquids. J Non Cryst Solids 353:2443
102. Mareš JJ, Šesták J (2005) An attempt at quantum thermal physics. J Therm Anal Calor 82:681–686
103. Gemmer J, Michel M, Mahler G (2009) Quantum thermodynamics: emergence of thermodynamic behavior within composite quantum systems. Springer, Heidelberg
104. Volz S (2007) Microscale and nanoscale heat transfer. Springer, Heidelberg
105. Mareš JJ, Šesták J, Hubík P (2011) Transport constitutive relations, quantum diffusion and periodic reactions. In: Šesták J, Mareš JJ, Hubík P (eds) Glassy, amorphous and nano-crystalline materials (Chapter 14), Springer, Heidelberg, pp 227–244
106. Adamovsky AS, Minakov AA, Schick C (2003) Scanning microcalorimetry at high cooling rate. Thermochim Acta 403:55–63
107. Adamovsky AS, Schick C (2004) Ultra-fast calorimetry using thin film sensors. Thermochim Acta 415:1–7
108. Höhne GWH (2003) Calorimetry on small systems—a thermodynamic contribution. Thermochim Acta 403:25–36
109. Wunderlich B (2007) Calorimetry of nanophases of macromolecules. Inter J Thermophys 28:958–967
110. Garden JL, Guillou H, Lopeandia AF, Richard J, Heron JS (2009) Thermodynamics of small systems by nanocalorimetry: from physical to biological nano-objects. Thermochim Acta 492:16–28
111. Perepezko JH, Glendenning TW, Wang JQ (2015) Nanocalorimnetry measurements of metastable states. Thermochim Acta 603:24–28
112. Zhao B, Li L, Lu F, Zhai Q, Yang B, Schick C (2015) Phase transitions and nucleation mechanisms studied by nanocalorimetry: a review. Thermochim Acta 603:2–23
113. Wautelet M, Duvivier D (2007) The characteristic dimensions of the nanoworld. Europ J Phys 28:953–959
114. Wautelet M, Shyrinian AS (2009) Thermodynamics: nano vs. macro. Pure Appl Chem 81:1921–1930
115. Šesták J, Mareš JJ (2014) Invited plenary lecture: composite materials and thermodynamics of nano-structured systems. Inter. Conference on composite nano-engineering in Saint Julian, Malta
116. Šesták J, Invited lectures (2015) Thermal physics of nanostructured materials: thermodynamic (top-down) and quantum (bottom-up) issues. Inter. Thermodynamic conference in Nizhny Novgorod (Russia) and European TA Conference in Ljubljana (Slovenia)
117. Kaptay G (2008) A unified model for the cohesive enthalpy, critical temperature, surface tension and volume thermal expansion of liquid metals and crystals. Mater Sci Eng A 495:19–26
118. Cantwell PR, Tang M, Dillon SJ, Luo J, Rohrer GS, Harmer MP (2014) Grain boundary complexions: overview. Acta Mater 62:1–48

Chapter 11
Thermo-kinetic Phenomena Occurring in Glasses: Their Formalism and Mutual Relationships

Roman Svoboda, Jiří Málek and Jaroslav Šesták

Abstract In the present chapter, the macroscopic (recorded by methods of thermal analysis) manifestation of the structural relaxation and cold crystallization phenomena occurring in the glassy matrices will be discussed. Present formalism and methodological background are reviewed. Equilibrium viscous flow is introduced as an interconnecting element between the two phenomena. The consequent part then deals with the rheological and viscosity-related aspects of the glassy state itself. Viscosity behavior in view of so-called fragility is renovated in terms of thermal sensitivity. The chapter contains 98 references.

11.1 The Kinetics of the Structural Relaxation and Crystallization Processes in Terms of the Tool-Narayanaswamy-Moynihan and Johnson-Mehl-Avrami Models

11.1.1 Structural Relaxation Kinetics by TNM Model

The Tool-Narayanaswamy-Moynihan (TNM) model [1–3] belongs nowadays to well-known and commonly used models describing structural relaxation in the glass transition region. Popularity of this concept dwells in its immense flexibility (given by the phenomenological character of the model), its general acceptance by the respective scientific community (the model reflects the main features [4, 5] of the structural relaxation processes—hysteresis, nonlinearity, memory effects, and

R. Svoboda (✉) · J. Málek
Department of Physical Chemistry, Faculty of Chemical Technology, University of Pardubice, Studentská 573, 532 10 Pardubice, Czech Republic
e-mail: roman.svoboda@upce.cz

J. Šesták
New Technologies Research Centre (NTC-ZČU), University of West Bohemia, Universitní 8, 30114 Pilsen, Czech Republic
e-mail: sestak@fzu.cz

J. Šesták et al. (eds.), *Thermal Physics and Thermal Analysis*, Hot Topics in Thermal Analysis and Calorimetry 11,
DOI 10.1007/978-3-319-45899-1_11

non-exponentiality), and its validity (the TNM model was shown to accurately describe structural relaxation data for large variety of glassy and amorphous materials; see e.g., [6–10]). In addition, the TNM model belongs among the few theoretical concepts that are actually algorithmized [11, 12] to provide description of the raw experimental curves obtained either by differential scanning calorimetry (DSC), dilatometry (DIL), or thermo-mechanical analysis (TMA).

The TNM model is a four-parameter phenomenological model, where the dependence of relaxation time τ on structure is based on the Tool's concept [1] of fictive temperature T_f. Narayanaswamy [2] and Moynihan [3] later modified this concept, and the resulting equation can be expressed as follows:

$$\tau = A_{\mathrm{TNM}} \left[\frac{x\Delta h^*}{\mathrm{RT}} + \frac{(1-x)\Delta h^*}{\mathrm{RT}_f} \right], \tag{11.1}$$

where A_{TNM} is the pre-exponential factor, x is the nonlinearity parameter, Δh^* is the apparent activation energy of the structural relaxation, R is the universal gas constant, T is temperature, and T_f is the fictive temperature. The nonlinearity of structural relaxation is in this model defined using the parameter x that determines the ratio of how much the relaxation is influenced by structure and temperature, respectively.

The second important requirement for the relaxation model is to reflect the distribution of relaxation times. That is in the TNM model realized by using the stretched exponential function:

$$F = \exp\left[-\left(\int_0^t \frac{\mathrm{d}t}{\tau} \right)^{\beta} \right], \tag{11.2}$$

associated with the names of Kohlrausch [13], Williams, and Watts [14] (referred to as the KWW equation). The exponent β ($0 \leq \beta \leq 1$) is inversely proportional to the width of distribution of relaxation times, and F is a conventional relaxation function.

The TNM model has been intensively tested over past decades. The pioneers of this model were Rekhson [15], Moynihan and co-workers [16], and Hodge and co-workers [11, 12, 17]—all these authors report remarkably good ability of the model to describe the characteristic features of structural relaxation. Nevertheless, the TNM model is nowadays known to have certain shortcomings. Firstly, it is based on the assumption of thermo-rheological simplicity; i.e., the distribution of relaxation times is expected to be independent from experimental conditions. This can in case of certain materials lead to only partially successful description of the relaxation data, where different relaxation parameters are obtained if the relaxation behavior is investigated for moderately and heavily relaxed glass, respectively. In addition, the endeavor of the TNM model to cope with the so-called τ_{eff} paradox reported by Kovacs [18] also gives rise to several discrepancies [7, 8].

However, despite these minor shortcomings, the TNM model is still THE choice if one needs to describe and interpret the structural relaxation behavior in the vicinity of T_g. Considering the relevant competing models and concepts, probably the closest regarding both performance and fundamental principle comes the Adam–Gibbs–Hodge equation [19, 20], which employs similar stretched exponential function [Eq. (11.2)] but uses different expression for the relaxation time:

$$\tau = A_{\mathrm{AGH}} \exp\left[\frac{Q}{T(1 - T_{\mathrm{K}}/T_{\mathrm{f}})}\right] \tag{11.3}$$

where A_{AGH} is the pre-exponential factor, Q is the parameter related to the activation energy of the relaxation process, and T_{K} is the temperature at which the configurational entropy of liquid would vanish (in practice this temperature is identical to the so-called Kauzmann temperature [21]). The AGH model is very similar to the TNM one and suffers from the same shortcomings; in fact, the similarity of the two models is so high that very good correlations exist between the parameters of the two models [6]. The AGH model usually provides slightly worse description of the experimental data; it has slightly better theoretical background [7] (its parameters Q and T_{K} do have physical meaning), but the practical structural interpretation of the TNM relaxation parameters that was recently developed [10] gives edge to the TNM model.

The second competing model is the coupling model [22] developed by Ngai:

$$F = \exp\left[-\left(\int_0^t \frac{\mathrm{d}t}{\tau^*}\right)^{1-n}\right], \tag{11.4}$$

$$\tau^* = \left[(1-n)\omega_c^n \tau_0\right]^{1/(1-n)}, \tag{11.5}$$

where the Eq. (11.4) is formally similar to Eq. (11.2)—parameter n represents the coupling parameter ($0 \leq n \leq 1$; strength of coupling increases with n. The relevant relaxation variable initially decays at a constant rate τ_0^{-1} but very soon at timescales for which $\omega_c t \gg 1$ (where ω_c is a critical frequency, typically in the range 10^9–10^{10} s^{-1}) the rate becomes explicitly time-dependent [22]. The main advantage of the coupling model is that the parameter n is inherently a function of both—temperature and structure, i.e., the model is thermo-rheologically complex. The latter allows the model to reproduce [23] very well the Kovacs τ_{eff} paradox (it is the value of the parameter n that determines the magnitude of the so-called expansion gap). Despite its larger potential, the coupling model was not yet adjusted to model the raw calorimetric or dilatometric relaxation data—various $n(t, T_{\mathrm{f}})$ dependences would have to be tested to determine the simplest suitable solution.

Although the TNM phenomenology bears potential for very precise and meaningful characterization of relaxation behavior, the true quality of the description of experimental data depends on the correctness and accuracy of the

determination of the model parameters. In this regard, there are generally two methodological approaches for treating the TNM parameters evaluation—curve-fitting and the application of indirect non-fitting methods. Recently a series of methodological guides [24–28] has been published regarding the detailed evaluation methodologies for the TNM relaxation parameters from DSC data. As the primary goal of most non-expert researchers is to determine activation energy of the glass transition process, special attention should be paid to [28], where a very accurate and precise method was developed for the determination of apparent activation energy Δh^* from so-called constant ratio [26] cycles:

$$-\frac{\Delta h^*}{R} = \left[\frac{\mathrm{d}\,\ln|q^+|}{\mathrm{d}(1/T_\mathrm{p})}\right]_{q^-/q^+=\mathrm{const.}}, \tag{11.6}$$

where q^+ and q^- are the applied heating and cooling rates (within the given cycle over T_g) and T_p is the temperature of the maximum of the relaxation peak. This equation, however, exhibits a slight systematic shift from the true Δh^* values (approx. 5% error for the most common materials). Precise value of Δh^* can then be calculated using the following relationship [28]:

$$\Delta h^*_{e.v.} = 4.218 \times 10^{-5} z^2 + 4.841 \times 10^{-2} z + \left[9.885 \times 10^{1}/(z - 1.276)\right], \tag{11.7}$$

where z stands for true value of $\Delta h^*/R$ and $\Delta h^*_{e.v.}$ represents the positive percent error of the evaluation by Eq. (11.6) [28]. It was further demonstrated [26] that this method is completely independent from most data-distortive effects and thus very reliable and easy to apply. Note that Eq. (11.6) formally reminds the Kissinger-type equations; however, one should bear in mind that these equations were derived for simple thermally activated processes and cannot be used (without the application of proper constant ratio cyclic thermal history where q^+/q^- = const.) to evaluate activation energy of glass transition [29, 30].

As was stated in the introductory text, the structural relaxation process can be correlated with various other thermo-kinetic quantities and processes. In particular, the dynamic viscosity η was found to exhibit similar value of activation energy of viscous flow E_η (determined in the glass transition range $\sim 10^{12}$–10^{13} Pa s) as was the value of Δh^* found for the same material [31–33]. This correlation is not surprising as the relaxation time is directly proportional to dynamic viscosity [34]:

$$\eta = G_\infty \cdot \tau, \tag{11.8}$$

where G_∞ stands for the infinite-frequency shear modulus. As a result, also the kinetic fragilities determined based on both structural relaxation and dynamic viscosity are believed to well correlate. Note that the extensive variability of material's behavior during the solidification can be recognized from both, steepness of the viscosity change with temperature and rate at which excess entropy changes at T_g. Angell [35] has introduced his viscosity classification based on the

differentiation of the material's behavior in-between the "strong" and "fragile" extremes, using T_g as a scaling parameter, with the corresponding quantity being denoted as "kinetic fragility". The kinetic fragility, m, is defined as [35]:

$$m = \left.\frac{\mathrm{d}\log\eta}{\mathrm{d}(T_g/T)}\right|_{T=T_g} \cong \frac{E_\eta/R}{T_g\ln(10)}, \tag{11.9}$$

while the enthalpic kinetic fragility m_{ent} is defined as [36]:

$$m_{ent} = \left.\frac{\mathrm{d}\log\tau}{\mathrm{d}(T_g/T)}\right|_{T=T_g} \cong \frac{\Delta h^*/R}{T_g\ln(10)}. \tag{11.10}$$

Nevertheless, recently a decoupling of the two types of kinetic fragilities was reported [37] for certain glassy systems. A possible explanation regarding the increased viscosity fragilities involves the influence of dynamic structural heterogeneity (density fluctuations and clustering of structural elements) on shear viscosity in the glass transition region. In particular, the observed decoupling seems to occur in case of the materials exhibiting moderate-to-high activation energy of relaxation processes and large structural cooperativity. The origin of the fragility decoupling may lie either in different molecular movements being involved in the two processes (viscous flow versus structural relaxation) or in their different manifestation in terms of volume and enthalpy behavior [37].

Regarding the cold crystallization process, there is no explicit direct interdependence between the crystallization and relaxation behaviors. However, the two processes do influence each other. It was shown in [38] that while the maximum of the relaxation peak (and thus Δh^* determined from the CR cycles) is not influenced by small degree of glass crystallinity, the curve-fitting and non-fitting evaluation of Δh^* from CHR cycles were significantly influenced, exhibiting larger values of apparent activation energy and smaller ΔC_p. The structural relaxation processes, on the other hand, can also to a certain extent influence the nucleation and crystal growth—there are number of materials that exhibit sub-T_g nucleation, where the formation and consequent behavior of the nuclei can be influenced by the state (compactness) of the surrounding structure. In addition, although above T_g, all structural relaxation effects produced by applied thermal history are erased, certain stress- and strain-induced defects persist and can either act as nucleation centers or accelerate crystal growth [39].

11.1.2 Crystallization Kinetics by JMA Model

The Johnson–Mehl–Avrami (JMA) model [40–43] belongs among the so-called sigmoidal models, the initial and final stages of which exhibit characteristic accelerating and decelerating behavior, respectively. In this way, the process rate

reaches its maximum at some intermediate degree of conversion α—contrary to e.g., power law models (only accelerating) or reaction order and diffusion models (only decelerating) [44]. The concept of the JMA model is based on the idea of the so-called extended volume V_e of the transformed phase, i.e., the volume the transformed phase would acquire if the overlap among growing nuclei was nonexistent. The essence of the JMA model can then be expressed by the following equation [40–43]:

$$\alpha(t) = 1 - e^{-V_e(t)}, \tag{11.11}$$

where the extended volume is a simple function of time (considering crystallization under isothermal conditions, where the nucleation rate N and crystal growth rate G are constant).

$$V_e = K(N, G)t^n. \tag{11.12}$$

The JMA parameter n can then be interpreted in terms of the dimensionality of the formed crystallites. The applicability of the JMA model originally required the following conditions: single isothermal crystallization mechanism based on the nucleation and consequent growth occurs, nucleation sites are distributed randomly throughout the glassy matrix, critical size of the nuclei is negligible, anisotropy of the growing crystals is low [40–43]. It was pointed out later [45, 46] that the JMA model validity can be extended to non-isothermal conditions if nucleation is completed during the early stages of the overall process and becomes negligible afterward.

In practice, the JMA model is used mainly to describe the crystallization data obtained by differential scanning calorimetry (DSC) or differential thermal analysis (DTA)—common studies involve either a set of non-isothermal measurements performed at different heating rates or set of isothermal measurements performed at different temperatures. The basic kinetic equations are as follows [47]:

$$\frac{d\alpha}{dt} = Ae^{-E/RT} f(\alpha), \tag{11.13}$$

$$\frac{d\alpha}{dt} = \frac{1}{q^+ \Delta H} \int \Phi dT, \tag{11.14a}$$

$$\frac{d\alpha}{dt} = \frac{1}{\Delta H} \int \Phi dt, \tag{11.14b}$$

where Eqs. (11.14a) and (11.14b) hold for the non-isothermal and isothermal conditions, respectively. The meaning of the particular symbols follows—$d\alpha/dt$ is reaction/transformation rate, Φ is the measured heat flow, ΔH is the crystallization enthalpy, A is the pre-exponential factor, E is the apparent activation energy of the process, R is the universal gas constant, q^+ is heating rate, and $f(\alpha)$ stands for an

expression of a kinetic model with α being conversion. The $f(\alpha)$ function for the JMA model can then be expressed as follows:

$$f(\alpha) = n(1-\alpha)[-\ln(1-\alpha)]^{1-(1/n)}. \tag{11.15}$$

As there are numerous methodological guides (see e.g., [44]) dealing with the kinetic analysis [enumeration of Eq. (11.13)] of simple crystallization processes, the following paragraphs will be focused on the so-called complex crystallization mechanisms. Complex processes can be characterized as those during which at least two different mechanisms proceed simultaneously. It was found only recently, that most real-life solid-state processes and reactions are in fact complex, and the occurrence (magnitude of manifestation) of the process complexity is only the question of applied experimental conditions. Nowadays, the topic of kinetic analysis of complex processes is strongly accentuated and starts to be of major interest for scientists dealing with solid-state kinetics.

The possibility to implement the JMA model into kinetic evaluations of the complex crystallization processes is therefore very important. There are basically three major approaches to the evaluation of complex kinetic processes: 1. kinetic analysis of the overall process (provides only qualitative information about the particular sub-processes), 2. mathematic deconvolution followed by single-process kinetic analysis, 3. kinetic deconvolution. Concerning the first approach, it involves application of the standard methods of kinetic analysis on the overall complex processes and the subsequent interpretation of the results. The isoconversional methods (Friedman [48] and modified Kissinger–Akahira–Sunose [49] methods being the most common) designed for determination of E are the especially important in this regard [44]. As these methods provide the dependence of E on degree of conversion α, using them, it is theoretically possible to determine the activation energies for the involved sub-processes by taking into account the appropriate α-intervals. However, in practice, the correct E values are obtained only in case when small overlaps occur and major parts [50]; otherwise, the activation energies are averaged within the overlap interval. On the other hand, it is quite common for the complex crystallization processes that all the sub-processes have similar apparent activation energy and in that case the averaging introduced by the isoconversional methods does not matter—this premise can be simply verified by comparing the raw DSC kinetic peaks obtained for the lowest and highest q^+ (if valid, the peaks will be of similar shape with similar degree of overlap) [50]. In addition to the isoconversional methods, also the simpler E calculations based on the temperature values corresponding to the maxima of the kinetic peaks (e.g., the original Kissinger equation [51]) can be utilized for the evaluation of complex crystallization processes; it was shown [50] that the E values provided by these methods correspond very accurately to the activation energy of the dominant/most rapid kinetic sub-processes. Apart from the activation energy E, certain information about the kinetic model can be also derived based on the simple kinetic analysis of the overall complex crystallization data. In case of only lowly overlapping sub-processes the combined kinetic analysis [52] can provide reliable information

on both of them even if the overall response is evaluated. On the other hand, in case of fully overlapped processes, it is the characteristic kinetic functions (master plots) [53] that can be used to extract some information—this methodology denoted as "advanced interpretation" [54] has, however, its limitations. Three cases are interesting in particular: firstly, if one of the sub-processes manifests only weakly, the master plots corresponding to the dominant sub-process are almost unaffected and can be interpreted with only little error. Secondly, in case of fully parallel overlapping JMA processes, the $z(\alpha)$ master plot correctly predicts the applicability of the JMA model and the $y(\alpha)$ master plot indicates the dimensionalities of all the types of occurring crystallites and the ratio of their representation [54]. Lastly, in case of generic apparent single-peak complex process, the master plots very reliably (unlike the E-α dependences) reveal the possible complex character of the crystallization (usually shoulders or double maxima occur) [54].

The second approach to the kinetic analysis of complex processes is based on a mathematic deconvolution of the complex kinetic data and the consequent analysis of the deconvoluted sets of data (corresponding to the particular sub-processes) by means of usual single-process methodologies [55]. Regarding the mathematic functions, the Fraser–Suzuki equation [Eq. (11.16)] [56] showed ability to accurately describe most kinetic models [56]. Note that selection of appropriate mathematic function is the key for the correct deconvolution—nowadays variety of unacceptable functions (e.g., Gauss, Lorentz, Voigt, and Pearson.) is still regularly used in literature.

$$y = a_0 \exp\left[-\ln 2\left[\frac{\ln\left(1+2a_3\frac{x-a_1}{a_2}\right)}{a_3}\right]^2\right]. \tag{11.16}$$

Nonetheless, even with the appropriate mathematic function, the deconvolution procedure does not need to be unambiguous (especially in case of largely overlapped processes) and an iterative approach to the deconvolution needs to be adopted. If the consequent kinetic analysis of deconvoluted data shows that some kinetic peaks were deconvoluted incorrectly (the results do not match the rest of the dataset), then during the repeated deconvolution certain restrictions should be applied to force the most clearly pre-determined kinetic parameter (usually the asymmetry of the peak). This approach is particularly beneficial in case of complex crystallization processes, where the JMA model is often used. It was shown in [57] that JMA kinetic peaks exhibit a characteristic asymmetry; hence, the appropriate restriction of parameter a_3 in Eq. (11.16) results in mathematic deconvolution with certainty of the resulting kinetic analysis leading to the JMA behavior. Regarding the main cons of the approach, major disadvantage of the mathematic deconvolution is the necessary assumption of the sub-processes being independent, the iterative procedure as such is also rather tedious and time-demanding. On the other hand, this is the only approach that can appropriately describe the highly complex

processes, where the complexity changes with experimental conditions (usually with q^+ and T for non-isothermal and isothermal measurements, respectively) [55].

The third approach to the kinetic analysis of complex processes is then represented by direct kinetic deconvolution of the whole set of measured data. The method of multivariate kinetic analysis [58] [Eqs. (11.17) and (11.18)] absolutely dominates in this field.

$$\mathrm{RSS} = \sum_{j=1}^{n} \sum_{k=\mathrm{First}_j i}^{\mathrm{Last}_j} w_{j,k} \left(Y\exp_{j,k} - Y\,\mathrm{cal}_{j,k} \right)^2, \tag{11.17}$$

$$w_{j,k} = \frac{\sum_{j=1}^{n} \left(\mathrm{Last}_i - \mathrm{First}_i \right)}{n\left(\mathrm{Last}_j - \mathrm{First}_j \right) \left[\mathrm{abs}\left(\mathrm{Max}\left(Y\exp_{j,k} \right) \right) + \mathrm{abs}\left(\mathrm{Min}\left(Y\exp_{j,k} \right) \right) \right]}, \tag{11.18}$$

where RSS is the sum of squared residua determined during curve-fitting, n is number of measurements, j is index of the given measurement, First_j is the index of the first point of the given curve, Last_j is the index of the last point of the given curve, Y $\exp_{j,k}$ is the experimental value of the point k of curve j, Y $\mathrm{cal}_{j,k}$ is the calculated value of the point k of curve j, and $\mathrm{w}_{j,k}$ is weighting factor for the point k of curve j. Note that the expression for $w_{j,k}$ [Eq. (11.18)] is optimized for the DSC measurements, so that each measured curve is weighted despite the different number of measured points and increased errors due to the magnifying influence of heating rate on measured heat flow [58].

The largest benefit of multivariate kinetic analysis is the direct provision of all the kinetic parameters for all involved sub-processes. It can be also accommodated to account for various dependences between the particular sub-processes (e.g., consecutive, parallel, competing, switching, inhibiting, catalyzing, or independent reactions) and to calculate with rather complex reaction schemes [58]. In this way, the multivariate kinetic analysis provides opportunity to either fit the observed kinetic behavior as accurately as possible (mostly for practical predictive purposes) or to conduct a detailed study regarding physically meaningful identification of the involved reaction mechanisms. Direct kinetic deconvolution by means of the multivariate kinetic analysis can also deal with some of the less common crystallization processes following either zero-order or even accelerating kinetics (usually surface-located fully defects-based growth) [58]. The only disadvantage of the above-described method is that it cannot easily account for the change of model mechanisms with experimental conditions (q^+, T)—here only a slightly easier iterative approach (compared to the modified Fraser–Suzuki approach introduced as the mathematical deconvolution) has to be adopted, based on the successive evaluations of data subsets corresponding to the acceptably narrow intervals of applied experimental conditions (with either fixed or variable E).

Since the multivariate kinetic analysis is not easily algorithmized, several other "hybrid" approaches were recently developed. Quite successful solution was introduced in [59], where the kinetic deconvolution using only the three-exponent autocatalytic Šesták–Berggren function (SB) [47] in the following form was used:

$$f(\alpha) = \alpha^M (1-\alpha)^N [-\ln(1-\alpha)]^P, \tag{11.19}$$

where M, N, and P are empirical parameters. Considering that Eq. (11.19) is a general expression from which the JMA model [Eq. (11.15)] can be derived, the kinetic deconvolution based on the SB function can be very beneficial with respect to the complex crystallization processes, where practically only the JMA and SB models are used. Another solution was introduced in [60], where a reverse deconvolution algorithm (simulation of large amount of data with slightly varying JMA or SB parameters and their consequent comparison with the experimental data; best correlation coefficient was the criterion of choice) was used. Both these approaches have, however, the disadvantage of assuming complex kinetic behavior with strictly independent sub-processes (in addition to not accounting for the possible variation of the reaction/crystallization mechanism with experimental conditions).

As was shown in the previous paragraphs, even in case of complex kinetic processes, a physically meaningful answer can be obtained if the state-of-art methodologies are utilized. This is particularly important for the complex macroscopic crystallization, where the JMA kinetic exponent n indicates dimensionality and general location (surface versus bulk) of the growing crystallites [54, 55]. Since the JMA model describes (in case of crystallization) the macroscopic manifestation of nucleation and crystal growth, the value of parameter n cannot be directly linked to the other thermo-kinetic phenomena (structural relaxation, viscous flow) mentioned in the introductory part. However, both the nucleation and crystal growth are already closely associated with these phenomena. As mentioned at the end of Sect. 11.1.1, the structural relaxation can (together with the corresponding viscous flow) in certain cases influence the nucleation of the material exhibiting sub-T_g formation of the nuclei. In addition, it was shown in [39] that for some materials the nucleation can be influenced by stress-induced and mechanically induced defects, the existence and persisting of which are also closely interlinked with the relaxation and viscous flow phenomena. Furthermore, the microscopic crystal growth is directly driven by viscosity via the Turnbull–Cohen formula [61]. Note that for number of materials the isothermal crystal growth rate corrected for thermodynamic driving force u_{kin} exhibits a weaker temperature dependence than viscosity: $u_{\text{kin}} \sim \eta^{-\xi}$ (where $\xi < 1$). This type of decoupling can be observed over many orders of magnitude for chemically quite dissimilar systems; hence, it appears to reflect a general behavior. In [62], it was claimed that this decoupling is caused by properties of the liquid and not by properties of crystal surface—the exponent ξ was found to be strongly correlated with fragility.

11.2 General Consideration Regarding Thermal Behavior in the Neighborhood of Glass Transition Temperature

11.2.1 Dynamic Cooperative Performance

In pursuit of promoting the life concept of late B. Hlaváček [63–76], liquids can be assumed to consist of a mechanically divided structure formed by blocks (or, if you like, floes, domains, clusters) [72, 73] and on the other hand by the individual "semi-evaporated" units, which are subjected to nonlinear anharmonic motions of high amplitudes [64–67]. Implicitly, the highly nonlinear oscillators maintain the particular character of their motions functioning as simple individual units about a monomer size. Conversely, the blocks are assumed to possess interconnected microstructure (see Fig. 11.1) and are composed of identical elastically bonded particles packed to the high density. Correspondingly, the glass [72, 76] is understood as a mechanically heterogeneous substance where that blocks are characterized by stiffed (glassy-solid) phase interconnected by short stretched molecules. Besides blocks in the glassy state, some embryonic states become existing as a certain precursor of cavities which get enlarging above the glass transformation temperature, T_g.

Above critical crossover temperature, T_{cr}, the termination of "bridge-over" effect can be acquainted with the level of shear modulus contributed by bridging descend down to zero. The isolated blocks can remind a structure as "floating icebergs" restricting the considerations on glassy system to a Newtonian-like liquid trying to avoid the entropic rubber-like share interrelated to elasticity. The scheme in [72, 73] provides furthermore an assessment toward the critical number of elements inside

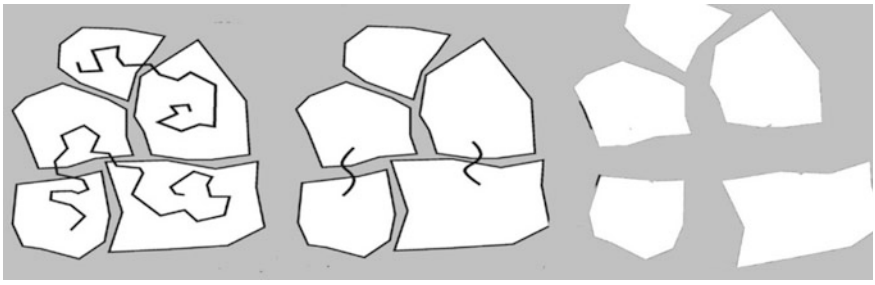

Fig. 11.1 Illustrative picture of a liquid-like (as well as derived glassy) structure composed of variously bonded blocks illustrating the degree of possible coupling below T_g, at T_{cr} and above. When the separation of blocks interconnected by macromolecules occurs above critical temperature, T_{cr} it results to rubber elasticity often associated with the so-called entanglement. Low molecular compounds, however, never achieve such a rubbery state and the dissection can be found on the basis of rheological measurements of shear viscosity. The internal energy related to shear module disappears above the crossover temperature T_{cr} for which the relation $T_g \approx 0.8\ T_{cr}$ holds approximately

the heterogeneity of domains which becomes determinable from the shear viscosity data. Surprisingly it furnishes an estimate of the universal number, n, in range of about 605–660 units regardless of the chemical structure of monomers [77]. Parameter n decreases with increasing temperature when considering the shear modulus arising through the deformation of observed body under a response cohesive energy.

Simply portrayed n can be perceived to apprehend on a sacred geometry arising out of the set of numbers from the Fibonacci series in which each number is the sum of the previous two (i.e.,…377 ↔ 610 ↔ 987…) often used to explain harmony, creation, and growth in nanoworld, i.e., from a number of petals on a flower to the arrangement of golden nanoparticles up to the grandiose architecture of galaxies [77]. It is also in a good agreement with literature [78] following the data from the extend relaxation spectra of main transition zone by Tobolsky [79] and an estimate for the size of acoustic segments by Heuer and Spiess [80].

The following sequence of characteristic temperatures can be esteemed as experimentally discriminated on liquid cooling, i.e., from the boiling point temperature, T_m, to crossover temperature T_{cr}, glass transition temperature, T_g, down to the Vogel's temperature T_v recognizing sequential link: $T_m \geq T_{cr} \geq T_g \geq T_v$. Just this sequence will follow the proposed model taking in account distinct characteristics of vibration modes at different temperature areas. It can be related to the shape of parallel form of van der Waals curve the bottom part on the liquid side, which plays the important role for the evaluation of nonlinear amplitude size. The onset of the spinodal part of the van der Waals curve seems to poses a sensible restrain on the upper amplitude of vibration motion. If exceeding this limit, it gives the lead to vacancy enlargement in which the particles in vicinity of high-amplitude oscillator have to take away the vibration energy of particle, by their own "avalanche-like" displacement. This type of energy withdrawal from high-amplitude vibrating particle can only be productively performed by particles in the vicinity below the liquid point T_m, without the destruction of a sample (through e.g., the configuration of a gas phase within the sample bulk). Between the crossover temperature T_{cr} and the boiling point, the high amplitudes of vibration are able to mechanically perturb the original bonding of blocks to such a level that shear module disappears. Below T_{cr}, the substantial rise in shear module G becomes a factor as a new component limiting the vacancy enlargement as the sample is capable to store the elastic energy connected to shear module [64–66]. Above the crossover temperature, the diffusion process is driven mainly by few particles standing out of the block areas, which are undergoing the amplitudes switch. Thus, the relation formed by product of viscosity, size of the diffusing particles, and diffusion coefficient cannot retain its figure. For approximate value on a hole number at T_g (so-called magic ratio 1/40) and accounting on the associated rheological point of view, the rapid fall of the shear module is caused as the substances start to flow while entering liquid-like state. The T_v state represents a starting point of the main transition zone with a subsequent thermal activation and the vacancies

development as the temperature rise toward T_g and the start of the validity of well-known Williams–Landel–Ferry (WLF) equation [81, 82].

$$\ln\left(\frac{\eta_T}{\eta_{T_g}}\right) = \ln a_T = \frac{-17.4(T - T_g)}{51.6 + (T - T_g)} \tag{11.20}$$

where T_g is used as a reference temperature (instead the original T_{ref}) settled on constructing the compliance master curve specifically for 17.4 = C_1 and 51.6 = C_2 where C's are WLF empirical constants adjusted to fit the values of the so-called superposition parameter a_T. Worth of reminding is that the classical Vogel–Fulcher–Tammann (VFT) equation is often used to explain the temperature dependence of the zero-shear viscosity η_T with respect to the relaxation times τ_T valid for not too high temperatures in the range between glass transition T_g and (T_g + 100) [in °C]. It mathematically looks like $\tau_T = \tau_o \exp(B/(T - T_o))$ making available a certain similarity with WLF through $C_2 = T_{ref} - T_o$ and $B = 2.303\ C_1C_2$ [83].

Roughly, we can assume that $T_v \approx 0.8\ T_g$, and above this temperature, all particles start to relocate while the diffusion process sets on which means that within hours, days, or even years the external shape of sample will change. The upswing in the C_p value takes place at T_v and at T_g; the expansion coefficient, α_{exp}, undergoes a stepwise change assuming $T_g \approx 1/3$ up to 2/3 of melting temperature according to the glass-forming tendency [84, 85].

11.2.2 Shear Viscosity, Fragility, and Thermal Sensitivity

In the main transition zone, the Angell's renowned equation [86–92] is dealing with the shear viscosity derivative relatively to inverse absolute temperature as introduced in connection to the substance fragility, i.e.,

$$m = \frac{\delta \ln \eta}{\delta\left(\frac{T_g}{T}\right)} = -\frac{\delta \ln \eta}{\delta \ln T}\left(\frac{T}{T_g}\right) \tag{11.21}$$

Here, we stay behind the specific symbolic originally employed by Hlaváček (δ, ω) [63–65]. This Eq. (11.21) is telling to some extent about the speed of viscosity decrease relatively to the temperature rise. Thus, it enables ranking and systematic classifications of the substances relatively to the viscosity behavior in view of so-called *fragility*. This quantity, however, should be better called the *thermal sensitivity* [76, 93] because of an alternative expression

$$m \cong \frac{\delta \ \ln \frac{G^{//}(\omega,T)}{\omega}}{\delta\left(\frac{T_g}{T}\right)} \tag{11.22}$$

where the quantity G represents the Young's module of elasticity in shear, the η_{Sh} stands for the shear viscosity assuming additionally $\omega \cong \gamma \cong 1/t$, where ω represents the angular frequency, γ is the steady shear velocity gradient, and t is the time of relaxation (eventually the time variable for the creep function). Matching the validity for the dynamical complex modulus $G^*\left(\ \omega\, a_T^*\ \right)$ and using the complex dynamical viscosity, Hlaváček [76, 93] concluded that

$$\eta^*\left(\omega a_T^*\right) = \frac{G^*\left(\omega a_T^*\right)}{\omega a_T^*} \tag{11.23}$$

while accepting the correspondence to real and/or imaginary components of module. For the linear viscoelastic measurements, the dynamical viscosity is related to the complex dynamical module G^* through the standard relationships. The module G^* contains the two components of real $G^{/}(\omega)$ and imaginary parts $G^{//}(\omega)$ of the dynamical module: $\eta^* = G^*/\omega$.

For the comparison of shear viscosity, η_{SH} (under a steady state constant gradient of velocity) and by action of the dynamical viscosity $\eta^* = G^*/\omega$, we can formulate termination which is valid over a large and expanded area of frequencies and gradients. It stems from the fact that the shortly observed quantity of viscosity or modulus in the logarithmic scale against temperature appears graphically in the main transition zone rather approximate. Therefore, the use of fragility should be preferably bound to the linear viscoelastic functions in time or to the frequency representations under dynamical experiments coining thus a new term of above mentioned generalized thermal sensitivity.

By keeping the Angel structure [86–95], such a more general expression can gain a recognition when reflecting the main transition interval in a broader time zone, temperature area, frequency, and the velocity gradients, e.g.,

$$\mathrm{m} \ = \frac{\delta \ \ln\left(\frac{\frac{T_g\ \rho_{T_g}}{T\ \rho_T}\left|G^*\left(\omega\, a_{T_g}^*\right)\right|}{\omega\, a_{T_g}^*} - \frac{\frac{T_g\ \rho_{T_g}}{T\ \rho_T}\left|G^*\left(\omega\, a_T^*\right)\right|}{\omega\, a_T^*}\right)}{\delta\left(\frac{T_g}{T}\right)} \tag{11.24}$$

The symbols ρ_T and ρ_{T_g} are corresponding to the densities of the substance at the temperatures T and T_g and $G^*\left(\omega\, a_T^*\right)$ expresses the dynamic module on basis of dynamic viscosity. $\eta^*\ (\omega\ a_T,\ T)$, see Eq. (11.23).

On bases of experimental observations, the stepwise change in derivative of the product of diffusion and viscosity π indicates the higher transition in liquid state at T_{cr}.

$$\pi = \frac{\delta(1/D\eta_{sh})}{\delta(1/T)} \tag{11.25}$$

where D is the diffusion coefficient, and δ is again the Hlaváček's symbol for derivative (traditionally d). It seems useful to mention that for the Newtonian liquids it takes place setting up that:

$$\frac{D\eta_{sh}\phi}{k_B T} \cong 0.154 \quad \text{for} \quad T \geq T_{cr} \tag{11.26}$$

where ϕ is the hard-core diameter of particles, which mildly depends on temperature, and k_B is the Boltzman's constant. Equation (11.26) reveals [72–74] that the parameter π changes a sign at $T = T_{cr}$ and the product of $1/\eta_{sk}$ decreases sharply for $T \leq T_{cr}$ by many decades. If the shear viscosity of sample reflects just the addition of individual particles viscosities to take part within the blocks, under the crossover temperature $T \geq T_{cr}$, a new quality emerges in a form of the samples elastic behavior.

Under T_{cr}, the response to shear force gets new contribution as a result of new structures of elastic bridges between the isolated blocks [64], cf. Fig. 11.1, so that for $T \leq T_{cr}$ we have to incorporate into the shear viscosity the part of viscosity arising from elasticity of new bridged structures, i.e.,

$$\eta_{sh} = \eta_{block} \quad \text{for} \quad T \geq T_{cr} \quad \text{and} \quad G(t,T) = 0 \tag{11.27}$$

$$\eta_{sh} = \eta_{block} + \Theta G(t,T) \quad \text{for} \quad T \leq T_{cr} \quad \text{and} \quad G(t,T) \geq 0 \tag{11.28}$$

where Θ is the relaxation time of sample, being about 10^{-7} s at $T = T_{cr}$ and about $10^2 - 10^3$ s at $\approx T_g$. As the consequence of bridging, a sudden grow in shear modulus $G_{t,T}$ from zero level at T_{cr} to level of about $10^9 - 10^{10}$ Pa at T_g will have major impact on the viscosity level in form of a viscoelastic contribution to viscosity.

The reflection on the micro-processes of diffusion bears also an important stimulus for a better understanding of quantum thermal physics [96] in relation to the quantum aspects of self-organized periodical chemical reactions [97, 98] which is subject treated in the other chapters of this compendium.

Acknowledgements This work was supported by the Czech Science Foundation under project No. 16-10562S (Svoboda, Málek) as well as by the Ministry of Education of the Czech Republic in the framework of CENTEM PLUS project (LO1402) operated under the "National Sustainability Program I" (Šesták).

References

1. Tool AQ (1946) Relation between inelastic deformability and thermal expansion of glass in its annealing range. J Am Ceram Soc 29:240–253
2. Narayanaswamy OS (1971) A model of structural relaxation in glass. J Am Ceram Soc 54:491–497
3. Moynihan CT, Easteal AJ, DeBolt MA, Tucker J (1976) Dependence of the fictive temperature of glass on cooling rate. J Am Ceram Soc 59:12–16
4. Scherer GW (1986) Relaxation in glass and composites. Wiley
5. McKenna GB (1989) Glass formation and glassy behavior. In: Comprehensive polymer science 2, pergamon
6. Hodge IM (1994) Enthalpy relaxation and recovery in amorphous materials. J Non-Cryst Sol 169:211–266
7. Angell CA, Ngai KL, McKenna GB, McMillan PF, Martin SW (2000) Relaxation in glass forming liquids and amorphous solids. J Appl Phys 88:3113–3157
8. Hutchinson JM (1995) Physical aging of polymers. Prog Polym Sci 20:703–760
9. Liška M, Chromčíková M (2005) Simultaneous volume and enthalpy relaxation. J Therm Anal Calorim 81:125–129
10. Svoboda R (2013) Relaxation processes in Se-rich chalcogenide glasses: Effect of characteristic structural entities. Acta Mater 61:4534–4541
11. Hodge IM, Berens AR (1982) Effects of annealing and prior history on enthalpy relaxation in glassy polymers. 2. Mathematical modeling. Macromolecules 15:762–770
12. Hodge IM, Berens AR (1985) Effects of annealing and prior history on enthalpy relaxation in glassy polymers. 5. Mathematical modeling of nonthermal presaging perturbations. Macromolecules 18:1980–1984
13. Kohlrausch F (1866) Beitrage zur Kenntniss der elastichen Nachwirkung. Ann Phys Chem 128:1–20
14. Williams G, Watts DC (1970) Non-symmetrical dielectric relaxation behavior arising from a simple empirical decay function. Trans Faraday Soc 66:80–85
15. Rekhson SM, Bulaeva AV, Mazurin OV (1971) Change in linear dimensions and viscosity of window glass during stabilization. Izv Akad Nauk SSSR Neorg Mater 7:714–715
16. DeBolt MA, Easteal AJ, Macedo PB, Moynihan CT (1976) Analysis of structural relaxation in glass using rate heating data. J Am Ceram Soc 59:16–21
17. Hodge IM (1987) Effects of annealing and prior history on enthalpy relaxation in glassy polymers. 6. Adam-Gibbs formulation of nonlinearity. Macromolecules 20:2897–2908
18. Kovacs AJ (1963) Transition vitreuse dans les polymers amorphes – Etude phenomenologique. Fortschr Hochpolym Forsch 3:394–507
19. Adam G, Gibbs JH (1965) On the temperature dependence of cooperative relaxation properties in glass-forming liquids. J Chem Phys 43:139–146
20. Hodge IM (1997) Adam-Gibbs formulation of enthalpy relaxation near the glass transition. J Res Natl Inst Stand Technol 102:195–205
21. Kauzmann W (1948) The nature of the glassy state and the behavior of liquids at low temperatures. Chem Rev 43:219–256
22. Ngai KL (1994) Disordered effects in relaxation processes. Springer
23. Rendell RW, Ngai KL, Fong GR, Aklonis JJ (1987) Volume recovery near the glass-transition temperature in polyvinylacetate—predictions of a coupling model. Macromolecules 20:1070–1083
24. Svoboda R, Málek J (2013) Description of macroscopic relaxation dynamics in glasses. J Non-Cryst Solids 378:186–195
25. Svoboda R (2014) How to determine activation energy of glass transition. J Therm Anal Calorim 118:1721–1732

26. Svoboda R (2014) Utilization of "q^+/q^- = const." DSC cycles for enthalpy relaxation studies. Eur Polym J 59:180–188
27. Svoboda R (2015) Utilization of constant heating rate DSC cycles for enthalpy relaxation studies and their influenceability by error data-distortive operations. J Non-Cryst Sol 408:115–122
28. Svoboda R (2015) Novel equation to determine activation energy of enthalpy relaxation. J Therm Anal Calorim 121:895–899
29. Svoboda R, Čičmanec P, Málek J (2013) Kissinger equation versus glass transition phenomenology. J Therm Anal. Cal 114:285–293
30. Svoboda R, Málek J (2013) Glass transition in polymers: (in)correct determination of activation energy. Polymer 54:1504–1511
31. Málek J, Svoboda R, Pustková P, Čičmanec P (2009) Volume and enthalpy relaxation of a-Se in the glass transition region. J Non-Cryst Solids 355:264–272
32. Hodge IM (1991) Adam-Gibbs formulation of non-linear enthalpy relaxation. J Non-Cryst Sol 131–133:435–441
33. Chromčiková M, Liška M (2006) Simple relaxation model of the reversible part of the StepScan DSC record of glass transition. J Therm Anal Calorim 84:703–708
34. Dyre JC, Christensen T, Olsen NB (2006) Elastic models for the non-Arhenius viscosity of glass-forming liquids. J Non-Cryst Sol 352:4635–4642
35. Martinez LM, Angell CA (2001) A thermodynamic connection to the fragility of glass-forming liquids. Nature 410:663–667
36. Yang G, Gulbiten O, Gueguen Y, Bureau B, Sangleboeuf JC, Roiland C, King EA, Lucas P (2012) Fragile-strong behavior in the As_xSe_{1-x} glass forming system in relation to structural dimensionality. Phys Rev B 85:144107
37. Svoboda R, Málek J (2015) Kinetic fragility of Se-rich chalcogenide glasses. J Non-Cryst Sol 419:39–44
38. Svoboda R, Honcová P, Málek J (2010) Apparent activation energy of structural relaxation for $Se_{70}Te_{30}$ glass. J Non-Cryst Solids 356:165–168
39. Svoboda R, Málek J (2014) Nucleation in As_2Se_3 glass studied by DSC. Thermochim Acta 593:16–21
40. Avrami M (1939) Kinetics of phase change I—general theory. J Chem Phys 7:1103–1112
41. Avrami M (1940) Kinetics of phase change. II—transformation-time relations for random distribution of nuclei. J Chem Phys 7:212–224
42. Avrami M (1941) Granulation, phase change, and microstructure—kinetics of phase change III. J Chem Phys 7:177–184
43. Johnson WA, Mehl KF (1939) Reaction kinetics in processes of nucleation and growth. Trans Am Inst Min (Metall) Eng 135:416–442
44. Vyazovkin S, Burnham AK, Criado JM, Pérez-Maqueda LA, Popescu C, Sbirrazzuoli N (2011) ICATC Kinetics Committee recommendations for performing kinetic computations on thermal analysis data. Thermochim Acta 520:1–19
45. Henderson DW (1979) Experimental analysis of non-isothermal transformations involving nucleation and growth. J Therm Anal 15:325–331; and (1979) Thermal analysis of non-isothermal crystallization kinetics in glass-forming liquids. J Non-Cryst Sol 30:301–315
46. Kemeny T, Šesták J (1987) Comparison of crystallization kinetics determined by isothermal and nonisothermal methods. Thermochim Acta 110:113–121
47. Šesták J (1984) Modeling reaction mechanism by use of Euclidean and fractal geometry, Chapter 10 in his book: thermophysical properties of solids, their measurements and theoretical analysis. Elsevier, pp 276–314 (ISBN 13978-0-444-51954-2); and (2015) The Šesták-Berggren equation: now questioned but formerly celebrated—what is right? J Therm Anal Calorim. doi:10.1007/s10973-015-4998-x
48. Friedman HL (1964) Kinetics of thermal degradation of char-forming plastics from thermogravimetry. Application to a phenolic plastic, Wiley

49. Starink MJ (2003) The determination of activation energy from linear heating rate experiments: a comparison of the accuracy of isoconversion methods. Thermochim Acta 404:163–176
50. Svoboda R, Málek J (2014) Is the original Kissinger equation obsolete today? J Therm Anal Calorim 115:1961–1967
51. Kissinger HE (1957) Reaction kinetics in differential thermal analysis. Anal Chem 29:1702–1706
52. Perez-Maqueda LA, Criado JM, Malek J (2003) Combined kinetic analysis for crystallization kinetics of non-crystalline solids. J Non-Cryst Sol 320:84–91
53. Málek J (2000) Kinetic analysis of crystallization processes in amorphous materials. Thermochim Acta 355:239–253
54. Svoboda R, Málek J (2011) Interpretation of crystallization kinetics results provided by DSC. Thermochim Acta 526:237–251
55. Svoboda R, Málek J (2014) Crystallization kinetics of a-Se, part 2: deconvolution of a complex process—the final answer. J Therm Anal Cal 115:81–91
56. Perejón A, Sánchéz-Jiménez PE, Criado JM, Pérez-Maqueda LA (2011) Kinetic analysis of complex solid-state reactions. A new deconvolution procedure. J Phys Chem B 115:1780–1791
57. Svoboda R, Málek J (2013) Applicability of Fraser-Suzuki function in kinetic analysis of complex processes. J Therm Anal Cal 111:1045–1056
58. Opferman J (2000) Kinetic analysis using multivariate non-linear regression. J Therm Anal Calorim 60:641–658
59. Nakano M, Wada T, Koga N (2015) Exothermic behavior of thermal decomposition of sodium percarbonate: kinetic deconvolution of successive endotermic and exothermic processes. J Phys Chem A 119:9761–9769
60. Honcová P, Svoboda R, Pilný P, Sádovská G, Barták J, Beneš L, Honc D (2016) Kinetic study of dehydration of calcium oxalate trihydrate. J Therm Anal Calorim 124:151–158
61. Turnbull D (1950) Formation of crystal nuclei in liquid metals. J Appl Phys 21:1022–1028
62. Ediger MD, Harrowell P, Yu L (2008) Crystal growth kinetics exhibit a fragility-dependent decoupling from viscosity. J Chem Phys 128:034709
63. Hlaváček B, Carreau PJ (1975) Correlation between linear and non-linear viscoelatic data for polymer solutions. In: Walters K, Hutton JF, Pearson JRA (eds) Theoretical rheology. Applied Science Publishers, London (ISBN 9780853346388)
64. Hlaváček B, Šesták J (2009) Structural changes in liquids, creation of voids, micromovemets of vibrational centers and built-in blocks toward the glass transition temperature. Chapter 18. In: Šesták J, Holeček M, Málek J (eds) Thermodynamic, structural and behavior aspects of materials accentuating non-crystalline states. OPS-ZČU Plzeň, pp 388–411 (ISBN 978-80-87269-06-00, second edition 2011 (ISBN 978-80-87269-20-6)
65. Šesták J, Hlaváček B, Hubík P, Mareš JJ (2013) Vibrational forms in the vicinity of glass transition, structural changes and the creation of voids when assuming polarizibility. Chapter 3. In: Šesták J, Mareš J, Hubík P (eds) Glassy, amorphous and nano-crystalline materials. pp 41–58. Springer, Berlin (ISBN 978-90-481-2881-5)
66. Šesták J (2004) Oscillation modes and modern theories of glassy state. Chapter 14. In: Heat, thermal analysis and society. Nucleus, Hradec Kralove, pp 242–247 (ISBN 8086225-54-2)
67. Šesták J (2015) Dynamic cooperative behavior of constituting species at the glass transition vicinity: inspirational links to B. Hlaváček (1941-2014) legacy. J Therm Anal Calor. 120:167–173
68. Hlaváček B, Černošková E, Prokůpek L, Večeřa M (1996) Transition points in liquid state and their molecular modeling. Thermochim Acta 280(281):417
69. Hlaváček B, Křesálek V, Souček J (1997) Anharmonicity of motion in the liquid state and its consequences. J Chem Phys 107:4658–4667
70. Hlaváček B, Souček J, Prokůpek L, Večeřa M (1997/1998) The thermal entropy concept and T_g transition. J Polym Eng 17:111–137

71. Hlaváček B, Shánělova J, Málek J (1999) The discontinuities in amplitudes of particles micromotions in liquid state. Mech Time-Depend Mater 3:351–370
72. Hlaváček B, Šesták J, Mareš JJ (2002) Mutual interdependence of partitions functions in vicinity T_g of transition. J Therm Anal Cal 67:239
73. Hlaváček B, Šesták J, Koudelka L, Mošner P, Mareš JJ (2005) Forms of vibrations and structural changes in liquid state. J Therm Anal Cal 80:271–283
74. Hlaváček B, Drašar Č, Kalendová A, Mencl P, Šesták J, Veselý D (2013) Glassy state, as the lawfully disarranged state: vibration uncertainty and chaos like movements. Phys Procedia 44:52–59 (ISSN: 1875-3892)
75. Málek J, Svoboda R (2013) Structural relaxation and viscosity behavior in supercooled liquids at the glass transition, Chapter 7. In: Šesták J, Šimon P (eds) Thermal analysis of micro, nano- and non-crystalline materials. Springer, Berlin, pp 147–174 (ISBN 978-90-481-3149-5)
76. Hlaváček B, Mareš JJ (2008) Fyzika struktur amorfních a krystalických materiálů. In: Šesták J (ed) Physics of structures of amorphous and crystalline materials. Public House of the Pardubice, Pardubice (in Czech - ISBN 978-80-7395-023-1)
77. Bradley P (2010) Great mysteries. New Holland, New York
78. Schultz JM (1974) Polymer material science. Prentice Hall, Englewood, New Jersey (ISBN 013-6870-38-4)
79. Tobolsky AV (1960) The properties and structure of polymers. John Wiley, New York (ISBN 047-1875-81-3)
80. Heuer A, Spiess HW (1994) Universality of glass transition temperature. J Non-Cryst Solids 176:294–299
81. Ferry JD (1961) Viscoelastic properties of polymers, 3rd edn. Wiley, New York (1980—ISBN: 978-0-471-04894-7)
82. Williams M, Landel R, Ferry JD (1955) The temperature dependence of relaxation mechanisms in amorphous polymers and other glass-forming liquids. J Amer Chem Soc 77:3701–3707
83. Liu CY, He JS, Keunings R, Bailly R (2006) New linearized relation for the universal viscosity-temperature behavior of polymer melts. Macromolecules 39:8867–8869
84. Šesták J (1985) Some thermodynamic aspects of the glassy state. Thermochim Acta 95:13–459
85. Queiroz C, Šesták J (2010) Aspects of the non-crystalline state. Phys Chem Glass Eur J Glass Sci Technol B 51:165–168
86. Angell CA (1988) Perspective on the glass transition. J Phys Chem Sol 49:863–871
87. Angell CA (1991) Relaxation in liquids, polymers and plastic crystals—strong/fragile patterns and problems. J Non-Cryst Solids 131(133):13–31
88. Beiner M, Huth H, Schroter K (2001) Crossover region of dynamics glass transition: general trends and individual aspects. J Non-Cryst Solids 279:126–135
89. Angell CA, Sichina W (1976) Thermodynamics of the glass transition: empirical aspects. Ann New York Acad Sci 279:53–67
90. Angell CA (1991) Thermodynamic aspects of the glass transition in liquids and plastic crystals. Pure Appl Chem 63:1387
91. Angell CA (1995) Formation of glasses from liquids and biopolymers. Science 267:1615
92. Angell CA (2013) Heat capacity and entropy functions in strong and fragile glass-formers relative to those of disordering crystalline materials. Chapter 2. In: Šesták J, Mareš J, Hubík P (eds) Glassy, amorphous and nano-crystalline materials. Springer, Berlin, pp 21–40 (ISBN 978-90-481-2881-5)
93. Hlaváček B, Šesták J (2014) Redefinition of the dependence of dynamical viscosity on temperature as the thermal sensitivity as an alternative of the familiar term known as Angell´s fragility. Uncompleted and unpublished
94. Kozmidis-Petrovič AF (2016) Impact of the stretching exponent on fragility of glass-forming liquids. J Thermal Anal Calorim, doi: 10.1007/s10973-016-5828-5

95. Kozmidis-Petrovič AF, Šesták J (2017) Glass transition temperature its exploitation and insight to fragility. J Min Metall B, submitted
96. Mareš JJ, Šesták J (2005) An attempt at quantum thermal physics. J Thermal Anal Calor 82:681–686
97. Mareš JJ, Stávek J, Šesták J (2004) Quantum aspects of self-organized periodical chemical reactions. J Chem Phys 121:1499
98. Mareš JJ, Šesták J, Hubík P (2013) Transport constitutive relations, quantum diffusion and periodic reactions. Chapter 14. In: Šesták J, Mareš J, Hubík P (eds) Glassy, amorphous and nano-crystalline materials: thermal physics, analysis, structure and properties. Springer, Berlin, pp 227–245 (ISBN 978-90-481-2881-5)

Chapter 12
Parameterization and Validation of Thermochemical Models of Glass by Advanced Statistical Analysis of Spectral Data

Jan Macháček, Mária Chromčíková and Marek Liška

Abstract Shakhmatkin and Vedishcheva proposed the associated solutions' thermodynamic model (SVTDM) of glasses and glass-forming melts. This model considers glasses and melts as an ideal solution formed from saltlike products of chemical reactions between the oxide components and the original (unreacted) oxides. The model does not use adjustable parameters; only the standard Gibbs energies of the formation of crystalline compounds and the analytical composition of the system considered are used as input parameters. A nonlinear regression treatment with the help of a genetic algorithm is used for the optimization of molar Gibbs energies by minimizing the sum of squares of deviations between experimental and calculated structure units' distributions. In such a manner, the non-ideality of glass systems is reflected. The proposed method of using the optimized effective parameters (i.e., reaction Gibbs energies) within the SVTDM copes with most frequently met weak points of this method, i.e., missing of thermodynamic data for some components of SVTDM; missing of some components in the SVTDM because of insufficient knowledge of particular phase diagram or because of taking into account only the stable crystalline phases (and ignoring, e.g., the metastable ones); the assumption of zero mixing enthalpy connected with the supposed ideality of the studied glass system; the assumption of regular mixing entropy connected with the supposed ideality of the studied glass system; and the uncertainty in the mixing entropy originating in the uncertainty of molecular weight of individual components.

J. Macháček
University of Chemistry and Technology, Technická 5, 166 28 Prague, Czech Republic
e-mail: Jan.Machacek@vscht.cz

M. Chromčíková · M. Liška (✉)
Joint Glass Center of IIC SAS, TnUAD, and FChPT STU, Vitrum Laugaricio, Študentská 2, 91150 Trenčín, Slovakia
e-mail: Marek.Liska@tnuni.sk

J. Šesták et al. (eds.), *Thermal Physics and Thermal Analysis*,
Hot Topics in Thermal Analysis and Calorimetry 11,
DOI 10.1007/978-3-319-45899-1_12

12.1 Introduction

The glass is commonly defined as the non-crystalline solid obtained by cooling the melt without crystallization [1]. Despite the fact that glass can be produced also by other ways, like by the solgel method or by the amorphization of crystalline solid [2], it is worth noting the uncommon situation when the method of preparation becomes a part of the definition of some kind of substance material. This indicates the importance of the kinetic factors connected with the glass formation. On the other hand, the kinetics—namely the kinetics of nucleation and crystal growth—is determined by the melt structure.

In contrast to the crystalline substances where the 3D translational symmetry takes place, the structure of glass cannot be quantified giving a small number of numeric data. The relatively uniform coordination polyhedra, such as SiO_4, AlO_4, BO_4, and BO_3, can be found in the oxide glass. Therefore, the glass structure has to be seen in different scales. The uniform coordination polyhedra correspond to the short-range order (SRO) or the nearest neighbor scale. Going to the next nearest neighbor, we can distinguish between various types of coordination polyhedra according to their structural position within the glass network. So the SiO_4 tetrahedra can be classified according to the number of bridging oxygen atoms, connecting them with the neighboring polyhedra. For instance, Q^i represents the SiO_4 polyhedron with i bridging oxygen atoms, i.e., $Si(–O–X)_i(–O^-)_{4-i}$ where X stands for any other network-forming atom (Si, Al, B, P, etc.). Going to the next nearest neighbor (and next-next nearest neighbor), we can reach the more detailed structural description corresponding to the medium-range order (MRO). The long-range order (LRO) structural information concerns the large extent of the polymerized 3D network, including the ring distribution [3]. Different glass properties are structurally influenced in a different extent of structural arrangement. So some optical properties are defined by the SRO, mechanical, electrical, and thermal properties depending on the MRO and LRO structures.

On the other hand, the usefulness and applicability of any kind of the structure description/quantification are limited by the experimental methods enabling its quantitative determination. So the nearest neighbor and next nearest neighbor description of network-forming coordination polyhedra is possible mainly due to the experimental techniques such as EXAFS, XANES, MAS NMR, and infrared and Raman vibrational spectroscopy.

12.2 Thermodynamic Models of Glass

The crucial point of each thermodynamic model is the definition of atomic groupings that will be considered as components of the system. This definition implies the structural range described by the particular model. On the SRO level, the components of the system are defined as the particular coordination polyhedra

(like Q-units). In fact, the term "thermodynamic" is used to indicate that thermodynamic equilibrium of properly defined structural entities is found at isothermal isobaric conditions by the minimization of the system Gibbs energy with respect to the relative abundance of considered system components. Assuming the ideal behavior, the system entropy can be described by regular mixing of system components, while the enthalpy is given by the sum of components' enthalpies and can be approximated by summing the bond energies. The equilibrium composition of the system is then obtained by the minimization of the Gibbs energy constrained by the stoichiometry of the system. Such type of models is critically reviewed in the works of Gurman and Conradt [4–6].

MRO structure is reflected in the thermodynamic models based on the (at least stoichiometric) definition of components as compounds. The computational complexity of the model depends on the number of components. In the model of Conradt [4, 5], the components are defined as having the stoichiometry of crystalline substances coexisting in equilibrium phase diagram. The mixture of these crystalline compounds with the overall stoichiometry given by the glass composition forms the so-called crystalline reference state (CRS). The definition CRS implies that only the coexisting phases are taken into account. Thus, the concentrations of all components are straightforwardly defined by the mass balance equations and can be obtained by solving a set of linear equations.

12.3 Thermochemical Model of Shakhmatkin and Vedishcheva

Shakhmatkin and Vedishcheva proposed the associated solutions' thermodynamic model (SVTDM) of glasses and glass-forming melts [7–15] that could be considered as the extension of the Conradt's model. This model considers glasses and melts as an ideal solution formed from saltlike products of chemical reactions between the oxide components and the original (unreacted) oxides. These saltlike products (also called associates, groupings, or species) have the same stoichiometry as the stable crystalline compounds, which exist in the equilibrium phase diagram of the system considered. The model does not use adjustable parameters; only the standard Gibbs energies of the formation of crystalline compounds and the analytical composition of the system considered are used as input parameters. Obviously, contrary to Conradt's model, the number of system components is greater than the number of oxides. Thus, the equilibrium composition cannot be obtained on the basis of mass balance equations. That is why, the authors present a calculation of the equilibrium system composition based on the values of particular equilibrium constants that are obtained from the Gibbs formation energies by the standard thermodynamic way. More generally, the minimization of the systems' Gibbs energy constrained by the overall system composition has to be performed with respect to the molar amount of each system component to reach the

equilibrium system composition [16]. The total Gibbs energy is expressed supposing the state of the ideal solution:

$$G(n_1, n_2, \ldots, n_N) = \sum_{i=1}^{N} n_i \Delta_f G_{m,i} + RT \sum_{i=1}^{N} n_i \ln \frac{n_i}{\sum_{j=1}^{N} n_j}, \tag{12.1}$$

where N is the number of components, n_i is the molar amount of ith component, T is the system temperature (i.e., the glass transition temperature, T_g, for particular glass), and $\Delta_f G_{m,i}$ is the molar Gibbs formation energy of pure ith component at the pressure and temperature of the system. The system components are ordered in a such way that X_i (i = 1, 2, …, $M < N$) are pure oxides (sulfides, arsenides, selenides, etc.) and X_i ($i = M + 1, M + 2, \ldots, N$) are compounds formed by reversible reactions

$$X_i \leftrightarrow \sum_{j=1}^{M} \nu_{i,j} X_j, \quad i = M+1, M+2, \ldots, N \tag{12.2}$$

Let us suppose the system composition given by the molar amounts of pure unreacted oxides n_{0i} (i = 1, 2, …, M). Then, the mass balance constraints can be written in the form:

$$n_{0,j} = n_j + \sum_{i=M+1}^{N} \nu_{i,j} n_i, \quad j = 1, 2, \ldots, M \tag{12.3}$$

The molar Gibbs formation energies of the melts of pure components may be used in more advanced version of this model. However, these thermodynamic data are relatively scarce that prevent the routine application of the model to the study of multicomponent systems. On the other hand, the errors caused by substituting the melt by the crystalline state are partially compensated when the reaction Gibbs energies, $\Delta_r G_{m,i}$, are calculated according to

$$\Delta_r G_{m,i} = \Delta_f G_{m,i} - \sum_{j=1}^{M} \nu_{i,j} \Delta_f G_{m,j} = -RT \ln K_i, \quad i = M+1, M+2, \ldots, N \tag{12.4}$$

where K_i is the equilibrium constant of the ith equilibrium reaction described by Eq. (12.2).

When the crystalline state data are used, the model can be simply applied to most multicomponent glasses including the non-oxide ones. In particular, the application of the model to the multicomponent industrially produced glasses can be very important. Taking into account that the common praxis resides in expressing most

of the multicomponent glass properties in the form of (mostly) additive functions of the glass composition expressed in percents (even weight and not molar!) of pure oxides [17–19], using the thermodynamic model unambiguously represents the significant progress.

The contemporary databases of thermodynamic properties (like the FACT computer database [20]) enable the routine construction of the SVTDM for various important multicomponent glass systems and not only for the silicate/oxide glasses [21–31]. It is worth noting that other methods of thermodynamic modeling of glasses and glass-forming melts (not discussed here, e.g., [32–34]) do not possess the possibility of routine application to multicomponent systems.

The above very strong feature of SVTDM is at least partially compensated by some weak points. However, as will be seen later, the proposed regression method gives the realistic opportunity for solving all these weaknesses.

First, for non-oxide multicomponent systems, the equilibrium phase diagram may be unknown. Moreover, in some specific cases, also some phase diagrams are not fully overlooked. Moreover, the definition of system components by the equilibrium crystal phases can be questionable, at least for some systems. Here, it can be emphasized that the glass-forming melt at the temperature range below the liquidus temperature but well above the glass transition temperature is in the metastable equilibrium state. Therefore, one can in principle expect the participation of some unstable/metastable crystalline compounds. This situation is typically manifested by the disagreement between the experimental structural information (e.g., the Q-unit distribution) on one side and the SVTDM prediction on the other.

The other weak point of the SVTDM can be in some cases seen in the assumption of ideal behavior, i.e., the assumption of zero mixing enthalpy and regular mixing entropy [represented by the second term on the right-hand side of Eq. (12.1)]. Some specific features of the assumption of ideal mixing enthalpy have to be mentioned here. From the mathematical point of view, this assumption is expressed by the multilinear dependence of system enthalpy H:

$$H = \sum_{i=1}^{N} n_i H_{\mathrm{m},i}, \tag{12.5}$$

where H is the system enthalpy and $H_{\mathrm{m},i}$ are the molar enthalpies of pure system components. For simplicity, we can illustrate this situation on the enthalpy of real binary system A–B (Fig. 12.1). The ideality assumption predicts the linear course of enthalpy connecting the points of molar enthalpies of pure compounds. Let us suppose the composition dependence of molar enthalpy of real solution with composition $x\mathrm{A}\cdot(1-x)\mathrm{B}$ in the form (in arbitrary units):

$$\begin{aligned} H_{\mathrm{m}} &= xH_{\mathrm{m,A}} + (1-x)H_{\mathrm{m,B}} + \xi_{\mathrm{A,B}}x(1-x) \\ &= 2x + 7(1-x) - 7x(1-x), \end{aligned} \tag{12.6}$$

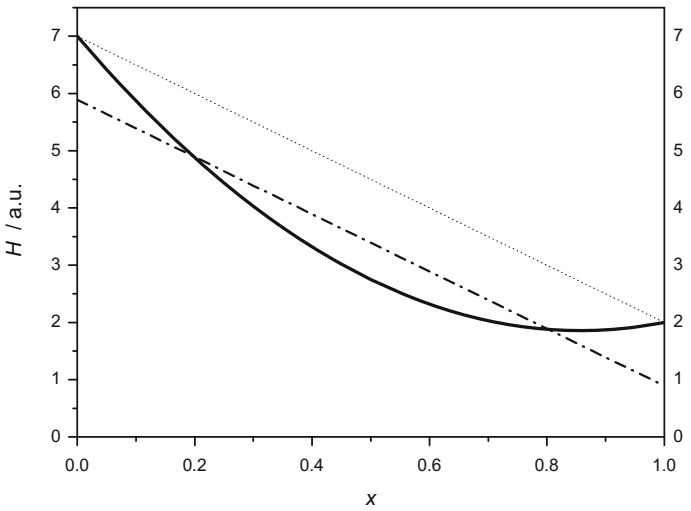

Fig. 12.1 Enthalpy of real binary system xA·(1 − x)B—*full line* [Eq. (12.6)]. Enthalpy dependence for ideal system [*dotted line*, Eq. (12.5)] and the optimized quasi-ideal linear enthalpy compositional dependence (*dash-dot line*) calculated using effective molar enthalpies of pure components [Eq. (12.7)]

where $H_{\mathrm{m,A}} = 2$, $H_{\mathrm{m,B}} = 7$, and the interaction parameter $\xi_{\mathrm{A,B}} = -7$. This behavior, known also as negative deviation from ideal behavior, causes systematic positive error in system enthalpy if this is calculated from true experimental values of molar enthalpies of pure components. This error is significantly decreased if instead of true molar enthalpies the effective optimized values $H_{\mathrm{m,eff,A}} = 0.89$, $H_{\mathrm{m,eff,B}} = 5.89$ are used in Eq. (12.5):

$$H_{\mathrm{m}} = xH_{\mathrm{m,eff,A}} + (1-x)H_{\mathrm{m,eff,B}} = 0.89x + 5.89(1-x) \tag{12.7}$$

The effective values of molar enthalpies were obtained by the minimization of sum of squares of deviations between the true [Eq. (12.6)] and effective [Eq. (12.7)] system enthalpy. This way, the non-ideality of the system can be reflected by using effective (i.e., shifted or not true) values of molar Gibbs energies of formation of system components $\Delta_{\mathrm{f}}G_{\mathrm{m,eff},i}$. This approach simultaneously reflects the deviations from supposed regular mixing. From the numerical point of view, there are only N–M independent values of Gibbs energies, i.e., the reaction Gibbs energies $\Delta_{\mathrm{r}}G_{\mathrm{m,eff},i}$ [Eq. (12.4)].

In connection with the mixing entropy, another weakness of SVTDM has to be reported. From the equilibrium phase diagrams, only the stoichiometry of the system components is taken and not the molecular weight. As a simple example, the P_2O_5 and P_4O_{10} component definitions can be reported. This uncertainty does not affect the value of system enthalpy, but it changes the value of the equilibrium molar amount of the particular component (due to changing the mixing entropy)

Table 12.1 Results of SVTDM obtained for $0.61CaO{\cdot}0.39P_2O_5$ glass with two different definitions of molar weight of system components X_i (M = 2; N = 5)

X_i	$-\Delta_f G_{m,i}$/kJ mol^{-1}	n_i/mmol	X_i	$-\Delta_f G_{m,i}$/kJ mol^{-1}	n_i/mmol
CaO	678.3	0.0	CaO	678.3	0.0
P_2O_5	1634.4	0.0	P_2O_5	1634.4	0.0
CaP_2O_6	**2663.8**	**170.1**	**$3CaP_2O_6$**	**7991.3**	**56.7**
$Ca_2P_2O_7$	**3549.6**	**219.9**	**$2Ca_2P_2O_7$**	**7099.1**	**110.0**
$Ca_3P_2O_8$	4378.5	0.052	$Ca_3P_2O_8$	4378.5	0.029

Gibbs energies taken from the FACT database, T = 795 K

and this way the equilibrium mole fractions x_i of all system components. Due to relatively low influence of the mixing entropy value for the definition of the position of the minimum of system Gibbs energy (i.e., the equilibrium molar amounts of all components), this effect is not substantial.

As an example, we present the SVTDM result obtained for the $0.61CaO{\cdot}0.39P_2O_5$ glass at $T = T_g$ = 795 K (Table 12.1). As the system components, the unreacted oxides were considered together with CaP_2O_6, $Ca_2P_2O_7$, and $Ca_3P_2O_8$. In the second example, the $3CaP_2O_6$ and $2Ca_2P_2O_7$ were considered. It can be seen that obviously, $\Delta_f G_m(3CaP_2O_6) = 3\Delta_f G_m(CaP_2O_6)$ and $\Delta_f G_m(2Ca_2P_2O_7) = 2\Delta_f G_m(Ca_2P_2O_7)$ hold. On the other hand, the relations between equilibrium molar amounts are very close to $n(CaP_2O_6) \approx 3n(3CaP_2O_6)$ and $n(Ca_2P_2O_7) \approx 2n(2Ca_2P_2O_7)$. Thus, we can conclude that of course, the equilibrium molar fractions of system components are changed by multiplying the molar weight (i.e., changing the "polymerization degree") of individual species. However, the equilibrium molar amounts are changed (almost) proportionally. Thus, any result obtained on the basis of equilibrium molar amounts of individual species (e.g., Q-distribution) is practically invariant to changes of their polymerization degree. Moreover, this effect is also partially compensated by using the effective values of reaction Gibbs energies.

Thus, in principle, using some feasible criterion, e.g., quantified difference between the experimental and calculated Q-distribution, the effective formal values of Gibbs reaction energies can be found by minimizing the difference between the experimental and predicted data.

12.4 Practical Aspects of Thermochemical Calculations

The basis of the SVTDM is the system of nonlinear equations for the equilibrium of simultaneous chemical reactions and mass balance. They are usually solved numerically in an iterative manner, even for simple systems comprising of few reactants (e.g., oxides) and several products (e.g., salts of reacting oxides). Currently, there is a wide range of commercial and public domain programs suitable for these thermochemical calculations. The FACTSage package should be

mentioned at least [20]. At present, it is probably the most popular thermochemical software.

Thermochemical calculations are much easier if particular software includes also some extensive thermochemical databases as it is in the case of FACTSage. On the other hand, if there are no source codes of such programs available and some special functions are required, e.g., inclusion of alternative relationships for excess quantities, then one has to develop his/her own program code. For this purpose, one may use the standard programming languages (e.g., Fortran and C) or integrated environments for applied mathematics (e.g., Maple and MATLAB). For non-programmers, there is one more interesting possibility of how to perform even quite complicated thermochemical calculations. This possibility is offered by common office software equipment, specifically the Microsoft Excel spreadsheet. From the version 2010, it is complemented with the Solver module which can be used for searching the global minima in optimization problems. The Solver employs a stochastic evolutionary algorithm developed by Frontline Systems, Inc. [35].

Experience shows that the major problem of the numerical solution of the thermochemical monophase equilibrium of simultaneous reactions is a situation when some of the chemical components are present in a system in negligible quantity only [16]. It causes huge problems in the calculation of equilibrium constants. Rounding errors and a division by zero may arise, and the speed of convergence decreases. In a rather simple case of the SVTDM, such problems may be overcome by a small change of chemical composition even when the gradient-based Newton–Raphson optimization method is used. The situation changes dramatically in the case of more complex optimizing problems, when the estimation of thermochemical parameters by the nonlinear regression analysis is performed in addition to solving chemical equilibrium. These thermodynamic parameters typically represent activity coefficients [36].

In the case of the SVTDM, the model predictions may in some cases differ from experimental structural and physical properties. In principle, the disagreement can be caused by either not including of some key compound into the model because this component is not found in the equilibrium phase diagram (if the phase diagram itself is known) or its thermodynamic properties are unknown, or by neglecting of non-ideality of a mixture or by neglecting of a non-equilibrium character of the glassy state, i.e., neglecting some metastable component that is not present in the equilibrium phase diagram. All these factors can be considered as a source of information which can be used for improving the original model. For example, if the model does not predict the presence of some structural unit and the experiment does, then one may input a compound containing this unit and determine its molar Gibbs energy of formation by the nonlinear regression.

In course of the nonlinear regression analysis, the value of the so-called fitness function is minimized. The fitness function is a sum of squares of deviations of structural or physical properties. The minimization is constrained due to preserving mass balance and chemical equilibrium. It shows that the problem is highly nonlinear. The fitness function has got a lot of local minima, and some of them are

related rather to numeric errors emerging during calculation. Consequently, there is a problem to determine even some acceptable initial guess of regression parameters which would lead to the global, i.e., true, minimum. The gradient optimization methods often provide an estimate parameters for the next step, which after putting into the model cause numerical instability and as a result the failure of calculation. From the above, it follows that the gradient optimization methods are not suitable for solving the complex thermochemical equilibrium of simultaneous reactions. The model of Shakhmatkin and Vedishcheva extended by the regression analysis is a particular case where difficulties arise.

12.5 Evolutionary Approach to Chemical Equilibrium Determination

A good optimization algorithm should lead a calculation to the global minimum, and it should be sufficiently stable, versatile, and as fast as possible. These conditions are met very well by stochastic evolutionary (genetic) algorithms [36–38]. Their basic idea follows, as their name suggests, from the analogy with evolutionary biology. With it, it also shares terminology, e.g., gene, chromosome, individual (phenotype), population, generation, natural selection, replication, crossover, and mutation. Contrary to evolutionary biology, it possesses some unique features, e.g., elitism; that is, the fittest individual is always automatically transferred (grafted) to the next generation. There is also possibility to combine the evolutionary approach with some other method; for example, in the first step, an evolutionary algorithm suggests some region where the global minimum is very probably located, and then, this minimum is precisely identified by a gradient-based algorithm.

The quality of the individual, which is a set of regression model parameters (variables), is given by the value of the fitness function. Allowable values of variables lay between upper and lower bounds defined at the beginning of calculation. The bounds should reflect physical properties of variables, e.g., molar fractions go from zero to unity and absolute temperature is positive. Each variable is encoded into a binary string of ones and zeros, which represents the gene. It can be done by many ways, for example, as follows:

Step 1	Transformation onto <0; 1> interval	$x' = \frac{x - x_{\min}}{x_{\max} - x_{\min}}$
Step 2	Setting precision by truncating decimal places, $a_{\max}$ is a large integer, $a_{\max}$ = 111…111 in binary numeral system	$a = \text{int}(x' a_{\max})$
Step 3	Binary string generation $b_{\min}$ = 000…000 $b_{\max}$ = 111…101	b = dec2bin(a)

A chromosome is a sequence of the genes, b, belonging to some individual. There are always more individuals (typically hundreds), and they form a population, e.g.,

	b_1	b_2	b_3
Individual 1	000111011101011	100100011010110	110011011010111
Individual 2	101111100100111	001001011100101	110011101110100
Individual 3	111001110001101	1101010001000011	110101000000000

The population evolves in cycles through generations (see Fig. 12.2). The initial population is typically created by a random number generator. Then, the fitness function, U_i, of each individual i in the population is evaluated. After that, a survival

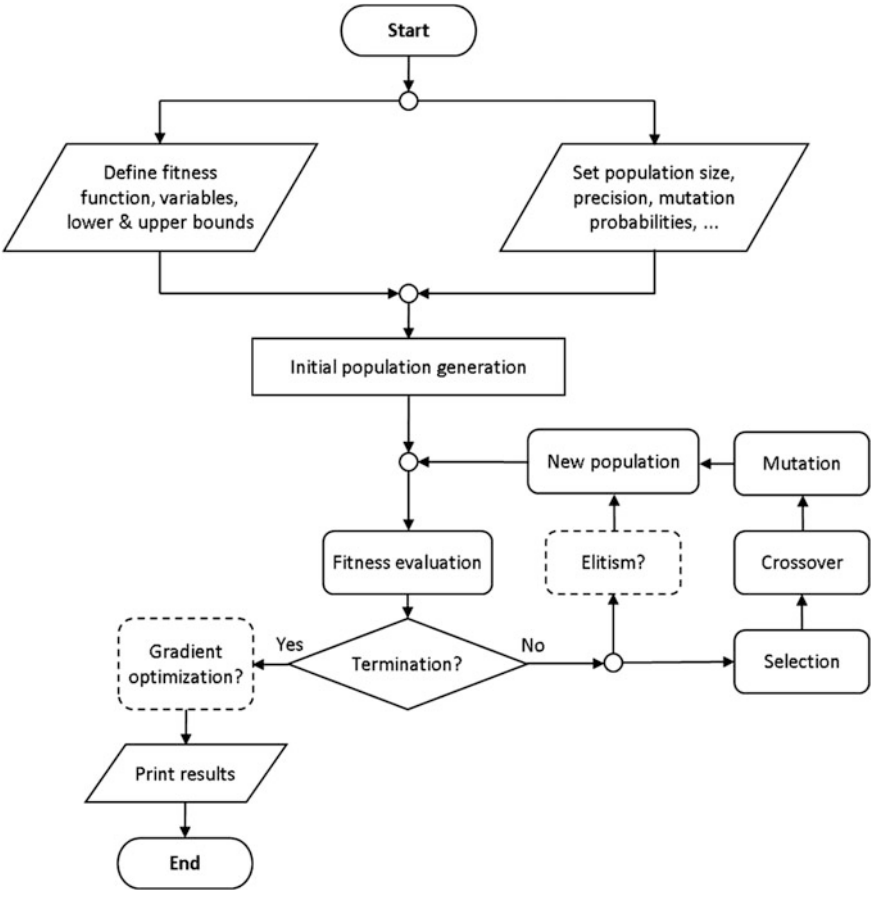

Fig. 12.2 Flowchart of genetic algorithm—freely [40]

probability is assigned to each individual according to its fitness function, i.e., the greatest-to-highest quality individual with the minimum value of the fitness function [37]. In this way, the probability p_i that the individual i survives is given by:

$$p_i = \frac{F_i}{\sum_{j=1}^{N_{\text{pop}}} F_j}, \tag{12.8}$$

where $F_i = -U_i$ and N_{pop} represents the individuals' number in the population.

Then, the random number generator selects the individuals for crossover. The position of crossover of binary strings (chromosomes) of two individuals is once again selected by the random number generator.

	↓ Position of crossover
Parent 1	0001110111010111001000011010110|1100110110101111
Parent 2	1011111001001111001001011001011|1100111011101000
Offspring	0001110111010111001001011001011|1100111011101000

Then, a random mutation follows with the set probability of flipping a bit from 1 to 0 or vice versa.

	↓ Mutation 1	↓ Mutation 2	↓ Mutation 3
Original	0001110111010111|1001000011010110|1100110110101111		
Mutant	0001010111010111|1001000010010110|1100111110101111		

Against the rules of evolution, the elite individual with the lowest value of the fitness function can be further inserted into the new population. The cycle closes by the evaluation of the fitness function in the new generation. The condition for the termination of the cycle is usually achieved when a given number of generations pass off, or the maximum number of generations without improvement of the fitness function passes off, or the maximum total calculation time is up, or the maximum value of the fitness function is achieved. None of these criteria does guarantee that the global minimum and even some local minimum were found. It seems that the operation of mutation is the main factor that guarantees the quality of searching the solution space. In contrast to this, the crossover operation helps in refining the location of some possible minimum.

For simple problems, the convergence of genetic algorithms is usually always slower than that in the case of the gradient algorithms. However, a considerable benefit follows from the possibility of finding the global minimum; hence, a longer running time of the algorithm is not usually a problem. The running time can be shortened by splitting a calculation into multiple parallel tasks. Most of the time is almost always consumed by the evaluation of the fitness function, and on the other hand, the operations with binary strings are very fast. Therefore, the parallelization efficiency is almost perfect.

12.6 Implementation of the Model into MS Excel

The specification of the fitness function is the major problem when transferring the SVTDM extended by the regression analysis into the spreadsheet editor MS Excel. The reason is that the minimization of the sum of squared deviations of the model and the experimental structural and physical properties and the application of mass balance and chemical equilibrium constraints must be performed simultaneously in a single step. The MS Excel allows sequential automatic optimization (i.e., a separate calculation of chemical equilibrium), but only using macros written in the Visual Basic for Applications (VBA). Experience shows that the best result gives a composite fitness function, U, in the form:

$$U = w_{\mathrm{e}} U_{\mathrm{e}} + w_{\mathrm{m}} U_{\mathrm{m}} + w_{\mathrm{p}} U_{\mathrm{p}} = \min, \tag{12.9}$$

where U_{e} is the partial fitness function for chemical equilibrium; U_{m} is the partial fitness function for mass balance; U_{p} is the partial fitness function for deviations of the model and the experimental structural and physical properties; and w_i are the respective weighting coefficients.

The SVTDM searches for the equilibrium of a set of N–M simultaneous chemical reactions for the formation of N–M products. The products are compounds of M reactants. The reactants are starting components, e.g., pure oxides.

$$\begin{gathered} v_{(M+1),1} X_1 + v_{(M+1),2} X_2 + \ldots + v_{(M+1),M} X_M \leftrightarrow X_{M+1} \\ v_{(M+2),1} X_1 + v_{(M+2),2} X_2 + \ldots + v_{(M+2),M} X_M \leftrightarrow X_{M+2} \\ \ldots \\ v_{N,1} X_1 + v_{N,2} X_2 + \ldots + v_{N,M} X_M \leftrightarrow X_N, \end{gathered} \tag{12.10}$$

where $v_{i,j}$ is the stoichiometric coefficient of the jth reacting component in the ith reaction. In chemical equilibrium, the equilibrium constant of the ith reaction, K_i, is given by:

$$\ln K_i = -\frac{\Delta_r G_{\mathrm{m},i}}{RT}, \tag{12.11}$$

where R is the molar gas constant; T is the thermodynamic temperature; and $\Delta_{\mathrm{r}} G_{\mathrm{m},i}$ is the reaction Gibbs energy of the ith reaction (i.e., formation of the product X_i—see the Eq. (12.4)).

The SVTDM supposes that all components form an ideal solution in thermodynamic equilibrium, and then, for the ith reaction, one may write:

$$K_i = \prod_{j=1}^{M} a_j^{v_{i,j}} == \prod_{j=1}^{M} x_j^{v_{i,j}} \tag{12.12}$$

or

$$\ln K_i = \sum_{j=1}^{M} v_{i,j} \ln x_j, \tag{12.13}$$

where a_j is the activity of the jth component; $v_{i,j}$ is the stoichiometric coefficient of the jth component in the ith reaction, and x_j is the molar fraction of the jth component in an equilibrium mixture. The set of N–M equilibrium Eq. (12.11) for N unknowns is completed with M mass balance equations of the reaction starting components:

$$n_j^0 = n_j + \sum_{i=M+1}^{N} v_{i,j} n_i, \tag{12.14}$$

where n_j^0 is the total number of moles of the jth starting component (e.g., oxide); n_j is the equilibrium number of moles of this component; n_i is the equilibrium number of moles of the ith compound; and $v_{i,j}$ is the stoichiometry coefficient (i.e., content) of the jth component in the ith compound.

The partial fitness function for chemical equilibrium, U_e, is given as the sum of the squares of the differences of left- and right-hand side of Eq. (12.11):

$$U_\mathrm{e} = \sum_{i=M+1}^{N} \left[\ln K_i - \left(-\frac{\Delta_\mathrm{r} G_{\mathrm{m},i}}{RT} \right) \right]^2 \tag{12.15}$$

and the partial fitness function for mass balance, U_m, is given as the sum of the squares of the differences of left- and right-hand side of Eq. (12.14):

$$U_\mathrm{m} = \sum_{j=1}^{M} \left(n_j^0 - n_j - \sum_{i=M+1}^{N} v_{i,j} n_i \right)^2 \tag{12.16}$$

If the calculation is performed simultaneously for several systems of a different chemical composition, then the partial fitness functions for chemical equilibrium and mass balance will be

$$U_\mathrm{e} = \sum_{s=1}^{S} \sum_{i=M+1}^{N} \left[\ln K_{i,s} - \left(-\frac{\Delta_\mathrm{r} G_{\mathrm{m},i}}{RT_s} \right) \right]^2, \tag{12.17}$$

$$U_\mathrm{m} = \sum_{s=1}^{S} \sum_{j=1}^{M} \left(n_{j,s}^0 - n_{j,s} - \sum_{i=M+1}^{N} v_{i,j} n_{i,s} \right)^2, \tag{12.18}$$

where S is the number of systems.

The physical/structural property of the system, P, can be calculated as the weighted average of the contributions, P_k, of starting components and compounds. The weights are the equilibrium molar fractions.

$$P = \sum_{k=1}^{N} x_k P_k \tag{12.19}$$

In the case of structural properties (e.g., Q-unit distribution), the fraction of structural units, P_α, is calculated as the sum of α-units present in the starting components and compounds normalized to the total number of units:

$$P_\alpha = \frac{\sum_{k=1}^{N} A_{\alpha,k} n_k}{\sum_{k=1}^{N} B_k n_k} \quad B_k = \sum_{\{\alpha\}} A_{\alpha,k}, \tag{12.20}$$

where $A_{\alpha,k}$ is the number of structural α-units in the kth component or compound and $\{\alpha\}$ is a set of all possible units α.

The partial fitness function for structural properties, U_p, for multiple systems of different composition is determined by the sum of squares:

$$U_\mathrm{p} = \sum_{s=1}^{S} \sum_{\{\alpha\}} \left(P_{\alpha,s}^{\mathrm{calc}} - P_{\alpha,s}^{\mathrm{exp}} \right)^2 \tag{12.21}$$

At the final calculation of the total cost function U, each system s (s = 1, 2,…, S) is required to preserve the chemical equilibria i ($i = M + 1, M + 2, \ldots, N$) and mass balance of input components j (j = 1, 2,…, M):

$$\left| \ln K_{i,s} - \left(-\frac{\Delta_r G_{\mathrm{m},i}}{RT_s} \right) \right| < \varepsilon_\mathrm{e}, \tag{12.22}$$

$$\left| n_{j,s}^0 - n_{j,s} - \sum_{i-1}^{M} \nu_{i,j} n_{i,s} \right| < \varepsilon_\mathrm{m}, \tag{12.23}$$

where ε_e and ε_m are adjustable convergence criteria that determine the accuracy of calculation of chemical equilibrium and mass balance. These are very small numbers. The convergence is largely affected by setting the weighting coefficients w_i in Eq. (12.9) (Fig. 12.3).

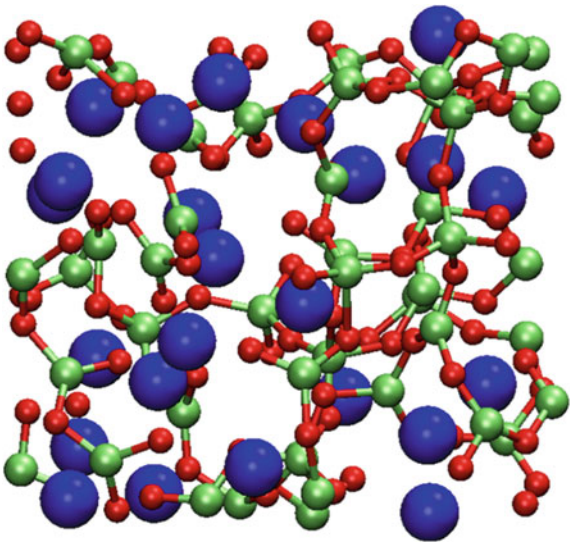

Fig. 12.3 Structure of $CaO{\cdot}B_2O_3$ glass, ab initio molecular dynamics simulation. Calcium atoms are *blue*, oxygen *red*, and boron *green*. BO_3 and BO_4 coordination polyhedra are clearly visible

12.7 Example: The Thermochemical Model of the CaO–B_2O_3 Glass System

Using X-ray diffraction, fractions of two coordinations of boron BO_3 and BO_4 were determined in the glass system CaO–B_2O_3 (see Fig. 12.4). It emerged that the SVTDM significantly increases the fraction of BO_3 at molar fractions of CaO greater than 0.35. This dramatic difference is due to the fact that the pure crystalline phases aCaO·$b$$B_2O_3$ with higher content of CaO do not contain four-coordinated boron, but three-coordinated only. And there is no way how to combine these phases to give the same fractions of BO_3 and BO_4 as the experiment suggests.

If we accept that the basic theses of the SVTDM are reasonable, then it is advisable to supplement the model with the missing compounds comprising a dominant fraction of BO_4 in addition to a large proportion of CaO. Figure 12.5 shows a phase diagram of CaO–B_2O_3. The list of all compounds is shown in Table 12.2. In the phase diagram and in the table, there are inserted also $2CaO{\cdot}3B_2O_3$ and $CaO{\cdot}3B_2O_3$ compounds which are not present in the original phase diagram, but they exist and their structural data are known [39].

Table 12.3 shows the number of structural units BO_3 and BO_4 in the considered system components. It is evident that most original system components contain solely BO_3. Only $CaO{\cdot}2B_2O_3$ contains also BO_4 in equimolar ratio with BO_3. The added compounds, i.e., $2CaO \cdot 3B_2O_3$ and $CaO \cdot 3B_2O_3$, contain both BO_3 and BO_4 in the ratios 1:2 and 2:1, respectively.

The standard Gibbs energies of formation of both added compounds are unknown; however, as a first step, they can be taken as free parameters whose value

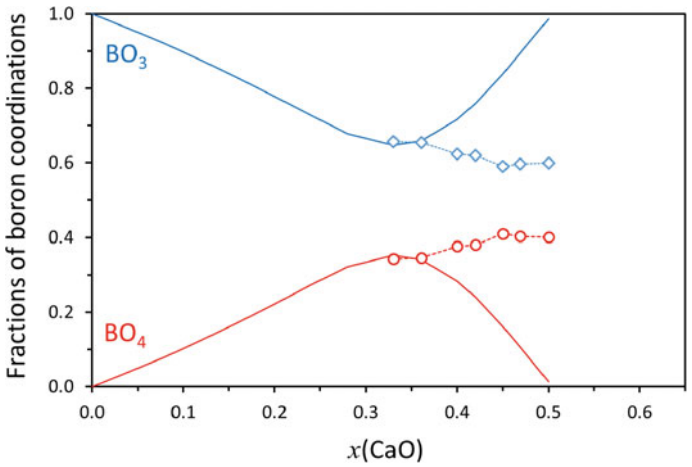

Fig. 12.4 Fractions of boron coordinations in binary $x\mathrm{CaO}(1-x)\mathrm{B_2O_3}$ glasses. Experimental data and the SVTDM (*solid lines*) at $T = 1000$ K (Tool's fictive temperature was considered constant, equal to 1000 K, in all systems.)

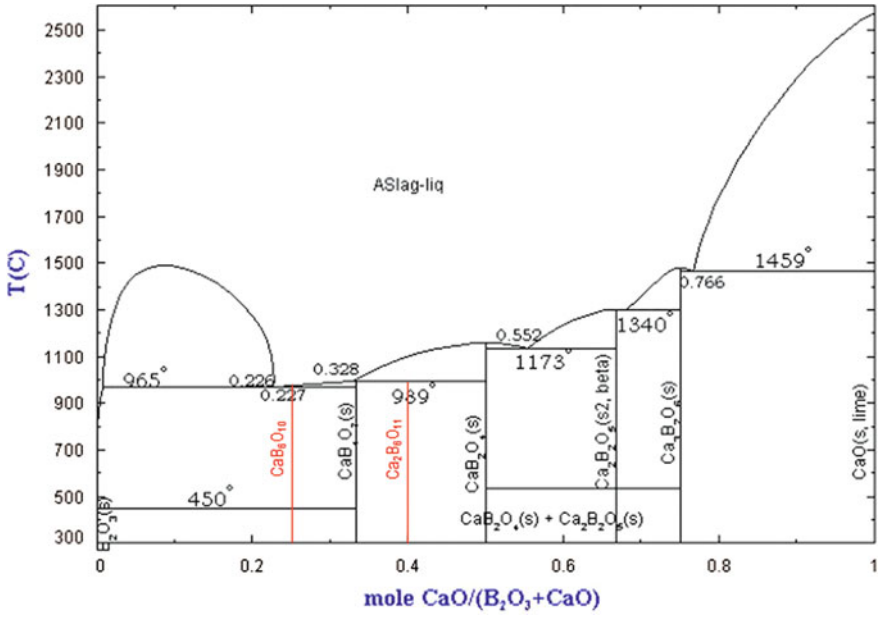

Fig. 12.5 Phase diagram of the binary CaO–B_2O_3 system [20]. Hypothetical $2\mathrm{CaO} \cdot 3\mathrm{B_2O_3}$ and $\mathrm{CaO} \cdot 3\mathrm{B_2O_3}$ phases are depicted in red color

Table 12.2 Stoichiometry of $a\mathrm{CaO}{\cdot}b\mathrm{B_2O_3}$ compounds considered in the model

	1	2	3	4	5	**6**	7	**8**
Compound	CaO	B_2O_3	$3CaO \cdot B_2O_3$	$2CaO \cdot B_2O_3$	$CaO \cdot B_2O_3$	**$2CaO \cdot 3B_2O_3$**	$CaO \cdot 2B_2O_3$	**$CaO \cdot 3B_2O_3$**
Abbrev.	C	B	C3B	C2B	CB	**C2B3**	CB2	**CB3**
CaO	1	0	3	2	1	**2**	1	**1**
B_2O_3	0	1	1	1	1	**3**	2	**3**
$\Delta_f G_{m,i}$	697	1370	3581	2890	2176	**?**	3565	**?**

Hypothetical $2CaO \cdot 3B_2O_3$ and $CaO \cdot 3B_2O_3$ compounds are presented in bold. In the last row, the $\Delta_f G_{m,i}$ (kJ mol^{-1}) values are given at $T = 1000$ K (the same temperature considered in all systems for simplicity)

Table 12.3 Numbers of boron coordinations in $a\mathrm{CaO}{\cdot}b\mathrm{B_2O_3}$ components considered in the model

Compound	CaO	B_2O_3	$3CaO \cdot B_2O_3$	$2CaO \cdot B_2O_3$	$CaO \cdot B_2O_3$	**$2CaO \cdot 3B_2O_3$**	$CaO \cdot 2B_2O_3$	**$CaO \cdot 3B_2O_3$**
BO_3	0	2	2	2	2	**2**	2	**4**
BO_4	0	0	0	0	0	**4**	2	**2**
Σ B	0	2	2	2	2	**6**	4	**6**

Table 12.4 Input data for the calculation

No. of glass systems, i.e., number of exp. data points	$S = 7$
No. of structure units, $\alpha \in \{BO_3, BO_4\}$	2
No. of reagents (i.e., CaO, B_2O_3)	$M = 2$
No. of compounds (i.e., $a\mathrm{CaO}{\cdot}b\mathrm{B_2O_3}$ salts, CaO, B_2O_3)	$N = 8$
No. of undetermined Gibbs energies of formation	$N_G = 2$
No. of unknown equilibrium molar fractions	$S \times N = 56$
No. of unknowns in nonlinear regression	$S \times N + N_G = 58$
Temperature (fictive) of all glass systems	$T = 1000$ K
Concentration limits for molar fractions	<0; 1>
Limits for undetermined Gibbs energies of formation	$<10^{-7}; 0>$
Convergence limit for chemical equilibrium	$\varepsilon_e < 10^{-4}$
Convergence limit for mass balance	$\varepsilon_m < 10^{-6}$
Initial weights of fitness function	$w_e = 1$; $w_m = 1$; $w_p = 1$
Final weights of fitness function	$w_e = 10^3$; $w_m = 10^6$; $w_p = 1$
Convergence of genetic algorithm in Solver	10^{-20}
No. of individuals in population	100
Mutation probability	0.075
Maximum time without improvement of fitness function	3600 s

is to be determined by the nonlinear regression procedure described in the previous chapter. Input data for the calculation are collected in Table 12.4.

A calculation progress is evaluated by the visual inspection of graphs of residuals, i.e., arguments of the partial fitness Eqs. (12.17), (12.18), and (12.21). At the beginning of calculation, weights of the total fitness function (12.9) were all set to one. This adjustment suppressed the influence of mass and equilibrium constraints and supported tendency to minimize differences between experimental data and the

model predictions. Later, during the run of calculations, mass and equilibrium weights gradually readjusted to much higher values to meet the convergence criteria as formulated in Eqs. (12.22) and (12.23). It was found based on many tests that this procedure leads to acceptable results much faster than that in the case of strong constraints applied in each iteration step.

After some time, when there is no further improvement of the fitness function, the calculation is finished and results saved. Figure 12.6 shows the fractions of boron coordinations in the binary $x\mathrm{CaO}\cdot(1-x)\mathrm{B_2O_3}$ glass after the nonlinear regression analysis. The agreement between experimental data and the model is now substantially better than it was in the case of the original SVTDM. On the other hand, the experimental data points are not scattered randomly along the model curve, but they cross the curve somewhere in the middle. It suggests that the model should be further revised from the point of incorporation of some other compounds and/or non-ideality (excess) terms. A hypothetical compound, which would improve the results, should have stoichiometry of $\mathrm{CaO}\cdot\mathrm{B_2O_3}$ but containing $\mathrm{BO_4}$ instead of $\mathrm{BO_3}$. To put it another way, the hypothetical compound should change the connectivity of the borate structure as follows:

$$\emptyset_2\mathrm{B}-\mathrm{O}^- \cdots \mathrm{Ca}^{2+} \cdots {}^-\mathrm{O}-\mathrm{B}\emptyset_2 \rightarrow (\emptyset_4\mathrm{B}^-)\cdots \mathrm{Ca}^{2+} \cdots (\mathrm{B}^-\emptyset_4), \qquad (12.24)$$

where Ø is the bridging oxygen and O^- is the non-bridging oxygen [41]. In the reaction (12.24), two non-bridging oxygens are transformed into two bridging oxygens and the connectivity of the network increases.

Figure 12.7 shows a model prediction of equilibrium amount of $a\mathrm{CaO}\cdot b\mathrm{B_2O_3}$ compounds in the $x\mathrm{CaO}$–$(1-x)\mathrm{B_2O_3}$ glass system. It is seen that both added compounds, i.e., $2\mathrm{CaO}\cdot 3\mathrm{B_2O_3}$ and $\mathrm{CaO}\cdot 3\mathrm{B_2O_3}$, contribute significantly to the

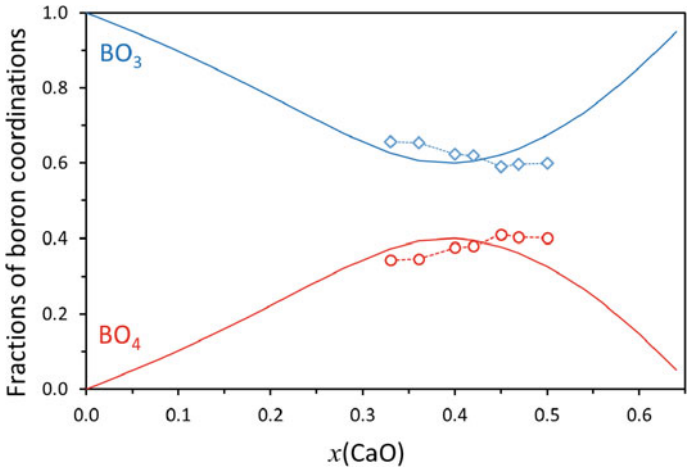

Fig. 12.6 Fractions of boron coordinations in the binary $x\mathrm{CaO}$–$(1-x)\mathrm{B_2O_3}$ glass system. Experimental data and the thermochemical model (*solid lines*)

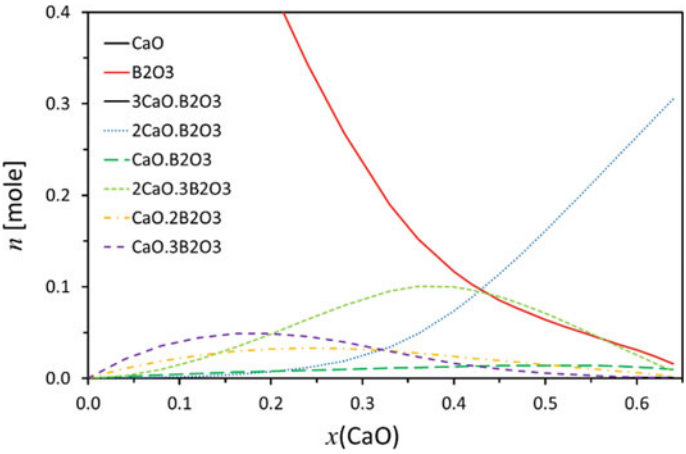

Fig. 12.7 Equilibrium amount of $a\text{CaO}\cdot b\text{B}_2\text{O}_3$ compounds in the binary $x\text{CaO}–(1-x)\text{B}_2\text{O}_3$ glass

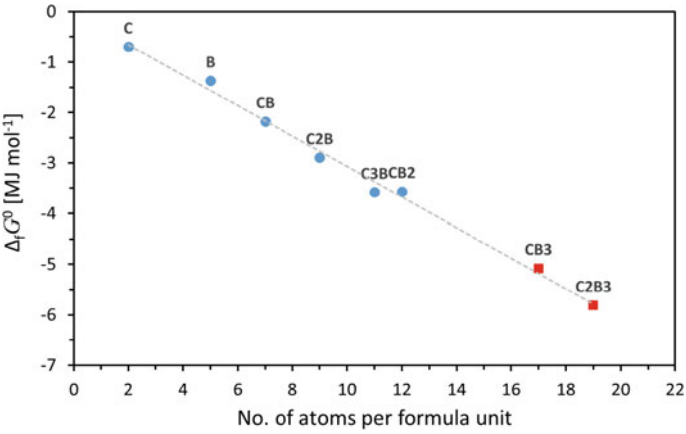

Fig. 12.8 Molar Gibbs energy of the formation of compounds in the binary $\text{CaO}–\text{B}_2\text{O}_3$ glass system in correlation with the number of atoms per formula unit. Experimental data (*blue disks*) and model data (*red squares*)

total composition. On the other hand, there is zero abundance of unreacted CaO and highly calcic $3\text{CaO}\cdot\text{B}_2\text{O}_3$.

The molar Gibbs energy of the formation of $2\text{CaO}\cdot 3\text{B}_2\text{O}_3$ and $\text{CaO}\cdot 3\text{B}_2\text{O}$ calculated by the nonlinear regression analysis is −5.812 and −5.079 MJ mol^{-1}, respectively. In Fig. 12.8, they are plotted on the correlation graph where the molar Gibbs energy of the formation of compounds is plotted against the number of atoms per formula unit. A linear dependence of the energy values is clearly seen. We can deduce that the estimated energies of the added compounds are quite reasonable.

12.8 Conclusion

The proposed method [30] of using the optimized effective parameters (i.e., reaction Gibbs energies) within the SVTDM copes with most frequently met weak points of this method, i.e.,

- Missing of thermodynamic data for some components of SVTDM.
- Missing of some components in the SVTDM because of insufficient knowledge of particular phase diagram or because of taking into account only the stable crystalline phases (and ignoring, e.g., the metastable ones).
- The assumption of zero mixing enthalpy connected with the supposed ideality of the studied glass system.
- The assumption of regular mixing entropy connected with the supposed ideality of the studied glass system.
- The uncertainty in the mixing entropy originating in the uncertainty of molecular weight of individual components.

However, the proposed treatment on the other side eliminates the most appealing strong feature of the SVTDM, i.e., the absence of any adjustable parameters. Thus, the results obtained by native SVTDM are in this respect unambiguous. Using effective values of parameters and adding to the system additional components may cause serious ambiguity of the obtained results. Therefore, such results have to be checked by an independent method. If the optimized parameterization is obtained on the basis of reproducing the solid-state MAS NMR structural data (e.g., the Q-distribution), the comparison of decomposition of Raman spectra obtained using the equilibrium molar amounts of system components with the multivariate curve resolution analysis of the same set of spectra may be used for the validation of the proposed model [25–31].

Acknowledgements This work was supported by the Slovak Grant Agency for Science under the grant VEGA 2/0088/16 and by the Slovak Research and Development Agency Project ID: APVV-0487-11. This work was also supported by the Grant Agency of the Czech Republic through the Grant No. P108/10/1631.

References

1. ASTM—C162 (1983) Standard terminology of glass and glass products, American society for testing and materials
2. Greaves GN, Sen S (2007) Inorganic glasses, glass-forming liquids and amorphizing solids. Adv Phys 56:1–166
3. Gedeon O, Liška M (2013) Rings in covalent glass and an evaluation of configurational entropy associated with rings. J Non-Cryst Solids 360:41–48
4. Conradt R (1999) Thermochemistry and structure of oxide glasses. In: Bach H, Krause D (eds) Analysis of the composition and structure of glass and glass ceramics. Springer, Berlin, pp 232–254

5. Conradt R (2004) Chemical structure, medium range order, and crystalline reference state of multicomponent oxide liquids and glasses. J Non-Cryst Solids 345&346:16–23
6. Gurman SJ (1990) Bond ordering in silicate glasses: a critique and resolution. J Non-Cryst Solids 125:151–160
7. Shakhmatkin BA, Vedishcheva NM, Shultz MM, Wright AC (1994) The thermodynamic properties of oxide glasses and glass-forming liquids and their chemical structure. J Non-Cryst Solids 177:249–256
8. Vedishcheva NM, Shakhmatkin BA, Shultz MM, Wright AC (1996) The thermodynamic modelling of glass properties: a practical proposition? J Non-Cryst Solids 196:239–243
9. Shakhmatkin BA, Vedishcheva NM, Wright AC (1997) Borate glasses crystals and melts. In: Wright AC, Feller SA, Hannon AC (eds) Society of Glass Technology, Sheffield, p 189
10. Shakhmatkin BA, Vedishcheva NM, Wright AC (2001) Can thermodynamics relate the properties of melts and glasses to their structure? J Non-Cryst Solids 293–295:220–236
11. Vedishcheva NM, Shakhmatkin BA, Wright AC (2001) Thermodynamic modelling of the structure of glasses and melts: single-component, binary and ternary systems. J Non-Cryst Solids 293–295:312–317
12. Vedishcheva NM, Shakhmatkin BA, Wright AC (2003) Thermodynamic modelling of the structure of sodium borosilicate glasses. Phys Chem Glasses 44:191
13. Vedishcheva NM, Shakhmatkin BA, Wright AC (2004) The structure of sodium borosilicate glasses: thermodynamic modelling versus experiment. J Non-Cryst Solids 345&346:39–44
14. Shakhmatkin BA, Vedishcheva NM, Wright AC (2004) Thermodynamic modelling of the structure of oxyhalide glasses. J Non-Cryst Solids 345&346:461–468
15. Vedishcheva NM, Wright AC (2014) Chemical structure of oxide glasses: a concept for establishing structure-property relationships. Chapter 5. In: Schmelzer JWP (ed) Glass—selected properties and crystallization. De Gruyter, Berlin
16. Vonka P, Leitner J (1995) Calculation of chemical equilibria in heterogeneous multicomponent systems. Calphad 19:25–36
17. Seward III. TP, Vascott T (2005) High temperature glass melt property database for process modeling. American Ceramic Society, Westerville, Ohio
18. Pye LD, Montenero A, Josephs I (2005) Properties of glass-forming melts. Taylor and Francis, Boca Raton
19. http://www.sciglass.info
20. Bale CW et al (2002) FactSage thermochemical software and databases. Calphad 26:189–228
21. Chromčíková M, Liška M, Macháček J, Šulcová J (2013) Thermodynamic model and structure of $CaO–P_2O_5$ glasses. J Thermal Anal Calorim 144:785–789
22. Chromčíková M, Liška M, Gašpáreková E, Teplanová M, Karell R (2013) Thermodynamic model and viscosity of selected zirconia containing silicate glasses. Ceramics-Silikáty 57:66–73
23. Chovanec J, Chromčíková M, Pilný P, Shánělová J, Málek J, Liška M (2014) Thermodynamic model and viscosity of Ge–S glasses. J Thermal Anal Calorim 116:581–588
24. Chromčíková M, Liška M, Macháček J, Chovanec J (2014) Thermodynamic model and viscosity of $Na_2O–MgO–CaO–SiO_2$ glasses. J Non-Cryst Solids 401:237–240
25. Chromčíková M, Liška M, Gavenda T, Macháček J (2014) Structure of $Na_2O–MgO–CaO–SiO_2$ glasses by combined Raman spectroscopy and thermodynamic modelling approach. J Therm Anal Calorim 118:835–840
26. Liška M, Chromčíková M, Holubová J, Černošek Z (2014) Thermodynamic model and structure of $As_2S_3–As_2Se_3$ glasses based on the MCR analysis of Raman spectra. Ceram Silikáty 58:95–98
27. Chromčíková M, Liška M, Holubová J, Černošek Z (2014) Structure of $As_2S_3–Sb_4S_4$ glasses by combined Raman spectroscopy and thermodynamic modelling approach. J Non-Cryst Solids 401:115–118
28. Liška M, Zemanová V, Lissová M, Plško A, Chromčíková M, Gavenda T, Macháček J (2015) Thermodynamic model and Raman spectra of $ZnO–P_2O_5$ glass. J Therm Anal Calorim 121:85–91

29. Chromčíková M, Liška M, Lissová M, Plško A, Hruška B, Gavenda T (2015) Thermodynamic model and Raman spectra of $CaO–P_2O_5$ glasses. J Therm Anal Calorim 121:269–274
30. Liška M, Macháček J, Chromčíková M, Gedeon O (2015) Thermodynamic model and structure of $ZnO–MoO_3–P2O_5$ glasses. Phys Chem Glasses Eur J Glass Sci Technol 56:63–66
31. Chromčíková M, Hruška B, Holubová J, Lissová M, Liška M (2016) The Raman spectra and structure of $PbO–WO_3–P_2O_5$ glasses. Phys Chem Glasses Eur J Glass Sci Technol 57:32–36
32. Mysen BO, Richet P (2005) Silicate glasses and melts—properties and structure. In: Developments in geochemistry, Vol 10. Elsevier, Amsterdam
33. Pelton AD, Wu P (1999) Thermodynamic modeling in glass-forming melts. J Non-Cryst Solids 253:178–197
34. Stolyarova VL (2008) Thermodynamic properties and structure of ternary silicate glass-forming melts: Experimental studies and modeling. J Non-Cryst Solids 354:1373–1377
35. Frontline Systems, Inc.: http://www.frontsys.com
36. Zhang H, Bonilla-Petriciolet A, Rangaiah GP (2011) A review on global optimization methods for phase equilibrium modeling and calculations. TOTHERJ 5(Suppl 1-M7):71–92
37. Montastruc L, Azzaro-Pantel C, Pibouleau L, Domenech S (2004) Use of genetic algorithms and gradient based optimization techniques for calcium phosphate precipitation. Chem Eng Process 43:1289–1298
38. Coley DA (1999) An introduction to genetic algorithms for scientists and engineers. World Scientific Publishing Co. Pte. Ltd., Singapore
39. Inorganic Crystal Structure Database, Release (2003) Fachinformationszentrum Karlsruhe, Germany, and the U.S. Department of Commerce
40. Vatani M, Asghari M, Vakili-Nejhaad G (2012) Application of genetic algorithm to parameter estimation in liquid-liquid phase equilibrium modeling. TJMCS 5(1):60–66
41. Sestak J, Liska M, Hubık P (2011) Oxide glass structure, non-bridging oxygen and feasible magnetic properties due to the addition of Fe/Mn oxides. In: Šesták J, Mareš JJ, Hubík P (eds) Glassy, amorphous and nano-crystalline materials, Springer, Berlin, pp 199–216 (ISBN 978-90-481-2881-5)

Chapter 13
Equivalence of the Arrhenius and Non-Arrhenian Temperature Functions in the Temperature Range of Measurement and Its Application in Isoconversional Kinetics

Peter Šimon, Tibor Dubaj and Zuzana Cibulková

Abstract It is shown that the kinetic data can be equivalently described in the temperature range of measurement by the Arrhenius, Harcourt–Esson and Berthelot–Hood temperature functions. The reason is that, in a narrow temperature range, $1/T$, ln T and T are linearly related to each other. Therefore, the kinetic parameters obtained from one function can be recalculated to the parameters from another one. This equivalence holds for the incremental and differential isoconversional methods only; due to their mathematical incorrectness, the equivalence does not take place for the integral isoconversional methods. It is reasoned that the temperature functions are equivalent not only in the case of the isoconversional methods, but also for the model-fitting methods. An incremental isoconversional method without any approximations or transformations of the experimental data and with a statistically well-grounded and physically justified objective function based on the maximum likelihood approach is mentioned.

13.1 Introduction

Thermoanalytical methods are widely used to study the condensed-state processes. Mechanisms of these processes are usually unknown or too complex to be characterized by a simple kinetic model. Methods based on the general rate equation are almost exclusively used to describe their kinetics [1, 2]. Within the general rate equation approach, rate of the process is expressed as

P. Šimon (✉) · T. Dubaj · Z. Cibulková
Faculty of Chemical and Food Technology, Institute of Physical Chemistry and Chemical Physics, Slovak University of Technology, Radlinského 9, 812 37 Bratislava, Slovakia
e-mail: peter.simon@stuba.sk

J. Šesták et al. (eds.), *Thermal Physics and Thermal Analysis*,
Hot Topics in Thermal Analysis and Calorimetry 11,
DOI 10.1007/978-3-319-45899-1_13

$$\frac{d\alpha}{dt} = k(T)f(\alpha) \tag{13.1}$$

where α is the conversion, t is time, T is temperature, $k(T)$ is a temperature function depending on temperature T and $f(\alpha)$ is a conversion function depending on the conversion of the process. There is a number of conversion functions applied in the kinetic analysis of thermoanalytical data [3]. On the other hand, the Arrhenius equation is almost exclusively employed as the temperature function.

The most popular class of methods used for determination of the kinetic parameters are model-free isoconversional methods. They can be divided into integral, incremental and differential methods [4]. The integral methods are based on an assumption that the conversion function holds in the whole range of conversions. In [5], it was proved that in the case of variable activation energy, the application of integral isoconversional methods leads to incorrect values of the kinetic parameters. In most thermoanalytical kinetic studies, conversion-dependent activation energy is reported; hence, the integral methods should be avoided. Theoretically, only the differential methods should provide the correct values of kinetic parameters. However, the drawbacks of these methods are that they are sensitive to noise and tend to be numerically unstable when applied to experimental data [3, 6]. Consequently, the best choice for the treatment of kinetic data is to employ the incremental methods where the values of kinetic parameters are assumed to be constant within sufficiently small conversion intervals. Moreover, conversion function is assumed to hold over these small increments of conversion which is much weaker assumption than that employed in integral isoconversional methods.

The isoconversional methods published so far are concentrated predominantly on obtaining the values of activation energy. This is obviously the consequence of interpreting the activation energy as a real activation barrier. Many times, the stability of materials is assessed from the values of activation energy where it is assumed that the higher the activation energy, the higher the stability. Our meaning is that, in the case of complex processes, the kinetic parameters have no clear physical meaning in general; however, the kinetic parameters enable to calculate objectively existing quantities such as isoconversional time, isoconversional temperature and degree of conversion. In this case, all the kinetic parameters are of equal importance; for example, for the Arrhenius temperature function, both the pre-exponential function and the activation energy are equally important. In our paper [6], we proposed an incremental isoconversional method where the regression model is directly fitted without any approximations or transformations of the experimental data and the error structure of the thermoanalytical data is taken into account. Further advantage is that a statistically well-grounded and physically justified objective function based on the maximum likelihood approach is optimized; thus, the parameters' uncertainties can be determined. Another advantage of the method is that it can be easily adapted to the kinetic analysis using non-Arrhenian temperature functions.

This chapter summarizes and extends the results from our previous work [7]. We demonstrate that, within the temperature range of measurement, other temperature functions provide description of experimental data of the same quality as the Arrhenius equation. From the various temperature functions reviewed in [8], we have selected the Harcourt–Esson and Berthelot–Hood equations. In this chapter, we limit ourselves mainly to the incremental isoconversional methods; the integral and differential isoconversional methods will be touched only marginally.

13.2 Theoretical Part

13.2.1 Complex Mechanisms and the Single-Step Approximation

As mentioned in the introductory part, the rate of the complex multi-step condensed-state process can be formally described by the general rate equation presented by Eq. (13.1). It resembles a single-step kinetic equation, but in fact, it is a representation of the kinetics of a complex process. From the probability point of view, the meaning of Eq. (13.1) is that temperature and conversion affect the rate of the process independently without any interaction.

The temperature function in Eq. (13.1) is in majority studies interpreted as the rate constant, and the conversion function is considered to reflect the mechanism of the process. In [2], it was discussed that this interpretation of the both functions may be incorrect, and the functions $k(T)$ and $f(\alpha)$ represent just the temperature and conversion components of the kinetic hypersurface. The kinetic hypersurface is a dependence of conversion as a function of time and temperature [2].

With only for few exceptions [9–16], the temperature function is expressed by the Arrhenius equation as follows:

$$k(T) = A'_{\mathrm{A}} \exp\left(-\frac{E}{RT}\right), \tag{13.2}$$

where A'_{A} is the apparent pre-exponential factor and E is the apparent activation energy, T is the absolute temperature and R stands for the gas constant.

Since according to [2], $k(T)$ represents just the temperature component of the kinetic hypersurface, there is no reason to be confined to the Arrhenius relationship [1, 2, 4]. Thus, use of two non-Arrhenian temperature functions was suggested as follows:

$$k(T) = A'_{\mathrm{HE}} T^m, \tag{13.3}$$

where A'_{HE} and m are parameters. Equation (3) is known as the Harcourt–Esson equation. The second one is the Berthelot–Hood equation and has the following form:

$$k(T) = A'_{\mathrm{BH}} \exp(DT), \tag{13.4}$$

where A'_{BH} and D stand for parameters.

13.2.2 Incremental Isoconversional Methods

In the incremental methods, the conversion axis is divided into n increments by $n + 1$ points, with the first point $\alpha_0 = 0$ at $t_0 = 0$ (or at $T_0 = 0$). The increments may not be necessarily of the same length; however, they should be short enough that the kinetic parameters could be considered constant.

Separation of variables in Eq. (13.1) and integration over the ith conversion increment leads to the result

$$\int_{\alpha_{i-1}}^{\alpha_i} \frac{\mathrm{d}\alpha}{f(\alpha)} = \int_{t_{i-1}}^{t_i} k(T)\,\mathrm{d}t \tag{13.5}$$

If the primitive function of the inverted conversion function, $1/f(\alpha)$, is denoted as $F(\alpha)$, then the following is obtained

$$1 = \frac{1}{F(\alpha_i) - F(\alpha_{i-1})} \int_{t_{i-1}}^{t_i} k(T)\,\mathrm{d}t \tag{13.6}$$

Equation (6) is general and can be applied for any time/temperature regime. At a constant temperature, the temperature function is constant and one can get as follows:

$$t_i - t_{i-1} = \Delta t_i = \frac{F(\alpha_i) - F(\alpha_{i-1})}{k(T)} \tag{13.7}$$

The difference Δt_i is the time needed to increase the conversion from α_{i-1} to α_i at the constant temperature. Combination of Eq. (13.7) with Eqs. (13.2)–(13.4) yields as follows:

$$\Delta t_i = A_{\mathrm{A}} \exp(E/RT) \tag{13.8}$$

$$\Delta t_i = A_{\mathrm{HE}}\, T^{-m} \tag{13.9}$$

$$\Delta t_i = A_{\mathrm{BH}} \exp(-DT) \tag{13.10}$$

The individual pre-exponential factors for the Arrhenius, Harcourt–Esson and Berthelot–Hood are then defined as follows:

$$A_{\mathrm{k}} = \frac{F(\alpha_i) - F(\alpha_{i-1})}{A'_{\mathrm{k}}} \tag{13.11}$$

The kinetic parameters for individual conversion intervals may differ. The time to reach the final conversion, t_α, is calculated as the sum of the individual time differences

$$t_\alpha = \sum_{i=1}^{n} \Delta t_i \tag{13.12}$$

In most thermoanalytical experiments, the linear heating regime is applied, where the temperature versus time relationship is expressed as follows:

$$T = T_0 + \beta t, \tag{13.13}$$

where T_0 is the starting temperature and β is the heating rate. Differentiating of Eq. (13.13) gives $\mathrm{d}t = \mathrm{d}T/\beta$, so that from Eq. (13.6) one can get as follows:

$$\beta = \frac{1}{F(\alpha_i) - F(\alpha_{i-1})} \int_{T_{i-1}}^{T_i} k(T)\,\mathrm{d}T = \int_{T_{i-1}}^{T_i} \frac{1}{\Delta t_{\mathrm{i}}(T)}\mathrm{d}T \tag{13.14}$$

Combination of Eq. (13.14) and Eqs. (13.8)–(13.10), for individual temperature functions leads to the following:

$$\beta = \int_{T_{i-1}}^{T_i} \frac{1}{A_{\mathrm{A}}\exp(E/RT)}\mathrm{d}T, \tag{13.15}$$

$$T_{\mathrm{i}} = \left[A_{\mathrm{HE}}(m+1)\beta + T_{i-1}^{m+1}\right]^{1/(m+1)} \tag{13.16}$$

$$T_{\mathrm{i}} = \frac{1}{D}\ln\left(A_{\mathrm{BH}}D\beta + e^{DT_{i-1}}\right) \tag{13.17}$$

An advantage of the application of temperature functions given by Eqs. (13.3) and (13.4) is that the temperature integral can be expressed in a closed form, as it can be seen from Eqs. (13.16) and (13.17).

13.2.3 Recalculation of the Kinetic Parameters

If the temperature functions are equivalent in the temperature range of the measurement, then either the isoconversional temperatures or times (or time increments)

should have the same values independently of the temperature function applied, since they reflect the physical reality. The isoconversional temperatures are expressed by Eqs. (13.15)–(13.17). The application of these equations for the recalculation of kinetic parameters would be difficult, since they are quite complicated. Moreover, the isoconversional temperature cannot be explicitly expressed from Eq. (13.15). On the other hand, it is very simple to employ Eqs. (13.8)–(13.10) for this purpose.

Let T_H and T_L be the highest and the lowest temperatures from the temperature range of measurement. Then, for the recalculation of the kinetic parameters of the Harcourt–Esson equation into the parameters of the Arrhenius equation, the following relationships hold:

$$A_A \exp(E/RT_H) = A_{HE} T_H^{-m}, \tag{13.18}$$

$$A_A \exp(E/RT_L) = A_{HE} T_L^{-m} \tag{13.19}$$

From Eqs. (13.18) and (13.19), it is straigthforward to obtain as follows:

$$E = R \frac{mT_L T_H}{T_H - T_L} \ln \frac{T_H}{T_L}, \tag{13.20}$$

$$A_A = A_{HE} \exp\left(-m \frac{T_H \ln T_H - T_L \ln T_L}{T_H - T_L} \right) \tag{13.21}$$

Equation (20) has already been derived by Dollimore et al. in [17]. An analogical procedure applied to the Berthelot–Hood equation gives the relationships as follows:

$$E = RDT_H T_L, \tag{13.22}$$

$$A_A = A_{BH} \exp[-D(T_H + T_L)] \tag{13.23}$$

13.3 Calculations

In [7], a simulated data set has been calculated by integrating Eq. (13.1) for the first-order kinetics with $f(\alpha) = 1 - \alpha$. The Arrhenius equation was chosen as the temperature function with the kinetic parameters $A'_A = 10^{12}$ min^{-1} and E = 100 kJ mol^{-1}. The integration has been carried out by the fourth-order Runge–Kutta method taking into account that $dt = dT/\beta$. The data are listed in Table 13.1.

The incremental isoconversional method based on the orthogonal distance regression has been employed to calculate the kinetic parameters of the Harcourt–Esson and Berthelot–Hood temperature functions. The program code can be found as a supplementary material to our recent paper [6].

Table 13.1 Simulated data set based on the first-order kinetics and the Arrhenius temperature function with the kinetic parameters $A'_A = 10^{12}$ min^{-1} and $E = 100$ kJ mol^{-1}

β/K min^{-1}	T_α/K																		
	0.05	0.1	0.15	0.2	0.25	0.3	0.35	0.4	0.45	0.5	0.55	0.6	0.65	0.7	0.75	0.8	0.85	0.9	0.95
1	365.03	372.71	377.5	381.07	383.98	386.48	388.69	390.72	392.61	394.4	396.12	397.82	399.51	401.22	403	404.9	407.02	409.54	413.01
3	376.89	385.07	390.16	393.97	397.08	399.74	402.11	404.28	406.29	408.21	410.05	411.87	413.67	415.51	417.41	419.45	421.71	424.41	428.13
5	382.66	391.09	396.34	400.27	403.47	406.22	408.67	410.9	412.98	414.95	416.86	418.73	420.6	422.49	424.46	426.56	428.9	431.69	435.54
7	386.55	395.15	400.51	404.52	407.79	410.6	413.09	415.37	417.5	419.52	421.47	423.38	425.28	427.22	429.23	431.38	433.77	436.62	440.55
10	390.77	399.55	405.03	409.13	412.47	415.34	417.89	420.22	422.4	424.46	426.45	428.41	430.36	432.34	434.4	436.6	439.05	441.97	445.99

Simulated data—isoconversional temperatures for various isoconversional levels and various heating rates

13.4 Results and Discussion

The results are summarized in Table 13.2. As seen, the kinetic parameters of the both temperature functions depend on conversion, although the input activation energy and pre-exponential factor used for the calculation of the simulated data set are constant.

Application of the Arrhenius and non-Arrhenian temperature functions led to the practically overlapping calculated curves as it can be seen in Fig. 13.1. In case of coinciding curves, there may be a possibility to recalculate the kinetic parameters occurring in various temperature functions.

13.4.1 Recalculation of Kinetic Parameters

The recalculation of the kinetic parameters was demonstrated on the simulated data set (Table 13.1). The simulated data set was used to ensure that the result from the recalculation is correct and not influenced by experimental noise. For the increment between *i*th and $(i - 1)$th isoconversional levels, we used the highest isoconversional

Table 13.2 Values of the kinetic parameters calculated by the incremental isoconversional method based on the Harcourt–Esson and the Berthelot–Hood temperature functions

α	Harcourt–Esson		Berthelot–Hood	
	m	ln A_{HE}	D/K^{-1}	ln A_{BH}
0.05	32.82	196.001	0.08967	35.128
0.10	31.47	188.073	0.08234	32.411
0.15	30.98	185.176	0.07970	31.448
0.20	30.60	182.983	0.07784	30.781
0.25	30.36	181.615	0.07656	30.338
0.30	30.14	180.328	0.07544	29.958
0.35	29.91	179.046	0.07440	29.614
0.40	29.83	178.620	0.07378	29.441
0.45	29.59	177.293	0.07281	29.133
0.50	29.50	176.869	0.07226	28.998
0.55	29.27	175.569	0.07135	28.726
0.60	29.25	175.546	0.07098	28.689
0.65	29.09	174.718	0.07028	28.524
0.70	28.93	173.878	0.06958	28.376
0.75	28.80	173.273	0.06896	28.286
0.80	28.68	172.747	0.06835	28.232
0.85	28.56	172.253	0.06770	28.214
0.90	28.37	171.483	0.06687	28.205
0.95	28.16	170.761	0.06587	28.318

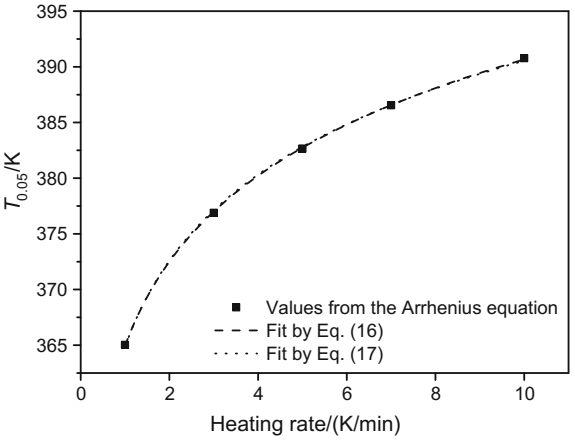

Fig. 13.1 Treatment of the simulated data from Table 13.1 for the isoconversional levels $\alpha_1 = 0.05$ and $\alpha_0 = 0$ by employing Eqs. (13.16) and (13.17)

temperature in the ith level as the temperature T_H and the lowest temperature in the $(i - 1)$th isoconversional temperature as the temperature T_L.

For the isoconversional level $\alpha = 0$, the isoconversional temperature in Eq. (13.14) (the lower integration limit) is being set as $T_0 = 0$ K. However, for the recalculation of kinetic parameters, the temperature $T_0 = 0$ K cannot be applied, since Eqs. (13.20) and (13.22) would lead to the zero value of the activation energy. Therefore, in the recalculations of the first interval, the extrapolated value of $\sqrt{T_H T_L}$ to zero conversion was estimated. For this purpose, also the isoconversional temperature for the 1% conversion at the heating rate 1 K min^{-1} was calculated ($T_{0.01}$(1 K min^{-1}) = 348.72 K). This procedure led to the value $\left(\sqrt{T_H T_L}\right)_0 = 365.96$ K.

In the recalculations, we calculated the values of the activation energy and pre-exponential factor from the values of kinetic parameters occurring in the Harcourt–Esson and Berthelot–Hood equations. The simulated data set was calculated for the first-order kinetics; hence, the pre-exponential factor A_A was recalculated into A'_A by rearranging Eq. (13.11):

$$A'_A = \frac{1}{A_A} \ln \frac{1 - \alpha_{i-1}}{1 - \alpha_i} \tag{13.24}$$

The activation energy and pre-exponential factor were calculated from the kinetic parameters of the Harcourt–Esson and Berthelot–Hood functions by applying Eqs. (13.20)–(13.23). As seen from Figs. 13.2 and 13.3, the recalculated values differ from the input values for the simulated data set within the round-off errors only. Our results demonstrate that the recalculation of kinetic parameters is a feasible procedure.

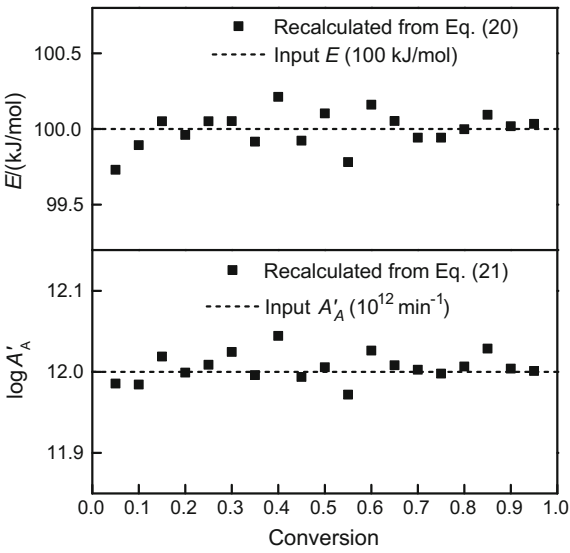

Fig. 13.2 Values of the activation energy and pre-exponential factor recalculated from the kinetic parameters of the Harcourt–Esson temperature function

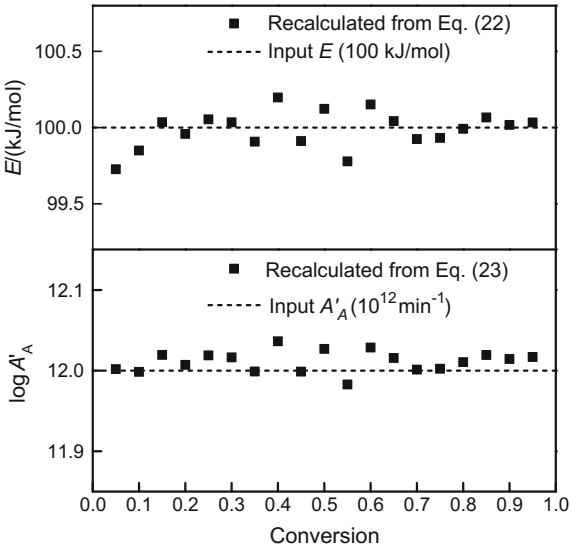

Fig. 13.3 Values of the activation energy and pre-exponential factor recalculated from the kinetic parameters of the Berthelot–Hood temperature function

13.4.2 Uncertainties of the Parameters

In this paper, the recalculation of the kinetic parameters is analyzed using a simulated data set. While the simulated data set is subject to only negligible round-off errors, this does not apply to experimental data. Hence, point estimates of the kinetic parameters from Eqs. (13.20)–(13.23) should always be supplemented with

their uncertainties. This can be accomplished by propagating the uncertainty of the non-Arrhenian kinetic parameters to the apparent pre-exponential factor and apparent activation energy. If the apparent activation energy is obtained by recalculation from the parameters of the Harcourt–Esson equation, then the corresponding standard error, SE(E), can be estimated as follows:

$$\mathrm{SE}(E) = R\frac{T_\mathrm{L}T_\mathrm{H}}{T_\mathrm{H}-T_\mathrm{L}}\ln\left(\frac{T_\mathrm{H}}{T_\mathrm{L}}\right)\cdot\mathrm{SE}(m) \tag{13.25}$$

Taking into account a strong positive correlation between $\ln A_\mathrm{HE}$ and m in Eq. (13.21), the standard error of $\ln A_\mathrm{A}$ is as follows:

$$\mathrm{SE}(\ln A_\mathrm{A}) = \sqrt{\mathrm{SE}(\ln A_\mathrm{HE})^2 + [\ln(\bar{T})\mathrm{SE}(m)]^2 - 2\ln(\bar{T})\mathrm{SE}(\ln A_\mathrm{HE})\mathrm{SE}(m)}, \tag{13.26}$$

where $\bar{T} = (T_\mathrm{H}^{T_\mathrm{H}}/T_\mathrm{L}^{T_\mathrm{L}})^{1/(T_\mathrm{H}-T_\mathrm{L})}$.

Analogous relationships can be derived in the case of the Berthelot–Hood equation as follows:

$$\mathrm{SE}(E) = RT_\mathrm{L}T_\mathrm{H}\mathrm{SE}(D) \tag{13.27}$$

and

$$\mathrm{SE}(\ln A_\mathrm{A}) = \sqrt{\mathrm{SE}(\ln A_\mathrm{BH})^2 + [(T_\mathrm{L}+T_\mathrm{H})\mathrm{SE}(D)]^2 - 2(T_\mathrm{L}+T_\mathrm{H})\mathrm{SE}(\ln A_\mathrm{BH})\mathrm{SE}(D)} \tag{13.28}$$

13.4.3 Integral and Differential Isoconversional Methods

The integral and differential methods can be considered special cases of the incremental method. In the integral methods, the lower integration limit is always set zero, so that there is only one increment. Equation (14) can be then rewritten as follows:

$$\beta = \int_0^{T_i}\frac{1}{t_i(T)}\mathrm{d}T \tag{13.29}$$

where T_i is the ith isoconversional level. In Fig. 13.4, there are summarized results for the recalculation of the kinetic parameters calculated by the integral methods based on the Harcourt–Esson and Berthelot–Hood equations. It can be seen that the recalculated data do not agree with the input data; there is a tendency of decrease in the activation energy with increasing conversion. The reason is that the kinetic

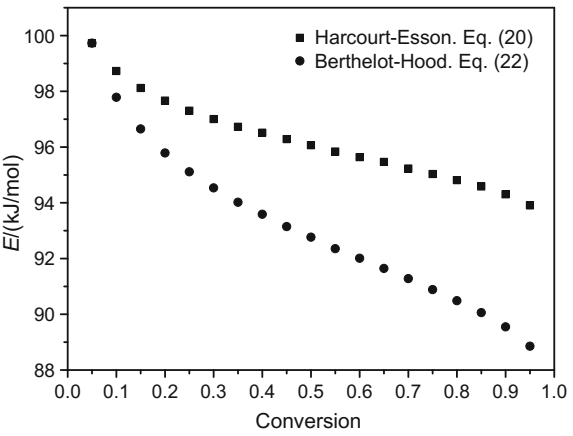

Fig. 13.4 Dependences of the activation energy recalculated from the kinetic parameters of the Harcourt–Esson and Berthelot–Hood temperature functions for the integral isoconversional method

parameters for the Harcourt–Esson and Berthelot–Hood equations vary with conversion so that the both integral methods are mathematically incorrect [5]. The same trend for the dependence of the activation energy on conversion for the integral isoconversional method based on the Harcourt–Esson temperature function was reported in [18].

Considering the differential methods, the increment is infinitesimally small so that the kinetic parameters are continuous functions of the conversion. In this case, for the Arrhenius temperature function, after separation of variables in Eq. (13.1), the time to reach the conversion α can be calculated as follows:

$$t_\alpha = \int_0^\alpha \frac{\mathrm{d}\alpha}{A_\mathrm{A}(\alpha)\exp[-E(\alpha)/RT]}, \tag{13.30}$$

where in this case, the parameter A_A is a product of $A'_\mathrm{A} f(\alpha)$ [4]. The conversion for the Harcourt–Esson and Berthelot–Hood equations can be calculated in an analogical way.

13.4.4 Equivalence of the Temperature Functions

Laidler [8] was probably the first person who explained the coincidence of the calculated kinetic curves when using the Arrhenius, Harcourt–Esson and Berthelot–Hood equations. The reason resides in the narrow temperature range usually employed in kinetic studies which is often only about 40–50 K and sometimes even less. For two neighbouring columns in the simulated data set (Table 13.1), the difference between the lowest and highest temperature is always below 40 K. For the three temperature functions mentioned, ln k depends linearly on $1/T$, ln T and T,

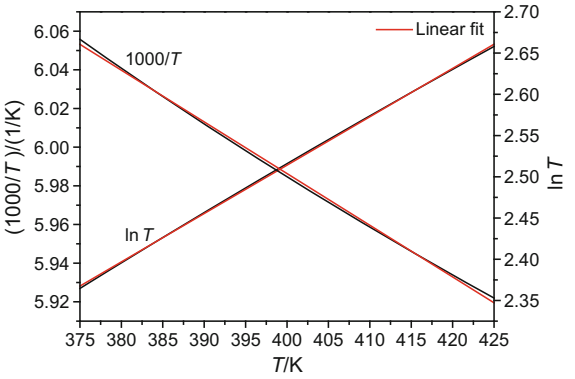

Fig. 13.5 Linear dependence of ln T and $1/T$ on temperature for the temperature range of 375–425 K

respectively. Thus, for the narrow temperature range, $1/T$, ln T and T are linearly related to each other [8]. This is illustrated in Fig. 13.5 where the dependences of $1/T$ and ln T on temperature are shown for 400 ± 25 K, i.e. for the temperature range of 50 K. It is seen that the linearity is almost perfect and the correlation coefficient is better than 0.999 for both dependences. The higher the temperature, the better the correlation. Hence, over the narrow temperature range, the three temperature functions represent just a linear transformation of each other so that they are equivalent.

13.5 Conclusions

The results obtained demonstrate that the studied temperature functions, i.e. the Arrhenius, Harcourt–Esson and Berthelot–Hood functions describe the kinetic data equivalently in the temperature range of measurement. The reason is that, in a narrow temperature range, $1/T$, ln T and T are linearly related to each other. This finding is not limited to the model-free methods so that it can be generalized also for the model-fitting methods. It is necessary to underline that the equivalence of the temperature functions holds in the temperature range of measurement only. When extrapolating the data out of the temperature range, the Arrhenius extrapolation mostly provides unrealistically overestimated isoconversional times. For the extrapolation, employment of non-Arrhenian temperature functions is advisable [19, 20].

The equivalence of the temperature functions enables the recalculation of the kinetic parameters from one function to another. This procedure was originally proposed in [17] for obtaining the Arrhenius parameters from the parameters of the Harcourt–Esson function. In this age of practically unlimited computational facilities, there is no valid reason not to calculate the kinetic parameters directly. The recalculation procedure can be very useful for comparison of the kinetic parameters obtained by methods based on various temperature functions.

Acknowledgements This work was supported by the Research and Development Operational Programme project "University Science Park of STU Bratislava", ITMS 26240220084, co-funded by the European Regional Development Fund. The financial support from the Slovak Scientific Grant Agency, grant No. VEGA 1/0592/15, is acknowledged.

References

1. Šimon P (2005) Considerations on the single-step kinetics approximation. J Therm Anal Calorim 82:651–657
2. Šimon P (2007) The single-step approximation: attributes, strong and weak sides. J Therm Anal Calorim 88:709–715
3. Vyazovkin S, Burnham AK, Criado JM, Pérez-Maqueda LA, Popescu C, Sbirrazzuoli N (2011) ICTAC kinetics committee recommendations for performing kinetic computations on thermal analysis data. Thermochim Acta 520:1–19
4. Šimon P (2004) Isoconversional methods—fundamentals, meaning and application. J Therm Anal Calorim 76:123–132
5. Šimon P, Thomas P, Dubaj T, Cibulková Z, Peller A, Veverka M (2014) The mathematical incorrectness of the integral isoconversional methods in case of variable activation energy and the consequences. J Therm Anal Calorim 115:853–859
6. Dubaj T, Cibulková Z, Šimon P (2015) An incremental isoconversional method for kinetic analysis based on the orthogonal distance regression. J Comput Chem 36:392–398
7. Simon P, Dubaj T, Cibulkova Z (2015) Equivalence of the Arrhenius and non-Arrhenian temperature functions in the temperature range of measurement. J Therm Anal Calorim 120:231–238
8. Laidler KJ (1984) The development of the Arrhenius equation. J Chem Educ 61:494–498
9. Dollimore D, Lerdkanchanaporn S, Alexander KS (1996) The use of the Harcourt and Esson relationship in interpreting the kinetics of rising temperature solid state decompositions and its application to pharmaceutical formulations. Thermochim Acta 290:73–83
10. Rodante F, Vecchio S, Catalani G, Guidotti M (2000) Thermal analysis and non-isothermal kinetic studies of some pesticides Part II: Chlorinate derivatives. J Therm Anal Calorim 60:605–622
11. Shih Y-F (2007) A study of the fiber obtained from the water bamboo husks. Biores Technol 98:819–828
12. Maitra S, Bandyopadhyay N, Pal J (2008) Application of non-Arrhenius method for analyzing the decomposition kinetics of $SrCO_3$ and $BaCO_3$. J Am Ceram Soc 91:337–341
13. Chen H, Liu N (2008) Approximation expressions for the temperature integral. Progr Chem 20:1015–1020
14. Chen H, Liu N (2010) Application of non-Arrhenius equations in interpreting calcium carbonate decomposition kinetics: revisited. J Am Ceram Soc 93:548–553
15. Zhao H, Yan H, Zhang C, Liu X, Xue Y, Qiao Y, Tian Y, Qin S (2011) Pyrolytic characteristics and kinetics of phragmites Australis Evid-Based Complement Altern Med Article, ID 408973. doi:10.1155/2011/408973
16. Li Y-B, Zhao J-Z, Pu W-F, Peng H, Zhong D, Hu Z-W (2014) A method based on the Harcourt and Esson equation to estimate the catalytic effect of metallic additives on light crude oil. J Alloys Compounds 585:7–13
17. Dollimore D, Tong P, Alexander KS (1996) The kinetic interpretation of the decomposition of calcium carbonate by use of relationships other than the Arrhenius equation. Thermochim Acta 282–283:13–27
18. Gotor FJ, Criado JM (2002) The abuse of the Harcourt and Esson relationship in interpreting the kinetics of rising temperature solid state reactions. Thermochim Acta 383:53–58

19. Šimon P, Hynek D, Malíková M, Cibulková Z (2008) Extrapolation of accelerated thermooxidative tests to lower temperatures applying non-Arrhenius temperature functions. J Therm Anal Calorim 93:817–821
20. Šimon P (2009) Material stability predictions applying a new non-Arrhenian temperature function. J Therm Anal Calorim 97:391–396

Chapter 14
Rationale and Myth of Thermoanalytical Kinetic Patterns: How to Model Reaction Mechanisms by the Euclidean and Fractal Geometry and by Logistic Approach

Jaroslav Šesták and Isak Avramov

Abstract Modeling tradition is reviewed within its historical maturity from Greek Plato to modern Penrose. Metaphors in non-isothermal kinetics achieved a wide application mostly employing models derived by means of undemanding isothermal descriptions. Geometrical basis of such modeling is revised and discussed in terms of symmetrical and asymmetrical (pentagonal) schemes. The properties of interface (reaction separating line) are found decisive in all cases of heterogeneous kinetics and can be acquainted with defects. The use of yet atypical fractal geometry is accredited, and associated formal kinetic models based on non-integral power exponents are acknowledged. Mathematical commencement and impact of logistic models are used highlighting the Sesták–Berggren (SB) equation and the impact of logistic approach as a generalized exploit. Typical erroneous beliefs are dealt with showing common kinetic misinterpretation of measured data and associated mathematical manipulability of kinetic equations. The correction of a measured DTA peak is mentioned assuming the effects of heat inertia and temperature gradients. The chapter contains 117 references.

14.1 Some Philosophical Thoughts as Introduction

The four basic (inventive) elements [1–4] *fire, air, earth,* and *water* (initiated by *Empedocles* 492–432) were the first known models and metaphors to signify the substantiality of which all subsistence is composed (i.e., *quantities* and

J. Šesták (✉)
New Technologies Research Centre (NTC-ZČU), University of West Bohemia,
Universitní 8 30114 Pilsen, Czech Republic
e-mail: sestak@fzu.cz

I. Avramov
Institute of Physical Chemistry, Bulgarian Academy of Sciences,
1113 Sofia, Bulgaria
e-mail: Avramov@ipc.bas.bg

J. Šesták et al. (eds.), *Thermal Physics and Thermal Analysis*,
Hot Topics in Thermal Analysis and Calorimetry 11,
DOI 10.1007/978-3-319-45899-1_14

interconnecting *qualities* such as warmness, dryness, coldness, and humidity). They were thought to possess the integrative and structural element or *quintessence* (after 'quint' meaning 'fifth') called *aether* or better *form* in the sense of an imperishable firmament (which in the modern world is interpreted as *in-**form**-ation*) [5–7]. Today however, mathematical modeling ensues differently not only from a further approved physical existence but also from an existence that is assigned by our more cultured mental perceptions. It is not just the precision but also the subtle sophistication and mathematical beauty of successful models that is profoundly mysterious. Mathematics is crucially concerned about *truth,* and philosophers would agree that there are some other fundamental (almost absolute) concerns, namely that *of beauty* and *of good,* which exist since the Platonic geometrical world of mathematical forms [7, 8]; however, it is the question of applicable to the portrayal of real processes.

The early modeling elements were first depicted by the metaphors of simple, equilateral triangles either pointing up, in order to escape (like air or fire), or pointing down, in order to rest (like water or earth). Later, Plato (427–347) used more explicit geometrical models spatially arranging multiple triangles, i.e., three triangles formed *tetrahedron* (∼fire), eight triangles—*octahedron* (∼air), six squares, or twelve triangles—*cube* (∼earth). Water, however, was represented by a more complex geometrical body called *icosahedra* (twenty triangles, cf. Fig. 14.1). In Greek culture, the term symmetry was interpreted as the harmony of different parts of an object. *Symmetria* (∼common measure) is composed of the prefix *sym* (∼common) and *meters* (∼measure). The Greek Gaius Plinius Secundus (23–82) provided the early fundament for crystallography (derived from Greek *cristal-los* ∼ piece of ice) as he gave primary rules for the plan-metric faces of crystals and their visually imagery shaping.

However, the most impressive historical treatise on crystallography was written by Johann Kepler (1571–1612), while resident in Prague (within the years 1600–1612) and was devoted to the description of snowflakes [9, 10]. In analyzing their numerous forms bearing a steady hexagonal symmetry, Kepler suggested a certain

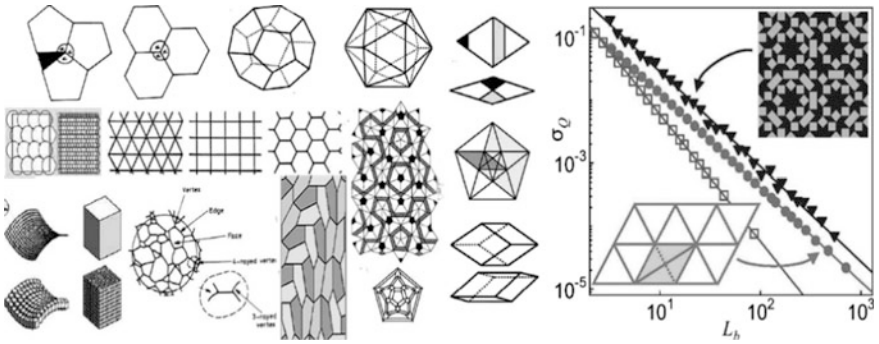

Fig. 14.1 *Left* Building faces (as construction blocks) available for geometrical modeling. *Right* The drawing portrayal of three-dimensional random scheme [20] for periodical boundary conditions with a block size L_b and the coordination number of fluctuations σQ

generalization model for the densest arrangement of rigid balls. Factually, he introduced the coordination-like number for a ball-like environment and declared the consistency of angles between analogical crystal planes and edges. It can be assumed that some implication of Platonian geometry was also inherent in Kepler's applications [10]. Though Auguste Bravais (1811–1863) was not sure that crystals are internally arranged in a repeatable manner, he mathematically modeled the fourteen geometrical figures that can be spatially arranged in a periodic mode [11, 12]. They can be characterized by a combination of one or more rotations and inversions in a lattice that is understood as a regular array of discrete points representing individual structural units (atoms, molecules, species), which thus appear exactly the same viewed from any point of the array. This discovery allows us to classify crystal shapes nowadays in the seven geometrically basic schemes: Area and/or *space can be filled completely* and symmetrically with tiles of *three, four, and six sides*. This is close to the Platonian conceptions of geometrical bodies but excludes, however, any *pentagonal* arrangement (also involved in the early Platonic bodies) because it is not possible to fill any area completely with its 5-fold symmetry. In the early 1970s, however, Roger Penrose (1931–) discovered that a surface can be wholly tiled in a specifically asymmetrical but non-repeating manner [13] providing some constructions similar to the cluster structure of liquid water [14] or glassy state of non-crystalline materials (like metallic glasses), which has been for a long run in the core of attention [15] (see Fig. 14.1).

These relations can be followed far back to history when the geometry of pentagon (and the pentagram inscribed within) bore its high metaphysical association as explored by the Pythagoreans (after *Pythagoras* 586–506): They considered it as an emblem of perfection. It was a doctrine that all things compose and proceed from numbers and the middle number five as being formed by the union of the odd and the first event was deemed of a peculiar value. In China, the central number five, similarly, represented the fifth additional element—the earth as the allied symbol of the great China [4, 16]. In astrology, geometrical figures kept engendering mystical and occult connotations such as with the supposed magical powers of pentagons and pentagrams. This effect lasted until recently as various occult guilds are often symbolized by five-leaved rose.

One consequence is the way how we fragment real-world entities into several categories: *things, events, and processes.* By things, we typically mean those entities which are separable, with identifiable shapes and size, and which persist in time. Events, on the other hand, have a relatively short duration and are composed of the interactions of several things of various sizes. Processes are, in this last property, similar to events but, like things, have a relatively long duration. However, many other entities may have a transient character such as vortices, flames, clouds, sounds, and ceremonies. There is an obvious difference between generic categories and particular entities because a category may be scale-thin in two different ways: generically (atoms, birds, etc.) or individually (geometrical concepts, etc.).

In the case of complex objects, there is a close relationship between their distribution over scales and a hierarchy of their structural, functional, and describable levels. We tend to assign objects of our concern into structural levels and events as

well as processes into functional levels. Obvious differences of individual levels yield different descriptions, different terminologies (or languages), and eventually different disciplines. Two types of difficulty, however, emerge, one caused by our limited understanding of whether and how distinct levels of a system can directly interact and, the other, related to the communication (words) barriers developed over decades of specialization of scientific disciplines [5, 17, 18] (providing the urgent need for a topic of *interdisciplinarity*).

14.2 On a General Execution of Mathematical Modeling

One of the first mathematical theories in science that dealt with interlevel interactions was Boltzmann's statistical physics, which is related to thermodynamics and to the study of collective phenomena. It succeeded in eliminating the lower (microscopic) level from the macroscopic laws by decomposing the phase space to what is considered macroscopically relevant subsets and by introducing new concepts, such as the mannered entropy principle. It requested to widely adopt the function of logarithm that was already and perpetually accustomed by nature alone (physiology, psychology [5, 6]). In comparison, another scaled sphere of a natural process can be mentioned here where the measure of coast or gradual evolution of living parts has been matured and completed in the log/log relations, called the *allometric* dependence, often penetrating to the kinetic evaluation methods [5, 7, 16].

Another relevant area is the study of order/disorder phenomena [5, 13, 15], acknowledging that microscopically tiny instability, the so-called *fluctuations*, can be somewhat 'immediately' amplified to a macroscopic scale. What seems to be a purely random event on one level can appear to be deterministically lawful behavior on some other level. Quantum mechanics may serve as an example where the question of measurement is actually the eminent question of interpreting macroscopic images of the quantum-scale uncertainty actions [5, 29]. Factually, we construct 'things' on the basis of 'information'; going from micro to macro in resemblance recalling the traditional case of engines as *information transducers* because they can be seen as transformers of energy without changing itself (not accounting on wearing by mechanical degradation).

Let us go inspecting the other construction manners while assembling basic geometrical blocks arising available for macroscopic modeling of makeup. Besides customarily adjustable hexagons, the pentagons (depicted in the upper raw of Fig. 14.1) reveal their incommensurability to compose a continuous web because of uncovered or overlapping areas. This can only be harmonized by curving their edges or adjusting angles (5-sided→convex and 7-sided→concave) or even employing asymmetrical tiles (far right). Classical symmetrical network, however, can only be satisfied with a collection of triangular, tetragonal, and hexagonal faces (middle) and their mutual combinations. For an array of equal balls and/or cubes (even when crimped), the restrictions are faced due to a strict Euclidean dimensionality, not found, however, in any actual microscopically observed electronic

images, which is often characterized (or observed) by typical 2-D cross sections (bottom right). Irregular grain structures (middle bottom) possess distinctive faces, which can best be characterized by the degree of vertices (4-rayed vertex decomposing to 3 as a spontaneous growth occurs). Some constructions (associable, e.g., with the clustered structure of liquid water [14]) are tiling in 5-fold symmetry, which were thought for long run as impossible to fill areas completely and regularly (Fig. 14.1 middle right). Upper right is revealed as dodecahedron (which Plato associated with heavenly firmament) interconnecting with the larger clusters of icosahedron (which Plato associated with water).

In Fig. 14.1, there are visualized the diamond (so-called Penrose) basic tiles [8] with a specific shape called 'rhombus,' where upper thick rhomb has longer diagonal equal to the 'golden ratio' phi (φ = 1.618034…, which is related to the number 5 by formulae $(1-\sqrt{5})/2$), fascinatingly playing a crucial role in various aspects of natural livelihood and also man-made art of constructions. The thinner rhomb has his shorter diagonal equal to $1/\varphi$. Both rhombs can be derived from a pentagon, whose five diagonals match ϕ and whose 5-side structure leaves gaps when used to be continuously repeated in space. On the other hand, the rhombs can fill the surface in an asymmetrical and non-repeating manner, which is known as *continuous but non-repeating structure* (sometimes called '*quasicrystals*'). On expanded tiling when covering greater areas, the ratio of the quantity of thick rhombs to thin ones approaches φ again and if the rhombs are marked by shadow strips, they form the unbroken structure (middle) where we can localize both the chains (like polymers) and pentagons (like water clusters), where the below connectivity map shows the molecules' orderliness within an icosahedron. Such a configuration can also be applied to a spatial distribution if the two kinds of rhombohedra are assembled to form icosahedrons matching thus the larger clusters (water again) but were never employed in the modeling of reaction solid-state species.

Not less important are modern issues while enforced drawing portrayal of three-dimensional random (so-called Voronoi) lattice (∇) or ($\sim$Delaunay) triangulation (o) following the Euler equation [20–22]. This characteristic is designed for its topological invariant χ equal to N − E + F − C where N are the lattice sites (with block size L_b, horizontal axis), E edges, F facets, and C frame the 3-D cells ($\sim$tetrahedras). For periodical boundary conditions, χ happens zero (otherwise involving an extra degree of freedom).

14.3 Modeling Roots Applied in Reaction Kinetics

In solid-state reaction kinetics [5, 6, 16, 23, 24], it is convenient to postulate a thought ('*gedenken*') model visualizing thus the feedback, which is usually separated into a sequence of possible steps then trying to identify the slowest event, which is considered to be the *rate-determining process* [23, 25]. Such models usually incorporate (often hypothetical) description of consequent and/or concurrent processes of interfacial chemical reactions and diffusion transport of reactants,

which governs the dimensionless degree of conversion α, the constitution of which is allocated by new phase formation (nucleation) and its consequent (crystal) growth. Such a modeling is often constructed within the perception of simplified geometrical structures (ideal Euclidian bodies), which are responsible to depict the incorporated particles, and such visualization exemplifies the reaction interfaces by *disjointing lines*. Such a derived kinetics then depends on all such physical, chemical, and geometrical events focused on the behavior of interface acting between the product and the initial reactant [5, 6, 16, 24, 26]. Accordingly, the space coordinates become rate-controlling rudiments responsible to create a heterogeneity consequence inevitably to be incorporated for solid-state samples. At the moment when interfaces are created, they should be identified with the underlying principle of defects conveniently symbolized by a pictographic contour (borderline curves) at our graphical representation. Hence, the mathematical description turns out to be much more complicated due to the fact that *no mean measure* (such as bulk concentration) but the *spot/site/defect assessment* (extent of phase interfaces) *carries out the most considerable information* undertaking and thus the posture of true rate-controlling process/execute associable with a reaction progress (cf. Fig. 14.2) not omitting the delivery task of reaction species moving to and/or from reaction boundary. It is challenged by introducing non-integral

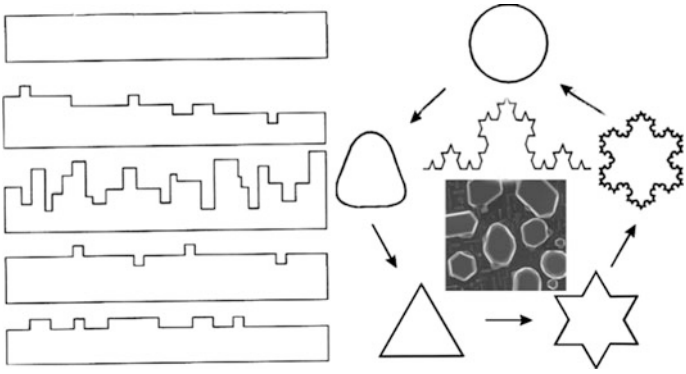

Fig. 14.2 *Left* Schematic reaction profile by Monte Carlo method [15] calculating interface in dependence on reaction temperature T_R, from above: ideally flat, growth occurring stepwise, rough interface at $T > T_R$, smooth interface at $T < T_R$, and under two-dimensional nucleation. *Right* Image of a circle continuous distortion, first into a triangle and hexagon continuing its deformation via the Koch Islands (*left*), which is composed of three congruent parts, each of them being a *Koch curve* (*inside*). Here, each line segment of the middle third is replaced by two new segments forming a tentlike angle. All endpoints of the generated line segments are part of the final curve. The circle (characterized by non-integral constant π) and its deformed constructions are topologically equivalent. Koch Island has a typical fractal (non-integral) dimension exhibiting infinite length but enclosing a finite area similar to that of the circle, which surrounds the original triangle. Moreover, such a famous pattern of this artificially created Koch 'snowflake' obviously bears the similarities with the real snowflakes found in nature (see the inset). These formations have typically many branches at all levels of details and belong to the comminuting objects called *dendrites* [5, 38]

(fractal-based) reaction rate mathematics [26–31]—see next. The conceptual shift [31–34] of the author's judgment toward modeling image can be best comprehended from seeing his two plenary lectures 1972–2006 [31, 33] and supplementary books [32, 34–38].

Early in 1950s, Smith [39] already proposed a classical approach emphasizing: 'normal grain growth result for the interaction between the topological requirements of space-filing and the geometrical needs of surface tension equilibrium.' We can distinguish that in both 2-D and 3-D (D = dimensional) arrangements, the structure consists of vertices joined by edges (sides), which surround faces, and in the 3-D case, the faces surround cells (see Fig. 14.1). The cells, faces, edges, and vertices of any cellular structure obey the conservation law (Euler's equation), i.e., $F - E + V = 1$ (for 2-D plane) and $F - E - C + V = 1$ (for 3-D space). Here, C, E, F, and V are, respectively, the number of cells, edges, faces, and vertices. Moreover, the number of edges joined to a given vertex settles its coordination number, z. For a topologically stable structure, i.e., for those in which the topological properties are unchanged by any small deformation, $z = 3$ (for 2-D) and $z = 4$ (for 3-D) are legitimate everywhere. This can be best illustrated for 2-D structure by a 4-rayed vertex, which will tend to be unstable decomposing into a two 3-rayed vertices, whose process is often termed as '*neighbor switching*.' For a 2-D structure, in which all boundaries have the same surface tension, the equilibrium angles at a vertex are 120°. The tetrahedral angle at 109°28′ is the equilibrium angle at a four-edged vertex in 3-D having six 2-D faces.

The grain growth in 2-D is inevitable unless a structure consists of an absolutely regular array of hexagons. If even one 5-sided polygon is introduced and balanced by a 7-sided one, then the sides of the grains must become *curved* in order to maintain 120° angles at the vertices. Grain boundary migration then tends to occur due to the curvature maneuver reducing boundary surface tension so that any grain with the number of edges above six will tend to grow because of concave and below six will incline to shrink because of convex sides.

It is clear that any reaction rate, particularly at the beginning of its 'acting-ion-exchange,' must depend upon the size of the solid grains, which undergo transformation (growth or dissolution). Reaction rate, $\vec{r}$, should thus be inversely proportional to the particle size, r, in the form of a certain power law, i.e., $\vec{r} = r^{Dr-3}$, where D_r is the *characteristic reaction dimension*, which can be allied with a *non-integral fractal* [27–29, 32, 40–42]. It is obvious that a mere use of strict integral dimensions, typically r^1 and r^2, would be an apparent oversimplification. Moreover, we have to imagine that the initial rate is directly proportional to the extent (true availability) of 'ready-to-react' surface and/or interface as well as to its coarseness (i.e., roughness as a kind of another characteristic with a non-integral dimension, again). It seems that such a concept can be discriminated as rather useful to describe the responding behavior of a reacting object toward the reaction impact characterized by *fractal dimension*. It recounts in-*self* summing all events occurring during the overall heterogeneous process. There, however, is not a regular polyhedron with plane sides subsisting exactly tetrahedral (angle 109°28′ between the edges). The nearest approach to space filling by a regular plane-sided polyhedron in

3-D is obtained by the Kelvin ideal tetra decahedra spaced on a body-centered cubic lattice. Even so the boundaries must become curved to assure equilibrium at the vertices so that a grain growth is likely to occur. It can be even illustrated by beer frost, which can be of two kinds: at-once draft beer with more interfacial fluid possessions (enabling mutual bubble slipping) and the already aged beer with a more rigid interfacial structure (∼'dry' hexagonal-like makeup). Apparently, both are unlike in experts' taste being capable to self-adjust by boundary migration and gas permeate through the cell membranes to equalize pressure of adjacent frost bubbles.

Using the simple Euclidean geometrical representation [5, 6, 16, 41–45], usually by means of models $f(\alpha)$, the reacting system can be classified as a set of spheres [41, 45] where each reaction interface is represented by the characteristic smooth curve. In any of such a created interfacial layer (i.e. geometrical deviding line), the separation endures thus the role of a *kinetic impedance.* The slower of the two associated elementary processes, i.e., *diffusion* to/from acting along with the chemical *interface reaction*, then become the *rate-controlling* process [5, 6, 16, 32, 42–45] becoming responsible for the *overall* reaction progression, α. We may indicate that the above-discussed kind of '*as-belief*' models depicts both the ideal situation of only single-reaction-controlling mode and a rigid spherical representation for ***all*** reacting particles. Inventory of such a geometrical manner of kinetic modeling was revised in detail in our previous book [45], the common focus being the simple shrinking core model based on a perfect globular particle. This, however, necessitates a sharp reaction boundary where each and every reaction interface is represented by similar characteristics of cutting reaction curve. Rationalization can be accomplished when assuming certain fractality [27, 28, 45–48], self-similarity and periodicity [49–51] or other coincidence model for improved geometrical fit incorporating some additional symmetry features. That can be a regularity adjustment of pattern-similar bodies (globe↔prism↔cube↔block↔hexahedral↔dodecahedral↔etc.). It somehow helps us to authorize the relation truthfulness and applicability of such (*oversimplified*) models when put into operation on more cogent (*irregular*) structures that we often decline or, at least, are anxious to observe. Even symmetry generalization does not facilitate an improved modeling to reach a full-scale matching of real morphologies (customarily witnessed in practice by microscopy). Thus, thermal analysis kinetics has remained a focal point of ongoing criticism [31, 52–54] due to simplifications enabling sorting processes in three domains only (Fig. 14.3).

In our kinetic practice, either we can survive with a simplified model-free description using a 'blank' modeling pattern [55–59] or we ought to adapt another philosophy of modeling the reaction mechanisms whichever learning how to employ more complex mathematics [49, 59] and/or providing a range of functions instead single numerical values (typically the activation energies often pointlessly pin down to decimal places). This tactic, however, may interfere with the principle of heat inertia [19, 60–62] often ignored [54, 61] even if exists for all samples under heating. The limiting cases of experimental setup touches either diminishing sample size to a certain threshold (thus incapable to distinguish the measured response of

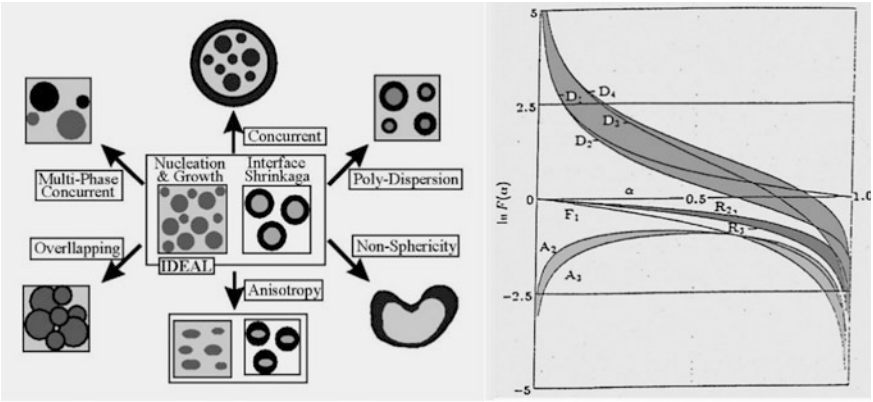

Fig. 14.3 *Left* displays a portrayal of distorted spherical particles because most common kinetic models are associated with the shrinking core of a globular particle, which maintains a *sharp* reaction boundary. Its right part shows conventional graph of a kinetic 'distinctiveness' often subsisting a plot of the model function of ln $f(\alpha)$ versus horizontalα showing thus three characteristic areas of self-similar models (shadowed) abbreviated as *nucleation* (*A*), phase boundary (*R*), and diffusion (*D*)-controlled processes. *The right plot* displays the wider variety of possible diffusion-controlled processes with a non-integral (fractal $\{1 - D)/D\}$) geometry when compared with the strict Euclidean geometry [5, 6, 16, 54, 55]. The *curves* involve such a modified course of model characterization, which allows the existence of intermediate cases (for $2 < D_D \leq 3$ holding $d\alpha/dt = \{(1 - \alpha)^{(1-D)/D} - 1\}^{-1}$ [6, 47, 55]). Such approach seemingly enables to envelop a larger area with the array of kinetic curves making possible their increased packing. The same curve swelling applies to the other groups of A's and R's indicating almost meaningless attempts to define precisely the solitary particularity of individual reactions, i.e., the serious kinetic differentiation (capacity to distinguish) of geometrical model of (still idealized) reaction mechanism falls within three categories only

bulk behavior from that of sample surface) or accelerating the imposed temperature changes ($\gg\phi$) probably getting in touch with an effect analogous to the uncertainty principle (unable to correspondingly determine each one of the independently measured parameters with an adequate precision, i.e., temperature and/or and its change—heat flux) [62]. Therefore, the future development of thermal analysis toward lower dimensions thermodynamics may become distinctive than that we presuppose today [62–65] see Chaps. 2, 5 and 18.

14.4 Use of yet Atypical Fractal Geometry

Always existing perturbations on the reaction interface can be imagined to encounter a driving force to accelerate growth that is usually expressed by the negative value of the first derivative of the Gibbs energy change, ΔG, with respect to the distance, *r*. For small superheating/cooling, we can still adopt the concept of constancy of the first derivatives, so that $d\Delta G$ equals the product of the entropy change, ΔS, and the temperature gradient, ΔT, which is the difference between the thermodynamic temperature gradient (associated with transformation) and the heat-imposed gradient at the reaction interface as a

consequence of external and internal heat fluxes. Because ΔS is often negative, a positive driving force will exist to allow perturbations to grow [62], only if ΔT is positive. This pseudo-thermodynamic approach gives the same result as that deduced from the concept of zone constitutional undercooling [38], and its analysis is important for the manufacturing advanced nanomaterials [62–65] such as fine metals, nanocomposed assets, quantum low-dimensional possessions (dots), composite whiskers, tailored textured configurations, and growth of oriented biologic structures.

The physical–geometrical models also neglect other important factors such as interfacial energy (immediate curvature, capillarity, tensions, nanograins radius), and particularly undistinguish internal and external transport of heat and mass (to and from the localized reaction boundary) resulting in a breakdown of smooth (planar) reacting interface which, at the process termination, are anyhow responsible for complex product topology [32, 39, 40, 66]. Variously activated disturbances are often amplified until a marked difference in the progress of the tips and depressions of the perturbed reacting interface occurs, making the image of resultant structures irregular and indefinable [66–68]. It creates difficulties in the correlation of traditional morphology observations with anticipated structures, becoming rather different from the originally assumed (simple, planar, 3-D) geometry. Depending on the directional growth conditions, the so-called *dendrites* (from the Greek *dendros* = tree) [5, 15, 38, 39] develop, their arms being of various orders and trunks of different spacing due to the locally uneven conditions of heat supply. This process is well known in metallurgy (quenching and casting of alloys [38, 62], water, and weather precipitates (such as snowflake formation or crystallization of water in plants) but also for less frequent types of other precipitation, crystallization, and decomposition processes associated with dissipation of heat, fluids, etc.

First, we should notice that there are sometimes fussy effects of particle radius, r, encompassing a wide range of reacting compacts. Besides affecting measurable point of phase changes [67–70], the most of derived model relations stay either for a simple reciprocity ($\sim 1/r$, if the whole reacting surface is exposed to ongoing chemical events) or for the inversely proportional square ($\sim 1/r^2$, if the diffusion across the changing width of reactant/product layer became decisive). It is clear that for a real instance, we can imagine such a situation when neither of these two limiting cases is unfailing so that the relation $1/r^n$ becomes effective and a new non-integral power exponent, n, comes into view falling to the *fractal region* $1 \leq n \leq 2$. It is somehow similar to the case of heat transfer across the layer d, which can similarly fall in between two optimal cases limited by $1/d$ and $1/d^2$. The associated cooling rate ϕ is essentially influenced by the heat transfer coefficient, Λ, and the thickness of cooled sample, d, and relatively less by its actual temperature, T. At the condition of ideal cooling, where we assume infinitely high coefficient of heat transfer, the cooling rate is proportional to $1/d^2$, while for the Newtonian cooling controlled by the character of phase boundary, ϕ correlates with $1/d$, only. In practice, we may adopt the power relation $\phi = 1/d^n$ (where n is a non-integral experimental constant $1 \leq n \leq 2$).

We can presuppose that transport properties due to fractal nature of percolation changes incorporate into the physical laws. For an enough randomly diluted system,

we can even admit that the localized modes occur for larger reacting frequencies, which can be introduced on the basis of bizarrely called '*fractons*' [67]. Inherent state density then shows an anomalous frequency behavior, and again, the power laws can characterize their dynamic properties. On fractal conductors, for example, the density is proportional to L^{d} and approaches zero for $L \rightarrow \infty$. If we increase L, we increase the size of the non-conducting holes, at the same time decreasing the conductivity, σ, which, due to self-similarity, decreases on all length scales, leading to the power law dependence defining the critical exponent, μ, as $\sigma \sim L^{-\mu}$. Due to the presence of holes, bottlenecks, and dandling ends, the diffusion is also slowed down on all length scales. Assuming the common example of 'random walker' [5, 47] and its probability to stay in place (using the standard relation, $x^2(t) = 2\mathrm{d}Dt$, where D is the diffusion constant and d is the dimension of lattice), the classical Fick's law [49] loses its orthodox validity. Instead, the mean square displacement is described by more general power law, i.e., $x^2(t) \cong t^{2/\mathrm{d}w}$, where the new exponent, d_w, is always greater than two. Both exponents can be related through the Einstein relation, $\sigma = e\ n\ D/(k_{\mathrm{B}}T)$, where e and n denote, respectively, the charge and density of mobile particles and k_{B} is a rate constant. As a result, $\mathrm{d}w = \mathrm{d}' - d + 2 + \mu$, where d' can be substituted by the ratio relation, log3 vs log2, so that dw becomes proportional to log5/log2, which, however, is not so easy to ascertain in the standard integer-like cases. In fact, it helped explicating various consequences of new phase formation [67–70] and formulating bases of logistic tactics [68, 71, 72] within which attitude we should not forget the role of percolation [73, 74].

First, it was Broadbent and Hammersley [73] who introduced the idea of percolation threshold P_{c} as critical concentration of contacts above which they form an infinite cluster. Transformation process can take place only if the corresponding concentration is higher than P_{c}. Examples of this are the spread of diseases, forest fire, crystallization of melts, etc. The restriction to exceed P_{c} explains why in countries governed by non-democratic regimes the plurality of public opinion is limited [74]. The so-called Arabic spring appeared only after Internet increased the possibilities of social contacts. To short distance L, the threshold concentration $P_{\mathrm{c}}(L)$ is lower. Most popular [74] is the approximation: $P(L) = P\ \{1 - (\mathrm{d}/L)^{\mu}\}$ where d is the length of single link and μ is the so-called critical exponent. So, if the concentration of links is limited below P_{c}, there is still possibility of appearance of transformation canters, each of size $\leq L$, separated from each other. On the other hand, lowering the threshold concentration leads to decrease of the activation energy barrier, correspondingly to higher kinetic constants.

14.5 Mathematical Commencement and Inspiration by Logistic Models

The mathematical basis emerges from a difference equation called *logistic mapping* (also polynomial diagram or iterative map equivalent to the recurrence relation) which is perceptibly arising from a quadratic transformation coming in different

forms [5, 47]. Often, it is a gradual transform $x' \rightarrow a\,x(1-x)$, where x are variables and a is a constant responsible for the system behavior. The instituted name may sound little peculiar as its origin resides in economics from which it gives us the term *logistic* to describe any type of planning process. It derives from the consideration of a whole class of problems in which appear two factors controlling the size of a changing population, x, varying between 0 and 1. This population passes through a succession of generations, labeled by the suffix n, so we denote the population in the nth generation by x_n. There is a birth process in which the number of populated species (nuclei, insects, and people) would deplete resources and prevent survival of them all. There is a negative depletion term proportional to the square of the population called starvation (density-dependent mortality) where the growth rate will decrease at a rate proportional to the value obtained by taking the theoretical 'carrying capacity' of the environment less than the current population. Putting these together, we have the nonlinear difference equation. By definition, the iteration is $x_{n+1} = a\,x_n(1-x_n)$ and we can illustrate the process graphically upon the superimposed parabola (x^2) and straight line (x) in the interval $0 \leq x \leq 1$. We can arrive at the two types of iterations by adjusting both the initial point, x_o, and the multiplying coefficient, a. It can exhibit either a sensitive irregular pattern or non-sensitive stable behavior. An important phenomenon subsists thus sensitivity, which can either magnify even the smallest error or dump the larger errors, if the system is finally localized in the stable state. This behavior is called *sensitive dependence on initial conditions* and is central to the problematic of chaos [46–48], though it does not automatically lead to chaos. The crucial difference between the discrete logistic system and its continuous derivative-like counterpart is the fact that it is plainly impossible for the dynamics of the differential equation to be chaotic. The reason is that in the one-dimensional system, no two trajectories, for the limit $\Delta t \rightarrow 0$, can cross each other, thus typically converging to a point or escaping to infinity, which, however, is not a general consensus in three-dimensional system often displaying chaos.

Today, logistic is related to a discrete-time demographic model [71, 75–86] analogous to the logistic equation first fashioned by Belgium professor Pierre Francois Verhulst (1804–1849), in the beginning of nineteen century [77]. Such S-shaped curves [5, 6, 71] are also called sigmoid curves (or sigmoidal functions from the Greek Σ—sigma) and also thought as a logistic '*ogive.*' Verhulst discovered that sigmoid curves are useful for describing population growth that small populations increase geometrically, because the supply of resources exceeds demand. Then, as supply and demand balance, population growth is constant. Finally, as demand exceeds supply, population growth decreases at the same rate that it had increased. Since computation is needed to predict the supplies an army requires, logistics has come to be also used for the movement and supply of troops. Realistic examples of systems with such a chaotic behavior are fluid flow around an obstacle being describable by such a nonlinear partial differential equation, which determines how the velocity changes in space and time. These types of differential equations are the most important tools for modeling straightforward ('vector') processes in physics and chemistry, though no particular analytical solution is

regularly available. The associated relationship can be transposable to write the form of a common kinetic equation: $d\alpha/dt \cong \alpha(1 - \alpha)$ [72, 87], where α can be the normalized extent of chemical conversion.

Verhulst [77], however, gave it the name *logistic* ('logistique' from the Greek *logistikos*—computational) since there is a connection with the logarithmic basis of the function (coined by John Napier, 1550–1617) from Greek logos (ratio, proportion, reckoning) and *arithmos* (number). Worth noting is Raymond Pearl (1879–1940) [78] who renewed Verhulst's terminology exhorting, however, researchers to use logistic curve or function in preference to autocatalytic curve because the latter is tied to a physically substantiated process. In 1944, his student Berkson [79] coined the term *logit* as a contraction of logistic unit to indicate the unit of measurement and popularized it in his application of the sigmoid curve to bioassay 'quantal' response. Logit is also used to characterize the logistic function in the way that '*probit*' (probability unit) characterizes the cumulative normal function. Finally, there appeared the term '*ogive*' indicating the shape of the logistic curve which is an architectural silhouette—a pointed arch. Modern mathematical use of ogive began in the late nineteen century by Francis Galton (1822–1911) [80] who characterized such a curve in its finite length infinitesimally coming over a certain endpoint (Galton's empirical maximum). Galton's curve can be idealized and its axes rotated to produce smooth shapes identifying the Verhulst's logistic figure [78–80]. The name ogive has been retained, even though the curve now likely resembles more an architectural 'ogee.' The merger logistic ogive as to identify the logistic curve was proposed by George Udny Yule (1871–1951) [81] who included tables of the numerical values of the logistic function suggesting three methods for the logistic curve parameter estimation. Recently, it was further exercised by Andersen [82] and practically explored elsewhere [78, 83–86].

Recently, the logistic approach became trendy in various scientific fields including reaction kinetics [47, 88–93]. Factually, this is a well-known form [72] of Akulov autogenesis [94] or Prout–Tompkins self-catalyzed [95] kinetic models naturally related to various aspects of opposing chemical reactions. However, life in the real kinetics of solid-state processes is far from being simple, and thus, almost in any physical–chemical system, the state cannot be described by a single variable or equation characterized by a simple integral power exponent (=1) as Kopelman introduced by his fractal extension [27, 28, 47]. Therefore, it was obvious that for generalized purposes of chemical kinetics, this logistic-like equation has inevitability acquired the completion by the non-integral random variables [72] m and n, as emphatically accomplished in the stylish form by Šesták–Berggren approach [5, 6, 54, 72, 96–104]. The involvedness of reactants (α) and products ($1 - \alpha$) is thus attuned to their actual physical–chemical transience (m) and productiveness (n) within the involved heterogeneity of solid-state system which is timely adjusted just by this type of power law fractals [26–28].

14.6 Impact of Logistic Strategy and the Origin of SB Equation

A simple relation consisting of two interrelated parameters α and reversing $(1-\alpha)$ is known since the middle of eighteen century as a logistic equation [76–78] beneficial to describe various forms of dissemination (diesis, reactions) [76, 81]. It reasonably involves interpretation of α as a kind of mortality involving the reactant disappearance and the complementary fertility of a reactant yet ready to proceed in response to $(1 - \alpha)$ [72, 97]. Such a logistic model makes possible to stay away from the orthodox classification of a reacting system employing conventional models based on a set of perfect geometrical (Euclidian) bodies (mostly ideal spheres) [41]. One hundred years later and still unacquainted of its logistic past, the α-relation was enriched by two arbitrary exponents n and m while introduced in the thermoanalytical practice [96–98]. Consequently coined by readers it became known as the Sestak–Berggren (SB) equation exhibiting recently as many as »800 citation responses [54, 98] (SCOPUS).

The SB equation was published in TCA 1971 [97] as a result of collaboration with Gunnar Berggren (1928–2013) carried out in the Swedish Nuclear Research Institute 'Atomenergy'. However, the publiaction missed the quotation of some early (then unavailable) books, which were uncovered by others much latter. Nevertheless, all of them affirmed the scheme analogy of SB relation without going into any deeper particulars. Such a source being merely a generally designed textbook [24, 94] (and not an original research paper) may not be pointed out as a fully immature quotation, moreover not even cited in the associated survey of Russian papers [100].

The essence of the author's thesis [22, 45, 97, 98] was in a detailed description and analysis of individual cases of plausible reaction mechanisms hidden behind the n–m equation following the basic (even if implicit) kinetic law [4, 5, 16], $\mathrm{d}\alpha/\mathrm{d}t = k(t)\,f(\alpha)$, where the reaction rate $\mathrm{d}\alpha/\mathrm{d}t$ is proportional to the product of two functions, temperature-dependent rate constant $k(t)$ and reaction degree-dependent reaction mechanism $f(\alpha)$ [23, 24, 41]. The main idea of this assumption turns out in the variable separation in order to decode the differential equation in the serviceable form $F(a) \equiv \int_0^{\alpha}(d\alpha)/f(\alpha) = \int_0^t k(t)\,\mathrm{d}t \equiv K(t)$. Further summarization of $f(\alpha)$ functions, endowed with its particular mathematical form, has been visualized across the world [42–45]. A substitutive prescription is provided by logistic equations [32, 76–78] making available an alternative insight toward the reaction interface-modeling which can be identified with an underlying principle of defects [47, 78] and their propagation alike illnesses dissemination [76–86]. It may thus become roots of antagonism of those who habitually operate with idealistic archetypes of particular $f(\alpha)$ [58, 72, 97]. It may possibly be replaced by simple

$$f(\alpha) = \alpha^n(1-\alpha)^m\{-\log(1-\alpha)^p \tag{14.1}$$

which is revealed in Table 14.1. This inventory clearly shows that the anticipated source (three-parameter) $m{-}n{-}p$ equation preserves its factual meaning only in the form of two-parameter variant [5, 45, 54, 98]:

$$f(\alpha) = \alpha^n(1-\alpha)^m \tag{14.2}$$

This form was examined and recommended in [71, 72, 96–103] displaying two arbitrary exponents m and n in the meaning of *two fractal variables,* and Eq. (14.2) can thus be legitimately called the *Sestak–Berggren equation.*

There are resources providing a choice of alternatives of m–n equation, all of them, however, exhibiting *specific numbers* for the exponents as manifestly recapitulated in Table 14.1. It includes the often-cited preliminary work of Kolmogorov [105] and the early summary by Hulbert [41] and others [4, 5, 16, 42, 44, 45, 71] following also the similar table published in the assessment work by Ng [87] and specified in our recent papers by Avramov [76]. It includes the less known work by Atkinson [106] successfully applied to unique kinetics of nanocrystal ('finemet') crystallization popularized by Illeková [42]. The essential study by Kopelman [26, 27] is also incorporated giving the basis of non-integral exponents within a fractal approach.

Worth noting is Yerofeev [117] who already shown that if a solid is involved with acting interfaces, the formation and growth of nuclei are describable by the above SB equation that coincides with $m = 2/3$ and $n = 2/3$ [71, 72]. It may include certain extension and correlation, for example, for $m = 1/2$, 2/3, 3/4, 4/5, consequently giving respective $n = 0.774$, 0.7, 0.664, 0.642, …, 0.556. It was shown [45, 107, 108] that such a two-parameter model may retain it physical–geometrical meaning only for $m \leq 1$ which can be even correlated with the classical nucleation growth equation (often abbreviated as JMAYK) staying factually the special case of SB equation (when approximating $\{-\ln(1-\alpha)\}^p$ through expansion by $\{\alpha\}^n$). Still, there is one important point distinguishing the use of either the term $\{-\ln(1-\alpha)\}^p$ or α^n. If α^n is involved, then for $t = 0$ the initial condition requires $\alpha(t = 0) \equiv \alpha_o \neq 0$. In other words, the process can start only under condition that minimal fraction of the system already existed in the new state. For instance, these are cases of developing new population or spread of disease, etc. On the other hand, if the term is $\{-\ln(1-\alpha)\}^p$, the process can start from 0, as is the case of nucleation and crystal growth. Also, different behavior of the system is predicted by these two terms at the final stages of the process, because there is $\lim(\{-\ln(1-\alpha)\}^p)_{\alpha\to 1} \to \infty$.

The increasing value of the exponent n indicates mounting 'mortality,' i.e., a more important role of the precipitated phase on the overall kinetics. It also appears that a higher value of the second exponent ($n > 1$) indicates an increasing reaction complexity; however, the temptation to relate the values of m and n to a specific reaction mechanism can be doubtful and should be avoided without complementary measurements. Besides, Málek shown [108] that there exists a relationship between the JMAYK robust exponents $r = 0 \to 1.5 \to 2 \to 3$ and SB exponents keeping on the respective values $m{-}n = 0\text{–}1 \to 0.35\text{–}0.88 \to 0.54\text{–}0.83 \to 0.72\text{–}0.76$.

Table 14.1 Individual power exponents n, m, and p of a generalized equation: $\alpha^n (1-\alpha)^m \{-\log (1-\alpha)^p\}$ related to particularized model cases developed all over the places [4, 5, 16, 42–46]

Exponents = n, m, p	$F(\alpha)$	Solution	Remarks
$n = 1$; $m = 1$, $p = 0$ $f(\alpha) = \alpha(1-\alpha)$	$\ln \frac{\alpha(1-\alpha_o)}{\alpha_o(1-\alpha)}$	$\alpha(t) = \frac{\alpha_o}{\alpha_o + \exp(-K(t))}$	Classical logistic function (Verhulst 1844) Autocatalytic (Prout–Tompkins 1944) Autogenesis (Akulov 1940)
n = random; $m = 0$ $(n \neq 1)$, $p = 0$ $f(\alpha) = \alpha^n$	$\frac{\alpha^{1-n}}{1-n} - \frac{\alpha_o^{1-n}}{1-n}$; $n \neq 1$	Unlimited growth $\alpha(t) = \left(\frac{1}{\left(\frac{1}{\alpha_o}\right)^{n-1} - (n-1)K(t)}\right)^{\frac{1}{n-1}}$ for $0 < K(t) < \frac{\left(\frac{1}{\alpha_o}\right)^{n-1} - 1}{(n-1)}$	Kopelman Fractal variant 1986
$n = 1$; $m = 0$, $p = 0$ $f(\alpha) = \alpha$	$\ln \frac{\alpha}{\alpha_o}$ if $n = 1$	$\alpha = \alpha_o \exp(K(t))$ for $0 \leq K(t) \leq -\ln \alpha_o$	Classical homogeneous reaction
$f(\alpha) = \alpha^n$ $n = 2$; $m = 0$, $p = 0$ $n = 3$	$\frac{1}{\alpha_o} - \frac{1}{\alpha}$ if $n = 2$ $\frac{1}{2\alpha_o^2} - \frac{1}{2\alpha^2}$; $n = 3$	$\alpha(t) = \frac{1}{\left(\frac{1}{\alpha_o}\right) - K(t)}$; for $n = 2$ $0 \leq K(t) \leq \frac{1}{\alpha_o} - 1$ $\alpha(t) = \sqrt{\frac{1}{\left(\frac{1}{\alpha_o}\right)^2 - 2K(t)}}$ for $n = 3$ $0 \leq K(t) \leq \frac{\left(\frac{1}{\alpha_o}\right)^2 - 1}{2} \approx \frac{1}{2\alpha_o^2}$	Homogeneous reaction: phase boundary reactions Contracting spheres
$n = 0$; m = random, $p = 0$ $f(\alpha) = (1-\alpha)^m$	$\frac{(1-\alpha)^{1-n} - 1}{n-1}$ if $n > 1$	$\alpha(t) = 1 - \frac{1}{[1 + [(n-1)K(t)]]^{\frac{1}{n-1}}}$	Power ranking at induction stages Mampel 1940
$f(\alpha) = (1-\alpha)^{-m}$	$\frac{1}{m+1}\left([1-\alpha_o]^{m+1} - [1-\alpha]^{m+1}\right)$	Parabolic law $\alpha(t) = \alpha_o + [(m+1)K(t)]^{\frac{1}{m+1}}$ for $0 < K(t) < \frac{(1-\alpha_o)^{m+1}}{m+1} \approx \frac{1}{m+1}$	One-dimensional diffusion (D1)
n = random, m = random, $p = 0$ $f(\alpha) = \alpha^m (1-\alpha)^n$	Hypergeometric series	Impracticable	Arbitrary reaction Sestak–Berggren (SB) equation 1971

(continued)

Table 14.1 (continued)

Exponents = n, m, p	$F(\alpha)$	Solution	Remarks
$\alpha^{2/3}\,(1-\alpha)^{\,2/3}$	$3\cdot x^{\frac{1}{3}}\cdot \text{hypergeom}\left[\begin{pmatrix}\frac{1}{3}\\ 1\end{pmatrix},\left(\frac{4}{3}\right),x\right]$	Impracticable	Roginskii–Shultz 1928 Interface reactions Kolmogorov 1937 Yerofeev 1961
$\alpha^{2/3}\,(1-\alpha)^{\,4/3}$	$3\sqrt[3]{\frac{\alpha}{(1-\alpha)}}$	$\alpha=\frac{1}{1+\left(\frac{3}{K(t)}\right)^3}$	Modified interface reactions Kolmogorov 1961
$\alpha^{1-\frac{1}{n}}(1-\alpha)^{1+\frac{1}{n}}$	$\frac{1}{n}\left[\frac{\alpha}{(1-\alpha)}\right]^{\frac{1}{n}}$	$\alpha=\frac{1}{1+\left(\frac{n}{K(t)}\right)^n}$	Modified logistic reactions Avramov 2013
$(1-\alpha)[-\ln(1-\alpha)]^{1-\frac{1}{p}}$	$[-\ln(1-\alpha)]^{\frac{1}{p}}$	$\alpha = 1$ - $\exp(-(K(t))^{\mathrm{p}})$	Nucleation growth (JMAK equation 1939)
$n = (1-w)$, $m = (1-q)$, $p = 0$ $f(\alpha)=\alpha^{1-q}(1-\alpha)^{1-w}$	Hypergeometric series	Impracticable	Early Jacobs and Tompkins relation 1955: Ng conjecture 1975

Such a universal façade of the above-quoted $m{-}n$ equation [72, 109, 116] is, however, the cause of mathematical difficulty if integrated [71] endowing with unfeasible hypergeometric series soluble only for specific values of exponents (e.g., 1 or 2/3) (see Table 14.1). In contrast to the renowned JMAYK model [42–45], that of SB equation misses opportunely its logarithmic term $\{-[\ln (1-\alpha)]^{P}\}$ which anyhow sounds *strange* in the logical strategy of reaction path portrayal. It can be customarily called as an accommodation function [6, 44, 107]. Moreover, the logarithm can be particularly expanded into a series [6, 71] providing thus a simplified solution in terms of the favorite double-exponent forms, i.e., transferring logarithmic term to the preferred $\alpha^{n'}$ and thus adapting the new value of n. Furthermore, such an intrinsic logarithm is a discarded source of a tribute damping which is particularly effective during supplementary kinetic evaluation when employing the process of multiple handling of logarithm [42].

Recently, there appeared an attempt to give the $m{-}n{-}p$ correlation a mathematical form [104], i.e., $1/P = \ln(1{-}\alpha) - \ln(1{-}\alpha)\, n - \{(1{-}\alpha)/\alpha\} \ln(1{-}\alpha) m$, which yields on simplification: $1/P = n - (3/4)\, m$. However, these attempts to associate the SB alternatives with a particular model of JMAYK seem to be somehow irrelevant because it is linking two ***incommensurable kinetics*** exhibiting divergent philosophical strategies [45, 54, 71, 72]: the geometrical JMAYK versus the logistic SB. Certainly, the values of n and m can be categorized and catalogued, but they better should serve as the characteristic values for the novel method of the so-called *non-parametric kinetics* [56] based on the so-called *model-free kinetics* [57–59]. Its acuteness can be substantiated by analyzing the most common kinetic models associated with the shrinking core of a globular particle, which requires a sharp reaction boundary which brings an unsolved question if the sharp boundary factually exists within each particle assuming homogeneous temperature distribution or if it resides jointly just inside the global entirety of the sample preventing individual particles from having their individual reaction front. It is worth noting that while traditionally modeling reaction mechanism, we use to assemble our considerations on a set of separate particles. Under a real measurement, we are actually exploring the sample's global behavior on the basis of averaged properties (temperature, volume, weight, etc.) within a shared experimental response of the sample entirety. Such a collective way of the reaction path investigation may thus better correlate with the logistic-like philosophy under a simplified model-free description using a 'blank' pattern within the m–n framework of SB equation [45, 54, 71, 72].

14.7 Further Prospects

It is clear that the so far conventionally idealized methods of kinetic modeling [41–45] are not fully sufficient for a sincerely advanced kinetic analysis in search of really truthful mechanism. These are, however, not disregarding precious studies on the discovering detailed mechanism of complicated solid-state processes which are well based and advance further branch of kinetics [116]. Distrust arises not only from the

overidealized geometrical archetypes [41] but before all from a permanent and highly conservative habit to take for granted the disconnected α- and t-functions, i.e., the above-mentioned $f(\alpha)$ and $k(t)$ separability [25, 31, 45, 54]. In view of mutually interactive impact of temperature with the sample reaction progress [62], it is indispensable to require a simultaneous modeling of the bridged thermal and conversional behavior. In this perspective, the enduring recommendations are somehow contraproductive and unsubstantiated when persistently declaring during the quarter of century (from early [109] to recent [110–114]), an almost unchanged counsel literally suggesting how to precisely evaluate and correctly publish somehow fictitious kinetic data [54, 115]. They are repeatedly telling public about the worth of the nonsense values of activation energies [52, 53]. It is a sad misfortune that even the most recent well-written kinetic book [114] is self-centerently folded on self-citations policy neglecting others (e.g., within its six hundred references there stays only a single reference [97] to the chapter authors and moreover as a subject of criticism). It is expectant that sample thermal 'deeds' must be in a little while integrated into the ICTAC Kinetic Committee perform in order to provide future kineticists the modern way [32] of solving non-isothermal kinetics [54].

Acknowledgements The present work was also supported by Institutional Research Plan of Institute of Physics ASCR, v.v.i., no. AV0Z1010052 as developed at its Join Research Laboratory with the New Technologies Centre of the University of West Bohemia in Pilzen (the CENTEM project, reg. no. CZ.1.05/2.1.00/03.0088 that is cofunded from the ERDF as a part of the MEYS—Ministry of Education, Youth and Sports OP RDI Program and in the follow-up sustainability stage supported through the CENTEM PLUS LO 1402). The abandoned support by the Grant Agency of ČR for the projected grant ′Thermal inertia and its significance for the analysis of DTA measurements′ (No 17-21840S-2016) is worth mentioning as an example of fatal misunderstanding of current needs of thermal science.

References

1. Russell B (1967) History of western philosophy, Routledge (reedit up to 1995). ISBN 0-415-07854-7.A
2. Partington JR (1970) A history of chemistry. Macmillan, London
3. Habashi F (2000) Zoroaster and the theory of four elements. Bull Hist Chem 25:109–116
4. Ball P (2004) The elements: a very short introduction. OUP Oxford, p 33. ISBN 9780191578250
5. Šesták J (2004) Heat, thermal analysis and society. Nucleus, Hradec Králové
6. Šesták J (2005) Science of heat and thermophysical studies: a generalized approach to thermal analysis. Elsevier, Amsterdam
7. Šesták J (2008) Some model classification of geometrical bodies and their development in historical applications. In: Wittwer A, Knut E, Pliska V, Folker G (eds) Chapter in book: Approaching scientific knowledge, Collegieum Helveticum, Zurich, pp 87–91
8. Penrose R (1994) Shadow of the mind: approach to the missing science of consciousness. Oxford University Press, Oxford
9. Kepler J (1611) Strena seu de nive sexangula (The six-cornered snowflake). ISBN 978-1-58988-053-5
10. Hales TC (2006) Historical overview of the Kepler conjecture. Discr Comput Geom 36:5–20

11. Bravais A (1846) Analyse mathématique sur les probabilités des erreurs de situation d'un point. Acad R Sci Inst Fr 9:255–332
12. Bravais A (1866) Études cristallographiques. Paris
13. Penrose R (2004) The road to reality: a complete guide to the laws of the Universe. Vintage, London
14. Šesták J, Zámečník J (2007) Can clustering of liquid water be of assistance for better understanding of biological germplasm exposed to cryopreservation. J Thermal Anal Calor 8:411–419
15. Chvoj Z, Šesták J, Tříska A (eds) (1991) Kinetic phase diagrams: nonequilibrium phase transitions. Elsevier, Amsterdam
16. Šesták J (1984) Thermophysical Properties of Solids: their measurements and theoretical thermal analysis. Elsevier, Amsterdam; and (1987) Teoretičeskij termičeskij analys. Mir, Moscow (in Russian)
17. Barrow JD (1994) The origin of the Universe. Orion, London
18. Barrow JD (1999) Impossibility: limits of science and science of limits. Vintage, New York
19. Šesták J, Holba P (2013) Heat inertia and temperature gradient in the treatment of DTA peaks: existing on every occasion of real measurements but until now omitted. J Therm Anal Calorim 113:1633–1643
20. Barghathi H, Vojta T (2014) Phase transitions on random lattices: how random is topological disorder? Phys Rev Lett 113:120602; and Okabe A, Boots B, Sugihara K, Chiu S (2000) Spatial tessellations: concepts and applications of Voronoi and delaunay diagrams. Wiley, Chichester
21. Giazitzidis P, Avramov I, Argyrakis P (2015) Variation of the critical percolation threshold with the method of system preparation. Eur Phys J B 88:331
22. Šesták J (1979) Philosophy of non-isothermal kinetics J Thermal Anal 16:503–520; and (1988) Nonisothermal kinetics: art, debate or applied science. J Thermal Anal 33:1263–1267
23. Jacobs PWM, Tompkins FC (1955) Classification and theory of solid reactions. In: Garner WE (ed) Chemistry of the solid state. Butterworth, London
24. Young DA (1966) Decomposition of solids. In: Tompkins FC (ed) Solid and surface kinetics. Pergamon, Oxford
25. Šesták J (1979) Thermodynamic basis for the theoretical description and correct interpretation of thermoanalytical experiments. Thermochim Acta 28:197–227
26. Kopelman R (1988) Fractal reaction kinetics. Science 241:620–625
27. Kopelman R, Parus SJ (1986) Fractals in reaction kinetics. In: Schaefer DW, Mandelbrot BB (eds) Fractal aspects of materials. Material Res. Soc. Boston
28. Avnir D (1989) Fractal approach to heterogeneous chemistry. Wiley, New York; and Schröde M (1991) Fractals, chaos and power laws. Freeman, New York
29. Šesták J (2002) The role of order and disorder in thermal science (I) and Universe, matter and society (II), J Mining Metal 38:1–6; and 2003; 39:1–7
30. Šesták J, Chvoj Z (2002) Irreversible thermodynamics and true thermal dynamics in view of generalized solid-state reaction kinetics. Thermochim Acta 388:427–431
31. Šesták J (2012) Rationale and fallacy of thermoanalytical kinetic patterns: how we model subject matter. J Thermal Anal Calor 110:5–16
32. Šimon P, Zmeškal O, Šesták J (2013) Fractals in solid-state processes. In: Šesták J, Šimon P (eds) Chapter 12 in book Thermal analysis of micro-, nano- and non-crystalline materials. Springer, Berlin, pp 257–290. ISBN 978-90-481-3149-5
33. Šesták J (2006) Plenary lectures: rationale and fiction of thermochemical kinetics. In: Vitez I (ed) The proceedings of the 34th conference of North American thermal analysis society. Bowling Green, pp 68–69; and Šesták J (1972) Plenary lectures: nonisothermal kinetics. In: Wiedemann HG (ed) The Proceedings of the thermal analysis conference 3rd ICTA in Davos, Birghausser, Basel, pp 3–9
34. Šesták J (ed) (1992) Reaction kinetics by thermal analysis. Special issue of Thermochim Acta, vol 203, Elsevier, Amsterdam

35. Šesták J, Sorai M (eds) (1995) Transition phenomena in condensed matter. Special issue of Thermochim Acta, vol 266. Elsevier Amsterdam
36. Šesták J, Mareš JJ, Hubík P (eds) (2011) Glassy, amorphous and nano-crystalline materials: thermal physics, analysis, structure and properties, vol 8. Springer, Berlin, Heidelberg. ISBN 978-90-481-2881-5
37. Kožíšek Z, Demo P, Sveshnikov A (2013) Kinetics of crystal nucleation in closed systems; and nucleation on strongly curved surfaces, In: Šesták J, Šimon P (eds) Chapters 9 and 19 in book Thermal analysis of micro-, nano- and non-crystalline materials: transformation, crystallization, kinetics and thermodynamics, vol 9. Springer, Berlin, Heidelberg, pp 190–208 and 419–428. ISBN 978-90-481-3149-5
38. Glicksman E (1984) Dendritic growth. Mater Sci Eng 65:45–55; and Lipton J, Glicksman ME, Kurz W (1984) Dendritic growth into undercooled alloy melts. Mater Sci Eng 65:57–63
39. Smith CS (1953) Microstructure and geometry. Trans Am Soc Metals 45:533–575; and (1964) Some elementary principles of polycrystalline microstructure. Metal Rev 9:1–17
40. Avnir D, Farin D, Pfeifer P (1984) Molecular fractal surfaces. Nature 308:261–263; and Bonde A, Havlin S (1991) Fractals and disordered systems. Springer, Berlin
41. Hulbert HF (1969) Models for solid-state reactions in powdered compacts: a review. J Br Ceram Soc 6:11–20; and Khawam A, Flanagan DR (2006) Solid-state kinetic models: basics and mathematical fundamentals J Phys Chem B 110:17315–17328
42. Illeková E, Šesták J (2013) Crystallization kinetics of metallic micro-, nano- and non-crystalline alloys. In: Šesták J, Šimon P (eds) Chapter 13 in book: Thermal analysis of micro-, nano- and non-crystalline materials, pp 257–290. Springer, Berlin. ISBN 978-90-481-3149-5
43. Málek J, Criado JM, Šesták J, Militký J (1989) The boundary conditions for kinetic models. Thermochim Acta 153:429–432; and Málek J, Mitsuhashi T, Criado JM (2001) Kinetic analysis of solid-state processes. J Mater Res 16:1862–1871
44. Koga N, Šesták J, Šimon P (2013) Some fundamental and historical aspects of phenomenological kinetics in solid-state studied by thermal analysis. In: Šesták J, Šimon P (eds) Chapter 1 in book: Thermal analysis of micro-, nano- and non-crystalline materials. Springer, Berlin, pp 1–45. ISBN 978-90-481-3149-5
45. Šesták J (2005) Modeling of reaction mechanism: use of Euclidian and fractal geometry. In: Chapter 10 in his book: Science of heat and thermophysical studies: a generalized approach to thermal analysis. Elsevier, Amsterdam, pp 276–314
46. Mandelbrot BB (2003) Gaussian self-similarity, fractals and 1/f noise. Springer, New York; and Falcone K (2002) Fractal geometry. Wiley, Chichester
47. Hiller R (ed) (1993) Application of fractional calculus in physics. World Sci, River Edge, NJ; and Milledr KS, Ross B (2000) Introduction to the fractional calculus and fractional differential equations. Wiley, New York
48. Fleschinger MF, Zaslavsky GM, Klaufter J (1993) Strange kinetics. Nature 363:31–33
49. Mareš JJ, Šesták J, Hubík P (2013) Transport constitutive relations, quantum diffusion and periodic reactions. In: Šesták J, Mareš J, Hubík P (eds) Chapter 14 in book Glassy, amorphous and nano-crystalline materials: thermal physics, analysis, structure and properties, pp 227–245. Springer, Berlin. ISBN 978-90-481-2881-5
50. Stávek J, Šesták Šípek M, Šesták J (2002) Application of the principle of least action to some self-organized chemical reactions. Thermochim Acta 388:440
51. Mareš JJ, Stávek J, Šesták J (2004) Quantum aspects of self-organized periodic chemical reaction. J. Chem Phys 121:1499–1503
52. Galwey AK (2004) Is the science of thermal analysis kinetics based on solid foundations? A literature appraisal. Thermochim Acta 413:139–183
53. Galwey AK (2006) What theoretical and/or chemical significance is to be attached to the magnitude of an activation energy determined for a solid-state decomposition? J Therm Anal Calor 86:267–286

54. Šesták J (2015) The quandary aspects of non-isothermal kinetics beyond the ICTAC kinetic committee recommendations. Thermochim Acta 611:26–35
55. Ozao R, Ochiai M (1993) Fractal nature and thermal analysis of powders. J Thermal Anal: 1331
56. Serra R, Nomen R, Sempere J (1998) Non-Parametric kinetics: a new method for kinetic study. J Thermal Anal Calor 52:933
57. Šimon P (2005) Single-step kinetic approximation employing non-Arrhenius T-functions. J Thermal Anal Calor 79:703; and (2007) Single-step approximation: attributes, strong and weak sides. J Therm Anal Calorim 88:709–715
58. Vyazovkin S (2006) Model-free kinetics: staying free of multiplying entities without necessity. J Thermal Anal Calor 83:45
59. Šimon P, Dubaj T, Cibulková Z (2015) Equivalence of the Arrhenius and non-Arrhenian temperature functions in the temperature range of measurements. J Therm Anal Calorim, 120: 231–238; and T. Dubaj, Z. Cibulková, P. Šimon (2015) An incremental isoconversional method for kinetic analysis based on the orthogonal distance regression. J Comput Chem 36: 392–398
60. Holba P., Šesták J. Sedmidubsky D (2013) Heat transfer and phase transition at DTA experiments. In: Šesták J, Šimon P (eds) Chapter 5 in book: Thermal analysis of micro-, nano- and non-crystalline materials. Springer, Berlin, pp 99–134. ISBN 978-90-481-3149-5
61. Holba P, Šesták J (2015) Heat inertia and its role in thermal analysis. J Thermal Anal Calor 121:303–307
62. Šesták J (2015) Kinetic phase diagrams as a consequence of radical changing temperature or particle size. J Thermal Anal Calor, 120:129–137; and Šesták J (2016) Measuring "hotness": should the sensor's readings for rapid temperature changes be named "tempericity"? J Thermal Anal Calor 125:991–999
63. Höhne GWH (2003) Calorimetry on small systems—a thermodynamic contribution. Thermochim Acta 403:25–36
64. Perepezko JH, Glendenning TW, Wang J-Q (2015) Nanocalorimnetry measurements of metastable states. Thermochim Acta 603:24–28
65. Barnard AS (2010) Modeling of nanoparticles: approaches to morphology and evolution—a review. Rep Prog Phys 73:6502–6554
66. Pfeifer O (1985) Macromolecules and colloidal aggregates—fractal dimension as concealed symmetry of irregular structures. Chimia 39:120
67. Alexander S, Orbach R (1982) Density of states on fractals—fractons. J Phys Lett 43:L625
68. Avramov I (2008) Diffusion coefficient of foreign particles in glass-forming melts. J Non-Cryst Sol 354(14):1537–1540
69. Karamanov A, Avramov I, Arrizza L, Pascova R, Gutzow I (2012) Variation of Avrami parameter during non-isothermal surface crystallization of glass powders with different sizes. J Non-Cryst Sol 358:1486–1490
70. Avramova K, Karamanov A, Avramov I (2015) Variations in non-isothermal surface crystallization kinetics due to minor composition changes, J Non-Cryst Sol 428:49–53; and Thieme K, Avramov I, Rüssel C (2016) The mechanism of deceleration of nucleation and crystal growth by the small addition of transitive metals. Sci Rep doi:10.1038/srep25451
71. Avramov I, Šesták J (2014) Generalized kinetics of overall phase transition explicit to crystallization. J Therm Anal Calorim 118:1715–1720
72. Šesták J (2016) Outline of hyperfree energy, equilibrium background and heat inertia opening new frontiers of thermal analysis. J Thermal Anal Calor doi:10.1007/s10973-016-5880-1
73. Broadbent SR, Hammersley JM (1957) Percolation processes. Math Proc Cambridge Philos Soc 53:629–641
74. Avramov I (2009) Rigid–floppy percolation threshold. J Phys Condens Matter 21:215402
75. Qiwu C, Lawson GJ (1982) Study on models of single population: an expanse of the logistic and exponential equations. J Theoret Biol 98:645–659
76. Avramov I (2007) Kinetics of distribution of infections in network. Phys A 379:615

77. Verhulst PF (1844) Recherches mathématiques sur la loi d'accroisement de la population. Mem Acad R Brux 18:1
78. Pearl R (1924) Studies in human biology. Williams & Wilkins, Baltimore
79. Berkson J (1944) Application of the logistic function to bio-assay. J Amer Stat Soc 39:357–365
80. Galton F (1875) Statistics by inter-comparison, with remarks on the law of frequency of errors. Phil Mag 49:33–46
81. Yule GU (1925) The growth of population and the factors which control it. J Roy Stat Soc 88:1–62
82. Andersen EB (1977) Sufficient statistics and latent trait models. Psychometrika 42:69–81
83. Latour B, Woolgar S (1979) The societal construction of scientific facts. Beverly Hills Sage Publ., London
84. Sakanoue S (2013) Ecological modeling 261/262:93–97
85. Ferretti NK, Rahman A (1988) Study of coupled logistic map and its applications in chemical physics. Chem Phys 119:275–288
86. Finkelshtein D, Kondratiev Y, Kozitsky Y, Kutoviy O (2015) The statistical dynamics of a spatial logistic model and the related kinetic equation. Math Models Methods Appl Sci 25:343–370
87. Ng WL (1975) Thermal decomposition in the solid state. Aust J Chem 28:1169–1178
88. ShaBian Lin-WeiDu, Yu-XiGao JianHuang, Gou Bao-Di, XiuhongLi YiLiu, Zhang Tian-Lan, Wang Kui (2012) Crystallization in aggregates of calcium phosphate nanocrystals: A logistic model for kinetics of fractal structure development. Cryst Growth Des 12:3481–3488
89. Burnham AK, Weese RK, Weeks BL (2004) Distributed activation energy model of thermodynamically inhibited nucleation and growth reactions and its logistic application to the b–d phase transition. J Phys Chem B 108:19432–19441
90. Cao R, Naya S, Artiaga R, Garcia A, Varela A (2004) Logistic approach to polymer degradation in dynamic TGA. Poly Degrad Stab 85:667–674
91. Naya S, Cao R, Lopez de Ullibarri I, Artiaga R, Barbadillo F, Garcia A (2006) Logistic mixture versus Arrhenius for kinetic study of material degradation by dynamic thermogravimetric analysis. J Chemom 20:158–163
92. Barbadillo F, Fuentes A, Naya S, Cao R, Mier JL, Artiaga R (2007) Evaluating the logistic mixture model on real and simulated TG curves. J Therm Anal Calorim 87:223–227
93. Tarrio-Saavedra J, Lopez-Beceiro J, Naya S, Francisco-Fernandez M, Artiaga R (2014) Simulation study for generalized logistic function in thermal data modeling. J Therm Anal Calorim 118:1253–1268
94. Akulov NS (1940) On the genesis of chemical reactions, Comp Rend Acad Sci URSS 28:135–138 (in Russian); and (1940) Comp Rend Acad Sci USSR 27:135–138 (English translation); and (1940) book: Basics of chemical dynamics. By Moscow State University; Moscow (in Russian)
95. Prout EG, Tompkins FC (1944) The thermal decomposition of potassium permanganate. Trans Faraday Soc 40:488–498
96. Šimon P (2011) Forty years of the Šesták-Berggren equation. Thermochim Acta 520:156–157
97. Šesták J, Berggren G (1971) Study of the kinetics of the mechanism of solid-state reactions at increasing temperature. Thermochim Acta 3:1–13
98. Šesták J (2017) The Šesták-Berggren equation: now questioned but formerly celebrated—what is right? J Therm Anal Calorim 127:1117–1123; and Militký J, Šesták J (2017) On the eliminating attempts toward Sestak-Berggren equation. J Therm Anal Calorim 127:1131–1133
99. Nolan PS, LeMay HE (1973) Evaluation of the non-isothermal rate equation proposed by Sestak and Berggren by computer methods. Thermochim Acta 16:179–186
100. Gorbachev VM (1980) Some aspects of Sesták's generalized kinetic equation in thermal analysis. J Therm Anal 18:193–197; and in Zh Fiz Khim USSR 51(1977) 1100 (in Russian)
101. Málek J, Criado JM (1991) Is the Šesták-Berggren equation a general expression of kinetic models? Thermochim Acta 175:305–309

102. Burnham AK (2000) Application of the Šesták-Berggren equation to organic and inorganic materials of practical interest. J Therm Anal Calor 60:895–908
103. Munteanu G, Segal E (2010) Sestak–Berggren function in temperature—programmed reduction. J Therm Anal Calorim 101:89–95
104. Arshad MA, Maaroufi A (2015) Relationship between Johnson-Mehl-Avrami and Šesták-Berggren models in the kinetics of crystallization in amorphous materials. J Non-Cryst Sol 413:53–58
105. Kolmogorov A (1961) Reaction rate of processes involving solids with different specific surfaces. In: The proceedings of the 4th international symposium reactivity of solids. Elsevier, Amsterdam, pp 273–282
106. Atkinson HV (1988) Theories of normal grain growth in pure single phase systems. Acta Metall 36:469–491
107. Šesták J (1991) Diagnostic limits of phenomenological kinetic models when introducing an accommodation function. J Therm Anal 36:1997; and Šesták J, Málek J (1993) Diagnostic limits of phenomenological models of heterogeneous reactions and thermoanalytical kinetics. Solid State Ionics 63/65:254–259
108. Málek J (1999) Crystallization kinetics by thermal analysis. J Thermal Anal Calor 56:763–769; and (2000) Kinetic analysis of crystallization processes in amorphous materials. Thermochim Acta 355:239–253
109. Perez_Maqueda LA, Criado JM, Sanchez-Jimenez PE (2006) Combined kinetic analysis of solid-state reactions: a powerful tool for simultaneous determination of kinetic parameters and the kinetic models without previous assumptions on the reaction mechanism. J Phys Chem A 110:12456–12462
110. Flynn JH, Brown M, Šesták J (1987) Report on the workshop: current problems of kinetic data reliability evaluated by thermal analysis. Thermochim Acta 110:101–112. A segment of the Special issue "Thermal analysis highlights" edited by V. Balek and J. Šesták, Elsevier, Amsterdam 1986
111. Vyazovkin S (2000) Computational aspects of kinetic analysis.: part C. The ICTAC Kinetics Project- the light at the end of the tunnel? Thermochim Acta 355:155–163
112. Vyazovkin S, Burnham AK, Criado JN, Perez-Maqueda LA, Popescu C, Sbirrazzuoli N (2011) ICTAC kinetics committee recommendations for performing kinetic computations on thermal analysis data. Thermochim Acta 520:1–19
113. Vyazovkin S, Chrissafis K, DiLorenzo ML, Koga N, Pijolat M, Roduit MB, Sbirrazzuoli N, Suñol JJ (2014) ICTAC Kinetics Committee recommendations for collecting experimental thermal analysis data for kinetic computations. Thermochim Acta 590:1–23
114. Vyazovkin S (2015) Isoconversional kinetics of thermally stimulated processes. Springer, Berlin, Heidelberg. ISBN 10: 3319141740
115. Šesták J (2014) Is the original Kissinger equation obsolete today—not obsolete the entire non-isothermal kinetics? J Thermal Anal Calorim 117:1173–1177; and Holba P, Šesták J (2014) Imperfections of Kissinger evaluation method and crystallization kinetics. Glass Phys Chem 40:486–449
116. Muravyev NV, Koga N, Meerova DB, Pivkinaa AN (2017) Kinetic analysis of overlapping multistep thermal decomposition comprising exothermic and endothermic processes: thermolysis of amonium dinitramide. Phys Chem Chem Phys doi:10.1039/c6cp08218a
117. Yerofeev BV (1961) Reaction rate of processes involving solids with different specific surfaces. In: The proceedings: 4th international symposium reactivity of solids. Elsevier, Amsterdam, pp 273–282

Chapter 15
The Role of Heat Transfer and Analysis Ensuing Heat Inertia in Thermal Measurements and Its Impact to Nonisothermal Kinetics

Pavel Holba and Jaroslav Šesták

Abstract The basic interrelations and consequences of heat transfer (1701 Newton cooling law) are analyzed showing its unambiguous importance and historical origin already known since 1933 in the form of basic caloric equation by Tian. It results in the heat inertia due to the sample heat capacity changes and undertakes two forms, integral and differential, the latter specific in providing s-shape background of DTA peaks. Its impact in the DTA measurements is examined showing misinterpretation by the origin work of Borchard and Daniels leading to further abandonment. The heat inertia correction was already suggested by authors in 1978 and verified on the basis of externally inserted rectangular heat pulses. Further corrections to heat inertia waited until 2009 (Netzsch commercial software). Relations following from general kinetic equation for the first-order reactions are substantiated, and the kinetic compensation effect explained as a correlation of pair activation energy pre-exponential factor and maximum rate temperature-heating rate. Kissinger erroneous assumption on temperature of maximum reaction rate is examined, and a correct solution is then suggested while determining the correct temperature of maximum reaction/transition rate and its correlation to the apex of a DTA peak. Both the kinetic equation and Kissinger equation are shown crucial when including the heat inertia term. Often forgotten influence of thermodynamic equilibrium as to kinetic equation is analyzed giving away its significance. New concept of a more sophisticated nonisothermal kinetics is suggested happy to be first when introducing the concept of equilibrium background which stays an important part of advanced kinetics anticipating that our innovative notions of temperature inertia, gradients, and even the operational meaning of temperature itself may facilitate modern

Pavel Holba—Deceased

P. Holba · J. Šesták
New Technologies Research Centre (NTC-ZČU), University of West Bohemia, Universitní 8, 30114 Pilsen, Czech Republic

J. Šesták (✉)
Division of Solid-State Physics, Institute of Physics, v.v.i., Czech Academy of Sciences, Cukrovarnická str. 10, 16200 Prague, Czech Republic
e-mail: sestak@fzu.cz

J. Šesták et al. (eds.), *Thermal Physics and Thermal Analysis*,
Hot Topics in Thermal Analysis and Calorimetry 11,
DOI 10.1007/978-3-319-45899-1_15

kinetic understanding. We believe that kinetic progress means practice-verified improvements while including detailed thermal phenomena of real thermoanalytical measurements, nor just making changes at any case. We neither should be afraid of changes while complicating our pervious practice nor should we feel troubled examining examples presented in this chapter. The chapter contains 72 references.

15.1 Introduction: Heat Inertia and Its Consequences

Chronicle of thermal science goes back to historic times of Isaac Newton (1642–1727) [1] who published his temperature scale in 1701 as well as its instrumental presentation of his famous law of cooling [2]. First cornerstone of the theory of warmth propagation was provided by Jean B.J. Fourier (1768–1830) [3] who also initiated the investigational problems of heat transfer, and it was Fick [4] who derived his famous laws of diffusion on the basis of Fourier. The entire roots of thermal analysis point back to the nineteenth century where temperature became an observable and experimentally sizeable quantity. Within the years 1903–1905, the term thermal analysis [5] was introduced by Gustav H.J. Tammann (1861–1938) who demonstrated the value of cooling curves for registration of temperature deviations between the sample and reference during sample state changes. The notion of temperature has been comprehended [6, 7], and the discipline of thermodynamics was established [8, 9] and applied to thermal analysis practice [10]. The thermal aspects were introduced into the first treaties on theoretical thermal analysis [11–16]; however, such knowledge has not been incorporated into thermoanalytical theoretical treatises [10] as much as it would have deserved, except [16–18]. The fact that *heat transfer takes time* (known since Newton's cooling law [2] and from the fundamental Tian's calorimetric equation [19]) was not adequately included in the recent theory of thermal analysis is the biggest mistake of non-isothermal kinetics extraordinarily needing correction.

Inertia as a tendency of body to *conserve a previous state* is unquestionably existing not only in mechanics (where the motional momentum, p, is related to mass, m, and velocity, v) but also in thermodynamics because changes of thermal state of bodies are also inclining preservation and heat transfer retard due to the feasible heat capacity. The action the relevant thermal 'momentum' is substituted by the allied inertia due to the material's heat capacity, C_p, and heat-change 'velocity' by the time derivative of the temperature difference, $d\Delta T/dt$. In 1701, Newton showed [2] that the temperature of a hot body decreases slowly according to *Newton's cooling law* which is still used to estimate even the hour of unexpected death in crime investigations. This first quantitative law dealing with heat and temperatures is easy to derive comparing the heat flow q from hot body (with temperature T_h) toward the cold surroundings (with temperature T_c) using a coefficient of proportionality K (thermal conductance) and difference between the rate of heat content changes of the hot body with heat capacity C_h and the cold surroundings with heat capacity C_c (if t means time).

Thus we have

$$q = K(T_h - T_c) = -C_h(\mathrm{d}T_h/\mathrm{d}t) + C_c(\mathrm{d}T_c/\mathrm{d}t) \tag{15.1}$$

Then, assuming $C_h \gg C_{c,}$ we obtain

$$K(T_h - T_c) = -C_h(\mathrm{d}T_h/\mathrm{d}t) \Rightarrow 0 = K(T_h - T_c)\mathrm{d}t + C_h\mathrm{d}T_h \tag{15.2}$$

Modifying Eq. (15.2) to

$$(K/C_h)\mathrm{d}t = -(1/(T_h - T_c))\mathrm{d}T_h = -\frac{\mathrm{d}T_h}{(T_h - T_c)} = -\mathrm{d}\,\ln(T_h - T_c) \tag{15.3}$$

and upon integrating (when $\mathrm{d}T_c/\mathrm{d}t \approx 0$ so that $T_c \approx$ const and assuming both C_h and K being also constant), we enter the following equation:

$$\begin{aligned}(t - t_o)/\tau &= -\ln(T_h - T_c)/(T_{ho} - T_c) \rightarrow (T_h - T_c) \\ &= (T_{ho} - T_c)\exp(-(t - t_o)/\tau)\end{aligned} \tag{15.4}$$

where $\tau \equiv C_h/K$ is called *time constant* of cooling.

There follows an important consequence that Newton's cooling law exists in two forms:

- *differential* form of Eq. (15.2) and
- *integral* form of Eq. (15.4).

The heat inertia was also included in the Tian's equation derived for microcalorimetry and published in 1933 [19], i.e.,

$$W\mathrm{d}t - P\mathrm{d}t - p(\Theta - \theta)\mathrm{d}t = -c\,\mathrm{d}\theta \tag{15.5}$$

Here, W is heat flow (in Watt) deliberated inside a sample, P is a compensating heat flow, p, which is heat flux necessary to reach temperature difference between the outer (surrounding) temperature Θ and inner (sample) temperature θ equal to 1 °C, and c is heat capacity of the sample. Equation (15.4) corresponds to the Newton's cooling law expressed by differential form of Eq. (15.2) (if symbols $\Theta = T_c$, $\theta = T_h$, $p = \Lambda$, and $c = C_h$ are used instead). It is enriched, however, by internal source of heat flux W (inside the sample signifying the hot body) and external compensation heat flux P. Historically, Tian illustrated the determination of quantity p by the following drawing, Fig. 15.1, conveyed from his fundamental paper [19], where the right side (falling) curve exemplifies the exponential shape of Newton's cooling law.

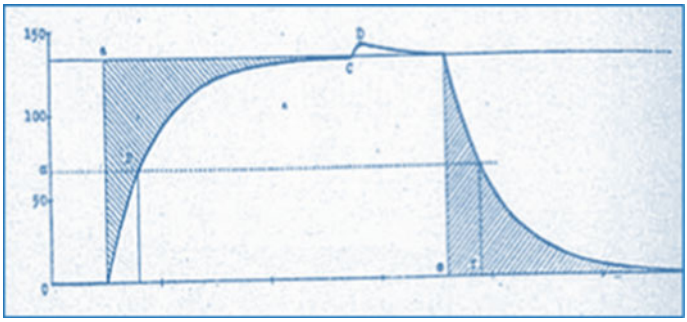

Fig. 15.1 Historical record of a heat calibrating pulse transferred from the original Tian's 1933 publication [19]. Descending part of the curve is traditionally used in calorimetry to determine the time constant

15.2 Application in Differential Thermal Measurements

One of the first attempts to describe equations involving heat fluxes in DTA apparatus was suggested in 1949 by Vold [20] who employed four temperatures T_s, T_r, $T_{w,}$ and T_o (as respective temperatures of sample under study, reference sample, furnace wall, and atmosphere) to express the heat flux balances for both samples, i.e.,

$$C_r \mathrm{d}T_r/\mathrm{d}t = K_r(T_w - T_r) + \sigma(T_r - T_s) + k_r(T_o - T_r) \tag{15.6}$$

$$\Delta H \mathrm{d}\alpha/\mathrm{d}t + C_s \mathrm{d}T_s/\mathrm{d}t = K_s(T_w - T_s) + \sigma(T_s - T_r) + k_s(T_o - T_s), \tag{15.7}$$

where C_r and C_s are heat capacities of reference and sample, respectively, and K_r, K_s, σ, $k_{r,}$ and k_s are heat conductivity coefficients for the fluxes between samples (using subscript sample s, reference r, furnace wall w, and atmosphere o). The derivative $\Delta H \mathrm{d}\alpha/\mathrm{d}t$ (which equals W in the Tian's Eq. (15.4)) is the internal heat source at an exothermic process when $\Delta H < 0$ or heat sink at an endothermic process when $\Delta H > 0$. It represented a reaction/transition rate $\mathrm{d}\alpha/\mathrm{d}t$ (α is the degree of conversion/transition) multiplied by integral enthalpy of the reaction/transition ΔH.

Substituting $T_s = T_r + \Delta T$, Eq. (15.6) becomes

$$\Delta H \mathrm{d}\alpha/\mathrm{d}t + C_s \mathrm{d}T_r/\mathrm{d}t + C_s \mathrm{d}\Delta T/\mathrm{d}t = K_s(T_w - T_r) - K_s\Delta T + \sigma\Delta T + k_s(T_o - T_r) - k_s\Delta T \tag{15.8}$$

On subtracting Eq. (15.6) from (15.7), the following equation (in correspondence with Eq. (15.5) in Ref. [20]) is found

$$(C_r - C_s)\mathrm{d}T_r/\mathrm{d}t - C_s\mathrm{d}\Delta T/\mathrm{d}t - \Delta H\mathrm{d}\alpha/\mathrm{d}t = (K_s + k_s)\Delta T + (K_r - K_s)(T_w - T_r) + (k_r - k_s)(T_o - T_r) \quad (15.9)$$

Assuming $K_r = K_s$, $k_r = k_s$ and substituting $K \equiv K_s + k_s$, $\Phi \equiv \mathrm{d}T_r/\mathrm{d}t$ a following simplified form is obtained

$$(C_r - C_s)\Phi - C_s\mathrm{d}\Delta T/\mathrm{d}t - \Delta H\mathrm{d}\alpha/\mathrm{d}t = K\,\Delta T \quad (15.10)$$

The middle term on left side of Eq. (15.6) has a nonzero value, and we featured $C_s\mathrm{d}\Delta T/\mathrm{d}t$ as the *heat inertia term* [21–25] without any connection with a thermal inertia concept in geology [26, 27].

The equation including the heat inertia term was also derived in publications by Faktor and Hanks [28] who, in addition, pointed out the cubic dependence of conductivity K (in Eq. (15.6)) on temperature T due to the participation of radiation on heat transfer:

$$K = A + BT^3. \quad (15.11)$$

Holba et al. [29, 30] published an algorithm for the transformation of original DTA curve $\Delta T(t)$ into kinetic curve $\mathrm{d}\alpha/\mathrm{d}t = f(t)$ using Eq. (15.6) including linear dependence of heat capacity of sample C_s on transition degree α as

$$C_s = C_s^o + \alpha\Delta C_s \quad (15.12)$$

where C_s^o is heat capacity of sample before transition, and ΔC_s (=$\mathrm{d}\Delta H/\mathrm{d}T$) is heat capacity change of sample due to transition. It was found that the activation energies for phase transition of $BaCO_3$ is calculated from the original DTA curve and the rectified kinetic curves revealing considerable inconsistency (namely activation energies 88 and 118 kcal/mole, respectively [30]).

It is worth manifestation that only few books on thermal analysis [16–18] have pointed out the inevitability to correct DTA curve using heat inertia term before kinetic evaluation. This situation is probably the consequence of article by Borchard and Daniels [31] who derived the similar equation as Vold [20]; nevertheless, they mistakenly supposed that value of the heat inertia term $C_s\mathrm{d}\Delta T/\mathrm{d}t$ is negligible with respect to the heat consumption/production term $\Delta H\mathrm{d}\alpha/\mathrm{d}t$. This crucial as well long passed belief of the $C_s\mathrm{d}\Delta T/\mathrm{d}t$ insignificant fittingness has been a *most regrettable mistake in theoretical thermal analysis* having impact until today [32].

15.3 Historical Misinterpretations

In the same year as Borchard and Daniels' paper by November 1957 [31], Kissinger published his famous and broadly cited work [33] where heat inertia term is not explicitly considered as it follows from his relation [34, 35]

$$\mathrm{d}\theta/\mathrm{d}t = f'(\mathrm{d}q/\mathrm{d}t)\left(\mathrm{d}^2q/\mathrm{d}t^2\right) \tag{15.13}$$

where θ is the difference in temperature of the centers of the two samples, $f(\mathrm{d}q/\mathrm{d}t)$ is a function of the reaction rate which also includes any secondary effects of the reaction, such as changes in volume, density, or thermal properties, and $\mathrm{d}q/\mathrm{d}t$ is the rate of heat generation due to a chemical reaction per unit volume of sample [32]. Kissinger assumed citing [33]: '*from* Eq. (15.6) *it is seen that when* $\mathrm{d}^2q/\mathrm{d}t^2$, *the derivative of the rate of heat absorption*, *is zero*, $\mathrm{d}\theta/\mathrm{d}t$ *is also zero. Since the rate of heat absorption is proportional to the rate of reaction*, *Eq.* (15.6) *states that the peak differential deflection occurs when the reaction rate is a maximum which becomes true only when the heating rate of the reference is constant …*'

A considerable support on such a simple kinetic studies [16, 24, 25, 27, 32, 36, 37] without paying any respect to the heat inertia term in DTA equation was supported by the widely cited paper of Piloyan et al. [38]. Negative impact can be seen in the context of recent kinetic studies supporting the customary effortless methodology while overlooking any reflection to the process specificity due to heat incorporation.

A new approach into the description of heat processes in dynamic calorimetry and DTA was brought by O'Neill [39] (affiliated at Perkin-Elmer Corp.) who utilized an analogy between balance of currents in electric circuit and balances of heat fluxes, using thermal resistance R instead of thermal conductivity K without notifying the resistance R which is the reciprocal of conductance $K = 1/R$.

The use of electrotechnical language for the description of heat fluxes was then accepted by further authors connected usually with TA Instruments, e.g., Danley [40] who derived for difference Δq of heat fluxes between the sample (subscript s) and reference (r) holders the equation:

$$\Delta q = \Delta p + (T_e - T_s)\left(\frac{1}{R_s} - \frac{1}{R_r}\right) - \frac{\Delta T}{R_r} + (C_r - C_s)\frac{\mathrm{d}T_s}{\mathrm{d}t} - C_r\frac{\mathrm{d}\Delta T}{\mathrm{d}t} \tag{15.14}$$

where $\Delta p = p_s - p_r$ means difference between heat productions in the s and r holders, T_e is temperature of enclosure, $\Delta T = T_s - T_r$, R_s, R_r are thermal resistances, and C_s, C_r heat capacities. If conductance $K_s = 1/R_s$, $K_r = 1/R_r$ are used instead of resistances R_s, R_r and $\Delta p = \Delta H$. When $\mathrm{d}\alpha/\mathrm{d}t$ is considered, then the equation turns out to be similar to that by Vold [20] (see Eq. 15.9) is obtained

$$\Delta q = -\Delta H\frac{\mathrm{d}\alpha}{\mathrm{d}t} + \Delta T_o(K_s - K_r) - \Delta T K_r + (C_r - C_s)\frac{\mathrm{d}T_s}{\mathrm{d}t} - C_r\frac{\mathrm{d}\Delta T}{\mathrm{d}t} \tag{15.15}$$

Another electrotechnical-like description of heat flux DSC was published by Kaisersberger and Moukhina [41] using five special thermal resistances to describe the heat fluxes for desmearing DSC signal including somehow the mathematically hidden effect of inertia. Significant is also an encouraging signals of distinction between the compensation and the heat flow DSC by Illekova et al. [42] who appropriately associated the term of heat inertia to individual methods.

It is worth noting that our recent papers [34–37] have been devoted to the clarification of the enduring problematic of kinetic evaluation via DTA experiments (eventually heat flux DSC), curves which ought to be corrected eliminating the influence of heat inertia. The curves obtained by compensation (Perkin-Elmer) DSC need not to include such a correction [16, 32, 39]. Exploitation of kinetic evaluation of TG curves is not an issue of our chapter; nonetheless, even such kinetic studies generally underestimate the influence of heat transfer on the course of a reaction process under sample weighing. For example, Gray [43] suggested the completely 'nonkinetic' model for TG curve in the form of the following equation (see Eq. (15.18) in his article [43]).

$$\mathrm{d}\alpha/\mathrm{d}t = m(C_s/\Delta H)(\mathrm{d}T_s/\mathrm{d}t) + \left(T_s - T_p\right)/(R\Delta H) \tag{15.16}$$

where t is time, $\mathrm{d}\alpha/\mathrm{d}t = (\mathrm{d}m/\mathrm{d}t)/\Delta m$ is rate of process derived from the thermogravimetric curve m versus t of mass related to full mass loss Δm of sample, and C_s, ΔH are heat capacity of sample and the enthalpy change of the process, respectively. Temperatures T_s and T_p serve for the sample (including its holder p) and for the sample surroundings, while R is the thermal resistance between the surroundings and the sample holder. The Gray's model [43] expresses the course of decomposition process excessively controlled by heat transfer citing '*thermal resistance between the sample and the furnace determines the rate at which heat can be provided to the sample*, *which for an endothermic reaction determines the rate of the reaction*, *which in turn determines the rate of weight loss.*' It is clear that the so far conventionally idealized methods of easy kinetic modeling [14, 15, 44, 45] are insufficient for a honestly sophisticated kinetic analysis while searching of a truthful reaction mechanism. It would look better as if we restrict kinetic analysis to a mediocre logistic approach [46]. It is apparent that the hitherto customary role of the popular figure of activation energy can serve as good agency for aptitude promotion *to easily reach a desired publication* [47]. It keeps sourcing a wide popularity reflected to numerators kinetic papers [48] without necessity to be refined by so far ignored effect of thermal inertia. In this modern time of computers [30], it is astonishing that the effect of heat inertia is being fearfully ignored by kineticists due to their traditional exploit of deep-rooted fashion of simple kinetic procedures [14].

The indisputable but overlooked existence of the term of *heat inertia* hangs over scientific community for many years [31, 32, 49] and seems to be a deterrent to all kineticists, who are accustomed to trouble-free calculations [14, 16, 45, 46]. The heat inertia term actually extends to all types of heat flux DSC and DTA measurements [49] and cannot be reduced by diminishing the sample size or reduced by mathematical practice of mere exchanging the measured temperature difference ΔT by heat flux Δq consequently adjusted by calibration (in order to reach an 'instrumental' likeness with DSC). Moreover, the incorporation of heat inertia would claim the modification of various software [30] (being often a traditional part of manufacture assessor package) and can in turn affect many already published articles connected with the determination of activation energies via DTA analysis

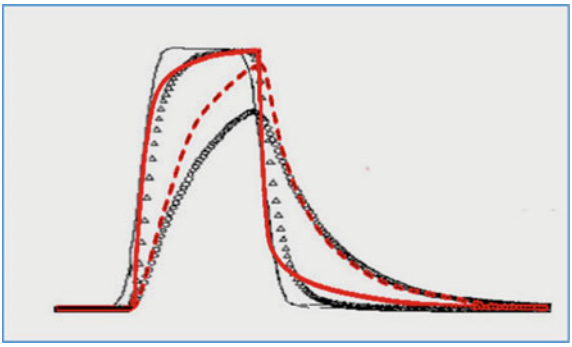

Fig. 15.2 A rectangular heat pulse was inserted into the sample by either method: **a** *circles*—the resistant heating inside the sample [51, 52] under the mode of linear heating and **b** *triangles*—the heat irradiation on sample surface [41] during the isothermal regime. Both pulses are normalized on the $<\Delta T$ versus $t>$ axis as to fine-tuning the same shape. The as-measured DTA response on the internally inserted pulses (*dashed read line*, resistant heating) was corrected on the heat inertia effect by differential method [30] to yield the rectified peak (*full red line*). The as-measured DTA feedback on the externally applied heat pulse (*small circle line*) was corrected by the standard Netzsch instrumental software [41] based on integral method giving a rectified peak (*small triangles line*). Both rectifications emerge from the matching character of corrections. The *upper left* area between rectified peak and inserted rectangular pulses results from yet uncorrected temperature gradients in the sample [32, 53]

[48]. Understandably, nobody would like to see any depreciation of his already published data. Disbelieving stance to the reality of inseparable inertia impact can be made clearer by simple graphical evidence visualized in Fig. 15.2. Two evaluation methods are explicitly compared, the one using DTA correction based on the differential form of Eq. (15.6) [30, 50, 51] with the other one, which is sourced on manufacture software based on integral form of Eq. (15.4) [41]. Though the as-measured DTA peaks are received under dissimilar experimental conditions, the shape and the character of consequent rectification provide almost identical consequence enabling to attain the original shape of the inserted rectangular pulses.

Nevertheless, it is clear that the legitimacy of thermal inertia in thermal measurements [37] has been ignored and would not receive desired recognition until accepted by a wider community of kineticists which would not take place until it will opportunely receive a substantial exploration by internationally recognized commissions [52].

15.4 Counterparting Impact of Gradients

Associated but yet unsolved intricacy is also due to the impact of temperature gradients ever existing in the bulk sample [25, 53] which was analyzed in detail in our previous book chapter [31] and early conferred elsewhere [53–56].

The manner of temperature sensing of the sample affects the relevance of heat inertia as illustrated in Fig. 15.3. The rectification process due to the heat inertia became complicated as the correction of DTA curves derived from temperatures measured on the sample surface and that from it integrated (bulk-mean) can be dissimilar and thus insufficient with respect to the correction necessary to find the actual (∼true) course of the process (∼transition) under study. It can be visualized by comparing a DTA curve obtained from continuous model (solid line: ΔT_{DTA}) with the correction obtained from integral temperature differences (dot-dashed line: $\Delta T_{\mathrm{prop}} - \Delta T_{\mathrm{DTA}}$) and the properly corrected DTA curve (dashed line: ΔT_{prop}), see Fig. 15.3.

The temperature profiles in a heated sample were thoroughly calculated in [31] regarding its simplest form as an infinite cylinder with external radius. The sample displays an endothermic first-order phase transition with the equilibrium transition temperature T_t during which the initial phase is changed into the final phase. When the sample is exposed to a linear heating, then four stages can be distinguished with respect to the temperature profile inside the finite sample. (1) Temperature at any part of the sample is lower than the (equilibrium) transition temperature so that the stabilized temperature profile occurs inside the sample. (2) When the temperature becomes higher than T_t in a part of the sample, the phase transition is in progress and the extent of transition inside the whole is lower than unity. The temperature profile is not stabilized since it is affected by so-called heat sink due to the running endothermic transition. (3) Temperature at any part of the sample occurs higher than T_t, while the extent of transition amounts to unity, the temperature profile is not yet stabilized, but it is tending to reach the stabilized state. Middle stage is illustrated in Fig. 15.4. Making problematic how to distinguish an appropriate picture of the process for mathematical modeling which can be approached using two geometrical version as: (1) a continuous and a (2) discontinuous—still open question to

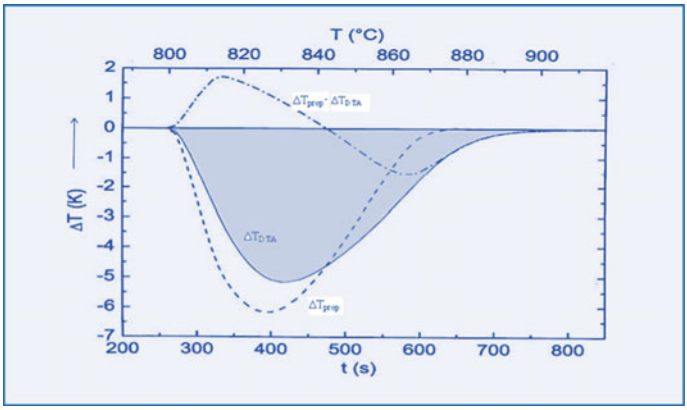

Fig. 15.3 Advisory consequence of twofold calculated impact of heat inertia (s-shaped) when assuming surface and mean-bulk measurements ΔT_{prop} on the as-received ΔT_{DTA} peak (*shadowed*)

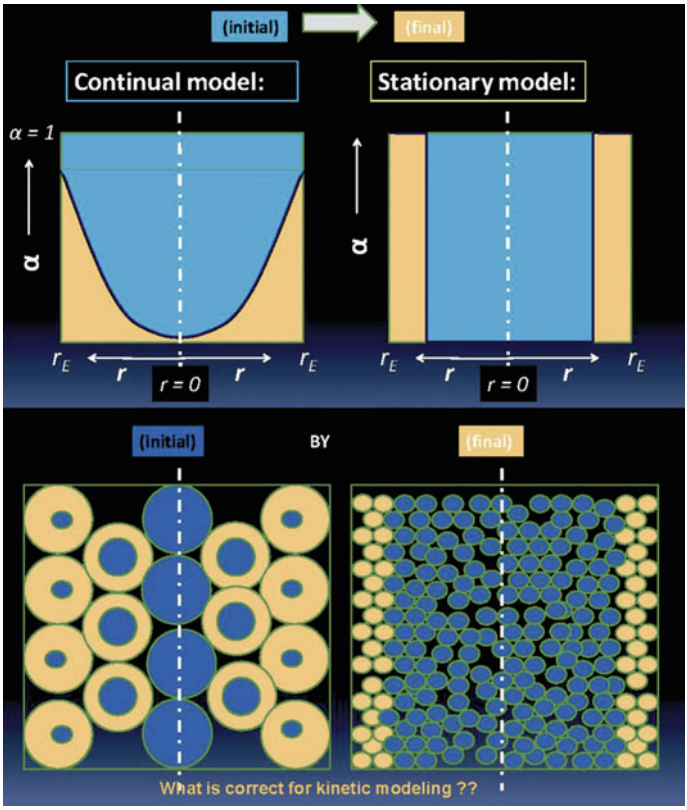

Fig. 15.4 Schematic pattern of two abridged cases possibly participating in a solid-state transformation shown within simple spherical images where *light shadow* areas show reacted and *dark* initial nonreacted material. Thorough analysis of temperature gradients and their calculations were revealed in Chapter 5 of previous Volume 8 [53]

researches how far they are able to introduce the radius-dependent reaction progress.

It is a matter of time when the peak rectification (DTA and heat flux DSC) becomes the standard means of sphere accessories using terms correcting both the heat inertia effect (term proportional to $d\Delta T_{DTA}/dt$) [29, 30] and the effect of varying temperature gradient inside the sample (the term proportional to the rate $d\theta_{SM}/dt$ of the difference θ_{SM} between the measured (outer) temperature of sample holder T_{EHS} and the temperature $T_{S\emptyset}$ averaged over whole volume of the sample [34]) will be introduced into both the private and commercial practice of instrumentally available software as already treated in [57, 58]. The gradient relations are important while forming a specific part of kinetically aimed analysis. However, the intricacy of an appropriate constitutive equation has been analyzed in detail previously [53, 59], but the topic of dynamic kinetics [10, 37] is so extensive thus falling beyond the restricted size of this chapter.

15.5 Relations Following from General Kinetic Equation for the First-Order Reactions

The basic equation of any kinetic launch appears to be the following unfussy relation (even if unknown from where it come form) [14]

$$\mathrm{d}\alpha/\mathrm{d}t = F(\alpha, T) = f(\alpha)k(T) \tag{15.17}$$

where variable α, t, and T customarily mean the degree of conversion of the process under study, time, and absolute temperature, respectively. Function $f(\alpha)$ represents (often isothermal) kinetic model [14, 16, 44–46], and $k(T)$ is the traditional fashion for temperature dependence of process (i.e., reaction or transition) rate. Although several models can be used for $k(T)$ (see, e.g., [8–14]), the Arrhenius equation $k(T) = A\ \exp(-E/RT)$ is the most popular one, where A is the so-called pre-exponential factor (with dimension s^{-1}), E is activation energy (in J/mol), and R is universal gaseous constant (in J/mol/K). Upon the combination, the legendary equation is obtained

$$\mathrm{d}\alpha/\mathrm{d}t = F(\alpha, T) = f(\alpha)\,A\exp(-E/RT) \tag{15.18}$$

serving as a traditional starting point for the derivation of equation for the maximum rate of the process connected with the temperature T_m at which this maximum is reached. For such a maximum of reaction/transition rate, the condition for maximum of the function $F(\alpha, T)$ (with respect to time) is used:

$$\begin{aligned}\mathrm{d}^2\alpha/\mathrm{d}t^2 = {} & (\mathrm{d}f(\alpha)/\mathrm{d}\alpha)\,(\mathrm{d}\alpha/\mathrm{d}t)[A\exp(-E/RT)] \\ & + f(\alpha)[A\exp(-E/RT)]\left(E/RT^2\right)\mathrm{d}T/\mathrm{d}t = 0\end{aligned} \tag{15.19}$$

After the mathematical rearrangements, the well-known modifications are obtained (where $\beta \equiv \mathrm{d}T/\mathrm{d}t$ for linear heating)

$$\begin{aligned}&(\mathrm{d}f(\alpha)/\mathrm{d}\alpha)(\mathrm{d}\alpha/\mathrm{d}t) + f(\alpha_m)\left(E/RT_m^2\right)\mathrm{d}T/\mathrm{d}t = 0 \\ &(\mathrm{d}f(\alpha)/\mathrm{d}\alpha)[f(\alpha)]A\exp(-E/RT_m) + [f(\alpha)]\left(E/RT_m^2\right)\mathrm{d}T/\mathrm{d}t = 0 \\ &(\mathrm{d}f(\alpha)/\mathrm{d}\alpha)A\exp(-E/RT_m) + \left(E/RT_m^2\right)\beta = 0\end{aligned} \tag{15.20}$$

with the resulting equation:

$$(\mathrm{d}f(\alpha)/\mathrm{d}\alpha)\exp(-E/RT_m) = -E\beta/ART_m^2. \tag{15.21}$$

Then, for 'classical' kinetic mechanism corresponding to the first-order reaction.

$$f(\alpha) = (1-\alpha)\ \rightarrow \mathrm{d}f(\alpha)/\mathrm{d}\alpha = -1 \tag{15.22}$$

Equation (15.21) is obtained in the form

$$\exp(-E/RT_m) = E\beta/ART_m^2$$
$$\text{or} \quad -E/RT_m = \ln(E\beta/AR) - 2\ln T_m \tag{15.23}$$

Using Eq. (15.23), we can unambiguously transform any pair of quantities E, ln A into pair T_m, β so that the information on the pair $T_m - \beta$ has the same importance as the information on the pair $E -$ ln A. This transformation at heating rate $\beta = 10$ K/min is shown in Fig. 15.5 and heating rates 2, 10, 60 K/min in Fig. 15.6.

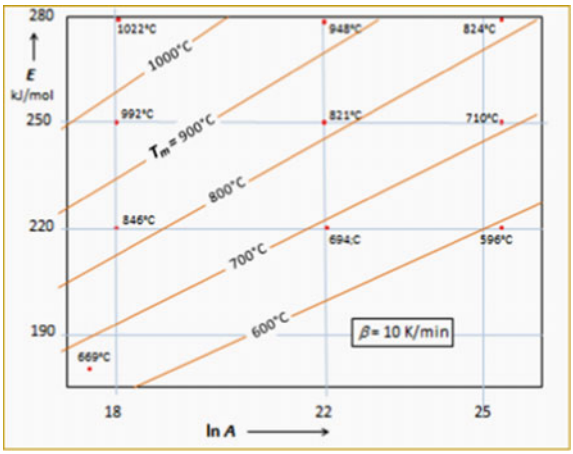

Fig. 15.5 Temperature T_m at inflection point in α versus T dependence for heating rate $\beta = 10$ K/min and values of activation energy E and logarithm of pre-exponential factor A

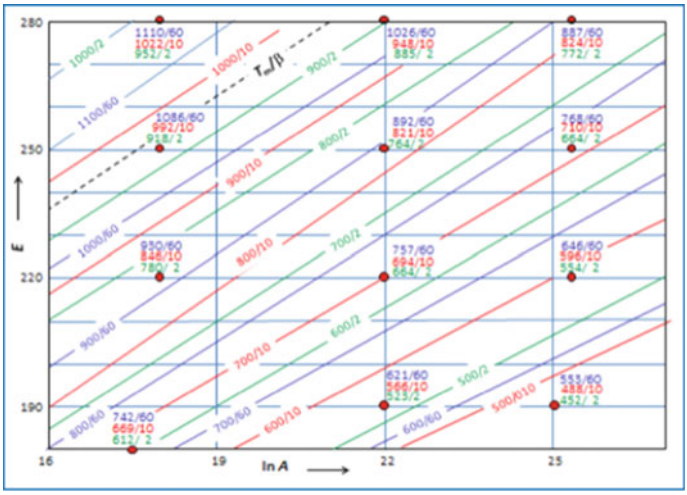

Fig. 15.6 Results of transformation of E, ln A into T_m, β for heating rates $\beta \in 2$, 10, and 60 K/min

We can further rewrite Eq. (15.21) into the form

$$E = -RT_m \ln(E\beta/RT_m^2) + RT_m \ln A = RT_m(\ln(RT_m^2/E\beta) + \ln A) \tag{15.24}$$

$$\text{or} \quad E/RT_m = \ln A + \ln(T_m/\beta) - \ln(E/RT_m) \tag{15.25}$$

where $\ln(E/RT_m)$ can be considered insignificant with respect to E/RT_m (i.e., $E/RT_m \gg \ln E/RT_m$) as well as with respect to $\ln(T_m/\beta)$ (i.e., $\ln(T_m/\beta) \gg \ln E/RT_m$) so that the legitimacy of kinetic compensation effect is thus approved [60] as also analytically derived by Roura and Farjas [61]. More detailed mathematical analysis can be found in our previous systematic chapter [62]. Worth noting is that the kinetic compensation effect was mathematically observed as early as in 1966 [63].

Another way to study the relation between the pair $E - \ln A$ and the pair $\beta - T_m$ can be based on the rules valid for partial derivatives. If we define the function $F \equiv F(E, A, \beta, T_m)$ using Eq. (15.25) as

$$F \equiv F(E, A, \beta, T_m) = \exp(-E/RT_m) - E\beta/ART_m^2 = 0. \tag{15.26}$$

By using rules valid for partial derivatives in general form for $F(x, y, z) = \text{const}$

$$(\partial y/\partial x)_z = -(\partial F/\partial x)_{y,z}/(\partial F/\partial y)_{x,z} \tag{15.27}$$

we can write

$$(\partial T_m/\partial \beta)_{E,A} = -(\partial F/\partial \beta)_{E,A,T_m}/(\partial F/\partial T_m)_{E,A,\beta} \tag{15.28}$$

The requested partial derivatives are then

$$(\partial F/\partial \beta)_{E,A,T_m} = -E/ART_m^2 \tag{15.29}$$

$$(\partial F/\partial T_m)_{E,A,\beta} = -\left(E/RT_m^2\right)\exp\left(-E/RT_m\right) + 2E\beta/ART_m^3 \tag{15.30}$$

so that

$$\begin{aligned}(\partial T_m/\partial \beta)_{E,A} &= E/ART_m^2/[2E\beta/ART_m^3 - \left(E/RT_m^2\right)\exp(-E/RT_m)] \\ &= 1/[2\beta/T_m - A\exp(-E/RT_m)]\end{aligned} \tag{15.31}$$

or according to general rule: $1/(\partial y/\partial x)_z = (\partial x/\partial y)_z$ we obtain

$$\begin{aligned}(\partial \beta/\partial T_m)_{E,A} &= [2\beta/T_m - A\exp\left(-E/RT_m\right)] \\ &\rightarrow (\partial \beta/\partial T_m)_{E,A} - 2\beta/T_m = A\exp\left(-E/RT_m\right)\end{aligned} \tag{15.32}$$

$$\rightarrow \ln[(\partial \beta/\partial T_m)_{E,A} - 2\beta/T_m] = \ln A - E/RT_m \tag{15.33}$$

15.6 Kissinger Erroneous Assumption on Temperature of Maximum Reaction Rate

In particular, Kissinger [33] started from Eq. (15.22) in the form

$$\beta/T_m^2 = -\mathrm{d}f(\alpha)/\mathrm{d}\alpha(AR/E)\exp(-E/RT_{mr}) \tag{15.34}$$

and its logarithmic form encompasses his famous equation [27, 48]

$$\ln(\beta/T_{mr}^2) = -E/RT_{mr} + \ln(AR/E) + \ln(-\mathrm{d}f(\alpha)/\mathrm{d}\alpha) \tag{15.35}$$

where T_{mr} represents the temperature at which the maximum rate of ongoing process $r \equiv \mathrm{d}\alpha/\mathrm{d}t$ is reached. For the first-order reaction ($f(\alpha) = 1 - \alpha$), we have $\mathrm{d}f(\alpha)/\mathrm{d}\alpha = -1$ (as it is used in Eq. 15.25) and we have $\ln(\beta/T_{mr}^2) = -E/RT_{mr} + \ln(AR/E)$, and neglecting $\ln(A/RE)$ with respect to E/RT_{mr} due to ($\ln(A/RE) \ll E/RT_{mr}$), the approximation equation is valid [33]

$$\ln(\beta/T_{mr}^2) \approx -E/RT_{mr} \tag{15.36}$$

For kinetic models other than first-order reaction, it should be fulfilled the condition $\mathrm{d}f(\alpha)/\mathrm{d}\alpha > 0$. In any case, Eq. (15.35) is usable only for positive heating rate $\beta > 0$ (not for cooling).

Kissinger used Eq. (15.36) as a base of procedure estimating activation energy E as a slope of approximating line in the plot of $\ln(\beta/T_{mr}^2)$ versus $-1/RT_{mr}$ where T_{mr} is substituted by temperature $T_{m\Delta}$ at which an extreme of the peak on DTA curve is reached, i.e., where the temperature difference $\Delta T = T_S - T_R$ between the sample under study (S) and the reference sample (R) reached its extreme value for which the condition is valid

$$\mathrm{d}\Delta_{m\Delta}T/\mathrm{d}t = 0. \tag{15.37}$$

However, Kissinger's assumption [33] is that the temperature $T_{m\Delta}$ in the point where temperature difference ΔT reaches the extreme value ($\Delta_{m\Delta}T$) is identical with temperature T_{mr} where the reaction rate $r = \mathrm{d}\alpha/\mathrm{d}t$ reaches its maximum *is not correct!* This Kissinger's assumption is that T_{mr} is identical with $T_{m\Delta}$ (on DTA curve) and is not valid [34, 35], and this identity can be assumed justifiable only for curves obtained by compensating DSC (Perkin-Elmer) method.

As far as $T_{mr} \neq T_{m\Delta}$ also applies to the spontaneous heat flux DSC (where spontaneous heat flux q is given as $q = K\Delta T$), the maximum deviation of such a DSC peak is reached at temperature T_{mq} which corresponds to incorrect temperature $T_{m\Delta}$. On the other hand, for compensating heat flux DSC (where compensating heat flux Q is given as $Q = \Delta h \cdot r$), the maximum deviation of DSC peak is reached at temperature T_{mQ} which corresponds to the correct temperature T_{mr}. The correct equation for a DTA curve $\Delta T_{(t,TR)}$ in the simplest form (after subtracting of the

baseline B_L: $\Delta T_S = \Delta T - B_L$) is revealed in above-mentioned papers by Vold [20], Factor and Hanks [28], Nevřiva et al. [22], Holba et al. [21, 29, 30, 35, 49], Šesták et al. [16, 23, 27, 32, 34], and Chen and Kirsh [17] which is given as

$$\begin{aligned} K\Delta T &= c_S(\mathrm{d}\,\Delta T/\mathrm{d}t) - \Delta h(\mathrm{d}\alpha/\mathrm{d}t) \\ \text{or} \quad \Delta T &= R_t[c_S(\mathrm{d}\Delta T/\mathrm{d}t) - \Delta h(\mathrm{d}\alpha/dt)] \end{aligned} \tag{15.38}$$

where K (dimension W/K) means thermal conductance between the sample environment and the sample holder, c_S (J/K) is the heat capacity of the sample under study including its holder, Δh is integral enthalpy (J) of the process under study, and $R_t \equiv 1/K$ is called thermal resistance.

Starting from Eq. (15.38), the maximum reaction rate should correspond to the condition

$$\mathrm{d}^2\alpha(T_{mr})/\mathrm{d}t^2 = (1/\Delta h)[c_s(\mathrm{d}^2\Delta T/\mathrm{d}t^2) - K(\mathrm{d}\Delta T/\mathrm{d}t)] = 0 \tag{15.39}$$

which can be modified into

$$\tau_S(\mathrm{d}^2\Delta_{mr}T/\mathrm{d}t^2) = (\mathrm{d}\Delta_{mr}T/\mathrm{d}t) \tag{15.40}$$

where $\tau_S \equiv c_S/K$ is called ti*me constant* of the system of the sample under study including its holder.

15.7 Determination of the Correct Temperature of Maximum Reaction/Transition Rate

The value of time constant τ_S could be estimated from the course of the tail (brush—index B) of DTA peak (the final part of peak where the reaction rate $\mathrm{d}\alpha/\mathrm{d}t$ equals zero, cf. Fig. 15.1) using the proper DTA Eq. (15.37) under the condition $\mathrm{d}\alpha/\mathrm{d}t = 0$

$$\begin{aligned} K\Delta_B T = c_S(\mathrm{d}\Delta_B T/\mathrm{d}t) \rightarrow \Delta_B T = \tau_S(\mathrm{d}\Delta_B T/\mathrm{d}t) \rightarrow 1 = \tau_s(d\ \ln\Delta_B\, T/\mathrm{d}t) \\ \rightarrow \tau_S = 1/(\mathrm{d}\ \ln\Delta_B T/\mathrm{d}t). \end{aligned} \tag{15.41}$$

Substituting (15.39) into (15.38), the condition for the determination of *correct* T_{mr} is given as

$$(\mathrm{d}^2\Delta_{mr}T/\mathrm{d}t^2)/(\mathrm{d}\Delta_{mr}T/\mathrm{d}t) = (\mathrm{d}\ln\Delta_B T/\mathrm{d}t) \tag{15.42}$$

which should be valid only at temperature T_{mr} where the maximum reaction rate is reached.

On the other hand, the use of Eq. (15.38), i.e., $\{K\Delta T = c_s(\mathrm{d}\Delta T/\mathrm{d}t) - \Delta h(\mathrm{d}\alpha/\mathrm{d}t)\}$, gives the following equation for the extreme of temperature difference at top of peak $\Delta_{m\Delta}T$

$$(K/c_s)\Delta_{m\Delta}T + (\Delta h/c_s)(\mathrm{d}\alpha/\mathrm{d}t)_{m\Delta} = \mathrm{d}\Delta_{m\Delta}T/\mathrm{d}t = 0 \tag{15.43}$$

where $(\mathrm{d}\alpha/\mathrm{d}t)_{m\Delta}$ is a reaction rate corresponding to the moment when peak extreme $\Delta_{m\Delta}T$ is achieved. From Eq. (15.43), the interesting conclusion can be derived in form of the relation

$$\Delta h/K = \Delta_{m\Delta}T/(\mathrm{d}\alpha/\mathrm{d}t)_{m\Delta} \tag{15.44}$$

which should stay independent on the heating rate β (if K is independent on β).

15.8 Kinetic Equation and Kissinger Equation After Including the Heat Inertia Term

The frequent fail in the use of Eq. (15.3), i.e., $\{\mathrm{d}\alpha/\mathrm{d}t = F(\alpha, T) = f(\alpha)A\ \exp(-E/RT)\}$, is its insertion into the equation values of the programmed temperature assuming $\mathrm{d}T/\mathrm{d}t = \beta$ constant. However, temperature of sample T_S differs from the programmed temperature (reference temperature T_R at any DTA method) by the difference $\Delta T = T_s - T_r$ which can be expressed from Eq. (15.38), i.e., $\{K{\cdot}\Delta T = c_s{\cdot}\mathrm{d}\Delta T/\mathrm{d}t - \Delta h{\cdot}\mathrm{d}\alpha/\mathrm{d}t\}$ as

$$\Delta T = (c_s/K)(\mathrm{d}\Delta T/\mathrm{d}t) - (\Delta h/K)\mathrm{d}\alpha/\mathrm{d}t \tag{15.45}$$

The starting kinetic Eq. (15.17) should be then used in the form

$$\mathrm{d}\alpha/\mathrm{d}t = f(\alpha)A\exp(-(E/R(T_R + \Delta T)) \tag{15.46}$$

and in logarithmic form

$$\ln r = \ln f(\alpha) + \ln A - E/(R(T_R + \Delta T)) \tag{15.47}$$

where $r \equiv \mathrm{d}\alpha/\mathrm{d}t$ is rate of process, and after modifications

$$E/R = (T_R + \Delta T)[\ln f(\alpha) + \ln A - \ln r] \quad \rightarrow \Delta T = -T_R + E/R\Sigma_{ln} \tag{15.48}$$

where $\Sigma_{\ln}$ (sum of logarithms) is given as

$$\Sigma_{\ln} \equiv [\ln f(\alpha) + \ln A - \ln r = \ln\ [f(\alpha)A/r] \tag{15.49}$$

The extreme of DTA curve means an extreme of temperature difference $\Delta_{ex\Delta}T$ where condition of local extreme has the form (assuming E/R is a constant)

$$\mathrm{d}\Delta_{ex\Delta}T/\mathrm{d}t = -\mathrm{d}T_R/\mathrm{d}t - (E/R)(D_{SL}/\Sigma_{\ln}^2) = 0 \tag{15.50}$$

where (assume that A is a constant)

$$D_{SL} \equiv \mathrm{d}\Sigma_{\ln}/\mathrm{d}t = \mathrm{d}\ln f(\alpha)/\mathrm{d}t - \mathrm{d}\ln r/\mathrm{d}t \tag{15.51}$$

and as consequence of equalities

$$\mathrm{d}\ln f(\alpha)/\mathrm{d}t = r(\mathrm{d}f(\alpha)/\mathrm{d}\alpha)/f(\alpha)) \tag{15.52}$$

$$\mathrm{d}\ln r/\mathrm{d}t = (\mathrm{d}r/\mathrm{d}t)/r \tag{15.53}$$

we have

$$\mathrm{d}\Delta_{ex\Delta}T/\mathrm{d}t = -\mathrm{d}T_R/\mathrm{d}t - (E/R)[(\mathrm{d}f(\alpha)/\mathrm{d}\alpha)(1/f(\alpha))r - (\mathrm{d}r/\mathrm{d}t)/r]/[\ln f(\alpha) + \ln A - \ln r]^2 \tag{15.54}$$

and for first-order reaction mechanism (cf Eq. 15.22), we have

$$(\mathrm{d}f(\alpha)/\mathrm{d}\alpha)(1/f(\alpha)) = -1/(1-\alpha) \tag{15.55}$$

so that $r_{m\Delta} \Rightarrow r_{ex\Delta}$

$$\mathrm{d}\Delta_{ex\Delta}T/\mathrm{d}t = -\beta_R + (E/R)[r_{ex\Delta}/(1-\alpha) + \mathrm{d}\ln(\mathrm{d}r_{ex\Delta}/\mathrm{d}t)]/[\ln(1-\alpha) + \ln A - \ln r_{ex\Delta}]^2 = 0$$
$$\rightarrow E/RT_{ex\Delta} = -(\beta_R/T_{ex\Delta})[\ln A(1-\alpha)/r_{ex\Delta}]^2/[r_{ex\Delta}/(1-\alpha) + \mathrm{d}\ (\ln r_{ex\Delta}/\mathrm{d}t)] \tag{15.56}$$

where $\beta_R \equiv \mathrm{d}T_R/\mathrm{d}t$ is programmed heating rate, and $r_{m\Delta}$ represents the reaction rate at sample temperature $T_{m\Delta}$ where maximum deviation ΔT is reached. The last equation is quite different from the equation derived from a simple famous Kissinger Eq. (15.46) based on incorrect equation of DTA curve

$$E/RT_{ex\Delta} \approx -\ln(\beta_R/T_{ex\Delta}^2) \leftarrow \ln(\beta_R/T_{ex}^2) \approx -E/RT_{\mathrm{ex}\Delta} \tag{15.57}$$

The ideal DTA peak $\Delta T(t)$ which is derived from a simple heating curve $T_s(t)$ is exemplified in Fig. 15.7., where furthermore the lines proportional to heat inertia term ($\mathrm{d}\Delta T/\mathrm{d}t$) and to transition rate ($\mathrm{d}\alpha/\mathrm{d}t$) are also drawn. At such an ideal peak, the peak area is given as a sum of areas $A + B$, while there are exposed three representations of B with the same surface areas: rectangle, rhomboid, and a tail with heights descent according to the exponential law. The surface area of rectangle under reaction rate line equals to surface area of the exponential tail, and a set of eight characteristic temperatures with ninth equilibrium temperatures is reduced to two temperatures, only. Through the heating rate at endothermic processes or by the

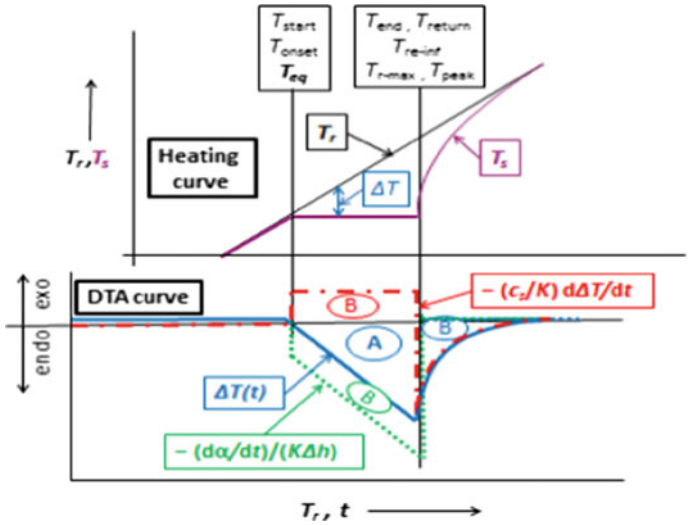

Fig. 15.7 Heating curve and DTA curve of process not influenced by energetically constrains. The area of peak equals to (A + B), where B is equal in three areas

cooling rate at exothermic processes, the maximum available transition rate is then limited due to fact that the maximum temperature deviation $\Delta T = T_s - T_r$ during the process (when sample has the temperature T_{eq}) cannot overcome the difference $\Delta T = T_{eq} - T_r$. If we substitute $T_r = T_{eq} + \beta(t - t_{eq})$ where t_{eq} is the time when temperature T_s reached T_{eq} and assume $T_{eq} = T_{\text{onset}}$ and $t_{eq} = t_{\text{onset}}$, we obtain $\Delta T = T_{eq} - T_{eq} - \beta(t - t_{\text{onset}})$. Using the relation $\mathrm{d}\Delta T/\mathrm{d}t = -\beta$, it follows that $\Delta T = -\beta(t - t_{\text{onset}}) = T_r - T_{eq}$ and transformed rate $\mathrm{d}\alpha/\mathrm{d}t$ yields a connection with $\{(T_r - T_{eq}) - \beta C_s\}$ curiously not involving any link with the ordinary kinetic parameters (as E, A).

15.9 Often Forgotten Influence of Thermodynamic Equilibrium Concerning Kinetic Equation

One of the main insufficiencies of general kinetic equation is its lack of concern in relation to thermodynamic equilibrium of the process [10]. The problem of *equilibrium background* of processes studied by the methods of thermal analysis was noted by authors as early as in 1972 [64] and later analyzed in more detail [65–68]. A possibility to solve this insufficiency resides in the reconstruction of the temperature-dependent function $k(T)$ to be a product which is proportional to two factors [68]. One is representing *thermodynamic driving force*, thus stimulating the run of the process, and the other one is being certain *kinetic opportunity* necessary

to conquer the energetic barrier hampering the process execution (appropriate term can be derived on basis of *kinetic braking force*) [75].

A more general way for introducing an influence of equilibrium state to reaction rate is to take the temperature dependence part of the general kinetic Eq. (15.17) as a product of Arrhenius function $k_A(T_S)$ and a driving force $D_f(T_S, T_{eq})$. In this way we can build up the relation involving equilibrium temperature of the process [66–68].

$$\begin{aligned} r(\alpha, T_S, T_{eq}) &= \mathrm{d}\alpha/\mathrm{d}t = f(\alpha)k_A(T_S)f(\alpha)D_f\left(T_S, T_{eq}\right) \\ &= \mathrm{f}(\alpha)A\exp(-B/T_S)D_f\left(T_S, T_{eq}\right) \end{aligned} \tag{15.58}$$

The driving force is assumed to be unity for *monotropic* processes[1] (changing from an unstable state into a stable state), while *enantiotropic* process (changing from low-temperature stable state into high-temperature stable state at heating—or vice versa at cooling). For such *enantiotropic* processes [64], it could be selected a dimensionless difference between logarithm of activity of the initial state of sample $\ln a_0$ and logarithm $\ln a_f$ of final activity (activity of a state of the sample reached after completion of a process under study)

$$D_f\left(T_S, T_{eq}\right) = \ln a_0 - \ln a_F = -\ln(a_F/a_0) = -(g_F - g_0)/RT_S = -\Delta g(T_S)/RT_S \tag{15.59}$$

where Δg (in J) is change of Gibbs free energy related to the amount of sample. Quantity Δg can be expressed through enthalpy change Δh and entropy change Δs as $\Delta g(T) = \Delta h - T\Delta s$, and for enantiotropic processes, at the equilibrium temperature T_{eq} , we have $\Delta g(T_{eq}) = \Delta h - T_{eq}\Delta s$. If temperature dependences of Δh and Δs are neglected, then we found

$$\Delta g(T_S) = \Delta h\left(1 - T_S/T_{eq}\right) = \Delta \mathrm{h}\left(T_{eq} - T_S\right)/T_{eq} \tag{15.60}$$

so that the driving force is given as

$$D_f\left(T_S, T_{eq}\right) = -\Delta H\left(T_{eq} - T_S\right)/\left(RT_S T_{eq}\right) = (\Delta h/RT_{eq})\left(T_S - T_{eq}\right)/T_S \tag{15.61}$$

where $\Delta H \equiv \Delta h/n_S$ (in J/mol) is *molar integral enthalpy change* of process going in sample substance, and n_S is molar amount of initial sample.

[1]Monotropy and enantiotropy are terms coined by Otto Lehman (1855–1922) in 1888 to distinguish two types of phase transitions (aragonite to calcite as monotropic transition and α-quartz to β-quartz as enantiotropic transition). In present paper, these terms are used more generally not only for phase transitions but also for decompositions. The process of change from an unstable state into stable state is called as *monotropic* process, while *enantiotropic* process is a change from low-temperature stable state into high-temperature stable state at heating (or from high-temperature stable state to low-temperature stable state at cooling).

Substituting Eq. (15.61) and using Arrhenius equation for $k_A(T)$ in Eq. (15.34), we go to the kinetic equation in the form including the influence of thermodynamic equilibrium

$$\mathrm{d}\alpha/\mathrm{d}t = f(\alpha)A\exp\left(-B_f/T_S\right)(\Delta H/RT_{eq})\left(T_S - T_{eq}\right)/T_S \tag{15.62}$$

where term $B_f \equiv E/R$ can be called as a *braking force*. Defining new constant $L = A\Delta H/RT_{eq}$ which is positive for endothermic process ($L > 0$ if $\Delta H > 0$) and negative for exothermic process ($L < 0$ if $\Delta H < 0$), Eq. (15.62) is transposed into

$$\mathrm{d}\alpha/\mathrm{dt} = f(\alpha)L\exp(-E/RT_S)\left(T_S - T_{eq}\right)/T_S$$

and for first-order reaction

$$\mathrm{d}\alpha/\mathrm{dt} = (1-\alpha)L\exp(-E/RT_S)\left(T_S - T_{eq}\right)/T_S \tag{15.63}$$

For isothermal reaction rate, we then have the simplest kinetic model which is exploitable as the continuous model of enantiotropic phase transition, see ref. [53]

$$\mathrm{d}\alpha/\mathrm{dt} = k_{\mathrm{iso}}(T_S)\,(1-\alpha)\left(T_S - T_{eq}\right) \tag{15.64}$$

where $k_{\mathrm{iso}}(T_S) \equiv (A\Delta H/RT_{eq}T_S)\ \exp(-E/RT_S)$. Differentiating Eq. (15.63) with respect to time and after rearrangement using $\mathrm{d}T_S/\mathrm{d}t = \mathrm{d}\Delta T/\mathrm{d}t + \beta_R$ (where $\beta_R = \mathrm{d}T_R/\mathrm{d}t$ is programmed heating rate indicated by the temperature of reference sample), we obtain for maximum reaction rate the equation

$$\begin{aligned}\mathrm{d}^2\alpha/\mathrm{d}t^2 = &-(\mathrm{d}\alpha/\mathrm{d}t)[L\exp(-E/RT_S)\left(T_S - T_{eq}\right)/T_S \\ &+ (\beta_R + \mathrm{d}\Delta T/\mathrm{d}t)\left(E/RT_S^2 + \left(T_{eq}/T_S\right)/\left(T_S - T_{eq}\right)\right)] = 0\end{aligned} \tag{15.65}$$

so that

$$\begin{aligned}A\Delta H/RT_{\mathrm{eq}}\exp\left(-E/RT_S\right)\left(T_S - T_{eq}\right) &= (\beta_R + \mathrm{d}\Delta T/\mathrm{d}t)\left[E/RT_S + T_{eq}/\left(T_S - T_{eq}\right)\right] \\ &= 0\end{aligned} \tag{15.66}$$

or

$$[A\Delta H/RT_{eq}\exp(-E/R/(T_R+\Delta T))(T_R+\Delta T - T_{eq})]/[E/R/(T_{R+}\Delta T) + T_{\mathrm{eq}}/(T_R+\Delta T - T_{eq})] = \beta_R + \mathrm{d}\Delta T/\mathrm{d}t$$

and after multiplying by $(T_R + \Delta T - T_{eq})/T_{eq}$ we obtain

$$[A\Delta H/RT_{eq}^2 \exp(-E/R/(T_R + \Delta T))(T_R + \Delta T - T_{eq})^2]/[E/RT_{\mathrm{eq}}(T_R + \Delta T - T_{\mathrm{eq}})/(T_{R+}\Delta T) + 1] = \beta_R + \mathrm{d}\Delta T/\mathrm{d}t$$

from which follows often accepted generalization

$$\text{if } (T_R + \Delta T - T_{eq}) = 0 \,\text{then}\, \mathrm{d}\Delta T/\mathrm{d}t = -\beta_R \tag{15.67}$$

as it is expected and observed at phase transition of temperature or enthalpy standards.

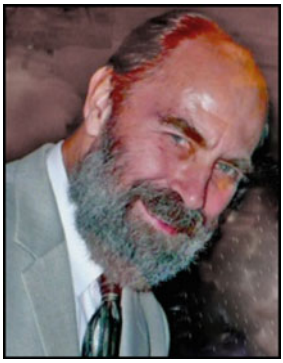

15.10 Conclusion

Pavel Holba (see the insert photo) was a thermodynamist who tried to incorporate thermodynamic background [21, 64, 67] into kinetic evaluations pointing out that activation energy is a process-dependent variable [67]. As shown in Eq. (15.23) the *E*-dependence [63] is a consequence of a primary kinetic equation habitually used in the form of Eq. (15.18) making thus no regard to thermodynamic equilibrium when temperature part $k(T)$ of the kinetic equation is given by only Arrhenius equation $k(T) = Z\ exp\ (-E/RT)$. The mathematical correlations between E and $ln\ Z$ [60, 63] make apparent that the transform of any pair of quantities $E - ln\ A$ and $T_m - \beta$ gives basis for unambiguous results. The solution of which is well presented in the work by Šimon [69] making use of the non-Arrhenius *T*-functions as a needed inventive approach to nonisothermal kinetics [37]. Inconsistency of E is further confused by often forgotten interference of the equilibrium temperature [64] repeatedly encountered in the study of carbonates [70], see Fig. 15.8 [67], which is the atmospheric cause for a spacious range of thermo-gravimetrically published *E*-data [16, 43, 62].

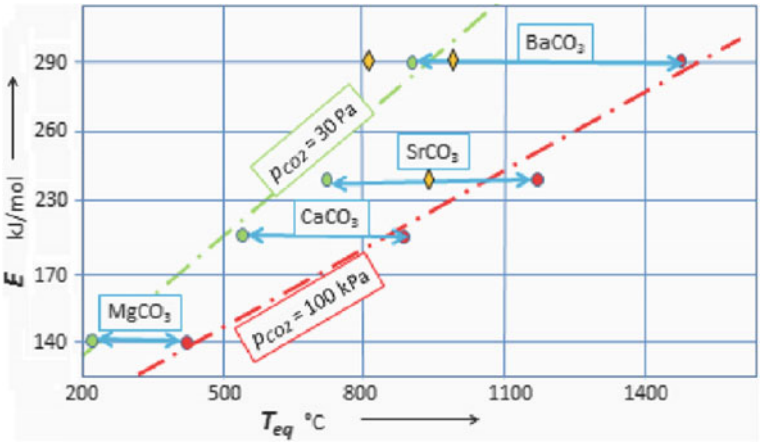

Fig. 15.8 Activation energies E (extracted from [71]) for the decomposition of carbonates in the temperature ranges 510–750°C ($MgCO_3$), 400–960°C ($CaCO_3$), 810–1000°C ($MgCO_3$) and 930–1155°C ($CaCO_3$) were plotted [67] against the equilibrium temperatures T_{eq} and calculated on basis of thermodynamic tables [72] for decomposition processes $MeCO_3$ (c) $\rightleftarrows$ MeO (ox) + CO_2 (g) at two different equilibria: (i) between tension (≅ partial pressure) of CO_2 in carbonate pCO2(c) and the tension of CO_2 in air atmosphere pCO2(g), i.e., pCO2(c) = pCO2(g) = 30 Pa (*green, upper*) and under (ii) hydrostatic equilibrium between tension of CO_2 in carbonate pCO2(c) and the pressure of air P_{air} : pCO2(c) = P_{air} = 100 *kPa* (*red, below*). The circular and rhombohedra points represent phase transitions of Mg-Ca and Sr-Ba carbonates respectively

In conclusion, it is worth noting that the present character and structure of thermoanalytical kinetics have been neither obvious at its conception is making use of Eq. (15.17) [14, 15] nor are we confirmed sure that it is the best possible when concerning yet unsolved effects of heat transfer consequences [30, 49, 53, 68]. We are happy when introducing the concept of equilibrium background [64–67] which developed into an important part of advanced kinetics. We also anticipate that our innovative notion of the operational meaning of temperature [73, 74] may facilitate development equally. We believe that progress means working out implementation and then improvements while comprising detailed effect of thermal phenomena [75] in the sphere of real thermoanalytical measurements. Just making changes at any case is not the aim; however, on the other hand, we should not be afraid of their consequences even if complicating our previously simple practice. Now, it is the turn of ICTAC Kinetic Committee [52] to incorporate and verify the suggested changes into the promoted kinetic practice [37, 76].

Acknowledgements This chapter is based on the life challenge of Pavel Holba (1940–2016) to establish an innovative concept of thermodynamics [75] while introducing it into thermoanalytical kinetics (see the other chapters in this volume). He completed the text of this chapter only a few days before his death and regrettably was no longer capable of its further corrections.

The work was developed at the Join Research Laboratory of the Institute of Physics CAS and the New Technologies Centre of the University of West Bohemia in Pilzen (the CENTEM project, reg. no. CZ.1.05/2.1.00/03.0088 that is co-funded from the ERDF as a part of the

MEYS—Ministry of Education, Youth and Sports OP RDI Program and, in the follow-up sustainability stage, supported through the CENTEM PLUS LO 1402). The abandoned support by the Grant Agency of ČR for the projected grant 'Thermal inertia and its significance for the analysis of DTA measurements' (No 17-21840S-2016) is worth mentioning as an example of fatal misunderstanding of current needs of thermal science. Deep thanks are due to the shared efforts by J. Czarnecki (formerly with Chan, USA), J.J. Mareš, P. Hubík, (Institute of Physics), M. Holeček, P. Martinec (West Bohemian University), M. Liška (Vitrum Laugaricio, Dubček University in Trenčín), J. Málek, R. Svoboda (University of Pardubice), N. Koga (Hiroshima University in Japan), and P. Šimon (President of the Slovak Chemical Society, Technical University in Bratislava) as well as to my wife semiconductor technologist Věra.

References

1. Newton I (1687) Philosophiæ Naturalis Principia Mathematica (Mathematical Principles of Natural Philosophy) Londini, jussi Societatus Regiae ac typis Josephi Streater; prostata pudplures bibliopolas
2. Newton I (1701) Scale graduum caloris. Calorum descriptiones & signa. Philos Trans 22:824–829
3. Fourier JBJ (1822) Théorie analytique de la chaleur. Paris, English transl.: The Analytical Theory of Heat. Dover Publications, Mineola/New York 2003
4. Fick AE (1855) Über Diffusion. Annalen der Phys. Chem. von Pogendorff 94:59
5. Tammann G (1905) Über die Anwendung der Thermische Analysen. Z Anorg Chem 45:289
6. Mach E (1896) Die Principien der Wärmelehre. Verlag von JA Barth, Leipzig
7. Mareš JJ. (2011) Hotness manifold, phenomenological temperature and other related concepts of thermal physics. Chapter 20 in book "Glassy amorphous and nano-crystalline materials". (Šesták J, Mareš JJ, Hubík P, editors) London: Springer; p. 327–45; and (2015) Do we know what temperature is? J Therm Anal Calorim. 120:223–30
8. Callen HB (1960) Thermodynamics: an introduction to thermostatics. New York: Wiley; and Tribus M. (1961) Thermostatics and thermodynamics: an introduction to energy, information and states of matter. New York: Nostrand
9. Zemansky MV (1968) Heat and thermodynamics. McGraw-Hill/Kogakuscha, Tokyo
10. Šesták J (1979) Thermodynamic basis for the theoretical description and correct interpretation of thermoanalytical experiments. Thermochim Acta 28:197–227; and Šesták J, Holba P (1975) Kinetics of thermal heterogeneous processes with the participation of solids. Chapter in: heterogeneous chemical reactions and reaction capability (Pavlyuchenko MM, Prodan I (eds)), Nauka Technika, Minsk, pp 519–531 (in Russian)
11. Berg LG, Nikolaev AV, Rode EY (1944) Thermography. Izd. AN SSSR, Moskva-Leningrad (in Russian)
12. Popov MM (1954) Thermometry and calorimetry Nauka, Moskva (in Russian)
13. Piloyan FO (1964) Introduction to thermography. Nauka, Moskva (in Russian)
14. Garn PD (1964) Thermoanalytical methods of investigation. Academic, New York
15. Wendlandt WW (1964) Thermal methods of analysis. Wiley, New York
16. Šesták J, Šatava V, Wendlandt WW (1973) The Study of Heterogeneous Processes by Thermal Analysis, Monograph as a special issue of Thermochimica Acta, Vol. 7, Elsevier, Amsterdam; and Šesták J (1984) Differential thermal analysis, Chapter 12 in his book "Thermophysical properties of solids: theoretical thermal analysis". Elsevier, Amsterdam (ISBN 0 444 99653 2), Czech origin by Academia, Praha 1982 and Russian translation by Mir, Moscow 1988
17. Chen R, Kirsh Y (1981) Analysis of thermally stimulated processes. Pergamum Press, Oxford, pp 109–110

18. Boerio-Goates J, Callen JE (1992) Differential thermal methods. Chapter 8 in book: determination of thermodynamic properties. (Rossiter BW, Beatzold RC, eds). Wiley, New York, pp 621–718
19. Tian A (1933) Recherches sue la calorimétrie. Généralisation de la méthode de compensation électrique: Microcalorimétrie. J de Chimie-Physiq 30:665–708
20. Vold MJ (1949) Differential thermal analysis. Anal Chem 21:683–688
21. Holba P (1976) Thermodynamic aspects in thermal analysis. Silikáty (Prague) 20:45–56 (in Czech)
22. Nevřiva M, Holba P, Šesták J (1976) Utilization of DTA for the determination of transformation heats. Silikáty (Prague) 29:33–39 (in Czech)
23. Šesták J, Holba P, Lombardi G (1977) Quantitative evaluation of thermal effects: theory and practice. Annali di Chimica (Roma) 67:73–87
24. Holba P (1974) On the applicability of isothermal kinetic equations for non-isothermal investigations of heterogeneous processes, Thermal Analysis Vol. 1. In: Buzas I (ed) Proc. 4th ICTA, Budapest, pp 33–46. AkadémiaiKiadó, Budapest 1975. (ISBN 963 05 0557 6)
25. Šesták J (2005) Thermometry and calorimetry, Chapter 12 in his book "Science of Heat and Thermophysical Studies: a generalized approach to thermal analysis". Elsevier, Amsterdam, pp 344–376
26. Xue Y, Cracknell AP. (1995) Advanced thermal inertia modeling, Int. J. Remote Sens 16:431–446; and Price JC (1977) Thermal inertia mapping: A new view of the Earth. J Geophys Res 82:(Oceans and Atmospheres) 2582–2590
27. Šesták J (2014) Is the original Kissinger equation obsolete today: not obsolete the entire non-isothermal kinetics? J Therm Anal Calorim 117:3–7
28. Faktor MM, Hanks R (1967) Quantitative application of dynamic differential calorimetry. Part 1—theoretical and experimental evaluation. Trans Faraday Soc 63:1122–1129
29. Holba P, Nevřiva M (1977) Description of thermoanalytical curves and the analysis of DTA peak by means of computer technique. Silikáty (Prague) 21:19–23 (in Czech)
30. Holba P, Nevřiva M, Šesták J (1978) Analysis of DTA curve and related calculation of kinetic data using computer technique. Thermochim Acta 23:223–231
31. Borchardt HJ, Daniels F (1957) The application of DTA to the study of reaction kinetics. J Am Chem Soc 79:41–46
32. Šesták J, Holba P (2013) Heat inertia and temperature gradient in the treatment of DTA peaks: existing on every occasion of real measurements but until now omitted. J Thermal Anal Calorim 113:1633–1643
33. Kissinger HE (1957) Reaction kinetics in differential thermal analysis. Anal Chem 29:1702–1706
34. Šesták J, Holba P, Živkovič Ž (2014) Doubts on Kissinger´s method of kinetic evaluation based on several conceptual models showing the difference between the maximum of reaction rate and the extreme of a DTA. J Min Metall Sect B-Metall 50:77–81
35. Holba P, Šesták J (2014) Imperfections of Kissinger evaluation method and crystallization kinetics. Glass Phys Chem 40:486–495. (ISSN 1087–6596. doi:10.1134/S1087659614050058) and in Russian: Fizika I Khimiya Stekla, 2014; 40:645–657
36. Šesták J (2012) Rationale and fallacy of thermoanalytical kinetic patterns: how we model subject matter. J Thermal Anal Calor 110:5–16
37. Šesták J (2015) The quandary aspects of non-isothermal kinetics beyond the ICTAC kinetic committee recommendations. Thermochim Acta 611:26–35
38. Piloyan GO, Ryabchikov IO, Novikova SO (1966) Determination of activation energies of chemical reactions by DTA. Nature 3067:1229
39. O´Neill MJ (1964) Analysis of the temperature controlled calorimeter. Anal Chem 36:1238–1246
40. Danley RL (2001) Power compensation differential scanning calorimeter EP 1136803 A1 (TA Instruments): http://www.google.com/patents/EP1136803A1
41. Kaisersberger E, Moukhina E (2009) Temperature dependence of the time constants for deconvolution of heat flow curves. Thermochim Acta 492:101–109

42. Illekova E, Aba B, Kuhnast FA (1992) Measurements of accurate specific heats of metallic glasses by DSC: analysis of theoretical principles and accuracies of suggested measurement procedure. Thermochim Acta 195:195–209
43. Gray AP (1968) Simple generalized theory for analysis of dynamic thermal measurements. In: Porter RS, Johnson JF (eds) Analytical calorimetry, vol. 1. . Plenum Press, New York, p 209
44. Málek J (1992) The kinetic analysis of non-isothermal data. Thermochim. Acta 200: 257–269; and (2000) Kinetic analysis of crystallization processes in amorphous materials. Thermochim. Acta 355: 239–253; and Málek J, Mitsuhashi T, Criado JM (2001) Kinetic analysis of solid-state processes. J Mater Res 16:1862–1871
45. Koga N (1997) Physico-geometric kinetics of solid-state reactions by thermal analysis. J. Therm. Anal. 49:45–56; and Koga N, Tanaka H (2002) A physico-geometric approach to the kinetics of solid-state reactions. Thermochim Acta 388:41–61
46. Avramov I, Šesták J (2014) Generalized kinetics of overall phase transition explicit to crystallization. J Therm Anal Calorim 118:1715–1720
47. Galwey AK (2006) What theoretical and/or chemical significance is to be attached to the magnitude of an activation energy determined for a solid-state decomposition? J Therm Anal Calor 86:267–286
48. Šesták J (2011) Citation records and some forgotten anniversary in thermal analysis. J Thermal Anal Calor 109:1–5
49. Holba P, Šesták J (2015) Heat inertia and its role in thermal analysis. J Thermal Anal Calor 121:303–307
50. Svoboda H, Šesták J. (1974) A new approach to DTA calibration by predetermined amount of Joule heat via rectangular pulses. In Thermal Analysis (Buzas I, ed), Proc. 4th ICTA, Akademia Kiado, Budapest, pp 726–731
51. Svoboda H, Šesták J. (1973) Use of rectangular and triangular heat pulses in DTA analysis. In TERMANAL—Proc. 9th TA Conf. at High Tatras, Publ House SVŠT, Bratislava, pp 12–17 (in Czech)
52. Brown ME, Maciejewski M, Vyazovkin S, Nomen R, Sempere J, Burnham A, Opfermann J, Strey R, Anderson HL, Kemmler A, Keuleers R, Janssens J, Desseyn HO, Chao-Rui Li, Tang TB, Roduit B, Malek J, Mitsuhashi T (2000) Computational aspects of kinetic analysis Part A: The ICTAC kinetics project-data, methods and results. Thermochim Acta 355: 125–143; and Vyazovkin S, Burnham AK, Criado JM., Pérez-Maqueda LA., Popescu C, Sbirrazzuoli N. (2011) ICTAC Kinetics Committee recommendations for performing kinetic computations on thermal analysis data. Thermochim Acta; 520:1–19
53. Holba P, Šesták J, Sedmidubský D (2013) Heat transfer and phase transition at DTA experiments. Chapter 5 in Thermal analysis of Micro-, nano- and non-crystalline materials, Šesták J, Šimon P (eds), Springer, Berlin, pp 99–134 (ISBN 978 90 481 3149 5)
54. Smyth HT (1951) Temperature distribution during mineral inversion and its significance in DTA. J Am Cer Soc 34:221–224
55. Barret P, Boumetain L (1961) Etude de la propagation dune reaction de dissociation thermique dans un systeme chmique conprenant une phase gazeuse at deux phases solides finement divisem. Bull Soc Chim France. 576
56. Proks I (1961) Influence of rate of temperature increase on the gradient quantities important for the evaluation of DTA curves. Silikáty 5:114 (in Czech)
57. Sánchez-Rodríguez D, Eloussifi H, Farjas J, Roura P, Dammak M (2014) Thermal gradients in thermal analysis experiments: criterions to prevent inaccuracies when determining sample temperature and kinetic parameters. Thermochim Acta 589:37–46
58. Lyon RE, Safronova N, Senese J, Stoliarov SI (2012) Thermokinetic model of sample centered response in non-isothermal analysis. Thermochim Acta 545:82–89
59. Mareš JJ. Šesták J, Hubík P (2011) Transport constitutive relations, quantum diffusion and periodic reactions. Chapter 14 in book: glassy, amorphous and nano-crystalline materials. In: Šesták J, Mareš JJ, Hubík P, eds, Springer, Berlin, pp 227–244
60. Koga N, Šesták J (1991) Kinetic compensation effect as a mathematical consequence of the exponential rate constant. Thermochim. Acta 182: 201; and Koga N (1994) A review of the

mutual dependence of Arrhenius parameters evaluated by the thermo-analytical study of solid-state reactions: the kinetic compensation effect. Thermochim Acta 244:1–10
61. Roura P, Farjas J (2009) Analytical solution for the Kissinger equation. J Mater Res 24:3095–3098
62. Koga N, Šesták J, Šimon P (2013) Some fundamental and historical aspects of phenomenological kinetics in the solid state studies by thermal analysis. Chapter 1 in book: Šesták J, Šimon P (eds) Thermal analysis of micro-, nano and non-crystalline materials, Springer, Dordrecht, pp 1–28 (ISBN 978-90-481-3149-5)
63. Šesták J (1966) Errors and interdependence of kinetic data obtained from TG curves at increasing temperature. Talanta 13:567
64. Holba P, Šesták J (1972) Kinetics with regard to the equilibrium of processes studied by non-Isothermal techniques, Zeit Physik Chem N.F. 80:1–20
65. Holba P (2010) Equilibrium background at heating under conditions of controlled atmosphere. In: Proc. 62nd Meeting of Czech and Slovak Chemical Associations, Pardubice University Press; and (2012) Chemické Listy 104:606–609 (both in Czech)
66. Holba P (2013) Equilibrium background of processes initiated by heating and the Ehrenfest classification of phase transitions, Chapter 2 in book: Thermal analysis of micro-, nano- and non-crystalline materials (Šesták J, Šimon P, eds), Springer Berlin, pp. 29–52 (ISBN 978-90-481-3149-5); and (2015) Ehrenfest equations for calorimetry and dilatometry. J Therm Anal Calorim 120:175–181
67. Holba P (2017) Temperature dependence of activation energy of endothermic processes and related imperfections of non-isothermal kinetic evaluations. J Therm Anal Calorim. doi:10.1007/s10973-017-6088-8
68. Šesták J, Holba P (2017) Quo Vadis of nonisothermal kinetics (in the course of preparation); and (2016) Piloyan method to determine the activation energy from DTA is defective in addition to other methods which do not take into account the thermal inertia. J Anal Bioanal Tech. doi:10.4172/2155-9872.1000331)
69. Šimon P (2005) Single-step kinetic approximation employing non-Arrhenius T-functions. J. Thermal Anal. Calor. 79: 703; and Šimon P, Dubaj T, Cibulková Z (2015) Equivalence of the Arrhenius and non-Arrhenian temperature functions in the temperature range of measurements. J Therm Anal Calorim, 120: 231–238; and Dubaj T, Cibulková Z, Šimon P (2015) An incremental isoconversional method for kinetic analysis based on the orthogonal distance regression. J Comput Chem 36:392–398
70. Maciejewski M (2000) Computational aspects of kinetic analysis. Part B: The ICTAC Kinetics Project - the decomposition kinetics of calcium carbonate revisited, or some tips on survival in the kinetic minefield. Thermochim Acta 355:145–154
71. Maitra S, Chakrabarty N, Pramanik J (2008) Decomposition kinetics of alkaline earth carbonates by integral approximation method. Cerâmica 54:268–272
72. Bale CW, Béliste E, Chartrand P, Decterov SA, Eriksson G, Hach K (2009) Thermochemical software and databases; recent developments. CALPHAD 33:295–31; and (2013) www.factsage.com
73. Šesták J (2016) Measuring, "hotness", should the sensor's readings for rapid temperature changes be named "tempericity"? J Therm Anal Calorim 125:991–999
74. Holba P (2016) Šesták's proposal of term "tempericity" for non-equilibrium temperature and modified Tykodi´s thermal science classification with regards to methods of thermal analysis. J Therm Anal Calorim. doi:10.1007/s10973-016-5659-4
75. Holba P (1994) Thermodynamics and ceramic systems. Chapter in book: structure and properties of ceramic materials (Koller A, eds), Elsevier, Amsterdam, pp. 17–113; and (2017) book: Thermal analysis and thermodynamics of phases, OPS Plzeň, uncompleted and thus never published
76. ICTAC Kinetics Committee Recommendations (2014) Collecting experimental thermal analysis data for kinetic computations. Thermochim Acta 590:1–23

Chapter 16
Thermal Gradients in Thermal Analysis Experiments

Jordi Farjas, Daniel Sánchez-Rodriguez, Hichem Eloussifi and Pere Roura

Abstract The concept of "sample temperature" in non-isothermal thermal analysis experiments is analyzed. From the analysis of the heat balance inside the sample, it is shown that the existence of such sample temperature is restricted to experimental conditions, where the thermal gradients are negligible. Two different sources of thermal gradients are studied: the sample thermal inertia and the heat of reaction that is not quickly removed. The conditions to prevent the formation of thermal gradients as well as the condition for a thermal runaway to occur are deduced. Finally, it is shown that the aspect ratio is a crucial parameter for the formation of thermal gradients within the sample.

16.1 Introduction

Thermal analysis (TA) methods denotes a set of techniques that monitor the evolution of a given system parameter as a function of the temperature of the sample when the sample is submitted to a controlled temperature program. Therefore, it is crucial to properly control and measure the sample temperature.

Three different temperature programs are commonly used: constant temperature (isothermal), constant temperature rise, $\beta = dT/dt = \text{const.}$ (non-isothermal), and rate-controlled thermal analysis (RCTA) [1, 2]. In RCTA measurements, the temperature is controlled to keep a constant transformation rate. Non-isothermal and RCTA experiments are preferred to isothermal experiments because they allow exploring a larger temperature range, they are faster, and they avoid the so-called non-zero initial degree of transformation problem [3]. However, mechanism identification is more difficult in non-isothermal experiments because they are less sensitive to the reaction model than isothermal ones [4, 5]. Conversely, RCTA experiments are more sensitive to the reaction model, but unfortunately most commercial apparatus do not include this option.

J. Farjas (✉) · D. Sánchez-Rodriguez · H. Eloussifi · P. Roura
University of Girona, Campus Montilivi Edif. PII, E17071 Girona, Catalonia, Spain
e-mail: jordi.farjas@udg.cat

J. Šesták et al. (eds.), *Thermal Physics and Thermal Analysis*,
Hot Topics in Thermal Analysis and Calorimetry 11,
DOI 10.1007/978-3-319-45899-1_16

In this contribution, we will focus our attention on non-isothermal experiments because they are the most commonly found in the literature. In non-isothermal experiments, the accuracy of the sample temperature measurement is lower than the temperature sensors' sensibility. The reason is that in most commercial equipment, the temperature sensor is located in contact or near the furnace walls [3]. Thus, there is a time delay between the sensor and the sample called "tau lag" that is related to the thermal inertia between the sample and the furnace [6–11]. In addition, the time constant related to the thermal inertia of the sample itself is called "sample thermal lag" [12, 13]. As a result, temperature gradients arise that are proportional to the time delay and to the heating rate, β.

Deviations related to tau lag can be corrected with proper calibration performed at different heating rates; in this case, the sample temperature accuracy depends on the accuracy of the calibration and on the particular heating rate. On the other hand, the sample thermal lag produces a thermal gradient within the sample. Therefore, there is no sample temperature but a temperature profile within the sample. Contrarily to the deviations introduced by tau lag, the artifacts introduced by tau signal cannot be corrected with calibration.

In this contribution, we study the heat balance inside the sample and we analyze the two main sources of thermal gradients within the sample: the sample thermal inertia and the heat evolved during sample transformation. We will quantify the temperature deviations as a function of the sample parameters and we will show that thermal gradients may be significant for samples in the form of powders. We will illustrate the artifacts induced in TA curves by thermal gradients. We will pay special attention to the occurrence of a thermal runaway. Finally, we will consider the effect of the sample aspect ratio on the heat balance.

16.2 Sample's Heat Balance: Conditions for the Formation of a Temperature Gradient

Heat balance inside the sample involves two contributions: the heat released by the system transformation and the heat transport through conduction.

The heat power released by the transformation is proportional to the transformation rate. We will consider a transformation that is governed by a single mechanism and that is thermally activated:

$$\frac{\partial \alpha}{\partial t} = A e^{-E_A/R_G T} f(\alpha), \tag{16.1}$$

where t is time, T is temperature, A is the pre-exponential constant, E_A is the activation energy, R_G is the universal gas constant, α is the degree of transformation ($\alpha = 0$ untransformed, $\alpha = 1$ totally transformed), and $f(\alpha)$ is a function describing the reaction mechanism. For the sake of simplicity, we will assume first-order transformation:

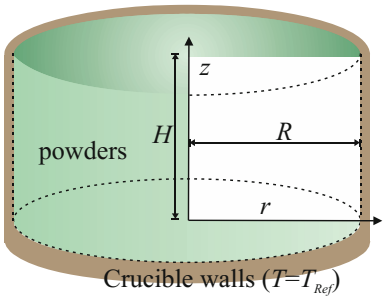

Fig. 16.1 Schematic representation of a cylindrical crucible filled with powders up to height H

$$f(\alpha) = 1 - \alpha. \tag{16.2}$$

In Fig. 16.1, we have schematically drawn a cylindrical crucible of internal radius R filled with powders up to height H. Thanks to the system symmetry, heat transport inside the sample can be reduced to a two-dimensional (2D) system of coordinates z and r (rectangle in Fig. 16.1). Thus, the heat balance is given by:

$$\rho c \frac{\partial T}{\partial t} = \lambda \left[\frac{1}{r} \frac{\partial}{\partial r} \left(r \frac{\partial T}{\partial r} \right) + \frac{\partial^2 T}{\partial z^2} \right] + \rho q \frac{\partial \alpha}{\partial t}, \tag{16.3}$$

where λ is thermal conductivity, ρ is the density, c is the specific heat capacity, and q is the specific heat of the transformation. The boundary conditions are as follows:

$$\left. \frac{\partial T}{\partial r} \right|_{r=0} = 0, \quad T(R, z) = T_{\text{Ref}}, \quad \left. \frac{\partial T}{\partial z} \right|_{z=H} = 0, \quad T(r, 0) = T_{\text{Ref}}, \tag{16.4}$$

where T_{Ref} is the *reference temperature* (i.e. the temperature of an empty reference pan)

$$T_{\text{Ref}} = T_0 + \beta t, \tag{16.5}$$

and T_0 is the initial temperature. We will assume that the transformation rate at $T = T_0$ is negligible; so the results do not depend on the particular value of T_0. Finally, the volume-averaged degree of transformation is given as:

$$\overline{\alpha}(t) = \frac{1}{V} \int \alpha(z, t) \, dV, \tag{16.6}$$

Note that in Eq. (16.4), we assume that the crucible temperature is constant and equal to T_{Ref}. This assumption is valid if the thermal diffusivity of the crucible is much larger than the sample's diffusivity, or the crucible wall thickness is much thinner than the sample's thickness. As we will see, this assumption is valid for powders inside a crucible because their diffusivity is at very least 10 times smaller than that of crucible.

We overlook heat losses from convection and radiation, and we also ignore the evolution of the system parameters during the transformation.

Finally, we will consider two limiting cases: a semi-infinite slab ($R \gg H$) and an infinite long cylinder ($H \gg R$) that allow reducing the heat transport to a 1D model. In the case of a semi-infinite slab or an infinite cylinder, the partial derivative with respect to r or to z in Eq. (16.3) can be neglected, respectively.

Two different effects may result in the formation of temperature gradients [11, 14, 15]: a relatively slow heat transport through the sample when compared to the furnace temperature rise rate and a relatively slow heat removal when compared to the rate of heat evolved from the sample transformation. In the following subsection, we will analyze Eqs. (16.1)–(16.5) to establish the timescales related to both effects. We will also set quantitative criteria to prevent the occurrence of thermal gradients within the sample.

16.2.1 Sample Thermal Inertia

In thermal analysis, it is assumed that an isenthalpic sample is thermalized, i.e., at any sample point the temperature is T_{Ref}. However, the sample thermal inertia introduces a time delay so that the temperature at any point is delayed with respect T_{Ref} [10, 13, 16–19]. The maximum temperature difference, ΔT, occurs at the farthest location from the crucible walls, and it is simply given by the product of the heating rate times the time delay:

$$\Delta T = \beta \cdot t_{\mathrm{Diff}}, \tag{16.7}$$

where t_{Diff} is the time delay related to heat diffusion,

$$t_{\mathrm{Diff}} = C\frac{d^2}{a}, \tag{16.8}$$

where d is a characteristic length of the system, C is a constant that depends on the system geometry and on the definition of d, and a is the heat diffusivity,

$$a = \frac{\lambda}{\rho c}. \tag{16.9}$$

Constant C can be derived from Eq. (16.3) imposing $q = 0$ (isenthalpic sample) [10, 13, 20]. In particular, for an infinite cylinder ($H/R \to \infty$):

$$t_{\mathrm{Diff},\infty}^{(1\mathrm{D})} = \frac{1}{4}\frac{R^2}{a}, \tag{16.10}$$

and for a semi-infinite slab ($H/R \to 0$):

$$t_{\mathrm{Diff},0}^{(1\mathrm{D})} = \frac{1}{2}\frac{H^2}{a}. \tag{16.11}$$

For a finite cylinder, we define d as the cubic root of the cylinder volume, V,

$$d^{(2\mathrm{D})} \equiv V^{1/3} = \sqrt[3]{\pi R^2 H}. \tag{16.12}$$

The geometrical factor $C^{(2\mathrm{D})}$ for the finite cylinder can be obtained assuming that two diffusion paths compete in parallel: an axial path and a radial path. Hence, the diffusion time for a finite cylinder is approximately [13],

$$\frac{1}{t_{\mathrm{Diff}}^{(2\mathrm{D})}} = \frac{1}{t_{\mathrm{Diff},\infty}^{(1\mathrm{D})}} + \frac{1}{t_{\mathrm{Diff},0}^{(1\mathrm{D})}}, \tag{16.13}$$

and substitution of Eqs. (16.8–16.11) into Eq. (16.13) gives:

$$C^{(2D)} = \frac{1}{2}\left(\frac{(H/R)^2}{\pi + 2\pi\sqrt{2}(H/R)^3}\right)^{2/3}, \tag{16.14}$$

The geometrical factor $C^{(2\mathrm{D})}$ depends on the aspect ratio H/R (see Fig. 16.2). Note that when $H/R > 3$ or $R/H > 3$, the longer path clearly dominates and the value of $C^{(2\mathrm{D})}$ coincides with that of an infinite cylinder or a semi-infinite slab, respectively. For intermediates values of H/R, $C^{(2\mathrm{D})}$ varies between 0.05 and 0.09.

According to Eqs. (16.7), (16.12), and (16.14), the temperature gradient depends on the heating rate, the thermal diffusivity, the volume of the sample, and its aspect ratio. For solids, $\rho c \approx 3 \times 10^6$ J/m^{3}K and $0.1 < \lambda < 300$ W/mK [22], thus $3 \times 10^{-8} < a < 10^{-4}$ m^2/s. Typically, the radius of the crucible is around

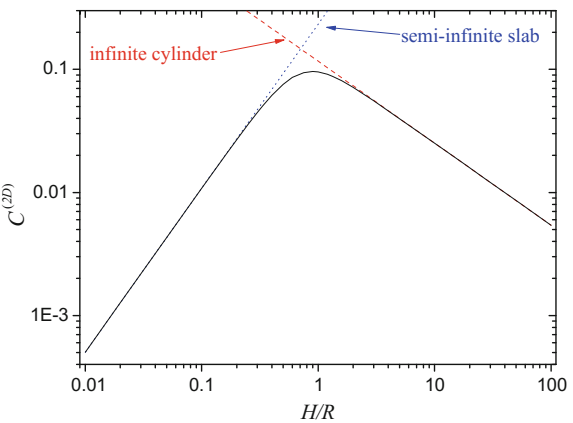

Fig. 16.2 Dependence of the geometrical factor $C^{(2\mathrm{D})}$ on the sample aspect ratio H/R, Eq. (16.14). *Dotted* and *dashed lines* are the limit cases when H/R tends to 0 and ∞, respectively

2.5×10^{-3} m and its volume is of the order of 10^{-7} m^3. In standard experiments, heating rates are well below 100 K/min (typically between 1 and 20 K/min). Therefore, for a highly insulating material ($\lambda = 0.1$ W/mK) the time lag in a 2.5-mm crucible with a volume of 10^{-7} m^3 is 47s. This delay results in temperature differences within the sample of 7.8 K when the heating rate is 10 K/min and 78 K when the heating rate is 100 K/min. Conversely, when sample exhibits a moderate conductivity (say $\lambda = 10$ W/mK), the time delay is 0.47 s and the temperature difference is less than 1 K for $\beta = 100$ K/min. Thus, apparently the sample thermal lag may be neglected in samples that exhibit a moderate or high conductivity.

However, TA measurements are often performed on samples in the form of powders. Their thermal conductivity is much lower (about 10–100 times) than that of their bulk counterparts [21–24]. For relative densities below 80% and small particle sizes (<100 μm), heat flow is governed by interparticle contact resistance [25]. This behavior makes metallic powders insulating as ceramic powders; thus, high-thermal gradients are likely to develop in samples in the form of powders.

From Eqs. (16.7) and (16.8), one can determine the critical sample size to prevent the formation of a significant gradient (ΔT) within the sample [13]:

$$m_{\mathrm{Crit}} = \rho \left(\frac{1}{C^{(2D)}} \frac{a}{\beta} \Delta T \right)^{3/2}. \tag{16.15}$$

If we impose that thermal gradients should be below 1 K for powders ($a \approx 3\ 10^{-8}$ m^2/s, $\rho \approx 1000$ kg/m^3 and $C^{(2D)} \approx 0.07$) the critical mass is around 4.1 and 0.13 mg for $\beta = 10$ and $\beta = 100$ K/min, respectively. Therefore, the rule of thumb of using sample masses below 1 mg for DSC and in the 1–10 mg range for TG experiments is not sufficient. Heating rate and sample thermal conductivity are the key parameters that should be considered, especially when dealing with samples in the form of powders.

The first consequence of a thermal lag due to the sample thermal inertia is a temperature shift to higher temperatures when the mass is increased [26]. In Fig. 16.3, we have plotted the simulated evolution of the transformation of yttrium trifluoroacetate $Y(CF_3COO)_3$ ($Y(TFA)_3$) powders. The parameters used in the simulation are summarized in Table 16.1 and have been determined experimentally [13, 27, 28]. To avoid any effect of the heat released during the decomposition, we have taken $q = 0$ (isenthalpic sample). Details of the numerical integration of Eqs. (16.1)–(16.5) are given in Ref. [13]. The values of the crucible inner radius and sample height are $R = 2.4$ mm and $H = 4.8$ mm, respectively. Thus, the sample mass is 100 mg and the time lag 23 s.

From Fig. 16.3, it is apparent that due to the thermal inertia of the sample, the transformation slows down so peaks are shifted to higher temperatures. Since the temperature shift is proportional to the heating rate, the faster the heating rate, the larger the peak shift. Also the peaks' shape is distorted. The points located near the crucible walls almost follow the expected kinetics while those located at farthest positions do not. Since the transformation rate peak is the convolution of these

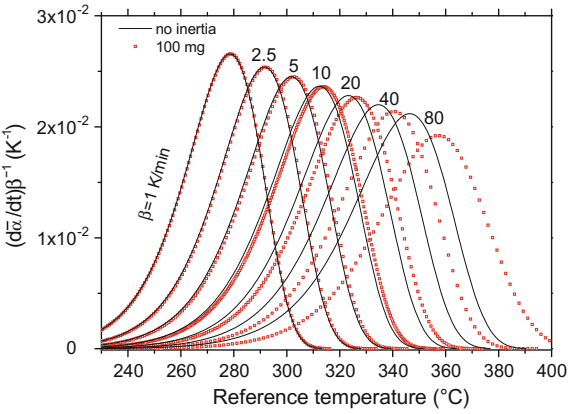

Fig. 16.3 2D simulations of the evolution with respect to the reference temperature of the thermal decomposition of $Y(TFA)_3$ with zero thermal inertia (*solid lines*) and for a mass of 100 mg and $R = 2.4$ mm (*squared symbols*). The simulation parameters are detailed in Table 16.1. To simulate an isenthalpic sample, we have imposed $q = 0$

Table 16.1 Physical parameters of the two metal-organic powders analyzed

	$Y(TFA)_3$	$Ba(TFA)_3$
Thermal conductivity, λ, W/(m K)	0.06	0.08
Specific heat capacity, c, J/(kg K)	875	2230
Density, ρ, kg/m^3	1114	1463
Thermal diffusivity, m^2/s	6.15×10^{-8}	2.45×10^{-8}
Specific heat of reaction, q, J/kg	2.75×10^5	1.0×10^6
Activation energy, E_A, J/mol	1.70×10^5	1.77×10^5
Pre-exponential constant, A, s^{-1}	3.4×10^{13}	4.5×10^{13}

contributions, the peak ends at higher temperatures, it becomes wider, and its height decreases.

Due to the delay introduced by thermal inertia, the kinetic analysis delivers an artificial evolution of the activation energy with the transformation degree as it is apparent in Fig. 16.4. More notorious is the fact that the apparent activation energy is significantly smaller than the actual value. The reason is that thermal lag increases the peak separation, so that the apparent activation diminishes [31].

16.2.2 Thermal Gradients Due to the Heat Evolved from the Sample

When the transformation is not isenthalpic ($q \neq 0$), the heat balance is controlled by two competing phenomena: the exothermic reaction that tends to increase the local temperature, and heat diffusion that dissipates the heat through heat conduction. The formation of a temperature gradient depends on the ratio between the

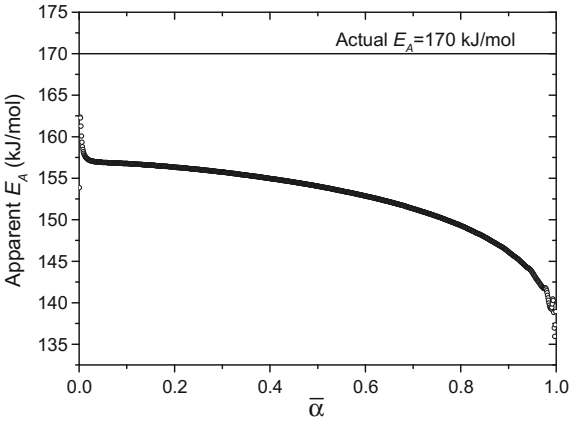

Fig. 16.4 Apparent activation energy of the evolutions shown in Fig. 16.3 determined with the Friedman's isoconversional method [29, 30]

rates of chemical reaction and heat dissipation. When the diffusion time is much smaller than the characteristic reaction time, heat is efficiently removed and thermal gradients are negligible.

As we have already seen in the previous section, the diffusion time in a cylindrical crucible can be expressed as:

$$t_{\text{Diff}} = C^{(2\text{D})} \frac{V^{2/3}}{a}. \tag{16.16}$$

For a single-step reaction with a rate constant that follows an Arrhenius temperature, the reaction time, t_R, defined as the full width at half maximum of the transformation rate peak, is given by [4, 32]:

$$t_R = \frac{c_R}{A e^{-E_A/R_G T_{\text{Max}}}}. \tag{16.17}$$

where T_{Max} is the temperature at which the reaction rate is maximum and c_R is a constant that depends on the reaction model. For instance, for a first-order reaction $c_R = 2.44639$ (values of c_R for various reaction models are given in [4]). Besides, T_{Max} is given by Kissinger's relationship [41]:

$$\frac{E_A}{R_G T_{\text{Max}}^2} = \frac{A}{\beta} e^{-E_A/R_G T_{\text{Max}}}. \tag{16.18}$$

T_{Max} can easily be calculated with high accuracy using the solution given in Ref. [31]. It has been shown [13] that temperature differences larger than 1 K occur when the sample mass is above a critical mass:

$$m_{\mathrm{Crit}} = \rho T_{\mathrm{Max}}^3 \left(c_R \frac{5 \times 10^{-5}}{C^{(2\mathrm{D})}} \frac{c}{q} \frac{a}{\beta} \right)^{3/2}. \tag{16.19}$$

When the sample mass is larger than m_{Crit}, the heat evolved is not efficiently removed and thermal differences larger than 1 K appear through the sample. This criterion not only depends explicitly on the thermal parameters of the system (c, a, q), the reaction model (c_R), and the heating rate, β, but also depends implicitly on the rate constant (A, E_A) through T_{Max}, Eq. (16.18).

To prevent local thermal gradients related to the heat evolved, as a rule of thumb, it has been proposed that the rate of generation must not exceed 8 mW [16]. The average heat flow released during the reaction can be calculated as:

$$\left\langle m \frac{dq}{dt} \right\rangle \approx \frac{q}{t_R} m. \tag{16.20}$$

The maximum heat flow allowed to prevent overheating can be obtained by substituting m_{Crit} in Eq. (16.20):

$$\left\langle m \frac{dq}{dt} \right\rangle_{Crit} = \rho \frac{E_A T_{\mathrm{Max}}}{R_G} \left(\frac{5 \times 10^{-5}}{C^{(2\mathrm{D})}} c a \right)^{3/2} \left(\frac{c_R}{q\beta} \right)^{1/2}. \tag{16.21}$$

Equation (16.21) shows that the critical heat flow is far from being constant; thus, the reference value of 8 mW is too rough a criterion to be considered seriously.

Contrarily to what has been stated in the previous section, the effect of local overheating is a peak shift toward lower temperatures. According to Eq. (16.1), the heat accumulated inside the sample accelerates the reaction; thus, when the sample mass is increased, the transformation is accelerated and the whole process shifts to lower temperatures (the opposite happens when the transformation is endothermic). This acceleration of the reaction when the mass is increased has been reported for different exothermic reactions: combustion of soot [33], thermal decomposition of $La(Fe(CN)_6)$ [34], and thermal degradation of barium trifluoroacetate Ba $(CF_3COO)_2$ ($Ba(TFA)_2$) [35].

In Fig. 16.5, we have plotted the measured evolution of the thermal decomposition of $Ba(TFA)_2$ together with the numerical simulations for a given heating rate (20 K/min) and different masses. The experimental conditions are described in Ref. [13]. The simulation parameters are summarized in Table 16.1. All the simulation parameters have been determined experimentally [13, 35, 36]. One can verify that both numerical and experimental results show the same trend; when the sample mass increases, the transformation shifts to lower temperatures. Indeed, according to (19) the critical mass for $Ba(TFA)_2$ and $Y(TFA)_3$ for a heating rate of 20 K/min and R = 2 mm, is 2.22 and 4.56 mg, respectively (the critical heat power is 18 and 10 mW, respectively). Thus, in the case of $Ba(TFA)_2$, an evolution of the TA curve

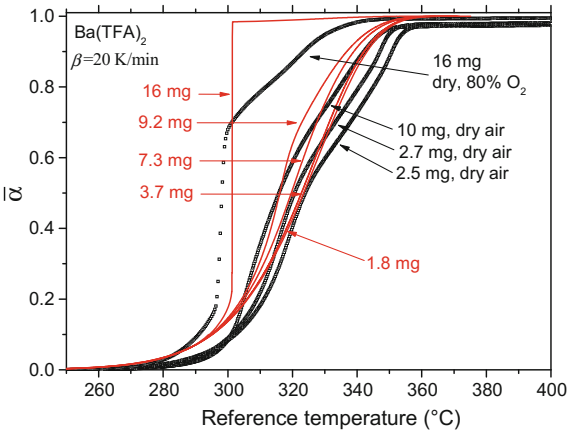

Fig. 16.5 Evolution versus the reference temperature of the thermal decomposition of $Ba(TFA)_2$ for different sample masses; squares (*black*) correspond to experimental data while lines (*red*) are numerical simulations. The simulation parameters are detailed in Table 16.1. Experimental details are given in [13]. The crucible inner radius is 2 mm for both experiments and simulations

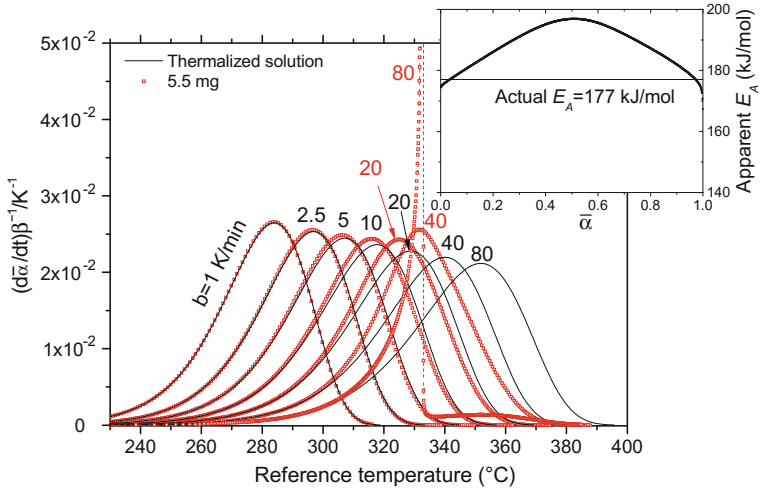

Fig. 16.6 2D simulations of the evolution with respect the reference temperature of the thermal decomposition of $Ba(TFA)_2$ without thermal gradients (*black solid lines*) and for a mass of 5.5 mg (*red squared symbols*). The simulation parameters are detailed in Table 16.1. The crucible inner radius is 2 mm. *Inset* Apparent activation energy calculated with Friedman's method [29, 30] (the evolution for β = 80 K/min has not been included because it undergoes a thermal runaway)

with the sample mass is expected for masses above 2.22 mg, such as it can be confirmed numerically and experimentally in Fig. 16.5.

Like what occurred in the previous section, the thermal gradients also affect the peak shape. The peak onset is not modified because, as long as there is no heat evolved, there is no overheating. Yet, once the reaction evolves, the heat accumulated accelerates the reaction so that the peak end shifts to lower temperatures. As a result, the peak width diminishes and the peak height increases. These effects are more pronounced at higher heating rates, as it is clearly seen in Fig. 16.6.

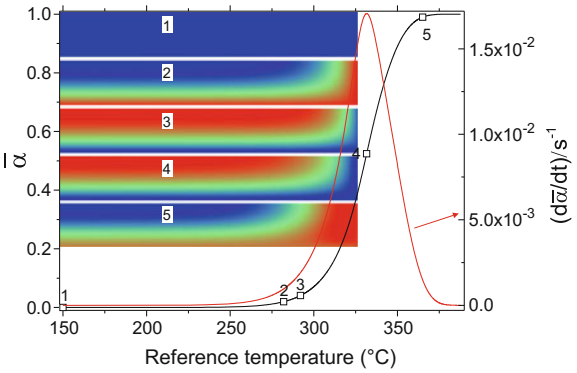

Fig. 16.7 Calculated evolution of $\overline{\alpha}$ with respect to the reference temperature for $Ba(TFA)_2$ decomposition. The sample mass is 5.5 mg, β = 40 K/min and R = 2 mm. The temperature distribution at five stages is shown. These stages are indicated with open symbols over the $\overline{\alpha}$ curve. Images *red* corresponds to the highest temperature while *blue* depicts the lowest one

The isoconversional kinetic analysis, inset of Fig. 16.6, also reveals an artificial evolution of the activation energy. Since the separation between peaks diminishes when the heating rate increases, the apparent activation energy is larger than the actual activation energy [31].

In Fig. 16.7, one can observe that, initially, the sample is thermalized (point 1) but when the reference temperature is raised, the thermal inertia makes the temperature next to the crucible higher than that of the center of the sample (point 2). However, as the reaction rate increases the temperature gradient flips over and the hottest part is located at the top center of the sample (points 3 and 4). The reason is that the crucible walls act as a thermal sink that allow fast heat dissipation. Eventually, the heat evolved from the reaction vanishes and the temperature gradient flips over again.

Another interesting aspect is that reaction takes place at a higher temperature that the one measured. TA apparatus records as sample temperature the temperature next to crucible walls. However, due to the heat accumulated, the average sample temperature is higher than that of the crucible walls. For instance, in Fig. 16.7, the temperature in the red region is 15 K above the temperature at the crucible walls (blue region). This effect is very pronounced when a thermal runaway takes place.

16.3 Thermal Runaway

As we have seen in the previous section, when heat production is not balanced by heat dissipation, heat accumulates locally. This local heating accelerates the reaction. So the heat generation rate also increases. Thus, above some critical conditions, the system undergoes a thermal runaway, i.e., the reaction becomes locally unstable and converges to a high-temperature state [37–42]. When a thermal runaway takes place, the reaction takes place faster that the reaction is virtually adiabatic; all the heat released by the reaction contributes to the sample temperature increase,

$$\Delta T_{AD} = \frac{q}{c}. \tag{16.22}$$

The transition from the "normal state" to this "high-temperature state" is abrupt. Below the critical conditions, the reaction is stable and the local overheating is moderate; above the critical conditions, the local overheating approaches or even overcomes ΔT_{AD}. Typically, c is of the order of 10^3 J/kg K and the enthalpy of many exothermic reactions is well above 10^5 J/kg, so that for many exothermic reactions ΔT_{AD} is well above 100 K. Indeed, combustion synthesis takes advantage of the short reaction time and large overheating related with thermal runaway to obtain materials that would otherwise imply high-temperature processing techniques [43, 44].

In Fig. 16.5, one can verify that for a mass of 16 mg the transformation of Ba $(TFA)_2$ is very abrupt; the transformation is over after a very short time period. Indeed, above a critical sample size, the decomposition of $Ba(TFA)_2$ undergoes a thermal runaway. Also in Fig. 16.6, we observe a very sharp peak for β = 80 K/min that is related to a thermal runaway. In Fig. 16.8, we observe that the evolution of the decomposition of an $YBa_2Cu_3O_{7-\delta}$ precursor strongly depends on the sample size. For small sample sizes, the evolution is smooth and the decomposition spans a wide temperature range. Conversely, above a critical size, the thermogravimetric curve shows a very abrupt mass loss and the differential thermal analysis (DTA) curve exhibits a very sharp peak; these two features are characteristic of a thermal runaway [33, 34, 45–47].

The condition for a thermal runaway to occur depends on two timescales: on the one side, the diffusion time that controls dissipation, and on the other side the ignition time, t_i, i.e., the duration of the induction period of a thermal runaway [48, 49]. When the crucible walls are kept at a constant temperature, the ignition time is given by [41, 49]:

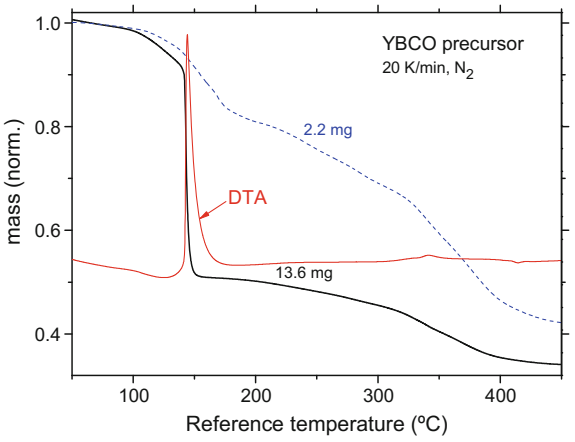

Fig. 16.8 Evolution of the decomposition of an aqueous solution of PEG, HNO_3, $BaCO_3$, Y_2O_3, and CuO that is a precursor of $YBa_2Cu_3O_{7-\delta}$ superconductor

$$t_i = t_R \frac{c}{q} \frac{RT_0^2}{E_A}. \tag{16.23}$$

where T_0 is the crucible temperature, and the reaction time under isothermal conditions is given by the reciprocal of the rate constant:

$$t_R = \left[A e^{-E_A/RT_0} \right]^{-1}. \tag{16.24}$$

Assuming that $\Delta T_{AD} \gg T_0$ and that the thermal runaway takes place at the early stages of the reaction, Frank-Kamenetskii showed that the critical size of the system is determined by a single parameter, δ, that is the ratio between the diffusion and ignition times:

$$\delta \equiv \frac{t_{\text{Diff}}}{t_i} = \rho \frac{q}{\lambda} \frac{E_A}{R_G T_0^2} d^2 A e^{-\frac{E_A}{R_G T_0}}, \tag{16.25}$$

Above a critical value, δ_C, the system undergoes a thermal runaway, i.e., when $t_{\text{Diff}} > \delta_C \cdot t_R$, heat diffusion is too slow to prevent a thermal runaway.

The critical value of δ depends on the definition of the characteristic length d and the geometry of the system. For instance, $\delta_C = 3.32$ for a spherical vessel with $d = R$, $\delta_C = 2.0$ for an infinite long cylinder with $d = R$ and $\delta_C = 0.88$ for a semi-infinte slab with $d = H$ [49–52].

For constant heating conditions, the reaction time is given by Eq. (16.17). Since for non-isothermal conditions, the timescale is determined by T_{Max}, under non-isothermal conditions the Frank-Kamenetskii parameter can be expressed as:

$$\delta = \frac{1}{5} \rho \frac{q}{\lambda} \frac{E_A}{R_G T_{\text{Max}}^2} d^2 A e^{-\frac{E_A}{R_G T_{\text{Max}}}} = \frac{1}{5} \frac{\rho q}{\lambda} \beta \left(\frac{E_A}{R_G T_{\text{Max}}^2} d \right)^2, \tag{16.26}$$

We have numerically verified Eq. (16.26) for heating rates ranging from 0.01 to 100 K/min and for an infinite long cylinder and a semi-infinte slab. Actually, the factor 1/5 is a free parameter that has been fitted to give the same values of δ_C than for the isothermal case.

Finally, for a finite cylinder, the critical value can be derived by assuming that two diffusion paths compete in parallel (see Eq. (16.13)):

$$\delta_C = 0.88 \times \left[\pi \left(\frac{R}{H} \right)^2 \right]^{2/3} + 2.0 \times \left[\pi \frac{H}{R} \right]^{2/3}, \tag{16.27}$$

From Eqs. (16.12), (16.26), and (16.27), the predicted critical sample mass for $Ba(TFA)_2$ decomposition is 9.0 mg (for $R = 2$ mm). This result is in fair agreement with the experimental and numerical results plotted in Fig. 16.5; no thermal runaway is observed for sample masses below 10 mg, while a thermal runaway occurs

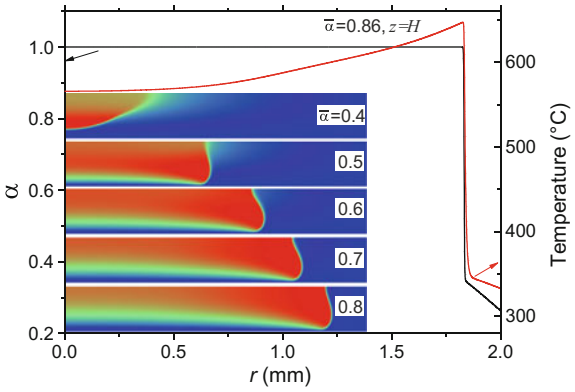

Fig. 16.9 Calculated α and temperature profiles along the radial direction for the thermal decomposition of $Ba(TFA)_2$. The temperature and α profiles correspond to the elapsed time where $\overline{\alpha}$ = 0.86 (t = 137 s). The sample mass is 5.5 mg, β = 40 K/min, and R = 2.4 mm. The images correspond to the temperature distribution for five different stages. The averaged degree of transformation achieved at each stage is indicated. *Red* corresponds to the highest temperature while *blue* depicts the lowest one

for a sample mass of 16 mg. Also, for a mass of 5.5 mg the critical heating rate is 55 K/min a result that is in agreement with Fig. 16.6 (a thermal runaway is only observed for β = 80 K/min).

From Fig. 16.9, we can realize that when a thermal runaway occurs, temperature variations are well above 100 K. The images of the temperature distribution show that the localized overheating propagates as a combustion front all along the material volume: from the top center of the sample toward the crucible walls. This propagation is very fast. The time elapsed between the first image ($\overline{\alpha}$ = 0.4) and the last image ($\overline{\alpha}$ = 0.8) is 0.42 s, a time much smaller than 15 s; the reaction time without overheating. Note that from the TA curve (Fig. 16.5), one may erroneously interpret that nearly all the transformation takes place at a relatively low constant temperature, whereas the transformation takes place at temperatures well above the sample temperature delivered by the TA apparatus [34].

16.4 Dependence on the Sample Aspect Ratio

A critical parameter to predict whether a thermal gradient appears or a thermal runaway occurs is the aspect ratio. As we have seen in the previous sections, the critical condition not only depends on the sample size but it also depends on the aspect ratio. The diffusion paths in the axial and longitudinal directions compete in parallel, so that the diffusion time is controlled by the shortest path. Using a wide crucible instead of a tall one will certainly reduce the thermal gradients inside the sample.

A particular case is that of films deposited on a substrate. In films, the ratio H/R is much smaller than 1. Therefore, the geometric coefficient, $C^{(2D)}$, in Eqs. (16.15) and (16.19) is typically well below 10^{-3}. Thus, under the usual TA experimental conditions, the formation of a significant thermal gradient inside films is virtually impossible.

In Fig. 16.10, we compare the evolution of the thermal decomposition of yttrium acetate in the form of powders and films. We observe in the case of powders that the evolution is smother when the sample mass is lower. The reason is that at higher masses, the accumulated heat accelerates the transformation. However, in the case of the film, the evolution is significantly smoother despite the fact that the total mass of the film is larger than that of the powders. In films, the higher aspect ratio ensures a much more efficient thermalization.

For instance, in the case of $Y(TFA)_3$ decomposition and for $\beta = 20$ K/min thermal gradients larger than 1 K occur in powders for sample masses above 3.2 mg ($R = 2$ mm), while in the case of films thicknesses above 220 μm are necessary. It is even more difficult to induce a thermal runaway in films; a mass of 16 mg is necessary for powders while combustion is only possible for film thicker than 860 μm. Experiments and simulation have confirmed that combustion occurs in the decomposition of $Y(TFA)_3$ for masses above 16 mg while in the case of thin films no temperature gradients are observed [45].

It has been recently claimed that combustion synthesis could be a straightforward route for the low-temperature synthesis of oxide-based electronic devices [54]. However, combustion on films was deduced from TA experiments performed on powders. When TA measurements were performed on these precursors in the form of thin films, the result was a smooth evolution of the decomposition course that rules out any thermal runaway [45]. Apart from the pronounced enhancement of heat diffusion in films, the much higher thermal conductivity of films (usually they are much more compact than powders) and the easier evaporation of fuels [55]

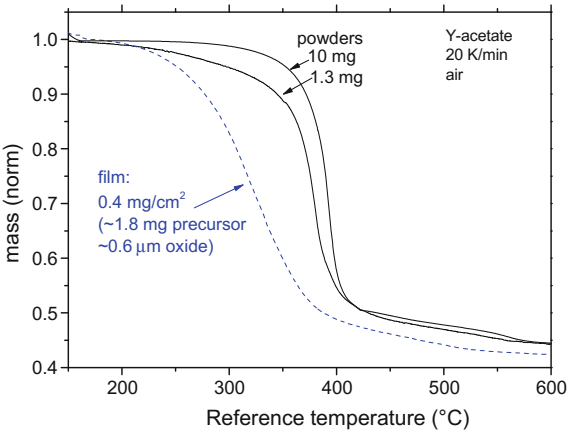

Fig. 16.10 Measured evolution of the thermal decomposition of $Y(CH_3COO)_3$ in the form of powders (*solid lines*) and as a film (*dashed line*). Experimental details are given in [53]

makes it virtually impossible to set a combustion front in thin films using a hot plate or a conventional furnace. To set a combustion front in films, other strategies should be foreseen.

Acknowledgements This work has been funded by the Spanish Programa Nacional de Materiales through project MAT2014-51778-C2-2-R and by the Generalitat de Catalunya contract No. 2014SGR-00948.

References

1. Málek J, Sesták J, Rouquerol F, Rouquerol J, Criado JM, Ortega A (1992) Possibilities of two non-isothermal procedures (temperature- or rate-controlled) for kinetical studies. J Therm Anal Calorim 38:71–87
2. Criado JM, Gotor FJ, Ortega A, Real C (1992) The new method of constant rate thermal analysis (CRTA): application to discrimination of the kinetic model of solid state reactions and the synthesis of materials. Thermochim Acta 199:235–238
3. Vyazovkin S, Burnham AK, Criado JM, Pérez-maqueda LA, Popescu C, Sbirrazzuoli N (2011) ICTAC Kinetics Committee recommendations for performing kinetic computations on thermal analysis data. Thermochim Acta 520:1–19
4. Farjas J, Butchosa N, Roura P (2010) A simple kinetic method for the determination of the reaction model from non-isothermal experiments. J Therm Anal Calorim 102:615–625
5. Vyazovkin S (2000) Kinetic concepts of thermally stimulated reactions in solids: a view from a historical perspective. Int Rev Phys Chem 19:45–60
6. Patt ME, White BE, Stein B, Cotts EJ (1992) Thermal time constants in differential scanning calorimetry. Thermochim Acta 197:413–424
7. Roura P, Farjas J (2005) Analysis of the sensitivity and sample–furnace thermal-lag of a differential thermal analyzer. Thermochim Acta 430:115–122
8. Siniti M, Schiets F, Alouani K, Claudy P (2007) Heat transfer in a disc-type DSC apparatus. J Therm Anal Calorim 89:45–50
9. Šesták J, Holba P (2013) Heat inertia and temperature gradient in the treatment of DTA peaks. J Therm Anal Calorim 113:1633–1643
10. Holba P, Šesták J, Sedmidubský D (2013) Heat transfer and phase transition in DTA experiments. In: Šesták J, Šimon P (eds) Therm Anal Micro, Nano-Non-Crystalline Mater Springer, Netherlands, pp 99–133
11. Blaine RL, Kissinger HE (2012) Homer Kissinger and the Kissinger equation. Thermochim Acta 540:1–6
12. Melling R, Wilburn FW, McIntosh RM (1969) Study of thermal effects observed by differential thermal analysis. Theory and its application to influence of sample parameters on a typical DTA curve. Anal. Chem. Am Chemical Soc 41:1275–86
13. Sánchez-Rodríguez D, Eloussifi H, Farjas J, Roura P, Dammak M (2014) Thermal gradients in thermal analysis experiments: criterions to prevent inaccuracies when determining sample temperature and kinetic parameters. Thermochim Acta 589:37–46
14. Coats AW, Redfern JP (1963) Thermogravimetric Analysis Analyst 88:906
15. Brown ME (2004) Introduction to thermal analysis. Kluwer Academic Publishers, New York
16. American society for testing and materials (ASTM International), test method E698 (2005) Method for Arrhenius kinetic constants for thermally unstable materials using differential scanning calorimetry and the Flynn/Wall/Ozawa method. Annu B ASTM Stand vol 14.02. ASTM International, West Conshohocken PA
17. Šesták J, Šatava V, Wendlandt WW (1973) The study of heterogeneous processes by thermal analysis. Thermochim Acta 7:333–334

18. Crighton JS, Wilburn FW (1992) The role of heat transfer in the production of DSC curves. Thermochim Acta 203:1–5
19. Mraw SC (1982) Mathematical treatment of heat flow in differential scanning calorimetry and differential thermal analysis instruments. Rev Sci Instrum 53:228–231
20. Merzhanov AG, Barzykin VV, Shteinberg AS, Gontkovskaya VT (1977) Methodological principles in studying chemical reaction kinetics under conditions of programmed heating. Thermochim Acta 21:301–332
21. Klemensiewicz Z (1949) Thermal conductivity of powders. Nature 164:589
22. Mukasyan AS, Rogachev AS (2008) Discrete reaction waves: gasless combustion of solid powder mixtures. Prog Energy Combust Sci 34:377–416
23. Sánchez-Rodríguez D, López-Olmedo JP, Farjas J, Roura P (2015) Determination of thermal conductivity of powders in different atmospheres by differential scanning calorimetry. J Therm Anal Calorim 121:469–473
24. Pujula M, Sánchez-Rodríguez D, Lopez-Olmedo JP, Farjas J, Roura P (2016) Measuring thermal conductivity of powders with differential scanning calorimetry. J Therm Anal Calorim 125:571–577
25. Goel NS, Gerboc JS, Lehmann G (1992) A simple model for heat conduction in heterogeneous materials and irregular boundaries. Int Commun Heat Mass Transf 19:519–530
26. Wendlandt WW (1986) Thermal analysis. Wiley, New York
27. Eloussifi H, Farjas J, Roura P, Camps J, Dammak M, Ricart S, Puig T, Obradors X (2012) Evolution of yttrium trifluoroacetate during thermal decomposition. J Therm Anal Calorim 108:589–596
28. Eloussifi H, Farjas J, Roura P, Ricart S, Puig T, Obradors X, Dammak M (2013) Thermoanalytical study of the decomposition of yttrium trifluoroacetate thin films. Thin Solid Films 545:200–204
29. Farjas J, Roura P (2011) Isoconversional analysis of solid state transformations. A critical review. Part I. Single step transformations with constant activation energy. J Therm Anal Calorim 105:757–766
30. Friedman HL (1964) Kinetics of thermal degradation of char-forming plastics from thermogravimetry. Application to a phenolic plastic. J. Polym. Sci Part C Polym 6:183–95
31. Farjas J, Roura P (2014) Exact analytical solution for the Kissinger equation: determination of the peak temperature and general properties of thermally activated transformations. Thermochim Acta 598:51–58
32. Farjas J, Roura P (2008) Simple approximate analytical solution for nonisothermal single-step transformations: Kinetic analysis. AIChE J 54:2145–2154
33. Neeft JPA, Hoornaert F, Makkee M, Moulijn JA (1996) The effects of heat and mass transfer in thermogravimetrical analysis. A case study towards the catalytic oxidation of soot. Thermochim Acta 287:261–278
34. Sánchez-Rodríguez D, Wada H, Yamaguchi S, Farjas J, Yahiro H (2015) Self-propagating high-temperature synthesis of $LaMO_3$ perovskite-type oxide using heteronuclearcyano metal complex precursors. J Alloys Compd 649:1291–1299
35. Farjas J, Camps J, Roura P, Ricart S, Puig T, Obradors X (2012) The thermal decomposition of barium trifluoroacetate. Thermochim Acta 544:77–83
36. Eloussifi H, Farjas J, Roura P, Ricart S, Puig T, Obradors X, Dammak M (2013) Thermal decomposition of barium trifluoroacetate thin films. Thermochim Acta 556:58–62
37. Varma A, Rogachev AS, Mukasyan AS, Hwang S (1998) Combustion synthesis of advanced materials: principles and applications. Adv Chem Eng 24:79–226
38. Patil KC, Aruna ST, Mimani T (2002) Combustion synthesis: an update. Curr Opin Solid State Mater Sci 6:507–512
39. Rabinovich OS, Grinchuk PS, Andreev MA, Khina BB (2007) Conditions for combustion synthesis in nanosized Ni/Al films on a substrate. Phys B Condens Matter 392:272–280
40. Thiers L, Mukasyan AS, Varma A (2002) Thermal explosion in Ni-Al system: influence of reaction medium microstructure. Combust Flame 131:198–209

41. Semenov N (1940) Thermal theory of combustion and explosion. Prog Phys Sci USSR 23:251–292
42. Semenov N (1928) Theories of combustion processes. Zeitschrift für Phys 48:571–582
43. Merzhanov AG, Khaikin BI (1988) Theory of combustion waves in homogeneous media. Prog Energy Combust Sci 14:1–98
44. Morsi K (2011) The diversity of combustion synthesis processing: a review. J Mater Sci 47:68–92
45. Sanchez-Rodriguez D, Farjas J, Roura P, Ricart S, Mestres N, Obradors X, Puig T (2013) Thermal analysis for low temperature synthesis of oxide thin films from chemical solutions. J Phys Chem C 117:20133–20138
46. Roura P, Farjas J, Eloussifi H, Carreras L, Ricart S, Puig T, Obradors X (2015) Thermal analysis of metal organic precursors for functional oxide preparation: thin films versus powders. Thermochim Acta 601:1–8
47. Boddington T, Hongtu F, Laye PG, Nawaz M, Nelson DC (1990) Thermal runaway by thermal analysis. Thermochim Acta 170:81–87
48. Merzhanov AG, Averson AEE (1971) The present state of the thermal ignition theory: an invited review. Combust Flame 16:89–124
49. Frank-Kamenetskii DA (1955) Diffusion and heat exchange in chemical kinetics. Princeton University Press, New Jersey
50. Chambré PL (1952) On the solution of the poisson-boltzmann equation with application to the theory of thermal explosions. J Chem Phys 20:1795
51. Gill W, Donaldson AB, Shouman AR (1979) The Frank-Kamenetskii problem revisited. Part I. boundary conditions of first kind. Combust Flame 36:217–232
52. Harley C, Momoniat E (2008) Alternate derivation of the critical value of the frank-kamenetskii parameter in cylindrical geometry. J Nonlinear Math Phys 15:69–76
53. Farjas J, Camps J, Roura P, Ricart S, Puig T, Obradors X (2011) Thermoanalytical study of the formation mechanism of yttria from yttrium acetate. Thermochim Acta 521:84–89
54. Kim M-G, Kanatzidis MG, Facchetti A, Marks TJ (2011) Low-temperature fabrication of high-performance metal oxide thin-film electronics via combustion processing. Nat Mater 10:382–388
55. Marchal W, De Dobbelaere C, Kesters J, Bonneux G, Vandenbergh J, Damm H et al (2015) Combustion deposition of MoO_3 films: from fundamentals to OPV applications. RSC Adv. 5:91349–91362

Chapter 17
The Physical Kinetics of Reversible Thermal Decomposition

J. Czarnecki and J. Šesták

Abstract A new theoretical basis, fitting thermal analysis of solids more adequately than the Arrhenius equation developed for reacting gas molecules, is proposed for gas-evolving reversible decompositions. Such complex processes are theoretically dissected into elementary steps, showing distinctions between micro-kinetics and macro-kinetics; only the slowest step being recordable thermoanalytically. Practical procedures of determination whether a thermoanalytical process is controlled by chemical kinetics on micro-level, or by physical macro-processes of heat- and gas-transport in the bulk, based on exposing the samples to changing degrees of heat transfer, and (separately) to the changing degree of exposure to the gaseous decomposition product, are postulated as a prerequisite before choosing the calculation model. It is shown that many typical processes of gas-evolving reversible decomposition are controlled not by chemical micro-kinetics, but by the physical processes of escaping of the gases and of the heat transfer. Even in smallest samples, the overlapping gradients of the temperature and of the gas concentration, plus two or three interwoven reaction fronts, invalidate micro-kinetic calculations and indicate that thermoanalytical data reflect globally the behavior of the sample as a whole, not of its individual grains or molecules—those two classes being completely different. The meaning of decomposition temperature is revisited. A family of TG curves obtained at the specified conditions enables distinguishing between the true decomposition temperature and the procedural one; only the latter being normally recorded. A pitfall of determination of decomposition temperature by CRTA is discussed. Implication for industrial processes are suggested.

J. Czarnecki (✉)
1554 Ironwood Ct., Brea 92821, CA, USA
e-mail: jpczarnecki@gmail.com

J. Šesták
New Technologies Research Centre (NTC-ZČU), University of West Bohemia,
Universitní 8, 30114 Pilsen, Czech Republic
e-mail: sestak@fzu.cz

J. Šesták et al. (eds.), *Thermal Physics and Thermal Analysis*,
Hot Topics in Thermal Analysis and Calorimetry 11,
DOI 10.1007/978-3-319-45899-1_17

17.1 Are Thermogravimetric Results Usable in Practice?

One of the reasons for creation of thermal analysis was the need of the industry for reliable predictions of the optimum temperature, optimum time, and the resulting yield of some industrial thermal processes. Some thermokinetic models, old and new, e.g., [1, 2], show ways to interpret TG results realistically and even predict them, but this is often limited to non-reversibly decomposing materials. In the area of gas-producing reversible decomposition processes of the type $A_{solid} \leftrightarrow B_{solid} + C_{gas}$ we presently cannot meet those expectations of the industry, so excessive amounts of costly energy are wasted due to using less-than-optimum parameters of e.g., calcination of limestone into lime, or industrial dehydration of gypsum. The parameters of those industrial processes are usually set according to the trial-and-error experience, without the expected help from thermal analysis.

Historically, when researchers were trying to understand the kinetics involved in thermal analysis in general, it seemed appropriate to use the help of the fundamental kinetic Arrhenius equation, in its standard exponential form $k = A\exp(-E/RT)$ where the symbols have their traditional meanings of reaction rate constant, pre-exponential factor, activation energy, gas-constant, and temperature. The researchers realized then that since the Arrhenius equation describes reactions between active collisions of gas molecules, then trade-offs would be unavoidable when that equation was to be applied to reactions in solids. Retrospectively, we can see now that the degree of this inherent incompatibility varies widely for different classes of substances. While many irreversibly decomposing materials, e.g., polymers or calcium oxalate, do conform to the sophisticated kinetic models, many carbonates, hydrates, and ammine/ammonia—transition-metal-salt complexes—evidently do not. The proven compatibility of the theoretical models with some classes of substances (mostly those decomposing irreversibly) has led to an unjustifiable extrapolation of the applicability to other classes of substances, in first place to those decomposing reversibly.

Regardless how hard and for how long we have been trying, the discrepancies and inconsistencies reported in the thermoanalytical literature are sometimes very large. Calcium carbonate (misleadingly) seems to be a straightforward, easy case for studying this problem in general. Its decomposition has been studied extensively, for several decades, prominently by Maciejewski [3–5], but the reported values of its temperature of decomposition (supposedly a "carved in stone" thermodynamic value) published by many authors are still scattered over a very wide range: from 923 K (650 °C) to 1323 K (1050 °C) [3, 4]. Some other calculated values are nonsensical, e.g., negative activation energies, or values of activation energy jumping by *tens of orders of magnitude* as caused by trivial changes of e.g., shape of the sample holder.

There is hardly any correlation of the values obtained from thermoanalytical experiments with large-scale industrial processes, as pessimistically expressed [6]:

"*there is no point in comparing the results of the thermal decomposition of a thin layer of limestone in vacuo with the technological process of firing pieces of limestone.*" This unfortunate fact can lead in two opposite directions: it can be used as an excuse for the flaws of the present "state of the art", or it can stimulate us to find a path for new, meaningful and adequate, theoretical models. Regrettably, most of us seem to have chosen the first option. We casually admit that thermoanalytical results pertaining to kinetics and thermal stability are valid only for the particular configuration of the sample at the particular set of the heating conditions, and that they do not characterize the substance itself. One could ask: if so, then what is the point of doing such research? Maciejewski's position [2–5] is "hybrid": While recognizing the crucial effects of the gaseous product (a macro-process), he keeps trying to find a reliable model within the micro-kinetics by making the micro-kinetic models even more sophisticated.

17.2 The Anatomy of a Gas-Producing Thermal Decomposition of Solids

Note: The following discussion is conceptual and is illustrated by graphs which are conceptual too, but it is based on hundreds of publications of TG data obtained at contrasting conditions, from the Liptay's monumental Atlas of Thermoanalytical Curves [7] to other families of TG curves, e.g., [8–10].

We will first analyze theoretical TG curves in the vicinity of the temperature of thermodynamic equilibrium. Let us assume an infinitely small sample, hypothetically approaching the size of a single molecule, of the substrate "A" (of the equation of the previous section), e.g., calcium carbonate, or another stable substance, heated linearly. The initial part of the TG curve will be perfectly horizontal, as can be expected from the marble sculptures lasting unchanged for millennia. Initially, the substance "A" is energetically advantaged, so if its molecule, energized randomly above the activation value, happens to decompose, the gas "C" will be re-absorbed by "B", recombining them back into the substrate "A". When the temperature of the thermodynamic equilibrium has been reached, a random temperature fluctuation above the average temperature, energetic enough to cover the reaction enthalpy, will make the molecule "A" decompose.

In Fig. 17.1, showing the concept (i.e., not empirical results), the above process is represented by the vertically stepped TG curve, vertically magnified here for visibility. The last part of the TG curve is a straight horizontal line, representing the mass of the solid product, CaO in this case.

Another sample of the same material, extremely small but of a more realistic size, kept under vacuum and heated linearly, will produce the other TG curve of Fig. 17.1. The region of stability and the starting point of decomposition are the

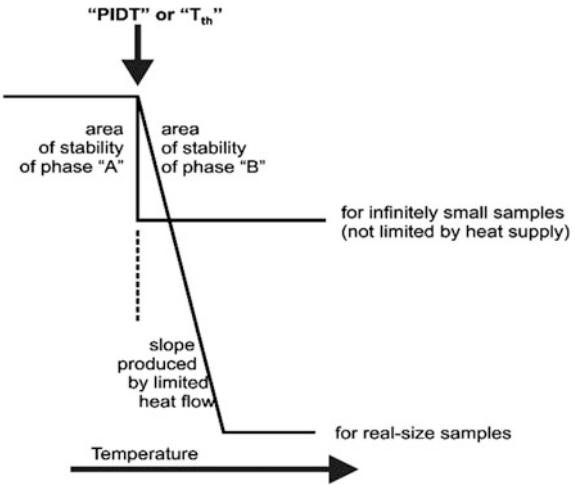

Fig. 17.1 Extremely small samples decomposing at the thermodynamic decomposition temperature; there is no hinderance for the gas escape

same as those of the previous case, but now the weight drop is not instantaneous but gradual, controlled by the flow of heat to cover the reaction's enthalpy.

These were TG curves with no hinderance of any kind involved. In reality, some hindrance is always present, and their effect on TG curves is discussed here extensively. Now, we will analyze details of reversible thermal decomposition.

A decomposition process of the type: $A_{solid} \leftrightarrow B_{solid} + C_{gas}$ involves more components than just breaking the chemical bonds and releasing the products; those concurrently proceeding elementary processes are as follows:

1. heat transfer to "A"
2. activation of "A"
3. breaking of the chemical bonds
4. desorption of "C" from "A"
5. collapsing of "A" structure
6. nucleation of crystal structure "B"
7. growth of crystal structure "B"
8. escape of gas "C".

Since the discussed reactions are reversible, there is always some concurrence of these elementary processes going *in the reverse direction*, but not of all of them. In the thermoanalytical conditions some steps are by-passed, for instance, steps (5–7) do not happen sometimes, e.g., amorphous structures [3] are involved instead. Notably, Hill [11] was able to study a small sphere of calcium carbonate without causing it to crumble, even though its after-the-reaction-front layers consisted of CaO, not of $CaCO_3$; but the not-crumbling down might have been a macro-phenomenon on the sample scale, not necessarily proving the lack of the

re-crystallization. Several of these elementary processes involve activation energy, but not those related to transport, that is steps (1) and (8). The term "transport" is used collectively for the gas escape and for heat transfer. Distinguishing between these two process-limiting factors is possible by "questioning the material", that is by varying the experiments' parameters in appropriate way.

The existence of the Arrhenius equation does not prove its applicability to a given case; indeed, a number of authors proved the opposite [8–12]. By its nature and by its intended design, the kinetic apparatus based on Arrhenius equation belongs to the "micro-world". Therefore, when macro-processes are involved, they should be dealt with using a different, adequate apparatus, and then the terms would re-gain their precise meanings. In thermal analysis, there is room for micro-kinetics, and there is room for non-Arrhenius macro-kinetics, too. There is also a place for the extreme sophistication of so many kinetic models, and there is a place for common sense, too. When we see the activation energy changing by tens of orders of magnitude, we know that an inadequate model was applied.

One can argue that there is nothing wrong with using the Arrhenius equation in thermal analysis of solids as long as we remember the merely formal nature of the terms and the relativity of the results. Very generally, it is correct that inadequate equations can be used as long as enough "fudge factors" are added, but when a mathematical apparatus and its applications are of the same "genre", the outcome is easier to handle and it is more reliable. A simplistic example: The Cartesian system of coordinates describes a circle as correctly as the radial system does, but in the latter it is easier to detect abnormalities or misinterpretations. While in this example, the inconvenience of the first choice is negligible, thermoanalytical kinetics is so complex that the additional complications caused by using inadequate equations can lead to impenetrable convolutions.

Which of these elementary processes (micro or macro) is controlling the particular process, that is often determined by "curve fitting", that is by comparing the plots of (mathematically processed) empirically obtained data, to the plots of the theoretic models; whichever of the theoretical plots fits best, that supposedly identifies the controlling process. Alas, the plots (usually logarithmic) of very different theoretical models differ only little, and so their differences often fall within the experiments' errors. A more reliable way of determining whether the process is controlled by "chemical" kinetics on the micro-level, or by the macro-processes in the bulk, is exposing the samples to changing degrees of the heat transfer, and (separately) to the changing degree of exposure of the material to the gaseous decomposition product. Determining whether it is gas "C" what controls a TG process can be done under controlled vacuum by changing the activity of that gas "C" being the only component of the sample's atmosphere: carbon dioxide for carbonates, water vapor for hydrates, ammonia for ammonium complexes etc.

17.3 Distinction Between Micro- and Macro-Kinetics of Reversible Thermal Decomposition of Solids

17.3.1 Micro-Kinetics

Processes on the molecular level and on the intra-crystal level. The decomposition is influenced by the following factors that are internal to the process:

- mobility of crystal lattice, affecting the transfer of heat (the equivalent of molecular collisions, that the Arrhenius equation was derived for);
- enthalpy of decomposition; activation energy needed for decomposition of molecules;
- crystal size and defects, affecting the surface energy (different from the energy in the bulk);
- structural differences between the reactant "A" and the solid product "B";
- nucleation and growth of "B";
- decomposition temperature (its thermodynamic value).

17.3.2 Macro-Kinetics

Sample-level intra-*container* processes. The decomposition is influenced by the following factors that are external to the process itself:

- concentration/partial pressure/activity of the gaseous product "C" in the immediate vicinity of the B–C interface;
- shape of sample holder;
- external gaseous envelope;
- granulation and porosity, which are becoming more loose as the decomposition progresses;
- inter-granular channels and obstructions of diffusion;
- pressure, composition, and flow of gas between the grains;
- catalytic capabilities, interface curvature, capillary effects;
- thermal conductivity of the sample (the porosity is changing),
- thermal resistance of the system: sample holder's walls + furnace walls + gap between them;
- heating rate in case of non-isothermal experiments.

Since thermogravimetric experiments record the integrated mass of the sample, then only the macro-kinetics is recordable. Chemical-type, or micro-kinetics, where the Arrhenius equation may apply to some degree, usually governs only one of the

steps of the thermal decomposition of a sample. Whether this step has a controlling role has to be determined (not assumed) in each experiment. Regardless how many elementary processes are occurring concurrently, at a given moment only one of them (the slowest one) is determining the actual (measured) reaction rate.

There is no question that micro-kinetic processes do take place; at the same time, the thermoanalytical literature is full of examples indicating diffusion (on the sample level) being the rate controlling process.

The lists (above) describe the concurrent elementary decomposition–recombination equilibria of a hypothetical *infinitely small* crystal. A real-world TG sample, even a milligram size, is usually a collection of clusters of crystals, with a labyrinth of channels affecting the escape of the gas product. Even if a single crystal is used as a TG sample, its surface may start crumbling due to re-crystallization the structure "A" to "B", and so that TG sample will become a multi-crystal pile of a mixture of those two phases.[1] This means an even smallest practical TG sample has several levels of gradients plus multiple local reaction fronts, very complicated indeed:

- gradients of temperature, continuously changing,
- gradients of the gas "C" concentration in the inter-granular air, continuously changing,
- moving reaction fronts within each crystal,
- moving reaction fronts within each crystal aggregate, and
- moving global reaction front within the entire sample—all of them proceeding simultaneously as shown in Fig. 17.2.

Up to this point, by "steps" we meant the process's component steps involved in a single chemical decomposition reaction. Many minerals, hydrates, carbonates, and coordination complexes decompose in more than one chemical reaction step, e.g., a copper sulfate penta-hydrate first produces tetra-hydrate, then bi-hydrate, followed by decomposition to copper oxide—most of these reactions being individual $A_{solid} \leftrightarrow B_{solid} + C_{gas}$. The kinetics of a single chemical reaction is complicated enough, so only one aspect of multiple chemical reactions: resolution, is discussed in this article. More about multiple decomposition reactions can be found in earlier publications [8, 9].

Note: the two drawings at the top of Fig. 17.2 are similar to those published by Garn [13].

[1]But see the remarks on amorphous structures in Sect. 17.2.

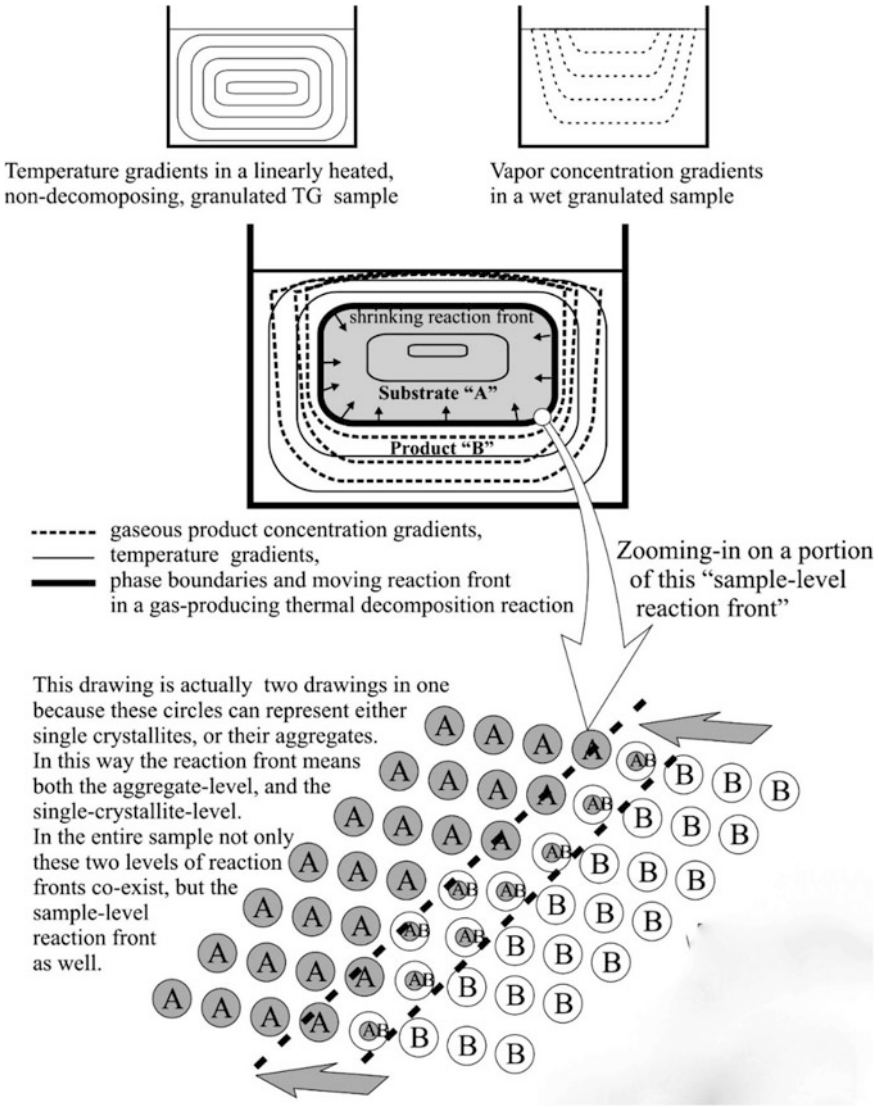

Fig. 17.2 Gradients of temperature and of the gaseous product concentration, and three levels of reaction fronts: crystallite-level front, aggregate-level-front, and sample-level front

17.4 How Is the Thermodynamic-Equilibrium Temperature Represented in TG Curves?

Note: TG curves are usually distorted by various disturbances and drifts, but blank-run corrections, if done properly, make possible precision within tens, or even single parts per million [14]. This in turn makes it possible to distinguish between perfectly horizontal sections and "almost horizontal" ones—a crucial distinction, as we will see. The TG curves of Fig. 17.3 are free of distortions.

While Fig. 17.1 was related to thermal decomposition free of hinderances; Fig. 17.3 extends this discussion to real-world conditions, where the decomposition is always obstructed and delayed, to some degree. This is a representation of typical changes in TG curves of reversible heterogeneous decomposition of granular solids heated linearly in time, at varying degrees of hindrance of escape of the gaseous product: from no hinderance (curve 1), that is a sub-milligram sample under vacuum, through intermediate hinderance, (curves 2–5) to the most hindered "self-generating atmosphere" (tightly packed sample holder covered with a lid, at ambient pressure), represented by curve 6.

TG curves like #1 of Fig. 17.1 can be obtained with sub-milligram samples heated linearly under vacuum. With the increasing temperature, the point of the thermodynamic equilibrium between "A" and "B" + "C", called "PIDT", will be reached. At the point of the thermodynamic equilibrium the decomposition and the recombination have equal likelihoods, since the gaseous product "C" is present in the immediate reaction zone. Above the PIDT point, the decomposition into "B" +

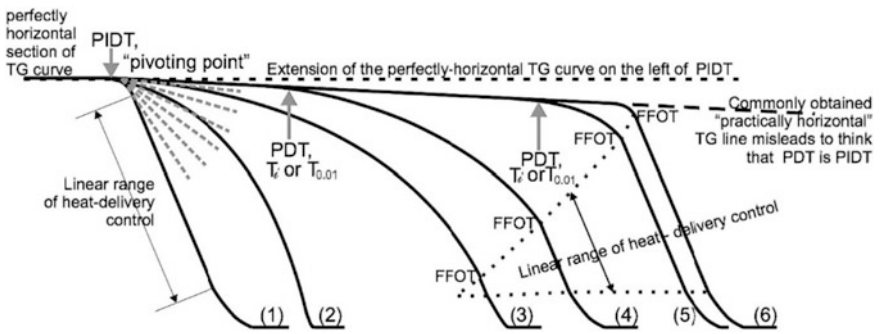

Fig. 17.3 Graphical illustration of the postulated mechanism of gas-producing reversible decomposition of granular samples at various degrees of hinderance of escape of the gaseous reaction products, at a linear heating rate: from completely un-hindered (TG curve 1) to the most hindered self-generating atmosphere (TG curve 6). Curves 2–6 represent intermediate degrees of the hinderance. The *upper dashed line* is the extension of the initial, perfectly horizontal section. The *lower dashed line* is the extension of the misleading "practically horizontal" section. *PIDT* procedure-independent decomposition temperature; thermodynamic decomposition temperature. *PDT* procedural decomposition temperature; literature equivalents: T_i, $T_{0.01}$. *FFOT* forced-flow onset temperature

"C_{gas}" is energetically favored, but kinetically the decomposition is always somewhat suppressed by the molecules "C". Above that PIDT temperature point, the TG curve of this elementary sample would drop sharply. The slope reflects the delivery rate of the heat covering the decomposition enthalpy. Then another perfectly horizontal line follows. Curve 1 of Fig. 17.3 represents a similar situation as it was shown in Fig. 17.1, but it is more diffused.

Now let us assume a somewhat larger sample of the same substance, also kept under vacuum; this is represented by curve (2) of Fig. 17.3. Up to the PIDT temperature point, no process is going on, and so the TG line is perfectly straight. Above the PIDT point however, the decomposition into "B" + "C_{gas}" is energetically favored but kinetically this decomposition is hindered by the molecules of "C_{gas}", always present in the immediate vicinity of the surface of the mixture of "A" and "B".

Above PIDT, both "A" and "B" phases co-exist in negative feedback loops of the dynamic equilibria. This is a kinetic meta-stability beyond the true thermodynamic-stability range, where decomposition is taking place, but it is hindered by that portion of the volatile product which has not escaped yet. This hinderance is reflected on TG curves by the TG line being more horizontal than the sharply dropping line of curve (1). The inclined section of the TG curve at right of PIDT means coexistence of "A" and "B". Such kinetic coexistence of "A" and "B" involves also the existence of multiple moving reaction fronts, as shown in Fig. 17.2. That kind of equilibrium is dynamic and changing continuously, it is a "pseudo-equilibrium". The gradually escaping gas is being replenished with more gas being supplied from the decomposing parts. When the escape of the gas is somewhat hindered, the slope of the *inclined* section (at the right of PIDT) is barely noticeable at first, then it increases, gradually curving downwards. With the increasing temperature the escape rate of gas "C" is becoming accelerated by the diffusion being faster at higher temperatures, and also by the increasing porosity of the sample due to the gradual loss of the material. This acceleration can be seen in the form of the curving, ever-increasing slope of the TG curve in that section. Finally, all the material "A" has decomposed, and the TG curve becomes horizontal again. This makes such TG curves highly non-symmetrical, which can be best noticed on their derivative form DTG.

Since the point PIDT is indistinguishable in such hindered TG curves, and no prior knowledge is available, then the researcher needs to deal with what is available. Customarily, a straight non-horizontal line is selected arbitrarily, and its point of intersection with the earlier, "practically horizontal" section produces a point called "procedural decomposition temperature"—"PDT". Although it is "the best guess available", the PDT point has almost no significance other than it misleadingly diverts the attention from the true, absolute value, to a merely procedural one. PDT misleads about the thermal stability, which sometimes leads to wrong, gravely dangerous assumptions. Determination of limits of thermal stability of materials is a very serious matter. How can we sort these problems out?

Let us return to the PIDT point that separates two sections of a TG curve: the *perfectly* horizontal section left of the PIDT point, and the start of the (initially unnoticeably) sloping down, almost horizontal section at the right side. At the left side of PIDT the curves are horizontal because the decomposition ***cannot take place*** due to thermodynamic factors; curves at the right side of PIDT are initially horizontal because decomposition ***cannot proceed*** due to accumulation of the product. PIDT may be difficult to see, but it makes a lot of difference. Even though the PIDT is often hidden, its value is fixed, contrary to the erratic variability of PDT. The PIDT cannot be read from a single TG curve, but it can be determined from a *family of curves* obtained at varying changing (in the subsequent TG runs) the degree of hinderance of the escape of "C". The PIDT becomes then readable as the ***pivoting point*** of the *initial* sloped sections of those curves, as it is shown in Fig. 17.3. Theoretically, if we could make the escape of gas "C" completely free, the PDT would disappear and the true PIDT (of thermodynamic significance) would emerge, but in practice, it is not possible, even with smallest samples under vacuum [8, 9]. Practical procedures allowing determination of the PIDT point are described in [15].

When the escape of the gas is extremely hindered (but not stopped, with narrow escape routes still available), the slope of the *inclined* section (right of the PIDT) decreases almost to none, then it starts dropping sharply and continues as a straight inclined line. This transition from the almost-not-sloping line to the sharply sloping one means that so much of the gas "C" had accumulated inside the sample holder, that its partial pressure exceeded the ambient pressure, forcing itself out of the vessel. This transition point is called "Forced-Flow Onset Temperature" (FFOT). From this point on, the decomposition rate is determined by the heat flux into the sample. It is so because the forced flow makes diffusion-based limitation meaningless—the gas "C" is simply pushing itself out, no diffusion is needed. Now all the incoming heat causes an equivalent portion of the sample to decompose. The heat flux rate, being almost constant, causes this section of the TG curve to be a straight line, too.

An inclined but straight section of any kind of a line means that its first derivative is horizontal, and so the straight, inclined section of a forced-flow-controlled TG curve has its DTG peak flatly cut off, a plateau. Unnoticed by thermoanalytical researchers, a plateau on a derivative curve in the science of chemical engineering is treated as an obvious proof for transport processes are the controlling (limiting) ones [12]. Plotting DTG curves, thus chances of seeing plateaus on them, became uncommon nowadays, but seeing a straight-line section in a TG curve is common, and those are one and the same thing.

Both curves obtained at the two extremes of the hinderance (curves 1 and 6) include similar straight, steeply inclined section, related to the heat transfer, but the reasons are different. For curve (1), diffusion is not limiting the process because of the small sample size and vacuum; for curve (6), because the velocity of the pressure-forced flow is much faster than the diffusion's, outflow is overwhelming

the restrictions. In both cases, the decomposition proceeds as fast as the heat flow is being supplied for the enthalpy of the decomposition.

The transition points PDT and FFOT may look similar, but their usefulness is very different. PDT is meaningless and misleading, FFOT is an equivalent of the boiling point; but none of them is the temperature border between the *thermodynamic* stability and the decomposition. The best usefulness of FFOT is visualization of separate steps of multi-step chemical decompositions.

The periods of the weight loss in the intermediate-hindrance curves (2–5) of Fig. 17.3 are dragging longer in time and it takes a longer portion of the linearly rising temperature, than those in the extreme curves 1 and 6. This is of importance for studying substances which decompose in several *chemical* steps, which often overlap, sometimes completely. Although such kinds of decomposition reactions are beyond the scope of this article, it is worth mentioning that their TG resolution is worst (not best, as commonly believed) for small samples. Curve (1) of Fig. 17.3 is hardly achievable in practice, probably due to the intra- and inter-granular diffusion hindrances, present even under vacuum; it is achievable only in exotically extreme conditions [8, 9]. For practical purposes, the best resolution can be achieved in the forced-flow conditions of the "self-generating atmosphere"; one just needs to remember the limits of the meaning of the FFOT temperature value. This reason for changing the number of the (chemical) decomposition steps seems to be a more reliable interpretation than "*a change in the reaction mechanism*", a not an uncommon postulate in the controlled rate (CRTA) research.

If we could conduct a TG experiment under controlled environment where there is no air (normally air obstructs the diffusion of gas "C"), but only the gas "C", dynamically maintained at constant pressure (any controlled, constant value of pressure, from vacuum to over-ambient), then the PDT and the FFOT merge, at temperature depending on the pressure in the same was as boiling point depends on the pressure. *Generally, the partial pressure/activity of the gaseous product has about the same significance for reversible thermal decomposition as the vapor pressure has for evaporation and boiling.*

Researchers' obligation is to avoid classifying empirical facts a priori, without proving the interpretation empirically. In our case, the bare facts are that some substances decompose when heated, releasing gases, and some of such processes are reversible; notably some carbonates, some hydrates, and some ammonia- and ammine-complexes of transition-metal salts. The assumption that chemical kinetics is controlling those processes is merely an assumption, not a fact.

Let us imagine a kettle, suspended from a recording balance and heated linearly. The bottom of this kettle is covered by a thick layer of wet sand. The set-up and the resulting curves will look like those shown in Fig. 17.4. One may say, it is silly to compare thermoanalytical kinetics to evaporation of water from a kettle, but industrial processes (which we are trying to understand, to model and predict) are closer to the water–kettle situation than to the gas molecules' collisions that the Arrhenius equation is based upon. And not only huge-scale industrial processes, but

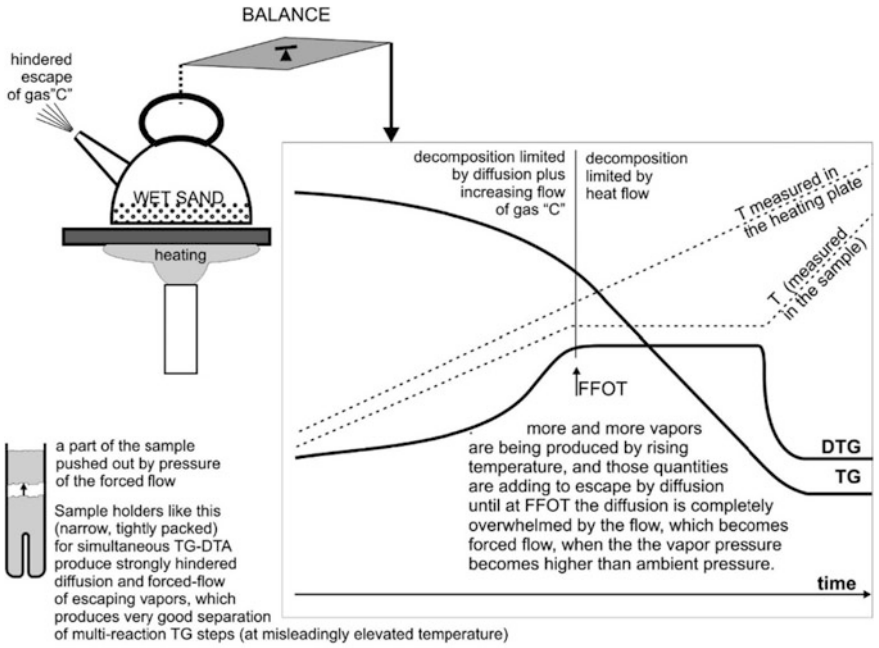

Fig. 17.4 Similarities of reversible, gas-producing thermal decomposition to escaping of vapors from granular samples

also the diffusion-restricted TG samples, kept in e.g., capillaries, or in labyrinth crucibles [6, 7] and in sample holders shaped as that shown in the lower-left corner of Fig. 17.4. They all produce exactly the same kind of TG curves as a water kettle does. At higher heating rates, it is not unusual to see a part of the sample having been pushed out of the vessel, like a steam engine's piston.

Let us be frank: If someone gave us the diagram of Fig. 17.4, telling us that it was a thermogravimetric recording, without adding "*of wet sand in a kettle*", are we sure that we would not be analyzing that process using the thermokinetic models? Unfortunately, real research never provides such a prior knowledge. Then, why are we usually sure that what we are recording in thermogravimetric experiments is micro-kinetics, and dismiss the possibility of the macro-type?

This multi-level gradient situation of a reaction: $A_{solid} \leftrightarrow B_{solid} + C_{gas}$ with all its complexity—is the macro-world. TG instruments record only the general over-lapping of those primary, secondary, and tertiary reaction fronts, the diffusion flow and the forced flow, and indirectly also the heat flow—and they record them only in the form of the over-all weight changes, which are blind to most of the processes involved. In view of Fig. 17.2, one can see that such coarse, global measurement as thermal analysis is, may be compared to trying to use EEG waves of a human brain to read that brain's thinking, equally impossible.

This is the difficulty, but when we abandon any attempts of catching the "tiny bacterium of micro-kinetics through thick glove of TG", and instead we describe just that the sample not the substance then the fog will clarify. After we decide to study the sample as a whole, and do not exclude transport processes a priori, then extrapolations will start making sense, and the road of thermal analysis to industrial applications will re-open again. This is a realistic and feasible task, waiting for open-minded researchers; in fact, waiting much too long already, since Gray [16] as early as 1968 showed: "thermal resistance between the sample and the furnace determines the rate at which heat can be provided to the sample, which for an endothermic reaction determines the rate of the reaction, which in turn determines the rate of weight loss." What is postulated [17] is not a model which would cover the enormous complexity of the dozen-or-so of the inter-related steps and fronts involved, but merely a postulate to *describe diffusion in diffusion-related terms, heat transfer in heat transfer terms*, rather than in terms of activation energy, reaction order, and the Arrhenius equation.

17.5 The Pathology and the Healthy Physiology of Temperature of Decomposition

Not only the physical meaning, but also the metrological aspects of decomposition temperature, that is "the lowest temperature at which the decomposition is measurable" do not seem to be consistent [18]. The symbols used are: "T_i (initial)", "$T_{0.01}$" (for the transformation ratio "α" reaching 1%), "*T*th"—temperature of thermodynamic equilibrium, defined as the "temperature at which the partial pressure of the gaseous product equals the ambient pressure". The physical meaning of the lowest temperature, at which the rate or the cumulative decomposition is *measurable*, is inevitably narrowed to the particular conditions and to the precision of the thermoanalytical experiment. In the first approximation, it has no absolute value; in the same way as the beginning of a TG-recorded evaporation of a liquid below its boiling point would be a merely procedural value, lacking any absolute physical meaning, since liquids evaporate at any temperature. It has very limited practical significance.

The drastic discrepancies between the published values of the thermal decomposition temperature for this class of heterogeneous decompositions are commonly known [2–12]. The error margins of ± 200 K for calcium carbonate, or ± 35 K for magnesium sulfate hepta-hydrate, or ± 30 K for copper sulfate penta-hydrate, speak for themselves. Moreover, the lower ends of the discrepancies for these two sulfates (very imprecise at the beginning of the heating) indicate that those hydrates were probably decomposing at room temperature, before the heating even started, and if the TG run were slow enough, it could record such room temperature decomposition.

The literature abounds in examples of appreciable decompositions recorded at temperatures much below the values generally accepted or expected. The data related to such discrepancies are scattered in the literature, but a Mettler publication [19] presents some pertaining examples in a well-organized, comprehensive way, which support the theses of this article. According to both the DSC curve of Example 17 (p. 19) and the "conventional" TG curve of Example 19 (p. 21), the first decomposition step of copper sulfate penta-hydrate begins about 328 K (550 °C) and ends at about 378 K (105 °C), peaking at about 368 K (95 °C). However, when using the "MaxRes" (a CRTA method), the first decomposition step completes at 336 K (63 °C). This means two things: (a) In all the three experiments: the DSC, the linear heating TG, and in the MaxRes TG, it took about 3 min to reach the beginning of the decomposition, so a possible decomposition near the room temperature was not given much time to reveal itself; (b) In the MaxRes run, the temperature increase stopped around 333 K (60 °C), and then all the water of that decomposition step had evaporated, without "waiting" for the water's boiling point. One can legitimately deduce that setting the temperature-ramping rate of the initial heating segment in the MaxRes algorithm at 1 K/min rather than 10 K/min would lower that first step from 333 K (60 °C) to about 303–308 K (30–35 °C).

The observed behavior of the hydrates can be explained as they are being thermodynamically unstable but kinetically suppressed by the limited rate of escape of the gaseous product "C" (water vapor in this case). The fact that a particular "temperature of decomposition" of water from those hydrates is lower than the boiling point of water is not surprising, since water (as well as other liquids) always has some vapor pressure and so it evaporates at any temperature.

From this particular viewpoint, the very beginning section of the TG experiment is the most interesting one. Unfortunately, that is also where the strongest disturbances usually occur. Characteristically, those *disturbances begin before the sample's temperature starts to increase*, since it is not the temperature itself, but its gradients, related to the heating power, what disturbs the gas [14, 20]. In the standard way of performing a TG experiment, the heating starts at, or close to, the start of the recording, and this spoils the opportunity for obtaining important data. It would be very informative to precede the heating with a (say) 1-h recording of the weight in a non-heating programming segment, with the gases flowing around the sample. That would require programming the starting temperature below that of the room to prevent a short, spurious heating. Interestingly, such weight recording without heating makes a TG instrument a recording balance (a now-extinct species), opening vast research opportunities [21].

The very nature of any reversible reaction is that an increase in the activity of the reaction product pushes that reaction to the reverse direction, but a decrease in its activity makes the reaction proceed. This is the case of copper sulfate penta-hydrate, whose decomposition is taking place even at room temperature, as long as, and only when the volatile product is being removed. If we spread that blue penta-hydrate on a plate, we will soon notice that each blue crystal starts crumbling down, shedding

white powder of the lesser hydrate. This means that the room temperature is already higher than the thermodynamic temperature of decomposition, and it is only the hindrance of escape of the water vapor (e.g., by keeping that substance in a closed jar) what makes us think that the penta-hydrate is stable at room temperature, and what misleads us to believe that the discrepant values of its decomposition temperature, determined by thermal analysis, are objective.

A counter-argument against comparing thermal decomposition to evaporation can be that hydrates are not mixtures but chemical compounds of fixed-number proportions and with chemical bonds which require energy to be broken; witness that a thinly spread layer of blue copper sulfate penta-hydrate does not lose water as rapidly as would the same thickness layer of wet sand; the chemical bonds are holding the water molecules in the crystals. This counter-argument does not address the fact that the values of the temperature of the thermodynamic equilibrium for these compounds demonstrate themselves to be lower than the ambient temperature; otherwise, the recombination, not decomposition, would be spontaneous. In the reality of such near-ambient decompositions, the energy needed for breaking the bonds has already been absorbed from the environment, so the decomposition has already taken place, but its *completion* is held back and limited by the diffusion of the water molecules inside each crystal through the outermost several molecular layers of the crystalline structure of "A".

Obviously, not all hydrates of salts are thermodynamically unstable at room temperature, but for copper sulfate penta-hydrate decomposing to tetra-hydrate, as well as for magnesium sulfate hepta-hydrate, and for ammonia and amine complexes with inorganic salts, this probably is the case.

These issues may seem confusing, since at one place, we say that heat transfer can be a limiting factor, in another that the energy needed for the reaction has already been supplied, so the gaseous product is free to escape; here is a clarifying summary:

(a) When the thermodynamic equilibrium temperature is located above the ambient temperature (e.g., calcium carbonate), a supply of energy is needed to cover the reaction enthalpy; activation energy is also an element of this situation. The saturation vapor pressure over the substrate is lower than it would be (at the same temperature) over that liquid alone.
(b) When the thermodynamic equilibrium temperature is located below the ambient temperature (e.g., the hydrates discussed), the substrate is thermodynamically unstable, the energy needed for breaking the bonds has already been absorbed from the environment, no extra energy is needed to break the bonds, no activation energy is involved, and even no evaporation energy is involved, since the water molecules in hydrate crystals are separate, not mutually bonded as they normally are in liquid form. All the water molecules would escape simultaneously if the escape routes were not mechanically obstructed. The saturation vapor pressure over the substrate is nearly the same as it would be over liquid water.

17.6 Practical Consequences

It is easy to say "*This process is diffusion-controlled*", but the consequences are noteworthy. For example, in converting limestone to produce burnt lime, the standard enthalpy of reaction required to make high-calcium lime is around 3.15 MJ/kg of lime. The old "batch kilns" were using 15 MJ/kg, so they were only 20% efficient. Modern shaft kilns are about 75% efficient (down to 4 MJ/kg), but the remaining 25% wasted is still economically significant.

On top of the issue of efficiency, there is also the issue of emission of carbon dioxide, which in this particular process has two meanings: (a) The environmental impact of the CO_2 produced by the calcinations reaction, and (b) the CO_2, being a part of the of the reactor-heating gases, is acting as an additional suppressor of the reaction. While 100% of the former will be later re-captured from the atmosphere by the lime during the brick bonding and other similar processes, the other kind of the CO_2 not only is unnecessary, but also is even harmful to the production process by chemically blocking that reversible decomposition. Replacing coal or coke by methane will lead to energy conservation thanks to reduced concentration of the reaction-suppressing CO_2 in methane's flame. This means that another example, gypsum processing, is not obstructed by CO_2, but if say methane (only one carbon atom per four hydrogen atoms) or natural gas, or still better—hydrogen or electricity—was used to calcinate limestone purged with air, then heating would produce less or none CO_2 not only directly, but also indirectly. The emission of CO_2 would be reduced or eliminated, and the decomposition process would be accelerated, now not hindered by CO_2 pushing the reaction backwards. This would also reduce the parasitic process of "re-calcination of lime". Dehydration of gypsum or calcination of limestone in rotating kilns would also be more economical; thanks to the faster removal of the gaseous products, hindering the process.

17.7 Simple Answers to Complex Questions Are Sometimes Wrong

Slow heating rates have many advantages, but they make TG experiments uneconomical. The controlled rate thermal analysis (CRTA) method, in its most popular variety, offers "the best of both worlds": the temperature is rising fast when no process is taking place, but this rising stops when the mass loss begins; then, the process continues at that constant temperature until completion. Very useful indeed. The problem is that determination of the characteristic process values (thermal stability, decomposition temperature) by dynamic CRTA is as imprecise as it is elegant.

There are several types of CRTA. The best known and most common is the dynamic heating rate method, and this particular variety is the subject of this

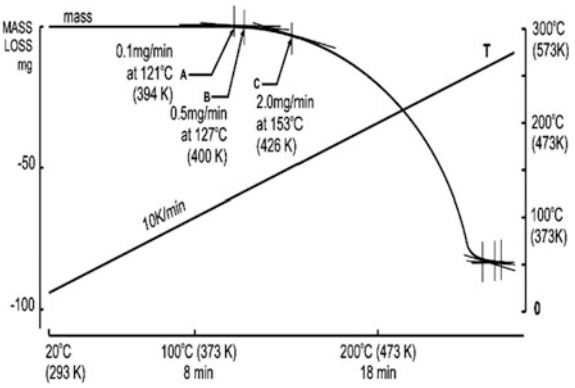

Fig. 17.5 A typical TG curve used for the analysis

section. For practical reasons, when CRTA is mentioned here, the dynamic heating rate method is meant. The other, "the stepwise isothermal method", has very different characteristics; albeit more complex it is more reliable.

A typical TG curve, shown in Fig. 17.5, was used to evaluate the CRTA procedures and their results. It shows the behavior of a sample (100 mg) of a theoretical substance whose true (thermodynamic) decomposition temperature is 110 °C (383 K),[2] heated at 10 K/min from room temperature to 275 °C (548 K).

The parameters read from the TG curve are as follows: The first detectable mass loss took place at 120 °C (413 K); it did not occur (as expected) at the thermodynamic value of 110 °C (383 K) due to the thermal inertia natural at the fast heating of 10 K/min, and also due to the diffusion delays. With the linear temperature increasing, the mass-loss rate was accelerating: from 0.1 mg/min at 121 °C (394 K) at point marked "A" to 0.5 mg/min at 127 °C (400 K) at point "B" and to 2.0 mg/min at 153 °C (426 K) at point "C"—until the decomposition completed at 266 °C (539 K), with the total loss of 90 mg.

Now, let us see what the CRTA method, applied to this kind of a sample, produces. This is a solely mathematical analysis based on the principles on which dynamic CTRA instruments work; no instrument was involved in this analysis.

The algorithm of the "dynamic heating rate CRTA" includes a pre-determined value of the mass-loss rate, which triggers switching the heating program to isotherming. Let us assume that in three CRTA experiments on that sample, the pre-determined value of the mass-loss rate is subsequently set to:

0.1, 0.5, and 2 mg/min. Figure 17.6 shows the resulting family of the mathematically generated CRTA curves, and Table 17.1 gives its numerical characteristics.

Evidently, this is a trade-off situation between the accuracy and the productivity.

So, what is the RCTA's answer to the question about the thermal stability of that substance? The right answer would be: "We cannot speak about the substance itself. Based on these measurements, we can say that for a 100 mg sample of this material,

[2]As determined separately. This value is not determinable in common TG practice.

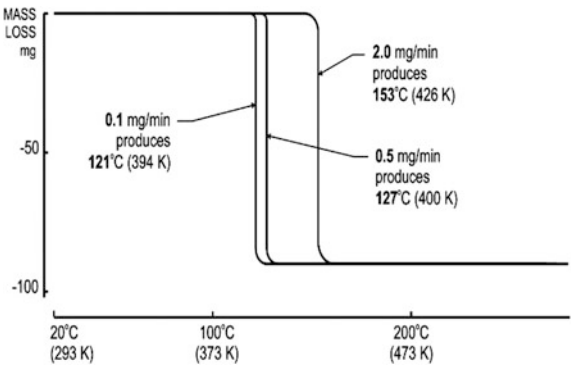

Fig. 17.6 Resulting CRTA curves

Table 17.1 Parameters of the mathematically generated CRTA curves for three values of the pre-set isotherm-triggering mass-loss rate

Mass-loss rate pre-set for CRTA (mg/min)	Resulted "decomposition temperature"	Duration of the CTRA-controlled decomposition	Error of the decomposition temperature determination (K)
0.1	121 °C (394 K)	5 h	+11
0.5	127 °C (400 K)	2 h 40 min	+17
2.0	153 °C (426 K)	44 min	+43

exposed to the CRTA procedure with the thermostating-triggering parameter set to 0.1 mg/min, the decomposition took place at 121 °C (394 K); when that parameter was set at 0.5 mg/min, it produced 127 °C (400 K); at 2.0 mg/min it produced 153 °C (426 K)."

Obviously, this is not the kind of answer most instruments' users want to hear. Some people trust procedures religiously, so they do not accept uncertainties in our knowledge.

Something needs to be done about this hidden unreliability of the dynamic heating rate CRTA method, aggravated by its misleading appearance of decisiveness. Neither users can be blamed for demanding straight answer, nor can the manufacturers for providing such answers. It is for the regulatory bodies such as ISO or ASTM to take action. ASTM has history of standardizing some aspects of thermogravimetry (ASTM E1582 "Standard Practice for Calibration of Temperature Scale for Thermogravimetry"). By no means is this merely an academic dispute: determination of limits of thermal stability of materials has consequences for economy and safety, so this issue is of a serious importance.

17.8 Does Decomposition Temperature Exist at All?

Reversible and irreversible transitions and reactions have been analyzed by Holba [22]. By definition, as long as the reaction is reversible, there is a never-ending competition between decomposition and recombination. At equilibrium, the gas molecules of "C" are constantly being produced and consumed, but if the liberated "C" molecules are being removed, then we have a non-equilibrium situation, and substance "A" decomposes irreversibly until it disappears completely. These processes take place at any temperature within the reversibility range.

A quotation [23]: "*Most such decompositions are endothermic and the entropy of decomposition is also positive, so the Gibbs energy change for decomposition will only be negative at high T and positive at low T (DG at temperature T will be given by RT ln* (Q_p/K_p) *or RT ln*(p/p_{eq})*, where* Q_p *is the reaction quotient, p is the actual pressure of C, and* p_{eq} *is the equilibrium pressure of C at T). When* ***p*** *is kept small, DG will be negative at all temperatures T, but the rate of decomposition will be determined by the Arrhenius equation. Therefore there is no unique decomposition temperature. The term "decomposition temperature" has a thermodynamic meaning of the switching point at which the decomposition reaction replaces the recombination reaction because of the thermodynamically favored process (with other conditions such as pressures of any gases held constant).*" This can be paraphrased as the three statements which say the same, with the wording stressing three different aspects:

- "*For substances which can decompose reversibly, the temperature of decomposition is the point separating the lower-temperature range, where the synthesis is irreversible, from the higher-temperature range, where the reactions of decomposition and synthesis are reversible.*"
- "*For reversible processes, the temperature of decomposition is the temperature, below which the synthesis is irreversible*."
- "*Within the temperature range of reversibility, decomposition temperature does not exist*."

17.9 How Can Thermogravimetry Restore Its Reputation in the Industry?

Due to the complexity of the thermoanalytical kinetics, it was necessary to focus this article on only one aspect of that kinetics. Interested readers can find a broader and deeper analytical review in [24]. The micro-kinetic approach has produced a wealth of impressively sophisticated science, but little of practically applicable results. New theories addressing transport of heat and mass can be developed, offering modeling for the industry, also by utilizing what has already bead

developed in chemical engineering. To obtain TG results which would have a practical meaning and can serve as modeling of industrial processes, we need to be able to study larger samples, and if we can study the transport processes by adding the appropriate vapor environment and controlled vacuum to our experiments, then we may find e.g., the optimum granulation for industrial substrates, maybe can postulate an added flow of air, and maybe using sources of heat which would not be chemically pushing the reactions back, as the flue gases in calcinations of lime presently do.

The thermal decomposition processes discussed in this article are not the only area of the industry's interest in thermoanalytical modeling of their processes, and materials characterization does not need to be the mainstream of thermogravimetry. Corrosion research, metallurgy, catalysis, volatility and outgassing of materials, cements, and wood industry are just several examples of the under-utilized potential of thermogravimetry.

All those require strong expansion of the instrumental capabilities in the first place an increase in the sample weight *and volume*. Capability of studying both small and large samples has three advantages: (a) Multiple TG steps are best identified in "self-generating atmosphere", which requires the samples to be large; (b) many kinds of industrial samples are inhomogeneous, or surface-coated, so they have to be large to produce meaningful data; (c) it is feasible to research part-per-million components in a 20-g sample, much less in a 1-g, or even smaller samples.

With discontinuation (in 2010) of Cahn TG-131, whose capacity was up to 20 ml and 100 g, and which could handle vacuum, vapors, corrosive, and contaminating gases, presently, no instrument of such capacity is available. These issues were discussed in article [21].

References

1. Ozawa T (1965) A new method of analyzing thermogravimetric data. Bull Chem Soc Japan 38(11):1881–1886. doi:10.1246/bcsj.38.1881
2. Maciejewski M (2000) Computational aspects of kinetic analysis. Part B: the ICTAC kinetics project—the decomposition kinetics of calcium carbonate revisited, or some tips on survival in the kinetic minefield. Thermochim Acta 355(1–2):145–154
3. Maciejewski M, Reller A (1987) How (un)reliable are kinetic data of reversible solid-state decomposition processes? Thermochim Acta 110:145–152
4. Lyahkov NZ, Maciejewski M, Reller A (1985) Theoretical considerations on the temperature and pressure dependence of the kinetics of reversible thermal decomposition processes of solids. J Solid State Chem 58(3):398–400
5. Maciejewski M, Baldyga J (1985) The influence of the pressure of the gaseous product on the reversible thermal decomposition of solids. Thermochim Acta 92:105–108
6. Sestak J (1984) Thermophysical properties of solids: theoretical thermal analysis. Elsevier, Amsterdam (Russian translation 'Těoretičeskij těrmičeskij analyz'. Mir, Moscow 1988)
7. Liptay G (1975) Atlas of thermoanalitycal curves. Akademiai Kiado, Budapest

8. Kemula W, Czarnecki J (1978) Mass- and heat transfer approach to reversible thermal decomposition of solids. Pol J Chem 52:613
9. Czarnecki J (1991) Heat- and mass-transfer approach to decomposition kinetics. In: Presented at 19-th annual north american thermal analysis society conference, Boston, MA; published in Solutions for Thermogravimetry. https://goo.gl/ABZX9y. Accessed 1 Dec 2015
10. Garn PD (1972) CRC Crit Rev Anal Chem 172:65
11. Hills AWD (1968) The mechanism of the thermal decomposition of calcium carbonate. Chem Eng Sci 23(4):297–320. doi:10.1016/0009-2509(68)87002-2
12. Rozovskii AY (1974) Kinetika Topo-Khimitsheskikh Reakcii, Izd. Khimija, Moscow
13. Garn PD (1965) Thermoanalytical methods of investigation. Academic Press, New York
14. Czarnecki J (2015) Precision thermogravimetry. J Therm Anal Calorim 120:139–147. doi:10.1007/s10973-014-4384-0
15. Czarnecki J (2014) Procedure for determination of thermodynamic values of thermal stability and decomposition temperature. Solutions for thermogravimetry. https://goo.gl/pQkBFv. Accessed 1 Dec 2015
16. Gray AP (1968) A simple generalized theory for the analysis of dynamic thermal measurement. Analytical Calorimetry, Plenum Press, New York
17. Czarnecki J (2009) The postulated new theoretical model of thermal decomposition that needs to be developed. Solutions for thermogravimetry. https://goo.gl/EHRYy8. Accessed 1 Dec 2015
18. Nikolaev AV, Logvinenko VA (1978) The problem of the utilizability of the starting temperature of thermal decomposition for the evaluation of the thermal stabilities of co-ordination compounds. J Therm Anal 13:253. doi:10.1007/BF01912297
19. Toledo M, Collected applications, thermal analysis, tutorial kit, pp 17–21. https://us.mt.com/dam/Analytical/ThermalAnalysi/TA-PDF/51709920_A_2012_PTFE.pdf (address shortened for typing: https://goo.gl/FN0Zuc), visited 1 Dec 2015
20. Czarnecki J, Koga N, Šestákova V, Šesták J (1992) Factors affecting the experimentally resolved shapes of TG curves. J Therm Anal 38:575–582
21. Czarnecki J, Sestak J (1915) From recording balances o thermogravietric instruments and back. J Therm Anal 120:157–166. doi:10.1007/s10973-014-4385-z
22. Holba P (2015) Ehrenfest equations for calorimetry and dilatometry. J Therm Anal Calorim. doi:10.1007/s10973-015-4406-6
23. Czarnecki J, Šesták J (2000) Practical thermogravimetry. J Therm Anal Cal 60(2):759–778
24. Šesták J (2014) The quandary aspects of non-isothermal kinetics beyond the ICTAC kinetic committee recommendations. Thermochim Acta 611(2015):26–35

Chapter 18
Thermodynamic Equilibria in Systems with Nanoparticles

Jindřich Leitner and David Sedmidubský

Abstract Thermodynamic description of systems with nanoparticles in the frame of the Gibbs theory of interfaces is presented. Although much attention has been paid to thermodynamic modelling of nanosystems, the calculation of phase diagrams of nanoalloys as well as the assessment of effects of surface-related phenomena on the solubility of nanoparticles and gas–solid reactions, some discrepancy still remains dealing with the expression of the surface contribution to molar Gibbs energy and chemical potential of components. It is shown that due to the non-extensive nature of the surface area, these contributions are different for molar and partial molar quantities. The consistent expressions for molar Gibbs energy and chemical potentials of components of spherical nanoparticles are put forward along with the correct forms of equilibrium conditions. Moreover, the applicability of the shape factor $\alpha = A_{\text{non-spherical}}/A_{\text{spherical}}$ ($V_{\text{non-spherical}} = V_{\text{spherical}}$) which is used in the expressions involving surface-to-volume ratio of non-spherical particles is addressed. A new parameter, the differential shape factor $\alpha' = \mathrm{d}A_{\text{non-spherical}}/\mathrm{d}A_{\text{spherical}}$ ($V_{\text{non-spherical}} = V_{\text{spherical}}$, $\mathrm{d}V_{\text{non-spherical}} = \mathrm{d}V_{\text{spherical}}$), is proposed which should be used in equilibrium conditions based on the equality of chemical potentials. The enhanced solubility of paracetamol nanoparticles in water and thermal decomposition of GaN nanowires are demonstrated as examples of size effect in nanosystems.

J. Leitner (✉)
Department of Solid State Engineering, University of Chemistry and Technology Prague, Technická 5, 166 28 Prague 6, Czech Republic
e-mail: jindrich.leitner@vscht.cz

D. Sedmidubský
Department of Inorganic Chemistry, University of Chemistry and Technology Prague, Technická 5, 166 28 Prague 6, Czech Republic
e-mail: david.sedmidubsky@vscht.cz

J. Šesták et al. (eds.), *Thermal Physics and Thermal Analysis*,
Hot Topics in Thermal Analysis and Calorimetry 11,
DOI 10.1007/978-3-319-45899-1_18

18.1 Introduction

Considerable attention has been paid to thermodynamic modelling of nanosystems [1–5], the calculation of phase diagrams of nanoalloys [6–13] as well as the assessment of effects of surface-related phenomena on nanoparticles solubility [14–16] and gas–solid reactions [17–21]. Although some special approaches have been proposed to solve these problems [22–26], a top-down approach based on the application of classical thermodynamics is most frequently used. Addition of a surface/interface term to the Gibbs energy of bulk material allows us to quantify the influence of interfaces on thermodynamic properties of nanophases and to evaluate surface-driving shifts of equilibrium relations. Surprisingly, some discrepancy still remains dealing with the expression of chemical potential of the involved components as well as the correct forms of equilibrium conditions.

18.2 Gibbs Energy of Nanophases

18.2.1 Single Component Systems

Suppose a solid body consisting of n moles of substance having a volume V and a surface area A. Let the spatial dimensions of such a body (denoted nanoparticle hereinafter) be in nanometer (1–100 nm) scale so the surface-to-volume ratio A/V is large and the surface contribution represents a significant part of the total Gibbs energy of the nanoparticle. The surrounding of this nanoparticle has a temperature T and a pressure p^{out}, while the nanoparticle has the same temperature but a higher inner pressure p^{in} due to surface stress. The Gibbs energy of this nanoparticle G^{np} can be expressed as

$$G^{\mathrm{np}} = G^{\mathrm{b}}(T, p^{\mathrm{in}}) + G^{\mathrm{s}} = G^{\mathrm{b}}_{\mathrm{m}}(T, p^{\mathrm{in}})n + \gamma A \tag{18.1}$$

The superscripts b and s stand for the bulk and surface terms, respectively, G_{m} is the molar Gibbs energy of the relevant substance and γ denotes the surface energy (reversible work which must be done to create a new surface/interface of unit area). The molar Gibbs energy of the nanoparticle is given as

$$G^{\mathrm{np}}_{\mathrm{m}} = \frac{G^{\mathrm{np}}}{n} = G^{\mathrm{b}}_{\mathrm{m}}(T, p^{\mathrm{in}}) + \gamma\frac{A}{n} = G^{\mathrm{b}}_{\mathrm{m}}(T, p^{\mathrm{in}}) + \gamma\frac{A}{V}V_{\mathrm{m}} \tag{18.2}$$

and the partial molar Gibbs energy of nanoparticle as

$$\overline{G}^{\mathrm{np}} = \mu^{\mathrm{np}} = \frac{\mathrm{d}G^{\mathrm{np}}}{\mathrm{d}n} = G^{\mathrm{b}}_{\mathrm{m}}(T, p^{\mathrm{in}}) + \gamma\frac{\mathrm{d}A}{\mathrm{d}n} = G^{\mathrm{b}}_{\mathrm{m}}(T, p^{\mathrm{in}}) + \gamma\frac{\mathrm{d}A}{\mathrm{d}V}V_{\mathrm{m}} \tag{18.3}$$

In general, a surface area of a solid body can be varied either by isomorphic change in its volume without any shape deformation or by change in its shape with

or without the volume variation. These two possibilities have some consequences which will be discussed later. Unless stated otherwise, only isomorphic changes are considered.

Spherical Nanoparticles

Consider a sphere of radius r as an example. Since $A/V = 3/r$ and $\mathrm{d}A/\mathrm{d}V = 2/r$

$$G_{\mathrm{m}}^{\mathrm{np}} = G_{\mathrm{m}}^{\mathrm{b}}(T, p^{\mathrm{in}}) + \frac{3\gamma V_{\mathrm{m}}}{r} \tag{18.4}$$

and

$$\overline{G}^{\mathrm{np}} = \mu^{\mathrm{np}} = G_{\mathrm{m}}^{\mathrm{b}}(T, p^{\mathrm{in}}) + \frac{2\gamma V_{\mathrm{m}}}{r} \tag{18.5}$$

The different multipliers (3 or 2) in Eqs. (18.4) and (18.5) are given by the fact that the surface contribution to the Gibbs energy G^{s} is a homogeneous function of the order 2/3 (degree of homogeneity $\lambda = 2/3$) of n. The surface contribution to the Gibbs energy of a spherical nanoparticle of radius r can be expressed as

$$G^{\mathrm{s}} = \gamma A = \gamma\left(4\pi r^2\right) = \gamma 4\pi\left(\frac{3V}{4\pi}\right)^{2/3} = \gamma 4\pi\left(\frac{3V_{\mathrm{m}}}{4\pi}\right)^{2/3} n^{2/3} = \gamma C_{\mathrm{A}} n^{2/3} \tag{18.6}$$

and

$$G^{\mathrm{s}}(kn) = \gamma C_{\mathrm{A}}(kn)^{2/3} = k^{2/3}\gamma C_{\mathrm{A}} n^{2/3} = k^{2/3} G^{\mathrm{s}}(n) \tag{18.7}$$

where $C_{\mathrm{A}} = (4\pi)^{1/3}(3\ V_{\mathrm{m}})^{2/3}$. Hence, it yields, according to the Euler theorem,

$$G^{\mathrm{s}} = \frac{3}{2}\overline{G}^{\mathrm{s}} n = \frac{3}{2}\frac{2\gamma V_{\mathrm{m}} n}{r} = 3\gamma V_{\mathrm{m}} n \frac{A}{3V} = \gamma A \tag{18.8}$$

At the same time, it holds

$$G^{\mathrm{s}} = G_{\mathrm{m}}^{\mathrm{s}} n = \frac{3\gamma V_{\mathrm{m}} n}{r} = 3\gamma V_{\mathrm{m}} n \frac{A}{3V} = \gamma A \tag{18.9}$$

It should be noted that the bulk contribution to Gibbs energy of a nanoparticle is considered at inner pressure p^{in} which is, due to the Young–Laplace (surface stress) effect, higher than the pressure of its surroundings p^{out}. This pressure difference for an isotropic spherical particle of radius r can be expressed in terms of the Young–Laplace equation in the form

$$p^{\mathrm{in}} - p^{\mathrm{out}} = \frac{2f}{r} \tag{18.10}$$

where f is the surface stress which is equal to surface energy in the case of liquids. The bulk contribution to the molar Gibbs energy of a spherical incompressible nanoparticle with radius r at surroundings pressure p^{out} can be expressed as

$$\begin{aligned} G_{\text{m}}^{\text{b}}(p^{\text{out}}) &= G_{\text{m}}^{\text{b}}(p^{\text{in}}) + \int_{p^{\text{in}}}^{p^{\text{out}}} V_{\text{m}}\mathrm{d}p = G_{\text{m}}^{\text{b}}(p^{\text{in}}) + V_{\text{m}}\left(p^{\text{out}} - p^{\text{in}}\right) \\ &= G_{\text{m}}^{\text{b}}(p^{\text{in}}) - \frac{2f}{r} V_{\text{m}} \end{aligned} \tag{18.11}$$

It is obvious that in this case, where the surface term is due to an elastic compression of particle, the factor two is involved in both the molar and the partial molar quantities.

Non-spherical Nanoparticles—Regular Polyhedra

In the case of non-spherical nanoparticles, it is possible to derive relevant expressions for A/V and $\mathrm{d}A/\mathrm{d}V$ from the formulas for surface area A and volume V and substitute them into Eqs. (18.2) and (18.3). These expressions for regular polyhedra are summarized in Table 18.1. It can be proved that, as in the case of sphere, relation $(A/V) = 2(\mathrm{d}A/\mathrm{d}V)/3$ holds for these bodies

$$A_{\text{poly}} = C_{\text{A}}a^2, \quad V_{\text{poly}} = C_V a^3, \quad \left(\frac{A}{V}\right)_{\text{poly}} = \frac{C_{\text{A}}}{C_V a} \tag{18.12}$$

$$\mathrm{d}A_{\text{poly}} = 2C_{\text{A}}a\mathrm{d}a, \quad \mathrm{d}V_{\text{poly}} = 3C_V a^2\mathrm{d}a, \quad \left(\frac{\mathrm{d}A}{\mathrm{d}V}\right)_{\text{poly}} = \frac{2}{3}\frac{C_{\text{A}}}{C_V a} = \frac{2}{3}\left(\frac{A}{V}\right)_{\text{poly}} \tag{18.13}$$

Another approach has been proposed in the literature: a so-called shape factor α has been introduced [27, 28]. It is defined as the ratio of surfaces of non-spherical (polyhedral) and spherical particles with the same volume

$$\alpha = \frac{A_{\text{poly}}}{A_{\text{sphere}}}, \quad V_{\text{poly}} = V_{\text{sphere}} = \frac{4}{3}\pi r_{\text{eqv}}^3 \tag{18.14}$$

Table 18.1 Ratios of A/V and $\mathrm{d}A/\mathrm{d}V$ and shape factors calculations according to Eq. (18.14)

Polyhedron	A/V	$\mathrm{d}A/\mathrm{d}V$	α
Tetrahedron	$6\sqrt{6}/a$	$4\sqrt{6}/a$	1,4900
Cube	$6/a$	4/a	1,2407
Octahedron	$3\sqrt{6}/a$	$2\sqrt{6}/a$	1,1826
Dodecahedron	$12\sqrt{(25 + 10\sqrt{5})}/(15 + 7\sqrt{5})a$	$8\sqrt{(25 + 10\sqrt{5})}/(15 + 7\sqrt{5})a$	1,0984
Icosahedron	$12\sqrt{3}/(3 + \sqrt{5})a$	$8\sqrt{3}/(3 + \sqrt{5})a$	1,0645

$$\left(\frac{A}{V}\right)_{\text{poly}} = \alpha\left(\frac{A}{V}\right)_{\text{sphere}} = \alpha\frac{3}{r_{\text{eqv}}} \tag{18.15}$$

where r_{eqv} is the radius of the "equivalent" sphere which has the same volume as a non-spherical particle: $r_{\text{eqv}} = (3V_{\text{non-sphere}}/4\pi)^{1/3}$. The values of α calculated for different regular polyhedra are also given in Table 18.1. In accordance with the preceding paragraphs, this (integral) shape factor can be used for an integral quantity only, for example in the expression

$$G_{\text{m}}^{\text{np}} = G_{\text{m}}^{\text{b}}(T, p^{\text{in}}) + \alpha\frac{3\gamma V_{\text{m}}}{r_{\text{eqv}}} \tag{18.16}$$

For partial molar quantities (chemical potentials), a differently defined (differential) shape factor α' should be used

$$\alpha' = \frac{\mathrm{d}A_{\text{poly}}}{\mathrm{d}A_{\text{sphere}}}, \quad V_{\text{poly}} = V_{\text{sphere}} = \frac{4}{3}\pi r_{\text{eqv}}^3, \quad \mathrm{d}V_{\text{poly}} = \mathrm{d}V_{\text{sphere}} \tag{18.17}$$

$$\left(\frac{\mathrm{d}A}{\mathrm{d}V}\right)_{\text{poly}} = \alpha'\left(\frac{\mathrm{d}A}{\mathrm{d}V}\right)_{\text{sphere}} = \alpha'\frac{2}{r_{\text{eqv}}} \tag{18.18}$$

Unlike α, this factor compares the "rate of change" of surface area with increasing volume of non-spherical and spherical particles having the same volume. It can be proved that for bodies whose geometry is dependent on a single parameter (sphere and regular polyhedra), α and α' shape factors are identical. It holds

$$\alpha' = \frac{\left(\frac{\mathrm{d}A}{\mathrm{d}V}\right)_{\text{poly}}}{\left(\frac{\mathrm{d}A}{\mathrm{d}V}\right)_{\text{sphere}}} = \frac{\frac{2}{3}\left(\frac{A}{V}\right)_{\text{poly}}}{\frac{2}{3}\left(\frac{A}{V}\right)_{\text{sphere}}} = \alpha \tag{18.19}$$

and thus

$$\overline{G}^{\text{np}} = \mu^{\text{np}} = G_{\text{m}}^{\text{b}}(T, p^{\text{in}}) + \alpha\frac{2\gamma V_{\text{m}}}{r_{\text{eqv}}} \tag{18.20}$$

This conclusion results from the fact that the surface area A is a homogeneous function of the order 2/3 of the amounts n in both cases. In fact, the validity of this result is more general—it holds for any variation of surface area of a solid body due to an isomorphic change in its volume.

Non-spherical Nanoparticles—Complex Geometry

The analysis performed above for regular polyhedra is rather complicated for bodies whose geometry is dependent on two or more parameters. Let us consider a cylinder of a radius ρ and a height h as an example. In this case, the surface area can be

changed either by volume variation at a constant aspect ratio $x = h/\rho$ (an isomorphic change) or by x variation at a constant volume (non-isomorphic change in shape). Writing the cylinder surface A and volume V in terms of h and ρ,

$$A_{\text{cylinder}} = 2\pi\rho^2 + 2\pi\rho h, \quad V_{\text{cylinder}} = \pi\rho^2 h, \quad \left(\frac{A}{V}\right)_{\text{cylinder}} = \frac{2}{h} + \frac{2}{\rho} \tag{18.21}$$

we infer that

$$\alpha = \left(\frac{2}{9}\right)^{1/3}\left[\left(\frac{\rho}{h}\right)^{2/3} + \left(\frac{h}{\rho}\right)^{1/3}\right] = \left(\frac{2}{9}\right)^{1/3}\left[x^{-2/3} + x^{1/3}\right] \tag{18.22}$$

It is obvious that the ratio $(A/V)_{\text{cylinder}}$ as well as α_{cylinder} is dependent on the relation between the h and ρ parameters. The lowest value of $\alpha_{\text{cylinder\_min}} = 1.145$ belongs to $h/\rho = 2$ and the relevant ratio $(A/V)_{\text{cylinder\_min}} = 3/\rho$ (Fig. 18.1).

The ratio $(\mathrm{d}A/\mathrm{d}V)_{\text{cylinder}}$ can be expressed as follows

$$\mathrm{d}A_{\text{cylinder}} = 2\pi[\rho\mathrm{d}h + (2\rho + h)\mathrm{d}\rho], \quad \mathrm{d}V_{\text{cylinder}} = \pi\left(\rho^2\mathrm{d}h + 2\rho h\mathrm{d}\rho\right) \tag{18.23}$$

$$\left(\frac{\mathrm{d}A}{\mathrm{d}V}\right)_{\text{cylinder}} = \frac{2[\rho\mathrm{d}h + (2\rho + h)\mathrm{d}\rho]}{\rho^2\mathrm{d}h + 2\rho h\mathrm{d}\rho} \tag{18.24}$$

At a constant $x = h/\rho$ ($h = x\rho$, $\mathrm{d}h = x\mathrm{d}\rho$), one can derive that

$$\left(\frac{\mathrm{d}A}{\mathrm{d}V}\right)_{\text{cylinder}\,[x]} = \frac{2[\rho x\mathrm{d}\rho + \rho(2 + x)\mathrm{d}\rho]}{\rho^2 x\mathrm{d}\rho + 2\rho^2 x\mathrm{d}\rho} = \frac{4}{3}\frac{x+1}{\rho x} = \frac{2}{3}\left(\frac{2}{\rho} + \frac{2}{h}\right) = \\ = \frac{2}{3}\left(\frac{A}{V}\right)_{\text{cylinder}} \tag{18.25}$$

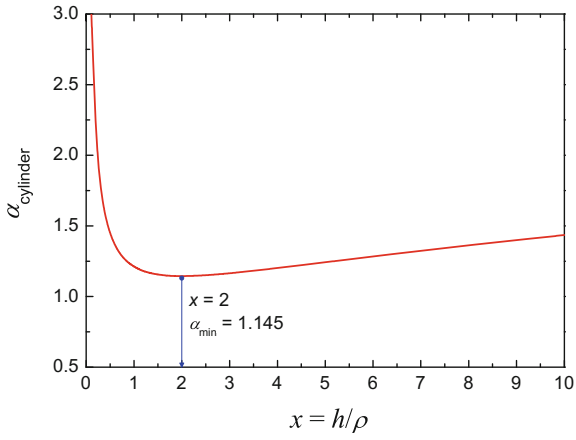

Fig. 18.1 Dependence of the shape factor of cylinder on its height-to-radius ratio

$$\alpha' = \frac{\left(\frac{\mathrm{d}A}{\mathrm{d}V}\right)_{\text{cylinder}\,[x]}}{\left(\frac{\mathrm{d}A}{\mathrm{d}V}\right)_{\text{sphere}}} = \frac{\frac{2}{3}\left(\frac{A}{V}\right)_{\text{cylinder}\,[x]}}{\frac{2}{3}\left(\frac{A}{V}\right)_{\text{sphere}}} = \alpha \tag{18.26}$$

It is a consequence of the same degree of homogeneity ($\lambda = 2/3$) of the surface areas A_{sphere} and $A_{\text{cylinder}[x]}$ as functions of the amounts n. Equation (18.20) holds in this case with α given by (18.22) and $r_{\text{eqv}} = (3x/4)^{1/3}\rho$.

Quite different relations can be given for a wire with a circular cross section. We can suppose that $h \gg \rho$ and $\rho/h \to 0$. Under this assumption, it follows from Eqs. (18.21) and (18.25) that

$$\left(\frac{A}{V}\right)_{\text{wire}} = \lim_{h\gg\rho}\left(\frac{A}{V}\right)_{\text{cylinder}} = \frac{2}{\rho} \tag{18.27}$$

$$\alpha_{\text{wire}} = \lim_{h\gg\rho}\alpha_{\text{cylinder}} = \left(\frac{2}{9}\right)^{1/3}\left(\frac{h}{\rho}\right)^{1/3} \tag{18.28}$$

$$\left(\frac{\mathrm{d}A}{\mathrm{d}V}\right)_{\text{wire}} = \lim_{h\gg\rho}\left(\frac{\mathrm{d}A}{\mathrm{d}V}\right)_{\text{cylinder}} = \frac{2\left[\frac{\rho}{h}\mathrm{d}h + \left(2\frac{\rho}{h}+1\right)\mathrm{d}\rho\right]}{\frac{\rho^2}{h}\mathrm{d}h + 2\rho\mathrm{d}\rho} = \frac{1}{\rho} = \frac{1}{2}\left(\frac{A}{V}\right)_{\text{wire}} \tag{18.29}$$

$$\alpha'_{\text{wire}} = \lim_{h\gg\rho}\alpha'_{\text{cylinder}} = \left(\frac{3}{32}\right)^{1/3}\left(\frac{h}{\rho}\right)^{1/3} = \frac{3}{4}\alpha_{\text{wire}} \tag{18.30}$$

In this case, the equality $\alpha = \alpha'$ does not apply and two different relations should be used for surface contribution to Gibbs energy

$$G_{\text{m}}^{\text{np}} = G_{\text{m}}^{\text{b}} + \alpha\frac{3\gamma V_{\text{m}}}{r_{\text{ekv}}} = G_{\text{m}}^{\text{b}} + 3\left(\frac{2}{9}\right)^{1/3}\left(\frac{h}{\rho}\right)^{1/3}\left(\frac{3\rho^2 h}{4}\right)^{-1/3}\gamma V_{\text{m}} = G_{\text{m}}^{\text{b}} + \frac{2\gamma V_{\text{m}}}{\rho} \tag{18.31}$$

$$\begin{aligned}\overline{G}^{\text{np}} = \mu^{\text{np}} &= G_{\text{m}}^{\text{b}} + \alpha'\frac{2\gamma V_{\text{m}}}{r_{\text{ekv}}} = G_{\text{m}}^{\text{b}} + 2\left(\frac{3}{32}\right)^{1/3}\left(\frac{h}{\rho}\right)^{1/3}\left(\frac{3\rho^2 h}{4}\right)^{-1/3}\gamma V_{\text{m}} \\ &= G_{\text{m}}^{\text{b}} + \frac{\gamma V_{\text{m}}}{\rho}\end{aligned} \tag{18.32}$$

It can be clearly seen that the inequality of $\alpha \neq \alpha'$ results from different degrees of homogeneity of the surface areas A_{sphere} ($\lambda_{\text{sphere}} = 2/3$) and $A_{\text{cylinder}[h\gg\rho]}$ ($\lambda_{\text{cylinder}[h\gg\rho]} = 1/2$) as functions of the amounts n. Let us now consider a body whose surface area A is a homogeneous function of the order λ. Then,

$$A = C'_{\mathrm{A}} n^{\lambda} \tag{18.33}$$

and it follows from the definitions of shape factors α and α', Eqs. (18.14) and (18.17), that

$$\alpha' = \frac{\mathrm{d}A}{\mathrm{d}A_{\mathrm{sphere}}} = \frac{\lambda\, C'_{\mathrm{A}} n^{\lambda-1} \mathrm{d}n}{\frac{2}{3} C_{\mathrm{A}} n^{-1/3} \mathrm{d}n} = \frac{n \cdot 3\lambda\, C'_{\mathrm{A}} n^{\lambda-1}}{n \cdot 2 C_{\mathrm{A}} n^{-1/3}} = \frac{3\lambda}{2} \frac{C'_{\mathrm{A}} n^{\lambda}}{C_{\mathrm{A}} n^{2/3}} = \frac{3\lambda}{2} \alpha \tag{18.34}$$

where $C_{\mathrm{A}} = (4\pi)^{1/3} (3V_{\mathrm{m}})^{2/3}$ (cf. Eq. 18.6). It should be noted that such a relation holds for bodies with a surface area being a homogeneous function of the amounts n. In other cases, e.g. a general cylinder whose surface area A_{cylinder}, Eq. (18.21), does not satisfy a condition of a homogeneous function of n, particular expressions for $\mathrm{d}A/\mathrm{d}V$ have to be assessed.

18.2.2 Multicomponent Systems

In multicomponent systems, Eqs. (18.1)–(18.3) have the following forms

$$G^{\mathrm{np}} = G^{\mathrm{b}}(T, p^{\mathrm{in}}) + G^{\mathrm{s}} = \sum_i \mu_i^{\mathrm{b}}(T, p^{\mathrm{in}}) n_i + \gamma A \tag{18.35}$$

$$G_{\mathrm{m}}^{\mathrm{np}} = \frac{G^{\mathrm{np}}}{n} = G_{\mathrm{m}}^{\mathrm{b}}(T, p^{\mathrm{in}}) + \gamma \frac{A}{n} = \sum_i \mu_i^{\mathrm{b}}(T, p^{\mathrm{in}}) x_i + \gamma \frac{A}{V} V_{\mathrm{m}} \tag{18.36}$$

$$\overline{G}_i^{\mathrm{np}} = \mu_i^{\mathrm{np}} = \left(\frac{\partial G^{\mathrm{np}}}{\partial n_i} \right)_{n_j} = \mu_i^{\mathrm{b}}(T, p^{\mathrm{in}}) + \gamma \frac{\mathrm{d}A}{\mathrm{d}n_i} = \mu_i^{\mathrm{b}}(T, p^{\mathrm{in}}) + \gamma \frac{\mathrm{d}A}{\mathrm{d}V} \overline{V}_i \tag{18.37}$$

Neglecting the excess volume of mixing, i.e. $\overline{V}_i = V_{\mathrm{m},i}$, the molar volume V_{m} of a multicomponent nanoparticle is given as

$$V_{\mathrm{m}} = \sum_i V_{\mathrm{m},i} x_i \tag{18.38}$$

The surface/interface energy γ of a multicomponent nanoparticle is composition dependent. Various models have been proposed to express such a dependence for different substances (metallic alloys, ionic melts, etc.) [29–35]. The Butler equation in the form

$$\gamma = \gamma_i + \frac{RT}{A_i} \ln \frac{x_i^{\mathrm{s}}}{x_i^{\mathrm{b}}} + \frac{1}{A_i} \left[\bar{G}_i^{\mathrm{E,s}}(x_i^{\mathrm{s}}) - \bar{G}_i^{\mathrm{E,b}}(x_i^{\mathrm{b}}) \right] \tag{18.39}$$

is frequently used for binary metallic alloys in liquid as well as in solid state. A_i means molar area of monatomic layer of the i-th component, $\overline{G}_i^{\mathrm{E}}$ is the partial excess Gibbs energy of the i-component and x_i^{s} is the molar fraction of the i-th component in the surface layer which is different from the bulk value x_i^{b} due to the segregation effect caused by differences in surface energies of components.

18.3 Thermodynamic Equilibria in Nanosystems

18.3.1 General Equilibrium Conditions for Systems with Nanoparticles

Due to the surface terms in expressions for Gibbs energy, the equilibrium conditions for nanosystems differ from those for macrosystems (bulk). Moreover, their forms significantly depend on spatial configuration of coexisting phases. The simplest topological model is that assuming a spherical nanoparticle [phase (α)] consisting of $n^{(\alpha)}$ moles of substance having a radius $r^{(\alpha)}$ surrounded by a fluid phase [phase (β)]. The pressure of surroundings p^{out} is constant, while the inner pressure of nanoparticle p^{in} is changed due to the change in radius $r^{(\alpha)}$ (see Fig. 18.2).

Considering a single component particle, it holds for the Helmholtz energy of such a system at constant [n, T, p^{out}]

$$\mathrm{d}F^{\mathrm{syst}} = \mathrm{d}F^{(\alpha)} + \mathrm{d}F^{(\beta)} + \mathrm{d}F^{(\sigma)} = -p^{\mathrm{out}}\mathrm{d}V^{\mathrm{syst}} \tag{18.40}$$

$$-p^{\mathrm{in}}\mathrm{d}V^{(\alpha)} + \mu^{(\alpha)}(p^{\mathrm{in}})\mathrm{d}n^{(\alpha)} - p^{\mathrm{out}}\mathrm{d}V^{(\beta)} + \mu^{(\beta)}(p^{\mathrm{out}})\mathrm{d}n^{(\beta)} + \gamma\mathrm{d}A = -p^{\mathrm{out}}\mathrm{d}V^{\mathrm{syst}} \tag{18.41}$$

Since $\mathrm{d}n^{(\beta)} = -\mathrm{d}n^{(\alpha)}$ and $\mathrm{d}V^{\mathrm{syst}} = \mathrm{d}V^{(\alpha)} + \mathrm{d}V^{(\beta)}$

$$-\left(p^{\mathrm{in}} - p^{\mathrm{out}}\right)\mathrm{d}V^{(\alpha)} + \left[\mu^{(\alpha)}(p^{\mathrm{in}}) - \mu^{(\beta)}(p^{\mathrm{out}})\right]\mathrm{d}n^{(\alpha)} + \gamma\mathrm{d}A = 0 \tag{18.42}$$

$$\mu^{(\alpha)}(p^{\mathrm{in}}) - \left(p^{\mathrm{in}} - p^{\mathrm{out}}\right)V_{\mathrm{m}}^{(\alpha)} - \mu^{(\beta)}(p^{\mathrm{out}}) + \gamma\frac{\mathrm{d}A}{\mathrm{d}V}V_{\mathrm{m}}^{(\alpha)} = 0 \tag{18.43}$$

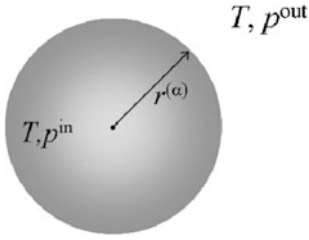

Fig. 18.2 Topological model for derivation of equilibrium condition: spherical nanoparticle continuously surrounded by fluid phase

For an incompressible nanoparticle, the sum of the first two terms in Eq. (18.43) gives the chemical potential at the surrounding pressure p^{out}, and the equilibrium condition can be expressed in the form

$$\mu^{(\alpha)}(p^{\text{out}}) + \gamma \frac{\mathrm{d}A}{\mathrm{d}V} V_{\text{m}}^{(\alpha)} = \mu^{(\beta)}(p^{\text{out}}) \tag{18.44}$$

which can be arranged for a spherical nanoparticle of radius $r^{(\alpha)}$ as

$$\mu^{(\alpha)}(p^{\text{out}}) + \frac{2\gamma V_{\text{m}}^{(\alpha)}}{r^{(\alpha)}} = \mu^{(\beta)}(p^{\text{out}}) \tag{18.45}$$

and for a non-spherical nanoparticle of equivalent radius $r_{\text{eqv}}^{(\alpha)}$ as

$$\mu^{(\alpha)}(p^{\text{out}}) + \alpha' \frac{2\gamma V_{\text{m}}^{(\alpha)}}{r_{\text{eqv}}^{(\alpha)}} = \mu^{(\beta)}(p^{\text{out}}) \tag{18.46}$$

Neglecting an excess volume of mixing, i.e. $\overline{V}_i = V_{\text{m},i}$, the equilibrium conditions in a multicomponent system acquire analogous forms [36–40]

$$\mu_i^{(\alpha)}(p^{\text{out}}) + \frac{2\gamma V_{\text{m},i}^{(\alpha)}}{r^{(\alpha)}} = \mu_i^{(\beta)}(p^{\text{out}}) \tag{18.47}$$

or for non-spherical nanoparticles

$$\mu_i^{(\alpha)}(p^{\text{out}}) + \alpha' \frac{2\gamma V_{\text{m},i}^{(\alpha)}}{r_{\text{eqv}}^{(\alpha)}} = \mu_i^{(\beta)}(p^{\text{out}}) \tag{18.48}$$

Considering another topological arrangements (see Fig. 18.3), one can derive different equilibrium conditions—for a two-particle system (a) in the form

$$\mu_i^{(\alpha)}(p^{\text{out}}) + \frac{2\gamma^{(\alpha)} V_{\text{m},i}^{(\alpha)}}{r^{(\alpha)}} = \mu_i^{(\beta)}(p^{\text{out}}) + \frac{2\gamma^{(\beta)} V_{\text{m},i}^{(\beta)}}{r^{(\beta)}} \tag{18.49}$$

and for core–shell structure (b) as

$$\mu_i^{(\alpha)}(p^{\text{out}}) + \frac{2\gamma^{(\alpha/\beta)} V_{\text{m},i}^{(\alpha)}}{r^{(\alpha)}} = \mu_i^{(\beta)}(p^{\text{out}}) + \frac{2\gamma^{(\beta)} \left(V_{\text{m},i}^{(\beta)} - V_{\text{m},i}^{(\alpha)} \right)}{r} \tag{18.50}$$

$\gamma^{(\alpha/\beta)}$ is interfacial energy on the (α)–(β) interface.

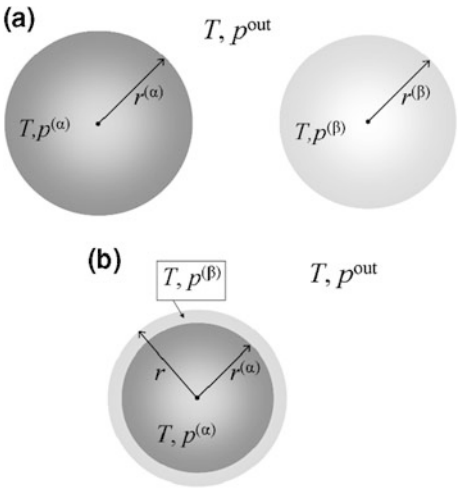

Fig. 18.3 Topological models for derivation of equilibrium condition: spherical nanoparticles of (α) and (β) phases continuously surrounded by fluid phase (**a**) and core (α)—shell (β) nanoparticle continuously surrounded by fluid phase (**b**)

18.3.2 Solid–Liquid Equilibria

In this section, a dissolution of nanosized paracetamol in water is presented as an example of solid–liquid equilibria. Higher solubility of solid nanoparticles in comparison with bulk materials has been known more than century. The Ostwald–Freundlich equation describes this effect for a nanoparticle of radius r

$$\ln \frac{c_{i,r}}{c_{i,\infty}} = \frac{2\gamma^{(\mathrm{s/l})} V_{\mathrm{m},i}^{(\mathrm{s})}}{RT \cdot r} \tag{18.51}$$

where an ideal solution of component i in relevant solvent is assumed. Although $\gamma^{(\mathrm{s/l})}$ stands for interfacial energy on the solid particle/saturated solution, it can be substituted by interfacial energy solid particle/solvent in the case of limited solubility.

We use a more general form of relevant equilibrium condition derived from Eq. (18.48)

$$\mu_i^{(l)} - \mu_i^{(\mathrm{s})} = \Delta G_{m,\infty}^{\mathrm{F}} + RT \ln a_{i,r} = \frac{2\gamma^{(\mathrm{s/l})} V_{\mathrm{m},i}^{(\mathrm{s})}}{r} \tag{18.52}$$

Since for a bulk material

$$\mu_i^{(l)} - \mu_i^{(\mathrm{s})} = \Delta G_{m,\infty}^{\mathrm{F}} + RT \ln a_{i,\infty} = 0 \tag{18.53}$$

it turns out that

$$\ln \frac{a_{i,r}(x_{i,r})}{a_{i,\infty}(x_{i,\infty})} = \frac{2\gamma^{(s/l)} V_{m,i}^{(s)}}{RT \cdot r} \tag{18.54}$$

As the solubility of paracetamol in pure water is very low (x = 0.0018 at 25 °C), the solution can be considered as ideal (in the Henry law sense) with a limiting activity coefficient of paracetamol being independent of composition. Thus, the activity ratio in Eq. (18.54) is equal to molar fraction ratio, and the relative enhancement of solubility can be calculated as

$$\frac{x_{i,r}}{x_{i,\infty}} = \exp\left(\frac{2\gamma^{(s/l)} V_{m,i}^{(s)}}{RT \cdot r}\right) \tag{18.55}$$

For non-spherical nanoparticles, the differential shape factor α' should be used to modify the equilibrium conditions (18.55) which then gains the form

$$\frac{x_{i,r}}{x_{i,\infty}} = \exp\left(\alpha' \frac{2\gamma^{(s/l)} V_{m,i}^{(s)}}{RT \cdot r_{eqv}}\right) \tag{18.56}$$

The temperature dependence of molar volume of monoclinic form (I) of paracetamol in the form

$$V_{m,par}(\mathrm{m^3\,mol^{-1}}) = 117.27 \times 10^{-6} \exp\left[1.462 \times 10^{-4}(T - 298.15)\right] \tag{18.57}$$

has been derived from XRD measurements [41]. A value of the interface energy $\gamma^{(s/l)}$ can be assessed from indirect experiments—kinetics of nucleation and contact angle measurements. A supersaturated solution of paracetamol in water is the relevant liquid phase in the former case, and the values 1.73 − 1.84 mJ m^{-2} [42], 1.83 mJ m^{-2} [43] and 2.91 ± 1.17 mJ m^{-2} [44] at 30 °C have been obtained. The contact angle of water droplets on solid paracetamol surface has been measured on compressed pellets [45, 46] as well as on various crystallographic planes of single crystals [46–48]. In their thorough study, Heng et al. [47] have measured contact angles on (001), (010), (011), (110) and (201) planes of a monoclinic crystal of paracetamol, and using the Owens–Wendt method, they calculated the respective surface energies $\gamma^{(s/g)}$.

A recalculation using the Young's equation gives the interface energies $\gamma^{(s/l)}$ in the range 2.4–8.4 mJ m^{-2}. The weighted average of this value $\gamma^{(s/l)}$ = 3.4 mJ m^{-2} was used for further calculations. The results calculated according to Eq. (18.55) are shown in Fig. 18.4. To demonstrate the influence of nanoparticles shape, the calculations were carried out according to Eq. (18.56) for cylindrical nanoparticles

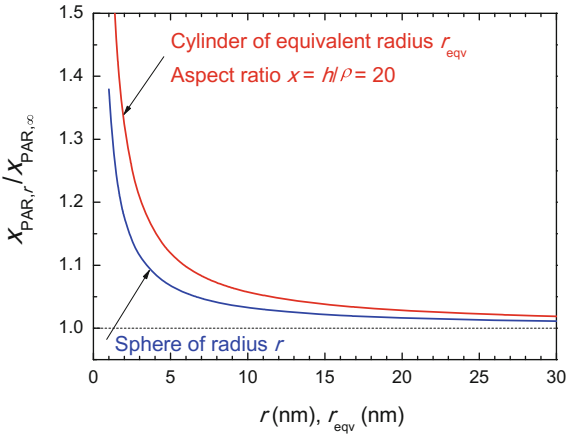

Fig. 18.4 Solubility of paracetamol nanoparticles in pure water at $t = 25$ °C in dependence of their size and shape ($r_{eqv} = \rho\ (3x/4)^{1/3}$, $x = h/\rho = 20$)

with the constant aspect ratio $x = h/\rho = 20$. Considering Eqs. (18.26) and (18.22), one can calculate the values of $\alpha' = \alpha = 1.7263$. The relation $\rho = r_{eqv}(4/3x)^{1/3}$ holds for cylinder radius ρ and equivalent radius r_{eqv} of sphere with the same volume.

18.3.3 Solid–Liquid–Gas Equilibria

To demonstrate the effect of nanosizing on the equilibria involving solid, liquid and gaseous phase, let us explore the decomposition of gallium nitride nanowires into liquid gallium nanodroplets and gaseous nitrogen. At normal total pressure, solid GaN is decomposed on heating according to the reaction

$$\mathrm{GaN(s)} = \mathrm{Ga(l)} + \frac{1}{2}\mathrm{N_2(g)} \tag{18.58}$$

For bulk materials, the relation between the equilibrium temperature and nitrogen pressure of GaN decomposition can be expressed as [49, 50]

$$\Delta_r G^{o,b} = -\frac{1}{2} RT \ln p_{N_2} = 160{,}770 - 116\,.\,T \tag{18.59}$$

The $T - p_{N_2}$ relation, as well as temperature and enthalpy of fusion, can be affected by surface-induced phenomena in nanosystems [51–54]. Considering the topology of Fig. 18.5—a cylindrical wire of GaN with radius ρ and length h ($h \gg \rho$) and totally non-wetting liquid Ga in the form of spherical nanoparticles of radius r. The equilibrium condition in the form

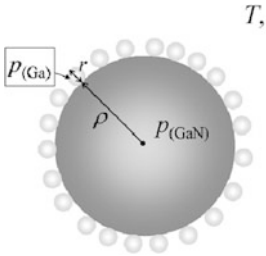

Fig. 18.5 Topological model for calculation of equilibrium relations $T - p_{N_2}$: cylindrical wire of solid GaN of radius ρ covered by nanospheres of liquid Ga (totally non-wetting surface)

$$\frac{1}{2}\left[G_{\mathrm{m}}^{\mathrm{o}}(\mathrm{N_2}) + RT\ \ln p_{\mathrm{N_2}}\right] + G_{\mathrm{m}}^{\mathrm{o,b}}(\mathrm{Ga}) + \gamma_{\mathrm{Ga}} V_{\mathrm{m,Ga}} \frac{\mathrm{d}A_{\mathrm{Ga}}}{\mathrm{d}V_{\mathrm{Ga}}} - G_{\mathrm{m}}^{\mathrm{o,b}}(\mathrm{GaN}) - \gamma_{\mathrm{GaN}} V_{\mathrm{m,GaN}} \frac{\mathrm{d}A_{\mathrm{GaN}}}{\mathrm{d}V_{\mathrm{GaN}}} = 0 \tag{18.60}$$

can be derived for this case.

By rearranging Eq. (18.60), we obtain

$$\frac{1}{2}RT\ \ln p_{\mathrm{N_2}} + \left[\frac{1}{2}G_{\mathrm{m}}^{\mathrm{o}}(\mathrm{N_2}) + G_{\mathrm{m}}^{\mathrm{o,b}}(\mathrm{Ga}) - G_{\mathrm{m}}^{\mathrm{o,b}}(\mathrm{GaN})\right] = \\ = \frac{1}{2}RT\ \ln p_{\mathrm{N_2}} + \Delta_{\mathrm{r}}G^{\mathrm{o,b}} = \frac{1}{2}RT\ \ln\frac{p_{\mathrm{N_2}}}{p_{\mathrm{N_2}}^{\infty}} = \gamma_{\mathrm{GaN}} V_{\mathrm{m,GaN}} \frac{\mathrm{d}A_{\mathrm{GaN}}}{\mathrm{d}V_{\mathrm{GaN}}} - \gamma_{\mathrm{Ga}} V_{\mathrm{m,Ga}} \frac{\mathrm{d}A_{\mathrm{Ga}}}{\mathrm{d}V_{\mathrm{Ga}}} \tag{18.61}$$

The surface term on the right-hand side of Eq. (18.61) can be expressed as [cf. Eqs. (18.5) and (18.32)]

$$\gamma_{\mathrm{GaN}} V_{\mathrm{m,GaN}} \frac{\mathrm{d}A_{\mathrm{GaN}}}{\mathrm{d}V_{\mathrm{GaN}}} - \gamma_{\mathrm{Ga}} V_{\mathrm{m,Ga}} \frac{\mathrm{d}A_{\mathrm{Ga}}}{\mathrm{d}V_{\mathrm{Ga}}} = \frac{\gamma_{\mathrm{GaN}} V_{\mathrm{m,GaN}}}{\rho} - \frac{2\gamma_{\mathrm{Ga}} V_{\mathrm{m,Ga}}}{r} \tag{18.62}$$

After substituting Eq. (18.62) into (18.61), we can write the final relation

$$\ln\frac{p_{\mathrm{N_2}}}{p_{\mathrm{N_2}}^{\infty}} = \frac{2\gamma_{\mathrm{GaN}} V_{\mathrm{m,GaN}}}{RT\rho} - \frac{4\gamma_{\mathrm{Ga}} V_{\mathrm{m,Ga}}}{RTr} \tag{18.63}$$

which allows us to calculate the equilibrium $T - p_{N_2}$ relation as a function of parameters ρ and r. Such a calculation was performed for a fix value of r = 1.5 nm and ρ = 2–50 nm. We used the following input data: the molar volume of GaN(s) $V_{\mathrm{m,GaN}} = 1.375 \times 10^{-5}\exp[1.551 \times 10^{-5}(T - 298.15) + 0.375 \times 10^{-10}(T^2 - 298.15^2) + 0.38952(1/T - 1/298.15)]$ [55], the molar volume of Ga(l) $V_{\mathrm{m,Ga}} = 69.723 \times 10^{-3}/[6077 - 0.611(T - 302.9)]$ [56], the surface energy of GaN(s) γ_{GaN} = 1928 mJ m^{-2} [57] and the surface energy of Ga(l) $\gamma_{\mathrm{Ga}} = 724 - 0.07$

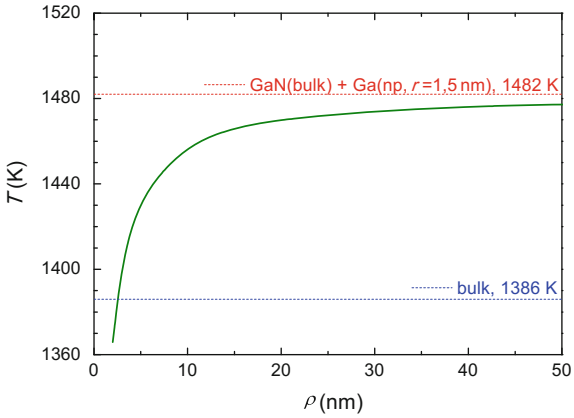

Fig. 18.6 Decomposition temperature of solid GaN nanowires of radius ρ (p_{N2} = 100 kPa) (Limiting value T = 1386 K stands for bulk equilibrium and T = 1482 K for equilibrium between bulk GaN and Ga(l) droplets of radius r = 1.5 nm)

(T − 302.9) mJ m^{-2} [58]. The dependence of decomposition temperature of solid GaN nanowires under 100 kPa nitrogen pressure on their radius ρ is shown in Fig. 18.6.

18.4 Conclusions

The surface terms of the Gibbs energy and chemical potential of spherical nanoparicles have been derived. The different multipliers, 3 and 2, occurring in the molar and partial molar quantity for spherical nanoparticles, respectively, result from the character of Gibbs energy surface term being a homogeneous function of the order 2/3 with respect to mole amount. For non-spherical nanoparticles, the respective shape factors α and α' can be introduced into the surface terms of Gibbs energy and chemical potential reflecting the A/V ratio and the variation of dA with dV relative to a sphere of the same volume. For a sphere and regular polyhedra, it has been demonstrated that $\alpha = \alpha'$ upon isomorphic changes in their surface areas, however, for more complex shapes such as long wire, this equality is not valid due to different degrees of homogeneity of the surface areas of a sphere and a long cylinder. Based on these geometry considerations, the equilibrium conditions for single- and multicomponent nanosystems have been expressed and applied to case examples involving solid–liquid (paracetamol–water) and solid–liquid–gas (GaN (s)–Ga(l)–N_2(g)) equilibria demonstrating the solubility enhancement and decomposition temperature depression with decreasing nanostructure size.

Acknowledgements This work was supported by Czech Science Foundation, grant number No. 13-20507S.

References

1. Goswami GK, Nanda KK (2012) Thermodynamic models for the size-dependent melting of nanoparticles: different hypotheses. Current Nanosci 8:305–311
2. Xue YQ, Zhao MZ, Lai WP (2013) Size-dependent phase transition temperatures of dispersed systems. Phys B 408:134–139
3. Li ZH, Truhlar DG (2014) Nanothermodynamics of metal nanoparticles. Chem Sci 5:2605–2624
4. Yang CC, Mai YW (2014) Thermodynamics at the nanoscale: a new approach to the investigation of unique physicochemical properties of nanomaterials. Mater Sci Eng R 79:1–40
5. Šesták J (2015) Kinetic phase diagrams as a consequence of sudden changing temperature or particle size. J Ther Anal Calorim 120:129–137
6. Eichhammer Y, Heyns M, Moelans N (2011) Calculation of phase equilibria for an alloy nanoparticle in contact with a solid nanowire. CALPHAD 35:173–182
7. Garzel G, Janczak-Rusch J, Zadbyr L (2012) Reassessment of the Ag-Cu phase diagram for nanosystems including particle size and shape effect. CALPHAD 36:52–56
8. Guisbiers G, Mejia-Rosales S, Khanal S, Ruiz-Zepeda F, Whetten RL, José-Yacaman M (2014) Gold-copper nano-alloy, "*Tumbaga*", in the era of nano: phase diagram and segregation. Nano Lett 14:6718–6726
9. Sim K, Lee J (2014) Phase stability of Ag–Sn alloy nanoparticles. J Alloys Compd 590: 140–146
10. Sopoušek J, Vřešťál J, Pinkas J, Brož P, Buršík J, Stýskalík A, Škoda D, Zobač O, Lee J (2014) Cu–Ni nanoalloy phase diagram—prediction and experiment. CALPHAD 45:33–39
11. Kroupa A, Káňa T, Buršík J, Zemanová A, Šob M (2015) Modelling of phase diagrams of nanoalloys with complex metallic phases: application to Ni-Sn. Phys Chem Chem Phys 17:28200–28210
12. Ghasemi M, Zanolli Z, Stankovski M, Johansson J (2015) Size- and shape-dependent phase diagram of In–Sb nano-alloys. Nanoscale 7:17369–17387
13. Bajaj S, Haverty MG, Arróyave R, Goddard FRSCWA III, Shankare S (2015) Phase stability in nanoscale material systems: extension from bulk phase diagrams. Nanoscale 7:9868–9877
14. Kaptay G (2012) On the size and shape dependence of the solubility of nano-particles in solutions. Int J Pharm 430:253–257
15. Du J, Zhao R, Xue Y (2012) Thermodynamic properties and equilibrium constant of chemical reaction in nanosystem: an theoretical and experimental study. J Chem Thermodyn 55: 218–224
16. Murdande SB, Shah DA, Dave RH (2015) Impact of nanosizing on solubility and dissolution rate of poorly soluble pharmaceuticals. J Pharm Sci 104:2094–2102
17. Navrotsky A (2011) Nanoscale effects on thermodynamics and phase equilibria in oxide systems. ChemPhysChem 2011:2207–2215
18. Chung SW, Guliants EA, Bunker CE, Jelliss PA, Buckner SW (2011) Size-dependent nanoparticle reaction enthalpy: oxidation of aluminum nanoparticles. J Phys Chem Solids 72:719–724
19. Kang SY, Mo Y, Ong SP, Ceder G (2014) Nanoscale stabilization of sodium oxides: implication for Na-O_2 batteries. Nano Lett 14:1016–1020
20. Li M, Altman EI (2014) Cluster-size dependent phase transition of Co oxides on Au(111). Surf Sci 619:L6–L10
21. Cui Z, Duan H, Li W, Xue Y (2015) Theoretical and experimental study: the size dependence of decomposition thermodynamics of nanomaterials. J Nanopart Res 17:321 (11 pp)
22. Hill TL (2001) A different approach to nanothermodynamics. Nano Lett 1:273–275
23. García-Morales V, Cervera J, Pellicer J (2005) Correct thermodynamic forces in Tsallis thermodynamics: connection with Hill nanothermodynamics. Phys Lett A 336:82–88

24. Turmine M, Mayaffre A, Letellier P (2004) Nonextensive approach to thermodynamics: analysis and suggestion, and application to chemical reactivity. J Phys Chem B 108: 18980–18987
25. Letellier P, Mayaffre A, Turmine M (2007) Solubility of nanoparticles: nonextensive thermodynamics approach. J Phys: Condens Matter 19:436229 (9 pp)
26. Letellier P, Mayaffre A, Turmine M (2007) Melting point depression of nanosolids: nonextensive thermodynamics approach. Phys Rev B 76:045428 (8 pp)
27. Qi WH, Wang MP (2004) Size and shape dependent melting temperature of metallic nanoparticles. Mater Chem Phys 88:280–284
28. Qi WH, Wang MP, Liu QH (2005) Shape factor of nonspherical nanoparticles. J Mater Sci 40:2737–2739
29. Tanaka T, Iida T (1994) Application of a thermodynamic database to the calculation of surface tension for iron-base liquid alloys. Steel Res 65:21–28
30. Tanaka T, Hack K, Iida T, Hara S (1996) Application of thermodynamic databases to the evaluation of surface tensions of molten alloys, salt mixtures and oxide mixtures. Z Metallknd 87:380–389
31. Picha R, Vřešťál J, Kroupa A (2004) Prediction of alloy surface tension using a thermodynamic database. CALPHAD 28:141–146
32. Tanaka T, Kitamura T, Back IA (2006) Evaluation of surface tension of molten ionic mixtures. ISIJ Int 46:400–406
33. Nakamoto M, Kiyose A, Tanaka T, Holappa L, Hämäläinen M (2007) Evaluation of the surface tension of ternary silicate melts containing Al_2O_3, CaO, FeO, MgO or MnO. ISIJ Int 47:38–43
34. Hanao M, Tanaka T, Kawamoto M, Takatani K (2007) Evaluation of surface tension of molten slag in multi-component systems. ISIJ Int 47:935–939
35. Egry I, Ricci E, Novakovic R, Ozawa S (2010) Surface tension of liquid metals and alloys—recent developments. Adv Colloid Interface Sci 159:198–212
36. Cahn JW (1980) Surface stress and the chemical equilibrium of small crystals—I. The case of the isotropic surface. Acta Metall 28:1333–1338
37. Jesser WA, Shneck RZ, Gile WW (2004) Solid-liquid equilibria in nanoparticles of Pb-Bi alloys. Phys Rev B 69:144121 (13 pp)
38. Cammarata RC (1997) Surface and interface stress effects on interfacial and nanostructured materials. Mater Sci Eng A 237:180–184
39. Cammarata RC (2008) Generalized surface thermodynamics with application to nucleation. Phil Mag 88:927–948
40. Cammarata RC (2009) Generalized thermodynamics of surfaces with applications to small solid systems. In: Egrenreich H, Spaepen F (eds) Solid state physics, vol 61. Elsevier, Amsterdam, p 1
41. Espeau P, Céolin R, Tamarit JL, Perrin MA, Gauchi JP, Leveiller F (2005) Polymorphism of paracetamol: relative stabilities of the monoclinic and orthorhombic phases inferred from topological pressure-temperature and temperature-volume phase diagrams. J Pharm Sci 94:524–539
42. Hendriksen BA, Grant DJW (1995) The effect of structurally related substances on the nucleation kinetics of paracetamol (acetaminophen). J Cryst Growth 156:252–260
43. Prasad KVR, Ristic RI, Sheen DB, Sherwood JN (2001) Crystallization of paracetamol from solution in the presence and absence of impurity. Int J Pharm 215:29–44
44. Omar W, Mohnicke M, Ulrich J (2006) Determination of the solid liquid interfacial energy and thereby the critical nucleus size of paracetamol in different solvents. Cryst Res Technol 41:337–343
45. Lerk CF, Schoonen AJM, Fell JT (1976) Contact angles and wetting of pharmaceutical powders. J Pharm Sci 65:843–847
46. Duncan-Hewitt W, Nisman R (1993) Investigation of the surface free energy of pharmaceutical materials from contact angle, sedimentation, and adhesion measurements. J Adhesion Sci Technol 7:263–283

47. Heng JYY, Bismarck A, Lee AF, Wilson K, Williams DR (2006) Anisotropic surface energetics and wettability of macroscopic form I paracetamol crystals. Langmuir 22: 2760–2769
48. Alander EM, Rasmusson AC (2007) Agglomeration and adhesion free energy of paracetamol crystals in organic solvents. AIChE J 53:2590–2605
49. Sedmidubský D, Leitner J (2006) Calculation of the thermodynamic properties of A^{III} nitrides. J Cryst Growth 286:66–70
50. Sedmidubský D, Leitner J, Svoboda P, Sofer Z, Macháček J (2009) Heat capacity and phonon spectra of $A^{III}N$. Experimental and calculation. J Therm Anal Calorim 95:403–407
51. Moon WH, Kim HJ, Choi CH (2007) Molecular dynamics simulation of melting behaviour of GaN nanowires. Scripta Mater 56:345–348
52. Wang Z, Zu X, Gao F, Weber WJ (2007) Size dependence of melting of GaN nanowires with triangular cross sections. J Appl Phys 101:043511 (4 pp)
53. Guisbiers G, Liu D, Jiang Q, Buchaillot L (2010) Theoretical predictions of wurtzite III-nitride nano-materials properties. Phys Chem Chem Phys 12:7203–7210
54. Antoniammal P, Arivuoli D (2012) Size and shape dependence of melting temperature of gallium nitride nanoparticles. J Nanomater 2012:415797 (11 pp)
55. Reeber RR, Wang K (2000) Lattice parameters and thermal expansion of GaN. J Mater Res 15:40–44
56. Assael MJ, Armyra IJ, Brillo J, Stankus SV, Wu J, Wakeham WA (2012) Reference data for the density and viscosity of liquid cadmium, cobalt, gallium, indium, mercury, silicon, thallium, and zinc. J Phys Chem Ref Data 41:033101 (16 pp)
57. Gomes MC, Leite DMG, Sambrano JR, Dias da Silva JH, de Souza AR, Beltrán A (2011) Thermodynamic and electronic study of $Ga_{1-x}Mn_xN$ films. A theoretical study. Surf Sci 605:1431–1437
58. Mills KC, Su YC (2006) Review of surface tension data for metallic elements and alloys: part 1—pure metals. Int Mater Rev 51:329–351

Chapter 19
Physico-chemical Analysis of Ceramic Material Systems: From Macro- to Nanostate

Vladimir Ya. Shevchenko

Abstract The historical aspects of ceramic production, as well as the modern approaches to the technical side of ceramic production, especially solgel technology as the path to modern nanotechnologies, are discussed. It is pointed out that the most essential significance of the nanostate for the applied sciences lies in the possibility of merging the inorganic, organic, and biological worlds, thus creating a prodigious number of new materials.

Glass and ceramics have been used in everyday life for thousands of years; they are a result of the industrial development of society. Ceramics is commonly referred to as the first industrial material. Some data on the overall production and consumption of various materials that have been created and that are presently produced in industrial society are listed in Table 19.1 [1].

Generally, ceramics comprises all materials based on the nonmetallic inorganic compounds produced by baking (firing), whereas glasses commonly imply substances in the amorphous metastable state. Among the artificial materials that are produced by the special treatment of natural raw materials or that have no natural analogs, ceramics occupies a special place. The main ceramics and glass technologies, the times of their advent, and the fields of human activity that changed drastically under the influence of the emerging new technologies are listed in Table 19.2 [2]. Egyptian faience was the first nonclay material, which was produced in Egypt and in the Middle East as long ago as about 4000 B.C. It consisted of a mixture of finely pounded quartz or sand, often with an admixture of lime, alkali metal oxides, and cuprate-based dyestuffs. Its optical properties significantly surpassed those of clay-based ceramics and could not be achieved in traditional pottery. In the history of the development of ceramics technology, it was the first step toward an artificial composition, and it fundamentally changed the methodology of ceramic materials science throughout the following time period.

V.Ya.Shevchenko (✉)
Institute of Silicate Chemistry of Russian Academy of Sciences,
nab. Makarova, 2, Saint-Petersburg 199034, Russia
e-mail: shevchenko@isc.nw.ru

J. Šesták et al. (eds.), *Thermal Physics and Thermal Analysis*,
Hot Topics in Thermal Analysis and Calorimetry 11,
DOI 10.1007/978-3-319-45899-1_19

Table 19.1 Production and consumption of the products of industrial society

Materials	Produced from	Production level today, millions of tons	Raw materials	Products
Wood (natural organic composite)	3,000,000 BC	Up to 5000	Reproducible, geographically limited	Building materials
Ceramics (nonmetallic inorganic materials including cements)	10,000 BC	10,000	SiO_2, Al_2O_3, CaO, MgO, Fe_2O_3, etc., everywhere	Porcelain, faience, insulators, refractories, optics, building materials, components for mechanical engineering, etc.
Metals	5000 BC	Iron, up to 500; other, <500	Ore, geographically uneven	All possible goods
Polymers	~1900	100	Oil	Containers, films, tars, etc.
Artificial composites	~1950	1	Mineral and organic raw materials	Machines and mechanisms
Semiconductors, ferroelectrics, etc.	~1940	0.01	Crystals and structures	Electronic

Metallurgy, which originated in the early thirtieth century B.C., employed ceramic materials for the fireclay lining of smelting furnaces, casting molds, and crucibles. Further extension of the variety of metal alloys called for the creation of new refractory materials. Some modern refractories have approximately the same composition as the refractories of ancient Rome and the *Middle Ages* (Fig. 19.1) [3].

Dating back to the times of the craftsmen of the *Bronze Age*, glass technology survived the technical revolution in the second century B.C. that gave rise to the development of new industrial technology for the mass production of glassware for all social strata of the Roman Empire and that spread out overall.

The achievements of Roman engineers, who created the technology of concrete for building blocks and producing structural elements, are impressive as well (Table 19.3) [4]. This led to the flourishing of civil engineering and the formation of townships. Chinese porcelain (celadon) also has a long history (Table 19.4) [5]. Its advent and improvement exerted a perceptible influence on the progress of civilization. Investigations in this field were begun more than 2000 years ago, and they still proceed today thanks to the infinite diversity of chemical processes in multicomponent silicate and oxide systems. Chinese porcelain was exported to many countries, including Egypt, Syria, and Turkey, where it was a household article of prosperous people. Let us recall a legend about Marco Polo, who brought a small porcelain bottle known as the "*Medici bottle*" when he returned to Venice in 1295. Possibly this was the first Chinese celadon article imported to Europe. Later,

Table 19.2 Methods of Egyptian faience manufacture by period and site

Period	Body manufactory	Glaze process	Factory evidence	Faience examined from these sites
Predynastic (4000–3100 BC)	Modeling a core for grinding	Experimental period	None	Naqada, Badari, El Amrah, Matraar, Harageh, Abadiya, Gerza
	Surface grinding	Application (?) Beck, Petrie)		
	Free-form modeling (rare)	Cementation		
		Efflorescence (?) (Binns)		
Protodynastic (3100–2686 BC)	Modeling Surface grinding Painting with slurry	Efflorescence	None	Hierakonpolis, Saqqara, Abydos, Bammamiya, Mahasna, Qau, Matmar, El Kab, Armant
Old kingdom (2686–2181 BC)	Layering (rare) Forming on a core (rare) Marbleizing (rare)			
I intermediate (2181–2040 BC)	Molding (?)			
Middle kingdom (2133–1786 BC)	Modeling molding on a form Forming on a core	Efflorescence (Noble) cementation (Kiefer and Allibert)	Kerma Lisht	Abydos, Kerma, El Kab, Haraga, Beni Hasan, Mostagidda
II intermediate (1786–1567 BC)	Marbleizing Layering Painting with a colored quartz slurry Incising Inlaying Resisting Painting with a pigment wash	Application as a liquid (Reisner)		
New kingdom (1568–1085 BC)	Molding on a form Pressing into open-face molds	Efflorescence Application as a liquid Finely powdered glass added to body or inlay	Amarna	Amarna, Abydos, Serabit el Khadim,Yahudiya, Lahun, Nebesha, Medinet, Ghurob, Akhmin

(continued)

Table 19.2 (continued)

Period	Body manufactory	Glaze process	Factory evidence	Faience examined from these sites
	Forming over a core Joining of molded parts with quartz slurry Layering Incising Inlaying with a quartz slurry Painting with pigment wash Throwing (?)	to extend color range (Kühne)		
Later periods (1085 BC–30 AD)	All new kingdom techniques and throwing (?)	Efflorescence Application as a liquid	Memphis Naucratis	Memphis, Abydos, Thebes, Giza, Matmar, Saqqara

? Hypothesis about this fact or method

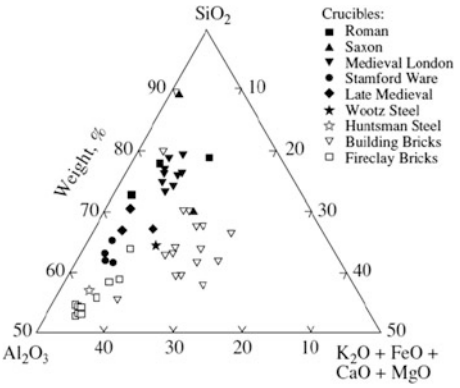

Fig. 19.1 Bulk compositions of crucibles compared with modern fireclay bricks and clay building blocks [3]

the import of celadon grew continuously and increased up to the eighteenth century. Meanwhile, persistent attempts by European craftsmen and researchers to reproduce the porcelain composition did not cease. It was not until as late as 1708 that the famous German alchemists *Chirnhaus*, *Pabst*, and *Böttger* from Meissen succeeded in obtaining firm white porcelain of a quality comparable to that of Chinese items. It is worthwhile to commend the role of *King Augustus of Saxony*, who lavishly sponsored not only the investigations of chemists but also the construction of a porcelain works that was enormous for that time. This fundamentally changed the economy of Saxony. France and England followed Saxony's example and thereby became prosperous exporters of porcelain (Fig. 19.2) [6].

Table 19.3 Macroscopic description of selected Roman cement-containing materials

Sample	Mortar matrix	Aggregate
Concrete wall Hadrian's tomb	Coherent, carbonated >20% (including ash <0.5 mm)	1. Trachytic tuff, rounded, vesicular to dense, 5–10 mm <70% 2. Volcanic ash, <1 mm, <10%
Rome ~139 AD Concrete wall Terme Caracalla	Coherent, carbonated >30% (including ash <0.5 mm)	1. Trachytic tuff, rounded 5–15 mm 2. Volcanic ash, <1 mm, >10%
Rome ~212 AD Concrete Forum	Mod. coherent to crumbly, carbonated >20% (including ash <0.5 mm)	1. Trachytic tuff, rounded angular, dense to vesicular, <5 mm, <60%
Rome ~60 AD Concrete wall Theater	Coherent, carbonated >20% (including ash <0.5 mm)	2. Leucite, feldspar, augite crystals <1 mm, >20%
		1. Trachytic tuff, rounded to angular, vesicular, 5–15 mm, >60%2 2. Leucite, augite crystals up to 1 mm, >10%
Ostia 200–300 AD		3. Volcanic ash, <1 mm, <10%

Table 19.4 Characteristic features of different Chinese celadons

Yue wares	Eastern Han-Tang dynasty 25–907 AD	The bodies are light gray in color, the body section is dense and vitrifiable, the glaze color is mugwort-leaf green, the surface is much brighter and with some small cracks, and the glaze thickness is thinner (~0.1–0.2 mm)
Fengsi's grave green ware	North dynasties 386–581 AD	The body is gray–white in color, the body section is dense and vitrifiable, the glaze color is green with a slight yellow cast, and the glaze layer is thicker (~0.25 mm)
Jiabi ware	Sui dynasty 581–618 AD	The body is gray–yellow in color, and the section is not sufficiently vitrified, but the glaze color appears green
Yixing ware	Tang dynasty 618–907 AD	The body appears deep gray in color, some little pores can be seen, the glaze color appears greenish yellow, and its thickness is ~0.2 mm
Yaozhou ware	North Song 960–1126 AD	The body is gray–white in color and is very dense, the glaze is olive green and bright, clear with much smaller cracks, and its carving pattern decoration especially is very fine
Ru ware	North Song 960–1126 AD	It is one of the five famous kilns of the North Song dynasty, but its body is not sufficiently vitrified, with a light gray color; the glaze is bright and clear with a greenish color, and the glaze thickness is ~0.6 mm
Linru ware	North Song 960–1126 AD	Although it was located in the same area as the Ru kiln site, their stiles are different. Its body is very dense

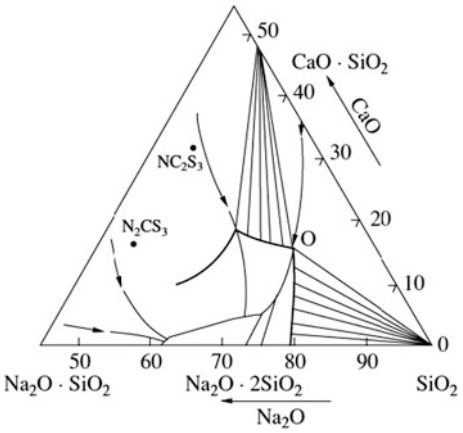

Fig. 19.2 Equilibrium phase diagram for the system Na_2O–CaO–SiO_2 illustrating the location of a typical French softpaste porcelain [6]

It can be seen from the presented data that practically all the mentioned technologies are based on the dissolution (hydration) and subsequent drying (firing) of a mixture of natural raw materials consisting mainly of metal oxides with additives of some other oxide mixtures for coloring and glazing purposes. Suitable compositions were selected for hundreds of years from the mineral raw materials in the nearest area and, of course, without any chemical analysis. Practically all of the minerals were assessed organoleptically.

A new stage in the development of these technologies came in the *Middle Ages*, when the Age of Alchemy began.

The old alchemy was not only deception and delusion. Proceeding from ancient notions of the unity of matter and basing their work on *Aristotle*'s doctrine of four basic elements (fire, air, water, and earth), the alchemists tried to separate, from the infinite diversity of substances, each elemental matter as the embodiment of some "basic" property or quality. For instance, according to their doctrines, mercury was assumed to correspond to the metallic luster property, sulfur to inflammability, and salt to indestructibility.

Alchemists observed a continuous disappearance of one substance and the appearance of another substance in its place. They saw how lead originated from litharge and mercury originated from cinnabar, neither of which look like metals at all. They had no reason to think that obtaining gold from lead is less possible. Their thinking was directed toward a search for the mystic "*philosopher's stone*," the possession of which allowed one to control all the transmutations of substances and to convert ordinary metals into gold, as well as to eliminate all evil diseases occurring from "evil elements."

Alchemy was closely woven with astrology and kabbalistic study. Alchemists were quite sure that all the substances being obtained, especially metals, and their transmutative abilities are in mysterious relationships with various forces and elements hidden in nature. Mercury was assumed to symbolize femininity, and sulfur,

masculinity. The Sun corresponded to gold, the Moon to silver; Venus meant copper; Mars, iron; Jupiter, tin; Saturn, lead; and Mercury, quicksilver.

The knowledge of alchemists was imparted in the darkness of secluded laboratories, among bizarre retorts, dried herbage, skeletons, and parchment books covered with mysterious signs and symbols borrowed from various Orient cults strangely mixed with the Christian religion. Dragons, snakes, ravens, and peacocks symbolized various substances and properties. Such "chemical" signs as planet symbols designating various metals were still in use in *Lomonosov*'s time (Tables 19.5 and 19.6) [7].

Tireless searching for the "philosopher's stone" required the alchemists to test everything that can be seen on the Earth's surface, found hidden in its bowels, or produced by flora and fauna. They made many observations and wonderful discoveries. They obtained sulfuric, nitric, and hydrochloric acids; potash; caustic; and iron vitriol. They brought into laboratory practice chemical furnaces, steels, filtrating, precipitation, and crystallization. But they worked at random and on the off chance.

The Age of Alchemy was concluded by the laying of the foundations of modern chemistry. This is colloidal chemistry, whose principles were first formulated by Ebelmen [8] and Graham [9] in the middle of the nineteenth century.

It will suffice to point out that, for instance, the absence of crystal forms, the presence of jellylike solid masses, the transition into solutions, and the setting up from those are, incidentally, the attributes of live organisms and, at the same time, characteristic features of colloids. Therefore, the study of colloids, especially those that originate from inert matter, is obviously the subject of highest importance for studying organisms. The general concept relating to this subject was formulated by *Graham*. Though the transition of silica into soluble and insoluble or jellylike states was known much earlier (for example, see [8]), he is renowned for his

Table 19.5 Working log of M.V. Lomonosov, 1751 (precipitation of colloidal gold)

(1) Solut. ʘ in ♀cum ☋multa aqua diluta praecipitata alcall animato dedit tincturam rubram coloris granati, quae per noctem subsedit in pulverem rubrum, ipsa flava facta
(2) Eadem solutio diluta pariter, primo cum calce Stannl eluta et in ♀eadem soluta affunderetur, turbabatur quidem et albes-cebat ad momentum, sed praecipitatum nullum promittebat at affuso alcali animato, statim viridis evasit pellucida 1-mo, tandem turbida et opaca. per noctem subsedit ⌣ tum liquor supra erat viridis
(3) Eadem liquore Stanni turbida flava
(4) Eadem ⌣ solutione cinerum clavellatorum turbida iactescens subflava
(5) Eadem ⌣ ta Wismuto in ☿fixo soluto. Nullae quidem turbae, sed solutio ad prasinam accedebat
(6) Eadem ⌣ ta Zinco in ϕ fixo soluto. Solutio statum evasit flavens turbida. Calida aqua erat
(7) Eadem ta solutione ♂ is in ϕ fixo. Nullae fere mutationes

Table 19.6 Working log of M.V. Lomonosov, 1751 (precious glaze of fine quartz and clays from Gzhel and Moscow)

	Massa ad vasa murrhea	Encaustum	Color encausti
1	∇Gzel. ex filtro p. I, cryst. subt. p. II		
2	----------p.I---------- p.III		
3	----------p.I---------- p.IV		
4	----------p.I*---------- p.II		
5	----------p.I---------- p.III		
---------- 1			2+
6	----------p.IV----------p.IV----------	2	2+
7	∇ Gzel. inspiss p. I, cryst. subt. p. II		
8	----------p.I---------- p.VI	8	2+
9	----------p.I---------- p.IV		2
10	----------p.I, cryst. rud. p. II		
11	----------p.I----------rudior p. III	9	
12	----------p.I---------- p.IV		
13	p I, cryst. Subtilissimae p. IV		
14	∇Mosqu. insp. p. I, cryst. subt. p. I3	3	2++
15	----------p.I---------- p.VI	4	2
16	----------p.I---------- p.IV		
17	----------p.I, cryst. gross. p. II		
18	----------p.I---------- p.VI		

generalization of such phenomena and for revealing the general rules that underlie such transitions. Thus, within the last decade, the origin of all research into organic substances forming the contents of animal bodies and plants was newly established. In this respect, silica (as well as alumina, tungsten hydrate, and so forth), with its easily occurring metamorphoses, will forever remain a typical subject for its simplicity and huge prevalence in nature.

Let us cite an excerpt from Mendeleev's work [10]. It does not seem plausible that the absence of crystallization should be considered the indication of colloids, because there are a lot of crystalline substances yet between them (hematocrystalline of proteins and tridymite of silica) and especially because there is only a quantitative rather than a qualitative difference between one and another. The difference between silica and quartz, which have specific weights of 2.2 and 2.6, respectively, does not at all mean that the former should be considered colloid and the latter should be considered crystalloid; it possibly means only that one of them is less polymerized. The difference between colloids and crystalloids should be rather sought only in the fact that the particles of the former have almost equal attraction in various directions, while those of the latter differ in attraction [10].

From the purely chemical point of view, colloids are of interest in various respects, which it would not be amiss to mention once again: All the colloids seem to be substances of complex composition; the particles are heavy in weight; they are large in size (alumina), and hence, they do not penetrate through membranes; they can be easily subjected to modifications of their chemical and physical properties; and they do not have an exact value of a chemical potential. All of the features mentioned above encourage special chemical interest in colloids.

Let us consider, for instance, pyroxene or augite. Its composition can be expressed by the formula $CaMgSi_2O_6$; i.e., it corresponds to hydrate H_2SiO_3, namely the bisilicate. It is very similar in various respects to another mineral referred to as lithium spoudumene, which has the composition $Li_6Al_8Si_{15}O_{45}$. Both minerals belong to the monoclinic system; the angles between the axes are 73° and 69°; the angles of prism inclining are 87°5′ and 87°; the specific weight of pyroxene is 3.4 and that of spoudumene is 3.18. Having reduced the formulas of both minerals to the equivalent content of silicon, one sees the following difference:

Lithium spoudumene	$Li_{12}Al_{16}Si_{30}O_{90}$
or	$(Li_2O)_6(Al_2O_3)_8 30SiO_2$;
Augite	$Ca_{15}Mg_{15}Si_{30}O_{90}$ or $(CaO)_{15}(MgO)_{15}30SiO_2$.

This means that all the difference is in the fact that the sum of magnesia and lime $(MgO)_{15} + (CaO)_{15} = 1440$ is substituted by the sum of lithium oxide and alumina $(Li_2O)_6 + (Al_2O_3)_8 = 1002.4$, and such sums are equal in a chemical sense because magnesium and calcium are intermediate between lithium and aluminum with due account of all the relations and in terms of oxidation forms and alkali power. Thus, the first sum may be substituted for the second sum.

Let us consider another purely empirical example. Augite from *Saal* contains 54.86 SiO_2, 0.21 Al_2O_3, 0.44 FeO, 0.42 MnO, 16.49 MgO, and 23.57 CaO. Similar

augite from *Vesuvium* contains 50.90 SiO_2, 5.37 Al_2O_3, 6.25 FeO, 14.43 MgO, and 22.96 CaO. The first one contains more silica, lime, and magnesia, while the second one, on the contrary, contains more alumina and iron protoxide. However, the sums may be equal to each other in the chemical sense.

It is necessary to mention briefly another kind of widely used silica compounds, namely cements (concretes). Ordinary lime and its mixture with sand, called in practice mortar or whitewash, is washed away by water, at least in the freshly prepared state. After some time, water destructs the cement formed by ordinary lime. However, some lime grades yield mortars that are not washed away by water and that are hardened under water. Generally, this is not characteristic of a mixture of lime with sand. Obviously, such hardening under water depends on the chemical composition of the mixture, which, in turn, depends on the origin of the source materials. Such lime grades are referred to as hydraulic lime or hydraulic cements. Incidentally, in technical terms, one should distinguish the proper hydraulic lime, which brings about mortar hardening under water, and cements, which usually make the mortar capable of hardening when mixed with lime. The hydraulic properties of lime are governed by admixtures of silica and alumina compounds. This is best proved in the method of artificial cement preparation. Lime should be taken mixed with clay ($\sim$25%), and the mixture should be subjected to some firing, so that the batch is not sintered but it loses the carbonic acid water that was contained in the clay. Such a batch, ground if it previously was homogeneous, forms a cement that hardens under water. The hardening process possibly involves the formation of chemical bonds between lime, silica, alumina, and water.

The theory and modern methodology of the solgel processes have been developing since the 1930s [11–13]. It is worthwhile to give modern definitions of sol and gel.

Sol (a colloidal solution) is a liquid colloidal system with particles of the dispersed phase (micelles) moving freely and independently of each other in Brownian motion. Sols with an aqueous dispersed environment are referred to as hydrosols, and those with an organic environment, as organosols.

Gel (from the Latin word *gelo*—to thicken) is a dispersed system with a liquid dispersed environment, in which the particles of the dispersed phase form a spatial network. Gels possess some solid-state attributes, i.e., form preservation ability, strength, and plasticity. Typical gels are formed, for instance, by sticking together the particles of sols, and they resemble jellylike sediments. By drying the gels, fragile microporous solids are produced, which are referred to as aerogels (silica gel, alumogel, etc.).

The generalized chemical formulas of solgel processes can be represented as follows:

The scheme of the general solgel process is shown in Figs. 19.3, 19.4, 19.5 and 19.6.

The solgel reaction is one of the best methods for preparing powders for technical ceramics among the methods from ancient inorganic chemistry and alchemy of ceramics that paved the way for modern nanotechnology (Figs. 19.7 and 19.8).

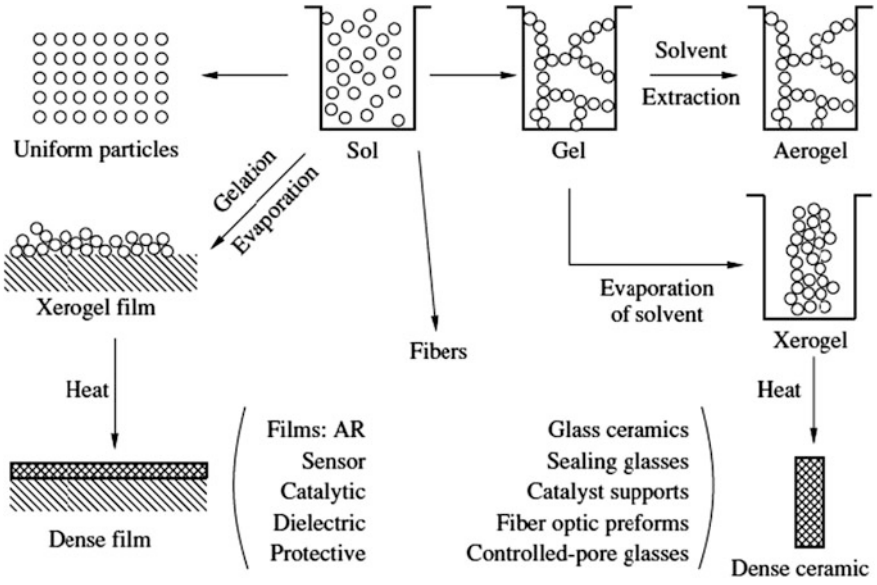

Fig. 19.3 Overview of the solgel process [11]

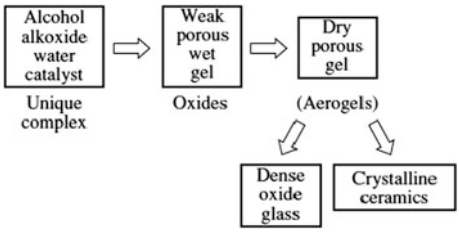

Fig. 19.4 Simplified overview of the first generation of the solgel process [12]

The nanostate problem is not new for materials science. *Zsigmondy* and *Svedberg* were the first scientists to be awarded *Nobel Prizes* (in 1925 and 1926, respectively) for important achievements in the chemistry of dispersed (nano) systems. To date, more than ten chemists have won *Nobel Prizes* for different aspects of research into the nanostate. The contribution of chemists in solving the nanostate problem is more essential than that of physicists. Along with scientists working in the field of inorganic chemistry, those involved in organic chemistry and biochemistry should be highlighted. Over the past seventy or eighty years, chemists have synthesized hundreds of fundamentally different kinds of nanoobjects, including particles, materials, and structures. These include centaur particles, coacervates, tactoids, phasoids, allophanes, giant icosahedral clusters, fullerenes, fumaroids, and nanotubes. It is important to note that all this diversity of forms exists within a limited size range (nanosizes) or consists of nanosized structural elements. Entering the nanoscale domain resulted in the discovery of many new

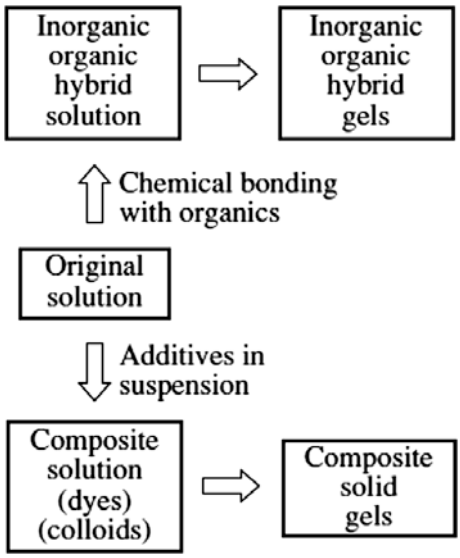

Fig. 19.5 Simplified overview of the second generation of the solgel process [12]

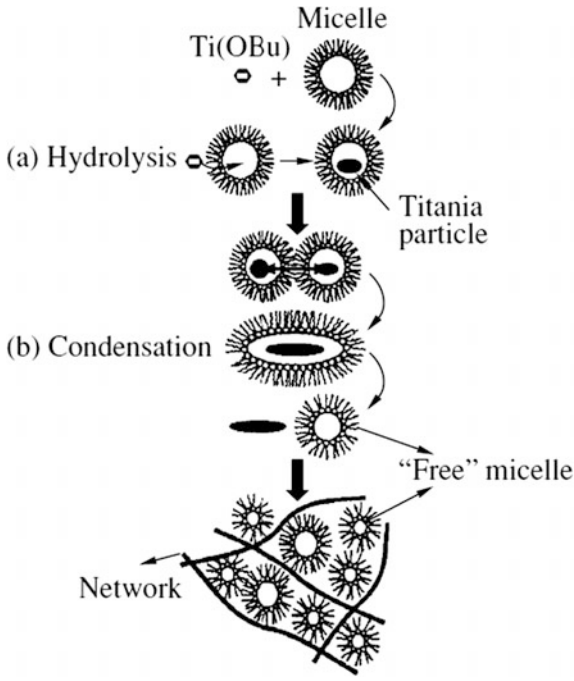

Fig. 19.6 Scheme of the solgel process in reverse micelles [13]

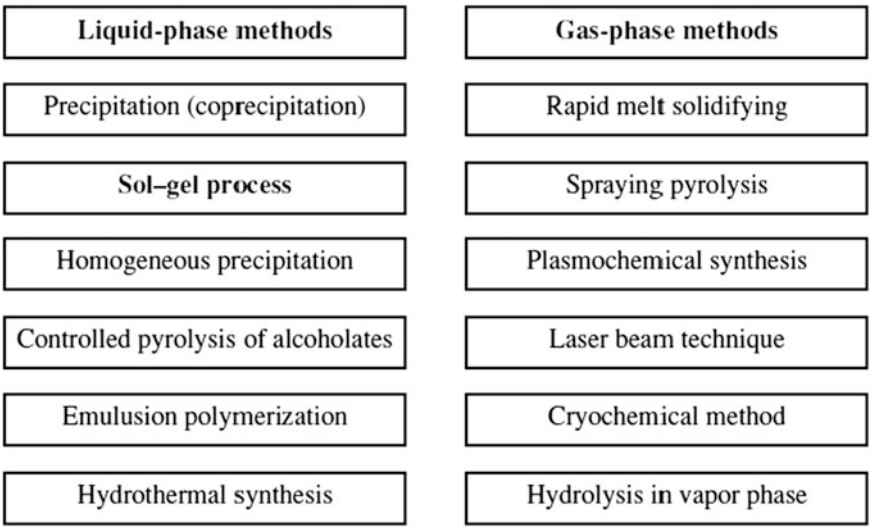

Fig. 19.7 Chemical methods of preparation of powders for technical ceramics

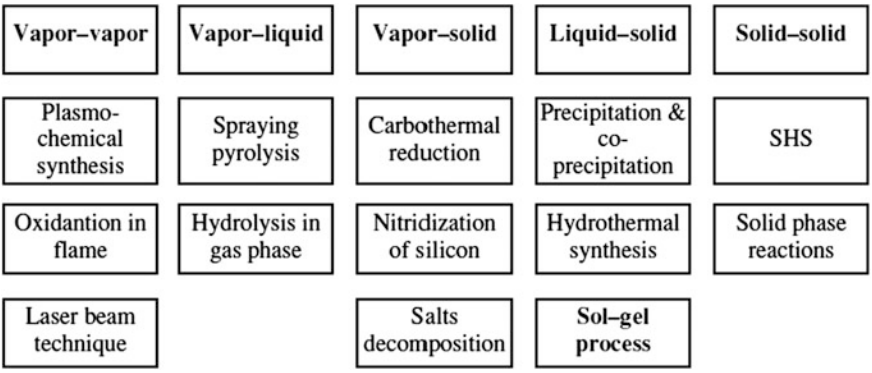

Fig. 19.8 Powder synthesis methods

structure types in inorganic chemistry that do not comply with the unshakeable macroworld laws of classical (generalized) crystallography [14–19] (Fig. 19.9). For example, screw axes of the fractional order are allowed [20] (Fig. 19.10).

Nanoparticles are characterized by quite different structural elements, such as one-, two-, and three-dimensional and fractal fragments and their various combinations. This brings up the following question: What is the cause of this diversity of structures in the nanoworld? The answer to this question can be found in the quantum nature of nanostates and in the specific statistical laws dominating the nanoworld. Owing to the developed surface, nanosystems are far from equilibrium.

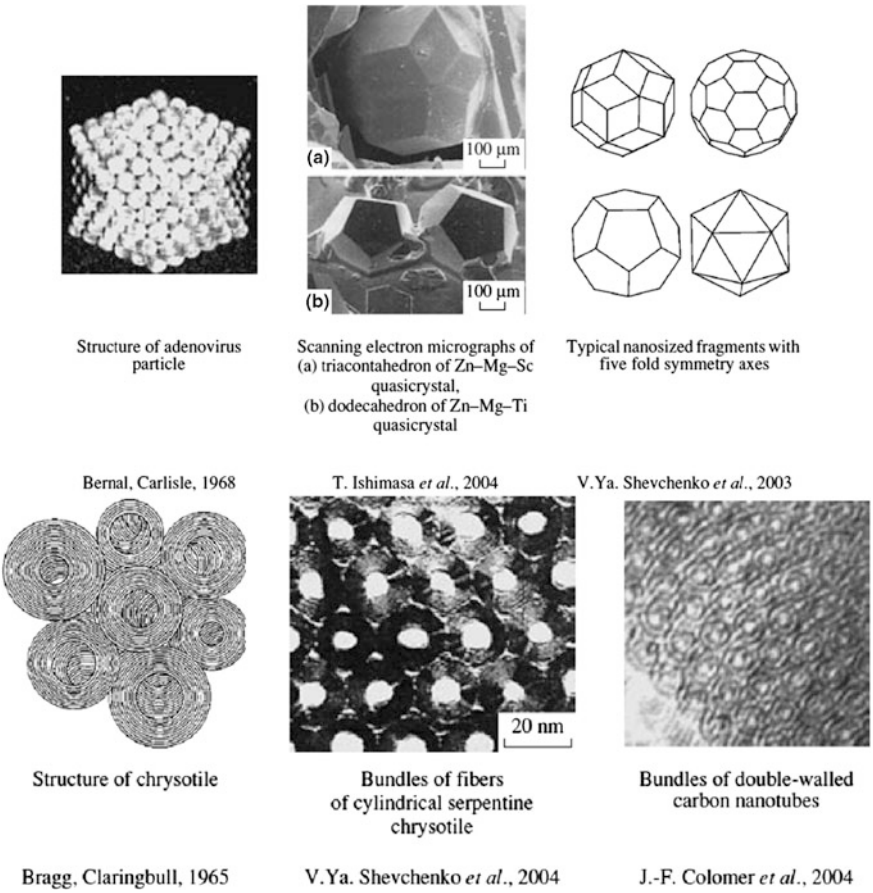

Fig. 19.9 Nanosize particles and structures that do not correspond to classical (generalized) crystallography [14–19]

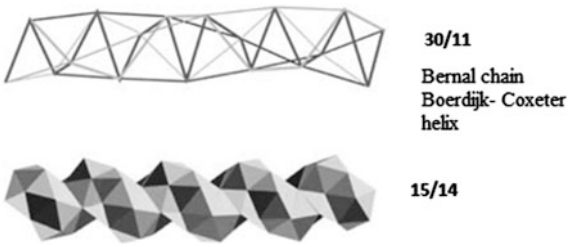

Fig. 19.10 Fractional order axes

Atomic sites in the vicinity of the surface differ geometrically and physically from those in the bulk of the crystal. The composition of a surface layer does not correspond to the stoichiometric composition of the chemical compound. The structural modulation can extend over a depth of several monatomic layers. These

effects suggest the existence of nonindependent surface phases and their pseudomorphic conjugation with the internal region of the particle.

The abatement of the restrictions of regular translational symmetry leads to the appearance of icosahedral packings with pentagonal symmetry for the inorganic particles. *Centaur* nanoparticles with coherent interfaces between various structure fragments of "incompatible" symmetry are also being realized [21]. To imagine how this happens, one can use the artistic outlines that wend their way into the fantastic (and now real) world of metamorphoses developed by the outstanding Dutch graphic artist Escher [22]. In his woodcut "*Metamorphoses*," one can see the gradually changing symmetry by step-by-step translation (Fig. 19.11).

The multivariance of nanostructures and nanoparticle states determines the accidental nature of their formation and implies the time dependence of the system parameters. To analyze the nanostate theoretically, one has to overcome the difficulties of its conceptual character. It is important that they are known. The *Wadsley–Andersson* paradigm implies, for example, that disordered arrays of blocks of ordered structures may be joined as in simple compounds (e.g., by corner or edge sharing) [23–25] (Fig. 19.12). Our "*centaur*" paradigm implies coherent joining and cross-linking of various fragments within the framework of the curved space formalism [14, 15, 26] (Fig. 19.13).

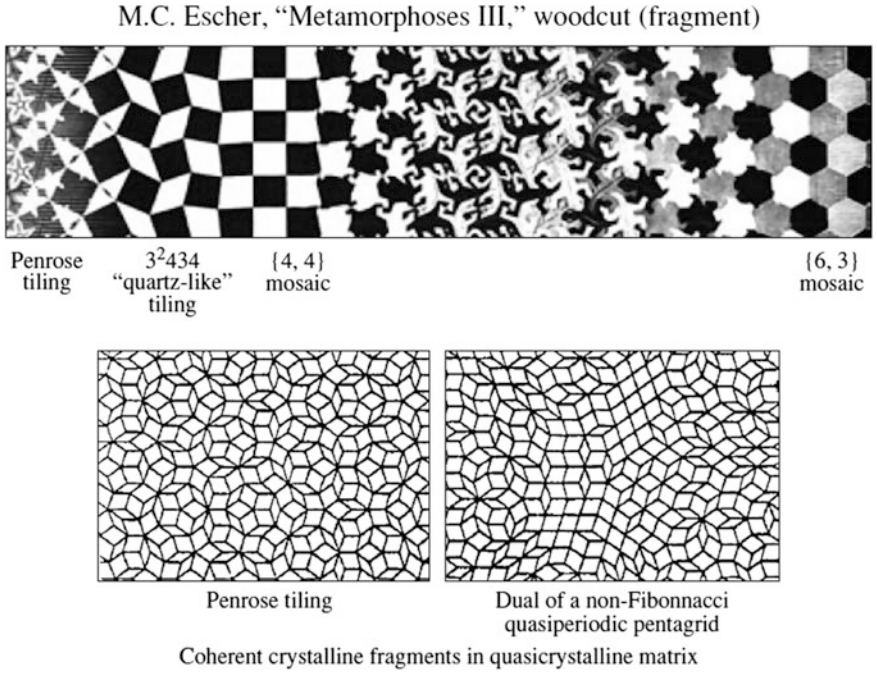

Fig. 19.11 Metamorphoses

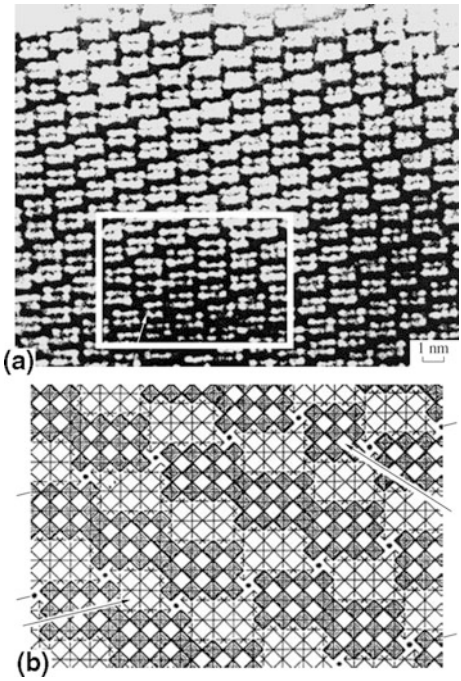

Fig. 19.12 Block structure of $TiO_2 \cdot 7Nb_2O_5$ (*arrows* indicate the presence of isolated 3 × 3 blocks in the matrix of 4 × 3 blocks) [25]

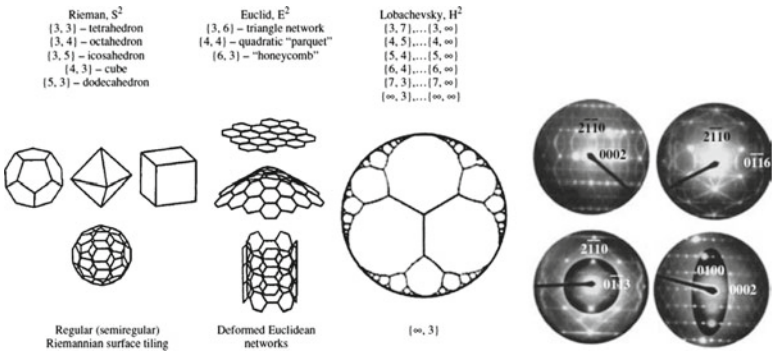

Characteristic curved (hyperbolic) diffuse intensity distribution for SiO_2-tridymite [26].

Fig. 19.13 Curved space formalism

The *Nobel Prize* winner *Feynman* said in 1959 that "there is plenty of room at the bottom," pointing out that, in the range of small sizes, there is much of interest. Many people suppose this comment to be the starting point of the ***Nano Age***. It does not hold true all the same.

Another *Nobel Prize* winner, *Prigogine*, said in 1977 that "we know now where the door is to this room."

The methods of high-resolution transmission electron microscopy and femtosecond spectroscopy have been being developed during the last 20 years for the investigation of chemical and physical processes. They make it possible to investigate the nanostate with open eyes and to determine many of its properties, which permits the next step to be made, that is, to move on to nanotechnologies. Let us assert that the door to Feynman's room is now open. (But there is surprisingly no light therein).

It was shown for the first time in [27] that structurally inhomogeneous zirconia nanoparticles consisting of interpenetrating fragments of different symmetries obey orientation relationships that are "incompatible" in terms of classical crystallography. We refer to the regularly oriented joining of structural fragments of various symmetries for which the rigorous requirements of classical crystallography are violated as centaur particles (nanostructures with coherent interfaces). This means that the interface between fragments does not need to be a plane, the orientation relationship does not need to be rational, the joining fragments are not necessarily crystalline fragments, etc.

From an analysis of the selected area electron diffraction patterns (SAED) and direct observations of structurally inhomogeneous ZrO_2 particles by high-resolution transmission electron microscopy (HTREM) [27], we have ascertained that structural inhomogeneity is the fundamental feature of the nanostate. There are a lot of experimental results confirming this principle for various materials. For example, the oriented noncrystallographic joining of the cubic and icosahedral phases in metallic alloys was observed in [28], whereby the interface was found to not be a plane and the rigorous orientation relationship was established to be irrational in both cubic and icosahedral indexing systems.

The local diffraction patterns from an individual nanoparticle represent the result of putting together two or more arrays of diffraction spots, namely the convolution of the corresponding reciprocal space mappings. Such nanoparticles are basically nonclassic. At the same time, the explanation of diffraction patterns is usually based on classical crystallography. Such a consideration reduces the description of the phenomenon to a simple superposition of diffraction patterns of two or more classical crystal phases. This basically contradicts the definition of the centaur nanoparticle as a single whole.

The spatial transitions from a region of some local symmetry to another region of a different symmetry can be considered as an example of the metamorphoses illustrated by the well-known woodcut by Escher (Fig. 19.11). The metamorphoses in a structure consisting of intergrowing fragments with various symmetries cannot be described by any Fedorov group. In Escher's graphic work, it is possible to distinguish the following fragments: one of the modifications of two-dimensional Penrose tiling, $\{3^2434\}$ tiling, various modifications of the regular *Euclidean mosaic* {4, 4}, various modifications of the mosaic {6, 3}, and transition layers. A nanoparticle with similar structure can be treated as a regular joining of the icosahedral, cubic, and hexagonal phases by coherent, but not plane, interfaces.

The depicted structure is built up of clusters, and it is possible to pinpoint the center for each of them. This structure can be interpreted as a set of points, which together form a base loaded with clusters (layers) so that the transition from one base point to another ensures cross-linking of the corresponding layers. Such an interpretation corresponds to the most simplified definition of the stratificated space as a special structure in terms of algebraic geometry, which is the mathematical basis of the "local" approach [29]. Within the framework of the local approach, the condensed structure (not necessarily crystalline) is considered to be built up from a set of special generating clusters, whereby the cross-linking rules are defined by the clusters themselves and by the space topology. The local approach is the basis of the generalized crystallography of the condensed state, which involves the formalism of an algebraic geometry that is more general than Euclidean geometry and includes classical crystallography as the limiting case.

A dodecahedron represents the regular map {5, 3} on a sphere (three pentagons join at each vertex) (Fig. 19.14). A decacycle represents a *Petrie polygon* (a consequence of the graph edges, for each of which two rather than three neighboring edges belong to a common side). Six decacycles embracing all 30 edges and 20 vertexes are isomorphic to the $\{10, 3\}_5$ map (the map closes into itself after five steps along the Petrie polygon) representing the tiling of the nonoriented (like the Mobius strip) surface. The $\{10, 3\}_5$ map is allomorphic to the $\{10, 3\}_5'$ map arising after the 2π disclination. Both are substructures of the incidence graph of the famous Desargues configuration in the projective geometry. All of these pure geometrical configurations correspond to the frequently occurring generating clusters in regular and defect crystals, structures of gas hydrates, *Frank–Kasper phases*, *quasicrystals*, etc.

Thereby, the mechanisms of the structural transitions between various structures can be described and predicted.

The model of a nanostructure with coherent interfaces between crystalline and quasicrystalline fragments is shown in Fig. 19.14. Thus, crystalline, diamond-like,

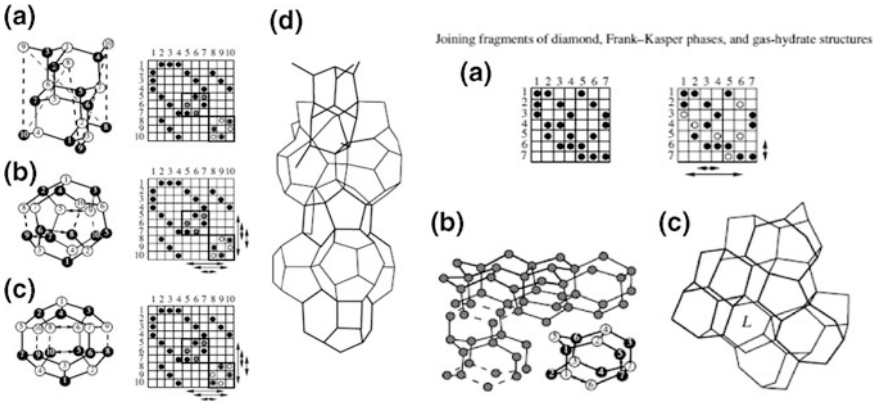

Fig. 19.14 Stratified space geometry

gas hydrate, quasicrystalline, and other structural fragments can be joined together without dangling bonds and without ruining the local symmetry.

So, what does one now mean by nanotechnologies? Formally, its elements are subjects with a characteristic size R in at least one direction that is comparable to 1 nm. Actually, the scope of the subjects and phenomena under discussion is much broader—from single atoms ($R < 0.1$ nm) to their agglomerates and organic molecules containing more than 10^9 atoms and that are as large as >1 μm in one or two dimensions. For various reasons (purely geometrical and physical), along with the decreasing size, the characteristic times of various processes occurring in the system decrease as well, and the potential processing speed increases. This is very important for electronics and computing. The achievable processing speed for typical computers is presently about *1* ns (10^{-9} s) per elementary operation, but it may be still shorter for some nanostructures.

It would be naive to suppose that nanosized objects and related processes were not used before the *Age of Nanotechnologies*. Biochemical reactions of macromolecules, of which all animate nature consists; photographic image processing; catalysis in the chemical industry; fermentation processes in wine, cheese, and baking; and many other processes proceed at a nanolevel scale. The "intuitive nanotechnology" that was first developed spontaneously without proper understanding cannot lay a reliable foundation for the future. Consequently, basic research that aimed at the development of new technological processes and products is of highest significance. Perhaps nanotechnologies will supersede some obsolete and ineffective technologies, but their most important application lies in new areas where traditional methods are basically inapplicable.

In between the macrolevel field on the one hand, in which the well-developed continual theories and computational methods of engineering run perfectly, and the quantum mechanical atomic level on the other hand, there is the huge and not yet settled vast field of mesahierarchical matter structure (mesos, from the Greek for middle, intermediate). At this level run important biochemical processes involving macromolecules of DNA, RNA, proteins, ferments, subcell structures, etc., which call for more profound understanding. Unprecedented products and technologies can thereby be created, which will be able to radically change life in human society. At the same time, there will be no need to spend raw materials, energy, and transport resources; industrial waste and pollution of the environment will diminish; and human labor will be more intellectual and healthy.

In other words, nanotechnology is a new strategy. Instead of the "top-down" technology (processing of components and finished products from intermediate ones by removing the superfluous parts), "bottom-up" technology (wasteless molecular design and self-assembling of products from elementary bricks of nature —atoms and molecules) will emerge as predominant.

The physical basis of such a new paradigm in technology is the knowledge of each type of atoms in *Mendeleev's* atomic table. Due to the action of interatomic forces, stable atomic configurations and associates can be formed. The smaller the particle and the lower the temperature, the more intensely its quantum properties are manifested. The sudden change of a particle's properties with respect to those of the

macroscopic particles of the same substance occurs, as a rule, well ahead of the approach to the quantum limits (at $R_c \leq 10 \ldots 100$ nm). This critical size may be dependent on the particular properties (mechanical, electrical, magnetic, chemical, etc.) of the substance.

The migration of atoms over the particle's surface occurs much faster than in its volume (especially at elevated temperatures). The attractive forces between them result in the self-organization and self-assembly of islandlike, columnlike, and other structures on the surface, which is commonly used for the creation of ordered heterostructures. The specific quantum size effects may arise at fairly small sizes and at low temperatures, which may be used in electronics, optics, and computer engineering. Vivid examples of such phenomena include quantum dots, wires, and rings.

Due to the strong dependence of the properties of the substance on the number of atoms in a cluster and, consequently, on the cluster size, the latter is sometimes even referred to as the third coordinate of *Mendeleev's* table.

The future of the nanosciences is not at all in the fact that nanoelectronics will supersede microelectronics, or that nanochemistry and nanobiology will emerge as subfields of the corresponding disciplines. The most essential significance of the nanostate for the applied sciences is the possibility of merging the inorganic, organic, and biological worlds, thus creating a prodigious number of new materials.

References

1. Shevchenko VYa (1993) Introduction to technical ceramics. Nauka, Moscow
2. Vandiver P, Kingery W (1986) Egyptian faience: the first high-tech ceramic. In: High-technology ceramics: past, present, and future. American Ceramic Society, pp 19–34
3. Freestone IM (1986) Title refractories in the ancient and preindustrial world. In: High-technology ceramics: past, present, and future. American Ceramic Society, pp 35–65
4. Lechtman HN, Hobbs LW (1986) Roman concrete and the roman architectural revolution. In: High-technology ceramics: past, present, and future. American Ceramic Society, pp 81–128
5. Gao-Zhen L, Ling-Xiang G (1986) Development of Chinese celadon and its influences. In: High-technology ceramics: past, present, and future. American Ceramic Society, pp 129–152
6. Kingery W (1986) The Development of the European Porcelain. In: High-technology ceramics: past, present, and future. American Ceramic Society, pp 153–180
7. Lomonosov M (1951) Working log 1751. In: Research in physics and chemistry. USSR Academy of Sciences, p 372
8. Ebelmen JJ (1846) Annals 57:331
9. Graham T (1864) J Chem Soc 17:318
10. Mendeleev DI (1860) Khim Zh 4:65
11. Brinker CJ, Sherer GW (1990) The physics and chemistry of sol-gel processing. Academic Press, Inc., Am Imprint of Elsevier, 908 p
12. Mackenzie JD (2003) Sol-gel research achievements since 1981 and prospects for future. J Sol-Gel Sci Technol 26:23–27
13. Marchi M, Megri RM, Bilmes SA (2003) Photophysical methods for the study of sol-gel transition and structure of titania gels. J Sol-Gel Sci Technol 26:131–135

14. Shevchenko VY, Madison AE, Shudegov VE (2003) Fragmentariness and metamorphoses of nanostructures. Fiz Khim Stekla 29(6): 809–816 (Glass Phys Chem (Engl transl), (2003) 29 (6):583–588]
15. Shevchenko VY, Madison AE, Shudegov VE (2003) The structural diversity of the nanoworld. Fiz Khim Stekla 29(6):801–808 (Glass Phys Chem (Engl transl), 2003 29(6):577–582)
16. Bernal JD, Carlisle CH (1968) Range of generalized crystallography. Kristallografiya 13 (5):927–951
17. Ishimasa T, Kaneko Y, Kaneko H (2004) New group of stable icosahedral quasicrystals: structural properties and formation conditions. J Non-Cryst Solids 1–7:334–335
18. Bragg W, Claringbull GF (1965) Crystal structures of minerals. Bell, London
19. Colomer J-F, Henrard L, van Tendeloo G, Lucas A, Lambin P (2004) Study of the packing of double-walled carbon nanotubes onto bundles by transmission electron microscopy and electron diffraction. J Mater Sci 14(4):603–606
20. Sadoc JF, Rivier N (1999) Boerdijk-Coxeter Helix and biological helices. Eur Phys J 12:309–318
21. Socolar JES, Steinhardt PJ (1986) Quasicrystals: II. Unit-cell configurations. Phys Rev B: Condens Matter 34(2):617–647
22. Locher JL (ed) (2000) Escher: the complete graphic work. Thames and Hudson Ltd., London, 349 p
23. Anderson S, Wadsley AD (1966) Nature (London) 211:581–583
24. Fére YG, Mellot-Draznieks C, Loiseau T (2003) Real, virtual, and not yet discovered porous structures using scale chemistry and/or simulation: a tribute to Sten Anderson. Solid State Sci 5(1):79–94
25. Bendersky LA, Gayle FW (2001) Electron diffraction using transmission electron microscopy. J Res Natl Inst Stand Technol 106(6):997–1012
26. Withers RL (2003) An analytical solution for the zero frequency hyperbolic RUM modes of distortion of SiO_2—Tridymite. Solid State Sci 5(1):115–123
27. Shevchenko VY, Khasanov OL, Madison AE, Lee JY (2002) Investigation of the structure of zirconia nanoparticles by high-resolution transmission electron microscopy. Fiz Khim Stekla 28(5):459–464 (Glass Phys Chem (Engl transl), 2002 28(5):322–325)
28. Alok Singh, Tsai AP (2003) On the cubic W phase and its relationship to the Icosahedral Phase in Mg–Zn–Y Alloys. Scr Mater 49(2):143–148
29. Samoylovich MI, Shevchenko VY, Talis AL (2004) Structural diversity of the nanoworld and the algebraic geometry constructions. In: Nanotechnologies and photonic crystals. Tekhnomash, Kaluga, pp 174–194

Chapter 20
Thermal Insulation and Porosity—From Macro- to Nanoscale

Dana Křemenáková, Jiří Militký, Mohanapriya Venkataraman and Rajesh Mishra

Abstract Porosity of textiles is one of the main factors influencing their thermal conductivity and insulation. Porosity in textile fabrics is the combination of fiber porosity, yarn packing density, and voids due to fabric construction. It is shown that assemblies from very fine fibers tend to suppress radiation and convection heat transfers because of huge total surface area, which restricts the free flow of air passing through them. For effective thermal insulation especially at low temperatures, it should be selected sufficiently high thickness of textile layer as well. Porosity is therefore decisive parameter for the evaluation of thermal comfort expressed in special units "clo." The main aim of this chapter is the prediction of the effect of porosity of fabrics and fibers on the thermal conductivity and insulation. The changes of thermal comfort due to the use of hollow fibers and multilayer corrugated nonwovens are described. The thermal properties of highly porous aerogel structures are discussed. Enhancement of insulation by their inclusion into textiles is investigated as well.

20.1 Introduction

Volume porosity is defined as the ratio of free space volume occupied within a material to the total volume of the material. Nonporous material is one that has a porosity of less than 0.25 and a porous material having usually a porosity greater than 0.4 [1]. Depending on the nature of the pores, three types of pores can be

D. Křemenáková (✉) · J. Militký · M. Venkataraman · R. Mishra
Department of Material Engineering, Faculty of Textile Engineering,
Technical University of Liberec, Studentská 2, 461 17 Liberec, Czech Republic
e-mail: dana.kremenakova@tul.cz

M. Venkataraman
Department of Materials Engineering, Indian Institute of Technology Madras, Chennai 600036, India

J. Šesták et al. (eds.), *Thermal Physics and Thermal Analysis*,
Hot Topics in Thermal Analysis and Calorimetry 11,
DOI 10.1007/978-3-319-45899-1_20

defined; blind pores are those that have one end closed, while interconnected pores are those that allow for the flow of fluids and closed pores refer to pores that are closed on all sides [2].

In terms of porosity, materials can be divided into two groups: porous and capillary-porous materials. This classification is based on the pore sizes. Porous materials are defined as those having a pore diameter greater than or equal to 100 nm, while materials with pore diameters of less than 100 nm are called capillary-porous materials [2].

According to this classification, textiles are generally highly porous structures characterized by the hierarchy of pores from nano- to macroscale. This volume porosity has major influence on their thermal conductivity and insulation.

The main aim of this chapter is to predict the effect of porosity in fabrics and fibers on the thermal conductivity and insulation. The thermal properties of highly porous aerogel structures are discussed. Enhancement of thermal insulation by their incorporation in textiles is investigated as well.

20.2 Porosity in Textile Structures

Porosity Po [−] is one of the main characteristics of textile structures. According to the IUPAC classification, there are three pore groups: micropores (dimension less than 2 nm), mesopores (dimension from 2 to 50 nm), and macropores (dimension over 50 nm). Micro- and mesopores are typical for fibers (typical fiber diameter is over 10 μm), and macropores are typical for fibrous assemblies (structural unit dimension in mm). Volume porosity is generally defined by the use of fabric density ρ_T and fiber density ρ_F or fabric volume V_T and fiber volume V_F or volume portion of fibrous phase $v_F = V_F/V_T$, as

$$\mathrm{Po} = 1 - \frac{\rho_T}{\rho_F} = 1 - \frac{V_T}{V_F} = 1 - v_F. \tag{20.1}$$

Basic characteristics of textile structures (woven, knitted, or nonwoven) are the planar mass—gsm W [kg m^{-2}] (usually [g m^{-2}]) and thickness H [m] (usually [cm]). The fabric density ρ_T is then defined as

$$\rho_T = \frac{W}{H} = \rho_F v_F + \rho_a(1 - v_F) = \rho_a + v_F(\rho_F - \rho_a). \tag{20.2}$$

where ρ_a is the density of air. At a temperature of 21 °C, 65% relative humidity, and 300 m elevation above sea level, the density of air is 1.15 kg m^{-3}. This is very low in comparison with the density of fibers (from 900 to 1600 kg m^{-3}), and then, Eq. 20.2 can be simplified as

$$\rho_{\mathrm{T}} = \frac{W}{H} \approx \rho_{\mathrm{F}} v_{\mathrm{F}}, \tag{20.3}$$

where fractional fiber volume, i.e., packing density is

$$v_{\mathrm{F}} \approx \frac{\rho_{\mathrm{T}}}{\rho_{\mathrm{F}}} = \frac{W}{\rho_{\mathrm{F}} H} = 1 - \mathrm{Po}. \tag{20.4}$$

The dependence of polyester fiber (ρ_{F} = 1360 kg m^{-3}) volume portion on fabric thickness for various planar masses is shown in Fig. 20.1a, and the dependence of polyester fiber volume portion on fabric planar mass for various small fabric thicknesses is shown in Fig. 20.1b. It is visible that the volume portion of fibrous phase for heavy fabrics and small thickness is nearly 15%. This corresponds to the total porosity 85%. Low planar mass and high thickness lead to the portion of fibers below 5%, i.e., porosity is over 95%.

Let us investigate the nonwovens composed of randomly oriented fibers with circular cross section of length l, radius r, and thermal emissivity ε. The number of fibers per unit volume N_{v} [m^{-3}] is related to the fractional fiber volume v_{F} by the relation

$$N_{\mathrm{v}} = \frac{(1 - \mathrm{Po})}{\pi l r^2}, \tag{20.5}$$

and surface area of the fibrous phase per unit volume S_{a} [m^2/m^3] is equal to

$$S_{\mathrm{a}} = N_{\mathrm{v}} 2 \pi r l = \frac{2(1 - \mathrm{Po})}{r}. \tag{20.6}$$

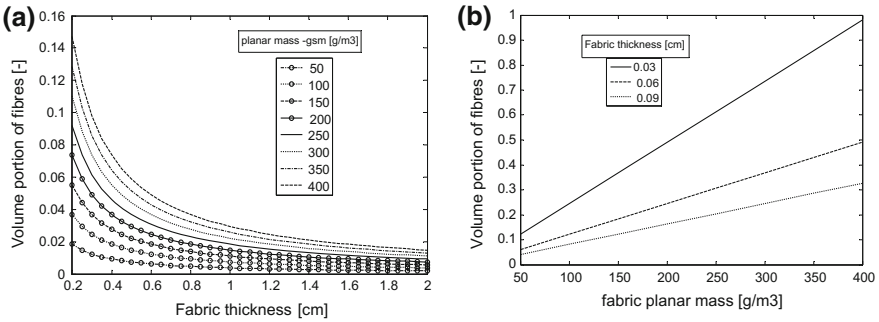

Fig. 20.1 **a** Dependence of fabric thickness on volume portion of fibers for various planar masses. **b** Dependence of fabric planar mass on volume portion of fibers for various small fabric thicknesses

Absorption constant β for randomly oriented fibers for radiation in both sides (see [3]) is equal to

$$\beta = \varepsilon S_a/2 = \frac{\varepsilon(1 - \mathrm{Po})}{r} \tag{20.7}$$

where ε is the fiber emissivity. For very thick sample, when a radiative conductivity model is appropriate, the coefficient of radiative conductivity λ_{rad} [W/(m K)] is equal to

$$\lambda_{rad} = 8\,\sigma\,T_0^3/\beta = \frac{8\sigma\,T_0^3 r}{\varepsilon(1 - \mathrm{Po})}, \tag{20.8}$$

where $\sigma = 5.67 \times 10^{-8}$ W m^{-2} K^{-4} is the Stefan–Boltzmann constant and T_o is related to skin temperature T_s and the surrounding air temperature T_a by the relation

$$T_o = \frac{T_s + T_a}{2}. \tag{20.9}$$

The radiative heat transfer is then

$$Q_r = -\lambda_{rad}\frac{T_a - T_s}{H}. \tag{20.10}$$

It is visible that finer fibers (with low radius) have smaller radiative heat transfer and higher radiation absorption. More porous structures have the adverse effect. Thermal convection depends on the airflow around the fibers. When the mean free path of gas molecules (>0.1 μm) becomes comparable to the fiber diameter, there is gas slip at the fiber surface, and more gas can flow through the fiber mass than would be expected based on the continuum flow assumptions. This is the same reason why nanofiber filters are unexpectedly effective. Very fine fibers tend therefore to suppress all kinds of convections because of their huge surface area, which restricts the free flow of air passing around the fibers.

20.3 Porosity and Thermal Insulation

Thermal conductivity (λ) of general thermal insulating materials (porous bodies) is described by the following equation:

$$\lambda = \lambda_{gc} + \lambda_{sc} + \lambda_c + \lambda_r, \tag{20.11}$$

where λ_{gc} is the thermal conduction through the air, λ_{sc} is the thermal conduction through the solid, λ_c is the heat transfer by convection, and λ_r is the heat transfer by

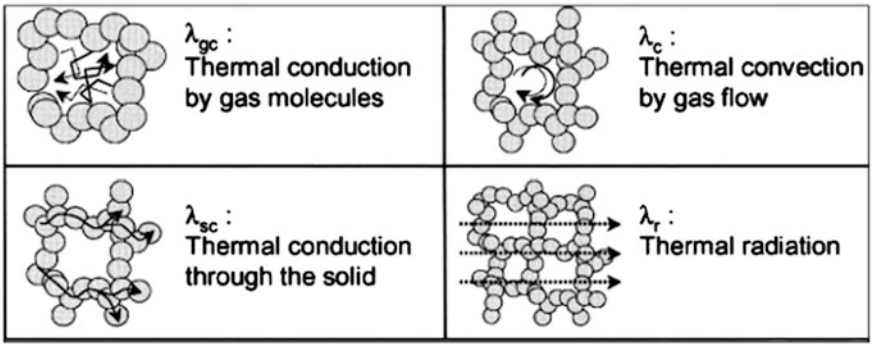

Fig. 20.2 Factors contributing to the thermal conduction through porous materials [4]

radiation. Each of these thermal conduction mechanisms is schematically shown in Fig. 20.2.

Here, the thermal conduction through the air can be regarded as a transport phenomenon with kinetic energy driven by the collision of gas molecules in the air under a temperature gradient. The thermal conductivity of a gas depends on the "mean free path" of a gas molecule (L_f) enclosed in a narrow space, the mean pore size (L_s), and the "mean free path" of the gas molecules in free space (L_g) [4], i.e.,

$$\frac{1}{L_f} = \frac{1}{L_s} + \frac{1}{L_g}. \tag{20.12}$$

Equation (20.12) can be expressed in the form

$$L_f = \frac{L_g}{1 + \frac{L_g}{L_s}} = \frac{L_g}{1 + Kn}. \tag{20.13}$$

Symbol Kn denoted the so-called Knudsen number. Knudsen effect appears if the mean free path of the gas molecules is larger than the pore diameter, i.e., $Kn > 1$. That is, a gas molecule located inside a pore will ballistically hit the pore wall and not another gas molecule.

Then, gas thermal conductivity, and thereby the overall thermal conductivity, becomes very low. It can be seen that when making the mean pore size (L_s) smaller than the "mean free path" of the gas molecules in space (L_g), L_f will be smaller and the overall thermal conduction can be less than that of the air. A rough relationship between the mean pore size (L_s) and the thermal conduction of the air is shown in Fig. 20.3.

Heat transfer by radiation increases as the fourth power of the absolute temperature and needs to be taken into account at high-temperature applications [4].

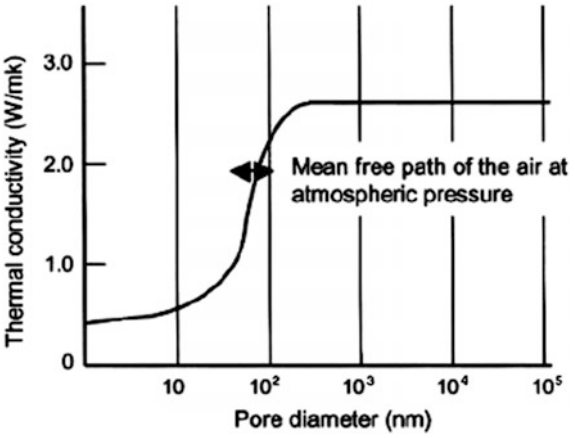

Fig. 20.3 Relationship between the mean pore size (L_s) and the thermal conduction of the air [4]

20.4 Thermal Conductivity Prediction

The physical (intensive, i.e., not dependent on geometry) parameter characterizing the thermal behavior of materials is thermal conductivity. Thermal conductivity $\boldsymbol{\lambda}$ [W m^{-1} K^{-1}] is defined as a factor in the well-known Fourier equation describing the steady-state one-directional transport of heat through the body of cross-sectional area A and thickness H due to the thermal difference ΔT

$$Q = \lambda A \, \Delta T / H, \tag{20.14}$$

where Q [W] is the transferred heat, H [m] is the thickness of the textile structure in the heat flow direction, and ΔT [K] is the difference of temperatures on the input and output from textile layer. Thermal conductivity of solid particles is about $\lambda = 1 - 5$ [W m^{-1} K^{-1}], for water $\lambda = 0.6$ [W m^{-1} K^{-1}], for ice $\lambda = 2.24$ [W m^{-1} K^{-1}], and for air $\lambda = 0.024$ [W m^{-1} K^{-1}]. For majority of fibrous polymers, it is $\lambda = 0.1 - 0.5$ [W m^{-1} K^{-1}].

Measurement devices are used to measure thermal resistance RT [W^{-1} K m^2] as reciprocal to thermal conductivity

$$\mathrm{RT} = H / \lambda. \tag{20.15}$$

It is visible that RT is extensive variable dependent on geometry (i.e., thickness). The RT is used for the calculation of thermal comfort characteristic expressed as thermal insulation I_c in ***clo*** units [5]. One ***clo*** corresponds to the intrinsic insulation I_c of business suit worn by sedentary resting male in a normally ventilated room at 21 °C and 50% RH and air ventilation of 0.1 m/s. In these conditions, the feelings of a man are quite comfortable. It is assumed that in these conditions, total metabolic heat equal to 1 Met = 58 W m^{-2} is produced. From this amount, 24% of heat is lost due to evaporation (temperature of skin in comfort conditions is 33°C) and

76% of heat, i.e., 44 W m^{-2}, is passing through clothing by the combination of conduction, convection, and radiation. Total thermal resistance of clothing RT is then (33 − 21)/44 = 0.2715 m^2 K W^{-1}. It is assumed that between body and clothing is existing air gap with the total thermal resistance 0.12 m^2 K W^{-1}.

Because air conductivity is 0.024 W m^{-1} K^{-1}, the thickness of this air gap is $H_a = 0.12 \times 0.024 = 0.0028$ m. Net thermal resistance caused by the clothing system only is then 0.2715 − 0.12 = 0.155 m^2 K W^{-1}. This is in fact $I_c = 1$ *clo*. Generally, it is valid that

$$I_c = \frac{H}{0.155\,\lambda}. \tag{20.16}$$

Cloths for standard winter condition have *clo* over 1, and for summer cloths, it has *clo* around 0.5.

Small portion of fibrous phase is the main reason why the total thermal conductivity is governed by porosity not by conductivity of fibers. This is shown in Fig. 20.4 where the thermal conductivity of fabric is computed form of

$$\lambda_T = 0.5\left((1-v_F)\lambda_a + v_F\lambda_f + \frac{\lambda_a\lambda_f}{(1-v_F)\lambda_f + v_F\lambda_a}\right). \tag{20.17}$$

Dependence of polyester fabric thermal conductivity (for polyester, it is $\lambda_f = 0.304$ W/(m K)) on the thickness for various planar masses is in Fig. 20.4a, and dependence of fabric thermal conductivity on the planar mass for selected thicknesses is in Fig. 20.4b.

Thermal properties of conventional noncircular and hollow fibrous materials were extensively studied. The typical fibers with holes or special cross section (Coolmax, Coolplus, Thermocool, Thermolite) and round polyester are shown in Fig. 20.5.

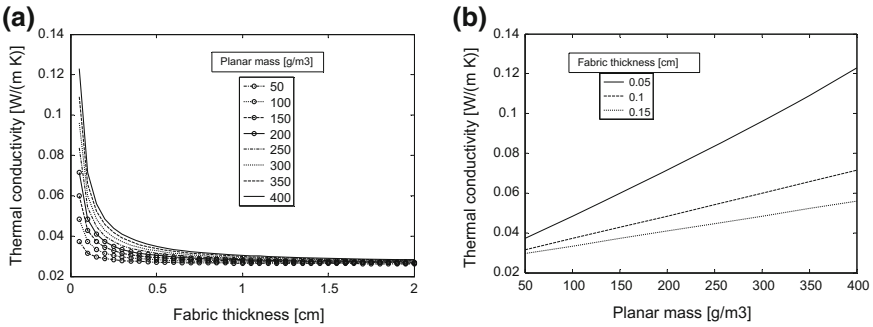

Fig. 20.4 **a** Dependence of fabric thermal conductivity on thickness for various planar masses. **b** Dependence of fabric thermal conductivity on planar mass for various small fabric thicknesses

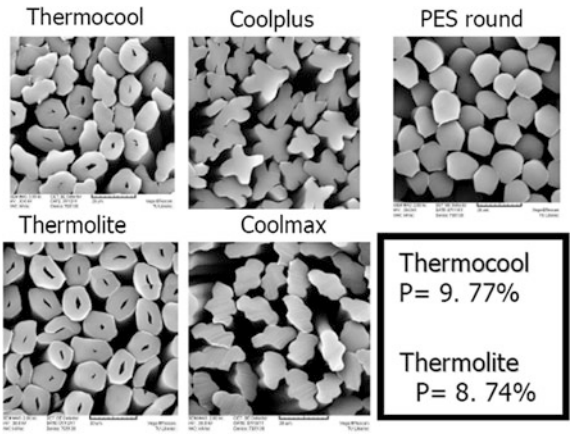

Fig. 20.5 Cross section of selected fibers

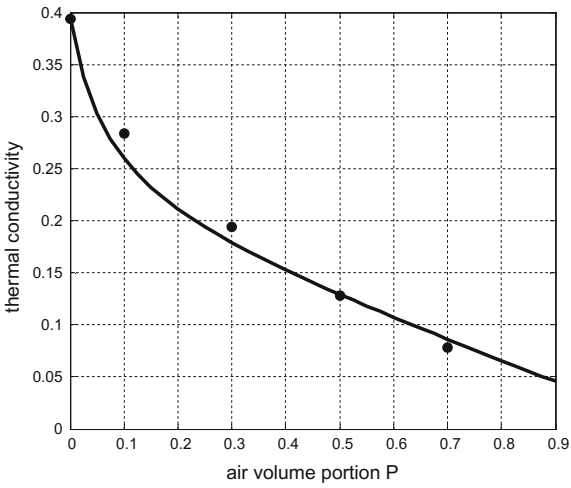

Fig. 20.6 Comparison of effective thermal conductivity of fibers with different hollow size calculated by commercial ANSYS package simulation (*dots*) and the mean thermal conductivity from Eq. 3.4 (*solid curve*)

Figure 20.6 shows the effective thermal conductivity of fibers with a different hollow size (black points). By numerical method, the thermal conductivity of solid fiber is 0.3935 W/(m K), which is 1.62% deviated from the fiber material. With the increase of air volume in fibers, the effective thermal conductivity decreases. When the air volume is up to 70%, the effective thermal conductivity is 0.0781 W/(m K).

Because the real fabric and nonwoven porosities are more than 70%, the influence of hole portion is not very important (see Fig. 20.7) and better thermal insulation can be obtained by the combination of planar mass and thickness.

In a study [6], the knitted structures created from the above-mentioned special fibers are deeply described and their thermal properties are discussed in detail. Here, it can be only mentioned that the differences between thermal conductivities for

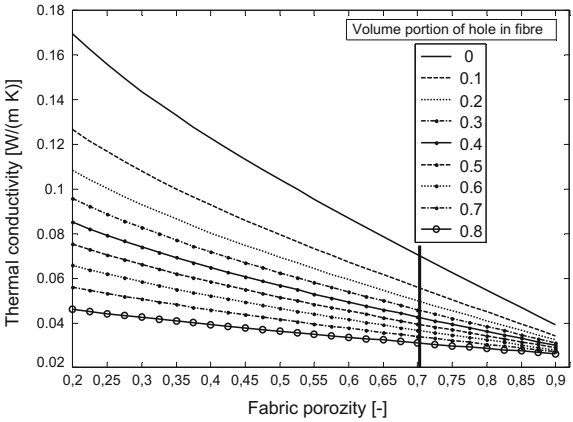

Fig. 20.7 Dependence of fabric thermal conductivity on their porosity for hollow fibers with various relative volumes of holes

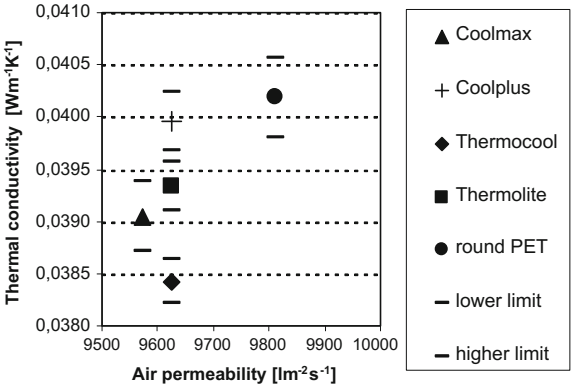

Fig. 20.8 Thermal conductivity of knitted fabrics as a function of air permeability

similar fibrous structures were very small. Much higher is the influence of fabric construction (see Fig. 20.7).

Thermal properties are generally strongly dependent on the fiber type and fabric porosity. Porosity is in this case closely connected with air permeability. Differences between Coolmax, Coolplus, Thermocool, and Thermolite knitted fabric's air permeability are statistically nonsignificant, but air permeability of fabric created from PET fibers with round profile is statistically significantly higher. It is the result of higher number of fibers in yarn cross section and lower fiber fineness (finer fibers) and higher porosity of this yarn. The dependence of thermal conductivity on air permeability for gray plain knitted fabric composed from fibers shown in Fig. 20.5 is given in Fig. 20.8.

It is visible that thermal conductivities of fabrics from conventional fibers and "hollow" fibers are similar.

20.5 Thermal Insulation

Thermal insulating properties of conventional and nonconventional products were extensively studied. The total heat resistance R_T is often calculated as the combination of resistance of textile layer R_o and resistance of air layer R_a between body and textile layer.

$$R_T = \frac{H}{\lambda} + \frac{1}{f_{cl}(k_R + k_p)} + R_a, \tag{20.18}$$

where H is the cloth layer thickness and λ is the cloth thermal conductivity. Thickness of intermediate air layer is usually selected as 2 mm. Coefficient of heat transfer by radiation $k_R = 1/R_R$ [W m^{-2} K^{-1}] has the form

$$k_R = 4\,\varepsilon\,\sigma\frac{A_r}{A_T}\left(273.15 + \frac{T_{cl} + T_r}{2}\right)^3, \tag{20.19}$$

where ε is the mean emissivity of cloth or body (usually $\varepsilon = 0.95$), σ [W m^{-2} K^{-4}] is the Stefan–Boltzmann constant, A_r [m^2] is the effective area of body radiation, and A_T [m^2] is the total body area. Ratio $f_{cl} = A_r/A_T$ for sitting humans is equal to 0.7, and for standing humans, it is equal to 0.73. Without external sources of heat and without sun shining, mean radiation temperature T_r is approximately the same as the air temperature T_a. Resistance to radiation for standard room condition is practically constant and equal to 4.7 W m^{-2} K^{-1}. For natural airflow (caused by the temperature difference only), k_p is estimated from the relation

$$k_p = \frac{0.021(0.72\,Gr)^{0.4}\lambda}{L}, \tag{20.20}$$

where L is the characteristic length of human body, $\lambda = 0.024$ [W K^{-1} m^{-2}] is the air thermal conductivity, constant 0.72 is the dimensionless Prandtl number for air, and Gr is the dimensionless Grashoff number expressed by the relation [7]

$$Gr = \frac{\alpha g\,\Delta T L^3}{v^2}, \tag{20.21}$$

where $\alpha = 3.42 \times 10^{-3}$ [K^{-1}] is the air temperature expansion coefficient, $v = 1.5 \times 10^{-5}$[m^2 s^{-1}] is the air kinematic viscosity, $\Delta T = T_{cl} - T_a$ is the thermal difference between cloth and ambient atmosphere, and g *is* the gravitational acceleration. For the case when the characteristic length of human body is $L = 1.8$, k_p is calculated from the simple relation $k_p = 0.9242\,\Delta T^{0.4}$. For temperature difference $\Delta T = 10$ °C, Grasshoper number is $Gr = 8.6937 \times 10^9$. Nusselt number Nu is defined as the ratio of the rate of heat transfer due to convection and conduction.

$$Nu = \frac{k_p L}{\lambda} = 0.021\, Ra^{0.4}, \tag{20.22}$$

where Ra is the Raleigh number $Ra \approx 0.72\, Gr$. For Grasshoper number $Gr = 8.6937 \times 10^9$, then, Nu is = 172.163. Under the conditions of natural airflow, heat transfer is realized predominantly by convection and contribution of conduction is relatively small. For Nu around 200, convection is turbulent. In the case of forced air convection caused by the rate of airflow in the surrounding atmosphere v, it is possible to use the relation

$$k_p = 12.1\sqrt{v}. \tag{20.23}$$

In the case when the wind velocity in the surrounding atmosphere is 0.05 m s^{-1}, then, k_p = 2.7056, which corresponds to the temperature difference between cloth and ambient air temperature which is roughly 15 °C. For sitting human (f_{cl} = 0.7) in the room, it is possible to select R_a = 0.0853 m^2 K W^{-1}, k_p = 3.1 W m^{-2} K^{-1}, and k_R = 4.7 W m^{-2} K^{-1}. The corresponding total thermal resistance is $R_T = R_c + 0.268$.

The optimal thickness H_{opt} of textile layer with thermal conductivity λ ensuring comfort in conditions below:

- human is sitting in the room at temperature T_a, without sweating, and metabolic rate is 1 *Met*,
- cloth is transferring 76% metabolic heat, i.e., 44.1963 W m^{-2}, and
- skin temperature is 33 °C,

is expressed by the equation

$$H_{opt} = \left(\frac{33 - T_a}{44.1963} - 0.268\right)\lambda. \tag{20.24}$$

For room temperature of 21 °C, the optimal textile layer thickness is equal to $H_{opt} = 0.00352\,\lambda$, and for temperature of −20 °C, it is H_{opt} = 0.9312 λ. One of the governing factors of thermal comfort is the thickness of textile layer H. The minimum thickness of the highest insulating textile layer (with the same thermal conductivity as air) ensuring that chosen *clo* is shown in Fig. 20.9.

It is clear that for required *clo* = 4, the minimal thickness of textile layer is equal to 15 mm. The influence of textile layer thermal conductivity λ [W m^{-1} K^{-1}] and thickness H on thermal insulation I_c in *clo* units is shown in Fig. 20.10.

It is clearly visible that for thickness H under 2 mm, the magnitude of thermal insulation in *clo* units is very low even for materials with the thermal conductivity on the level of air (λ_a = 0.024 [W m^{-1} K^{-1}]). For effective thermal insulation especially at low temperatures, it should be selected *sufficiently high thickness* of textile layer. Another important factor influencing the thermal comfort is textile structure porosity which is the combination of fiber porosity, yarn packing density, and fabric construction. Porosity is the decisive parameter for value of fabric

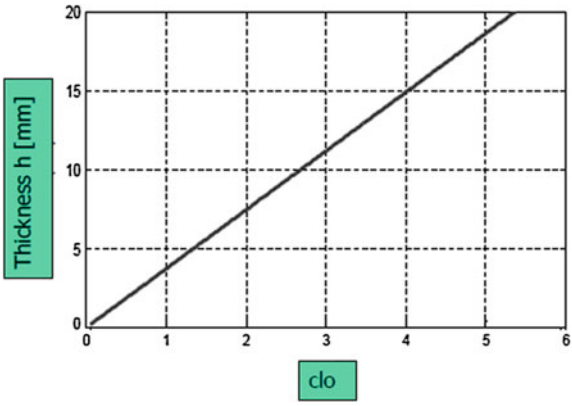

Fig. 20.9 Minimum thickness of the highest insulating textile layer (with the same thermal conductivity as air) for different *clo*

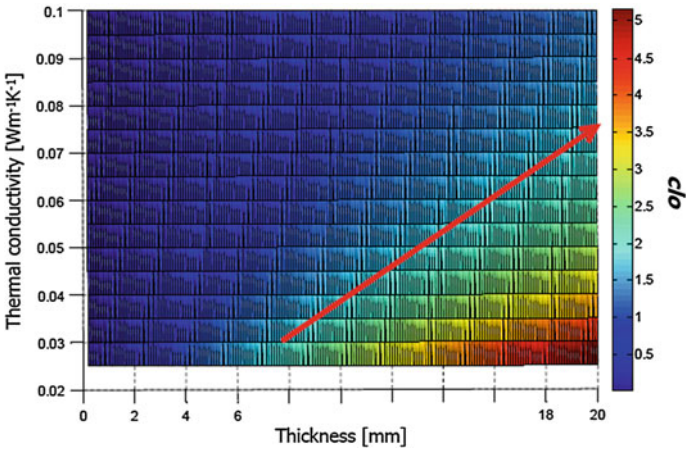

Fig. 20.10 Influence of textile layer thermal conductivity λ and thickness on thermal insulation in *clo*

thermal conductivity (increase of porosity leads to decrease of λ). For more porous materials, lower thickness is sufficient to obtain the same insulation, i.e., *clo*. For relatively high thermal conductivity of textile fabric 0.06 W m^{-1} K^{-1}, a thickness of 2 cm is sufficient for obtaining *clo* over 2.

One possibility is to use high-insulation layer as starting lap and create thicker product by the described technology. The Polartec Alpha (PES multifil, PES staple, PES/VS multifil)—*sample1* was selected as insulation layer. By Rotis technology, the two-*sample2* and three-*sample3* layers composed from POP 1.5 dtex nonwoven

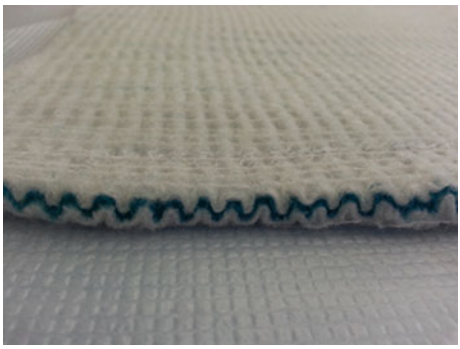

Fig. 20.11 Three-layer Rotis with Polartec Alpha in center

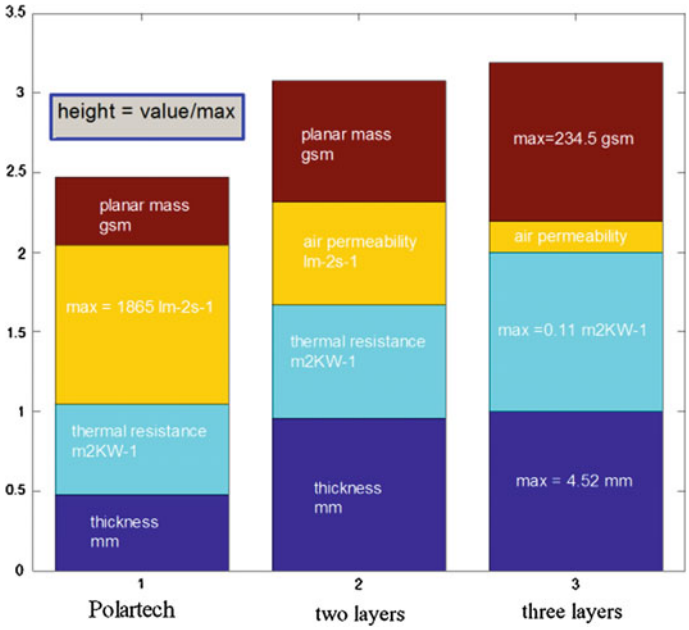

Fig. 20.12 Selected properties of multilayer high-insulation samples

web covering Polartec Alpha layer were prepared. Three-layer Rotis structure is shown in Fig. 20.11.

The properties of these samples are summarized in Fig. 20.12.

It is visible that thermal resistance of three-layer structure is approximately two times higher in comparison with single Polartec Alpha structure.

20.6 Aerogels

Aerogels are special materials with the promising thermal insulation. In 1930, Kistler invented a process for making a porous inorganic silica product called aerogel. Aerogel is also known as frozen smoke, solid smoke, solid air, or blue smoke. It is characterized by low-density solid with high surface area. As per IUPAC, aerogel is defined as a gel comprised of a microporous solid in which the dispersed phase is a gas. Aerogels are transparent, highly porous, open cell, and low-density foams. The microstructure of aerogels is comprised of nanosized pores and linked primary particles. Aerogels have the lowest thermal conductivity, refractive index, sound velocity, and dielectric constant of any solid ever tested due to its unique microstructure [8]. Aerogels, together with vacuum insulation panels, are one of the new promising high-performance thermal and acoustic insulation materials for wide industrial applications. Application of aerogel for thermal insulation in high-performance textiles is described in the review [4].

Skeletal densities of silica aerogels have been found in the range of 1700–2100 kg/m^3 [9]. But the full density of silica is 2200 kg/m^3, and the difference is attributed to microporosity in the primary particles comprising of the aerogel backbone [8]. Thermal transport in aerogel occurs via gaseous conduction, solid conduction, and infrared radiative transfer. One way to lower the thermal conductivity of an aerogel is to suppress the gaseous conduction [8]. The radiative transport in aerogels is governed by infrared adsorption. Characteristics are the high absorption region above 10 μm and the low absorption region between 3 and 5 μm [8]. The thermal insulating property of silica aerogels is their first important attribute as their total thermal conductivity, usually below 0.02 W/(m K) in air at ambient conditions, is much smaller than other traditional insulating materials and even smaller than the stagnant free air, about 0.026 W/(m K) [10]. Aerogel is distinguished by their very fine pore sizes (from about 1 to 20 nm) shown in Fig. 20.13. The very small pores are synonymous with very high surface areas

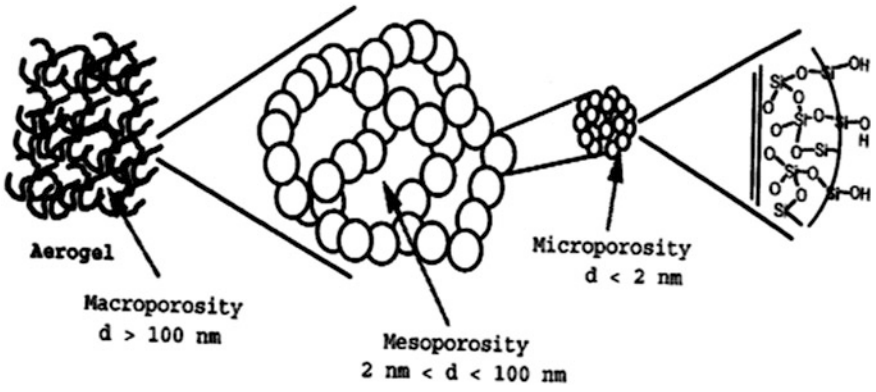

Fig. 20.13 Complex aerogel pore structure [37]

(such as from 800 to 1100 m square per gram) of the internal structures. It can be made to have ultralow densities.

Aerogel is a superinsulation material with open-cell nanoporous and tenuous skeleton structure [7, 8, 10, 11]. The extremely small sizes of the nanoparticles (2–20 nm) and nanopores (1–100 nm) give aerogel a very high specific surface area (>400 m^2/g). The thermal conductivity models for silica aerogels are needed to understand the relationship between the material structure, the properties, and the thermal performance [12–26].

Two problems limit the application of silica aerogels as thermal insulators. One is the fragility of SiO_2 solid skeleton since the aerogel matrix is made up of interlocking long chains of loosely bonded amorphous silica nanoparticles. The other is the dramatically increased radiative heat transfer at higher temperatures since silica aerogels have low extinction coefficients for wavelengths of 2–8 μm [7, 8, 10, 23, 27]. Microscale fiber is usually incorporated into the aerogel matrix to mechanically strengthen the silica aerogels [23, 28]. The proper fiber selection canal so strongly reduces the infrared radiative transfer by increasing the scattering and absorption [29, 30]. Convective heat transfer is negligible when the pore sizes are smaller than 1 mm [11, 15, 17, 29, 30]. The extinction coefficient, which represents the scattering and absorption, is a key parameter in radiative heat transfer models. The optical properties, size, and orientations of the fibers govern the radiation transport through the composite. Recent advances in the technology of producing nanofibers have revealed a gap in our knowledge about the heat transfer behavior of low-density nanofibrous layers. Flexible electrospun nanofibrous layers embedded with silica aerogel powder and granules were produced via electrospinning by using Nanospider device (see Fig. 20.14).

Nanospider is a modified electrospinning method which requires the use of a high-voltage electrostatic field to create an electrically charged stream of polymer solution or melt. The idea of the Nanospider is based on the possibility of producing

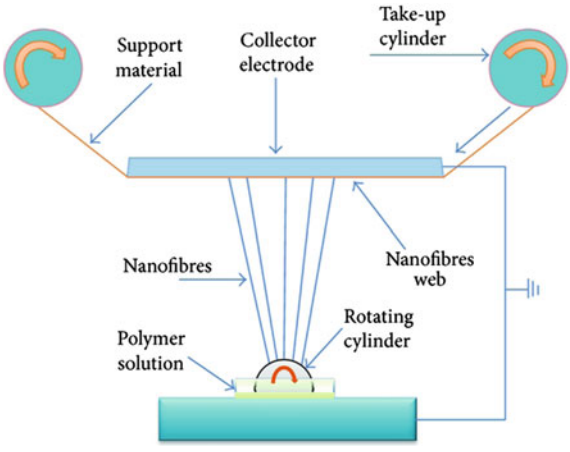

Fig. 20.14 Schematic of electrospinning setup —"Nanospider" [31]

Table 20.1 Parameters for the production of PUR nanofibrous web containing aerogel

Parameter	Specifications
Distance of electrode	175 mm
Wire speed	0.2 mm/s
Substrate speed	15 mm/min
Carriage speed	380–430 mm/s on 500 mm distance
Substrate	SB blue
Voltage	10/60 kV
Size of the girder	ø 0.7
Airflow	90/100 m^3/h
Humidity	With dry box

Table 20.2 Air temperature/humidity and size of the girder specifications

Samples	Air temperature and humidity	Size of the girder
PUR 1	22.7%/23 °C	ø 0.7
PUR 2	20.3%/23.6 °C	ø 0.7
PUR 3	20.8%/23.3 °C	ø 0.7
PUR 4	23.1%/24.4 °C 23.1%/24.2 ° C	ø 0.7/ø 0.8/ø 1.0
PUR 5	23.1%/24.8 °C (first layer)	ø 0.9
	21.5%/26 °C (second layer)	ø 0.9

nanofiber from a thin layer of liquid polymer. Taylor cones (the source of nanofiber) are here created on the surface of a rotating roller, immersed in a polymer solution. Because the Taylor streams are formed throughout the entire length of the roller, this process has many advantages, as high productive rate. In addition, Nanospider has the ability to process a wide range of polymers in diameters of 50–300 nm into nonwoven webs [31]. Parameters for the production of PUR nanofibrous web are given in Tables 20.1 and 20.2.

The electrospun PUR nanofibrous microstructures were fabricated by using DMF as solvent and then used to reinforce the SiO_2 aerogel and to attach them on the subsurface of fabrics. Details about the tested samples are given in Table 20.3.

Figure 20.15 shows the morphologies and microstructures of electrospun PUR nanofibrous layers. The electrospun nanofibrous layers have good integrity and flexibility. The different microstructures could be observed with and without aerogel particles present which were electrospun from the solutions with the concentration of 18 wt%.

Thermal conductivity measured by the ALMBETA device as a function of areal density for PUR electrospun nanofibrous layer embedded with silica aerogel is

Table 20.3 Electrospun PUR nanofibrous layer containing silica aerogel

Samples	Type	Sample description (spun PP + NFA)	Areal density [g/m^2]	Thickness [mm]	Thermal conductivity [W m^{-1} K^{-1}]	Thermal resistance, r [K m^2 W^{-1}] × 10^{-3}
SPUR1	Aerogel nanofibrous layer with spunbonded PP backup	Only PUR	34.01 (±1.71)	0.290 (±0.014)	0.036 (±0.0170)	7.68 (±0.381)
SPUR2		PUR + aerogel (powder)	33.11 (±1.65)	0.254 (±0.013)	0.0325 (±0.0060)	8.12 (±0.410)
SPUR3		PUR + aerogel (granular)	35.28 (±1.76)	0.300 (±0.015)	0.310 (±0.0260)	8.88 (±0.472)
SPUR4		PUR + aerogel (powder)	35.29 (±1.65)	0.390 (±0.020)	0.0326 (±0.0670)	11.48 (±0.572)
SPUR5		PUR + aerogel (granular)	38.58 (±1.93)	0.370 (±0.019)	0.0322 (±0.0090)	11.44 (±0.072)
PUR1	Aerogel nanofibrous layer	Only PUR	6.01 (±0.31)	0.083 (±0.004)	0.0303 (±0.0510)	3.10 (±0.255)
PUR2		PUR + aerogel (powder)	5.11 (±0.26)	0.089 (±0.005)	0.0298 (±0.0730)	5.42 (±0.072)
PUR3		PUR + aerogel (granular)	7.28 (±0.03)	0.112 (±0.006)	0.0287 (±0.0040)	5.66 (±0.208)
PUR4		PUR + aerogel (powder)	7.29 (±0.07)	0.206 (±0.010)	0.0275 (±0.0170)	7.35 (±0.084)
PUR5		PUR + aerogel (granular)	10.58 (±0.21)	0.248 (±0.012)	0.0282 (±0.0230)	8.78 (±0.092)

Note "±" is the upper and lower 95% confidence intervals of the mean

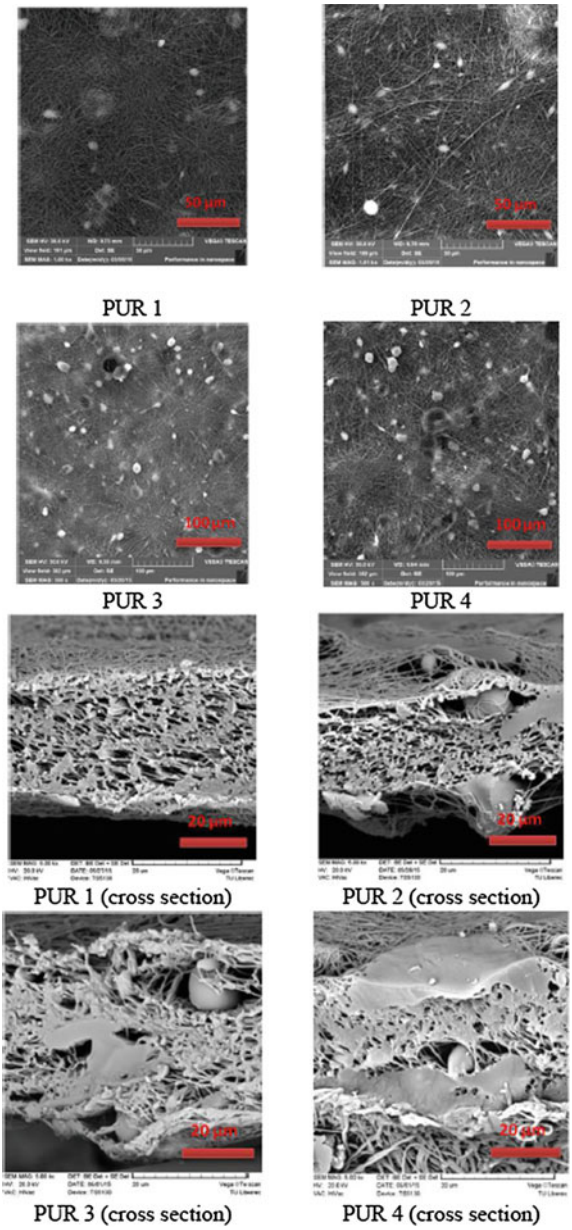

Fig. 20.15 Morphology and microstructure of electrospun PUR nanofibrous layers embedded with SiO_2 aerogel from 18 wt%

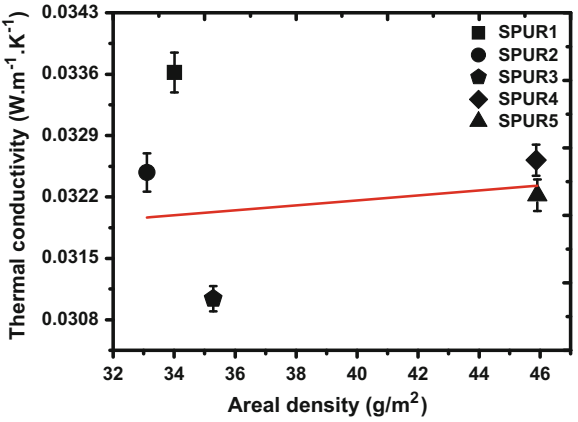

Fig. 20.16 Thermal conductivity versus GSM for PUR samples with spunbonded PP

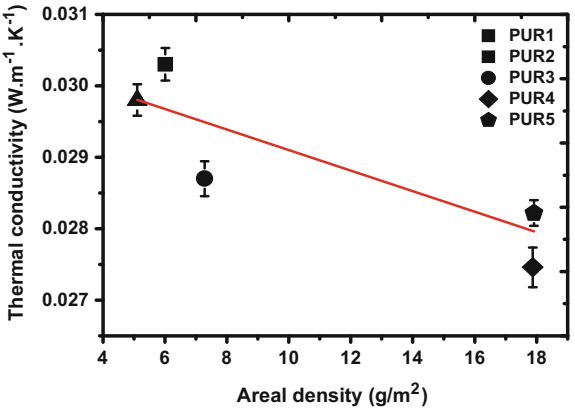

Fig. 20.17 Thermal conductivity versus gsm (electrospun PUR nanofibrous layers embedded with silica aerogel)

shown in Figs. 20.16, 20.17, 20.18, and 20.19. It is clearly visible that thermal conductivity of the electrospun nanofibrous layer decreased with the increase in density.

This can be explained by the fact that as the density increases, it makes the fibrous structure more packed. This causes the mean free path (distance traveled by a photon before it collides with another fiber surface [32] for a photon movement to decrease, thus causing a decrease in the heat transfer because of radiative conduction.

When the density comes to a critical point, the increase in conduction through solid phase (fibers) and decrease in radiation conductivity result in an increase in total thermal conductivity [33, 34]. In fact, in fibrous structures, the small size of the pores and the tortuous nature of the air channels present prevent any heat transfer by convection [35]. Moreover, in fibrous insulation materials because of low fiber

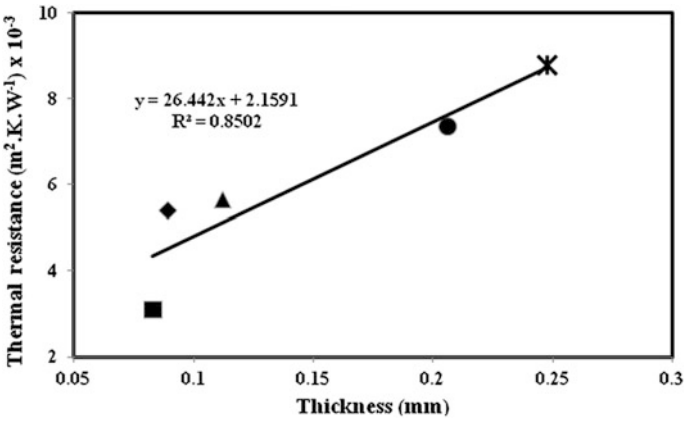

Fig. 20.18 Thermal resistance versus thickness (electrospun PUR nanofibrous layers embedded with silica aerogel)

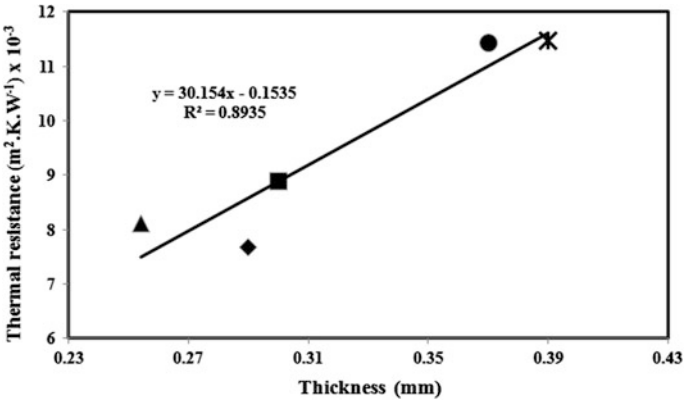

Fig. 20.19 Thermal resistance versus thickness (electrospun PUR nanofibrous layers with silica aerogel backed up with spunbonded PP)

volume fraction, heat conduction through the solid phase (the fibers) is not significant and conduction through air is usually considered to be the conductivity of still air that is poor at room temperature. Thus, radiative conductivity is the prevalent mechanism of conductivity since it has a high porosity percentage of fibrous structures. By adding a nanofiber web, thermal conductivity was enhanced noticeably that is believed to be because of their extremely fine fiber and very high porosity of web.

The superfine fibers in the web have better radiation absorption and extinction since their higher surface area-to-volume ratio leads to decrease in the thermal conductivity. Moreover, smaller pore size between nanofibers decreases the mean

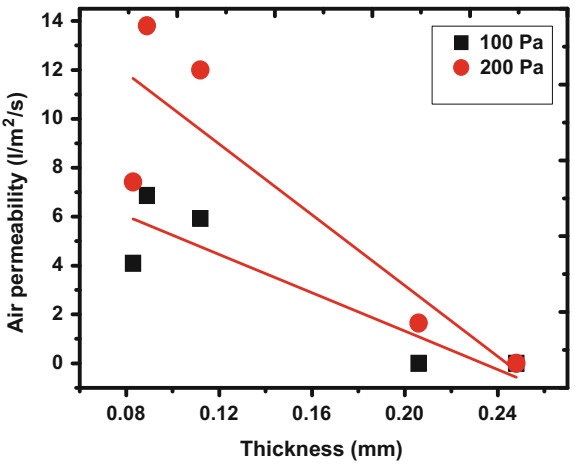

Fig. 20.20 Air permeability (electrospun PUR nanofibrous layer with silica aerogel)

free path for photon movement resulting in lower radiative energy transfer. This improvement becomes more significant when bulk density is increased. In high densities, increase in the thermal conductivity of the sample containing web was diminished which may be attributed to the presence of nanofiber and their natural compact structure that could compensate for increased thermal conductivity.

According to the thermal conductivity curves, decrease in the average nanofiber diameter leads to the lower limit of conductivity. Higher specific surface of thinner fibers means more surface area for radiative absorption that results in lower thermal conductivity [36].

Further, higher porosity of the web with a nanofiber diameter around 150 nm could be the other reason for their lowest thermal conductivity. Another explanation for reduction in conductivity can be smaller pore size in the web containing thinner nanofibers leading to lower radiative conductivity.

Electrospun PUR nanofibrous layers showed excellent reduction in overall heat transfer compared to the standard low-density fibrous insulating materials (at areal densities above 40 g/m^2).

Thermal conductivity testing confirmed that decreasing fiber diameter tends to increase the thermal resistance of fibrous insulation materials. However, the nanofiber/aerogel becomes an effective insulator since the aerogel structure suppresses conduction and convection, and the fibers reduce radiation heat transfer while increasing the strength of the brittle and weak aerogel structure. Although the aerogel/nanofiber combination shows good thermal properties, the volume fraction of fiber must be fairly high to support and protect the aerogel matrix. Thus, the aerogel materials cannot achieve the same thermal conductivity at densities as fibrous insulation, but they do achieve better thermal resistance for an equivalent thickness of material. High porosity of electrospun fibrous mesh is able to trap air which potentially gives it a good thermal insulation property.

As mentioned previously, nanofiber/aerogel has shown superior insulation properties for applications where the thickness is of concern.

With respect to fibrous insulation materials with high porosity, aerogel/nanofiber has excellent insulation growing linearly with the thickness, as is shown in Figs. 20.18 and 20.19.

From the figures, it can be seen that the thermal resistance increases with the increase of thickness.

Air permeability is a very important parameter for thermal insulation of electrospun nanofibrous layer. Lower air permeability causes lower airflow and consequently more thermal insulation. The air permeability of electrospun nanofibrous layers is shown in Fig. 20.20.

As can be seen, by increasing the number of nanofibrous layers, lower air permeability was achieved, confirming the relation of this important parameter with thermal insulation ability.

20.7 Conclusion

The influence of fabric construction, fiber fineness, and overall porosity on thermal insulation characteristics of fabrics and nonwovens was quantified. It was shown that the hollow fibers have only gradual influence on thermal insulation. Thickness of fibrous layer has the major influence on thermal insulation [3].

The effects of electrospun PUR nanofibrous layers embedded with silica aerogel on thermal behavior were studied. The results show the enhancement in thermal insulation by increasing the number and the weight per unit area of both nanofibrous layers. Higher thermal resistance was observed in the case of samples containing PUR nanofibrous layers, which can be attributed to the low air permeability and fiber diameter. Moreover, thermal measurements show that embedding silica aerogel in nanofibrous layers leads to increased thermal insulation. We have shown in this study that our experimental insulation material can enhance the thermal resistance. Furthermore, weight and thickness can be reduced by means of nanofiber layers. The work presented in this paper did not show nanofibers to be useful for high-loft thermal insulation. However, they may be useful as components in hybrid battings with high bulk densities. Fibers below 1 μm in diameter are not thermally efficient at low fiber volume fractions; this corresponds with the previous research on fiberglass insulation. Performance gains in existing thermal insulation materials may be possible by incorporating a proportion of nanofibers into the structure, but large diameter fibers would still be necessary for durability and compression recovery. Although the electrospun nanofibrous layers have been proposed to strengthen the aerogel, the preparation technique of the electrospun nanofibrous layers embedded with aerogel with larger size and lower thermal conductivity has to be further developed.

References

1. Krokida MK, Maroulis ZB (1997) Effect of drying method on shrinkage and porosity. Drying Technol 15:2441–2458
2. Datta AK (2007) Porous media approaches to studying simultaneous heat and mass transfer in food processes. I. Problem formulations. J Food Eng 80:80–95
3. Farnworth B (1983) Mechanisms of heat flow through clothing insulation. Text Res J 53:717–725
4. Venkataraman M, Mishra R, Kotresh T M, Militky J and Jamshaid H (2016) Aerogel for thermal insulation in high-performance textiles, Text Prog 48(2):55–118
5. Pl Gagge A et al (1941) A practical system of units for the description of heat exchange of man with his environment. Science 94:428–430
6. Petrulis D (2004) Fundamental study of the effect of the fiber wall thickness on the structure of polyamide and polypropylene hollow fibers. J Appl Polym Sci 92:2017–2022
7. Lu X, Caps R, Fricke J et al (1995) Correlation between structure and thermal-conductivity of organic aerogels. J Non-Cryst Solids 188:226–234
8. Fricke J, Tillotson T (1997) Aerogels: Production, characterization and applications. Thin Solid Films 297:212–223
9. Woignier T, Phalippou J (1987) Skeletal density of silica aerogels. J Non-Cryst Solids 93:17–21
10. Lu X, Arduinischuster MC, Kuhn J et al (1992) Thermal-conductivity of monolithic organic aerogels. Science 255:971–972
11. Wei GS, Liu YS, Zhang XX et al (2011) Thermal conductivities study on silica aerogel and its composite insulation materials. Int J Heat Mass Transf 54:2355–2366
12. Fu B, Luo H, Wang F et al (2011) Simulation of the microstructural evolution of a polymer crosslinked templated silica aerogel. J Non-Cryst Solids 357:2063–2074
13. Xiao X, Streiter R, Ruan G et al (2000) Modelling and simulation for dielectric constant of aerogel. Microelectron Eng 54:295–301
14. Chen ZQ, Cheng P, Hsu CTA (2000) Theoretical and experimental study on stagnant thermal conductivity of porous media. Int Commun Heat Mass 27:601–610
15. Fei H, Hao X, Li Y (2005) Study on thermal properties of aerogels. Mater Rev 19:20–22
16. Li SY, Chu HS, Yan WM (2008) Numerical study of phonon radiative transfer in porous nanostructures. Int J Heat Mass Transf 51:3924–3931
17. Lee OJ, Lee KH, Yim TJ et al (2002) Determination of mesopore size of aerogels from thermal conductivity measurements. J Non-Cryst Solids 298:287–292
18. Liu H, Li Y, Zhao X, Tao W (2015) Study on unit cell models and the effective thermal conductivities of silicaaerogel. J Nanosci Nanotechno 15(4):3218–3223
19. Zeng SQ, Hunt A, Greif R (1995) Mean free-path and apparent thermal-conductivity of a gas in a porous-medium. J Heat Trans-Transf ASME 117:758–761
20. Zeng SQ, Hunt A, Greif R (1995) Transport-properties of gas in silica aerogel. J Non-Cryst Solids 186:264–270
21. Hrubesh LW, Pekala RW (1994) Thermal-properties of organic and inorganic aerogels. J Mater Res 9:731–738
22. Gross J, Fricke J, Pekala RW et al (1992) Elastic nonlinearity of aerogels. Phys Rev B45:12774–12777
23. Wang J, Kuhn J, Lu X (1995) Monolithic silica aerogel insulation doped with TiO_2 powder and ceramic fibers. J Non-Cryst Solids 186:296–300
24. Swimm K, Reichenauer G, Vidi S et al (2009) Gas pressure dependence of the heat transport in porous solids. Int J Thermophys 30:1329–1342
25. Hemberger F, Weis S, Reichenauer G et al (2009) Thermal transport properties of functionally graded carbon aerogels. Int J Thermophys 30:1357–1371
26. Zhao JJ, Duan YY, Wang XD et al (2012) A 3-D numerical heat transfer model for silica aerogels based on the aggregate structure. J Non-Cryst Solids 358:1287–1297

27. Zeng JS, Greif QR, Stevens P (1996) et al. Effective optical constants n and k and extinction coefficient of silica aerogel. J Mater Res 11:687–693
28. Deng ZS, Wang J, Wu AM et al (1998) High strength SiO_2 aerogel insulation. J Non-Cryst Solids 225:101–104
29. Lee SC, Cunnington GR (2000) Conduction and radiation heat transfer in high-porosity fiber thermal insulation. J Thermophys Heat Transf 14:121–136
30. Cunnington GR, Lee SC (1996) Radiative properties of fibrous insulations: theory versus experiment. J Thermophys Heat Transf 10:460–466
31. Rozek Z et al (2008) Potential applications of nanofiber textile covered by carbon coatings. J Achievements Mater Manufacturing Eng 27:35–38
32. Li Y, Holcombe BV (1998) Mathematical simulation of heat and moisture transfer in a human-clothing-environment system. Text Res J 68:389–397
33. Fohr JP, Treguier G (2002) Dynamic heat and water transfer through layered fabrics. Text Res J 72:1–12
34. Sukigara SHY, Fujimoto T (2003) Compression and thermal properties of recycled fiber assemblies. Text Res J 73:310–315
35. Reim M et al (2005) Silica aerogel granulate material for thermal insulation and daylighting. Sol Energy 79:131–139
36. Venkataraman M, Mishra R, Jasikova D, Kotresh TM, Militky J. Thermodynamics of aerogel treated nonwoven fabrics at subzero temperatures. J Ind Text (in print)
37. Warrier P, Yuan YH, Beck MP et al (2010) Heat transfer in nanoparticle suspensions: modeling the thermal conductivity of nanofluids. AIChE J 56:3243–3256

Chapter 21
Biomaterials and Nanotechnology Approach to Medical Enhancement

Tomáš Kovářík, Tomáš Křenek, Petr Bělský and Jaroslav Šesták

Abstract Over the past few decades, biomaterial science has emerged as a new field in which a regeneration or replacement of damaged tissue has become one of the main focuses. Also, great advances in the application of multifunctional nanoparticles for biomedical applications have been made. Implementation of nanomedicine in cellular, preclinical, and clinical studies has led to exciting advances ranging from fundamental to applied research. This chapter will examine the key aspects of application of traditional biomaterials, their physicochemical properties, and behavior in biological system. Moreover, the unique properties of nanomaterials are highlighted in relation to their vast nanostructural characteristics and the field of application. With 164 references.

21.1 Introduction

In the last 50 years, the field of biomaterials has developed greatly. Vast enhancements in orthopedic, dental, haemic, neurological, cartilage, and cardiovascular applications have been achieved. The progress is essentially linked with research in industry and academia focused toward the development of innovative biomaterials. Such an endeavor is strongly supported by a need to solve medical problems related to tissue regeneration, lost or damaged organs, traumatic injuries, diseases, or aging.

T. Kovářík (✉) · T. Křenek · P. Bělský · J. Šesták
New Technologies Research Centre (NTC-ZČU), University of West Bohemia,
Universitní 8, 30114 Pilsen, Czech Republic
e-mail: toko@ntc.zcu.cz

J. Šesták
Division of Solid-State Physics, Institute of Physics v.v.i., Czech Academy of Sciences,
Cukrovarnická 10, 16200 Prague, Czech Republic
e-mail: sestak@fzu.cz

J. Šesták et al. (eds.), *Thermal Physics and Thermal Analysis*,
Hot Topics in Thermal Analysis and Calorimetry 11,
DOI 10.1007/978-3-319-45899-1_21

Biomaterials are widely used in medical applications as implants for bone regeneration/replacement or fracture repair [1–3], dental implants [4, 5], orbital implants and ocular prostheses [6], and artificial skin and muscles [7] and for biosensors, bioactuators, bioseparators, blood-contacting biomedical devices [8], etc. Additionally, various biotechnological applications are utilized in medical procedures such as colloidal particles for drug and gene delivery [9, 10], cancer imaging and therapy [11, 12], purification of assorted types of molecules or enrichment/detection of proteins [13], enzyme immobilization/encapsulation [14, 15], functionalized membranes for protein ultrafiltration [16] and wastewater cleaning [17], and biosensors devices [18].

Furthermore, biomaterials of human origin have attracted considerable attention in tissue engineering and therapeutics. Several types of blood-derived products, naturally occurring proteins or extracellular matrices, are utilized in clinical practice. Besides, non-expanded stem cells for tissue engineering provide new approaches for the advancement of clinically regenerative therapies [19, 20]. Biomaterial technologies provide appropriate scaffolds with desirable structural and biochemical properties to fulfill the requirements for successful tissue regeneration. The design of such scaffolds must strictly adhere to the mechanical, structural, biochemical, and biological requirements as presented in the diagram in Fig. 21.1.

Nowadays, health difficulties with medical implants are usually related to infection, rejection, accelerated bone loss, and poor osseointegration with loosening of the implant. The most frequent cause for failure is insufficient bone formation around the biomaterial immediately after implantation [21, 22]. This implies that implant surface and tissue interface are critical zone, where tissue responses are mainly dictated by processes controlled at the nanoscale. Current prospects for nanotechnology in biomaterials engineering for medical applications appear to be excellent with promising potential for further progress.

21.2 Biomaterials

Generally, the functional aspects of use and application of biomaterials also include manufacturing, packaging, sterilizing, and surgical placement. The importance of these considerations has been emphasized through the need of safety and functionality of medical implants or drug formulations. It is evident that physicochemical properties of applied materials will be decisive for the most relevant applications and examples. The specific applications of these materials are provided in various forms: porous, dense, powders, injectable mixtures, viscous cements, and coatings.

Implants for bone replacement or fracture repair in load-bearing situations are made of materials that provide the appropriate mechanical characteristics, such as Ti_6Al_4V or Co–Cr–Mo alloys used for a total hip or knee joint replacement, shoulder, and elbow prostheses [23]. Also, fixation plates, wires, and screws for the repair of fractures in the long bones or craniofacial regions are applied. Moreover,

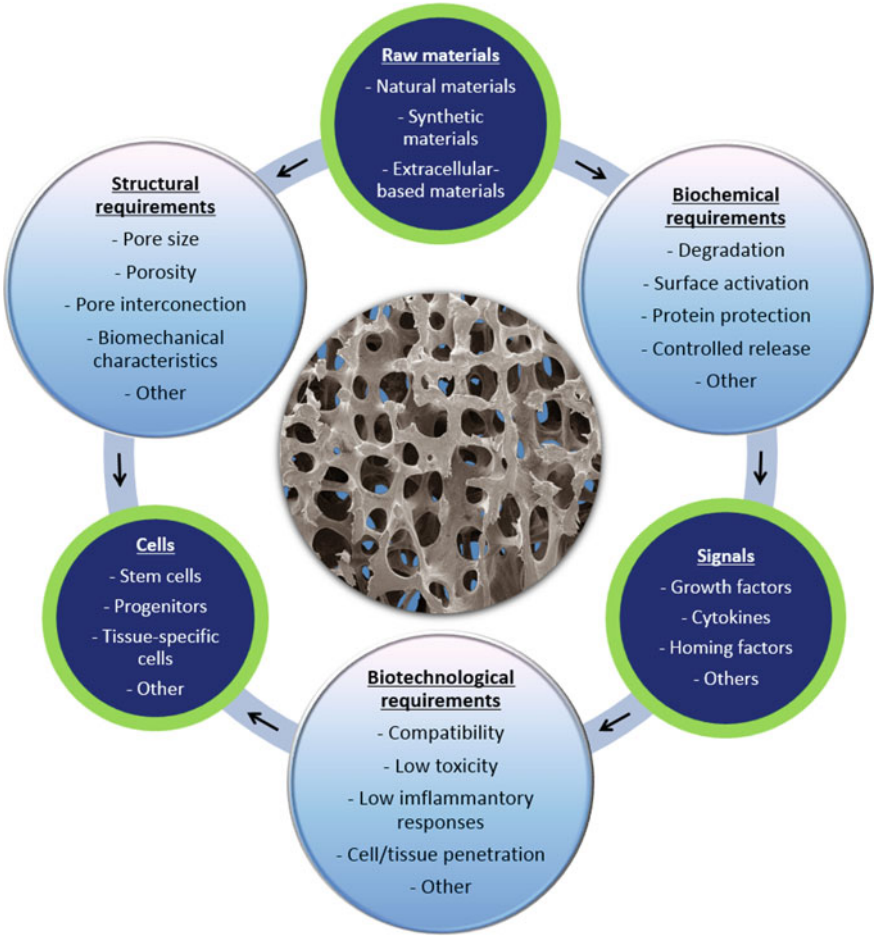

Fig. 21.1 Schematic presentation of key factors for scaffold design

low-carbon stainless steel (grade 316L) has been widely used in orthopedic applications and fracture fixation devices. Lately, several magnesium alloys have been investigated as a new class of biomaterials owing to their excellent biodegradability as potential biomaterials for implantable medical devices, specifically in the applications that require degradation and subsequent disappearance of the device after cure [24]. Typical examples of such applications include a pin or a screw in orthopedic devices and a stent for vascular reconstruction [25]. In particular, the in vitro cytocompatibility of Mg–Y–Zn–Zr alloys has been investigated using cell lines L-929 [26]. Thus far, several studies have reported in vitro or in vivo studies on the potential use of magnesium alloys in orthopedic applications [27] and implanting the alloys into soft tissues or bones [28].

Currently, a major challenge is the design and fabrication of scaffolds for specific defect sites [29]. Because of the differences in the architecture of cortical and cancellous bone, their mechanical and structural properties (compressive, flexural, and tensile strength, elastic modulus, and porosity) differ significantly. The comparison of basic properties such as compressive, flexural, and tensile strength, elastic modulus, and porosity of selected materials is presented in Table 21.1. It should be pointed out that the mechanical characteristics are strongly related to the manufacturing process, heat treatment, and solidification procedures resulting in specific microstructure of polycrystalline alloys.

Ceramic materials, of course, are another group of biomaterials. They include bioactive glasses [30] and glass ceramics [31], synthetic calcium phosphates [32], and ceramic composites [33]. According to the type of bioceramics and their interaction with the host tissue, they can be classified as bioactive or bioinert (resorbable/non-resorbable). Bioceramics are now used in various applications throughout the human body, primarily for skeletal repair and reconstruction of diseased or damaged hard tissue. As with other materials, the physical and biochemical/biotechnological properties of ceramic implants are strictly related to the structural state (polycrystalline, semicrystalline, and non-crystalline/amorphous), surface properties (chemical composition, bonding capabilities, and surface architecture), and form (dense, porous, granules/filler, multifunctional particles, and coatings). Well-known examples are zirconia and alumina, which are primarily used in the fabrication of femoral heads [34]. Among these, ceramics can react with the physiological fluids forming biological-type apatite, e.g., calcium phosphates, and several compositions of glasses and ceramic glasses [35]. Ordered mesoporous silica materials revealed interesting properties behaving as bioactive glasses, but including a pore channel system with dimensions that allow the inclusion of different molecules with biological activity [36]. These materials allow

Table 21.1 Mechanical characteristics of metals and related properties of human bone [147–151]

	316L	Ti_4Al_4V	Co–Cr–Mo alloy	Cortical bone	Cancellous bone
Compressive strength (MPa)	170–310	990	–	100–150	2–12
Flexural strength (MPa)	180–330	~1000	965	135–193	10–20
Tensile strength (MPa)	550–650	897–1205	864–1280	50–151	1–5
Modulus elasticity—tension (GPa)	193–200	114	241	10–20	0.1–5
Fracture toughness (MPa $m^{1/2}$)	150–200	75	–	2–12	0.1–0.8
Elongation (% in 50 mm)	40–50	10–18	8–10	–	–
Density (g/cm^3)	8.0	4.4	8.3–8.8	2–2.2	1.4–1.6
Porosity (%)	–	–	–	5–10	50–90

loading biologically active molecules such as drugs, peptides, proteins, or growth factors. Hence, they play a release function for biologically active molecules which may help and improve bone regeneration [37].

Also, there are a large number of polymeric materials that have been used as implants or part of implant systems, as presented in Table 21.2. In most of these applications, polymers have little or no competition from other types of materials. Their uniqueness consists in combination of following properties: Flexibility, resistance to biochemical attack, good biocompatibility, low weight, and available in a wide variety of compositions with adequate physical and mechanical properties, which can be easily manufactured into products with the desired shape. The polymeric systems include acrylics, polyamides, polyesters, polyethylene, polysiloxanes, polyurethane, and a number of reprocessed biological materials. Some of the applications include the use of membranes of ethylene-vinyl acetate (EVA) copolymer for controlled release and the use of poly(glycolic acid) for use as a resorbable suture material. Some other typical biomedical applications, in which polymeric materials are utilized, are artificial hearts, kidneys, livers, pancreases, bladders, bone cement, catheters, contact lenses, cornea and eye-lens replacements, external and internal ear repairs, heart valves, ventricular assist device (VAD), implantable pumps, joint replacements, pacemakers, encapsulations, soft tissue replacements, artificial blood vessels, artificial skin, and sutures. As bioengineers search for designs of ever-increasing capabilities to meet the needs of medical practice, polymeric materials alone and in combination with metals and ceramics are becoming increasingly incorporated into devices used in the body.

It has been confirmed that bioactive organic–inorganic hybrids could have mechanical properties comparable to those of connective tissues. For example, SiO_2–PDMS (polydimethylsiloxane) organic–inorganic hybrids, which showed unusual rubber-like mechanical properties [38], were modified with CaO to induce in vitro bioactivity. Organically modified SiO_2-based ceramics, known as "ormosil" or "creamer," are important organic–inorganic hybrids, which are usually prepared by using solgel method [39]. These materials can be fabricated at relatively low temperatures that allow the direct incorporation of biologically active materials [40]. For instance, formation of apatite layer was achieved on the surface of an

Table 21.2 Examples of polymers in medical use [152]

Application	Polymer
Knee, hip, shoulder joints	Ultrahigh molecular weight polyethylene
Finger joints	Silicone
Sutures	Polyactic and polyglycolic acid, polyamide
Tracheal tubes	Silicone, acrylic polymers, polyamide
Heart pacemaker	Polyethylene, polyurethane
Blood vessels	Polyester, polytetrafluoroethylene, polyvinyl chloride
Facial prostheses	Polydimethyl siloxane, polyurethane, polyvinyl chloride
Bone cement	Polymethyl methacrylate

organically modified silica in a simulated body fluid (SBF) with ion concentrations similar to those of the human blood plasma [41, 42].

21.3 Historical Aspects of Glasses and Bioactivity

Glass manufacturing in the twentieth century was significantly linked to the technology progress in glass chemistry, heat treatment procedures, and machinery industry. For example, the development of the twin-roller technique enabled to make sheet glass a few mm in thickness and a couple of meters in width, or the invention of the float process, in which melts are poured continuously from a furnace onto a shallow bath of molten tin, made possible to produce optical smooth and parallel surfaces. The chemical glass modifications, such as doping with rare earth ions and coloring with added oxides, halides/chalcogenides, or surface functionalization, allowed adjusting various physicochemical and structural properties of produced glasses [43]. This led to an increased interest in such materials in the field of electro-optics, optoelectronics, and microelectronics. Further attention of both the industrial and academic researches was devoted to the study of thermal properties of solid-state structures, phase changes/phase separations, or viscosity properties [44].

A series of questions was addressed regarding the properties of the bonding between living tissues and non-living implant materials. The glass composition of 45% SiO_2, 24.5% Na_2O, 24.5% CaO, and 6% P_2O_5 was selected to provide a large amount of CaO with some P_2O_5 in a Na_2O–SiO_2 matrix. In vivo and in vitro tests provided an explanation for the interfacial bonding of the implant to the bone, and the "bioglass" became highly attractive for further research [30]. Since the discovery of Bioglass by Hench [45], various kinds of bioactive materials have been found and clinically used. Their high bioactivity opens qualitatively new application fields, especially for anchoring of the implant in the host tissue, with practical use in orthopedics, stomatology, neurosurgery, oncology, craniofacial surgery, and other fields [46].

For many years, it was accepted that placing any man-made material in the body would result in a foreign body reaction and that a non-adherent scar tissue would always form at the interface between the original tissue and the implanted material. Thus, for decades, biomaterials research was focused toward materials that were as inert as possible to the physiological environment. This understanding was completely changed when a special composition of soda lime–phosphate silicate glass was synthesized and implanted in the femurs of rats. This glass composition was an invert glass containing only 45 wt% of SiO_2. The content of network modifiers was 24.5% Na_2O and 24.5% CaO and 6% P_2O_5 to provide the CaO and P_2O_5 constituents of hydroxyapatite (HA), the inorganic mineral phase of bone. The glass, designated as 45S5 Bioglass®, did not form interfacial scar tissue. Instead, Bioglass® implants bonded to the living bone and could not be removed from their implant site [47]. Bioactive materials, including bioactive glasses and glass

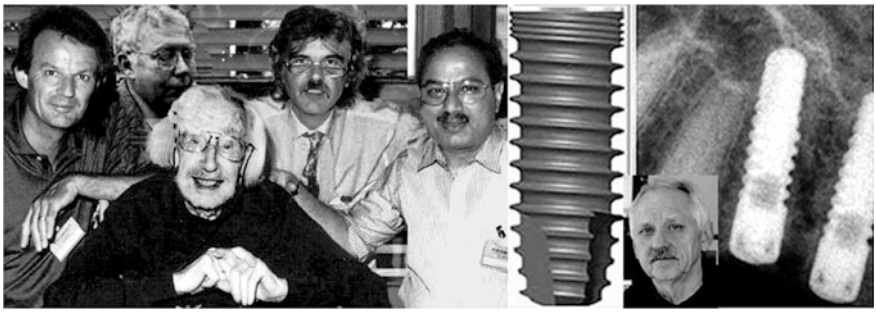

Fig. 21.2 *Left* Think tank at the US Missouri University in Rolla at the turn of seventies headed by the legendary glasses-progenitor Norbert Kreidl (*middle*) with his disciples and new topic architects (*upper from left*) Peter Schultz (glassy fibbers for communication), Larry Hench (bioglasses for implantation), Jaroslav Šesták (oxide glasses for magnetic applications), and Edward Boulos (engineering glasses for industry). *Right* Thirty years later, the manufactured dental Ti-implants, double surface treated (acid-alkali [51, 52] nanolayering), were produced by the Czech company LASAK © (www.lasak.cz Prague) and successfully presented to the dentistry market (founded by Z. Strnad, bioactivity designer—*inset*)

ceramics, have special compositions and consist typically of the Na_2O–CaO–MgO–P_2O_5–SiO_2 system [48]. However, the presence of P_2O_5 is not necessary [49] for triggering bioactivity, the degree of which can be well esteemed quantitatively using the principle of non-bridging oxygen [50–52] which was described in detail in our previous book (Volume 9) [53] (Fig. 21.2).

The bond to bone occurs at different rates depending upon the composition. Materials with the fastest rates of bone bonding also bond to soft tissues. When a particulate of bioactive glass, ceramic, or glass ceramic is used to fill a bone defect, both the rate and extent of bone recovery depend on the material's composition [54, 55]. The bone is regenerated to a larger extent in the presence of bioactive glass 45S5 than when synthetic HA or other calcium phosphate ceramic particulates are used. After weeks of regeneration, more than twice as much of new bone material forms in the defect when bioactive glass is used for the repair. The quantity, architecture, and mechanical properties of the recovered part of the bone match to those of the original bone [56].

21.4 Porous Materials

Another way how to enhance fixation of implants to the bone is the production of porous biomaterial. Mismatch of Young's moduli of the implanted biomaterial and the surrounding bone has been identified as a major reason for implant loosening due to the stress shielding of bone [57]. A suitable balance between strength and stiffness represents an important factor. This can be achieved by the formation of materials with significant surface or total bulk porosity of implant.

Another challenge of porous materials is their high surface area for the bone ingrowth for long-term biologic fixation in biomedical applications [58]. Porous implants should exhibit specific features such as filling bone defect cavities, pore interconnectivity, and pore architecture that promote bone formation as well as facilitate the exchange of nutritional components and oxygen to enhance bone ingrowth [59], and sufficient strength to support physiological loading. From the early 1970s, various studies on porous materials have been reported. Ceramic [60], polymeric [61], and metallic porous materials [62] have to be demonstrated in animal studies to be promising candidates for porous implants that exhibit suitable bone ingrowth. Despite excellent corrosion and wear resistance of ceramics implants, their intrinsic brittleness excludes this material from the utilization as load-bearing implants. Similarly, porous polymeric materials do not possess mechanical strength high enough to endure loads in orthopedic implants. The most promising group of porous materials for load-bearing implants showed to be porous metals, especially titanium and its alloy (Ti_6Al_4V), Co–Cr alloys, and 316L stainless steel. Their suitable fracture and fatigue resistance characteristics predispose them for load-bearing applications [63]. Numerous methods of the formation of both closed-cell as well as open-cell porous metal materials have been developed. Table 21.3 gives a brief summary of them.

The quality of fixation of the bone into the porous coating is strongly dependent on the geometry of the porous layer. However, no significant difference in biologic response as a function of pore shape has been reported [64]. The size of interconnecting pores has been confirmed as one of the critical factors for bone ingrowth [65]. Although the ideal pore size desired for implant fixation remains undefined, there is a common agreement that in order to optimize mineralized bone ingrowth, pore sizes between 100 and 400 μm are needed [66]. Despite several studies

Table 21.3 Summary of various fabrication techniques for porous metals and their categorization according to the resulting pore distribution

Fabrication methods for porous metals		
Closed-cell	Random distribution	Gas injection into the metal melt [153]
		Decomposition of foaming agents [154]
	Graded pore distribution	Plasma spraying [62]
Open-cell	Non-homogenous	Sintered metal powders [155]
		Sintered metal fibers [156]
		Space holder method [157]
		Replication [158]
		Combustion synthesis [159]
		Plasma spraying [62]
	Homogenous	Orderly oriented wire mesh [160]
		Vapor deposition [161]
		Ferromagnetic fiber array [162]
	Functionally graded	Rapid prototyping [163]
		Electro discharge compaction [164]

showing excellent bone ingrowth into porous metallic systems, there have been a number of cases in which prostheses with porous surfaces were retrieved with minimal or no bone ingrowth present [67].

The basic condition for an artificial material to bond to natural bone is the formation of a biologically active bone-like apatite layer on its surface in the living body [68]. Thin, plasma-sprayed hydroxyapatite coatings over powder-made, porous Ti surfaces have shown increased rates of bone ingrowth due to the hydroxyapatite coating [69]. HA coatings on Ti and Ti alloys were produced by a myriad of different techniques ,e.g., plasma-spray [70], thermal [71], microvave [72], microarc oxidative [73], solgel [74], electrolytic [75], electrophoretic [76], electron-beam [77], ion-beam [78], pressure-less sintering [79], hot isostatic pressing [80], dipping [81], magnetron-sputtering [82], and laser-induced [83] deposition.

There are some differences in the composition and the degree of crystallinity of HA and bone mineral, since bone mineral—$(Ca, M)_{10}(PO_4,Y)_6(OH, X)_2$, where M (Mg, Na, K) and Y (Cl, F) stand for metal and halogen ions—is typically calcium deficient and contains carbonate moieties. It is also known that the substitution of the silicate ions for the phosphate ions in HA enhances osteoblast cell activity, which leads to higher rate at which bone cells adhere and proliferate on HA coatings [84, 85]. Attempts have been therefore made to prepare and examine a carbonate-substituted HA (C-HA) with carbonyl groups exchanged with hydroxyl or phosphate groups [86, 87] and an (Si-HA) with a moderate incorporation of silicon [88]. The formation of the TiO_2 interface layer improves adhesion between the HA coating and the Ti substrate and leads to better osseointegration of the HA-coated implant.

21.5 Nanoparticles in Modern Medicine

Over the years, many novel functions of nanophase/nanoscale materials have been investigated in a wide range of medical domains, such as orthopedy, dentistry, urology, neurology, vascular medicine, cartilage medicine, and many others. Also, nanoarrays have been established as the preferred method for carrying out genetic, biological, or drug analyses on massive scale [89].

In particular, nanoscale science and engineering have accelerated the development of drug and gene delivery systems (multifunctional capsules) [90]; contrast agents for magnetic resonance imaging [91]; nanofibrous scaffolds [92]; nanoporous membranes for sorting, sensing, isolating, and releasing biological molecules [93]; immunoisolation devices [94]; nanoporous/crystalline thin films for sensing [95]; and many others. Nanoparticles have become highly attractive for many biological and medical applications due to their unique size-dependent properties, high reactivity, very high specific surface area (surface-to-mass or surface-to-volume ratio), and catalytic activity. Of course, there still remain

questions regarding the safety of nanoparticles in the human body and their incorporation into biological environment/living organism.

The major contributions of nanoparticles to modern medicine, already advanced to clinical use or in vivo experiments, are related to:

- ***Fluorescent biological labels—Quantum dots/rods***

Inadequate fluorescence and photobleaching are the most frequent problems in conventional imaging of cells and tissues. Quantum dots (QDs) are nanoparticles composed of inorganic semiconductor molecules emitting strong fluorescent light under ultraviolet illumination [96, 97]. The wavelength of the emitted fluorescent light depends sensitively on particle size and narrow size distribution. In order to interact with biological target, a biological or molecular coating acting as a bio-inorganic interface is attached to the nanoparticle. Furthermore, more than one type of molecule can be attached to each QD, giving it multiple functionalities. This leads to specific in vivo characteristics and to applications such as imaging of lymph nodes, lung blood vessels, and tumors. It was demonstrated that ZnSn-capped CdSe QDs can be directed to the lungs of mice by coating the QD surface with a peptide sequence [98]. QDs made of CdTe capped with CdSe are capable of light emission under near-infrared excitation which led to ability to map lymph nodes up to 10 mm below the skin surface without the need for surgical incisions [99]. In addition, biomolecules can be conjugated with QDs through non-covalent bonds, such as the interactions of biotin/avidin or nickel nitrilotriacetic acid (Ni-NTA)/histidine-tagged peptides [100]. Also, biological coatings may include antibodies, biopolymers, or monolayers of small molecules that make the nanoparticles biocompatible [101].

Detonation nanodiamonds (NDs) have emerged as carbon materials favorable for modern nanomedical applications, such as biocompatible nanoparticle drug delivery systems [102], adsorbents for removal/purification of various compounds [103], nanostructured coatings for implants [104], capacitive-based biosensors [105], and imaging probes [106]. Considering recent studies, fluorescent nanodiamond (FND) particles have unique surface or structural features that markedly improve their performance as imaging agents compared to clinical and nanoparticle standards [107]. The extreme photostability of NDs with negatively charged nitrogen vacancy (N-V) emerged as an excellent candidate for long-term cellular imaging over commonly used fluorophores. Upon continuous exposure to a 100 W lamp power for 480 min, the red fluorescent NDs (100 nm) remained stable with no observed photobleaching, whereas similarly sized red fluorescent polystyrene nanospheres photobleached within the first 30 min of photoexcitation [108, 109].

- ***MRI contrast enhancement***

Magnetic resonance imaging (MRI) technique is closely linked with contrast agents, which are important for precise and detailed observation of biological tissues [110]. MRI utilizes magnetic resonance spectroscopy to analyze hydrogen atoms that are naturally present in tissue (water, cell membrane proteins, etc.).

The MRI contrast agents are generally categorized according to their effect on the longitudinal (T_1) and the transverse (T_2) relaxation times, which is characterized by the corresponding relaxivities r_1 and r_2. The area where fast T_1 relaxation takes place appears bright, whereas T_2 relaxation results in dark areas in the MR images [111].

Compounds of gadolinium have been successfully applied for several years as high-spin paramagnetic contrast agents with the ability to study such areas as kidneys and brain. Other contrast agents were developed in order to replace Gd^{3+} ions or to be used for complementary purposes: iron and manganese compounds, nitroxide radicals, and PEG/HA nanoparticles containing manganese ions [112]. Recently, improved hydrophilicity and contrast enhancement were described for Gd-coated Au nanoparticles [113]. Also, mesoporous manganese silicate-based nanomaterial is a promising candidate as T_1 contrast agent and anticancer drug delivery carriers for the theranostics of tumor [114]. Superparamagnetic iron oxide (SPIO) nanoparticles have emerged as effective contrast agents for T_2 relaxations. The colloidal nanoparticles contain an iron oxide core, whose composition and physicochemical properties vary continuously from magnetite Fe_3O_4 to maghemite γ-Fe_2O_3.

- ***Drug and gene delivery***

Among the different application areas of nanoparticles, drug delivery is one of the most advanced ones. Generally, the aim of nanoparticles is entrapment of drugs and enhanced delivery to (or uptake by) target cells and/or reduction of the toxicity of the free drug to nontarget organs [115]. The main issues in the research of nanoparticles for bioengineering are (i) increase in specificity of targeted drug delivery, (ii) reduction of toxicity while maintaining the therapeutic effects, (iii) safety and biocompatibility, and (iv) multifunctionality. The composition of the engineered nanoparticles may vary from materials of biological origin such as phospholipids, lipids, lactic acid, dextran, and chitosan to chemical compounds such as polymers, carbon, silica, and metals. The release of active agent is controlled by its diffusion across a membrane, or it is released from a biodegradable polymer after its degradation or by erosion of nanoparticle shell or by a combination of diffusion and erosion of the shell. Most of the nanoparticles contain biodegradable polymers resulting in drug release after their degradation.

Also, several coatings can be used to prevent agglomeration and keep the particles in colloidal suspension including various polymers such as polyethylene glycol (PEG), poly(vinylpyrrolidone) (PVP), or natural polymers such as dextran, chitosan, pullulan, or surfactants such as sodium oleate and dodecylamine. Recently, noble metals such as silver, gold, and platinum demonstrated better antibacterial, antifungal, and antiviral effects when conjugated with biopolymers [116]. The biopolymer-decorated metal nanoparticles have been tested for combating various diseases caused by microbial pathogens [117].

Moreover, thermosensitive nanoparticles may be used for selective release of the contents after specific localization. For example, an enhanced cytotoxicity of

doxorubicin was observed in vitro at 42 °C compared to 37 °C when using nanocarriers consisting of copolymers of PEG and PLLA [118]. Also, pH-responsive nanocarriers have remarkable properties that allow them to circumvent biological barriers and achieve targeted intracellular drug delivery as schematically presented in Fig. 21.3 [119, 120].

Nanodiamond-based drug delivery systems against cancer are one of the most developed biomedical applications of NDs, which may also have a therapeutic role [121]. ND-mediated drug delivery may serve as a powerful method for overcoming chemoresistance in cancer stem cells and markedly improving overall treatment of hepatic cancer. In this case, delivery of epirubicin by NDs was demonstrated to overcome ATP-binding cassette transporters, which is the mechanism of resistance against an effective treatment of cancer stem cells [122].

The intracellular localization of the NDs suggests that these nanoparticles have the potential to be employed for the intracellular delivery of small therapeutic molecules. It should be noted that internalization of NDs into cells is strongly dependent upon their surface characteristics and other physical parameters such as size, shape, and aggregation of particular particles [123].

- ***Cancer treatment***

Nanoparticle-based drugs and delivery systems have made a tremendous impact on the treatment of various types of cancer [124]. Hyperthermia (also called thermal therapy or thermotherapy) is one of the possible treatments being widely studied and focused on heating certain organs or tissues to a temperature between 41 and 46 °C. This can also be achieved through heat transfer to specific sites by oscillations of nanoparticles. At present, ferrite nanoparticles are the most common material for hyperthermia because of the low toxicity, good magnetic properties, and straightforward synthesis by eco-friendly routes, where the spinel structures can be obtained with high crystallinity degree. Thus, the heating efficiency in aqueous colloids of these materials is well established [125, 126].

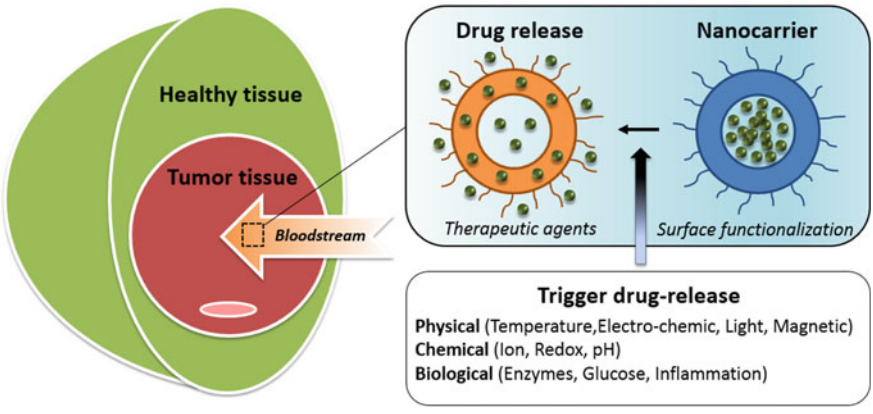

Fig. 21.3 Schematic representation of targeted drug delivery and release

Also, laser-selective photothermolysis and hyperthermia mediated by gold nanoparticles were introduced. Gold nanoclusters (AuNCs) were studied on the basis of targeting cancer tissue through physical transportation or conjugating with antibodies or virus. After reaching the target site, AuNCs were irradiated with short laser pulses of sufficient energy that make these nanoclusters explode. The explosion of these particles may be accompanied by optical plasma, shock wave generation, and particle fragmentation, which collectively aid to kill the cancer cells [127].

Nanocrystalline diamond (NCD) surfaces were functionalized, and morphogenetic protein in its active form was interacted strongly when NCD was oxygen terminated. Strong physisorption was shown to be directly related to the unique properties of NCD. Functionalized hydrophilic NCD surfaces were able to promote osteogenic induction in human stromal cells in vitro [128]. Various biological molecules can be assembled on the ND hydrogel film deposited onto the polylysine (PLL)-coated glass substrate [129]. Considering recent studies, ND-drug films can be implanted immediately after surgical removal of a tumor to target residual cancerous cells so as to effectively prevent the tumor from recurring [130].

- ***Tissue engineering***

Scaffolds provide support to the regenerating tissue, and they can also be used to deliver bioactive molecules to accelerate the healing process. In addition, the scaffolds for bone tissue engineering need to be biocompatible, osteoinductive, osteoconductive, and osteointegrative [131]. Various nanomaterials have enhanced these characteristics and/or exhibited superior physicochemical properties (i.e., mechanical, electrical, optical, catalytic, and magnetic) [132]. These materials include nanoparticles, nanoclusters, nanocrystals, nanotubes, nanofibers, nanowires, nanorods, and nanofilms.

The reason for using nanotechnology for regenerative medicine becomes obvious when examining bone as a structural nanocomposite. Bone tissue itself represents a biological nanocomposite composed of a protein-based soft hydrogel template (i.e., collagen, non-collagenous proteins—laminin, fibronectin, and vitronectin) and water. Hard inorganic components dominantly consist of nanocrystalline hydroxyapatite components, with a hierarchical structure ranging from the macroscale down to the nanoscale (Fig. 21.4) [133]. For example, 70% of the bone matrix is composed of nanocrystalline HA which is typically 20–80 nm long and 2–5 nm thick [134]. Studies have demonstrated that nanostructured materials with cell favorable surface properties may promote specific protein interactions more intensely compared to conventional materials and thus to stimulate the new bone growth more efficiently [135]. In a recent study, a biodegradable nanohydroxyapatite/polyphosphazene microsphere 3D scaffold was fabricated, which had suitable mechanical properties and cytocompatibility properties for bone tissue engineering applications [136]. Also, in vivo studies demonstrated that nanocrystalline HA accelerated new bone formation on tantalum scaffolds when used as an osteoconductive coating compared to uncoated or conventional micron-size-HA-coated

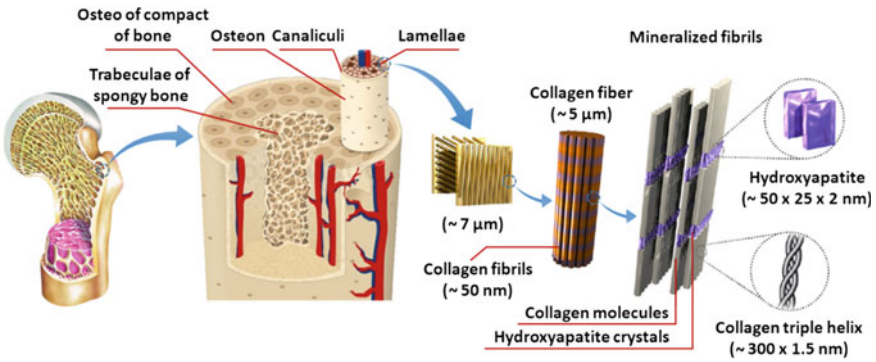

Fig. 21.4 Illustration of bone structure from macroscopic level down to nanostructured objects

tantalum [137]. Similar tendencies have been reported for other nanoceramics including aluminum, zinc, and titanium oxide. Furthermore, nanophase zinc oxide, nanophase titania, and nanofiber alumina enhanced collagen synthesis, alkaline phosphatase activity, and calcium mineral deposition by osteoblasts compared to conventional equivalents [138]. As is known, significantly improved osteoblast adhesion has been observed on helical rosette nanotubes regardless of whether they are incorporated into hydrogels or coated on titanium [139]. Against this background, due to their superior cytocompatible, mechanical, and electrical properties, carbon nanotubes/nanofibers (CNTs/CNFs) are ideal scaffold material candidates for bone tissue engineering applications [140].

As mentioned above, NDs have several unique properties giving them vast application platform. The versatility of surface functionalization and the anisotropic distribution of charges on the ND surface enables antimicrobial applications such as infection treatment using NDs functionalized with saccharides to detect and capture bacteria [141]. Also, partially oxidized and negatively surface-charged NDs were utilized to mediate potent antimicrobial activity against both Gram-negative and Gram-positive bacteria [142].

It was demonstrated that toxicity of NDs can vary depending upon their surface chemistry, the type of cell line, and the composition of the treatment medium [143, 144]. Nevertheless, comparative in vitro studies have been conducted with graphene, CNTs, and NDs to understand the similarities and differences in nanocarbon toxicity. Whereas CNTs and graphene exhibited similar rates of toxicity with increasing carbon concentration, NDs appeared to be less toxic [145]. In addition, cellular studies in vivo have been conducted to evaluate the toxicity of NDs demonstrating that intravenous administration of modified NDs did not cause any destruction of blood cells or death of experimental animals [146].

Acknowledgements The result was developed within the CENTEM project, reg. no. CZ.1.05/2.1.00/03.0088, cofounded by the ERDF as part of the Ministry of Education, Youth and Sports OP RDI program and, in the follow-up sustainability stage, supported through

CENTEM PLUS (LO1402) by financial means from the Ministry of Education, Youth and Sports under the National Sustainability Program I. This action was also supported by the Technology Agency of the Czech Republic, Program ALFA, project no. TA04020860. Shared aims by LASAK ©—The Laboratory for Glass and Ceramics in Prague (Doc. Zdeněk Strnad, Ing. Jan Riedel and Dr. Jakub Strnad) as well as by Universität Bremen in Germany (Dr. Michael Maas) are appreciated.

References

1. Fu Q, Saiz E, Rahaman MN, Tomsia AP (2011) Bioactive glass scaffolds for bone tissue engineering: state of the art and future perspectives. Mater Sci Eng C 31:1245–1256
2. Ginebra MP, Espanol M, Montufar EB, Perez RA, Mestres G (2010) New processing approaches in calcium phosphate cements and their applications in regenerative medicine. Acta Biomater 6:2863–2873
3. Arcos D, Vallet-Regí M (2010) Sol–gel silica-based biomaterials and bone tissue regeneration. Acta Biomater 6:2874–2888
4. Lemons JE, Misch-Dietsh F, McCracken MS (2015) Biomaterials for dental implants. In: Dental implant prosthetics. St. Louis (Chapter 4, ISBN 9780323078450)
5. Babu ARS, Ogle O (2015) Tissue response: biomaterials, dental implants, and compromised osseous tissue. Dent Clin North Am 59:305–315
6. Baino F, Perero S, Ferraris S, Miola M, Balagna C, Verné E, Vitale-Brovarone Ch, Coggiola A, Dolcino D, Ferraris M (2014) Biomaterials for orbital implants and ocular prostheses: overview and future prospects. Acta Biomater 10:1064–1087
7. Ullah F, Othman MBH, Javed F, Ahmad Z, Akil H (2015) Classification, processing and application of hydrogels: a review. Mater Sci Eng C 57:414–433
8. Hsiao ChR, Lin ChW, Chou ChM, Chung ChJ, He JL (2015) Surface modification of blood-contacting biomaterials by plasma-polymerized superhydrophobic films using hexamethyldisiloxane and tetrafluoromethane as precursors. Appl Surf 346:50–56
9. Zhang Q, Liu F, Nguyen KT, Ma X, Wang X, Xing B, Zhao Y (2012) Multifunctional mesoporous silica nanoparticles for cancer-targeted and controlled drug delivery. Adv Funct Mater 22:5144–5156
10. Kozlova D, Chernousova S, Knuschke T, Buer J, Westendorf AM, Epple M (2012) Cell targeting by antibody-functionalized calcium phosphate nanoparticles. J Mater Chem 22:396–404
11. Yu MK, Park J, Jon S (2012) Targeting strategies for multifunctional nanoparticles in cancer imaging and therapy. Theranostics 2:3–44
12. Mahmoudi M, Sant S, Wang B, Laurent S, Sen T (2011) Superparamagnetic iron oxide nanoparticles (SPIONs): development, surface modification and applications in chemotherapy. Adv Drug Deliv Rev 63:24–46
13. Burtea C, Laurent S, Mahieu I, Larbanoix L, Roch A, Port M (2011) In vitro biomedical applications of functionalized iron oxide nanoparticles, including those not related to magnetic properties. Contrast Media Mol Imaging 6:236–250
14. Broberg Kristensen J, Meyer RL, Horsmans Poulsen C, Kragh KM, Besenbacher F, Sogaard Laursen B (2010) Biomimetic silica encapsulation of enzymes for replacement of biocides in antifouling coatings. Green Chem 12:387–394
15. Kawachi Y, Kugimiya S, Nakamura H, Kato K (2014) Enzyme encapsulation in silica gel prepared by polylysine and its catalytic activity. Appl Surf 314:64–70
16. Rovira-Bru M, Giralt F, Cohen Y (2001) Protein adsorption onto zirconia modified with terminally grafted polyvinylpyrrolidone. J Colloid Interface Sci 235:70–79
17. Ciston S, Lueptow RM, Gray KA (2008) Bacterial attachment on reactive ceramic ultrafiltration membranes. J Membr Sci 320:101–107

18. Largueze J-B, Kirat KE, Morandat S (2010) Preparation of an electrochemical biosensor based on lipid membranes in nanoporous alumina. Colloids Surf B 79:33–40
19. Chow D, Nunalee ML, Lim DW, Simnick AJ, Chilkoti A (2008) Peptide-based biopolymers in biomedicine and biotechnology. Mater Sci Eng R Rep 62:125–55
20. Chen F-M, Liu X (2016) Advancing biomaterials of human origin for tissue engineering. Prog Polym Sci 53:86–168
21. Tomsia AP, Launey ME, Lee JS, Mankani MH, Wegst UGK, Saiz E (2011) Nanotechnology approaches for better dental implants. Int J Oral Maxillofac Implants 26:25–49
22. Christenson EM, Anseth KS, van den Beucken LJJP, Chan CK, Ercan B, Jansen JA, Laurencin CT, Li WJ, Murugan R, Nair LS, Ramakrishna S, Tuan RS, Webster TJ, Mikos AG (2007) J Orthop Res 25:11–22
23. Mahapatro A (2015) Bio-functional nano-coatings on metallic biomaterials. Mater Sci Eng C 55:227–251
24. Mochizuki A, Kaneda H (2015) Study on the blood compatibility and biodegradation properties of magnesium alloys. Mater Sci Eng C 47:204–210
25. Ma J, Zhao N, Betts L, Zhu D (2015) Bio-adaption between magnesium alloy stent and the blood vessel: a review. J Mat Sci Tech (ISSN 1005–0302, http://dx.doi.org/10.1016/j.jmst.2015.12.018)
26. Fan J, Qiu X, Niu X, Tian Z, Sun W, Liu X, Li Y, Li W, Meng J (2013) Microstructure, mechanical properties, in vitro degradation and cytotoxicity evaluations of Mg–1.5Y–1.2Zn–0.44Zr alloys for biodegradable metallic implants. Mat Sci Eng C 33:2345–2352
27. Scheideler L, Füger C, Schille C, Rupp F, Wendel H-P, Hort N, Reichel HP, Geis-Gerstorfer J (2013) Comparison of different in vitro tests for biocompatibility screening of Mg alloys. Acta Biomat 9:8740–8745
28. Hänzi AC, Gerber I, Schinhammer M, Löffler JF, Uggowitzer PJ (2010) On the in vitro and in vivo degradation performance and biological response of new biodegradable Mg–Y–Zn alloys. Acta Biomat 6:1824–1833
29. Alvarez K, Nakajima H (2009) Met Scaffolds Bone Regeneration 2:790–832
30. Hench LL (2006) The story of Bioglass®. J Mater Sci Mater Med 17:967–978
31. Kokubo T, Shigematsu M, Nagashima Y, Tashiro M, Nakamura T, Yamamuro T, Higashi S (1982) Apatite- and wollastonite-containing glass ceramics for prosthetic applications. Bull Inst Chem Res 60:260–268
32. Bohner M, Gbureck U, Barralet JE (2005) Technological issues for the development of more efficient calcium phosphate bone cements: a critical assessment. Biomaterials 26:6423–6429
33. Fidancevska E, Ruseska G, Bossert J, Lin Y-M, Boccaccini AR (2007) Fabrication and characterization of porous bioceramic composites based on hydroxyapatite and titania. Mat Chem Phys 103:95–100
34. Huet R, Sakona A, Kurtz SM (2011) Strength and reliability of alumina ceramic femoral heads: review of design, testing, and retrieval analysis. J Mech Behav Biomed Mat 4:476–483
35. Gil-Albarova J, Garrido-Lahiguera R, Salinas AJ, Román J, Bueno-Lozano AL, Gil-Albarova R, Vallet-Regí M (2004) The in vivo performance of a sol–gel glass and a glass-ceramic in the treatment of limited bone defects. Biomaterials 25:4639–4645
36. Taguchi A, Schüth F (2005) Ordered mesoporous materials in catalysis. Micropor Mesopor Mat 77:1–45
37. Balas F, Manzano M, Colilla M, Vallet-Regí M (2008) L-Trp adsorption into silica mesoporous materials to promote bone formation. Acta Biomater 4:514–522
38. Salinas AJ, Merino JM, Babonneau F, Gil FJ, Vallet-Regí M (2007) Microstructure, macroscopic properties of bioactive CaO–SiO2–PDMS hybrids. J Biomed Mater Res 81:274–282
39. Mackenzie JD, Huang Q, Iwamoto T (1996) Mechanical properties of ormosils. J Sol-Gel Sci Technol 7:151–161

40. Manzano M, Aina V, Aren CO, Balas F, Cauda V, Colilla M, Delgado MR, Vallet-Regí M (2008) Studies on MCM-41 mesoporous silica for drug delivery: effect of particle morphology and amine functionalization. Chem Eng J 137:30–37
41. Chen Q, Miyata N, Kokubo T, Nakanura T (200) Bioactivity, Mechanical properties of PDMA-modified CaO-SiO2-TiO2 hybrids prepared by sol-gel process. J. Biomed. Mater. Res. 51:605–611
42. Tsuru K, Ohtuki C, Osaka A (1997) Bioactivity of sol-gel derived organically modified silicates. J Mater Sci Mater Med 8:57–61
43. Skorospelova VI, Stepanov SA (1974) Behavior of iron ions in glasses of the K2O–Al2O3–B2O3 system. Izv Akad Nauk SSSR Neorg Mater 10:1864–1871
44. Šesták J, Mareš JJ, Hubík P (2011) Glassy, amorphous and nano-crystalline materials, thermal physics, analysis, structure and properties, hot topics in thermal analysis and calorimetry 8, Springer (ISBN 978-90-481-2881-5)
45. Hench LL, Splinter RS, Allen WS (1971) Bonding mechanisms at the interface of ceramic prosthetic materials. J Biomed Res Symp 2:117
46. Brånemark PI (1969) Intraosseous anchorage of dental prostheses. Scand J Plast Reconstr Surg 3:81–93
47. Hench LL, Clark Jr. AE, Schaake HF (1972) Int Int J Non-Cryst Sol 8–10:837
48. Hench LL, Wilson J (1999) An introduction to bioceramics. Singapore World Scientific 1–23:41–62
49. Strnad Z (1992) Role of the glass phase in bioactive glass-ceramics. Biomaterials 13:317–321
50. Koga N, Strnad J, Strnad Z, Šesták J (2003) Thermodynamics of non-bridging oxygen in silica bio-compatible glass-ceramics. J Therm Anal Calorim 71:927–938
51. Strnad J, Strnad Z, Šesták J (2007) Physico-chemical properties and healing capacity of potentially bioactive surfaces. J Therm Anal Calorim 88:775–779. (2007) Bio-activated titanium surface utilizable for mimetic bone implantation in dentistry: surface characteristics and bone-implant contact formation. J Phys Chem Solids 68:841–8
52. Šesták J, Strnad Z, Strnad J, Holeček M, Koga N (2008) Biomedical thermodynamics and implantology aspects of biocompatible glass-ceramics and otherwise modified inorganic materials and Ti-surfaces. Adv Mat Res 39–40:329–333. Strnad J, Protivinsky J, Veltruská K, Helebrant A, Šesták J, Strnad Z (2004) Interaction of acid and alkali treated titanium with dynamic simulated body environment. J Thermal Anal Calor 76:17
53. Šesták J, Koga N, Šimon P, Foller B, Roubíček P, Wu N-L (2013) Amorphous inorganic polysialates: geopolymeric composites and the bioactivity of hydroxyl groups. In: Thermal analysis of micro, nano- and non-crystalline materials: transformation, crystallization, kinetics and thermodynamics. Springer, London, pp 441–460 (ISBN: 978-90-481-3149-5)
54. Marx RE, Carlson ER, Eichstaedt RM, Schimmele SR, Strauss JE, Georgeff KR (1998) Platelet-rich plasma: growth factor enhancement for bone grafts. Oral Surg Oral Med Oral Pathol Oral Radiol Endod 85:638–646
55. Marx RE (2000) In: Davies JE (ed) Platelet concentrate: a strategy for accelerating and improving bone regeneration in bone engineering. EM Squared Inc.
56. Hench LL (1991) Bioceramics: from concept to clinic. J Am Ceram Soc 74:1487–1570. (1997) Glasses and genes: a forecast for the future. Glastech Ber Glass Sci Tech 70:439–48. (1996) Life and death: the ultimate phase transformation. Thermochim Acta 280/281:1–14
57. Robertson DM, Pierre L, Chahal R (1976) Preliminary observations of bone ingrowth into porous materials. J Biomed Mater Res 10:335–344
58. Levine B (2008) A new era in porous metals: applications in orthopaedics. Adv Eng Mater 10:788–792
59. Hollister SJ, Murphy WL (2011) Scaffold translation: barriers between concept and clinic. Tissue Eng Part B Rev 17:459–474
60. Klawitter JJ, Weinstein AM (1974) The status of porous materials to obtain direct skeletal attachment by tissue ingrowth. Acta Orthop Belg 40:755–765

61. Spector M, Michno MJ, Smarook WH, Kwiatkowski GT (1978) A highmodulus polymer for porous orthopedic implants: biomechanical compatibility of porous implants. J Biomed Mater Res 12:665–677
62. Hahn H, Palich W (1970) Preliminary evaluation of porous metal surfaced titanium for orthopedic implants. J Biomed Mater Res 4:571–577
63. Ryan G, Pandit A, Apatsidis DP (2006) Fabrication methods of porous metals for use in orthopaedic applications. Biomaterials 27:2651–2670
64. Turner TM, Sumner DR, Urban RM, Rivero DP, Galante JO (1986) A comparative study of porous coatings in a weight-bearing total hiparthroplasty model. J Bone Joint Surg Am 68:1396–1409
65. Clemow AJ, Weinstein AM, Klawitter JJ, Koeneman J, Anderson J (1981) Interface mechanics of porous titanium implants. J Biomed Mater Res 15:73–82
66. Cameron HU, Pilliar RM, Macnab I (1976) The rate of bone ingrowth into porous metal. J Biomed Mater Res 10:295–302
67. Collier JP, Mayor MB, Chae JC, Surprenant VA, Surprenant HP, Dauphinais LA (1988) Macroscopic and microscopic evidence of prosthetic fixation with porous-coated materials. Clin Orthop Pract 235:173–180
68. Kokubo T (1991) Bioactive glass ceramics: properties and applications. Biomaterials 12:155–163
69. Cook SD, Thomas KA, Dalton JE, Volkman TK, Whitecloud TS III, Kay JF (1992) Hydroxylapatite coating of porous implants improves bone ingrowth and interface attachment strength. J Biomed Mater Res 26:9891001
70. De Groot K, Geesink R, Klein CP, Serekian P (198–7) Plasma sprayed coatings of hydroxyapatite. J. Biomed. Mater. Res. 21:1375–1381
71. Li H, Khor KA, Cheang P (2003) Impact formation and microstructure characterization of thermal sprayed hydroxyapatite/titania composite coatings. Biomater 24:949–957
72. Siddharthan A, Kumar TS, Seshadri SK (2010) In situ composite coating of titania–hydroxyapatite on commercially pure titanium by microwave processing. Surf Coat Technol 204:1755–1763
73. Yan F-Y, Shi Y-L, Ni J-H (2011) n-SiO2 Embedded HA/TiO2 composite coatings deposited on pure titanium substrate by micro-arc oxidation. In: Turkyilmaz I (ed) Implant dentistry—The most promising discipline of dentistry, vol 13. In Tech. (ISBN 978-953-307-481-8)
74. Kim HW, Koh YH, Li LH, Lee S, Kim HE (2004) Hydroxyapatite coating on titanium substrate with titania buffer layer processed by sol-gel method. Biomat 25:2533–2538
75. Lin CM, Yen SK (2004) Characterization and bond strength of electrolytic HA/TiO_2 double layers for orthopedic applications. J Mater Sci Mater Med 15:1237–1246
76. Besra L, Liu M (2007) A review on fundamentals and applications of electrophoretic deposition (EPD). Progr Mater Sci 52:1–61
77. Kim DH, Kong YM, Lee SH, Kim H-E, Lee I-S, Heo S-J, Koak J-Y (2003) Composition and crystallization of hydroxyapatite coating layer formed by electron beam deposition. J Am Ceram Soc 86:186–188
78. Chen TS, Lacefield WR (1994) Crystallization of ion beam deposited calcium phosphate coatings. J Mater Res 9:1284–1290
79. Shahrjerdi A, Mustapha F, Bayat M, Sapuan SM, Majid DLA (2011) Fabrication of functionally graded hydroxyapatite-titanium by applying optimal sintering procedure and powder metalurgy. Int J Phys Sci 6:2258–2267
80. Hero H, Wie H, Jorgensen RB, Ruyter IE (1994) Hydroxyapatite coatings on Ti produced by hot isostatic pressing. J Biomed Mater Res 28:343–348
81. Lee J, Aoki H (1995) Hydroxyapatite coating Ti plate by a dipping method. Biomed Mater Eng 5:49–58
82. Volke JGC, Van Dijk K, Schaeken HG, De Groot K, Jansen JA (1994) Study of the surface characteristics of magnetron-sputter calcium phosphate coatings. J Biomed Mater Res 28:1477–1484

83. Cotell CM (1993) Pulsed laser deposition and processing of biocompatible hydroxylapatite thin films. Appl Surf Sci 69:140–148
84. Thian ES, Huang J, Best SM, Barber ZH, Bonfield W (2005) A new way of incorporating silicon in hydroxyapatite (Si-HA) as thin films. J Mater Sci Mater Med 16:411–415
85. Porter AE, Patel N, Skepper JN, Best SM, Bonfield W (2003) Comparison of in vivo dissolution processes in hydroxyapatite and silicon-substituted hydroxyapatite bioceramics. Biomat 24:4609–4620
86. Driessens FCM, Verbeeck RMH, Kiekens P (1983) Mechanism of substitution in carbonated apatites. Z Anorg Allg Chem 504:195–200
87. Porter A, Patel N, Brooks R, Best S, Rushton N, Bonfield W (2005) Effect of carbonate substitution on the ultrastructural characteristics of hydroxyapatite implants. J Mater Sci Mater Med 16:899–907
88. Romo LA (1954) Synthesis of carbonate-apatite. J Am Chem Soc 76:3924–3925
89. Wang H, Branton D (2001) Nanopores with a spark for single-molecule detection. Nat Biotechnol 19:622–623
90. Gao JH, Gu HW, Xu B (2009) Multifunctional magnetic nanoparticles: design, synthesis, and biomedical applications. Acc Chem Res 42:1097–1107
91. Cheon J, Lee JH (2008) Synergistically integrated nanoparticles as multimodal probes for nanobiotechnology. Acc Chem Res 41:1630–1640
92. Woo KM, Jun JH, Chen VJ, Seo J, Baek JH, Ryoo HM, Kim GS, Somerman MJ, Ma PX (2007) Nano-fibrous scaffolding promotes osteoblast differentiation and biomineralization. Biomat 28:335–343
93. Adiga SP, Jin C, Curtiss LA, Monteiro-Riviere NA, Narayan RJ (2009) Nanoporous membranes for medical and biological applications. Interdiscip Rev Nanomed Nanobiotechnol 1:568–581
94. Lioni L, Boiarski A, Desai TA (2002) Characterization of nanoporous membranes for immunoisolation: diffusion properties and tissue effects. Biomed Microdev 4:131–139
95. Singh SP, Arya SK, Pandey P, Malhotra BD, Saha S, Sreenivas K, Gupta V (2007) Cholesterol biosensor based on RF sputtered zinc oxide nanoporous thin film. App Phys Lett 91:1–3
96. Cho M, Contreras EQ, Lee SS, Jones ChJ, Jang W, Colvin VL (2014) Characterization and optimization of the fluorescence of nanoscale iron oxide/quantum dot complexes. J Phys Chem C 118:14606–14616
97. Fu A et al (2007) Semiconductor quantum rods as single molecule fluorescent biological labels. Nano Lett 7:179–182
98. Akerman ME, Chan WCW, Laakkonen P et al (2002) Nanocrystal targeting in vivo. Proc Natl Acad Sci 99:12617–12621
99. Kim S, Lim YT, Soltesz EG et al (2004) Near-infrared fluorescent type II quantum dots for sentinel lymph node mapping. Nat Biotechnol 22:93–97
100. Bailey RE, Smith AM, Nie S (2004) Quantum dots in biology and medicine. Phys E Low Dimens Syst Nanostruct 25:1–12
101. Sinani VA, Koktysh DS, Yun BG, Matts RL, Pappas TC, Motamedi M, Thomas SN, Kotov NA (2003) Collagen coating promotes biocompatibility of semiconductor nanoparticles in stratified LBL films. Nano Lett 3:1177–1182
102. Vaijayanthimala V, Lee DK, Kim SC, Yen A, Tsai N, Ho D, Chang HC, Shenderova O (2015) Nanodiamond-mediated drug delivery and imaging: challenges and opportunities. Expert Opin Drug Deliv 12:735–749
103. Lai L, Barnard AS (2014) Anisotropic adsorption and distribution of immobilized carboxyl on nanodiamond. Nanoscale 6:14185–14189
104. Behler KD, Stravato A, Mochalin V, Korneva G, Yushin G, Gogotsi Y (2009) Nanodiamond-polymer composite fibers and coatings. ACS Nano 3:363–369
105. Qureshi A, Gurbuz Y, Howell M, Kang WP, Davidson JL (2010) Nanocrystalline diamond film for biosensor applications. Diam Relat Mater 19:457–461

106. Chen T, Lu F, Streets AM, Fei P, Quan J, Huang Y (2013) Optical imaging of non-fluorescent nanodiamonds in live cells using transient absorption microscopy. Nanoscale 5:4701–4705
107. Dolenko TA, Burikov SA, Vervald AM, Vlasov II, Dolenko SA, Laptinskiy KA, Rosenholm JM, Shenderova OA (2014) Optical imaging of fluorescent carbon biomarkers using artificial neural networks. J Biomed Opt 19:117007
108. Yu SJ, Kang MW, Chang HC, Chen KM, Yu YC (2005) Bright fluorescent nanodiamonds: no photobleaching and low cytotoxicity. J Am Chem Soc 127:17604–17605
109. Kaur R, Badea I (2013) Nanodiamonds as novel nanomaterials for biomedical applications: drug delivery and imaging systems. Int J Nanomed 8:203–220
110. Kim BH, Lee N, Kim H, An K, Park Y et al (2011) Large-scale synthesis of uniform and extremely small-sized iron oxide nanoparticles for high-resolution T1 magnetic resonance imaging contrast agents. J Am Chem Soc 133:12624–12631
111. Huh YM, Jun YW, Song HT et al (2005) In vivo magnetic resonance detection of cancer by using multifunctional magnetic nanocrystals. J Am Chem Soc 127:12387–12391
112. Mornet S, Vasseur S, Grasset F et al (2004) Magnetic nanoparticle design for medical diagnosis and therapy. J Mater Chem 14:2161–2175
113. Zeng C, Shi X, Wu B, Zhang D, Zhang W (2014) Colloids containing gadolinium-capped gold nanoparticles as high relaxivity dual-modality contrast agents for CT and MRI. Colloids Surf B Biointerfaces 123:130–135
114. Li X, Zhao W, Liu X, Chen K, Zhu S, Shi P, Chen Y, Shi J (2016) Mesoporous manganese silicate coated silica nanoparticles as multi-stimuli-responsive T1-MRI contrast agents and drug delivery carriers. Acta Biomater 30:378–387
115. Masood F (2016) Polymeric nanoparticles for targeted drug delivery system for cancer therapy. Mat Sci Eng C 60:569–578
116. Shah M, Naseer MI, Choi MH, Kim MO, Yoon SC (2010) Amphiphilic PHA–mPEG copolymeric nanocontainers for drug delivery: preparation, characterization and in vitro evaluation. Int J Pharma 400:165–175
117. Rai M, Ingle AP, Gupta I, Brandelli A (2015) Bioactivity of noble metal nanoparticles decorated with biopolymers and their application in drug delivery. Int J Pharma 496:159–172
118. Rahimi M, Kilaru S, Sleiman GEH, Saleh A, Rudkevich D, Nguyen K (2008) Synthesis and characterization of thermo-sensitive nanoparticles for drug delivery applications. J Biomed Nanotech 4:482–490
119. Liu J, Huang Y, Kumar A, Tan A, Jin S, Mozhi A, Liang X-J (2014) pH-Sensitive nano-systems for drug delivery in cancer therapy. Biotech Adv 32:693–710
120. Nogueira DR, Scheeren LE, Vinardell MP, Mitjans M, Infante MR, Rolim CMB (2015) Nanoparticles incorporating pH-responsive surfactants as a viable approach to improve the intracellular drug delivery. Mat Sci Eng C 57:100–106
121. Xi G, Robinson E, Mania-Farnell B, Vanin EF, Shim KW, Takao T, Allender EV, Mayanil CS, Soares MB, Ho D, Tomita T (2014) Convection-enhanced delivery of nanodiamond drug delivery platforms for intracranial tumor treatment. Nanomed 10:381–391
122. Wang X, Low XC, Hou W, Abdullah LN, Toh TB, Rashid MMA, Ho D, Chow EK-H (2014) Epirubicin-adsorbed nanodiamonds kill chemoresistant hepatic cancer stem cells. ACS Nano 8:12151–12166
123. Martín R, Álvaro M, Herance JR, García H (2010) Fenton-treated functionalized diamond nanoparticles as gene delivery system. ACS Nano 4:65–74
124. Greef MD, Kok HP, Correia D, Bel A, Crezee J (2010) Optimization in hyperthermia treatment planning: the impact of tissue perfusion uncertainty. Med Phys 37:4540–4545
125. Sharifi I, Shokrollahi H, Amiri S (2012) Ferrite-based magnetic nanofluids used in hyperthermia applications. J Mag Mag Mat 324:903–915
126. Gonzalez-Fernandez MA, Torres TE, Andrés-Vergés M, Costo R, Presa P, Serna CJ, Morales MP, Marquina C, Ibarra MR, Goya GF (2009) Magnetic nanoparticles for power

absorption: optimizing size, shape and magnetic properties. J Sol State Chem 182:2779–2784
127. Letfullin RR, Joenathan C, George TF, Zharov VP (2006) Laser-induced explosion of gold nanoparticles: potential role for nanophotothermolysis of cancer. Nanomed 1:473–480
128. Kloss FR, Gassner R, Preiner J, Ebner A, Larsson K, Hachl O, Tuli T, Rasse M, Moser D, Laimer K, Nickel EA, Laschober G, Brunauer R, Klima G, Hinterdorfer P, Steinmuller-Nethl D, Lepperdinger G (2008) The role of oxygen termination of nanocrystalline diamond on immobilisation of BMP-2 and subsequent bone formation. Biomat 29:2433–2442
129. Huang HJ, Pierstorff E, Osawa E et al (2008) Protein-mediated as-sembly of nanodiamond hydrogels into a biocompatible and biofunctional multilayer nanofilm. ACS Nano 2:203–212
130. Zhu Y, Li J, Li W et al (2012) The biocompatibility of nanodiamonds and their application in drug delivery systems. Theranostics 2:302–312
131. Zhang L, Webster TJ (2009) Nanotechnology and nanomaterials: promises for improved tissue regeneration. Nano Today 4:66–80
132. Zhang L, Sirivisoot S, Balasundaram G, Webster TJ (2010) In: Basu B, Katti D, Kumar A (eds) Advanced biomaterials: fundamentals, processing and applications. Wiley, New Jersey (ISBN: 978-04-701-9340-2)
133. Okamoto M, John B (2013) Synthetic biopolymer nanocomposites for tissue engineering scaffolds. Prog Polym Sci 38:1487–1503
134. Sadat-Shojai M, Khorasani M-T, Dinpanah-Khoshdargi E, Jamshidi A (2013) Synthesis methods for nanosized hydroxyapatite with diverse structures. Acta Biomat 9:7591–7621
135. Webster TJ, Schadler LS, Siegel RW, Bizios R (2001) Mechanisms of enhanced osteoblast adhesion on nanophase alumina involve vitronectin. Tissue Eng 7:291–301
136. Nukavarapu SP, Kumbar SG, Brown JL, Krogman NR, Weikel AL, Hindenlang MD, Nair LS, Allcock HR, Laurencin CT (2008) Polyphosphazene/nano-hydroxyapatite composite microsphere scaffolds for bone tissue engineering. Biomacromol 9:1818–1825
137. Sattler KD (2010) Handbook of nanophysics: nanomedicine and nanorobotics. CRC Press, Taylor & Francis Group, US (ISBN 9781420075465)
138. Webster TJ, Hellenmeyer EL, Price RL (2005) Increased osteoblast functions on theta + delta nanofiber alumina. Biomat 26:953–960
139. Zhang L, Chen Y, Rodriguez J, Fenniri H, Webster TJ (2008) Biomimetic helical rosette nanotubes and nanocrystalline hydroxyapatite coatings on titanium for improving orthopedic implants. Int J Nanomed 3:323–333
140. Supronowicz PR, Ajayan PM, Ullmann KR, Arulanandam BP, Metzger DW, Bizios R (2002) Novel current-conducting composite substrates for exposing osteoblasts to alternating current stimulation. Biomed Mater Res 59:499–506
141. Hartmann M, Betz P, Sun Y, Gorb SN, Lindhorst TK, Krueger A (2012) Saccharide-modified nanodiamond conjugates for the efficient detection and removal of pathogenic bacteria. Chemistry 18:6485–6492
142. Wehling J, Dringen R, Zare RN, Maas M, Rezwan K (2014) Bactericidal activity of partially oxidized nanodiamonds. ACS Nano 8:6475–6483
143. Xing Y, Xiong W, Zhu L, Osawa E, Hussin S, Dai L (2011) DNA damage in embryonic stem cells caused by nanodiamonds. ACS Nano 5:2376–2384
144. Williams OA, Hees J, Dieker Ch, Jäger W, Kirste L, Nebel ChE (2010) Size-dependent reactivity of diamond nanoparticles. ACS Nano 4:4824–4830
145. Zhang XY, Hu WB, Li J, Tao L, Wei Y (2012) A comparative study of cellular uptake and cytotoxicity of multi-walled carbon nanotubes, graphene oxide, and nanodiamond. Tox Res 1:62–68
146. Puzyr AP, Baron AV, Purtov KV, Bortnikov EV, Skobelev NN, Mogilnaya OA, Bondar VS (2007) Nanodiamonds with novel properties: a biological study. Diam Relat Mater 16:2124–2128

147. Lin Ch-W, Ju Ch-P, Lin J-HCh (2004) Comparison among mechanical properties of investment-cast c.p. Ti, Ti–6Al–7Nb and Ti–15Mo–1Bi Alloys. Mater T Jim 45:3028–3032
148. Henriques B, Gasik M, Souza JCM, Nascimento RM, Soares D, Silva FS (2014) Mechanical and thermal properties of hot pressed CoCrMo–porcelain composites developed for prosthetic dentistry. J Mech Behav Biomed 30:103–110
149. *Henry D (2009) Materials and coatings for medical devices: cardiovascular. ASM International, Materials Park (ISBN-13: 978-1-61503-000-2)
150. Ivanova EP, Bazaka K, Crawford RJ (2014) In new functional biomaterials for medicine and healthcare. Woodhead Publishing (ISBN: 9781782422655)
151. Ratner BD, Hoffman AS, Schoen FJ, Lemons JE (2013) Biomaterials science: an introduction to materials in medicine, 3rd ed. Academic Press (ISBN 9780123746269)
152. Ramakrishna S, Mayer J, Wintermantel E, Leong KW (2001) Biomedical applications of polymer-composite materials: a review. Compos Sci Technol 61:1189–1224
153. Korner C, Singer R (2000) Processing of metal foams–challenges and opportunities. Adv Eng Mater 2:159–165
154. Banhart J (2001) Manufacture, characterization and application of cellular metals and metal foams. Progr Mater Sci 46:559–632
155. Oh IH, Nomura N, Masahashi N, Hanada S (2003) Mechanical properties of porous titanium compacts prepared by powder sintering. Scr Mater 49:1197–1202
156. Martell JM, Pierson RH III, Jacobs JJ, Rosenberg AG, Maley M, Galante JO (1993) Primary total hip reconstruction with a titanium fibercoated prosthesis inserted without cement. J Bone Joint Surg Am 75:554–571
157. Bram M (2000) High-porosity titanium, stainless steel, and superalloy parts. Adv Eng Mater 2:196–199
158. Li JP, Li SH, de Groot K, Layrolle P (2002) Preparation and characterization of porous titanium. Key Eng Mater 218:51–54
159. Li BY, Rong LJ, Li YY, Gjunter VE (2000) A recent development in producing porous NiTi shape memory alloys. Intermetallics 8:881–884
160. Ducheyne P, Martens M (1986) Orderly oriented wire meshes as porous coatings on orthopaedic implants. I: morphology. Clin Mater 1:59–67
161. Bobyn J, Hacking S, Chan S, Toh K, Krygier J, Tanzer M (1999) Characterization of a new porous tantalum biomaterial for reconstructive orthopaedics. A Scientific Exhibit at the Annual AAOS, AnaheinCA
162. Markaki AE, Clyne TW (2004) Magneto-mechanical bone growth stimulation by actuation of highly porous ferromagnetic fibre arrays. In: SPIE international symposium of smart materials, and micro-smart systems, biomedical applications of micro and nanoengineering II. Australia, Sydney
163. Thieme M, Wieters KP, Bergner F, Scharnweber D, Worch H, Ndop J, Kim TJ, Grill W (2001) Titanium powder sintering for preparation of a porous functionally graded material destined for orthopaedic implants. J Mater Sci Mater Med 12:225–231
164. Okazaki K, Lee WH, Kim DK, Kopczyk RA (1991) Physical characteristics of Ti–6A1–4V implants fabricated by electro discharge compaction. J Biomed Mater Res 25(12): 1417–1429

Chapter 22
Thermal Analysis Scheme Anticipated for Better Understanding of the Earth Climate Changes: Impact of Irradiation, Absorbability, Atmosphere, and Nanoparticles

Jaroslav Šesták, Pavel Hubík and Jiří J. Mareš

Abstract Methodological scheme of thermal analysis is used for portraying the Earth environmental research and climate changes, showing particularly the history, effect of atmosphere reflection (albedo), and absorption (so-called greenhouse effect included). The net behavior of the Earth as a black body is reviewed. The most influential on climate changes is the alteration of the geometry of the Earth trajectory and the irradiative power of the Sun (as a standard thermoanalytical pair of the sample and radiator). Thermodynamic basis of water vapor impacts is pointed out, the absorption spectra of atmosphere are emphasized, and temperature gradients are indicated. The historical course of the Earth temperature and CO_2 concentration is put in analogy with the method of gas desorption analysis, which supports the view that the variation of CO_2 concentration recorded in the past may not be alone blamed for temperature changes. The influences of atmosphere nanoparticles on weather, climate, and human health are discussed, as well. With 91 references.

22.1 Mid-European Prologue

According to Czech legends [1, 2], the Bohemian forefather named 'Čech' during his mythic travels stopped on Mount Rip and landscape of forests, meadows, and rivers impressed him so much that he with his entourage settled there. The diversity of the natural features is conditioned by the change of seasons alternating thus

J. Šesták (✉)
New Technologies Research Centre (NTC-ZČU), University of West Bohemia, Univerzitní 8, 30114 Pilsen, Czech Republic
e-mail: sestak@fzu.cz

P. Hubík · J.J. Mareš
Division of Solid-State Physics, Institute of Physics, Czech Academy of Sciences, Prague, Czech Republic

J. Šesták et al. (eds.), *Thermal Physics and Thermal Analysis*,
Hot Topics in Thermal Analysis and Calorimetry 11,
DOI 10.1007/978-3-319-45899-1_22

different types of weather phenomena. For the temperate climate of Central Europe, the fluctuations in the form of floods, droughts, etc. were, are and will be commonplace. In some periods, they are more frequent and stronger, and sometimes, they occur only rarely. Historically, a large part of the Czech landscape was modeled by water and shaped by floods. But even human beings in its entire history have tried to suit the changes to their needs in the Czech basin landscape observing continuous struggle of man with the landscape while changing the forests and meadows in the fields and the cities. Water is, however, an element that cannot be easily bound. Water, the same applies as for fire, is a good servant but evil master. Flood statistics tell us that during the recent centuries, major floods in the Czech country almost did not occur. After the disruption of the Charles Bridge in 1890, a big flood was as waited more than 100 years. In the last 15 years, however, the Czech Republic was experiencing a period of more frequent occurrence of flood of all kinds. In the years 1997, 2002, 2006, and 2013, the Czech Republic was affected by large rainfalls in its entirety. In 1995, 1996, 1998, 2009, and 2010, isolated areas were affected by extreme floods with unprecedented power and rapid onset. When such a review is completed by extreme droughts in 2000, 2003, and 2015, strong European windstorms Kyrill (2007) and Emma (2008), as well as severe frosts and heat waves in 2012, then we have a lot to think over the course of the weather.

However, it is not right to associate any single extreme situation with climate change. Yet it often happens not only in our country. Our historical weather records showed [1] that in the past it was plentifully freezing, even in summer when snow fell (note the years 763, 962, 1074, 1252, 1282, 1371, 1407, 1524, 1607), while other times, it was enormously warm winter and sweltering summer (988, 1087, 1156, 1420, 1470, 1561, 1660), sometimes providing double harvesting. It is obvious that the intense climate changes have exist and will exist and that our ancestors coped with them (better: survived them) and that only the future will show whether our followers will handle them and how they will be prepared to withstand yet unseen changes. It, however, is good to bring to mind that no civilization ceased because of overheating even if politicians warn public before warming.

22.2 Introduction

From the outer space looks our livable world, the Earth, rather fragile. It is covered by a somewhat thin blanket of atmosphere underneath which is a very thin habitable layer capable to bring the miracle of life. First in the Earth history, this layer contains self-reliant entity of mankind, which is becoming to exceedingly wear out its adjacent surrounding by plentiful utilization of raw materials, overburning fossil resources, abundant traffic, and making superfluous wastes, which in fact destroys the living conditions on the planet. Inherent biological network interacts with the ecosystem treated as a thermal structure which is no more a passive stage but has a character of a “living architecture” sometimes assimilated to the image of the Earth goddess “Gaia” (Greek Γαῖα, which paradigm describes a productive confluence

between scientific understandings of Earth as a living system with cultural understandings of human society as a seamless continuum of that system) [3]. The global treatment stimulates better understanding of the concept of global steadiness governing a distribution of local non-equilibriums [2].

We are living in an interglacial period, but about 20,000 years ago, massive glaciers were spread far away from poles [4]. Glaciers have come and gone many times, but the climate may fluctuate even within shorter phases. For example, in the period 1400–1800, the year-averaged temperature dropped by about 1.5 °C comparing today (even called as "little Ice Age") [1, 4, 5], while within 1910–1940, the global warming (increase of the average temperature by ∼0.5 °C [5]) appeared which was too big to be caused by "greenhouse" effect alone. So it is the question whether our planet is under an unusual course of warming or is yet recovering from the little Ice Age, which may bring Greenland back its farming stage as it was 1000 years ago during the medieval climate optimum [6]. Looking at such historical records, we can make a thought ("gedanken") thermal analysis experiment and put resulting figures into a certain correspondence with similar thought experiments, e.g., evolved gas analysis (desorption of greenhouse gases, especially of CO_2). Understandably, we cannot cover herewith all articles dealing with associated phenomena so a certain profile is only offered. All politically motivated issues and reports, however, are avoided because they often reflect rather financial interests instead of the objective ecological aspects.

22.3 Earth Irradiation Treated in the Frame of Thermal Analysis

Thermal analysis (TA) is traditionally exploited for a quantitative determination of thermal changes which occur in various samples under monitored heating/cooling, often on mesoscopic and microscopic scales [7]. Such an arrangement requires a suitable instrumental setting for controlled and homogeneous sample heating provided by the surrounding furnace/thermostat. Temperature conditions are averaged by heat convection, conduction, and radiation. The sample temperature is, as a rule, measured either in a single place or, less commonly, is monitored over various points of the sample [7, 8]. In some cases, the sample is heated by directional light source and the equilibration of temperature is achieved by the sample rotation [9]. Samples are surrounded by ambient atmosphere (sometimes interacting/decomposing) which is under the influence of the gravitation forces. The presence of the atmosphere helps to equalize the temperature gradients by local heat fluxes [6, 7, 10]. The distance between the heater and the sample is usually kept constant, only in some special arrangements the temperature program is realized by the controlled motion of a sample along the stationary gradient in the furnace [7, 8]. In some cases, a shielding reflector is inserted between the heater and sample in order to modify locally the radiation (and consequently the temperature gradients).

Amazingly, the formalism of thermal analysis can provide heating characteristics used in various applications. For instance, the ancient Roman baths were described with respect to their architectural aspects where the heat loss from the reconstructed bath was calculated, allowing for the estimation of temperatures and thermal conductivities [10]. Apparently, the thermal analysis can be used for describing the Earth's climate changes as the Sun–Earth system exhibits some analogous features of the furnace sample assembly, which, certainly, must be imagined on much larger macroscopic scale. Directional heater, the Sun, and the one-way irradiated sample, the Earth, are in permanent interaction which controls the most important observable Earth's temperature [7, 11, 12]. Other possible cause of the modification of Earth's surface temperature, the heat coming from Earth's core, can be neglected as the relevant heat flow surface density is by more than three orders of magnitude smaller than that of the Sun [13–24]. The dynamical thermal equilibrium essentially due to the position and rotation of the Earth is modified by the presence of surrounding atmosphere with its varying composition, local motions, and heat and mass fluxes [11–37]. Therefore, the irradiative input is complexly distributed vertically and horizontally including the advection, convection, and diffusion in atmosphere. The warm is spread out within ocean with its long-standing convectional flows due to the changes of both temperature and salinity, thus standing as a stock for climate inertia ("thermohaline oceanic heat exchanger and reservoir"). In order to study these effects, the temperature is measured at multiple points on the Earth surface, marine, and in the adjoining atmosphere and also includes the remote service of orbiting satellites. Similarly, the surface and atmosphere are scanned over various wavelength regions in the way traditionally known as "thermography" [7].

The heat exchange near the Earth is realized through the adhering atmosphere layer, which is bound by the centripetal gravitational force, further surrounded by the near-vacuum space avoiding thus successive heat/mass transport by outward convection. On the interplanetary separation scale, the only mechanism remaining for the heat exchange is radiation, which requires taking into account Earth's reflection ("albedo") and absorption. These effects including also the popular "greenhouse effect" are extensively discussed in the literature [2, 11–13, 25–28].

Consequently, the weather has a regular component which is due to the diurnal and annual rotations of the Earth and a somewhat chaotic component due to the atmospheric circulation driven by the irradiative energy of the Sun. The climate is then understood as an integral of weather over the periods lasting more than one year. Because of numerous analogies, we are convinced [27]. The relevant method for theoretical description of such a complexity can be found in the theory of thermal analysis [7, 9, 14–28]. The experience with thermal analysis clearly reveals that the decisive effect on the sample (Earth) temperature should have the behavior of furnace (Sun) and their mutual position and feasible shielding.

22.4 History of Research into the Earth Climate and Atmosphere Thermodynamics

The original concept of the so-called atmospheric greenhouse effect can be traced back to the work of Jean B.J. Fourier (1768–1830) [29] who in the year 1822 realized that the Earth atmosphere is relatively transparent to solar radiation but highly absorbent for the terrestrial reradiation, which results in a relative increase of the temperature of the Earth surface. Michael Faraday (1791–1867) [30] called the attention to the atmospheric CO_2, which has a positive environmental effect on the growth of plants and animal population as well, helping to maintain their diversity. However, it was only Svante A. Arrhenius (1859–1927) [31] who in the year 1896 laid the formal foundation of the theory linking the variation of concentrations of atmospheric gases to the climate changes. His main goal was the estimation of the surface temperature rise due to the increase in the content of carbon dioxide. This research matured to a more detailed model of the radiation balance between the atmosphere and the surface and particularly led to the discovery of importance of water vapor which determines the sensitivity of climate to greenhouse gases.

As the Earth catches warming, the saturation pressure (p_s) of water vapor would increase exponentially with temperature (T) according to the classical Clausius–Clapeyron relation [5, 7, 16–23, 25, 27] $d\ \ln(p_s)/\mathrm{d}T = \Delta H/(RT^2)$ (ΔH being molar heat of evaporation). The increased saturation pressure would enhance the water vapor concentration, further amplifying the greenhouse effect. On the other hand, oversaturation of water vapor would lead to the condensation and formation of clouds increasing the outside reflection ("albedo") and suppressing thus the internal greenhouse effect. The associated release of heat (ΔH) plays an important role in the control of atmospheric temperature because it affects, on macroscopic scale, the balance of evaporation/condensation and the coexistence of liquid/gas phases. Moreover, for micro-/nanoscale of condensing droplets, the effect of surface tension (γ) and its curvature (radius r) becomes decisive. The actual saturated vapor pressure (p_{sr}) with respect to that over the flat surface (p_∞) is given by the Kelvin equation $RT\ \ln\ (p_{sr}/p_\infty) = 2\gamma V_m/r$, where V_m is the molar volume of water. It is clear that with decreasing of r, the ratio p_{sr}/p_∞ increases, causing the instability of cloudy systems, where tiny droplets evaporate, yielding then the vapor supersaturation and making the re-establishment of liquid water phase difficult. The condensation thus frequently needs an auxiliary (catalytic) stimulus of external (often heterogeneous) condensation nuclei, such as dust and aerosols (called CCN—cloud condensation nuclei), the occurrence of which additionally decreases the irradiative absorption. (This very often ignored Twomey's effect [32] is very likely responsible for most changes of rainfall activity [33].) There are some other dimension-dependent thermal effects [23, 34], in which detailed explanation falls beyond the frame of this contribution.

Early laboratory absorption measurements (accomplished by Tyndall [35] on the CO_2 and H_2O vapors) became important to see the foremost influence on the terrestrial rays and associated climate changes. It was followed by direct

observations of an atmospheric transmission by Langley [36] who designed a high-precision temperature detector, called bolometer, capable to record numerous data regarding the solar and even the lunar spectra. The birth of the quantum mechanical theory in the early twenties of twentieth century announced the beginning of theoretical spectroscopy and expansion of relevant experiments, which led eventually to the availability of reliable spectroscopic data [37–41] such as those by Goody [40] and others [38, 41].

Natural cycles of atmospheric greenhouse gases and associated clouds have become a subject of many theoretical studies involving thermodynamic analysis [5, 7, 14–25], which showed that the immediate Earth weather and long-lasting trends in global climate are very sensitive phenomena which are dependent on a plenty of variables having very often chaotic behavior [42, 43]. For example, recent estimates based solely on energy balance disturbances because the changes of atmosphere composition (e.g., CO_2) have shown that in comparison with the variability of solar irradiation, just this factor should dominate the climate [16, 27, 28, 44].

Such an "energy argument," however, is not reliable for highly nonlinear, extremely complex systems such as the coupled structure of atmosphere–ocean–cryosphere–biosphere and their power inputs and interrelations. It is well known that any multifaceted systems can behave bizarrely, i.e., can follow very different paths after the smallest perturbation. Chaos in climate (copious and meager years) and weather conditions is thus something "normal" revealing unpredictable fluctuations or drifts (see Fig. 22.1). In an uneven structure with large reservoirs of latent energy (such as the atmosphere–ocean–biosphere), global redistributions of energy can be triggered by unexpectedly small inputs, a process that may depend far more on their spatial and temporal pattern than on their magnitude, and it is the question whether the man-made (anthropogenic) effects are influential enough. Worth mentioning is the work by Lorenz [42] who stressed that only non-periodic systems suffered by limited predictability. External periodic or quasi-periodic systems can positively impose their rhythm on the climate. This is not only the case of the periodic diurnal changes and of the Milankovič cycles (see later) which satisfy these conditions, but also of 11-year sunspot cycle in solar energy output playing no role in the practice of predictions.

For serious analysis of climate changes [44–46] are thus needed exact, extended, and continuous measurements of atmospheric conditions. Such a data are, unfortunately, available only since about last century; for larger periods, we are dependent on historical records and on a somewhat fuzzy approach, which is based on the methodology analogous to "computing" with words describing subjective sensations instead of with numbers [23].

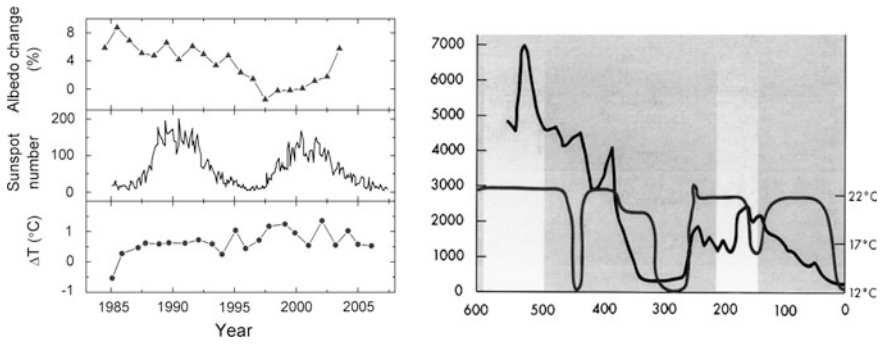

Fig. 22.1 *Left* Brief span records of major effects influencing the regional temperature changes (ΔT) due to the time-dependent irradiative power of Sun (affected by sunspots, *middle*) and the relative changes of the confined Earth albedo showing rather irresolvable upshot in long-lasting trends (composed on basis of various sources, e.g., [26, 52]). *Right* The exploratory lifelong profiles of historical figures for the CO_2 concentration (in ppm—*upper blacker line with the left scale*) and associated temperatures (in °C—*lighter line with the right scale*) related to the assumed historical continuation in the past (in millions of years—*bottom scale*) [45, 48, 70, 71]. Two *lighter strips* indicate the steady temperature period associated with the major geological periods of Cambrian and Jurassic, and the 0 point on the *right side* shows the present-day relatively low content of CO_2 ($\sim$370 ppm, close to the lower limit of the CO_2 content, $\sim$120 ppm, which may be even adjacent to the extinction of life). Note the era of global icing 300 million years ago, with markedly low temperatures close to 10 °C. Remind that such a plot looks like that common for the procedure of evolved gas analysis and the figures are factually based on the chromatographic analysis of the bygone atmospheric content of ice-trapped microbubbles. Such examination toward climatologic history is often accompanied by isotopic testing of the ratio of heavy vs. normal ($^{18}O/^{16}O$) oxygen, thus indicating the olden temperatures ("paleontological indicator") as well as by determination of the isotope ^{10}Be revealing in this fashion the intensity of cosmic radiation and thus also the amount of bygone sun energy

22.5 Influence of the Sample Position—Geometrical Anomalies of the Earth's Orbit

Regarding the living conditions of mankind, the Earth's orbit is the most important attribute, which course, opportunely, is within an appropriate distance from the Sun and moves around it along the ellipse very close to a circle (cf. Fig. 22.2 right). Under the gravitational force of the Sun combined with those of the distributed masses of the giant planets (Jupiter, Saturn) and nearest planets (Mars, Venus), the elliptical orbit revolves over the course of the year, but its effect is too weak ($\approx$3%) to cause the instant change of seasons (the full revolutions with respect to the stars take about 112,000 year), but strong enough for to have a long-term impact. Now, the Earth reaches perihelion (closest point toward the Sun) in early January, but this date does not remain fixed but slowly regresses. Tropical year is measured between two subsequent vernal equinoxes (being the base of our Gregorian calendar), while between two perihelia lies the anomalistic year (about 25 min longer), which moves completely through the tropical year in about 21,000 years, i.e., it advances by

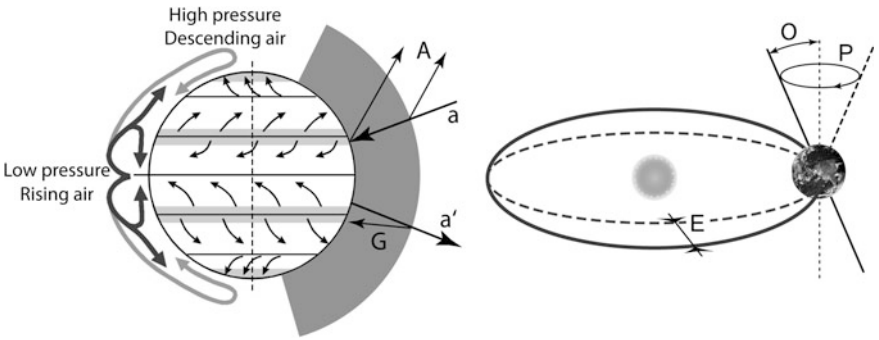

Fig. 22.2 *Right* Macroscopic arrangement of the sample (the Earth) and the furnace (the Sun) showing a schematic picture of the Earth orbital irregularity (eccentricity *E*, precession *P* and obliquity *O*). *Left* Behavior of the sample—the Earth including the portrayal of its energetic balance accounting on incoming (*a*) and outgoing (*a′*) energy fluxes, albedo (*A*), and greenhouse effect (*G*) and showing the major stream of atmosphere, which are leveling uneven surface heating (this effect is on the microscale of standard TA samples unobservable)

about one full day every 58 years. This effect is a combination of the above-mentioned orbit revolution with the precession of the Earth's rotation axis, i.e., a slight cyclic movement of the direction of the axis with a period of 26,000 years. Thanks to the gyroscopic effect of the Moon, the anomalies of the Earth revolution are well stabilized.

The eccentricity of the Earth's orbit varies complexly with the resulting roughly periodic changes within the timescale of about 100,000 years (maximum distance between Earth and Sun is 1.52×10^{11} m, and minimum occurs at 1.47×10^{11} m), so that it can be significant for climate changes if modulated together with the 21,000 cycle of perihelion. Another 41,000-year variation is given by changes of the angle between Earth's axis and Earth's orbital plane (from 22.1° to 24.5°). These astronomical phases are often called the Milankovič cycles (after the theory of Serbian civil engineer Milutin Milankovič (1879–1958) [47]), but their true pattern [43] and impact on climate changes are not yet fully comprehended [48] though they were forecasted by French mathematician Joseph Adhemar (1797–1862) and Scot James Croll (1821–1890) in that time, however, disbelieved (in light of persistence obsolete "quadricglacial hypothesis"). It is of no doubt, nevertheless, that pronounced climatic changes during the past two millions years (glacial of about 100,000 years and interglacial of about 15,000 years each) emerged as a result of the simultaneous periodically repeating changes of the Earth orbit parameters (as shown in more detail by Huybers [45]) accompanied at the same time with the variability of the Sun radiation [49] (see below). However, it is not clear why these alterations did not show sooner (as at the turn of Tertiary and Quaternary) as they likely proceeded during the whole existence of our planet and could have puzzlingly amalgamated with the early shifts of planetary plates below continents or with other yet unidentified upshots.

International IPCC estimated, however, the potential increase in global average temperature of the Earth in the years 1906–2005 to reach a change $dT \approx 0.74$ °C, while for the period 1901–2000, it was only $dT \approx 0.6$ °C, and it should be recalled that the last decade was the warmest. It turns out that land is warming faster than ocean and that mid-troposphere is somewhat consistent with the warming of the Earth's surface. The process of warming proceeds inconsistently because the northern hemisphere has a $dT \approx 0.6$ °C while the south only $dT \approx 0.3$ °C. Also, different geographical locations differ as to the position of 65° north latitude and is $dT \approx 1.5$ °C above global change 0.4 °C pointing out that the trend of evaporation of water vapor over the oceans every ten years is increased by 1.2%, which can explain the increase in extreme precipitation (and temperatures) in the last decade. Emission scenarios foresee every ten years, the increase of interior temperatures 0.2 °C which is still unpredictable due to the blending of various climatologic phenomena. It prospers the view that climate change is a reality being regionally heterogeneous, but what is important is that the influence of human activities can be neither exaggerated nor underestimated.c

22.6 Influence of the Radiator—Irregularities in the Energy Emission of the Sun

From various records in the current literature [49–54], we can deduce that the fluctuations of the heat source, Sun, play a major role in natural climatic changes on the timescales of decades and centuries. The measurements from spacecrafts reveal the irradiation changes ranging from minutes to decades, including the pronounced cycle of roughly eleven years, often related to sunspots and other forms of solar activity. Besides, there are long-time averaged drifts of the total radiation produced by the Sun. However, this effect does not seem essential for the variation of the Earth climate in present. For example, within past 150 years, the mean global temperature at the Earth surface increased about 0.5 °C and the amount of CO_2 measured at the Earth's atmosphere increased about 25% as a consequence of our enormous, continuously escalating, and shabbiest burning of fossil fuels (instead their sparing for a more perspective future with further energy-sophisticated technologies). However, stellar and isotopic findings suggest an increase in solar total radiation of roughly 0.25%. Let us note that the global mean temperature did not rise steadily as some statistics claim to show; the significant year-to-year and decade-to-decade variability, reaching $\sim 0.2\%$ from one month to the next one, is namely possibly consistent with the 27-day period of rotation of the Sun.

It becomes clear that the primary cause of the solar modulation of cosmic rays is not the level of the mentioned sunspot activity, but rather the variations of the strength of the solar wind [50–56]. This supersonic outflow of plasma originates in the very hot corona of the Sun and carries ionized particles together with the magnetic lines of force from the Sun. A steady stream of charged particles flowing continuously outward from the Sun impacts and deforms the Earth's extended

magnetic field. The upper layers of the atmosphere (ozone layer and ionosphere) are strongly affected by the flow of high energetic solar particles; some of these particles even enter the lower parts of the atmosphere where they provide the condensation nuclei enabling easier formation of rainy clouds changing the Earth's albedo.

Most important, however, are solar cycles, which are without exception related to the Sun's fundamental oscillations about the center of mass of the whole solar system, into which the cycles of different length, but similar function, are integrated. In the simplest model, the dynamics of the magnetic sunspot cycle is driven by the Sun's rotation. Yet this theory only takes into account the Sun's spin momentum, related to its rotation about its axis, but not its orbital angular momentum, linked with irregular oscillations about the center of mass of the solar system as a whole, which is related also to the motion of giant planets (Jupiter and Saturn). The orbital momentum carries more than $\sim 99\%$ of the angular momentum in the solar system (while the Sun's spin momentum is confined to less than $\sim 1\%$). So there is a high potential of angular momentum to be transferred from the outer planets to the revolving Sun and eventually to the spinning Sun. Recent considerations showed that such an effect in fact determines the length of the doubled period of sunspot activity (22.1-year magnetic cycle) and overall cycles called "big fingers" and "big hand" having a mean length of 35.8 and 178.8 years, respectively. Interestingly enough, varied climatic phenomena in different regions of the world show synchronized phases in a cycle of 33–37 years. The magnetic sunspot cycle of 22.1 years (often called the Hales cycle) is the true cycle of solar activity as groups of sunspots are usually composed of preceding and following spots with different magnetic polarities. With the commencement of a new cycle, the polarity reverses and the original polarity is only restored every second 11-year cycle. Some authors suspect that in Pleistocene, the impact of the Sun activity was physically more powerful than that of Milankovič cycles, which, however, dominated in warmer interglacial periods [45, 46, 48]. The Milankovič theory [47] in its modern form shows that the decrease in solar irradiation of $\sim 0.1\%$, effective during a very long interval, can release a real Ice Age and that there may be some congruent modulation between eccentricities of the Sun and the Earth [45, 46, 50–57]. It may be thus expected that the Gleissberg cycle of sunspot activity having a characteristic time of 90–120 year and which super-modulates the intensity of the 11-year cycle possesses a considerable potential to accumulate an effective surplus of irradiance, or, quite contrary, to induce a steadily decreasing radiant flux density—who can be knowledgeable about?

22.7 The Earth as a Black Body Sample—Heat and Entropy Fluxes

Income of irradiative power on the Earth, $J_E(E)$, is about 1.2×10^{14} kW, which is a negligible fraction ($\sim 10^{-9}$) of the power totally emitted by the Sun ($J_S(E) \cong 10^{23}$ kW). Even though the total energy of the Earth remains constant, there is

a definite change in the entropy flux, $J(S)$, because of the temperature disparity [20, 23, 58] in partial terms $J_{in}(S)$ and $J_{out}(S)$. It reads as $J(S) = J_{in}(S) - J_{out}(S) = 4/3\ (J_E(E)/T_S - J_E(E)/T_E) = 4/3 \times 1.2 \times 10^{14} \times (1/5800 - 1/290) = -5.2 \times 10^{11}$ kW/K. This flux can be related to one square meter of the Earth so that divided by $4\pi R_E^2$ yields the value of about 1 $WK^{-1}\ m^{-2}$. About 94% of entropy is produced during the absorption and re-emission of the radiant energy (the Earth serves as a transducer), and the rest can be attributed to material changes and motions of the atmosphere, oceans, and Earth core ($\sim$0.07 $WK^{-1}\ m^{-2}$). Assuming that the whole mankind consumes roughly 10^{10} kW, it produces entropy about 3×10^7 kW/K being at about 0.1% of the total production associated with material changes (photosynthesis, atmosphere circulation, phase changes of water, heating of the Earth surface, etc.).

Most important is an estimate of hypothetical balance of the Earth behavior assumed as a black body, in which we can take into account two decisive processes: the reflection (albedo—A) and the absorption (greenhouse effect—G) of radiation, see Fig. 22.2, left:

- a incoming radiation from the Sun ($T \cong 5800$ K, $\lambda_{max} = 497$ nm)
- a' outgoing radiation from the Earth ($T \cong 290$ K, $\lambda_{max} = 9.9$ μm)
- A total albedo, which is averaged over various angles and altitudes providing the recent value $\sim$35%, strongly depending on the surface quality (e.g., wet surface considerably increases albedo)
- G part of radiation which is returned back to the Earth surface due the interaction with atmosphere (dependent on its composition exhibiting the recent value $\sim$45%)
- T Earth temperature$T = T_{bb}\{(1 - A)/(1 - G)\}^{1/4}$ (where T_{bb} is the temperature of black body equal to $(S/4\sigma)^{1/4} \cong 278.6$ K, S is the solar constant (density of the radiation power from the Sun at the distance of the Earth orbit) $\sim 1.365 \times 10^3$ W/m^2, and σ is the Stefan–Boltzmann constant $\sim 5.67 \times 10^{-8}$ W/m^2K^4).

From these data, we can calculate the following idealized conditions governing on the Earth surface, namely

for $A = 35$, $G = 45 \Rightarrow T \cong 17$ °C (present state)
for $A = 0$, $G = 0 \Rightarrow T \cong 5.4$ °C (ideal black body without any atmosphere)
for $A = 35$, $G = 0 \Rightarrow T \cong -23$ °C (without greenhouse effect)
for $A = 0$, $G = 45 \Rightarrow T \cong 50$ °C (without albedo).

These estimates illustrate very well the extraordinarily beneficial setting of the Earth in the space. Taking into account the parameters of orbits and atmosphere reflectivity G of the neighboring planets Mars (G is negligible) and Venus (G exceeds 70), we obtain much unfavorable figures. Relative thermal stability of the Earth together with reasonably small scatter of its surface temperatures ($\Delta T \approx \pm 50$ °C) around the water freezing point at 0 °C is an amazement, thus allowing the mounting miracle of life. Notice that such a difference between

maximal and minimal temperatures is insignificant in comparison with the usual extent of temperatures encountered in the universe. Certainly, the actual temperature is not only the function of A and G, but is sensitively related to the Sun activity if the validity of Wien's law $T \cong 2.884 \times 10^{-3}/\lambda_{max}$ is assumed. Moreover, our evaluation shows that the Earth temperature is probably more sensitive to the changes of actual temperature of the Sun surface than the changes brought about by variations of coefficients inherent in its vivacity through A and G.

What more, the Earth temperature stability is curiously reinforced by the sudden change of the natural course of gradually falling temperature at tropopause (~15 km) to the positive gradient reversing again at stratopause (~50 km) (see Fig. 22.3), which prevents the escape of the Earth atmosphere into the outer cosmic space and ensures the existence of ultraviolet shielding, the ozonosphere.

The relative changes of the mean Sun radiation incident to the Earth's atmosphere during the twentieth century can be estimated as no more than 0.15%. On the other hand, the mean Earth's surface temperature is raised by 0.9 K during the same period [44]. If the Earth is considered as a black body radiator (see above), the relation (valid for small changes) $dT/T \sim 1/4\ dS/S$ takes place which shows that a possible change of the temperature due to the variation of the irradiation from the Sun should not be more than ~0.11 K. Hence, this simple estimate indicates that other effects, like the change of atmosphere compositions, have to be likely considered to explain an increase of the Earth temperature in the last century. Such a deduction agrees very well with the conclusions based on complex approaches [44].

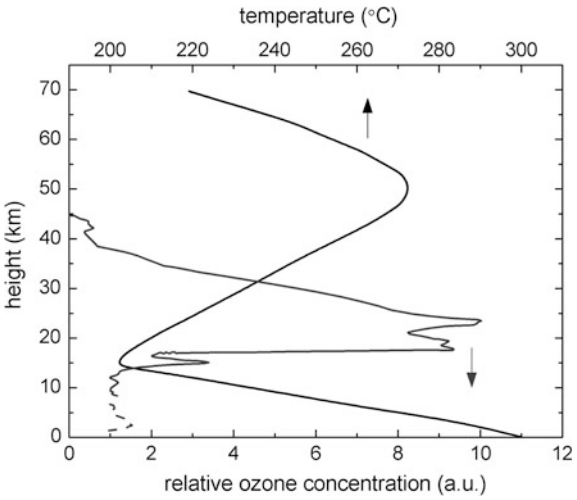

Fig. 22.3 Negative (troposphere) and positive (stratosphere) temperature gradients (*upper scale*) in the Earth atmospheric envelope (*left*) and associated distribution of ozone (*bottom*) as a far-reaching thermal measurement. Besides the gravitation, this rare temperature distribution assures the life crucial preservation of atmospheric layer in order to stick firmly onto the Earth surface

22.8 Composition of the Atmosphere, Greenhouse Effect, and the Recent Views of Climate Changes

Let us recall that the water vapor is the major agent of the atmosphere absorption naturally controlling the Earth surface temperature, which is spontaneously fluctuating under the influence of other phenomena that are yet poorly understood [59, 60]. High temperature enhances evaporation, and the enhanced amount of water vapor increases greenhouse effect and temperature of the Earth. Nevertheless, enhancement of water vapors in the atmosphere may have also a quite opposite effect.

Saturated vapors in the presence of small disturbances tend to condensate and increase the albedo, which consequently decreases the temperature and activates further vapor condensation releasing the latent heat and so on. The interplay of these antagonistic trends with random disturbances cannot converge to some equilibrium steady state but is rather a source of permanent chaos.

The dominating role of water vapors on greenhouse effect and allied processes in the atmosphere was confirmed by US satellite 2001 observations [61]. They revealed often overlooked fact that the actual effect of individual gases on the degree of greenhouse effect may be estimated as follows (probable percentage of natural/anthropogenic effect): H_2O as much as ≈99/0.10, CO_2—0.12/0.01, and the rest mainly CH_4—0.1/0.05 (cf. also Fig. 22.4).

The second most significant greenhouse gas is carbon dioxide. Let us make a balance estimate of the total human industrial production of CO_2, primarily from the use of fossil fuel, production of cement, and automobile industry, which is about 8 Gt of carbon (C) per year, while humans exhale mere 0.6 Gt of C. Overall, human CO_2 production is still negligible as compared to that residing in the ocean and biosphere [62–67]. Hence, the sources and absolute amounts of CO_2 in the atmosphere are likely of secondary importance and are thus rather insignificant to the hypothesis of human-caused global warming, because the overall rather weak absorption effect of CO_2 itself seems to be overestimated with respect to that caused by H_2O. Nevertheless, historical records reveal that even insignificant changes in the energy partaking (due to volcano eruption and meteorite collision) may cause the consequent far-reaching climate modification; thus, the impact of exponentially increasing mankind and their brutal Earth exploration may become a yet unknown instigative mechanism influencing living conditions on the Earth in an unprecedented manner.

One of the most unfavorable figures for the manufacture release of carbon dioxide is provided by the Czech Republic with CO_2 annual production per capita of about 1.3×10^4 kg with a definitely highest energetic cost of 2.2 USD per one kilogram of the created CO_2 (which is the amount of needed production energy related to the gross national product). These values are closely followed by Poland and Slovak Republic ($\sim 0.8 \times 10^4$ kg at ~ 1.8 USD/kg). The highest CO_2 production shows USA with almost 2.1×10^4 kg/cap but at only 0.6 USD/kg followed by Canada and Australia. The most favorable data exhibit Scandinavian countries, Japan, and

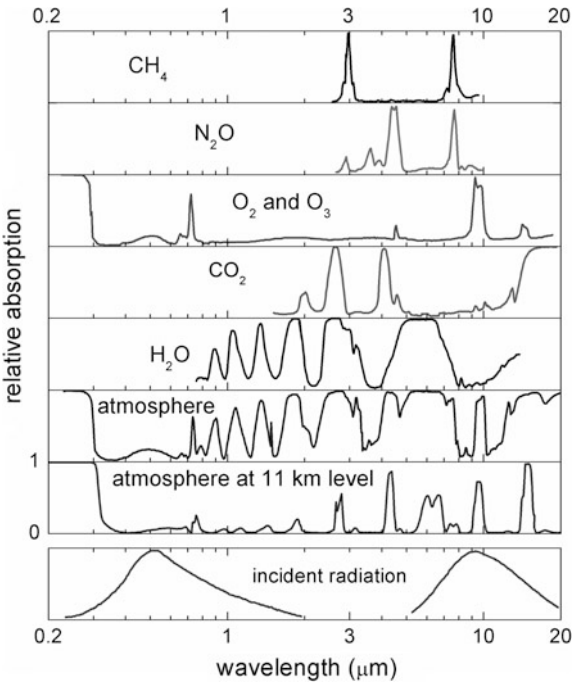

Fig. 22.4 Absorption bands of individual gases presented in the Earth atmosphere in various contents contributing thus the greenhouse effect (in comparison with the incoming (*left*) and outgoing (*right*) radiation shown *bottom*)

Switzerland with 0.5–0.8 $\times$ 10^4 kg/capita at mere 0.1–0.3 USD/kg. Certainly, it ensues an everlasting inquiry whether such a momentous industrial production of CO_2 (generated by the nature-unexpected combustion of fossil deposits collected through the extended geological history) really affects the crucial circulation of carbon between air, land, and water. Terrestrial vegetation uses about 10^9 tons of carbon a year to grow so that this demand would exhaust CO_2 in the atmosphere if not constantly replenished through plant respiration and decomposition of organic matter. Only Atlantic Ocean plants keep removing billions of tons of CO_2 from air and water—not accounting for the further CO_2 dissolution capability and its consequent redeposition in the form of solid carbonates. However, the presence of CO_2 vigorous sinks is critical for the moderation of the human made buildup of CO_2, which has recently increased by about 30% (when comparing with the preindustrial levels). It is well known that major climate shifts of the past half million years, as an alternation of Ice Ages and interglacial periods, never triggered a spike in atmospheric CO_2 content like the one recorded in the past 150 years. In particular, air trapped in ice cores from the Antarctica iceberg was analyzed showing that the CO_2 content approximately oscillated every 100,000 years from about 200 to 280 ppm (parts per million) roughly matching the shift of periods. It is the question whether the stable range of CO_2 concentration ended with the modern era's unprecedented burning of petrified fuels, which has currently increased CO_2 content up to the never detected amount of 350 ppm, and whether, as predicted, doubling of CO_2 content will be already attained by the year 2100.

22.9 Often Underestimated Effect of Nanoparticles and Allied Health Risks

Based on the above given figures, one can take almost for granted that the recent effect of extra man-made exhalations of greenhouse gases alone cannot be so significant as it is believed by, e.g., protagonists of Greenpeace movement. This fact provides strong arguments for the opposition claiming that the greenhouse effect together with global warming is nothing else but baloney [48, 55] proclaimed by so-called 'eco-terrorists'. Both these opinions are, however, fatally simplifying the real situation. Greenhouse effect, a physical effect par excellence stabilizing for millions years the conditions on the surface of the Earth, does exist. Global warming (if existent and till now of not fully known origin) may be discernible in recent decades by fast disappearance of glaciers and unusual catastrophic behavior of weather. These effects, however, must be properly accounted for and not only proclaimed or denied [67–71]. Therefore, in conclusion, we would like to point out some important aspects which should be subjected to further research [27].

In order to separate anthropogenic and natural effects, the influence of temporal changes of irradiation of the Earth by the Sun regardless of its origin (changes of the Earth's orbit, activity of the Sun or of yet unknown impact of cosmic rays) should be eliminated first (very helpful may be here just a simple TA approach). As the main greenhouse effect and albedo in the atmosphere of the Earth are very likely due to the water, the interactions resulting in phase transformations of the water changing dramatically absorption of radiation in atmosphere, electric potential [72, 73], and its ion content [54, 74–79] have to be studied. Among the agents triggering the phase transitions of water belong heavy ions [74], nanoparticle dust [33, 34, 75, 78], chemically active gases (perhaps even "greenhouse" ozone), as well as a nucleation making caused by cosmic rays collision with atmosphere. The significance of these "agents" is due especially to the facts that they are efficient even in extraordinary small concentrations. Some of them can be produced in an appreciable amount by human activity [77, 78]. The attention should not thus be paid only to the increase of concentration of greenhouse gases but rather to other components of exhalations, to heavy ions, and especially to nanoparticles [74–79]. It is evident that the fabrication of CO_2 by combustion is always accompanied by the production of such nanoparticles, the life of which is more persistent (due to the negligible sedimentation controlled by Brownian motion) than that of CO_2 which takes a part in the natural circulation (dissolution, precipitation). Very important become then the diurnal effects such as rise of ions and charged nuclei and their dissipation [72–74], which are localized especially near the large agglomeration (cities, factories) where there is the greatest introduction of dangerous nuclei into atmosphere, thus completing the natural cosmic background. It concerns the importance of (often neglected) knowledge of the values of the electric potential gradient at the Earth´s surface [72, 73], which, for example, is remarkably low in fine weather, while, on contrary, fog and dust produce high potential gradients not only harmful to human health but also affecting weather. Striking proof of such a

pollution effect was measured at a remote island (Samos) as early as in 1937 [27, 72]) showing a marked increase in the diurnal variation of potential gradient (>50%, reaching up to 300 V/m) due to mere festival barbecue on holiday days; more crucial effects are detectable in the vicinity of big sources of man-made pollution. This yet undervalued subject can likely turn soon into the center of pollution policy linked to the climate change and can substitute the recently fashionable target of greenhouse gases and their gradual increase [39].

Since humans have always been exposed to tiny particles from dust storms, volcanic activity, and other natural processes, our bodily systems have become well adapted to protect us from these potentially harmful intruders [79, 80]. The reticuloendothelial system actively neutralizes and eliminates foreign matter in the body, including viruses and non-biological particles. Particles originating from human activities have existed for millennia, e.g., smoke from combustion and lint from garments, but the recent development of industry and combustion-based engine transportation has profoundly increased anthropogenic particulate matter pollution [79]. Significantly, technological advancement has also changed the character of particulate pollution, increasing the percentage of nanometer-sized fragments, nanoparticles, and expanding the variety of chemical compositions. Recent epidemiological studies have shown a strong correlation between particulate air pollution levels and respiratory, brain and cardiovascular diseases, various cancers, and resulting mortality [80–84]. Probable explanation is that the nanoparticles are less efficiently removed from the organism than larger particles by the macrophage clearance mechanisms in the lung, causing lung damage being translocated through the circulatory, lymphatic, and nervous systems to many tissues and organs, including the brain. Examples of toxic effects include tissue inflammation and shifted cellular redox balance toward oxidation, causing abnormal function or cell death.

As an example may serve the oil wells burning from horizon to horizon during the 1991 Gulf War. It looked like an apocalypse with less than 1% of the sun's visible light penetrating through dove-gray plumes rich of NaCl and $CaCl_2$ crystals and full of uncombusted oil droplets, hydrophobic in nature and immune to cloud scavenging. The plumes were expected to rise to the top of the planetary boundary layer (>3000 m) where smog and other pollutants use to stabilize. According to the atmospheric models, sunshine would heat the upper atmosphere via the black soot, making it rise further through a process called "self-lofting" (known from extensive natural wildfires). But it turned out that the soot particles had a lot of sulfate mixed in, which makes them to absorb water and act like cloud condensation nuclei so that a black plume in corner of the Gulf disappeared by the time and got to the Indian Ocean. It is clear that some other oils, with less favorable composition, can have a great climatic impact if ignited, so that we were lucky not to face the effects of their out-of-control burning. Certainly, we should be vigilant to any signal or evidence of weather changes due to our everyday doings. For example, we cannot even exclude that the higher frequency of unwanted rainy weekends is caused by gradual collection of dust in the atmosphere during working days, which culminates as the last working day approaches, forming nucleation sites and ease consequent vapor

condensation. In any case, a more violent alteration of weather (extreme windstorms, hurricanes, and tornados) may be a sign of inattentive changes caused by mankind or nature self.

Nanoparticles (NPs) [74–79] are thought to play an important role in dust cloud formation after being released into the environment as they coagulate and form dust cloud [29]. 70% of the brown clouds over South Asia are made up of soot from the burning of biomass; largely wood and animal dung are used for cooking and mainly contain particulate matters and carbon NPs from unprocessed fuel [28, 30]. The regional haze, known as atmospheric brown clouds, contributes to glacial melting, reduces sunlight, and helps create extreme weather conditions that impact agricultural production. The pollution clouds also reduced the monsoon season in India [32]. The weather extremes may also contribute to the reduced production of key crops such as rice, wheat, and soybean.

The hydroxyl radical, which is one of the most reactive free radicals in the environment, plays an important role in the photochemical degradation of natural organic matter and organic pollutants in the environment. NNPs being very reactive immediately bind with hydroxyl radicals and ultimately result in the overall reduction of hydroxyl radicals [35, 36]. As hydroxyl radicals are strong oxidants and thereby degrading many pollutants, its reduction is responsible for the increase in greenhouse gases, which are ultimately responsible for ozone layer depletion (cf. Fig. 22.4) and cause severe environmental damage. Furthermore, it increases the exposure to UV radiation [38], which leads to the increase in incidences of various types of skin cancer.

NPs in the troposphere interact with molecular hydrogen accidentally released from hydrogen fuel cells and other sources [39]. Molecular hydrogen along with NPs moves up to the stratosphere, resulting in the abundance of water vapor in the stratosphere. This will cause stratospheric cooling, enhancement of the heterogeneous chemistry that destroys ozone, an increase in the so-called noctilucent clouds changing tropospheric chemistry, and atmosphere–biosphere interactions. Noctilucent clouds are composed of tiny crystals of water ice 40–100 nm in diameter and exist at a height of about 76–85 km, higher than any other clouds in Earth's atmosphere. As the more familiar lower altitude clouds, the noctilucent clouds are formed from water collecting on the surface of nanosized dust particles. The sources of both the dust and the water vapor in the upper atmosphere are not yet known with certainty. The dust is believed to come from micrometeorites, although volcanoes and dust from the troposphere are also possibilities. The moisture could be lifted through gaps in the tropopause as well as formed from the reaction of methane with hydroxyl radicals in the stratosphere.

Human's exposure to NPs mainly occurs through natural routes (oral, pulmonary, or skin uptake) [80–84]. Exposure assessment is difficult but necessary. Furthermore, many intentional processes such as medical applications may directly inject engineered NPs (ENPs) into the human body. Under practical conditions, the most important routes of uptake for ENPs are inhalation or oral uptake, but this has not been specifically studied. More information is available for accidentally released NPs from combustion engines especially diesel exhaust. In case of aerosolized silver-containing

NPs that are widely used in consumer products due to their antimicrobial properties, environmental and human health risk was reviewed in detail. NPs come in the direct contact with skin as they are widely used in various cosmetics and personal care products, and hence, the assessment of toxicity due to dermal route of exposure is very critical. Since NPs are already present in food products such as ketchup, intake of NPs through food is another area where exposure assessment is crucial. Unfortunately, there is very little information available about influence on population exposures through ingestion. In order to facilitate the toxicity assessment of NP exposure of human, the establishment of exposure registries was recommended to conduct large-scale prospective multicenter epidemiologic studies.

22.10 Thermal Inertia, Climate Feedbacks, and Ecosystem Thermodynamics

For planetary surface materials, thermal inertia [85] is a key property controlling the daily and seasonal surface temperature variations and is typically dependent on the physical properties of near-surface geologic materials. Thermal inertia represents a complex combination of particle size, their moisture, rock abundance, bedrock outcropping, and the degree of indurations [86]. A rough approximation to thermal inertia is sometimes obtained from the amplitude of the diurnal temperature variation. The temperature of a material with low thermal inertia changes significantly during the day, while the temperature of a material with high thermal inertia does not alter so drastically. Understanding the thermal inertia of the surface can help to recognize small-scale features of that surface. In conjunction with other data, thermal inertia can help to characterize surface materials and the geologic processes responsible for forming these materials. Inertia is a widespread inherent characteristic of the climate, ecological, and socioeconomic systems. Therefore, some impacts of anthropogenic climate change may be slow to become apparent, if some critical thresholds (whose positions may be poorly known) are crossed in rate or magnitude, and some climate change can be irreversible.

Remote sensing (e.g., from satellites [86]) can be utilized to measure the thermal inertia of the Earth surface. An algorithm has been developed which relates thermal inertia to remote measurements of surface temperature and reflectance. Application to geosynchronous satellite data illustrates the contrast between irrigated and desert areas in the region north of, e.g., Gulf of California. The effect of local weather conditions (latent and sensible heat transfer to the atmosphere) must be estimated before precise values for thermal inertia can be specified.

Thermal inertia [85–90] (P) can be defined as $P = (Kc\rho)^{1/2} = c\rho(k)^{1/2}$, where c is specific heat capacity and ρ is density of a given material. The term k is related to thermal conductivity K and is known as thermal diffusivity having units of centimeters squared per second. This parameter governs the rate of temperature change within a material measuring a substance's ability to transfer heat in and out of that portion that received from solar heating during the day and cools at night. P is a

measure of the heat transfer rate from the material volume to its boundary. Because materials with high P (e.g., wet soil) possess a strong inertial resistance to temperature fluctuations at a surface boundary, they show less temperature variation per heating/cooling cycle than those with lower thermal inertia (air).

The term thermal inertia is a scientific analogy but is not directly related to the mass-and-velocity term used in mechanics, where inertia is that which limits the acceleration of an object [91]. In a similar way, thermal inertia is a measure of the thermal mass and the velocity of the thermal wave which controls the surface temperature of a material. However, such understood thermal inertia is different from that derived on the basis of Newton cooling law and is applied in differential thermal measurement (DTA) [91].

Based on different values of thermal inertia [85–90], the atmosphere heats more quickly than the oceans (and of course icy bodies). Perhaps obviously, as the heat comes almost entirely from above, the near surface of the oceans heats more quickly than the depths, and just the surface temperature is usually included with that of the atmosphere to get a near-surface temperature. The average atmospheric/surface ocean temperature has risen by 0.8 °C, but the ocean alone down to about 700 m has risen by only 0.45° within the period of decades. In the case of ice bodies, heat transfer can be measured by the volume melted, where that is known. A small amount of heat is transferred daily into and out of the solid Earth, and some is transferred daily and over longer time periods into and out of land surface water bodies. Lethargy of the ocean temperature, when compared with the atmosphere, forms many implications for the Earth's weather and climate being out of the scope of this short overview.

The power per square meter of the Earth's surface is a relatively small number (see Sect. 22.7), but this is a modest but imperative gift what the nature has given us. Generations of dinosaurs lived in equilibrium with this number for a hundred millions years and humankind also managed it for several millennia until started to expand its population and advanced its technology. Finally, in the last thirsty century, insignificant with respect to history, a small percentage of humankind has developed a trend for fossil energy consumption, which has become out of tune with the natural orders of magnitude of power that likely the cosmic evolution has decided to give us. Sometimes, it is hard to believe that we are not clever enough, acting without scientific conscience, just simply driven by allurement of increasing growth.

The biological network interacts with the thermodynamic system (is factually "thermodynamically living") so that it is not a passive stage but a lively architecture. The global treatment induces better understanding of the concept of global steadiness governing a distribution of local disequilibrium. If the Earth had an irregular orbit, the problem would not admit a globally steady-like solution, and if, in addition to the daily and annual periodicity, there were additional irregular movements, there would be neither global steadiness nor the less restrictive property of global periodicity. The significant complication is the variation in either the solar emission or mutual orbit geometry, which implies changes in the input conditions for the Earth ecosystem and which is known to happen in certain

often-repeating short (30, 70 or 150 years) or lengthy (thousand and million years) intervals depending chiefly on the Sun, but having also many chaotic components (eruptions). However, within a cosmological scale, the concept of an isolated system becomes no longer practicable because the definition even of our neighborhood boundaries is tricky (as the Sun is enveloped by far-reaching dispersion layer full of whirlpools and jets, and at the same time our terrestrial atmosphere is diffuse and full of motion, containing rarefied ions with outwards super-fast streams) and the equations of fluid motion fail to hold. These alterations in the input conditions bring about yet new dynamical regime of atmospheric and oceanic motions (apart from changes in composition, structure, etc.). As these modifications are nonlinear again, nobody can predict, or know, what could be the resulting effect with respect to what we have experienced or can resolve from history.

If the solid Earth were a black rigid sphere with radius R_E, and with transparent atmosphere, the inward and outward fluxes would give simple condition for the temperature at R_E (see Sect. 22.7). The relative motion of the Earth and the Sun is described by a periodic function with the period p, which embodies the mass continuity, Navier–Stokes equation, and energy balance relations for the atmosphere (still very far from authenticity). According to Sertorio [16], the stationary distribution of the sustained equilibrium can be found compatible to a capacity of mechanical power that may be expressed by distribution of an infinite number of Carnot's-like engines whose global efficiency can be mathematically formulated in certain generalized terms. It can be approximated by the relation, $\eta_{global} = \int \lambda \left[(T_1 - T_2)^2 / \max(T_1, T_2) \right] \mathrm{d}S / R_E^2 \sigma T^4$, where λ and σ are, respectively, the overall Newton thermal conduction (fixed as 8 W/m^{2}K) and Stefan–Boltzmann radiation constants (providing $\sigma T^4 \approx 1384$ W/m^2). Such calculated values of η_{global} subsist in the neighborhood of one hundredth [16, 23].

It is clear that good ideas for the theory of the ecological human shelter may come from the study of dissipative learning systems, i.e., such adaptive systems that are matching survival. The Earth has the necessary vitality, complexity, and equilibrium-like stability, which is the prerequisite for its survival [3]. The hierarchy of interactions may help to formulate the concept that mankind is not a deterministic system, but rather a teleological system, or better a control system. However, the ecosystem species have rather simpler external interaction and the whole ecosystem (a giant engine being very complex inside) has its relatively uncomplicated and almost negligible interaction with the far Universe, which enables us to see Earth's ecosystem as yet deterministic world. Therefore, it is the profound mystery to see the existence of islands of order that promote the possibility of intelligent life reinforcement. The study and wider application of truly non-equilibrium thermodynamics and the theory of chaos makes sense. However, there is a great, unexplored domain beyond that, particularly regarding off-equilibrium behavior of the Earth environment itself which shielding aspects are distinguishable from the impacts of greenhouse gases and nanoparticles.

Acknowledgement J. Šesták acknowledges the support of Ministry of Education of the Czech Republic in the framework of CENTEM PLUS project (LO1402) operated under the "National Sustainability Program I."

References

1. Strnad J (1790) Chronologisches Verzeichniss der Naturbegebenheiten in Böhmen vom Jahre 633–1700, Prag. Studnička JF (1878) Entertainment Astronomical. Kolář, Praha, p 104 (in Czech)
2. Šesták J (2008) How is it with the warming of our planet Earth and what is the role of greenhouse gases. Energetika (Prague) 10:392–395 (in Czech)
3. Lovelock J (2000) Gaia: a new look at life on the Earth. Oxford University
4. Clark PU, Dyke AS, Shakun JD, Carlson AE, Clark J, Wohlfarth B, Mitrovica JX, Hostetler SW, McCabe AM (2009) The last glacial maximum. Science 325:710. Moberg A, Sonechkin DM, Holmgren K, Datsenko NM, Karlén W (2005) Highly variable northern-hemisphere temperatures reconstructed from low- and high-resolution proxy data. Nature 433:613
5. Climate Change 2007 (2007) Synthesis report, an assessment of the intergovernmental panel on climate change. http://www.ipcc.ch/pdf/assessment-report/ar4/syr/ar4_syr.pdf
6. McGovern TH (1980) Cows, harp seals, and church bells: adaptation and extinction in Norse Greenland. Human Ecol 8:245
7. Šesták J (1984) Thermophysical properties of solids: theoretical thermal analysis. Elsevier, Amsterdam. (1988) Its Russian version 'Teoreticheskij termicheskij analiz'. Moscow; Mir. (2005) Science of heat and thermophysical studies: a generalized approach to thermal analysis. Elsevier, Amsterdam
8. Czarnecki JP, Koga N, Šestákova V, Šesták J (1992) Factors affecting the experimentally resolved thermoanalytical curves. J Therm Anal 38:575. Czarnecki JP, Šesták J (2015) From recording balances to thermogravimetric instruments and back. J Therm Anal Calorim 120:157–166
9. Šatava V, Šesták J (1973) Mechanism of thermal decomposition of sulphate hemihydrates by isothermal and nod isothermal thermogravimetry using light-aided heating. Anal Chem 35:154. Šesták J (1993) Thermal treatment and analysis. J Therm Anal 40:1293
10. Basaran, T, Ilken Z (1998) Thermal analysis of the heating system of the small bath in ancient Phaselis. Energy Build 27:1–11. Athienitis AK, Santamouris M (2000) Thermal analysis and design of passive solar buildings. Routledge (ISBN-13: 978-1902916026)
11. Hartmann DL, Ramanathan V, Hunt GE (1986) Earth radiation budget data and climate research. Rev Geophys 24:439
12. Raval A, Ramanathan V (1989) Observational determination of the greenhouse effect. Nature 342:758
13. Wallace JM, Hobbs PV (1977) Atmospheric science: an introductory survey. Academic Press, London
14. Zemansky RW, Dittman RH (1952) Heat and thermodynamics. McGraw Hill, New York
15. Eskinazi S (1975) Fluid mechanics and thermodynamics of our environment. Academic Press, New York
16. Sertorio L (1991) Thermodynamics of complex systems: an introduction to eco-physics. World Science, London
17. Peixoto JP, Oort AH (1992) Physics of climate. American Institute of Physics, New York
18. Odum HT (1996) Environmental accounting: energy and decision making. Wiley, New York
19. Bohren CF, Albrecht BA (1998) Atmosphere thermodynamics. Oxford University Press, New York
20. Maršík F, Dvořák I (1998) Biothermodynamics. Academia, Prague (in Czech)

21. Curry JA, Webster PJ (1999) Thermodynamics of atmosphere. Academic, New York
22. Berdwell A, Hoden L (2003) Weather and climate studies. Prentice Hall, New York
23. Šesták J (2004) Society, science and ecology: progress against survival (Chapter 16). Heat, thermal analysis and society. Nucleus, Hradec Králové, p 277
24. Day JA (2005) The book of clouds. Sterling. Kiehl JT, Ramanathan V (eds) (2006) Frontiers of climate modeling. Cambridge University Press
25. Robinson AB, Robinson NE, Soon W (2007) Environmental effects of increased atmospheric CO_2. J Amer Phys Surg 12:81. (1999) Climate Res 13:171. http://www.oism.org/pproject/s33p36.htm
26. Šesták J (2007) Consideration on economic and ecological book Vaclav Klaus: global warming and the immensity of energy resources. Chem Listy (Prague); 101:832 (in Czech). www.fzu.cz/∼sestak
27. Šesták J, Hubík P, Mareš JJ (2010) Thermal analysis scheme aimed at better understanding of the Earth's climate changes due to the alternating irradiation. J Therm Anal Calorim 101:567–575
28. Šesták J (2006) On the availability, exploitability and sustainability of our energy resources (Chapter 9). In: Knut E, Pliska V, Folkers G (eds) Promises of science. Collegium Helveticum, Zurich, p 69
29. Fourier JB (1822) Theorie analytique de la chaleur. Paris
30. Faraday M (1860) Chemical history of candle. Royal Inst, London
31. Arrhenius S (1896) On the influence of carbonic acid in the air upon the temperature of the ground. Phil Mag 41:237
32. Twomay S (1974) Pollution and the planetary albedo. Atmos Environ 8:1251
33. Teller A, Levin Z (2006) The effects of aerosols on precipitation and dimensions of subtropical clouds: a sensitivity study using a numerical cloud model. Atmos Chem Phys 6:67
34. Guisbier G, Buchaillot L (2009) Universal size/shape-dependent law for characteristic temperatures. Phys Lett A 374:305. Vanithakurami SC, Nada KK (2008) Universal relation for the cohesive energy of nanoparticles. Phys Lett A 372:6930
35. Tyndall J (1861) On the absorption and radiation of heat by gases and vapors. Philos Mag 22:169, 173
36. Langley SP (1884) Researches on solar heat and its absorption by the Earth atmosphere. Report of the Mt. Whitney expedition. Governmental Printing, Washington
37. Kaplan LD (1959) The atmosphere and the sea in motion. Rockefeller Inst. Press, New York (in particular, the chapter "Calculation of infrared fluxes" pp. 170)
38. Poynting JH (1904) Radiation in the solar system. Phil Trans A 202:525
39. Tverskoy PN (1951) Course on meteorology: atmospheric physics. Hydrometeorol Izdatelstvo, Leningrad (in Russian)
40. Goody RM (1964) Atmospheric radiation: theoretical basis. Clerandon, New York
41. Bednář J (1989) Special phenomena in the Earth atmosphere. Academia, Prague (in Czech)
42. Lorenz EN (1963) Deterministic nonperiodic flow. J Atmos Sci 20:130
43. Sussman GJ, Wisdom J (1992) Chaotic evolution of the solar system. Science 257:56
44. Lean JL (2010) Cycles and trends in solar irradiance and climate. Wiley interdisciplinary reviews: climate change 1:111–122. Haigh J (2011) Solar influences on climate. Grantham Institute for Climate Change, Briefing paper No 5, London, Imperial College
45. Huybers P (2007) Glacial variability over the past two million years. Quat Sci Rev 26:37
46. Oeschger H, Langway CC (eds) (1989) The environmental record in glaciers and ice sheet. Wiley, New York
47. Milankovitch M (1920) Theorie Methematique des Phenomenes Thermiques produits par la Radiation Solaire. Gauthier-Villars, Paris
48. Kutilek M (2008) Rationally about the global warming. Prague, Dokořán (in Czech)
49. Clough HG (1905) Synchronous variations in solar and terrestrial phenomena. Astrophys J 22:42

50. Christensen EF, Lassen K (1991) Length of the solar cycles as an indicator of solar activity closely associated with the Earth's climate. Science 254:698. (1995) J Atmos Terr Phys 57:835
51. Haigh J (1996) On the impact of solar variability on climate. Science 272:767
52. NASA/Marshal Solar Physics. The sunspot cycle. Websites: http://solarscience.msfc.nasa.gov/SunspotCycle.shtml
53. Hoyt DV, Schatten KH (1997) The role of the Sun in climate changes. Oxford University Press, New York
54. Svensmark H, Christensen EF (1997) Variation of cosmic ray flux and global cloud coverage—a missing link in solar climate relationships. J Atmos Sol Terr Phys 59:1225. Svensmark H, Pedersen JOP, Marsh ND, Enghoff MB, Uggerhoj UI (2007) Experimental evidence for the role of ions in particle nucleation under atmospheric conditions. Proc R Soc A 463:385
55. Singer SF, Awery DT (2007) Unstoppable global worming every 1500 years. Rownan-Littefield, Lanham
56. Landscheidt T (1997) Klimavorhersage mit astronomischen Mitteln? Fusion 18:58
57. Arnold VI (1963) Small denominators and problems of stability in classical and celestial mechanics. Russian Math Surv 18:85 (in Russian)
58. Maršík F (1999) Thermodynamics of continuum. Academia, Prague
59. Pauluis OM (2005) Water vapor and entropy production on the Earth's atmosphere. In: Kleidon A, Lorens RD (eds) Nonequilibrium thermodynamics and production of entropy. Springer, Heidelberg, pp 107–119
60. Adams DL, Renno NO (2005) Thermodynamic efficiencies of an idealized global climate model. Clim Dyn 25:801–813
61. Singer SF (2001) Satellite observations of atmospheric gases. Wall Street Journal, Sept. 10 (data from US Weather Satellite Service)
62. Ramanathan V (1987) The Role of ocean-atmosphere interaction in the CO_2 climate problem. J Atmos Sci 38:918. (1987) The role of Earth radiation budget in climate and general circulation research. J Geophys Res 38:4075
63. Zámostný P, Kukula P, Young JS (1999) Possible green house gases and global climate change. Chemické listy (Prague) 93:238 (in Czech)
64. Houghton RA (2007) Balancing the global carbon budget. Ann Rev Earth Planet Sci 35:313
65. Romanova V, Lohmann G, Grosfel K (2006) Effect of land albedo, CO2, orography and ocean heat transport on extreme climate. Clim Past 2:31
66. Rodhe H (1990) A comparison of the contribution of various gases to greenhouse effect. Science 248:1217
67. Burgmeister J (2007) Missing carbon mystery: case solved? Nat Rep Clim Change 3:37
68. Petit JR (1999) Climate and atmospheric history of the past 420,000 years from the Vostok Ice Core, Antarctica. Nature 399:429–436
69. Humlum O, Stordahl K, Solheim J (2013) The phase relation between atmospheric carbon dioxide and global temperature. Glob Planet Change 100:51–69
70. Kuo C, Lindberg CR, Thorson D (1990) Coherence established between the atmospheric CO_2 and global temperature. Nature 343:709
71. Henderson GE (2006) Caving into new chronologies. Science 313:620. (2007) Orbital and millennial Antarctic climate variability over the past 800,000 years. A collective report. Science 317:793
72. Chalmers JA (1957) Atmospheric electricity. Pergamon, London
73. Rycroft MJ, Harrison RG, Nicoll NA, Mareev AE (2008) An overview of earth's global electric circuit and atmospheric conductivity. Space Sci Rev 137:83–105. Harrison RG, Ambaum MHP (2009) Observed atmospheric electricity effect on clouds. Environ Res Let 4:4
74. Harrison RG, Carslaw KS, (2003) Ion-aerosol-cloud processes in the lower atmosphere. Rev Geophys 41. Buseck PR, Adachi K (2008) Nanoparticles in the atmosphere. Elements 4:389. doi:10.1029/2002RG000114

75. Smita S, Gupta SK, Bartonova A, Dusinska M, Gutleb AC, Rahman Q (2012) Nanoparticles in the environment: assessment using the causal diagram approach. Environ Health 11 (Suppl 1):S13
76. Stone V, Nowack B, Baun A, van den Brink N, Kammer F, Dusinska M, Handy R, Hankin S, Hassellöv M, Joner E, Fernandes TF (2010) Nanomaterials for environmental studies: classification, reference material issues, and strategies for physico-chemical characterization. Sci Total Environ 408:1745–1754
77. Kulmala M, Kerminen VM (2008) On the formation and growth of atmospheric nanoparticles. Atmos Res 90:132–150
78. Biswas P, Wu C (2005) Nanoparticles and the environment. Air Waste Manage Assoc 55:708–746
79. Buzea C, Pacheco II, Robbie K (2007) Nanomaterials and nanoparticles: sources and toxicity. Biointerphases 2:MR17–MR71
80. Xia T, Li N, Nel AE (2009) Potential health impact risk of nanoparticles. Ann Rev Pub Health 29:137–150
81. Nel A, Xia T, Mädler L, Li N (2006) Toxic potential of materials at the nanolevel. Science 311:622–627
82. Oberdörster G, Sharp Z, Atudorei V, Elder A, Gelein R, Kreyling W, Cox C (2004) Translocation of inhaled ultrafine particles to the brain. Inhal Toxicol 16:437–445
83. Simkó M, Mattsson MO (2010) Risks from accidental exposures to engineered nanoparticles and neurological health effects: a critical review. Part Fibre Toxicol 7:42
84. Lockman PR, Koziara JM, Mumper RJ, Allen DD (2004) Nanoparticle surface charges alter blood-brain barrier integrity and permeability. J Drug Target 12:635–641
85. Price JC (1977) Thermal inertia mapping: a new view of the Earth. J Geophys Res (oceans and atmospheres) 82:2582–2590. Xue Y, Cracknell AP (1995) Advanced thermal inertia modeling. Int J Remote Sens Environ 16:431–446
86. Carlson TY, Dodd JK, Benjamin SG, Cooper JN (1981) Satellite estimation of the surface energy balance, moisture availability and thermal inertia. J Appl Meteorol 20:67–87
87. Nearing SG, Moran MS, Scott RL, Ponce-Campos G (2012) Coupling diffusion and maximum entropy models to estimate thermal inertia. Int J Remote Sens Environ 119:222–231
88. Murray T, Verhoef A (2007) Moving towards a more mechanistic approach in the determination of soil heat flux from remote measurements: a universal approach to calculate thermal inertia. Agric For Meteorol 147:80–87
89. Wang J, Bras RL, Sivandran G, Knox RG (2010) A simple method for the estimation of thermal inertia. Geophys Res Lett 37:L05404 doi:10.1029/2009GL041851
90. Wang J, Bras RL (1999) Ground heat flux estimated from surface soil temperature. J Hydrol 216:214–226
91. Holba P, Šesták J (2015) Heat inertia and its role in thermal analysis. J Therm Anal Calor 121:303–307. Šesták J (2014) Is the original Kissinger equation obsolete today: not obsolete the entire non-isothermal kinetics while ignoring thermal inertia? J Therm Anal Calorim 117:3–7

Chapter 23
Thermodynamics and Economics

Jürgen Mimkes

Abstract Thermodynamics and economics have developed independently through the last centuries. Only in the last three decades, scientists have realized the close relationship between economics and physics. The name of the new field is econophysics: In double-entry accounting, the sum of monetary and productive accounts is zero. In calculus, monetary and productive accounts may be represented by Stokes integrals. In engineering, Stokes integrals lead to the two levels hot and cold of Carnot motors. In production, Stokes integrals lead to the two-level process: buy cheap and sell expensive. In economics, the two-level mechanism of capital and labor is called capitalism. A heat pump can extract heat from a cold river and heat up a warm house. A monetary circuit extracts capital from a poor population and makes a rich population richer! A running motor gets hotter, the efficiency, the difference in temperatures, grows with time. A running economy gets richer, the efficiency, the difference between rich and poor, grows.

23.1 Introduction

Economics is a field of philosophy based on the experience and tradition rather than on mathematical foundations. Economic laws are stated as principles that have been developed by different schools beginning with Adam Smith and classical economics in the late eighteenth century. *Economics* today is considered to be a field of *social science*, cooperation, and competition as well as buying and selling are closely related to game theory and *psychology*. Business is entangled with contracts, and public *law*, banking, and money are tied to properties such as hope and trust that are clearly part of *social sciences*.

J. Mimkes (✉)
Physics Department, University of Paderborn, Paderborn, Germany
e-mail: juergen.mimkes@upb.de

J. Šesták et al. (eds.), *Thermal Physics and Thermal Analysis*,
Hot Topics in Thermal Analysis and Calorimetry 11,
DOI 10.1007/978-3-319-45899-1_23

However, if the early economists had stated their principles by calculus that had been developed by the British natural scientist Isaac Newton (1643–1727) and the German mathematician Gottfried Wilhelm Leibniz (1646–1716), economic science would perhaps be a completely different field of science. In the early days of natural production, people worked in the fields to obtain food and shelter. Work, food, heat are measured in energy units, in kWh or in calories. Energy is an element of natural science, of *biology*. Work, again, is an element of mechanics and indicates a close relationship to *physics.* Cooperation and competition are well known from chemistry. People, like atoms, attract each other and cooperate, repel each other, and dissociate, or are indifferent and integrate. Cooperation, segregation, and integration have the same structure in social science and in chemistry. Only the forces are different: In chemistry, we have electromagnetic forces between atoms; in societies, we have social bonds like love, hate, or indifference between people. Obviously, economics is linked to *chemistry.* Trade follows the law: buy cheap–sell expensive! Every shop has to buy a product at a low price and has to sell it at a higher price in order to make a profit. This process is repeated and requires labor to keep the economy running. If the price for buying and selling is the same, trade will stop. The same mechanism is known for heat engines or motors: Cold air is sucked in by the motor and hot air is blown out. This process is repeated and repeated and requires energy to keep the motor running. If the two temperatures of the motor are the same, the motor will stop. Production and trade apparently are closely linked to *engineering!* Banks, surprisingly, rarely use the term trust, and they prefer the term risk, the reciprocal of trust: Low trust is high risk and high trust means low risk. The term risk is again linked to statistics and to *statistical mechanics*. Accordingly, *economics* seems to be very close to the fields of *natural science*.

Indeed, since 1990 natural scientists have started to investigate economics, finance, and social sciences by means of statistics, calculus, and tools of theoretical physics. The new field has been called econophysics [1–9]. Presently, the name econophysics is mainly focused on finance. But many authors use the terms econophysics or complexity for the combination of social and natural sciences.

23.2 Neoclassical Problems

There is a widely accepted economic theory, the neoclassical approach [10, 11]. However, this theory is not based on calculus and shows deficits that can be solved by calculus-based theory:

23.2.1 Solow Model

The Solow model of neoclassical theory claims income (Y) to be a function of capital and labor:

$$Y = F(K, L). \tag{23.1}$$

Income (Y) is a function (F) of capital (K) and labor (L). The function $F(K, L)$ is called production function.

Every investor would like to know how much he will earn in the investment period. But income (Y) is an *ex post* term, we can file our income tax only at the end of the year. Income can only be determined when the money is earned. In contrast, a function (F) may be calculated at any time, in the beginning or at the end of the year. Functions (F) are called *ex ante* terms. *Ex ante* cannot be equal to ex *post*! Either we know beforehand or not. This means income (Y) cannot be a function (F):

$$Y \neq F(K, L)! \tag{23.2}$$

This puzzle will be solved by exact (*ex ante*) and not exact (*ex post*) differential forms in calculus-based economic theory.

23.2.2 The Neoclassical Misinterpretation of a Monetary Balance as a Circular Flow

Neoclassical theories consider monetary circuits as ring-like flows: Income (Y) flows from industry to households and flow back to industry as consumption costs (C). The surplus (S) flows from households to the bank, from where the money flows back into the economic circuit as investment (I) of industry.

However, this cannot be true, if we put in the numbers of the balance: A company pays 100 € per day to each worker and gets back only 90 € for consumption cost. The company has to withdraw ΔM = 10 € from the bank to be able to pay the workers 100 € again the next day!

This neoclassical model cannot work! (Fig. 23.1)

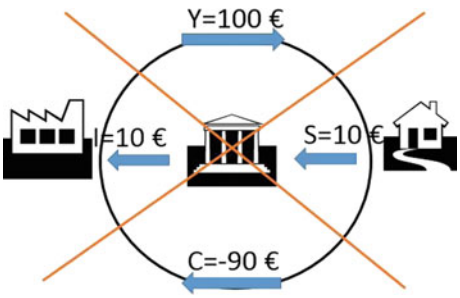

Fig. 23.1 A monetary balance cannot be a closed circuit flow. If a company pays 100 € per day to each worker and gets back only 90 € for consumption cost, the company has to withdraw 10 € from the bank to be able to pay the workers 100 € again the next day! This neoclassical model cannot work! Again, this problem will be solved by Stokes integrals in calculus-based economic theory

23.3 The Double-entry Balance

Balances are the fundament of economics. Every merchant has to look at his economic balance.

A monetary balance is an account of numbers measured in monetary units such as €, US$, and £. The account must indicate the economic unit, the person, the household or the company to which it refers. We may indicate the numbers by symbols and the economic unit by a suffix such as Y_H for income of a household, or C_{In} for industrial costs, and ΔM_X for the annual surplus of the company. The balance overlooks a well-defined time interval, such as a day, a month, or a year.

Example 3.1 A household (H) works in industry (In) earning $Y_H = 100$ € per day and spending $C_H = 90$ € for food and goods. The daily surplus is $\Delta M_H = 10$ €.

We may summarize the balance of Example 3.1 by an equation,

$$Y_H - C_H = \Delta M_H \tag{23.3}$$

A positive balance (ΔM) is a surplus; a negative balance (ΔM) is a deficit.

23.3.1 The Monetary Balance as Excel Calculation

The excel sheet is the most popular tool for calculating a balance like in Example 3.1 (Fig. 23.2).

23.3.2 The Monetary Balance as a Spiral

The monetary balance may be repeated every day and is often considered as a cycle. But is this really a circle? If we put in numbers, we start at $Y_1 = 100$ € and get to costs $C_1 = 90$ €. This leaves a surplus $\Delta M_1 = 10$ € at the first day. At the next day, we continue with $Y_2 = 100$ € and get to costs $C_2 = 90$ € with a surplus $\Delta M_2 = 10$ €. This leaves a surplus of $\Delta M_2 + \Delta M_1 = 20$ € at the second day. The surplus leads to a higher level each day, after n days the total surplus will be $\Delta M_n = n \cdot 10$ €. The continuous monetary balance is a spiral! With positive surplus, the spiral will go up, with permanent deficit the spiral will go down, Fig. 23.3.

$Y_H =$	100	€
$C_H =$	-90	€
$\Delta M_H =$	10	€

Fig. 23.2 Excel calculation. Examples for similar calculations are shopping receipts store or bank accounts

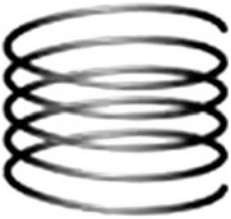

Fig. 23.3 A positive balance is a spiral that goes up and a negative balance is a spiral that goes down. ΔM is the lift after each round. The balance of Example 3.1 may be regarded as a spiral going up by 10 € every day

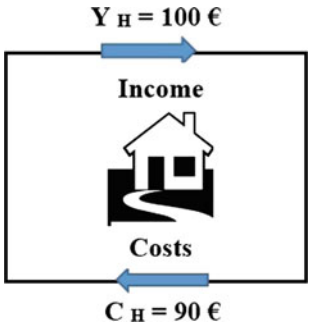

Fig. 23.4 The monetary circuit of households is a closed spiral, in this figure we are looking into the spiral. We may present the circuit in rectangular or circular shape

23.3.3 The Monetary Balance as a Closed Stokes Line Integral

In Chap. 3.1, we have discussed the monetary balance of households (Fig. 23.4).

We may interpret the monetary balance as a closed Stokes line integral:

$$\oint \delta M = Y_{\mathrm{H}} - C_{\mathrm{H}} = \Delta M_{\mathrm{H}}. \tag{23.4}$$

If the monetary Stokes integral is positive, the spiral goes up after each round by ΔM_{H}. If the monetary Stokes integral is negative, the spiral goes down after each round by ΔM_{H}. Equation (23.4) is equivalent to Eq. (23.3).

23.3.4 The Double-entry Balance

The double-entry balances consider the monetary and the productive circuits by adding both accounts: the sum is always zero. This equivalence of monetary and productive accounts is the origin of the word "balance" in accounting.

a. **The double-entry balance as an excel calculation**

The double-entry balance adds the monetary balance and the productive balance in monetary units by an excel sheet:

$Y_H = 100$ €	$W_H = -100$ €
$C_H = -90$ €	$G_H = 90$ €
$\Delta M_H = 10$ €	$\Delta P_H = -10$ €
Monetary account + productive account = 0	

In double-entry accounting, the monetary balance and the productive balance always add to zero. Households obtain income (Y_H) = 100 € by investing labor worth 100 €. They have costs (C_H) = −90 € receiving goods worth 90 €. Accordingly, the sums always add up to zero!

b. **The double-entry balance in circuits**

Figure 23.5 shows the sum of monetary (M) and productive (P) circuits of a household: the sum is zero. In this figure the household receives wages (+100 €) and gives away labor (−100 €), the household pays consumption costs of (−90 €) and obtain consumption goods for (90 €). Both circuits are nonzero and run into the opposite direction.

c. **The double-entry balance in spirals**

We may also interpret Fig. 23.5 as two spirals that wind in opposite directions. The monetary spiral winds upward and the productive spiral winds downward. The sum of both movements remains zero.

Courses on double-entry bookkeeping also include accounts for deficits and credits. This makes bookkeeping more complex and difficult to handle, but the basic idea remains the same: All corresponding double-entry accounts add to zero. This is the most important result of double-entry bookkeeping, and we will now try to translate this important result into economic equations.

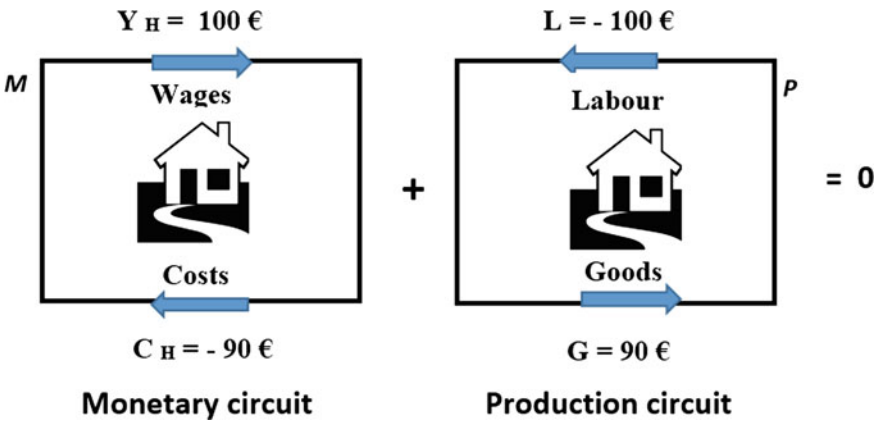

Fig. 23.5 The equivalence of monetary and productive circuits for a household. Both circuits run in opposite direction, the sum of both circuits is zero

d. **The double-entry balance as fundamental integral of economics**

We may also express the results of double-entry bookkeeping by Stokes integrals:

$$\oint \delta M + \oint \delta P = 0 \tag{23.5}$$

The sum of the monetary circuit (δM) and the production circuit (δP) is zero, but each Stokes integral is not equal to zero.

The closed Stokes line integral is the fundamental law of economics and represents the balance of every economic system.

23.4 The Laws of Economics in Integral Form

Equation (23.5) may be written as

$$\oint \delta M = -\oint \delta P \tag{23.6}$$

The monetary circuit measures the productive circuit. This is the fundamental law of economics in integral form based on double-entry accounting.

23.4.1 The Monetary Circuit

The monetary circuit is a closed Stokes integral:

$$\oint \delta M = \int_{\text{ln}}^{\text{H}} \delta M_1 + \int_{\text{H}}^{\text{ln}} \delta M_2 = Y_{\text{H}} - C_{\text{H}} = \Delta M_{\text{H}}. \tag{23.7}$$

If the monetary Stokes integral is positive, the spiral goes up after each round by ΔM_{H}. The term ΔM_{H} is the output of production of households. The value depends on the path of the integral, of the special way of production. If the monetary Stokes integral is negative, the spiral goes down after each round by ΔM_{H}. Equation (23.7) is equivalent to Eq. (23.1).

Income (Y_{H}) and costs (C_{H}) of households are part of a closed monetary circuit or integral:

Along path (1), industry (In) pays income (Y_{H}) to households (H),

$$Y_{\mathrm{H}} = \int_{\mathrm{ln}}^{\mathrm{H}} \delta M_1 \tag{23.8}$$

Along path (2), households (H) pay consumption costs (C_{H}) to industry (In),

$$C_{\mathrm{H}} = \int_{\mathrm{H}}^{\mathrm{ln}} -\delta M_2 \tag{23.9}$$

Output, income, and costs depend on the path of integration, on the way of production and cannot be calculated in advance. Output, income, and costs are always related to a certain system, to a household, a company, or an economy.

23.4.2 The Productive Circuit

The productive circuit—like the monetary balance in Eq. (23.7)—is again a closed Stokes integral. Labor and goods are Stokes line integrals of the same closed circuit.

$$\oint \delta P = \int_{\mathrm{ln}}^{\mathrm{H}} \delta P_1 + \int_{\mathrm{H}}^{\mathrm{ln}} \delta P_2 = L_{\mathrm{H}} - G_{\mathrm{H}} = \Delta P_{\mathrm{H}}. \tag{23.10}$$

Along path (1), industry (In) sends goods (G_{H}) to households (H),

$$G_{\mathrm{H}} = \int_{\mathrm{ln}}^{\mathrm{H}} \delta P_1. \tag{23.11}$$

Along path (2), households (H) invest labor (L_{H}) at work in industry (In),

$$L_{\mathrm{H}} = -\int_{\mathrm{H}}^{\mathrm{ln}} \delta P_2. \tag{23.12}$$

Output (ΔM_{H}), income (Y_{H}), cost (C_{H}), labor (L_{H}), and goods (G_{H}) are terms in neoclassical theory, but only calculus-based theory clarifies the ex post character of these economic terms.

23.5 The Laws of Economics in Differential Forms

In Sect. 23.4, we have found the fundamental law of economics of money-based societies in Eq. (23.6),

$$\oint \delta M = -\oint \delta P.$$

The monetary circuit measures the production circuits in monetary units. This integral law is also the basis for the laws of economics in differential forms.

23.5.1 The First Law of Economics

The first law of economics in differential forms is

$$\delta M = \mathrm{d}K - \delta P. \tag{23.13}$$

Integrating Eq. (23.13) by a closed integral leads back to the fundamental law, Eq. (23.6). The new term (dK) is an exact differential form, and the closed integral of (dK) will be zero. The first law of economics contains three differential forms with the common dimension *money*:

δM is inexact and refers to the *ex post* terms of income (δY), costs (δC), and surplus or profit.

δP is also inexact and refers to the *ex post* term of production, to goods (G), and to labor (W). Production is not just the number of laborers, but real physical work.

dK is exact and (K) a function. The meaning of (dK) is capital, the fields of the farmer, the company of the entrepreneur, the industries of an economy, and the earth of all beings. Capital of an economic system includes property, firms, houses, and money in cash. We will come back to this in a separate chapter.

The first law is the balance of every economic system: *Profits* (δM) *depend on capital* (dK) *and labor* (δP). This result is well known in economics, but so far, it has not been stated in a proper mathematical form by a differential equation.

The first law corresponds to the statement by Adam Smith in "Wealth of Nations" (I.6.11): "*It was not by gold or by silver, but by labour, that all the wealth of the world was originally purchased; and its value, to those who possess it, and who want to exchange it for some new productions, is precisely equal to the quantity of labour which it can enable them to purchase or command.*"

23.5.2 The Second Law of Economics

According to calculus a not exact differential form (δM) may be transformed into an exact differential form (dF) by an integrating factor λ,

$$\delta M = \lambda \mathrm{d}F. \tag{23.14}$$

We may call this the second law of economics. (δM) is inexact or *ex post*. For positive values, (δM) refers to production output, profits, or income (δY). At negative values, (δM) refers to losses or costs (δC).

For positive values, (δM) may be replaced by income (δY),

$$\delta Y = \lambda \mathrm{d}F. \tag{23.14a}$$

Equation (23.14a) replaces the erratic Solow equation $Y = F(K, N)$ in Eq. (23.1) due to the rules of calculus:

1. Complete or exact differential forms (dF) lead to a function (F) by a Riemann integral.
2. Incomplete or inexact differential forms (δY) do not have a stem function Y! The Stokes integral of not exact differentials (δY) is not a unique function, but depends on the path of integration. Income as an *ex post* term cannot be a function, it must be a not exact differential form: (δY)!

23.5.3 The Third Law of Economics

The second law replaces the inexact differential form (δM) by an exact differential form (dF) and an integrating factor (λ). In the same way, we may replace the inexact form of production (δP) by the exact differential (dV) and the integrating factor (p),

$$\delta P = -p\,\mathrm{d}V. \tag{23.15}$$

We have, presently, deducted Eq. (23.15) formally, but this needs further discussion of the new economic terms (p) and (V). People go to work in the fields or in industry. Why do they work? The answer: Everybody gets periodically hungry. Hunger is an inner pressure (p) to obtain food. This is true for all creatures. Even in modern times, where nobody needs to be hungry, there is a public pressure (p) for everybody to work.

The function (V) corresponds to space, to the area, that we need for living, for agriculture, for industries. Pressure (p) and space (V) are two possible production factors that we may apply to economics.

23.5.4 Economics and Thermodynamics

The differential laws of calculus-based economics have the same mathematical structure as the laws of thermodynamics:

$$\delta Q = \mathrm{d}E - \delta W. \tag{23.16}$$

In thermodynamics, heat (δQ) and work (δW) are not exact differential forms. The not exact differential of heat (δQ) may be linked to an exact differential form ($\mathrm{d}S$) by an integrating factor (T):

$$\delta Q = T\mathrm{d}S(E, W). \tag{23.17}$$

Also Eq. (23.15) corresponds to thermodynamics, where the not exact form of work (δW) is replaced by an exact form of volume ($\mathrm{d}V$) and an integrating factor of pressure (p):

$$\delta W = -p\mathrm{d}V. \tag{23.18}$$

But this is not only a formal coincidence but rather an identity:

1. In Eq. (23.10) labor is part of the closed cycle of production. In neoclassical economics, labor (L) is interpreted as the number (N) of laborers. But 10 people standing around in a field will stay hungry unless they go to work and pick the crops. Labor may be measured in energy units and is equivalent to physical work (W), $L = W$!
2. The oil price is an international standard to transform capital (K) into energy (E) and vice versa. We may conclude: $K = E$!
3. Income (δY) like capital is measured in monetary units. With the oil price, income may be turned into a quantity (δQ) measured in energy units, $\delta Y = \delta Q$.

Table 23.1 shows the corresponding functions in economics and thermodynamics:

Table 23.1 shows the corresponding functions of economics and thermodynamics resulting from the first and second laws. In addition, we may compare thermodynamic pressure to economic or social pressure, and volume of materials to space of economic systems.

23.5.5 Standard of Living as Economic Temperature

The integrating factor (λ) exists in all economic systems, in production, in markets, and finance. In interacting economic systems and efficient markets, we always find a common economic level (λ). A market will lead to a common price level (λ) for each commodity, and an economy will have a common mean standard of living (λ).

Table 23.1 Corresponding functions of economics and thermodynamics

Symbol	Economics	Unit		Symbol	Thermodynamics	Unit
Y	Income, costs	€, $, £. ¥	↔	Q	Heat	kWh
K	Capital	€, $, £. ¥	↔	E	Energy	kWh
L	Production, labor	€, $, £. ¥	↔	W	Work	kWh
λ	Mean capital	€, $, £. ¥	↔	T	Mean energy	kWh
F	Production function	–	↔	S	Entropy	–
N	Number	–	↔	N	Number	–
p	Pressure		↔	p	Pressure	
V	Space		↔	V	Volume	

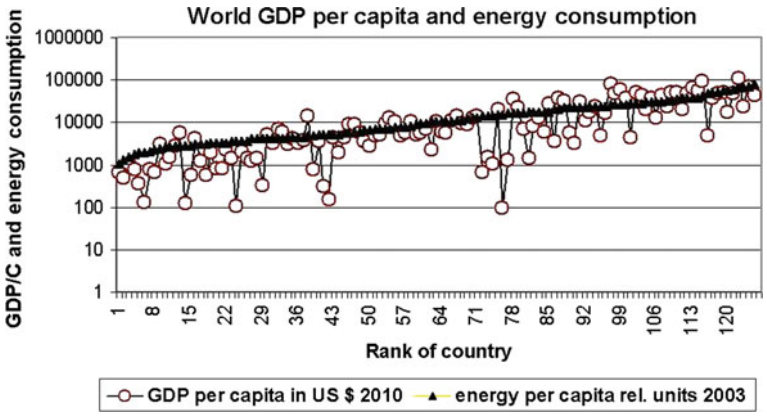

Fig. 23.6 GDP per capita and energy consumption per capita follow the same line for most of the 126 largest countries in the world. Both, mean capital and mean energy consumption are equivalent and may be regarded as economic temperature

The integrating factor λ is the mean capital and equivalent to temperature (T) as the mean energy, $T = \lambda$.

This equivalence of (T) and (λ) is shown in Fig. 23.6: GDP per capita and energy consumption per capita are equivalent for most of the 126 largest countries in the world. Both, mean capital and mean energy consumption follow the same line (Fig. 23.6).

The standard of living (λ) may be defined by the mean capital per capita

$$\lambda = K/cN. \tag{23.19}$$

It is proportional to the economic temperature or energy consumption per capita

$$T = E/cN. \tag{23.20}$$

The constant c may be called specific income and reflects the degrees of freedom to obtain income from work, stocks, etc. It corresponds to the specific heat or degrees of freedom in thermodynamics.

23.5.6 Capital

According to the first law capital, (dK) is the only monetary term that is represented by an exact differential form (dK) and exists "ex ante." Capital corresponds to energy in thermodynamics.

The difference between capital (*ex ante*) and income (*ex post*) is clear for a boy that goes out to work at a restaurant. He has five dollars in his pocket, which will be his capital tonight. But he does not know how much he will earn from tips at the restaurant. He will count his income afterward. For the boy, capital is the cash money in his pocket.

According to Eq. (23.13), capital is also equivalent to all goods that do not lose in value ($\delta M = 0$):

$$\delta M = \mathrm{d}K - \delta P = 0. \tag{23.21}$$

The capital of a farmer is given by the fields; they are the basis for production and profit. The capital of a company is the production plant, the machines, and investments. The capital of countries is resources such as water, air, land, and oil. But capital is also knowledge, technology, industry, cities, houses, universities, education, and infrastructure.

23.5.7 Entropy as the New Production Function

A most important result is the equivalence of production function (F) and entropy (S), $F = S$. Entropy is linking thermodynamics to statistical mechanics,

$$S = \ln P(N) \tag{23.22}$$

$P(N)$ is the probability of arrangement of the N elements (atoms) in the thermodynamic system.

In a system with (i) different elements (atoms), the entropy may be calculated from the relative number is $x_\mathrm{i} = N_\mathrm{i}/N$ of atoms,

$$S = N \Sigma x_\mathrm{i} \ln x_\mathrm{i}. \tag{23.23}$$

This is called the Shannon entropy.

Accordingly, the production function of an economic system of (i) different elements (goods, people, etc.) may be calculated from the relative number $x_i = N_i/N$ of people, goods, etc.

$$F = N \Sigma x_i \ln x_i. \tag{23.24}$$

The function is shown in Fig. 23.7.

Entropy replaces the Cobb Douglas production function of neoclassical economics

$$F = -N(x_i)^{\alpha}(x_j)^{\beta}. \tag{23.25}$$

Both functions are very similar, but according to Figs. 23.14 and 23.15, entropy is larger by a factor 1, 4. Entropy is the natural and optimal production function.

Indeed, entropy in Fig. 23.7 is the natural production function, which is always more optimal than the Cobb Douglas function in Fig. 23.8. In addition, there is no

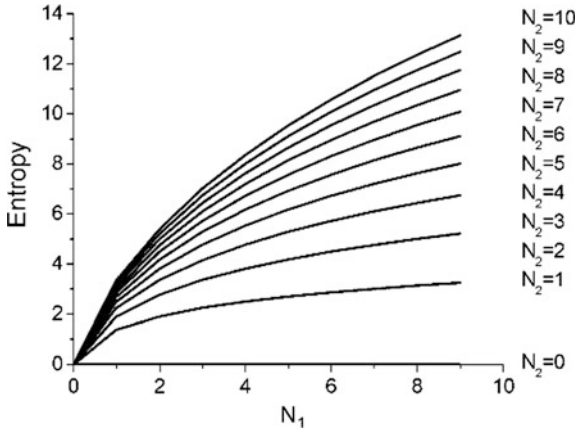

Fig. 23.7 The entropy production function $F(N_1, N_2)$ in Eq. (23.24) is plotted versus N_1 in the range from 0 to 10. The parameter N_2 is in the range from 0 to 10

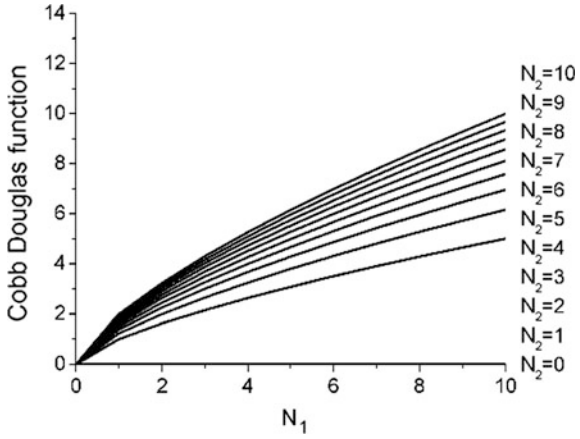

Fig. 23.8 The Cobb Douglas production function $F(N_2) = A\, N_1^{\alpha}\, N_2^{1-\alpha}$ in Eq. (23.25) is plotted versus N_1 in the range from 0 to 10. The parameter is N_2 in the range from 0 to 10. The parameters are $N = 1$ and $\alpha = 0, 7$

elasticity in calculus-based economics, which is used in standard economics to adjust to real data. Entropy needs no adjustment to data. In addition, entropy is the natural logarithm of probability P(N) and leads to microeconomics and to statistical economics.

23.5.8 Entropy and Work

The new production function entropy is a measure of disorder. This leads to a new understanding of entropy in thermodynamics and economics:

1. Thermodynamics: Combining the first and second law of thermodynamics, we obtain

$$T\,\mathrm{d}S = \mathrm{d}E - \delta W. \tag{23.26}$$

   A light breeze in a park with the energy (dE) will easily empty a paper basket and generate more and more disorder (T d$S > 0$). The paper will distribute throughout the park and never come back into the basket. Positive entropy means creating disorder or distributing items. But a janitor may work (δW) and sweep the paper together and put it back into the basket. Work reduces disorder: (T d$S < 0$). Negative entropy means reducing disorder or ordering, collecting items.
2. Economics: In the same way, we may combine the first and second laws of economics,

$$\lambda\,\mathrm{d}F = \mathrm{d}K - \delta P. \tag{23.27}$$

   The capital (dK) you pay for a snack will easily empty your purse and distribute (λd$F > 0$) the money to the shop keeper. The money will never come back into the purse. But in the afternoon, you may work (δP) in the office and the money will come back into your purse.

   We may solve Eq. (23.27) for (δP):

$$\delta P = \mathrm{d}K - \lambda\,\mathrm{d}F. \tag{23.28}$$

Labor (dP) increases capital (dK) and reduces disorder ($-\lambda$ dF). Work means ordering (Fig. 23.9).

Entropy reduction also applies to mental work: Mental work orders ideas like in a puzzle:

$$\text{Brain work: g} + \text{i} + \text{r} + \text{r} + \text{n} + \text{o} + \text{d} + \text{e} \rightarrow \text{ordering}$$

Fig. 23.9 Production of automobiles requires the ordering of many parts: screws, nuts and bolts, wires, tires, wheels, etc. All parts have to be placed in the correct position and in the right order, hence entropy $dF < 0$

Medical doctors order deficiencies within a body; teachers order or develop the minds of young people. Housewives have known for long times that making order is hard (unpaid) work! This may be one reason that today most women prefer to work as professionals outside of the house.

23.5.9 Production Costs

According to Eq. (23.28), production costs (δP) depend on capital or energy costs (dK), on the amount of ordering ($-dF$), and on the standard of living (λ) of the producing country. Many companies produce cars with the same energy costs and parts in the same order (dF) in Europe and China. However, wages are much lower in China than in Europe due to the lower standard of living (λ) in China.

23.6 The Mechanism of Capitalistic Production

In mathematics, the closed production circuit is a Stokes integral. In physics, this is called the Carnot cycle of motors. In economics, it is the mechanism of capitalistic production.

23.6.1 The Carnot Production Cycle of Capitalism

We now come back to the productive and monetary circuits in Sect. 23.3. The equivalence of productive and monetary circuits, Eq. (23.6), and the second law, Eq. (23.14), which replaces profits (δM) by ($\lambda\ dF$), lead to the fundamental equation of production and trade:

$$-\oint \delta P = \oint \delta M = \oint \lambda\, dF. \tag{23.29}$$

Productive and monetary circuits are now depending on the production factors (λ) and (F), and we can give the productive and monetary circuits proper coordinates:

The factor (λ) is the Y-axis and represents the value or price. The entropy (F) is the X-axis: (+dF) corresponds to distributing or selling products and (−dF) to collecting or buying products. The integrals of Eq. (23.29) are not exact and depend on the path of integration. Carnot proposed an ideal path of integration, which was first used to explain the steam engine: integration along (F) at constant (λ) and then integration along (λ) at constant (F). In this way, we obtain four different lines of the line integrals Eq. (23.29) in Fig. 23.10.

According to Carnot, the production process is divided into four sections:

1–2: Workers of a company collect or assemble (−dF) industrial goods at low price (λ_1);
2–3: Products are refined to create a higher value (dλ) or are transported (exported) to a region, where the products are more valuable (λ_2);
3–4: Products are distributed (+dF) and sold to customers at higher price (λ_2);
4–1: After longer time of use, the products will break and must be transported at lower value (λ_1) to centers of recycling. Without recycling, the process starts directly again at point (1).

The Carnot production process is a two-level mechanism at two price levels, λ_2 and λ_1.

Example 6.1 The production circuit of European import of clothes from Bangladesh

The details of the clothes production circuit are derived from the law of production, Eq. (23.28),

$$\delta P = c\,N\,\mathrm{d}\lambda - \lambda\,\mathrm{d}F \tag{23.30}$$

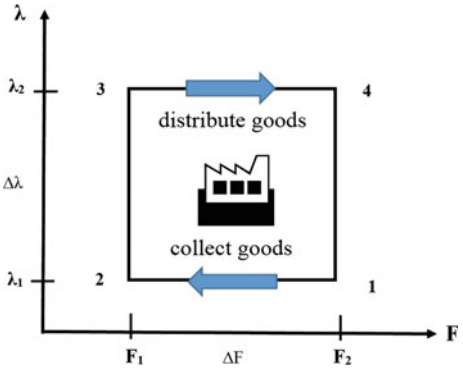

Fig. 23.10 The mechanism of capitalistic production is a Carnot production process: produce cheap and sell expensive! The Carnot production process is an ideal process originally used to explain a steam engine

1–2: A Bangladesh export company collects clothes ($-\mathrm{d}F$) produced by workers (seamstresses) at low costs (λ_1) and brought to the airport of Dhaka.

$$\delta P_1 = \lambda_1(-\mathrm{d}F) \tag{23.31}$$

(P_1) is the value of labor input and depends on the amount of seaming ($-\mathrm{d}F$) and of the very low standard of living of the workers (λ_1) in Bangladesh. This corresponds to an isothermal process in thermodynamics.

2–3: Clothes are flown to Frankfurt in Europe, where clothes have a higher value (λ_2):

$$\delta P_2 = c\,N\,\mathrm{d}\lambda \tag{23.32}$$

During transport or export by car, train, ship, or plane, the value (λ) of clothes rises, but the clothes stay together, the entropy (F) is constant. This is called an adiabatic process in thermodynamics.

3–4: Clothes are distributed and sold to customers in Europe at a higher price (λ_2),

Within one season, the price (λ_2) stays constant; this is again an *isothermal* process in thermodynamics.

$$\delta P_3 = \lambda_2 \mathrm{d}F \tag{23.33}$$

4–1: In time, the clothes become old fashioned or may break. They are transported to recycling centers. The value of the used clothes has declined ($\mathrm{d}\lambda$),

$$\delta P_4 = -c\,N\,\mathrm{d}\lambda \tag{23.34}$$

During transport, e.g., in a container, the products stay together, this means constant entropy (F), transport is again adiabatic. Without recycling, the last step may be omitted. The new Carnot cycle of capitalism starts again at point (1).

Example 6.2 The production cycle of automobiles in a factory

1–2: The workers of an automobile factory are collecting, ordering ($\mathrm{d}F < 0$), and putting together a large number of parts to construct the automobile at constant wages (λ_1).

2–3: The automobile company transports (exports/imports) the produced cars from the factory to the car dealer, where cars may be sold at a higher price (λ_2). During transport by truck, train, or ship, the cars stay together, the entropy (F_1) does not change.

3–4: The car dealer distributes or sells ($\mathrm{d}F > 0$) the cars to customers at a high price (λ_2).

4–1: After years of use, cars will break or rust and must be transported to a recycling center for a low price (λ_1).

Example 6.3 The production cycle of potatoes at a farm

1–2: On a farm, workers collect ($\mathrm{d}F < 0$) potatoes in the fields at constant low wage (λ_1).
2–3: The farmer transports (exports/imports) the collected cheap potatoes (λ_1) from the fields to the market, where potatoes may be sold at a higher price (λ_2). Since the collected potatoes stay in the basket during the transport, the entropy (F_1) does not change.
3–4: At the market, the farmer distributes or sells ($\mathrm{d}F > 0$) the potatoes to customers at a constant high price (λ_2).
4–1: As the next year (cycle) starts with new potatoes, recycling may be omitted.

23.6.2 The Monetary Cycle of Capitalism

The monetary circuit (δM) runs opposite to the production circuit (δP), Eq. (23.29)

$$-\oint \delta P = \oint \delta M = \oint \lambda \, \mathrm{d}F. \tag{23.35}$$

In the productive circuit in Fig. 23.10, goods, commodities, and manufactured products are collected from workers and distributed to customers. In the monetary circuit of Fig. 23.11, money is collected from customers and distributed to workers:

The monetary circuit is again divided into four sections:

4–3: A company outlet store collects ($-\mathrm{d}F$) money from customers for manufactured products. During one season, the high price (λ_2) of the products stays constant. This money is the income (Y) of the company.
3–2: The company outlet store sends money for manufactured products to the financial center of the company, and transporting the money in a safe is a process of constant entropy (F_1).

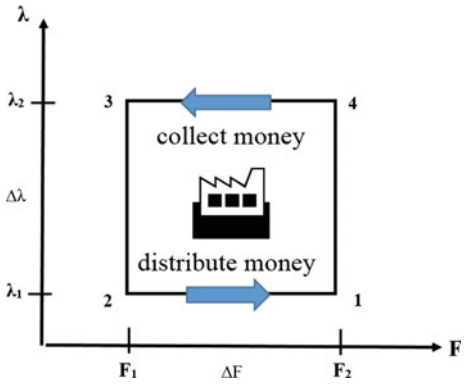

Fig. 23.11 The monetary circuit of capitalism in industry according to Carnot: Earn (collect) much and pay (distribute) little! The monetary circuit runs opposite to production

2–1: The low wages (λ_1), which are distributed (dF) to workers, are the labor costs (C) of the company.
1–4: The production company pays for materials to be recycled. Without recycling, the Carnot process starts again directly at point (1).
4-3-2-1-4: The area of the Carnot cycle, $Y_{\mathrm{Ind}} - C_{\mathrm{Ind}} = \Delta M_{\mathrm{Ind}}$ is the profit of the company,

$$\oint \delta M = \oint \lambda \, \mathrm{d}F = Y_{\mathrm{F}} - C_{\mathrm{F}} = (\lambda_2 - \lambda_1)\Delta F. \tag{23.36}$$

Again, the Carnot production process is a two-level mechanism at two price levels, λ_2 and λ_1.

Example 6.4 The monetary circuit of European import of clothes from Bangladesh

4–3: The importer of clothes collects money ($-\mathrm{d}F$) from European customers for Bangladesh clothes at constant high price (λ_2). This money is the income (Y_2) of the import company,

$$Y_2 = \lambda_2 \Delta F \tag{23.37}$$

Within the same season, the price level (λ_2) is constant, and this is called an isothermal process in thermodynamics.

3–2: Importers in Europe send money for clothes to the exporting company in Bangladesh; transporting (money) is again an adiabatic process, $\Delta F = 0$,

$$\Delta M_1 = \lambda \Delta F = 0. \tag{23.38}$$

2–1: Industry pays (dF) workers for their products a constant low price (λ_1). Labor costs of industry are the incomes of the workers.

$$C_2 = \lambda_2 \Delta F \tag{23.39}$$

1–4: Industry pays recycling centers for materials that may be recycled in the next production circuit.

$$\Delta M_2 = \lambda \, \Delta F = 0 \tag{23.40}$$

4-3-2-1-4: The area of the Carnot cycle, $Y_{\mathrm{Ind}} - C_{\mathrm{Ind}} = \Delta M_{\mathrm{Ind}}$, is the profit of the company.

Example 6.5 The monetary cycle on a potato farm

4–3: At the market, the potato farmer collects money ($\mathrm{d}F < 0$) a constant high price (λ_2) from the customers.

3–2: The farmer transports the collected money in his pocket at constant low entropy (F_1) from the market to the fields, and transport (export/import) is again an adiabatic process.
2–1: In the fields, the farmer distributes constant low wage (λ_1) to the workers.
1–4: The farmer pays for fertilizer.
4-3-2-1-4: The area of the Carnot cycle, $Y_{\mathrm{Ind}} - C_{\mathrm{Ind}} = \Delta M_{\mathrm{Ind}}$, is the profit of the farmer.

23.6.3 Production and Trade

Production and trade are closely linked together. In productive companies, the products are produced cheaply (λ_1) and sold at a higher price (λ_2). In trade-oriented companies, products are bought cheaply (λ_1) and sold more expensively (λ_2). Both follow the Carnot mechanism: money and goods have to be traded at two different price levels, λ_2 and λ_1!

At one levels (λ_1), the exchange of money and goods does not change the total capital of buyers or sellers, as demonstrated in double-entry bookkeeping. This may be expressed by the first law

$$\delta P + \delta M = \mathrm{d}K = 0 \tag{23.41}$$

The action of buying or selling is an *isocapital* process and corresponds to an *isothermal* process in thermodynamics. Nobody can get rich by a single exchange of money and goods, unless he cheats with false money or manipulated goods. A profit is only possible by a second exchange of money and goods at a new level (λ_2)!

Trade like production is a Carnot process, the exchange of money and goods at two different price levels, the simultaneous combination of a productive and a monetary circuit. The profit according to Eq. (23.29) is:

$$\oint \delta M = \oint \lambda \, \mathrm{d}F = Y_{\mathrm{F}} - C_{\mathrm{F}} = (\lambda_2 - \lambda_1)\Delta F. \tag{23.42}$$

The profit of trade and production is the difference between incomes (Y_{F}) and costs (C_{F}). Profit grows with the amount of ordering ΔF and the improvement of the value $\Delta\lambda$ of products. The difference in value ($\lambda_2 - \lambda_1$) may be obtained in many ways:

1. The product may be refined by the workers: Metals may be gilded or shaped into a new form, potatoes may be cooked in a restaurant, threads may be woven into a garment, etc.
2. Another way of raising the value of a product is exporting the product to a new location, where the product has a higher value.
3. A third way is waiting for a certain time period, until the product is more valuable.

23.6.4 Production and Trade Are Two-level Mechanism: λ_2 and λ_1

The production mechanism applies to all economic activities, to labor of households, to farmers, to production in industrial plants, to import of commodities from China, coal from South Africa, or the financial activities of a savings bank. In thermodynamics, the Carnot mechanism applies to heat engines such as motors, generators, heat pumps, or refrigerators.

Production always requires two separate constant levels λ_1 and λ_2 or classes, and vice versa; production always generates a two-class society: In companies, we have capital and labor; in markets, we have buyers and sellers; in societies, we find rich and poor; in the world economies, we have first- and third-world counties. In physics, a motor always requires two temperatures, hot and cold. The Carnot process in factories and in motors runs on the same fuel: oil.

23.6.5 Efficiency

The efficiency η of the Carnot process is proportional to

$$\eta \sim (\lambda_2 - \lambda_1). \tag{23.43}$$

The efficiency grows with the difference in levels of (λ). The higher the difference $(\lambda_2 - \lambda_1)$, the more efficient is the process. A cold motor does not run, only after a few cycles of heat production, the inside of the motor will become hotter and the efficiency rises, if the outside is cooled down by air or water. This efficiency applies to motors as well as to economies.

23.6.6 Scissor Effect

In most economies, we observe a growing difference between rich and poor. This is sometimes called the scissor effect, Fig. 23.12. This corresponds to thermodynamics: As soon as a refrigerator is turned on, the inside will get colder and the outside will get warmer. And as soon as a motor has started, the heat produced during a cycle is distributed to the inside and the motor will get hotter and more efficient.

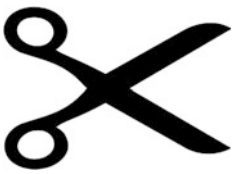

Fig. 23.12 The growing difference between rich and poor is due to the growing efficiency of the Carnot production process. This is often called the scissor effect. The mechanism corresponds to the growing temperature of a running motor or the falling temperature of an operating refrigerator

23.6.7 Efficiency and Socioeconomic Models

Efficiency is the basis of socioeconomic programs of political parties and states:

Capitalism: Capital favors a high efficiency, $\boldsymbol{\eta \rightarrow \max}$! This means: high prices and low wages, which leads to a strong economy, and according to the scissor effect to a rising gap between rich and poor. A good example in Europe is Germany. In order to avoid aggressions between high- and low-income classes, the government of a strong economy can level out differences in incomes by taxes and by support of unemployed and other problem groups.

Socialism (**Labor**): Labor favors a lower efficiency, $\boldsymbol{\eta \rightarrow \min}$! This means: low prices and high wages. This leads to a weaker economy and a slowdown of the scissor effect between rich and poor. A good example in Europe seems to be France. The lower-income classes still have a rather good standard of living, but the state cannot raise enough taxes to support problem groups.

Communism: Communism calls for a one-class society in which the capital is owned by the workers, the proletarians. In a one-class society ($\lambda_2 = \lambda_1 = \lambda_0$), the efficiency will be zero.

$\boldsymbol{\eta \rightarrow 0}$**!** This has been observed for all the communist states and has led to the downfall of all the communist regimes in Europe.

In order to make a refrigerator work, we have to close the door, inside and outside have to be separated. In the same way, rich and poor classes have to be separated to make the Carnot production process work.

23.6.8 Economic Growth of Countries

Capital growth of a country may be calculated from capital as a function of standard of living and the population:

$$K = c\,N\,\lambda \tag{23.44}$$

$$\mathrm{d}K = c\,N\,\mathrm{d}\lambda + \lambda\,c\,\mathrm{d}N \tag{23.45}$$

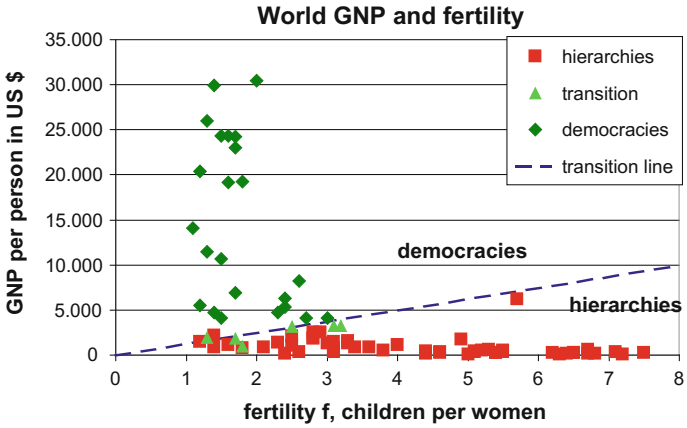

Fig. 23.13 GNP and fertility for the 90 biggest countries in the world

In every country, the growth of capital is given by a change in standard of living and a change in population. We will discuss four different cases:

(a) At constant capital, the standard of living will drop with rising population.
(b) At constant standard of living, the population will rise.
(c) At constant population, the standard of living will rise.
(d) A rising capital with rising population and rising standard of living is rarely observed.

Figure 23.13 demonstrates that people invest either in pension funds or in children. People in rich and democratic countries have a high standard of living and low fertility. People in poor and not democratic countries have a low standard of living and a high fertility.

This distribution may only be changed by reducing fertility in poor countries. In many countries like Egypt, economic growth being is eaten up by the growing population. Countries like India, especially in Kerala, have managed to reduce fertility drastically by building hospitals with controlled birth and by investing in the Internet for jobs in rural areas. Similar programs must be installed in all poor areas to raise local economic growth and reduce population growth.

23.7 Conclusion

Calculus-based economic theory leads to economic laws that are identical to those in thermodynamics. The new economic theory defines many terms of neoclassical economics in differential forms referring to economic properties such as “ex ante” and “ex post.” Experimental data on “GDP and energy consumption” support the

result that economic output depends on energy (E) and physical labor (W) rather than on capital (K) and the labor force (N).

The theory may be expanded further to economic growth, to microeconomics and finance using the new production function entropy as a gate to probability and statistics. This field is called econophysics and has been widely investigated in recent years.

Another field is the application of thermodynamics to social sciences. Countries with people of different national or religious background are heterogeneous many agent systems. They follow the same laws of integration or segregation, that have been found for alloys or other heterogeneous many particle systems. These results have been discussed elsewhere [12–16].

References

1. Mantegna RN, Stanley HE (2000) Introduction to econophysics. Correlations and complexity in finance. Cambridge University Press, Cambridge, USA
2. Mimkes J (2006) A thermodynamic formulation of economics. In: Chakrabarti BK, Chakraborti A, Chatterjee A (eds) Econophysics & sociophysics: trends & perspectives. Wiley-VCH Verlag, Weinheim, Germany
3. Aruka Y, Mimkes J (2006) An evolutionary theory of economic interaction—introduction to socio- and econo-physics. Evol Inst Econ Rev 2(2):145–160
4. Mimkes J (2006) Concepts of thermodynamics in economic growth. In: Namatame A, Kaizouji T, Aruka Y (eds) The complex networks in economic interactions. Lecture notes in economics and mathematical systems. Springer, Berlin, Heidelberg
5. Yakovenko VM, Rosser JB (2009) Colloquium: statistical mechanics of money, wealth and income. Rev Mod Phys 81:1703
6. Mimkes J (2010) Putty and clay—calculus and neoclassical theory. Dyn Socio-Econ Syst 2 (1):1–8
7. Mimkes J (2010) Stokes integral of economic growth: calculus and the Solow model. Phys A 389:1665–1676
8. Mimkes J (2012) Introduction to macro-econophysics and finance, continuum mechanics and thermodynamics. Springer 24(4–6):731–737
9. Richmond P, Mimkes J, Hutzler S (2013) Econophysics and physical economics. Oxford University Press
10. Cobb CW, Douglas PH (1928) A theory of production. Am Econ Rev 18(Mar 28 Supplement):139–165
11. Solow ARM (1956) Contribution to the theory of economic growth. Q J Econ 70:65–94
12. Mimkes J (1995) Binary alloys as a model for the multicultural society. J Thermal Anal 43:521
13. Mimkes J (2000) Society as many particle system. J Thermal Anal Calor 60:1055
14. Šesták J (2004) Thermodynamics and society—laws versus feelings. In: Chapter 18 in book "Heat, thermal analysis and society". Nucleus, Hradec Kralove, Czechia, pp 298–302. ISBN 8-86225-54-2
15. Šesták J (2005) Thermodynamics, econophysics and societal behavior. In: Chapter 8 in book "Science of heat and thermophysical studies: a generalized approach to thermal analysis. Elsevier, Amsterdam, Netherlands, pp 230–246. ISBN 444 51954 8
16. Mimkes J (2006) A thermodynamic formulation of social science. In: Chakrabarti BK, Chakraborti A, Chatterjee A (eds) Econophysics & sociophysics: trends & perspectives. Wiley-VCH Verlag, Weinheim, Germany

Chapter 24
On the Mathematical Structure of Physical Quantities

Jiří J. Mareš, Pavel Hubík and Václav Špička

The infinity is a square without corners (Chinese proverb).

Abstract The choice of the mathematical structure of physical quantities, which is natural for the description of finite physical reality and related problems, is discussed from the historical and the epistemological points of view. We show that for the establishment of physical quantities is fully sufficient the system of rational numbers which are equivalent to the finite ordered sets of integers, while the currently used system of real numbers is quite redundant for such a purpose. These facts may have far reaching consequences not only for pure epistemology but for the interpretation of many fundamental physical phenomena as well. Finally, the relation between the chosen structure of physical quantities and the so-called Principle of conformity of physics and mathematics is shortly discussed.

24.1 Introduction

Explanations concerning the mathematical structure of physical quantities form a separate discipline either of *dimensional analysis* [1, 2] or of *measurement theory* [3]; both of them are generally considered as well as established and more or less closed parts of physics and other sciences. However, making recently an attempt to define the phenomenological temperature utilizing Mach's concept of hotness manifold [4, 5], we have recognized that the requirement put on the physical quantities in the frame of standard measurement theory, namely that the ratio of a physical quantity and its unit is expressible just only by a *real number* is redundant and in fact hardly tenable. Therefore, keeping in mind that the critical inquiry into the well-established fundamental concepts and "truths" is extremely important subject of scientific research, in this contribution we discuss an alternative structure of physical quantities which can do without *continuum* and without system of *real numbers*, using only *rational* ones.

J.J. Mareš (✉) · P. Hubík · V. Špička
Institute of Physics, Czech Academy of Sciences,
Cukrovarnická 10, 16200 Praha 6, Czech Republic
e-mail: maresjj@fzu.cz

J. Šesták et al. (eds.), *Thermal Physics and Thermal Analysis*,
Hot Topics in Thermal Analysis and Calorimetry 11,
DOI 10.1007/978-3-319-45899-1_24

This chapter is organized as follows: Prior to the derivation of possible consequences of our hypothesis for epistemology and physical theory, it is useful to introduce relevant concepts and shortly review a few diverse items related in some way to our very complex subject. These items are discussed in following sections called arithmetization of geometry, physical conception of measurement and quantity, measurement error, measurement theory and representation of real numbers. These sections are followed by the key section on a certain epistemological consequence formulated as the central theorem on redundancy of real numbers in physics. It provides a basis for the following section in which we discuss a lesser known Principle of conformity of physics and mathematics together with some of its consequences.

24.2 Arithmetization of Geometry

Practically every ancient culture contributed to the mathematical knowledge of mankind by creating elementary concepts of number, geometrical figure and by establishing the relationship between these two entities. For the development of mathematics in Europe of special significance was the school of Pythagoras (sixth-century BCE) which transmitted the mathematical knowledge of Egypt and Babylonia into this region [6]. Besides, Pythagoreans achieved also outstanding original results in number theory and geometry, discovering. e.g. incommensurability of certain segments ([7], see later). Undoubtedly, the first exact measurements were the measurements of lengths, belonging to the scope of geometry. No wonder that the first formally satisfying scientific introduction of "quantities" belongs to the geometry too. This is due to Greek astronomer Eudoxus of Knidos (fourth-century BCE) who established theory of proportions remarkable till present. Axiomatic exposition of his theory as is given in Euclid's *Elementa* ([8] book V) carefully translated by N. Tartaglia (sixteenth-century CE) into Italian initiated deep changes in the interpretation of geometry. This allowed also rigorous treatment of other continuous quantities and became the basis for quantitative work in science until the calculus with non-numerical ratios was step by step replaced by the method of Descartes, i.e. computing with segments according to algebraic rules. Such an arithmetization of geometry from our modern point of view almost trivial was in fact quite a difficult task. It should be stressed here, namely that for Euclid and Middle Age scholars, the numbers were collections of units, i.e. integers, differing by nature from geometrical segments. For ancient Greeks, there were also no fractions in our sense. Parts of a unit were treated in terms of units of lower order (introduced through corresponding Egyptian unit fractions), preserving thus a character of integers. That is also why the contents of Euclid's book V and of arithmetic book VII, being the same for us, represented for the author apparently quite different subjects [9]. It was therefore only Legendre [10] in the eighteenth century who started to deal with segments and numbers as with the identical entities. Further research has shown, however, that Legendre's pragmatic approach

was too simplifying. One can easily show that a number can be assigned to each segment, while the converse theorem that each number corresponds to a segment has to be viewed as an axiom, or as equivalent to the assumption of continuity of the line. In order to clarify these questions with sufficient rigour, a big effort of excellent mathematicians, such as Bolzano [11], Dedekind [12], and others (see e.g. [13]), was necessary. The result of their struggle for the identification of straight line with a set of real numbers was, according to the analysis due to P. du Bois-Reymond, somewhat ambiguous. As he has shown, the problem can be approached from two points of view that are drastically opposed to one another: the *idealistic* and the *empiric* one [14]. Idealists believe in the reality of extensions of the concepts that go beyond the imagination but are necessitated by our thought process. They thus assume real existence of ideal objects such as point, line, and number continuum and of actual infinity (*aphorismenon*) as well. Empiricists stop at the fact that the unit segment contains unlimitedly many points (*apeiron* of things) giving up the possibility to distinguish dense and continuum sets by means of an experiment. Unfortunately, it is impossible to decide between idealistic and empiric points of view on the ground of pure logic. Nevertheless, there is a valuable side-product of P. du Bois-Reymond's analysis, namely the observation that the discovery of irrational numbers is a direct consequence of arithmetization of geometry. Quite a natural continuation of this arithmetization process is, in a certain sense, G. Cantor's set theory [15, 16], canonizing actual infinity and continuum. It has opened the doors to the abstract mathematical paradise from which "no one shall ever evict us" [17]. Using P. du Bois-Reymond's classification, modern mathematics represents an idealistic attitude having far reaching consequences. Indeed, for Euclid the axiom was a statement specifying as well as possible fundamental properties of a real object, while for modern mathematician, believer in Cantor's credo "*Das Wesen der Mathematik liegt gerade in ihrer Freiheit*" ("The essence of mathematics is just in its freedom"), the content of an axiom can be arbitrary if only it is not in contradiction with other axioms of a particular system. Let us mention an example of our concern: Fraenkel-Zermelo's Axiom VII postulates the existence of a specially constructed set which is per definition an actually infinite set [16]. Based just on this axiom, the infinite chain of transfinite sets can be constructed. Without assuming the validity of this axiom, however, there would be in mathematics no actually infinite set at all. Particularly, there would not be the set of real numbers or any continuum. Taking thus into account such a trend, we have to ask how strong the link between present mathematics and reality is. In this connection, the sceptic words of C. F. Gauss should be mentioned giving his opinion about the objectivity of human mathematical constructs [18]: "*...we have to concede with humility, that, since the number is just the product of our spirit, the space has extra our spirit also a reality, to which we cannot a priori prescribe completely its laws*". In this connection, also Kronecker's opposition to the mathematics exploiting actual infinity should be mentioned [19]. His program (precursor of *intuitionism*) based on the "innate" act of enumeration, i.e. counting of natural numbers, was in strict contradiction with the "inhuman" introduction of various kinds of numbers in the frame of set theory. Besides, he pointed out the fact that

many fundamental constants of geometry have astonishingly simple arithmetical structure as Leibnitz series [20]:

$$\pi/4 = 1 - 1/3 + 1/5 - 1/7 + \cdots \tag{24.1}$$

It further supported his conviction that the whole body of mathematics can be reduced to the arithmetic of integer numbers and their properties.

24.3 Physical Conception of Measurement and Quantity

There is no perfect consensus as concerns the meaning of the terms *physical measurement* and *physical quantity*; therefore, we have to specify what will be understood under these terms in this paper. As we are reluctant to the strong belief of psychologists that whatever exists at all exists in some amount and whatever exists in some amount can be measured, we admit more "conservative" physical conception of measurement as is discussed in a fundamental work by N. Campbell [21]. Accordingly:

(i) Measurement is an assignment of numbers to entities and events according to certain rules to represent their properties and relations. Results of measurement are called quantities.

In order to perform measurement, an *operational definition* of measurement [22], i.e. description of measuring instrument, measuring procedure and rules enabling comparison of physical properties belonging to different systems or to the same system treated differently, is necessary. The rules for assigning the numbers to entities are in compact form, represented by the so-called *scales of measurement*. There are essentially four types of such scales which can be classified according to their invariance with respect to various mathematical operations [23]. One can thus distinguish *nominal*, *order*, *interval* and *ratio scales* which are invariant to permutation, order-preserving, linear and similarity group of transformations, respectively. In physics, in contrast to psychology, we are satisfied only with the most perfect type of scale, ratio scale, which provides the basis for the introduction of corresponding physical quantity. If then, exists for two physical properties of the same kind A and B an operational definition of the ratio $A/B = q$, and the properties are called *physical quantities* [2]. Taking thus, say, property B for a standard, we can perform an (extensive) measurement via an operation called *concatenation*. Concatenation operation means the counting how many times must be a physical realization of a unit B, having the sense of French word *étalon* (possibly its convenient fraction or multiple), linked together with a measured object in order to achieve the same extent. The physical realization of a unit, etalon, has its individual name, $[Q]$, which should be attached to the result of every concatenation operation. The quantities capable of sustaining concatenation are called *extensive quantities*. They include mass, time, electrical resistance, and plane angle, which are known in

metrology as *base quantities.* Other quantities for which the realization of concatenation operation is not possible (it is not that these quantities are not quantifiable!) are called *intensive quantities*. Such quantities are in fact conventional combinations of two or more extensive quantities. Although there are devices enabling direct measurement of intensive quantities (e.g. manometer measuring pressure), the extensive quantities virtually involved can be, if necessary, re-extracted. From this point of view, the intensive quantities should be considered as derived or indirectly measurable quantities. This important property is widely used by constructing energy terms from couples of extensive and intensive quantity, where the latter one implicitly involves the former one. As examples may serve volume–pressure, charge–electric potential, momentum–velocity and many others couples. The operation of concatenation being the basis of practical measurements has been, quite naturally, reflected in axiomatic systems of geometry [24] and measurement theory [25], too. Relevant axiom, the axiom of Archimedes has, however, many different forms and interpretations. For example, it can express the absence of infinite or infinitesimal elements in a given set, or be a precursor of continuity. Nevertheless, for our "conservative" interpretation of a physical quantity, the most illustrative is the following formulation where the quantities are represented, for the sake of simplicity, by segments:

(ii) Axiom of Archimedes: If the smaller one of the two given segments is marked off a sufficient number of times, it will always produce a segment larger than the larger one of the original two segments.

Accordingly, the Archimedean property of a measured system ensures the existence of its upper bound expressed as a product of a unit (corresponding to smaller segment) and number of steps of concatenation procedure. Making thus unit smaller and simultaneously increasing the number of steps, the lowest upper bound of the system can be approached as exactly as we please. Since the unit is for particular concatenation a constant, the measuring procedure itself is *linear*. Such a property, assumed for quantities encountered in physics, enables one to treat quite generally a quantity measured in ratio scale as a product of number and unit. Formally expressed, a result of any scientific measurement may be thus written as:

$$Q = q \times [Q], \tag{24.2}$$

where Q is the magnitude of the quantity, q is the real number and $[Q]$ is the unit magnitude of the same kind. Physical laws can then be expressed as numerical relations between measured quantities. Putting in (24.2) $q = 1$ systematically, we can combine instead of different quantities only the "names" of units obtaining in this way "algebra of units" (A. Lodge [26]), which provides the basis of *dimensional analysis* [1].

Interestingly, the classical definition of physical quantity due to J. C. Maxwell [27] serving for generations as a standard contains practically all attributes of this concept as specified above, having only somewhat different reading. ("*Every expression of a Quantity consists of two factors or components. One of these is the*

name of a certain known quantity of the same kind as the quantity to be expressed, which is taken as a standard of reference. The other component is the number of times the standard is to be taken in order to make up the required quantity. The standard quantity is technically called the Unit, and the number is called the Numerical Value of the quantity".) In modern textbooks, there are lots of definitions dealing with physical quantities but they are hardly much better. The definition of physical quantity is extremely difficult because of the strong demand for generality. In addition, the definitions involve seemingly lot of elements of arbitrariness since various authors put emphasis on different aspects. In spite of that, we cannot fully agree with A. Einstein who claims [28] that all physical quantities are freely invented abstractions, in some cases not quite close to the experience. Taking into account, namely the fact that the physical quantity has a meaning only in terms of the instrument to measure it [22], just the physical realization of the particular instrument, which inevitably follows the laws of Nature, objectifies also the corresponding quantity.

24.4 Measurement Error

The most important proposition being imparted during school laboratory practice is that any measured physical quantity has some unavoidable intrinsic fuzziness. The students are instructed that no physical measurement can be made with absolute accuracy or precision, and the evaluation of experimental error is a compulsory part of their laboratory reports. However, even from the fairly naive application of the principle of causality [29] we can learn us just the opposite. Indeed, how do we actually know that any of our measurements are in error? Being honest, we do not! In fact, there is no a priori reason to suppose that our measurements are in error at all, simply because every obtained result is a resultant of all natural forces involved. The repetition of any measurement performed in a different time thus provides different reading not because the measurement has "intrinsic error", but quite causally, because it was made at different time under slightly changed conditions. It is then thinkable that by careful step-by-step elimination of all apparent and hidden influences which change experimental conditions, we will achieve a perfect reproducibility of our measurement. Notice that this is also exactly the way how the precision of measurements is increased in common metrological practice. From this point of view, the terms such as "measurement error, approximation, fuzziness, and accuracy of the method" are only the alternative names for our limited ability to identify all physical processes taking part in our experiments or of constructing a satisfactory theory. Such an essentially subjective nature of experimental fuzziness is the reason why the classical measurement theory deals with measurement errors only marginally [30] and considers in fact only "true values" of physical quantities.

However, in spite of this almost agnostic criticism, the concept of experimental error apparently does exist and plays an important role in many practical considerations. Fortunately, the engineers designing aircrafts and bridges would not likely

agree with our scepticism above, denying the existence of experimental error at all. After all the stochastic properties of physical observations are known already from the time of Galileo! What is then the nature and cause of this remarkable phenomenon?

The central assumption of the theory of measurement error is the existence of *true value* of measured quantity to which the results of actual measurement are related. *Observational (measurement) error* of a particular experimental reading is then defined as a deviation between measured and corresponding true values. Making thus at intently unchanged conditions the measurements repeatedly one obtain, as a rule, a set of inconsistent readings, which can be interpreted as the values of given quantity influenced just by the observational error. However, the quantification of such an error is impossible without making additional assumptions concerning the true value. In classical case, represented by the founders of theory of errors, P. S. Laplace, A. M. Legendre and C. F. Gauss [31], and which was inspired mainly by measurements performed in astronomy and geodesy, it is assumed that the true value of measured quantity is not experimentally accessible in principle. Simultaneously, it is believed that for sufficiently large collection of measured values, the true value is approximated, under some conditions, by arithmetic mean of measured values. On the basis of such a hypothesis can be the observational error evaluated and the sources of error classified. The two components of observational error are usually identified, namely the *random error* (error of inconsistency) which is caused by inherently unpredictable fluctuations in readings and the *systematic error* (error of method), a typically constant error shifting the values in one direction which is due to the imperfections of method of observation. While the random error cannot be eliminated but only reduced by making more measurements, the systematic error, in case where the source of error is identified, can often be eliminated. For the consequent treatment of these facts, an important question should be solved, namely how can the error be measured? Notice, measuring of error is not directly analogous to measuring of extensive quantities because there is no definite set of errors apt for concatenation operation. The characteristics of error thus rather reflect the distribution or frequency of occurrence of deviations. In conformity with the splitting of error into random and systematic, two characteristics of observational error are of general use, namely the *precision* and the *accuracy* of measurement. The precision of measurement related to the random error, sometimes also called *reproducibility*, is the degree to which repeated measurements under unchanged conditions yield the same results. Under the term accuracy, characterizing the systematic error of method is meant the proximity of measurement results to the true value. Classical methods of determination of these characteristics are based on quite general assumptions, partially belonging to the theory of probability [32] and having the nature of axioms. For example, according to the well-known least square hypothesis, arithmetical mean of several observations provides the most probable estimate of the true value [33]; the hypothesis that the error arises from the joint operation of a large number of independent sources of error then implies that grave errors must be less frequent than minor ones, etc. Such qualitative conclusions are involved in various quantitative "*laws of error*" or

distributions of errors the most appreciated of which is the famous Gauss's law $\varphi(x)$:

$$\varphi(x) = (h/\sqrt{\pi}) \exp[-h^2(x-a)^2], \tag{24.3}$$

where x is the measured quantity, h is the parameter controlling its distribution and a is the mean ("true") value of x; $\varphi(x)$ has then the meaning of the relative number of readings within an interval $(x, x + \mathrm{d}x)$. Assuming the validity of a particular law of errors, the precision of the measurement represented by an ensemble of observed values $x_1, x_2, \ldots, x_N$ can be evaluated.

In contrast to such a classical approach, we can imagine that we were able to remove, by improving of our methods of observation, all systematic errors. Since the observed random errors are in fact unidentified systematic errors [21], any of our ultimately improved measurements will provide an exact true value of the physical quantity we are interesting in. The measurement where the true values are observed, however, can by identified with the concept called in the literature the *quantum measurement* [34]. As can be easily recognized, such a quantum measurement has also some features already awarded to the errorless measurement in the introductory part of this section.

24.5 Measurement Theory

What is now considered to be a modern *measurement theory* has only a little to do with the theory of making physical measurement. It is rather a branch of applied mathematics concerning with the problem how to specify the homeomorphism of some empirical structure into a numerical one. Nevertheless, it deals also with general properties of quantities and as such must be a subject of our interest. Axiomatic form of measurement theory begins practically with Hölder's "*Die Axiome der Quantität und die Lehre vom Mass*" [25] in which the axioms for extensive quantities were concisely formulated. Dedekind axiomatized the classical concept of quantity in such a way that ratios of magnitudes could be expressed as *positive real numbers*. This conclusion was a direct consequence of his concept of continuity [12] as an essential feature of the scientific concept of quantity. Very similar opinion is found by other researchers working in this subject—Helmholtz [35], Frege and Russell [36]. Contemporary theory of measurement is dominated by so-called *representational theory* (Krantz, Luce, Suppes and Tversky [37]), which extends and generalizes the approach just mentioned. Accordingly, the very task of measurement theory is how a given empirical structure is represented in some numerical structures. Less formal is the program of *conventionalists*, which also sounds more "physically" [3]. They mean that our job is to investigate rather the physical reality of the world in which we live then our abstractions. They thus put emphasis on careful observations, clear definitions, correct use of language and logic and on tracing of sharp borderline between physics and metaphysics. For them

is of primary importance finding out the extent to which the choices made in adopting physical conventions are constrained by empirical facts, theories, considerations of convenience, formal simplicity and so on, and to what extent their adoption appears to be arbitrary. Quite an opposite attitude brought in the measurement theory is the epistemological *holism*. Its founder, W. Quine, proposed [38] that it is the whole field of science and not a single statement that to be verified. Since all scientific statements are interconnected, the talking about the empirical content of a single statement is misleading. Moreover, any statement can be held as true, if only the right changes are made somewhere else in the system. Particularly, the results of a single measurement are of no value if not simultaneously considered together with all other possible measurements made in the universe. The holistic attitude is, of course, absolutely true but due to its generality mostly useless. For example, although we have to concede holistic point of view that scientific problems concerning psychological effects of the battle of Hastings and surface tension of fresh water at 20 °C are interconnected, we are inclined to study them separately.

In spite of the dramatic diversity in philosophical attitudes to the measurement theory just showed, different classical as well as modern theories of measurements requires univocally continuity as an intrinsic feature of the scientific concept of quantity. As we are convinced, however, such a requirement of continuity of physical quantities entered into the physics and other sciences not as a discerned necessity but only historically being derived from the geometry where the continuity was an intuitive concept. It is thus the very matter of fact that at present quantitativeness per se is closely connected with the mappings into the sets of real numbers ($\in\mathbf{R}$).

24.6 Representation of Real Numbers

Putting aside for a moment philosophical and physical aspects of our subject, we ought to recall some relevant facts concerning the set of real numbers ($\in\mathbf{R}$) and its representations. Common representations of real numbers perform *positional numeral systems* constructed for different bases g. For example, the decimal system ($g = 10$) quite familiar in elementary arithmetic is very convenient for making current computations, while the binary system ($g = 2$) fits better to computers or to theoretical considerations. In spite of the verbal contradiction involved, all positional numeral systems are usually called decimal systems. Under the well-specified conditions, these systems provide unambiguous representations of real numbers. For example, for base $g = 10$ the following theorem is valid [39].

Any positive number $x \in \mathbf{R}$ may be expressed as a decimal $A_1A_2 \ldots A_{S+1} \,.\, a_1a_2a_3 \ldots$, where $0 \leq A_1 < 10, 0 \leq A_2 < 10, \ldots, 0 \leq a_n < 10$ are integers, not all A's and a's are 0, and an infinity of the a's is less than 9; S is a non-negative integer. If

$x \geq 1$, then $A_1 > 0$. Under these conditions, there is a one-to-one correspondence between the numbers and the decimals, and

$$x = A_1.10^S + A_2.10^{S-1} + \ldots + A_{S+1}.10^0 + a_1/10 + a_2/10^2 + \ldots . \tag{24.4}$$

Of course, the extension of the theorem to the range ≤ 0 is trivial.

The representation (24.4) of real numbers with respect to their arithmetic nature reveals a remarkable *trichotomy* in expansions after the separating (decimal) point. In the case where the expansion is *finite (terminating)*, x is a rational number, which is equivalent to the fraction where g^K divides denominator, in which K is a certain natural number. If the corresponding expansion is *infinite and recurring*, the number x is again a rational number [40]. The last possibility where the expansion is *infinite and non-recurring* corresponds to irrational numbers. However, this trichotomy has only a relative validity. For example, the fact that a given number belongs to the first or the second class may depend on the particular choice of the base g. Indeed, the form of decimal expansions of one-third recorded in bases $g = 10$ and $g = 3$ differ essentially:

$$1/3 = (0.3333\ldots)_{10} = (0.1)_3. \tag{24.5}$$

Moreover, regardless of base g, every terminating decimal expansion can be, if we want, rewritten as an infinite periodic decimal too. It can be illustrated using a previous example where we immediately obtain for number 1.0 two alternative records

$$(1.0)_{10} = 3 \times 1/3 = 3 \times (0.3333\ldots)_{10} = (0.9999\ldots)_{10}, \tag{24.6}$$

one terminating and another one infinite periodic. The facts just discussed may be more rigorously formulated as the following theorem [41]:

(iii) Any real number can be unambiguously represented by infinite decimal expansion, and two expansions are equal only if they are identical digit by digit.

This theorem, unifying format of records of all real numbers, makes it simultaneously impossible, by means of finite number of operations to establish whether a given number is rational or irrational. And this is also one of the reasons why the positional numeral expansions are not quite suitable for deeper studies into the arithmetic nature of real numbers. Fortunately, there is an alternative method how to record and study real numbers more effectively, namely the method of continued fractions.

Continued fractions, which clearly reveal the arithmetic and metric nature of numbers and provide much insight into many mathematical problems are, however, rather inconvenient for performing the mathematical operations. This is likely the reason why the continued fractions are not widely used in common praxis. Let us

here therefore recall the notation and basic properties of this beautiful mathematical tool in more detail. An expression of the form

$$x = a_0 + \cfrac{1}{a_1 + \cfrac{1}{a_2 + \cfrac{1}{a_3 + \cdots}}}, \tag{24.7}$$

where a_0, a_1, …, a_{n-1}, a_n, … are integer quotients ($a_i > 0$ for $i > 0$) is called a *simple continued fraction* or sometimes shortly a continued fraction [42]. Nevertheless, the illustrative way (24.7) of writing continued fractions (*scriptio plena*), being the nightmare of typographers, is for larger expansions not very convenient and comfortable. Instead, as a rule, the more condensed notation (*scriptio defectiva*) is used, namely

$$x = [a_0; a_1, \ldots, a_{n-1}, a_n, \ldots], \tag{24.8}$$

where the integer part a_0 of the number x is from the rest of the quotients separated with a semicolon. It can be proved [43] that the expressions (24.8) are the most effective and unambiguous representations of real numbers $x \in \mathbf{R}$. The effectiveness of this representation is, roughly speaking, due to the fact that by expanding a given number x into the continued fraction, we are computing, in contrast to the decimal systems, in every step of approximation a new g basis fitting best to the particular number. Moreover, the representation of real numbers by continued fractions reveals remarkable *dichotomy* in expansions, which can be expressed by following important theorem [44].

(iv) The continued fraction expression of a real number $x \in \mathbf{R}$ is finite if and only if the real number is rational (i.e. $x \in \mathbf{Q}$). If a real number $x \in \mathbf{R}$ is irrational, then its continued fraction expression is infinite.

The expansions of real numbers into the continued fractions are unique with the following proviso. It is known [45] that for any rational number $x = p/q$, the quotients in corresponding expansion into continued fraction (24.7) are in fact partial remainders in Euclidean algorithm for the "highest common divisor" $D(p, q)$ and as such they inevitably yield exactly one sequence. However, the last term of this sequence $a_n > 1$ can be obviously substituted by an equivalent couple of terms $(a_n - 1) + 1/1$, so that

$$x = [a_0; a_1, \ldots, a_{n-1}, a_n] = [a_0; a_1, \ldots, a_{n-1}, a_n - 1, 1]. \tag{24.9}$$

This property may be also formulated as follows [44]:

(v) Any rational number $x \in \mathbf{Q}$ can be expressed as a finite continued fraction in which the last term can be modified so as to make the number of terms in the expansion either even or odd.

The uniqueness of representations of rational numbers by continued fractions (finite expansions) can thus be ensured by means of a simple convention, while the

uniqueness of representations of irrational numbers (infinite expansions) is, due to the absence of the last quotient, guaranteed automatically.

An obligatory part of doctrine of continued fractions is their conversion into common or decimal fractions and vice versa. For this purpose are used recurrent relations for evaluation of so-called *convergents*, i.e. fractions in lowest terms approximating a given real number x. The numerators p_k and the denominators q_k of the k-th convergent ($k = 1, 2, 3, \ldots n, \ldots$) of the continued fraction $[a_0; a_1, \ldots, a_{n-1}, a_n, \ldots] = x$ satisfy the relations

$$\begin{aligned} p_k &= a_k p_{k-1} + p_{k-2} \\ q_k &= a_k q_{k-1} + q_{k-2} \end{aligned} \tag{24.10}$$

with initial values

$$\begin{aligned} p_{-1} &= 1, \quad p_0 = a_0 \\ q_{-1} &= 0, \quad q_0 = 1. \end{aligned}$$

The series of convergents is remarkable in itself. For example, for numerator p_k and denominator q_k of a convergent = p_k/q_k, for all $k \geq 0$, the following relation is valid:

$$(p_{k-1}q_k - p_k q_{k-1}) = (-1)^{k+1}. \tag{24.11}$$

This equation among others enables one to determine the difference between following convergents as

$$(p_{k-1}/q_{k-1} - p_k/q_k) = (-1)^k/(q_{k-1}q_k). \tag{24.12}$$

Accordingly, the series of convergents oscillates in such a way that the series of even convergents is decreasing while that of odd convergents is monotonically increasing. *Precision of approximation* of real number x by the k-th convergent is then given by a formula

$$|x - (p_k/q_k)| \leq 1/(q_k q_{k+1}). \tag{24.13}$$

Approximating the number x by a fixed k-th convergent, we can formally write

$$x = [a_0; a_1, a_2, \ldots, a_k, \ldots, a_n] = [a_0; a_1, a_2, \ldots, r_k], \tag{24.14}$$

where the rational number r_k represented by a continued fraction

$$r_k = [a_k, a_{k+1}, \ldots, a_n] \tag{24.15}$$

is called *k-th remainder* of x [42]. Remainder r_k reflects arithmetical structure of the "tail" of x, serving as a magnifying glass for details smaller then that given by the

estimate (24.13). Inquiry into the remainders of continued fraction is thus very effective for recognition of arithmetical nature of number as a whole.

24.7 An Epistemological Consequence—Physical Quantities Are Rational

Confronting the above real number representations with our ability to realize the corresponding record, it is quite clear that writing down or reading an infinite expansion of irrational number is for any human being or any finite human-made contrivance, which are confined in both time and space, impossible in principle. On the same grounds, it can be concluded that the results of physical measurements performed in a finite time cannot be represented by irrational numbers. We can even claim that all the results of physical measurements ever made till now and also of those which will be made in the future are represented just only by rational numbers. Reflecting these facts, we can complete our definition of measurement and of quantity (i) by the following theorem (formulated for scalars only):

(vi) Any value of physical quantity is expressed by a rational number $\in \mathbf{Q}$, which can be rewritten as the finite ordered set of integers.

From our analysis above, it is apparent that the concept of infinity is in some way entangled in contemporary physical considerations. We have to ask then, how the (actual) infinity entered physics and which role infinity plays there. From the previous paragraphs, it is clear that the primary source of acceptance of infinity in physics was a geometrical model of a straight line, precursor of continuum. Furthermore, the isomorphism between the straight line and a physical quantity is traditionally considered to be self-evident. But it should be stressed here that the continuity of a straight line is a result of axioms of geometry (i.e. of a certain thinking process inspired by observation) and not the result of experimental observation itself. To this point, let us mention the fact that it is impossible to distinguish by experiment whether the straight line is continuous or dense, while in common speech these two concepts merge together. According to naive argumentation, if we insert in every visible gap of a drawn straight line a "sufficient" number of points (what actually means mathematically dense system), finally all the gaps are filled and naturally, the line without gaps must be a continuous line! The confusion is crowned by establishment of equivalence between the straight line and a set of real numbers, which is the consequence of the fact that both the systems of axioms, Hilbert's for geometry [24] and Fraenkel-Zermelo's [16] for real numbers, implicitly contain axioms of the existence of actual infinity. The subsequent transfer of this property on physical quantities is supposed to be "intuitively" clear. But what is missing here is just the idea of how actual infinity, the product of human

imagination, can be observed experimentally. We dare to claim that there is no way for making it. Accepting then epistemological paradigm that the belief in something what cannot be observed is inadmissible for experimental scientists [46], we have logically also to abandon the system of real numbers (**R**) in physics, because it is the system rooting in non-observable entity, actual infinity.

Moreover, there is another important aspect worth mentioning. A set of real numbers **R** consists almost entirely of irrational numbers and **Q** is a very exclusive subset of **R**. Indeed, a set of rational numbers **Q** is countable and, as can easily be proved [39], any countable set $\subset$**R** is with respect to **R** measure zero. Similarly, the results of physical measurements perform also a countable set. Why should we then use an excessively redundant system of real numbers, in which all results of physical measurements ever made represent a set measure zero? Straightforward application of *principle of parsimony* (Ockham's razor) according to which "what is not necessary is redundant" leads us again to the above conclusion (vi), namely that the values of a physical quantity must $\in$**Q**.

Since the numerical value of any quantity is in fact *a ratio* (quotient) of two commensurable entities, the one of them being measured and the other one serving as a unit, it belongs again by definition to the set of rational numbers, $\in$**Q**. The statement that the value of any physical quantity is irrational, i.e. $\in$**R**, is in fact an *oxymoron*. (The most apposite term for such a situation would be "*incommensurability*" of quantity and unit.) Notice that formal transformation of a commensurable quantity into incommensurable one by multiplying original rational unit by an irrational coefficient, say by $\sqrt{2}$ or $(1/4\pi)$, is evidently only of a little help, because such an irrational unit etalon cannot be realized. (As an example of a unit which cannot be realized practically may serve radian.)

We should also exclude *infinite values* of physical quantities from our considerations, because of an important property of infinity, according to which a part of an infinite set can be equivalent to the whole set. This property violating the VIII-th axiom of Euclid ("*The whole is larger than its part*". [8]) denies the very sense of physical measurement, i.e. quantitative comparison of physical objects.

In order to illustrate our attitude, we add two examples. The first one is concerning a number $\sqrt{2}$ sometimes called Pythagorean constant. For Pythagoreans, integer numbers were the symbols by means of which all ideas concerning the nature of things were possible to explain. They particularly believed that all numbers can be expressed as the ratio of integers. It was then a terrible shock for them to discover that there is an "everyday quantity", corresponding to the diagonal of a square, which does not fit their picture of the world. From this nightmare, the Pythagoreans never recovered [7, 9]. Geometrical proof of irrationality of $\sqrt{2}$ (see Elementa [8], book X) starts with an obvious assumption that there exists a square having a diagonal. Quite elementary consideration then led to the conclusion that the diagonal of a square is not commensurable with its side, i.e. in modern notation, $\sqrt{2}$ is irrational and as such cannot be expressed as a ratio of two integers. Taking

into account, e.g. the continued fraction expansion of $\sqrt{2} = [1;\ 2,\ 2,\ \ldots]$, Pythagorean constant can be evaluated to arbitrary digit after the decimal point,

$$\sqrt{2} \approx 1.41421356237309504880168872420969807856967187537694 8\ldots \tag{24.16}$$

On the other hand, however, accuracy of any experimental realization of a square having, say 1 m side, is limited to ångstrom range, i.e. to 10th digit, so that the construction and observation of an exact square cannot be realized experimentally. Since there is then no exact square in the universe, either constructed or observed, the geometrical proof of incommensurability of its diagonal and side is only an abstract exercise.

Invincible difficulties are encountered also by solving another problem to set in the electrical circuit a current having exactly π A. Ramping our current source from say 3.14 to 3.15 A, one can believe that the value of π must be inevitably passed through. But such a belief is based solely on our arbitrary mathematical assumption (e.g. Fraenkel-Zermelo's axiom) that such a value actually exists. An alternative, setting the infinite expansion of π digit by digit, is for any experimentalist obviously hopeless.

As we can thus see, the mathematics appropriate for physics should abandon the actual infinity and should be exclusively based on rational numbers $\in \mathbf{Q}$ which ensure measurability and commensurability of physical quantities. Speaking in slogans, we can say, Aristotle was right—*Infinitum actu non datur* (Actual infinity does not exist) and also Pythagoras was right—the real physical world is controlled by integers. On the other hand, G. Cantor's idealistic Paradise involving actual infinity, irrationals, continuum and transfinite numbers should be avoided because it belongs rather to metaphysics than to physics. Symptomatically, even so ardent advocate of Cantor's set theory as D. Hilbert admitted [17], pressed by the facts, that "… The infinite is nowhere realized. Neither is it present in Nature nor is it admissible as a foundation of our rational thinking—a remarkable harmony between being and thinking". Indeed, infinity often generates contra-intuitive paradoxical consequences which are in odds with experimental observations.

As an example may serve the renormalization problem, a déjà vu appearing in different branches of physics, e.g. quantum field theory, hydrodynamics and others. Treating the space and time as a continuum, statistical or quantum-mechanical constructions are in the vicinity of certain singular points ill-defined. In order to compel a regular behaviour of physical quantities also in these singularities a highly sophisticated "renormalization procedure" must be invented for every particular case. However, as we believe the necessity of renormalization will very likely disappear just with the abandonment of continuity of space and other physical quantities.

Interestingly enough, just the same sharp borderline between physics and metaphysics can be found in many religious systems over the world. For example, in neo-pythagorean tradition as preserved in Jewish Kabbalah (likely compiled in

the thirteenth-century CE, e.g. [47]), the whole field of metaphysics is covered just by a single concept of "infinity", (Én-súf). Also B. Bolzano crossed the same borderline, making an ultimate decision in favour of existence of actual infinity on theological rather than on mathematical grounds [11]. Nevertheless, just these facts are in a perfect accord with our paradigm that entities belonging to the scope of physics must be inevitably finite, i.e. particularly represented by rational numbers.

At the end of this section, it should be stressed that the similar critical views concerning the concept of infinity as presented above can be found, less frequently, in arXiv publications [48] and, more often, also on various blogs. The internet chats are, however, mostly focused on the "reality" of different types of infinity in mathematics and on attempts to prove or disprove the existence of infinity there, using mathematical or traditional philosophical arguments (cf., e.g. [49]); the impact on physics is discussed only marginally. Considering the attempts for expelling infinity from mathematics purposeless, we have thus rather concentrated our attention on the role of infinity in physics and on physical arguments allied.

24.8 Principle of Conformity

In physics, it is generally taken for granted that the physical quantities are apt to express the observed laws of nature or fully reflect the physical properties of a given material system. Since there are no apparent limits for the validity of such a belief, this idea ought to be extrapolated to the mathematical structure of physical quantities itself. *Eo ipso*, there must be a structural correspondence or mapping between some physical aspects of a material systems and the arithmetic properties of numeral system used for the construction of its relevant description. This principle, which has been never satisfactory proved or substantiated, is sometimes called the *Principle of conformity of physics and mathematics* (cf. [50]). However, among scientists, a strong scepticism prevails with respect to this principle. As we are convinced, it is mainly due to the fact that a set of real numbers reveals no apparent structure; two different intervals of real numbers having the same length are topologically indistinguishable, providing quite a neutral and homogeneous system. Therefore, the direct correspondence between the sets of real numbers and highly diversified matter seems also unlikely. On the other hand, the room for the resemblance between the rational and especially integer numbers and material objects is much larger. For example, integers can be even or odd, revealing thus remarkable twofold symmetry. Moreover, any sufficiently long interval of integers has its own characteristic quasi-random distribution of primes, i.e. the individuality ("fingerprint") so typical for material objects.

If we thus accept the principle of conformity and our theorem (vi), according to which we have just only finite ordered sets of integers for description of physical systems in our disposal, we have to conclude that any material system is, at its ultimately lowest level, consisting of a finite number of discrete entities—"particles" revealing definite symmetry, order or distribution. Such a conclusion is,

however, essentially nothing but the message which should be, according to R. Feyman, in case of some cataclysm, transmitted to future generations (viz. *Atomic Hypothesis* [51]: "…all things are made of atoms - little particles that move around in perpetual motion etc"). At this connection should be also mentioned Fredkin's IT-related *Finite Nature Hypothesis* [52], according to which "…all things are discrete rather than continuous, grainy rather than smooth, step-wise rather than flowing. The most compelling model for meaningful transformation of one finite set to another is the computer, and in particular the computer architecture known as *Cellular Automata*". The universe is thus interpreted as a giant but finite computing machine. On the other hand, an assumption of continuity of physical quantities would immediately evoke a rather obsolete idea of impenetrability of matter and models of real bodies known, e.g. from mechanics of continua and field theory.

The *principle of conformity* may also serve for a long time searched rational basis of the so-called *physical numerology*. This contested branch of physics consists mainly of attempts to derive exact values of dimensionless monomials composed of physical constants solely by operations with mathematical constants and functions. Certainly, because of the absence of fundamental causal ("*Platonic*") theory behind, the numerological explanations are usually not trusted [53] and in fact no numerological explanation has ever been generally accepted by the physical community. However, the situation will change essentially if we interpret the principle of conformity as a true physical law and admit the fact that the physical quantities are expressible in terms of integers [proposition (vi)]. In such a case, the whole subject of physics would be covered by the *Theory of numbers,* and the conclusions based on the physical numerology will became a legitimate part of physical reasoning. The authors are aware of the boldness of such an approach, but the attempts already made in this direction, e.g. [50, 54–57], cannot be classified as completely unsuccessful and should be thus taken seriously. From this point of view, the systematic comparison of the relations known from the theory of numbers with those which are valid among physical quantities can perform a promising field of the future research.

Last but not least, we should mention here some symptoms of conformity or analogy between behaviour of rational number expressed in the form of continued fraction and that of a physical quantity measured with increasing precision. Indeed, according to relation (24.13) the improving of approximation of a rational number x means to proceed to the further convergent in the corresponding expansion. Since the every k-th convergent must fall between the $(k-1)$th and the $(k-2)$th convergents [cf. formula (24.12)], the neighbourhood of number x effectively behaves like a dense set. Nevertheless, if one reaches the last convergent, to keep doing further "better approximation" is not possible because the continued fraction reproduces the value of the last convergent with an absolute precision. Quite similarly, increasing step by step the precision of measurement of a macroscopic physical quantity x, the particular readings will densely fill a certain interval of values. Finally, however, by exceeding some precision limits, the values of the quantity start to be resolved into a single discrete eigenvalue which is exact and no more sensitive to the further increasing of measurement precision. Evidently, such a

type of conformity existing between rational numbers, $\in\mathbf{Q}$, and physical quantities cannot be extended to a set of real numbers $\in\mathbf{R}$. By increasing the precision of approximation of some values of real variable x, there is no reason to observe a jump to an exact value as described above but a continuous convergence to the limiting value of x is expected. As we are convinced, just the facts above are root of the persisting enigma of the transition from "classical (i.e. continuous)" to "quantum (i.e. discrete)" behaviour of physical quantities.

Further interesting details of "quantum-like" properties of physical quantities $\in\mathbf{Q}$ which can be described in terms of metric theory of remainders [42] and in terms of multiplicative properties or commutativity of remainders [45] are, however, out of the scope of this introducing paper.

24.9 Conclusions

In conclusion, our analysis has shown that the mathematical structure of physical quantities should essentially differ from that presented in the contemporary current literature. We have formulated a central theorem (vi) claiming that any physical quantity has to be expressed not by a real but just by a rational number ($\in\mathbf{Q}$). The most important consequence of this statement is the fact that the results of all physical observations ever made can be presented in the form of ordered finite sets of integers and that the actual infinity is quite redundant for the description of physical phenomena. The elimination of actual infinity from the physical reasoning ensures, among others, the commensurability of physical quantities and enables one to draw a sharp borderline between physics and metaphysics. The rationality of physical quantities fits also better to the actually observed granularity of matter, finiteness of observed universe and makes it possible to introduce in a meaningful way the conformity between mathematical and physical objects. Moreover, by admitting the usage of finite mathematics in physics one can quite naturally interpret the gradual transition from classical to discrete ("quantum") description as a direct consequence of increasing precision of measurement.

References

1. Palacios J (1964) Dimensional analysis. Macmillan & Co., Ltd., London
2. Cariñena JF, Santander M (1988) Dimensional analysis. In: Hawkes PW (ed) Advances of electronics and electron physics. Academic Press Inc., Boston
3. Savage CW, Ehrlich P (eds) (1992) Philosophical and foundational issues in measurement theory. LEA-Publishers, New Jersey
4. Mareš JJ (2011) Hotness manifold, phenomenological temperature and other related concepts of thermal physics. In: Šesták J et al (eds) Glassy, amorphous and nano-crystalline materials. Springer, Berlin, p 327
5. Mareš JJ (2015) Do we know what the temperature is? J Therm Anal Calorim 120:223–230

6. Cantor M (1907) Vorlesungen über Geschichte der Mathematik. B.G. Teubner, Leipzig
7. von Fritz K (1945) The discovery of incommensurability by Hippasus of Metapontum. Ann d Math 46:242–264
8. Euclid of Alexandria: Elements. There are a number of critical editions in various languages; authors used Základy (Elementa), Czech transl. by Servít F (1907) J.Č.M., Praha
9. Tropfke J (1930) Geschichte der Elementar-Mathematik. W. de Gruyter & Co., Berlin
10. Legendre AM (1823) Éléments de géométrie avec des notes, 2nd edn. F. Didot, Paris
11. Bolzano B (1850) Paradoxien des Unedlichen. Orig. ed.: F. Přihonsky, Budissin, Reprint: (2006) Verlag Dr. Müller, Saarbrücken
12. Dedekind R (1887) Was sind und was sollen die Zahlen? Stetigkeit und Irrationale Zahlen. Vieweg & Sohn, Braunschweig
13. Perron O (1921) Irrationalzahlen. Walter de Gruyter & Co., Berlin
14. du Bois-Reymond P (1882) Die Allgemeine Functionentheorie. H. Laupps, Tübingen
15. Cantor G (1932) Grundlagen einer allgemeinen Mannigfaltigkeitslehre; Ein mathematisch-philosophischer Versuch in der Lehre des Unendlichen. In: Zermelo E (ed) G. Cantor—gesammelte Abhandlungen mathematischen und philosophischen Inhalts. B. G. Teubner, Leipzig, pp 165–208
16. Fraenkel A (1923) Einleitung in die Mengenlehre. Springer, Berlin
17. Hilbert D (1926) Über das Unendliche. Math Annalen 95:161–190
18. Gauss CF (1860) Letter from 12 July 1831. Briefwechsel Gauß-Schumacher II, Altona, p 269
19. Kronecker L (1887) Ueber die Zahlbegriff. J Reine Angew Math 101:337–355
20. Kronecker L (1901) Vorlesungen über Mathematik. B. G. Teubner, Leipzig
21. Campbell NR (1920) Physics—the elements. Cambridge University Press, Cambridge; Reprint (1957) Foundations of science, New York, Dover
22. Bridgman PW (1927) The logic of modern physics. MacMillan, New York
23. Stevens SS (1946) On the theory of scales of measurement. Science 103:677–680
24. Hilbert D (1899) Grundlagen der Geometrie. In: Festschrift zur Feier der Enthüllung des Gauss-Weber-Denkmals in Göttingen, B.G. Teubner, Leipzig; English translation (1959) The foundations of geometry. The Open Court Publishing Co., La Salle, Ill
25. Hölder O (1901) Die Axiome der Quantität und die Lehre vom Mass. Berichte über die Verhandlungen der Königlich Sächsischen Gesellschaft der Wissenschaften zu Leipzig, Mathematisch-Physikalische Classe, Bd. 53:1–64
26. Lodge A (1888) The multiplication and division of concrete quantities. Nature 38:281–283
27. Maxwell JC (1873) A treatise on electricity and magnetism. Clarendon Press, Oxford
28. Einstein A (1923) The meaning of relativity. Princeton University Press, Princeton
29. Frank P (1932) Das Kausalgesetz und seine Grenzen. Springer, Wien
30. Kyburg Jr HE (1993) Measuring errors of measurement. In: Ref [3]
31. Sheynin OB (1979) C. F. Gauss and the theory of errors. Arch Hist Exact Sci 20:21–72
32. Czuber E (1932) Wahrscheinlichkeitsrechnung und ihre Anwendung auf Fehlerausgleichung. B.G. Teubner, Leipzig
33. Rényi A (1962) Wahrscheinlichkeitsrechnung mit einem Anhang über Informationstheorie. VEB Deutscher Verlag der Wissenschaften, Berlin. Czech transl. (1972) Teorie pravděpodobnosti. Academia, Praha
34. Lévy-Leblond J-M, Balibar F (1990) Quantics—rudiments of quantum physics. North-Holland, Amsterdam
35. von Helmholtz H (1887) Zählen und Messen, erkenntnisstheoretisch betrachtet. In: Philosophische Aufsätze, Eduard Zeller zu seinem fünfzigjährigen Doctotorjubiläum gewidmet, Fues' Verlag, Leipzig, pp 17–52
36. Russell B (1903) Principles of mathematics. Norton, New York
37. Krantz D, Luce RD, Suppes P, Tversky A (1971) Foundations of measurement: additive and polynomial representations. Academic Press, New York
38. Quine WVO (1951) Two dogmas of empiricism. Philos Rev 60:20–43
39. Hardy GH, Wright EM (2011) An introduction to the theory of numbers, 6th edn. Oxford University Press, Oxford

40. Leman A (1952) Vom periodischen Dezimalbruch zur Zahlentheorie. B. G. Teubner, Leipzig
41. Niven I (1961) Numbers: rational and irrational. The Mathematical association of America, Washington
42. Khinchin, AY (1949) Tsepnye droby. GITL, Leningrad; English transl (1964) Continued fractions. University Press, Chicago
43. Perron O (1913) Die Lehre von den Kettenbrüchen. B. G. Teubner, Leipzig
44. Olds CD (1963) Continued fractions. Random House Inc., New York
45. Sushkevich AK (1956) Teoriya chisel—elementarnyi kurs. Izdatel'stvo Kh. Uni., Khar'kiv
46. Heisenberg W (1925) Über quantentheoretische Umdeutung kinematischer und mechanischer Beziehungen. Z Phys 33:879–893
47. Bischoff E (1903) Die Kabbalah, Einführung in die Jüdische Mystik. Grieben's Verlag, Leipzig
48. Mueckenheim W (2008) The infinite in sciences and arts. In: Proceedings of the 2nd international symposium of mathematics and its connections to the arts and sciences. University of Southern Denmark, Odense, pp 265–272, arXiv:0709.4102 [math.GM]
49. Rodych V (2011) Wittgenstein's philosophy of mathematics. In: Zalta EN (ed) The Stanford encyclopedia of philosophy, http://plato.stanford.edu/archives/sum2011/entries/wittgenstein-mathematics/
50. Hartman RS (1942) Prime number and cosmical number. Philos Sci 9:190–196
51. Feynman R, Leighton RB, Sands M (1964) The Feynman's lectures on physics, vol I. Addison-Wesley, New York
52. Fredkin E (1992) Finite Nature. In: Proceedings of the XXVIIth Rencontre de Moriond, Les Arcs, Savoie, France
53. Good IJ (1988) Physical numerology. Technical Report No. 88–26, Dep. of Statistics, Virginia Tech., Blacksburg, VA24 601
54. McGoveran DO, Noyes HP (1989) Physical numerology? SLAC-PUB-4929, pp 1–17
55. Fürth R (1929) Über einen Zusammenhang zwischen quantenmechanischer Unschärfe und Struktur der Elementarteilchen und hierauf begründete Berechnung der Massen von Proton und Elektron. Z Phys 57:429–446
56. Kritov A (2013) A new large number numerical coincidences. Prog Phys 10:25–28
57. Eddington A (1939) The philosophy of physical science. Cambridge University Press, Cambridge

Chapter 25
Professional Value of Scientific Papers and Their Citation Responding

Jaroslav Fiala and Jaroslav Šesták

Quo usque tandem, scientometrics? or voice in the desert

Abstract In the course of the last thirty years, science enjoys a remarkable quantitative boom. For example, the total number of substances, registered in the Chemical Abstracts Service Registry File (CAS RF) at the end of the year 1985, was about 8 millions while at the end of the year 2015 it reached up to 104 millions. But, still more and more behind this quantitative boom of science are some of its qualitative aspects. So, e.g., the x–y–z coordinates of atoms in molecules are presently known for no more than 1 million of substances. For the majority of substances registered in CAS RF, we do not know much on their properties, how they react with other substances and to what purpose they could serve. Gmelin Institute for Inorganic Chemistry and Beilstein Institute for Organic Chemistry, which systematically gathered and extensively published such information since the nineteenth century, were canceled in 1997 (Gmelin) and 1998 (Beilstein). The number of scientific papers annually published increases, but the value of information they bring falls. The growth of sophisticated 'push-and-button' apparatuses allows easier preparation of publications while facilitating ready-to-publish data. Articles can thus be compiled by mere combination of different measurements usually without idea what it all is about and to what end this may serve. Driving force for the production of ever growing number of scientific papers is the need of authors to be distinguished in order to be well considered in seeing financial support. The money and fame are distributed to scientists according to their publication and citation scores. While the number of publications is clearly a quantitative criterion, much hopes have been placed on the citation, which promised to serve well as an adequate measure of the genuine scientific value, i.e., of quality of the

J. Fiala (✉) · J. Šesták
New Technologies Research Centre (NTC-ZČU), University of West Bohemia,
Universitní 8, 30114 Pilsen, Czech Republic
e-mail: fialjar@seznam.cz

J. Šesták
e-mail: sestak@fzu.cz

J. Šesták
Division of Solid-State Physics, Institute of Physics, v.v.i., Czech Academy of Sciences,
Cukrovarnická Str.10, 16200 Prague, Czech Republic

J. Šesták et al. (eds.), *Thermal Physics and Thermal Analysis*,
Hot Topics in Thermal Analysis and Calorimetry 11,
DOI 10.1007/978-3-319-45899-1_25

scientific work. That, and why these hopes were not accomplished, is discussed in detail in our contribution. Special case of Journal of Thermal Analysis and Calorimetry is discussed in more particulars.

25.1 Introduction: 'Publish or Perish'

Since 1969, the field of thermal analysis is well represented by the Journal of Thermal Analysis and Calorimetry (JTAC) and from 1970 also by Thermochimica Acta (TCA) both, with $IF_{2016} \geq 2$ [1] which belong to the family of about 70 000 scientific journals publishing annually about millions of papers while employing an order higher amount of pages. Moreover, almost half of the submitted manuscripts are in general view rejected directly or consequently during peer-reviewing. It is known that about half of the published papers are never read (or even noticed), and a mere one percent of publications receive over half of the citations from the total number of responses. About 90% of all actual information is never referred significant citation representing only several thousand scientific papers. In contrast to the seventeenth century science where a scientist could read almost all so far published books, a today's average scientist does not possess capacity to read even the papers related to their own specialization thus reliant to separate abstracts service only. Most scientists, however, do not even care to read anything else than their own previously published data, almost bothered by others' information and concentrated to reach as many citation responses as possible, and get financed under any circumstances.

What is the driving force for the production of such mounting number of scientific papers? Besides the original and natural need to share and disseminate the latest knowledge, there is now prevailing need to be distinguished in order to be well considered in seeing financial support. This fact was succinctly captured in the popular dictum '*Work-finish-publish*' attributed to M. Faraday (1791–1867) [2], which in this process saw the notoriously applauded phrase: '*publish or perish*' [3], see also [4], which is more and more worthy of serious reconsideration particularly in the age of computer's facilitated production of papers.

Almost twenty years ago, we published an assay [5] describing the storage and citation manners utilized in the sphere of scientific literature [6] noting '*if the aim of science is pursuit of truth, then the pursuit of information may even drive people from science.*' Since then the demand for a more extensive data dissemination accelerated because most scientific evaluations account on the need to be *seen* (reaching 'publicity'), which is rated according to the so-called journals' *impact factors* (pervasive ***IF***), journal rating, which is a position within the same periodical and scientifically aimed species (i.e., JournalUpdate) and the authors '*citation feedback*' (i.e., readers' responsiveness). Specific databases have been established and the available records are attentively followed to provide basis for a more unprejudiced scientific appraisal though the absolutely objective assessment is yet unreachable. Most common is the ISI '*Web of Science*' (WOS) which is a standard

in providing easy accessible data on a searched journal, paper, and/or author yielding figures on the total citation and annual citation record as well as partial data on the yearly mean responsiveness (including IF and H-index). However, for older data (before 1972) WOS requests application of a more specific search. In addition, there is another somehow largest database of peer-reviewed literature by Elsevier—SCOPUS [7], which needs somehow more concern in the process of searching and is mostly preferred when exploring more recent data (after 1990).

In the recent evaluative practice, all IF Journals surface from the Journal Citation Report (JCR) and are a product of Thomson ISI, providing thus a desired quantitative tool for journals appraisal. The IF is a measure of the frequency with which the so-called average article in a given journal has been cited within an agreed period of time (often a two-year interval). It is determined by dividing the number of such links (in x) to the publication of this journal in the previous two years (N_{cit}, x) and a number of publications in this journal (N_{pub}) in the same period of time. Thus, IF can be considered to be the average number of times published papers being cited up to two years after publication. Alternatively, a personalized sum of citations of the author's work is usually regarded as a representative indicator of his scientific success (i.e., readers' popularity). However, a higher informative value stays the average citations per publication or so signifies the newly introduced and widely accepted H-index (by American physicist J. Hirsch at 2005) which is used to measure the productivity of an individual (or group or institution) and is calculated by taking into account the balance between the number of publications and the number of citations per publication. The author's citation expressed in H-index has a value of N, if his publications have been cited at least N times and other publications less than N times. For example, the author's H-index of 22 tells us that he has 22 publications which received 22 citations on each paper or more. After all, the other *Proceedings Citation Index* is determined as a specific number of evaluating points for papers in the international journals with IF employing formula $J_{\mathrm{imp}} = 295 \times 10 + f$, where $f = (1 - N)/(1 + (N/0.057))$. Value of N is a normalized sequence within the given journals, $N = (P - 1)/(P_{\mathrm{max}} - 1)$, where P is the order of the periodical in the field sequenced according to Journal Citation Report in a row in descending order of the IF Journals. For illustration, the values for selected J_{imp} journals in which guidelines and application touch the field of thermal analysis and applied thermodynamics most published are summarized in Table 25.1.

25.2 Citation Strategy and Forgery

Recently, the structure of information has dramatically changed as the average library removed about 200 outdated volumes each year because of the shortage of space nowadays, moving to the space-saving digitalized records and robotic databasing. The last twenty years, we are also increasingly talking about the actuality how to evaluate the growing amount of scientific work often based on the citation analyses which put on view some of its problematic aspects [8–14]. It is

Table 25.1 Quantitative parameters of professional quality of selected journals quoting the year 2010 (courtesy by J. Leitner)

Journal	ISSN	IF_{2010}	Category (P_{max})	P	N_{av}	J_{imp}
J. Therm. Anal. Calor.	1388-6150	1.752	Chem., Analyt. (73)	39	0.562	21.9
			Chem. Phys. (127)	76		
Thermochim Acta	0040-6031	1.908	Chem., Analyt. (73)	33	0.500	25.1
			Chem. Phys. (127)	71		
J. Alloy Comp.	0925-8388	2.138	Chem. Phys. (127)	63	0.255	50.2
			Mater. Sci. Multi (225)	50		
J. Non-Cryst. Sol.	0022-3093	1.492	Mater. Sci. Ceram. (25)	4	0.252	50.7
			Mater. Sci. Multi (225)	86		
J. Chem. Thermodyn.	0021-9614	2.794	Chem. Phys. (127)	46	0.199	62.7
			Thermodynamics (51)	3		

surprising that in spite of the existing practices there was long ago recommended its termination [15], however, still in the year 2012 the statement condemning specific international initiatives DORA (San Francisco Declaration of Research Assessment) [16] stays alive. On the other hand, it should be indicated that a certain usefulness of citation analyses as an aid in the search for scientific information cannot be put in doubt.

What are the current problems? Mounting extent of publishable figures requires some of their inspections which are difficult to realize in the jungle of unreliable information and contradictory approaches due to a plethora of manuscripts and repetitive data. High-impacted journals use to refuse more than half of the manuscripts right away by the direct response of editors without peer-reviewing which led to increasing the supremacy of editors resulting in their dominancy rights to discriminate what are seen unsubstantiated, suspicious, and scholarly not purposed thoughts or what is correct or incorrect to publish in the given scientific journals. Even if the authors are responsible for their published figures, the rightness of which can be properly disapproved by reviewers but not subjected to individually motivated exclusion sometimes leading to an in-collusion establishment (∼almost editorial mafia). Having no friends, an anonymous author has little chance to get through the editorial manager of a respected journal often being rejected right away. Moreover, as put it by Max Planck (1858–1947): '*A new scientific truth does not win by convincing opponents but rather because opponents will die and a new generation grows up under the new truth that she will own.*'

What is a result? The hunt for published papers forces, however, on new and new journals establishment, providing thus the additional space for desired publicity. Because the published papers create money, it inspires as a source of financing for such a freshly founded periodical that brings the picture use avoiding the feared peer-reviewing or other fictive data revision and providing thus easy-to-reach papers. They keep riding on the name of the prestigious journal, misleading their names by reordering words, parasite on renowned names, and putting on a notional amount of different assessment factors, in whose name confusingly used the variation phrase of IF

such as 'Global Impact Factor' or 'Universal Impact Factor.' This new sort of periodical plagiarism coined even its own name 'predator journals.' More than 1000 such journals are listed in [17] where 50 of them are panderly labeled as 'International Journal of Advance of …? something?…' having even its Wikipedia site and providing stand-alone predator journals, see [17]. In 2013, a shocking news appeared that the so-called predator journals published about 420 thousand papers while in 2010 it was only 53 thousand so that many of the second-rate scientists helped starting there on their career. In this trend, another rank of consequent 'superpredatory' periodicals may occasionally appear to fill the 'gap after the gap.'

Divergent scientific results and impenetrability of certain novel ideas resulted in the formation of two spheres of science: one traditional—saying conservative, and the other dissident—saying too revolutionary. For example, this is the fate of dissident alternative to the mainstream physics discussing the future of physics paradigm and yielding 'intricate' journals such as Apeiron or Galilean Thermodynamics. Their challenges are often expressed as questions: Are changes in Newton's law of gravity necessary?; Can we believe that the Maxwell equations are universally applicable?; Is Einstein's light postulate still valid?; Are critical cosmological data being ignored?; Could rearrangement the primary building blocks of the current physics paradigm provide lead to new theories?; What are the connections between electricity and gravity?, What is dark matter?; Do the laws of motion and space-time need to be reexamined?; Is the universe finite or infinite?, etc., providing thus an enormous sphere for discussions and new imaginings.

Moreover, the growth of sophisticated 'push-and-botton' apparatuses allows easier preparation of publications while facilitating ready-to-print data and newly synthesized samples can be sent to investigation into different places easing multiple referencing. Articles can thus be compiled by mere combination of different measurements usually without idea what it all is about, without needed a scientific enrichment. Consequently, the journals are overflowed by formally perfectly written papers which describe various measurements on the mixture of materials; however, nobody is bothering to note them down at all. Such an administrator attitude is requiring more and more institutional approaches by a specialist cultured

in formal writing but underestimating those educated scientifically who are looking for a scientific development in extreme founding specialized institutes just devoted to professional perfecting (hopefully already yet scientific) inscription. Particular research began to gradually separate from its formal valuation. On limited financial resources, it has begun to rival university, academic, departmental, and industrial workplaces, so that the division between good and bad results is transferred from the utility to the formality. For example, the success rate of grant applications proposed in Czechia 2012 (GAČR) was 1/6 of submitted projects. From the statistics, it can be inferred that in the selection event when a statistical sample is less than 1/3 it becomes biased and objectiveness can be achieved only by *drawing lots*. It gives a subtle difference between the objective judgment and the biased verdict healthier based on some objective measures even if imperfect but still far better than a personal decision by preselected even so far renowned personalities.

Worth noting is the special role of Internet as a rising feed of everything that can not only give the desired resource finding but also provide otherwise deficient initiative for the compilations. It seems that it may even spontaneously replace dwindling databases, but without the crucial organization, systematization and feedback control. As an endless source of plagiarism, it has been found serving not only students—altogether it would be a subject for another chapter.

25.3 Scientific Information ⇒ Money and Fame

The point is that scientific publications (articles, journals, books, proceedings, and their parts) can be indexed (recognized and retrieved) by the materials they cite. This idea was published in 1955 [18] and implemented by Eugene Garfield in 1963 when his Institute for Scientific Information issued the first Science Citation Index (SCI) (annual edition: 9 volumes, 20 000 pages). Since then, SCI has been published regularly every year, being extended, updated, and improved continuously to make it possible for the readers to look up relevant information much more effectively than in any other way.

The great success of citation indexing in the scientific literature soon aroused the interest of administrators of scientific institutions in application of the citation analysis for the performance assessment of people who produce the scientific information [19, 20], for until then, scientific activities were simply expressed by the number of publications (articles, books, etc.), i.e., by a purely quantitative criterion, similarly as chemical activity (a) was measured by concentration (c) back in 1867 when Guldberg and Waage formulated their law. It was not sooner than in 1886 that van't Hoff came up with an idea that in addition to concentration (quantity), the chemical effects of a component of a reaction mass also depend on what the component is like, i.e., on its quality, with this effect being expressed by activity coefficient γ, i.e.,

$$a = c \,.\, \gamma.$$

The value of the activity coefficient, which represents the qualitative feature of the chemical activity, is determined by measuring partial pressures or electromotive forces [21]. An idea then occurred quite obviously: to evaluate similarly the scientific performance of an individual not only by the number of citation but also by the rate of citation of his or her publications, because '*the more frequently a publication is cited, the more it has been used by people in their own scientific work and, therefore, the higher is its scientific contribution.*' This idea is believed to be presented first by Robert K. Merton in his foreword to Garfield's book on citation indexing [22]. Garfield, himself, speaks about it in the last chapter of his book [23], also mentioning the problems that could arise when the citation criterion of scientific work quality is applied in an all-inclusive, routine manner without any more detailed deliberation. And problems really did come, as we have noted right at the beginning. The book 'The web of knowledge' published to honor Eugen Garfield on the occasion of his 80th birthday [24] discusses this on 151 out of the total 565 pages. It showed that the mere rate of citation of a publication was not, in many cases, an adequate measure of its scientific value. There were a number of modifications recommended and further more ingenious criteria developed, taking into account other aspects in addition to the rate of citation, such as H-index [25], G-index [26], and others [27], yet with no considerable improvement. What is behind the failure of the attempts to 'measure science'? It is the idea that the main thing that motivates the men of science in their work is money and the honors distributed on the basis of the results of such a measurement.

25.4 Light and Truth

Which are a tragic mistake and also the main reason behind the dissatisfaction of the scientific community with the manner its activities are assessed these days? Also the efficiency of citation indexing as a tool of retrieving scientific information has decreased greatly since the time citation started being used to assess scientific work. It is because information, i.e., communicable knowledge, admittedly, is the principal product of science but not its goal. After all, the goal of science is to know (i.e., to learn and recognize) the truth quoted by Goethe [28]:

> that I may detect the inmost force
>
> which binds the world, and guides its course;
>
> its germs, productive powers explore,
>
> and rummage in empty words no more!.

Citations of information products excellently help improve the efficiency of their retrieval (identification) but are completely unsuitable for the assessment of individual scientists. It is because, inter alia, scientists and their products are abundant,

so the laws reigning in this area are of statistical nature and are relevant for large sets only. The citation analysis can be used to compare the scientific activities of (approximately equally) big countries or giant scientific institutions or magazines that publish a great number of articles year by year, and even in this case only with great care and rather for longer periods of time than for the episodes of the lifetime careers of single authors [29, 30]. The material support and social recognition of individuals are based on the evaluation of their scientific activities. But the resources of both are limited, which tempts to establishing confidential agreements between the citing and the cited subjects and creating clans with the aim to win an exclusive position in procuring funds and fame. This probably is what the King of Bohemia and Holy Roman Emperor Charles IV had in mind when establishing in the Foundation Charter of the Prague (Charles') University in 1348 the duty of students to swear that they would continue devoting themselves to science after leaving the University '*not for filthy profit or passing fame but to propagate the truth and to brighten its light upon which the human welfare rests.*' Money and fame are the temporary worldly possessions but the truth is eternal and transcendent, really the 'light of the world' … '*Mehr Licht !*' Goethe said, dying. And '*I am the light of the world,*' Jesus said [31]. Moral weakness leads human sons and daughters to strive for their personal profits and fame more than for learning the truth. Evaluation of scientists based on the citations only strengthens this trend and disintegrates the scientific community internally. As '*every kingdom divided against itself is brought to desolation*' [32], evaluation of scientists based on the citation becomes the driving force of decline of the scientific community and of the human race in general. '*There will be no hope for honesty, peace and abundance in the world should individuals only pursue their own interests according to their ideas and should they not be attracted to and connected with something in common to understand clearly that only together they can achieve success in everything*' (Jan Amos Komenský, 1592–1670). If scientists are evaluated by citations, it means that they (owing to the cartelization of the scientific community), after all, only evaluate themselves. But for such an evaluation, to be fair, it is beyond their control: '*it is not in man that walked to direct his steps*' [33].

25.5 In the Depth of the Heart

That is why Englishmen used to say that if one wanted to do science, he had to have a good manor and a reliable administrator to fetch one thousand pounds every fortnight to London for him. This was the way of doing science by Joseph Achille le Bel (1847–1930), who, together with van't Hoff, suggested an idea that the four bonds of carbon are not oriented randomly, but have a specific spatial arrangement. Thanks to the wealth of his family, he did not have to work to earn his living and could set up his own private laboratory. Or, John William Strutt, Baron Raleigh (1842–1919), who inherited an estate with seven thousand acres of land (which his younger brother agreed to manage) but engaged himself in the theory of wave motion and its applications in acoustics, optics, and electromagnetism (Nobel Prize for physics in 1904). If one who has no such proverbial good manor wants to do science, he must earn his living himself and then do science as a hobby. He is the sponsor of his own scientific work, which he performs with love and pleasure as the best way ever of making its results useful for the mankind.

Like the women who did a proper portion of excellent scientific work while raising their children and, moreover, taking care of their husbands [34], such as Marie Skłodowska Curie (1867–1934), double Nobel Prize laureate (1903 and 1911), or Dorothy Mary Hodgkin (1910–1994), Nobel Prize laureate for the X-ray diffraction research of structures of biologically important substances (1964). Or like Johannes Kepler (1571–1630), who made his living as an astrologer for the Holy Roman Emperor Rudolph II, whereby he could do a lot of scientific work in astronomy and optics and also to write the essay titled 'Strena seu de nive sexangula' (1612) considered by the International Union of Crystallography to be the very first scientific monograph in crystallography. The laureate of the first Nobel Prize for physics, Wilhelm Conrad Roentgen (1845–1923), worked as a professor and an academic worker at the universities of Würzburg and Munich. He discovered the 'X-rays' called Roentgen radiation here and there in the world in remembrance of the discovery. But Roentgen was not supported for the purpose of discovering X-rays, all the more so that no one ever anticipated that anything like X-rays existed. In the afternoon of December 8, 1895, not even Roentgen himself had any faintest idea that there were any X-rays he would discover later that evening (in his apartment). And he even refused to have the discovery patented. When prompted to do so by Thomas Alva Edison, Roentgen said that he must have felt ashamed should he assume even if a small part of what X-rays could bring to the mankind. He donated the money he received together with the Nobel Prize to the University of Würzburg. He was ascetically modest. He was not interested in any honorary degrees and functions and he even did not accept the Order of the Crown through which Prince Luitpold of Bavaria promoted him to nobility in 1896 [35]. Unlike him, Thomas Alva Edison (1847–1931) left a big wealth after his death. For his exploring activities (the results of which could be envied by many renowned scientists), this talented and unprecedentedly hardworking man did not need any grant support, earning his living as a private person in his laboratories in

Menlo Park, New Jersey. With his life's credo—four hours of daily sleep is a need, five hours means leisure, and six hours means laziness—he could not use the money he earned through his work in anything else than again in his work and on his way to further discoveries. And that the scientific productivity does not need to be supported with social honors was proved by Josiah Willard Gibbs (1839–1903), for example. This man, whom Albert Einstein appraised as one of the most original thinkers-scientists the USA gave the mankind, father of vector analysis, coauthor of statistical physics, and pioneer in the physical chemistry of interfaces, never aspired to membership in scientific institutions and, in the USA, his works came to recognition as late as a couple of years after publishing.

Copper, silver, and gold are only slightly magnetic substances. When put into a magnetic field, small magnetic moments are only induced in their atoms in a direction opposite to that of the external magnetic field, thereby becoming only slightly weakened. At a room temperature, iron is a strongly magnetic (ferromagnetic) metal. Its atoms possess large magnetic moments. They are so strong that, by their mutual interaction, they are oriented spontaneously in the so-called Weiss domains even outside the external magnetic field. When placed in an external magnetic field, they turn to be aligned with its direction, increasing it considerably. If iron is heated up above Curie temperature, the heat will disturb the arrangement of the magnetic moments of its atoms, iron will stop being ferromagnetic and its ability to increase the external magnetic field will be reduced by several decimal orders of magnitude. Already Aristoteles recognized that human beings had the innate spontaneous interest in learning the truth. This interest is the intrinsic driver of science. The money and fame allocated by the authorities on the basis of some problematic scientometric criteria can suppress the interest in seeking truth in many of us …

25.6 Particularity of Thermal Analysis

Let us focus on the field of thermal analysis [1] where the outmost quotation reveals the JTAC paper by Ozawa [36] exceeding 1000 citations. This is still far below the responses to the most famous kinetic paper by Kissinger [37] exceeding 8000 citations which, however, bears some long overlooked errors [38]. The kinetic theme is followed in JTAC by the second best cited paper [39] exceeding 500 citations, which is one of hundred papers modifying the Kissinger method [37]. Only the third position keeps the paper from a different area of novel techniques [40] exceeding 300 citations becoming later widely functional.

These citation figures are comparable with the output of TCA, namely with the so-called SB equation [41] exhibiting uppermost 1000 responses followed by methodically oriented papers on thermoporometry [42] as well as the modulated DSC [43] with over 400 citations coauthored by the famous US thermoanalysts, Bernhard Wunderlich (1930–2012, with H-index >70 and citation response >17 000). Recently, a well cited has become recommendations of the ICTAC

Kinetic Committee [44] which, however, have been somehow contra-productive while declaring untouched guidance literally suggesting how to precisely evaluate and correctly publish false kinetic data [38]. Even if the consequences of heat transfer hindrance are inexcusably known since the time of legendary Newton cooling law [45] and Tian calorimetric equation [46], it has not been incorporated [38] as yet into theoretical treaties properly enough [47] which is the biggest transgression of modern thermal science.

Just a selection of best cited papers should not subsist as an optimum evaluation of the journal impact as we are also supposed to take care on the birth of new disciplines such as the field of geopolymers [48, 49], kinetic phase diagrams [50, 51], or econophysics [52, 53]. Such linked forward-looking prospects of thermal sciences have been recently investigated on the pages of three consequent books [54, 55] (including the present issue) published in the Springer series '*Hot topics of thermal analysis*' (2011, 2013, and 2017). We wish good luck to all those who will mold the evolution for the further upgrading of thermoanalytical theories and interpretations which is at this point in time needed very much.

25.7 Quality Time Quantity Is Constant

The number of scientific publications increases quickly. This can be illustrated by, e.g., the rate of growth of the number of substances registered in the Registry File (RF) of the Chemical Abstracts Service (CSA). During the first year of its building (1965), 211 934 substances were registered. During the year 2000, 6 031 378 substances, including 5 131 250 biosequences (amino acids in proteins and bases in nuclear acids) were registered, so that in December 31, this year, 28 499 942 substances including 10 938 676 biosequences were registered in the RF altogether. (The Abstracts File—AF, the second large database which CAS has been building since 1907, increased in the course of the year 2000 by 725 195 abstracts, the total number of abstracts in AF reaching 19 754 207 by the end of this year.) The growth of the number of registered substances from 1965 till 2000 is shown in the Table 25.2. After the year 2000, the number of registered substances has been increasing even more swiftly. So, e.g., 41 911 919 organic and inorganic substances and 60 642 927 biosequences were registered in CAS RF at 04:57:16 EST in 19.1.2009. The number of substances registered during the last six years is given in Table 25.3.

Unfortunately, the number of registered substances (≈100 000 000 substances) is much greater than the number of substances for which we know the (metrical data on) molecular structure, i.e., x–y–z coordinates of atoms in molecule (no more than 1 000 000 substances at all). And the difference between these two numbers quickly increases. This is important, e.g., in pharmacy, as knowledge of (metrical data on) molecular structure is required for each new medicament along with successful passing difficult tests the price of which is estimated to about 1 000 000 000 $. In the year 2000, some 160 new medicaments were successfully

Table 25.2 Growth of the number of substances registered in the database Chemical Abstracts Service Registry File

Year	ΔΣ	Year	ΔΣ		
1965	211 934	211 934	1983	418 905	6 346 713
1966	313 763	525 697	1984	563 390	6 910 103
1967	270 782	796 479	1985	544 618	7 454 721
1968	230 321	1 026 800	1986	628 966	8 083 687
1969	287 048	1 313 848	1987	610 480	8 694 167
1970	288 085	1 601 933	1988	602 465	9 296 632
1971	351 514	1 953 447	1989	615 987	9 912 619
1972	277 563	2 231 010	1990	663 342	10 575 961
1973	437 202	2 668 212	1991	684 252	11 260 213
1974	319 808	2 988 020	1992	690 313	11 950 526
1975	372 492	3 360 512	1993	680 230	12 630 756
1976	347 515	3 708 027	1994	777 212	13 407 968
1977	369 676	4 077 703	1995	1 186 334	14 594 302
1978	364 226	4 441 929	1996	1 269 246	15 863 548
1979	346 062	4 787 991	1997	1 376 942	17 240 490
1980	353 881	5 141 872	1998	1 679 913	18 920 403
1981	424 230	5 566 102	1999	3 548 161	22 468 564
1982	361 706	5 927 808	2000	6 031 378	28 499 942

Table 25.3 Total number of organic and inorganic substances (without biosequences) registered in the last years (counts in December of the current year)

Year	Count
2010	56 259 436
2011	64 765 463
2012	70 082 806
2013	76 705 260
2014	91 022 519
2015	104 228 986

developed, while only 10 new medicaments arose in 2012 … For the majority of substances registered in CAS RF, we do not know much on their properties, how they react with other substances and to what purpose they could serve. Such detailed information on inorganic and metal-organic substances was systematically gathered and extensively published by the Gmelin Institute for Inorganic Chemistry in Gmelin Handbook of Inorganic Chemistry—first German edition published in 1817. The institute was in the last years of its existence staffed by about 120 full-time employees, of whom about 80 had doctorates. Gmelin Handbook (GH) presented many valuable tables of numerical data, curves, and other graphic material, including diagrams of apparatus. GH reported of the applied or 'practical aspects' and methods of manufacture and included about 20% of patents considered. With regard to the detailed, in-depth processing of the work, the new volumes

of GH appeared with 2–25 years delay against the original data. Altogether 760 volumes of GH were issued on more than 240 000 pages, plus the 'Gmelin Formula Index' in 35 volumes. In the year 1997, the publishing of GH was stopped and the Gmelin Institute canceled. The basic reference work (database) on organic compounds is Beilstein Handbook of Organic Chemistry, which was published by the Beilsten Institute for Organic Chemistry in Frankfurt am Main. In the last years of its existence, the Institute had 160 full-time employees, of which 110 had a doctorate in chemistry and more than 500 outside contributors. Beilsten Handbook (BH) reported structural diagrams, information on natural occurrence and techniques of isolation from natural products, methods of preparation and manufacture, physical properties alone and in mixture with other compounds, chemical properties, methods of analytical determination as well as data of salts and addition compounds. The time lag between the publication of original data and the issue of the pertinent volume of BH was about 20 years. Altogether 503 volumes of BH were issued on 440 814 pages. In the year 1998, the publishing of BH was stopped.

The amount of substances registered by CAS RF during the past 50 years (m = 100 000 000) is stately. But in practice, we use mostly mixtures of substances rather than pure substances. And important is how the substances do behave to each other, how they react with each other. We would need information on $m \cdot (m - 1) = 10^{16}$ binary mixtures and on $m \cdot (m - 1) \cdot (m - 2) = 10^{24}$ mixtures … More useful—from scientific, technological, and economical points of view—would provide information on binary mixtures of 10 000 substances or on ternary mixtures of 470 substances than on those (pure) 100 000 000 substances which are registered today. It is better to know more on a small number of substances than little on a great number of substances.

Among the large number of registered substances, there are certainly not a few that (in the mixture with other substances) would prove to be remarkable catalysts, medicines, explosives, or maybe structural materials. The problem consists in the

fact that for 99% of the 100 000 000 of registered substances there are no reference spectra of identification features, with the help of which those substances could be recognized (the world's largest database for identification of substances—Powder Diffraction File of the International Centre for Diffraction Data—contains at present only about 800 000 X-ray diffraction reference spectra). Along with continued registration of new substances, we should also create the database of reference spectra of all substances that have already been registered; the spectra with the help of which those substances could—at least theoretically—be identified. But even in case that such a database would exist, the identification of substances registered in CAS RF will face serious problems. Expressing the reference spectra (IR, XRD, MS, NMR …) by n-dimensional pattern vectors [56–59], the identification of an unknown substance (unknown mixture of substances) means to find m numbers $c_1, c_2, \ldots, c_m$, which minimize the value of the residual misfit

$$\left| \vec{x} - \sum_{j=1}^{m} c_j \vec{y}_j \right|$$

where $\vec{x} = [x_1, x_2, \ldots, x_n]$ is the pattern vector (vectorial representation of the spectrum of identification features) of the unknown substance and $\vec{y}_j = \left[y_{j1}, y_{j2}, \ldots, y_{jn} \right]$; $j = 1, 2, \ldots, m$ are reference pattern vectors. Among the m reference spectra (pattern vectors), there are only n independent vectors, and each other pattern vector can be expressed as a linear superposition of those n independent pattern vectors. After the identification technique used, n amounts to several hundred or at most a few thousands. And that is why the identification of $m = 100\ 000\ 000$ substances would be hopelessly ambiguous. Unless the identified substance is composed of only several (not more than four or five) components, the spectrum of (such a simple) mixture is similar to spectra of each of its components in such a degree that the procedure in which the spectrum of the unknown is compared finally only with those reference spectra, which are mostly similar to the spectrum of unknown, does work. Efficiency of such a procedure can be even raised using factor analysis. The analyzed mixture (with the pattern vector $\vec{x}$) is separated onto $p - 1$ fraction and their spectra $\vec{x}_1 \equiv \vec{x}, \vec{x}_2, \ldots, \vec{x}_p$ are determined. Designating the spectra of (unknown) components of the analyzed substance $\vec{z}_1, \vec{z}_2, \ldots, \vec{z}_k$, then the vectors

$$\vec{x}_i = \sum_{j=1}^{k} c_{ij} \vec{z}_j; \quad i = 1, 2, \ldots, p$$

form a k-dimensional subspace (of the n-dimensional space of pattern vectors) with the base $\vec{z}_1, \vec{z}_2, \ldots, \vec{z}_k$, which can be from the p (2265 k) vectors $\vec{x}_1, \vec{x}_2, \ldots, \vec{x}_p$ of this subspace determined (reconstructed) by factor analysis—[60]—see Appendix: Factor analysis. As these are spectra of 'pure' substances (single-component 'mixtures'), their identification with the help of database $\{\vec{y}_1, \vec{y}_2, \ldots, \vec{y}_m\}$ of

reference spectra of known substances is easy. Of course, as far as we have at disposal a database of reference spectra of all substances which we want to identify. If we do not want to identify some substances once, then it is perhaps needless that they are registered …

Acknowledgements The present work was developed at the Join Research Laboratory of the Institute of Physics CAS and the New Technologies Centre of the University of West Bohemia in Pilzen (the CENTEM project, Reg. No. CZ.1.05/2.1.00/03.0088 that is cofunded from the ERDF as a part of the MEYS—Ministry of Education, Youth and Sports OP RDI Program and, in the follow-up sustainability stage supported through the CENTEM PLUS LO 1402). The paper is based on a long-lasting close letter friendship of J. Fiala with E. Garfield. Deep thanks are due to the shared efforts by J. Czarnecki (formerly with Chan, USA), I. Kraus Czech Technical University in Prague), J. Leitner (Institute of Chemical Technology in Prague), J.J. Mareš, P. Hubík, D. Kindl, V. Špička (Institute of Physics), P. Holba^{+}, M. Holeček, P. Martinec (Westbohemian University), M. Liška (Vitrum Laugaricio, Dubček University in Trenčín), J. Málek (University of Pardubice), A. Kállay-Menyhárd, J. Simon (Budapest University of Technology and Economics), and P. Šimon (President of the Slovak Chemical Society, Technical University in Bratislava). Cartoons (adapted) by courtesy of M. Barták and J. Jurčák.

Appendix: Factor Analysis

Spectra (pattern vectors of identification features) $\vec{z}_1, \vec{z}_2, \ldots, \vec{z}_k$ of components and their abundances in an analyzed mixture can be reconstructed (synthesized, extracted) from the spectra of this mixture $\vec{x}(\equiv \vec{x}_1)$ and its $(p-1)$ fractions $\vec{x}_2, \vec{x}_3, \ldots, \vec{x}_p (p \geq k)$, which can be obtained by separation of the mixture under consideration [60, 61]. Expressing the vectors $\vec{x}_1, \vec{x}_2, \ldots, \vec{x}_p$ by linear superposition of transposed eigenvectors $\vec{q}_1', q_2', \ldots, \vec{q}_n'$ of the Gramian matrix $\widehat{X}' \widehat{X}$ of the data matrix

$$\widehat{X} = \begin{bmatrix} \vec{x}_1 \\ \vec{x}_2 \\ \cdots \\ \vec{x}_p \end{bmatrix} = \begin{bmatrix} x_{11} & x_{12} & \ldots & x_{1n} \\ x_{21} & x_{22} & \ldots & x_{2n} \\ \ldots & \ldots & \ldots & \ldots \\ x_{p1} & x_{p2} & \ldots & x_{pn} \end{bmatrix}$$

associated with the eigenvalues $\lambda_1, \lambda_2, \ldots, \lambda_n$

$$\widehat{X}' \widehat{X} \vec{q}_j = \lambda_j \vec{q}_j, \quad j = 1, 2, \ldots, n,$$

arranged in descending order $(\lambda_1 \geq \lambda_2 \geq \cdots \geq \lambda_n)$ then

$$\vec{x}_i \sum_{j=1}^{n} u_{ij} \sqrt{\lambda_j} \vec{q}_j', \quad i = 1, 2, \ldots, p.$$

From this it is obvious that eigenvectors associated with the largest eigenvalues are most important and eigenvectors associated with the smallest eigenvalues are least important. So, retaining only the first k eigenvalues, which are significant at an accepted level, we have for $i = 1, 2, \ldots, p$

$$\vec{x}_i \doteq \sum_{j=1}^{k} v_{ij}\vec{q}'_j. \quad \text{Due to the fact that } \vec{x}_i = \sum_{j=1}^{k} d_{ij}\vec{z}_j$$

it holds, within the same tolerance, as well

$$\vec{z}_j = \left[z_{j1}, z_{j2}, \ldots, z_{jn}\right] \doteq \sum_{m=0}^{k} t_{jm}\vec{q}'_m; \quad j = 1, 2, \ldots, k.$$

The coefficients t_{jm} (elements of the matrix $\widehat{T} = \left[t_{jm}\right]_{j=1,\ldots,k}^{m=1,\ldots,k}$) are then determined making use of the fact that intensities of lines of the components of analyzed mixture in the spectra of the mixture and its fractions are nonnegative

$$\widehat{Z} = \begin{bmatrix} \vec{z}_1 \\ \vec{z}_2 \\ \cdots \\ \vec{z}_k \end{bmatrix} = \begin{bmatrix} z_{11} & z_{12} & \cdots & z_{1n} \\ z_{21} & z_{22} & \cdots & z_{2n} \\ \cdots & \cdots & \cdots & \cdots \\ z_{k1} & z_{k2} & \cdots & z_{kn} \end{bmatrix} = \begin{bmatrix} t_{11} & t_{12} & \cdots & t_{1k} \\ t_{21} & t_{22} & \cdots & t_{2k} \\ \cdots & \cdots & \cdots & \cdots \\ t_{k1} & t_{k2} & \cdots & t_{kk} \end{bmatrix} \cdot \begin{bmatrix} \vec{q}'_1 \\ \vec{q}'_2 \\ \cdots \\ \vec{q}'_k \end{bmatrix} = \widehat{T} \cdot \widehat{Q} \geq \widehat{O}$$

where

$$\widehat{Q} = \begin{bmatrix} \vec{q}'_1 \\ \vec{q}'_2 \\ \cdots \\ \vec{q}'_k \end{bmatrix} = \begin{bmatrix} q'_{11} & q'_{12} & \cdots & q'_{1n} \\ q'_{21} & q'_{22} & \cdots & q'_{2n} \\ \cdots & \cdots & \cdots & \cdots \\ q'_{k1} & q'_{k2} & \cdots & q'_{kn} \end{bmatrix},$$

and also abundances $d_{i,j}$ of those components in the analyzed mixture and their fractions are nonnegative

$$\widehat{D} = \begin{bmatrix} d_{11} & d_{12} & \cdots & d_{1k} \\ d_{21} & d_{22} & \cdots & d_{2k} \\ \cdots & \cdots & \cdots & \cdots \\ d_{p1} & d_{p2} & \cdots & d_{pk} \end{bmatrix} = \widehat{X}\widehat{Q}'\widehat{T}'\left(\widehat{T}\widehat{Q}\widehat{Q}'\widehat{T}'\right)^{-1} \geq \widehat{O}$$

(the Procrustes problem of quadratic programming).

References

1. Šesták J (2012) Citation records and some forgotten anniversaries in thermal analysis. J Thermal Anal Calorim 108:511–518; and Šesták J, Fiala J, Gavrichev SK (2017) Evaluation of the professional worth of scientific papers, their citation responding and the publication authority of Journal of Thermal Analysis and Calorimetry. J Thermal Anal Calorim doi:10.1007/s10973-017-6178-7
2. http://en.wikiquote.org/wiki/Michael Faraday
3. http://en.wikipedia.org/wiki/Publish or parish
4. Garfield E (1996) What is the primordial reference for the phrase 'Publish or parish'? Scientist 10:11
5. Fiala J, Šesták J (2000) Databases in material science: contemporary state and future. J Thermal Anal Calorim 60:1101–1110
6. Fiala J (1987) Information flood: fiction and reality. Thermochim Acta 110:11–22
7. Burnham JF (2006) SCOPUS database: a review. Biomed Digit Libr 3:1
8. Seglen PO (1997) Why the impact factor of journals should not be used for evaluating research. Br Med J 314:498–502
9. Adam D (2002) Citation analysis: the counting house. Nature 415:726–729
10. Scully C, Lodge H (2005) Impact factors and their significance; overrated or misused? Br Dent J 198:391–393
11. Lehmann S, Jackson AD, Lautrup BE (2006) Measures for measures. Nature 444:1003–1004
12. Editorial (2008) Papers about papers. Nature Nanotechnol 3:633
13. Frey BS, Rost K (2010) Do rankings reflect research quality? J Appl Ecol 13:1–38
14. Editorial (2013) Beware the impact factor. Nat Mater 12:89
15. Editorial (2003) Deciphering impact factors. Nat Neurosci 6:783
16. Ylä-Herttuala S (2015) From the impact factor to DORA and the scientific content of articles. Mol Ther 23:609
17. http://scholarlyoa.com/individual-journals/ and Beall J, Criteria for determining predatory open-access publishers. http://scholarlyva.com/
18. Garfield E (1955) A new dimension in documentation through association of ideas. Science 122:108–111
19. Johnson AA, Davis RB (1975) The research productivity of academic materials scientists. J Met 27(6):28–29
20. Roy R (1976) Comments on citation study of materials science departments. J Met 28:29–30
21. Mannchen W (1965) Einführung in die Thermodynamik der Mischphasen. VEB Deutscher Verlag für Grundstoffindustrie, Leipzig
22. Garfiel E (1979) Citation indexing. Wiley, New York
23. Garfield E (1979) Perspective on citation analysis of scientists, Chap 10. In Garfield E (ed) Citation indexing. Wiley, New York
24. Cronin B, Atkins HB (eds) (2000) The web of knowledge. Information Today, Medford
25. Hirsch JE (2005) An index to quantify an individual's scientific research output. Proc Natl Acad Sci USA 102:16569–16572
26. Eghe L (2006) Theory and practise of the G-index. Scientometrics 69:131–152
27. Bornmann L, Mutz R, Hug SE, Daniel H-D (2011) A multilevel meta-analysis of studies reporting correlations between the H-index and 37 different H-index variants. Informetrics 5:346–359
28. Goethe JW (1870) Faust a tragedy, translated by Bayard Taylor, Part I, Scene I. Night, Houghton Mifflin Company, Boston and New York
29. Ketcham CM (2007) Predicting impact factor one year in advance. Lab Invest 87:520–526
30. Garfield E (1999) Journal impact factor: a brief review. Can Med Assoc J 161:979–980
31. The Gospel according to St. John 8:12
32. The Gospel according to St. Matthew 12:25
33. The Book of the prophet Jeremiah 10:23

34. Kraus I (2015) Ženy v dějinách matematiky, fyziky a astronomie (Ladies in the history of mathematics and physics), Česká technika – nakladatelství ČVUT, Praha
35. Kraus I (1997) Wilhelm Conrad Röntgen, dědic šťastné náhody (Wilhelm Conrad Röntgen: the heritage of lucky coincidence), Prometheus, Praha
36. Ozawa T (1970) Kinetic analysis of derivative curves in thermal analysis. J Thermal Anal 2:301–324
37. Kissinger HE (1957) Reaction kinetics in differential thermal analysis. Anal Chem 29:1702–1706
38. Šesták J (2014) Is the original Kissinger equation obsolete today—not obsolete the entire non-isothermal kinetics? J Thermal Anal Calorim 117:1173–1177; and (2014) Imperfections of Kissinger evaluation method and crystallization kinetics. Glass Physics Chem 40:486–449
39. Augis JA, Bennet JE (1978) Calculation of Avrami parameters for heterogeneous solid-state reactions using a modification of Kissinger method. J Thermal Anal 13:283–292
40. Reading M, Elliot D, Hill VL (1993) A new approach to the calorimetric investigations of physical and chemical transitions. J Thermal Anal Calor 40:949–955
41. Šesták J, Berggren G (1971) Study of the kinetics of the mechanism of solid-state reactions at increasing temperatures. Thermochim Acta 3:1–12
42. Brun M, Lallemand A, Quinson JF, Eyraud C (1977) New method for simultaneous determination of size and shape of pores—thermoporometry. Thermochim Acta 21:59–88
43. Wunderlich B, Jin YM, Boller Y (1994) A mathematical description of DSC based on periodic temperature modulations. Thermochim Acta 238:277–293
44. Vyazovkin S, Burnham AK, Criado JN, Perez-Maqueda LA, Popescu C, Sbirrazzuoli N (2011) ICTAC Kinetics Committee recommendations for performing kinetic computations on thermal analysis data. Thermochim Acta 520(1–19)
45. Newton I (1701) Scale graduum Caloris. Calorum Descriptiones & Signa. Philosophical Trans 22:824–829
46. Tian A (1933) Recherches sue la calorimétrie. Généralisation de la méthode de compensation électrique: Microcalorimétrie. J de Chimie-Physiq 30:665–708
47. Holba P, Šesták J (2015) Heat inertia and its role in thermal analysis. J Thermal Anal Calor 121:303–307
48. Davidovits J (1989) Geopolymers and geopolymeric materials. J Thermal Anal 35:429–441; and (1991) Geopolymers: inorganic polymeric materials. J Thermal Anal 37:1633–1656; and Šesták J, Foller B (2012) Some aspects of composite inorganic polysialates. J Thermal Anal Calor 109:1–5
49. Davidovits J (2015) Geopolymer Chemistry and Applications. Institut Géopolymère, Saint-Quentin (previously 2008 and 2011). ISBN 9782951482098
50. Šesták J, Chvoj Z (1987) Thermodynamics of kinetic phase diagrams. J Thermal Anal 32:325–333; and (1991) Nonequilibrium kinetic phase diagrams in the $PbCl_2$-AgCl eutectic system. J Therm Anal 43:439–448
51. Chvoj Z, Šesták J, Tříska A (eds) (1991) Kinetic phase diagrams: non-equilibrium phase transitions. Elsevier, Amsterdam
52. Mimkes J (1995) Binary alloys as a model for the multicultural society. J Thermal Anal 43:521; and (2000) Society as many particle system. J Thermal Anal Calor 60:1055
53. Richmond P, Mimkes J, Hutzler S (2013) Econophysics and physical economics. Oxford University Press, Oxford; and Šesták J (2005) Thermodynamics, econophysics and societal behavior, Chap 8. In: Šesták J (ed) Science of heat and thermophysical studies: a generalized approach to thermal analysis. Elsevier, Amsterdam
54. Šesták J, Mareš JJ, Hubík P (eds) (2011) Glassy, amorphous and nano-crystalline materials: thermal physics, analysis, structure and properties, vol 8. Springer, Berlin, Heidelberg. ISBN 978-90-481-2881-5
55. Šesták J, Šimon P (eds) (2013) Thermal analysis of micro-, nano- and non-crystalline materials: transformation, crystallization, kinetics and thermodynamics, vol 9. Springer, Berlin, Heidelberg. ISBN 978-90-481-3149-5

56. Fiala J (1972) Algebraic conception of the powder diffraction identification system. J Phys D: Appl Phys 5:1874–1876; and (1976) Optimization of powder-diffraction identification. J Appl Crystallogr 9:429–432
57. Fiala J (1980) Powder diffraction analysis of a three-component sample. Anal Chem 52:1300–1304
58. Fiala J (1982) A new method for powder diffraction phase analysis. Cryst Res Technol 17:643–650
59. Fiala J, Říha J (2014) X-ray diffraction analysis of materials. Hutnické listy 67:2–7
60. Malinowski ER, Howery DG (1980) Factor analysis in chemistry. Wiley, New York
61. Martens H, Naes T (1989) Multivariate calibration. Wiley, Chichester

Index

J. Šesták et al. (eds.), *Thermal Physics and Thermal Analysis*,
Hot Topics in Thermal Analysis and Calorimetry 11,
DOI 10.1007/978-3-319-45899-1